

LA-8843

①

I-182

lh. 119

Los Alamos National Laboratory is operated by the University of California for the United States Department of Energy under contract W-7405-ENG-36.

MASTER

The Los Alamos Geostationary Orbit Synoptic Data Set

A Compilation of Energetic Particle Data



Los Alamos

Los Alamos National Laboratory
Los Alamos, New Mexico 87545

DISTRIBUTION OF THIS DOCUMENT IS UNLIMITED

**THE LOS ALAMOS GEOSTATIONARY
ORBIT SYNOPTIC DATA SET**
A Compilation of Energetic Particle Data

by

D. N. Baker, P. R. Higbie, R. D. Belian, W. P. Aiello, E. W. Hones, Jr.,
E. R. Tech, M. F. Halbig, J. B. Payne, R. Robinson, and S. Kedge

ABSTRACT

Energetic electron (30 to 2000 keV) and proton (145 keV to 150 MeV) measurements made by Los Alamos National Laboratory sensors at geostationary orbit $6.6 R_E$ are summarized. The data are plotted in terms of daily average spectra, 3-h local time averages, and in a variety of statistical formats. The data summarize conditions from mid-1976 through 1978 (S/C 1976-059) and from early 1977 through 1978 (S/C 1977-007). The compilations correspond to measurements at 35°W , 70°W , and 135°W geographic longitude and, thus, are indicative of conditions at 9° , 11° , and 4.8° geomagnetic latitude, respectively. Most of this report is comprised of data plots that are organized according to Carrington solar rotations so that the data can be easily compared to solar rotation-dependent interplanetary data. As shown in prior studies, variations in solar wind conditions modulate particle intensity within the terrestrial magnetosphere. The effects of these variations are demonstrated and discussed. Potential uses of the Synoptic Data Set by the scientific and applications-oriented communities are also discussed.

I. INTRODUCTION

The geostationary orbit is a region of considerable human interest in space. At this location, $6.6 R_E$ (42 000 km from the center of the earth), a spacecraft appears to remain fixed above a given point on the earth's geographic equator because the orbiting satellite completes one revolution as the earth completes one rotation each day. This geostationary orbit is therefore very useful for many satellite applications to weather, communication, and military needs when it is desirable for a spacecraft to maintain a constant position relative to particular geographic locations or land masses.

Scientifically, $6.6 R_E$ is also a very interesting position within the terrestrial magnetosphere. As illustrated, for

example, on the cover of this report, the geostationary orbit is at the outer terminus of the terrestrial trapped radiation region (outer radiation zone) and is also at the inner edge of the magnetotail plasma sheet. From a geostationary spacecraft platform, therefore, scientific instrumentation can probe the highly dynamic outer magnetosphere and can assess both the trapped (Van Allen) radiation environment and plasma sheet conditions, the latter being strongly modulated by geomagnetic activity.

The Los Alamos National Laboratory has provided energetic particle sensors for a variety of geostationary satellites. Each of these energetic particle instruments, consisting of several subsystems, is called a Charged Particle Analyzer (CPA) experiment. Each

CPA provides an environmental monitoring function for the satellite of which it is part and also provides a global assessment of magnetospheric conditions in a variety of ways, which we will discuss.

From mid-1976 to the present, CPA instruments have collected data almost continually on the geostationary orbit environment. It is the purpose of this report to further describe the nature of the CPA measurements and to present a summary of all available CPA energetic particle measurements made from 1976 through 1978. Because the form of the geostationary data presented here is an overview of a very detailed data set that we have acquired, we refer to our compilation as the Los Alamos Synoptic Data Set. In this report, we describe the Synoptic Data Set (SDS), its observational basis, and its potential uses for the scientific and applications-oriented communities.

II. SPACECRAFT AND INSTRUMENTATION

The data described in this report were acquired by the CPA instruments onboard spacecraft (S/C) 1976-059 and 1977-007. The data from S/C 1976-059 extend from July 1976 through the end of 1978 (Appendix A), and the data from S/C 1977-007 extend from February 1977 through 1978 (Appendix B). CPAs on three geosynchronous satellites continue to return data to the present time. Data acquired after 1978 from various satellites will be the subject of future reports. Before February 1977, S/C 1976-059 was positioned at $\sim 35^\circ\text{W}$ geographic longitude (at a magnetic latitude of 9°). From February 1977 through 1978, S/C 1976-059 was at $\sim 70^\circ\text{W}$ and S/C 1977-007 was located at $\sim 135^\circ\text{W}$. These latter longitudinal positions correspond, respectively, to magnetic latitudes of $\sim 11^\circ$ and $\sim 4.8^\circ$.

The CPA instruments have been described in some detail in prior reports.¹⁻³ Each CPA consists of separate electron and proton sensor systems. The electron detectors are designated LoE (low-energy electron) and HiE (high-energy electron). LoE consists of a fan of five separate detector-collimator units at 0° , $\pm 30^\circ$, and $\pm 60^\circ$ to the spacecraft equatorial plane. The spacecraft rotate with a 10-s period about an axis that points continually toward the center of the earth. Thus, complete (over the unit sphere), continuous pitch-angle measurements of the electron distribution are made by LoE each 10 s for essentially all magnetic field orientations. Each LoE sensor-collimator unit has a geometric

factor of $3.6 \times 10^{-3} \text{ cm}^2\text{-sr}$ and is sensitive to electrons between 30 and 300 keV (in six channels). The basic CPA sampling rate is 8 ms, so that each energy channel of each sensor is sampled 40 times per 10-s spacecraft rotation (that is, 1200 total samples per rotation).

The HiE subsystem consists of a single detector-collimator unit that is pointed radially outward in the spacecraft equatorial (0°) plane. The HiE geometric factor is $1.8 \times 10^{-2} \text{ cm}^2\text{-sr}$ and its range of sensitivity is between 0.2 and ~ 2 MeV. Because a single collimator unit (half-angle of acceptance $\sim 4^\circ$) is used in HiE, only a relatively narrow band of the unit sphere is sampled as the spacecraft rotates. For normal, approximately dipolar magnetic field orientations, nearly all pitch angles would be sampled by HiE, but for nondipolar (taillike) magnetic field configurations often encountered near midnight at $6.6 R_E$, very limited pitch-angle sampling is possible.

Both LoE and HiE have relatively thick aluminized mylar windows immediately in front of the sensitive solid-state detector elements. This window eliminates contamination by sunlight, by very low energy ($\lesssim 10$ keV) electrons, and by protons below ~ 250 -300 keV. Because of this feature, LoE provides a "clean" measurement of the $\lesssim 300$ -keV electron component and is free of proton or low-energy pileup contributions. In the case of HiE, the measurement relies on the soft spectral nature and low relative flux ratio of the $\gtrsim 300$ -keV proton (ion) component⁴ to effect the 0.2- to 2.0-MeV electron measurement in the presence of background ions.

The energetic proton measurement at $6.6 R_E$ is made by two separate CPA particle telescope systems: low-energy proton (LoP) and high-energy proton (HiP). LoP is a single, thin ($\sim 40\text{-}\mu$) surface barrier solid-state detector in front of an anticoincidence scintillator element. A sweep magnet is part of the LoP collimation system and eliminates electrons with energy $\lesssim 0.5$ MeV from entering the LoP sensors. LoP has a geometric factor of $3.9 \times 10^{-3} \text{ cm}^2\text{-sr}$ and measures ions, which we identify as primarily protons, from 145 to 560 keV (10 channels). The HiP is a four-element telescope consisting of three solid-state detectors encased in the fourth sensor element, which is a plastic anticoincidence scintillator cup. HiP also has a strong sweeping magnet to eliminate contamination by $\lesssim 1.0$ -MeV electrons. The high-energy proton telescope measures protons between 0.4 and 150 MeV in 16 quasi-logarithmic differential energy channels with a geometric factor of $4.4 \times 10^{-2} \text{ cm}^2\text{-sr}$ ($\sim 8 \times 10^{-2} \text{ cm}^2\text{-sr}$ for $E_p > 25$ MeV).

As in the case of the electron sensors, LoP and HiP have passive window elements to maintain a light-tight operation. Like HiE, the proton sensors consist of one collimation view direction (0° in the spacecraft equatorial plane) so that pitch-angle coverage is complete for a dipolar magnetic field orientation, but is incomplete for a nondipolar (taillike) magnetic field. More thorough descriptions and illustrations of the LoP and HiP elements of the CPA (and results therefrom) are contained in Refs. 4, 6, and 7.

III. DATA PROCESSING

From 1976 through 1978, CPA data were processed by a set of "Phase I" analysis computer codes. The basic directional count rate arrays were read in by the programs on a rotation-by-rotation basis, particle anisotropies were calculated,⁸ spin-averaged count rates were formed, and 2-h per frame microfiche plots of all quantities were generated. Thus, a high time resolution (10-s) archival data set of fiche plots was produced. In addition, as the spin-averaged data set was generated, CPA data were stored to form a broader average data set (with a basic 1-h resolution) for all particle parameters. The concatenated hour-averaged data tapes from the CPAs on S/C 1976-059 and S/C 1977-007 form the basis for the present SDS presentation. The hour-averaged synoptic data have been previously reported in a study of the low-energy electron anisotropy (for different geomagnetic conditions as measured by the planetary K_p index) as a function of local time (LT).⁹

Using the hour-averaged data tapes, a subsequent computer program sorted data for each day into eight local time bins 3 h wide: 0-3, 3-6,..., 21-24 LT. The sorted LT samples were then averaged together to give mean particle count rate values, etc., for each of the eight LT sectors. This LT sorting in the SDS was expected to take account of the strong LT (diurnal) variability that energetic particles exhibit because of, for example, drift-shell splitting effects.

Interplanetary conditions substantially affect the energetic particle population at geostationary orbit.^{3,4,10,11} This effect, or control, appears to operate primarily through the effect of solar wind bulk speed. The solar wind parameters often undergo a recurrent and quasi-periodic variability because of the long-lived solar wind streams that emerge from the sun.¹² Thus, various researchers^{3,10} found that long-term energetic particle flux variations could be well-organized by plotting data

in terms of solar rotation periods. Just as Feldman et al.¹² used Carrington 27-day solar rotations to organize interplanetary data, we used Carrington solar rotations to organize the SDS.

Using the LT sorted 3-h averages, we broke the days of data into Carrington Rotations, blocking CPA data into ~13 solar rotation periods for each year. LT and solar rotation breakdowns of the data form the bulk of this report. After the above sorting was accomplished, detector counting rates were converted to differential particle fluxes ($\text{cm}^{-2}\text{-s}^{-1}\text{-sr}^{-1}\text{-keV}^{-1}$) and plotted as described in Sec. IV. Daily count rate averages (that is, averages over all LTs) were also converted to fluxes for the "stacked spectrum" plots discussed below.

The 1-h average data were used for several types of statistical analyses in the rest of this report. These statistical studies involve, for example, assessments of probabilities that the flux of a particular energetic particle component would exceed any given flux value. These statistical studies are based on similar analyses performed, for example, by Paulikas et al.¹³

IV. SYNOPTIC DATA PLOT FORMATS

The SDS plots in this report are divided into two parts: S/C 1976-059 (Appendix A) and S/C 1977-007 (Appendix B). As discussed above, the periods of data coverage from the two spacecraft largely overlap and instrumentation is essentially identical. Therefore, differences between the measurements made at the same time by the CPAs aboard the two satellites must be primarily the effects of magnetic latitude, which can be quite large,¹⁴ or else LT effects.

For each solar rotation, we show three pages of data. As illustrated by the first plots (for Carrington Rotation No. 1955) in Appendix A, the first page in each solar rotation series illustrates pseudo-three-dimensional stacked spectrum plots. For both electrons and ions, we have averaged all LT data and calculated the daily average particle differential energy spectrum. Then, for each day of the solar rotation, we plot the logarithm (base 10) of the electrons or protons ($\text{cm}^{-2}\text{-sr}^{-1}\text{-keV}^{-1}$) vs the logarithm of the particle kinetic energy (in keV). The third (or perspective) dimension of each plot is solar rotation day number (from 1 to 27) running to the right.

The upper part of each daily spectrum page illustrates the variation in electron distribution functions between ~30 and 2000 keV. To aid in the three-dimensional representation of the spectral variation on each plot, four

dashed lines are added, which run across the solar rotation period, connecting the spectra at four specific energy channel points. These dashed lines are intended to help the user visualize the "spectral surface" determined by the CPA for each solar rotation period.

The lower part of the daily spectrum page illustrates the variation in proton (ion) distribution functions above 145 keV. As noted for Carrington Rotation No. 1955 data, proton fluxes typically reach a background level of $\sim 10^{-2}$ ($\text{cm}^2\text{-s-sr-keV}^{-1}$) at $E_p \approx 1000$ keV. Thus, although the CPA makes proton measurements up to 150 MeV, we typically show the proton energy range only up to ~ 20 MeV. The proton stacked spectrum plot is identical to that of the electron plot, including the use of dashed lines to aid in emphasizing the spectral surface features.

Additional labelling on each spectrum plot includes (1) spacecraft identification (for example, S/C 1976-059) in the upper left-hand corner, (2) the start time of each solar rotation period in month-day-year in the lower left-hand corner (day 1 of the rotation corresponds to the start date), and (3) the Carrington Rotation number of the solar rotation in the lower right-hand corner.

On both the second and third pages of each solar rotation grouping there are four frames of data. As noted at the top center in each frame, the data in each case correspond to 3-h LT averages. From the upper left-hand corner of page 2 to the bottom right-hand corner of page 3 we show data running from 0-3 hours LT to 21-24 hours LT.

Within each major 3-h LT frame there are three panels. (1) The upper panel in each case plots the log of the electron flux (that is, electrons/ $\text{cm}^2\text{-s-sr-keV}^{-1}$) for selected differential channels vs day of the solar rotation. Table I shows the energy ranges and plotting symbols used for the electron plots. (2) The second panel shows the proton fluxes measured by the LoP portion of the

TABLE II. LoP Proton Solar Rotation Flux Plots

Curve Number	Plotting Symbol	Energy Range (keV)
1		145-160
2	o	175-190
3	△	215-245
4	+	290-340
5	x	400-480

CPA in terms of the log of the proton flux (protons/ $\text{cm}^2\text{-s-sr-keV}^{-1}$) vs solar rotation day number. Table II shows the details of the panel 2 information. (3) The third panel shows the proton fluxes measured by the HiP portion of the CPA. This panel is also shown in terms of the log of the proton flux (protons/ $\text{cm}^2\text{-s-sr-keV}^{-1}$) vs solar rotation day number. Table III shows the details of the HiP plotted information.

In the general run of data, especially in the case of HiP (panel 3), fluxes are often below meaningful baseline levels. When this is the case, that is, when counting statistics are very poor, we simply do not plot a data point for that day in that 3-h LT period.

When no data were acquired by the CPA because of telemetry dropouts or other data handling problems, a gap occurs in the time sequence at all energy levels, which is shown by an absence of plotting symbols in all channels.

Each major 3-h frame of the solar rotation flux plots is labelled with a spacecraft identification number, solar rotation (Carrington) number, and start date of the solar rotation.

The stacked spectrum plots give an overview of the spectral and temporal variability of the energetic particle

TABLE I. Electron Solar Rotation Flux Plots

Curve Number	Plotting Symbol	Energy Range (keV)
1	□	30-45
2	o	65-95
3	△	140-200
4	+	200-300
5	x	430-630
6	◊	930-1360

TABLE III. HiP Proton Solar Rotation Flux Plots

Curve Number	Plotting Symbol	Energy Range (MeV)
1	□	0.4-0.5
2	o	0.5-0.6
3	△	0.6-0.8
4	+	0.8-1.0
5	x	

populations for any given solar rotation period. These relatively coarse, somewhat qualitative results are complemented by the more detailed LT-sorted data provided in the two-dimensional flux-time plots. Beyond this level of detail, for example, for evaluation of very detailed particle variation features, pitch-angle effects, and other high-frequency phenomena, one must use the SDS as a guide and return to the fundamental archival high-resolution data for detailed analysis.

The last part of the SDS deals with very broad statistical analyses of the CPA data base. Here the 1-h data tapes were used as input and statistical evaluations were made over long periods compared to a solar rotation. These plots are expected to be of interest for instrument design, spacecraft engineering, and environmental monitoring. They may be of especial interest to operators looking at energetic particle data in real time by providing a baseline for the interpretation or prediction of rapid variations in particle fluxes.

The flux probability plots summarize the chances that, at any given energy, the integral particle flux ($\text{cm}^{-2} \cdot \text{s}^{-1} \cdot \text{sr}^{-1}$) will exceed a particular value. We present these statistical plots following the set of daily average spectrum and solar rotation plots. In the case of S/C 1976-059, for example, we give three sets of flux probability plots. The first set of plots covers 07/20/76 to 12/31/76. Within this set we present five electron graphs and five proton graphs, which correspond to five different LT groupings as labelled in the upper left-hand corner of each plot: 21-03 LT, 03-09 LT, 09-15 LT, 15-21 LT, and all LTs. These LT breakdowns cover the midnight sector (where substorm particle injections are often seen), the local dawn region, local noon (where drift-shell splitting often produces the highest average flux), and local dusk.

Statistical plots of identical format for S/C 1976-059 are also presented separately for 1977 and 1978. These data can allow analysis of long-term temporal variations of particle fluxes at $6.6 R_E$. For S/C 1977-007, we present statistical plots in a format identical to that described above: one set for 1977 and one set for 1978. Table IV shows the integral electron and proton thresholds used in the statistical (flux probability) plots and the plotting symbols corresponding to each.

The final type of plot shown in this report summarizes the average diurnal variations of electrons and protons throughout 1976-78. For each of the several selected energy channels, we plot the mean flux (50% probability) value as well as the 10 and 90% flux probability values. From such curves, it is possible to judge what the

TABLE IV. Integral Energy Thresholds Used in the Flux Probability Plots

Electrons		Protons	
Energy	Plotting Symbol	Energy	Plotting Symbol
>30 KeV		> 145 keV	
65	o	175	o
140		215	
200	+	290	+
430	x	400	x
930	◊	500	◊
		1000	

average energetic particle environment would be at $6.6 R_E$ for any given LT. It is also possible to judge what the likely extreme conditions of either low flux (90% probability) or high flux (10% probability) might be.

V. APPLICATIONS AND SCIENTIFIC USES OF THE SDS

The SDS is a broad compilation of information concerning the radiation environment at geostationary orbit. As discussed in Sec. I., the geostationary orbit is useful both to the applications and to the scientific community. Here we discuss a few of the potential uses of the SDS.

By the term "applications community" we mean those persons and organizations who are using the atmosphere and/or outer space for commercial, engineering, or military purposes. This community often needs to know the geomagnetic and magnetospheric environmental conditions to better carry out its tasks (that is, spacecraft design, communication, or satellite operations).

We believe that the statistical studies presented in this report will be particularly useful for this community. Our statistical results clearly indicate what flux levels of energetic particles may be expected to be encountered at geostationary orbit. The probability levels assigned to various flux levels of the different particle components should allow better assessment of design criteria for future geostationary satellite missions, as an example.

We expect that the SDS can also be useful in evaluating events of interest to the applications community long after these events have occurred. For

example, spacecraft operational anomalies or atmospheric disturbances (affecting radio propagation) can at times be interpreted in terms of energetic particle enhancements in the outer magnetosphere. The data presented here (and data that continue to be collected by CPAs on orbit) are readily available for use by the applications community. Data are also available from these satellites in real time for qualified users in the applications community for environmental monitoring purposes.

Within the scientific community, a major goal is to better understand magnetospheric structure and dynamics. Relevant questions include where energetic plasma particles originate, how the particles are subsequently transported, and how they are eventually lost (precipitated into the terrestrial atmosphere). Long-term overviews of the time variations of energetic particle fluxes such as given by the SDS can lead to a better predictive capability in the future.^{3,4,9-11,15,16}

Also, the International Magnetospheric Study (IMS) was organized to gain an improved understanding of the terrestrial magnetosphere. The observational phase of the IMS extended from 1976 through 1979. Therefore, the SDS as presented here overlaps the IMS observational period and provides a very relevant data base for IMS comparative studies. We strongly encourage the scientific community to use the SDS as a basis for evaluating general energetic particle conditions in the magnetosphere and we look forward to cooperative studies of magnetospheric processes with other interested researchers.

ACKNOWLEDGMENTS

Because this is a report on a synoptic data set, it is appropriate to make a general acknowledgment to our associates in this program who have helped and encouraged us over the years. During the 10 years of this program, many people have contributed to the success of the CPA instrument series. S. Singer, J. Conner, B. Martin, M. Montgomery, R. Greenwood, W. Everett, W. Workman, P. Farmer, G. Voos, F. Woods, P. Max, and D. Smith are a few of the present and former members of the Space Science Office at the Los Alamos National Laboratory who have been directly involved with the CPA instrument. The aid of R. Hostetler and H. Gottlieb at Sandia National Laboratories, Albuquerque has been essential to our success and is gratefully acknowledged. Many individuals in the US Air Force, the Defense and

Space Systems Group of TRW, and the DOE have been very helpful to us.

The authors express thanks to J. B. Blake (Aerospace Corporation) and D. T. Young (University of Bern) for many helpful conversations and suggestions. The authors would also like to apologize to the many whose names were left off the above lists in the interest of brevity or through oversight.

The authors also thank Dan Morse and colleagues in Los Alamos Group IS-7 for their help in the graphics reproductions for this report.

REFERENCES

1. D. N. Baker, P. R. Higbie, E. W. Hones, Jr., and R. D. Belian, "High-Resolution Energetic Particle Measurements at 6.6 R_E , 3, Low-Energy Electron Anisotropies and Short-Term Substorm Predictions," *J. Geophys. Res.* **83**, 4863 (1978).
2. D. N. Baker, P. Stauning, E. W. Hones, Jr., P. R. Higbie, and R. D. Belian, "Strong Electron Pitch-Angle Diffusion Observed at Geostationary Orbit," *Geophys. Res. Lett.* **6**, 205 (1979).
3. D. N. Baker, P. R. Higbie, R. D. Belian, and E. W. Hones, Jr., "Do Jovian Electrons Influence the Terrestrial Outer Radiation Zone?", *Geophys. Res. Lett.* **6**, 531 (1979).
4. D. N. Baker, R. D. Belian, P. R. Higbie, and E. W. Hones, Jr., "High-Energy Magnetospheric Protons and Their Dependence on Geomagnetic and Interplanetary Conditions," *J. Geophys. Res.* **84**, 7138 (1979).
5. P. R. Higbie, R. D. Belian, and D. N. Baker, "High-Resolution Particle Measurements at 6.6 R_E , 1, Electron Micropulsations," *J. Geophys. Res.* **83**, 4851 (1978).
6. R. D. Belian, D. N. Baker, P. R. Higbie, and E. W. Hones, Jr., "High-Resolution Energetic Particle Measurements at 6.6 R_E , 2, High-Energy Proton Drift Echoes," *J. Geophys. Res.* **83**, 4857 (1978).
7. R. D. Belian, D. N. Baker, E. W. Hones, Jr., P. R. Higbie, S. J. Bame, and J. R. Asbridge, "Timing of

- Energetic Proton Enhancements Relative to Magnetospheric Substorm Activity and its Implication for Substorm Theories," *J. Geophys. Res.* **86**, 1415 (1981).
8. P. R. Higbie and W. R. Moomey, "Pitch-Angle Measurements from Satellites Using Particle Telescopes with Multiple View Directions," *Nucl. Instrum. Methods* **146**, 439 (1977).
9. P. R. Higbie, D. N. Baker, E. W. Hones, Jr., and R. D. Belian, "Pitch-Angle Distributions of >30 KeV Electrons at Geostationary Altitudes," *Quantitative Modeling of Magnetospheric Processes*. 21, *Geophys. Monograph Series*, W. P. Olson, Ed. (1979), p. 203.
10. G. A. Paulikas and J. B. Blake, "Energetic Electrons at Synchronous Altitude 1967-1977," Aerospace Corp. report TR-0078(3860-05) (March 1978).
11. G. A. Paulikas and J. B. Blake, "Effects of the Solar Wind on Magnetospheric Dynamics: Energetic Electrons at the Synchronous Orbit," *Quantitative Modeling of Magnetospheric Processes*, 21, *Geophys. Monograph Series*, W. P. Olson, Ed. (1979), p. 180.
12. W. C. Feldman, J. R. Asbridge, S. J. Bame, and J. T. Gosling, "Long-Term Variations of Selected Solar Wind Properties: IMP 6, 7, and 8 Results," *J. Geophys. Res.* **83**, 2177 (1978).
13. G. A. Paulikas, J. B. Blake, and J. A. Palmer, "Energetic Electrons at Synchronous Altitude: A Compilation of Data," Aerospace Corp. report TR-0066(5620-20)-4 (November 1969).
14. D. N. Baker, P. R. Higbie, and R. D. Belian, "Multispacecraft Observations of Energetic Flux Pulsations at $6.6 R_E$," *J. Geophys. Res.* **85**, 6709 (1980).
15. P. R. Higbie, D. N. Baker, V. Domingo, W. L. Imhof, R. L. McPherron, W. N. Spjeldvik, D. J. Williams, J. R. Burrows, and M. Hayakawa, "Short-Term Magnetospheric Particle Variations ($1 \text{ min} < T < 1 \text{ day}$)," in *Solar-Terrestrial Predictions Proceedings*, Vol. 2, R. R. Donnelly, Ed. (1979), p. 433.
16. H. I. West, Jr., R. M. Buck, G. Davidson, "Study of Energetic Electrons in the Outer Radiation-Belt Regions Using Data Obtained by the LLL Spectrometer on OGO-5 in 1968," Lawrence Livermore report UCRL-52807 (July 1979).

APPENDIX A

**DATA FOR S/C 1976-059, July 1976—December 1978
(SOLAR ROTATION NUMBERS 1955—1987)**

TABLE I. Electron Solar Rotation Flux Plots

Curve Number	Plotting Symbol	Energy Range (keV)
1		30-45
2	o	65-95
3	..	140-200
4	+	200-300
5	x	430-630
6	◊	930-1360

TABLE III. HiP Proton Solar Rotation Flux Plots

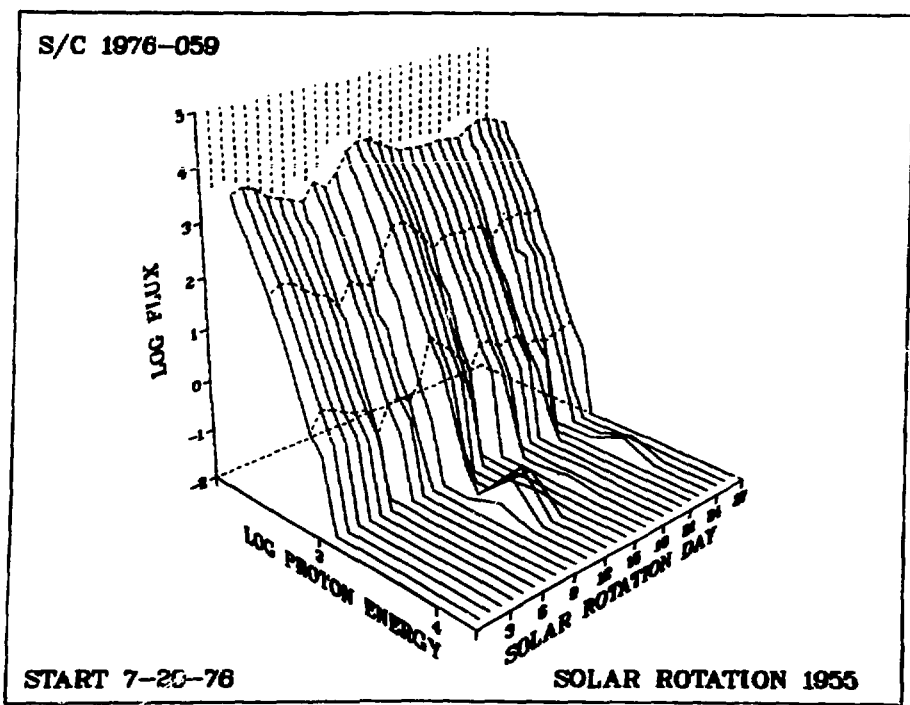
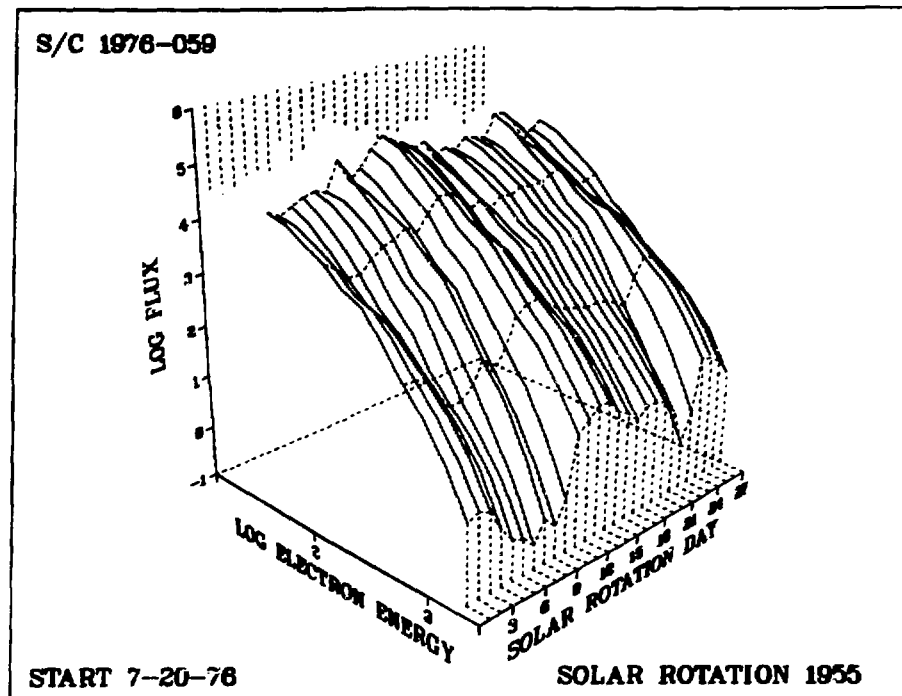
Curve Number	Plotting Symbol	Energy Range (MeV)
1		0.4-0.5
2	o	0.5-0.6
3	..	0.6-0.8
4	+	0.8-1.0
5	x	

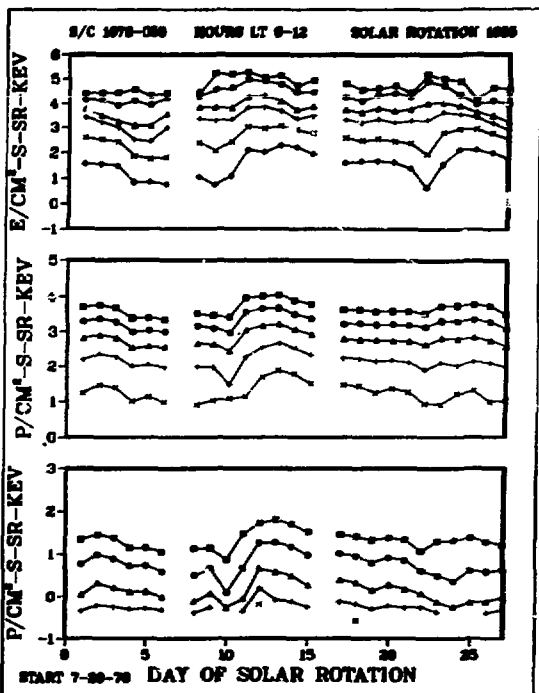
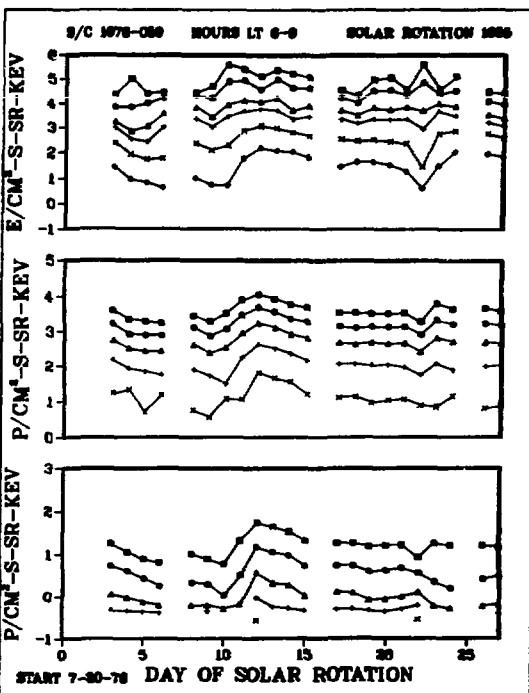
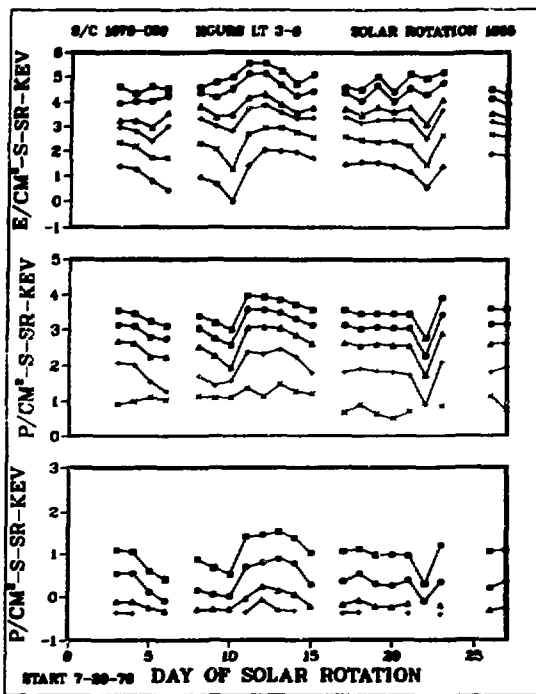
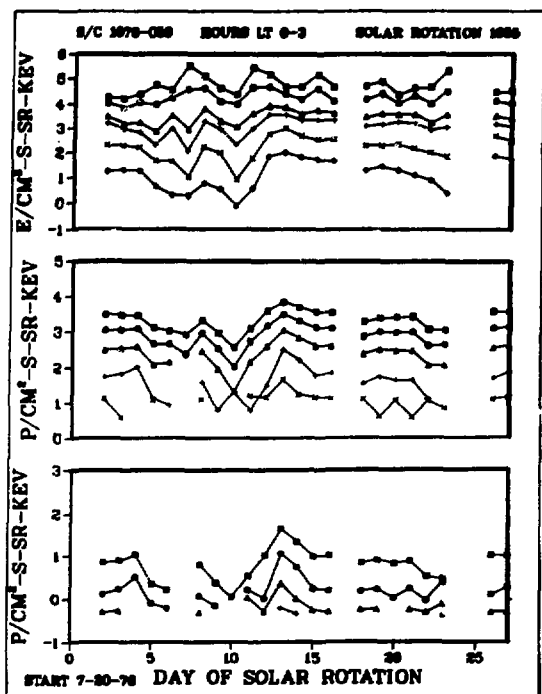
TABLE II. LoP Proton Solar Rotation Flux Plots

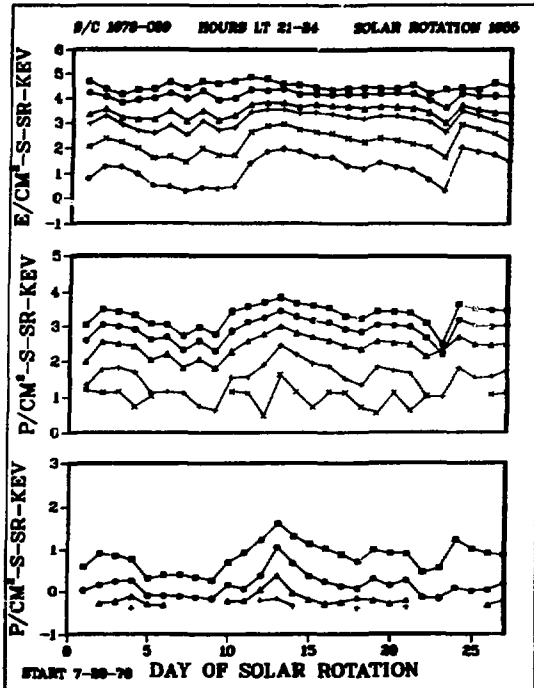
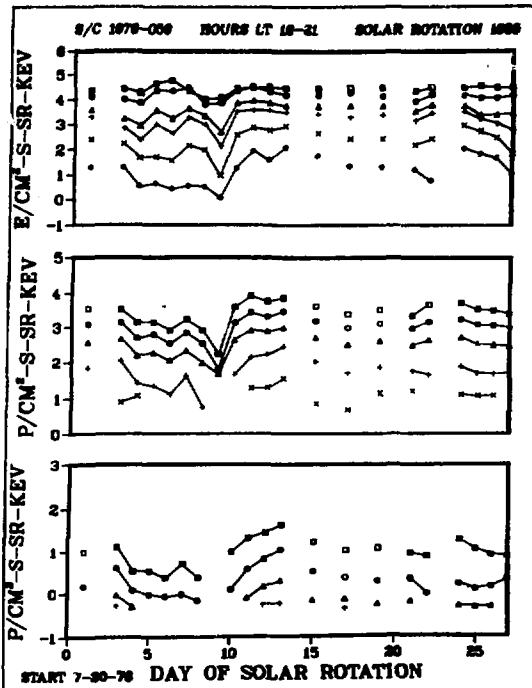
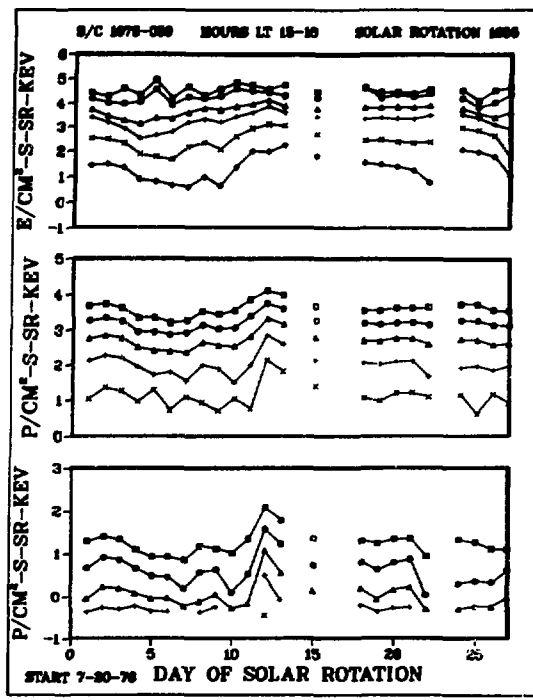
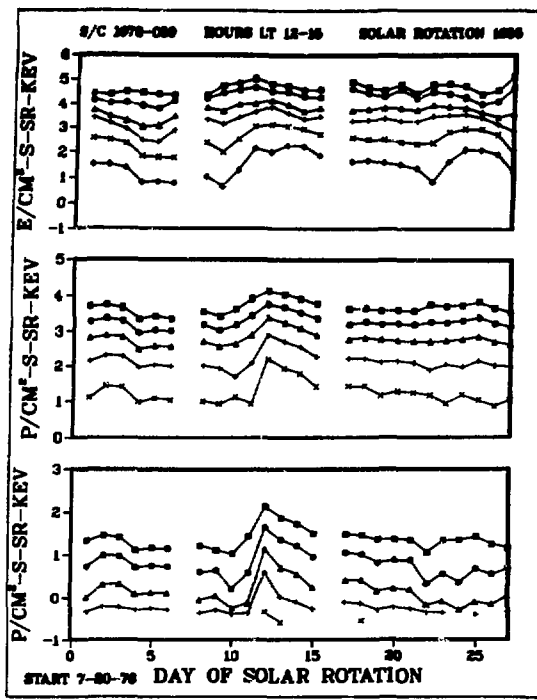
Curve Number	Plotting Symbol	Energy Range (keV)
1		145-160
2	o	175-190
3	..	215-245
4	+	290-340
5	x	400-480

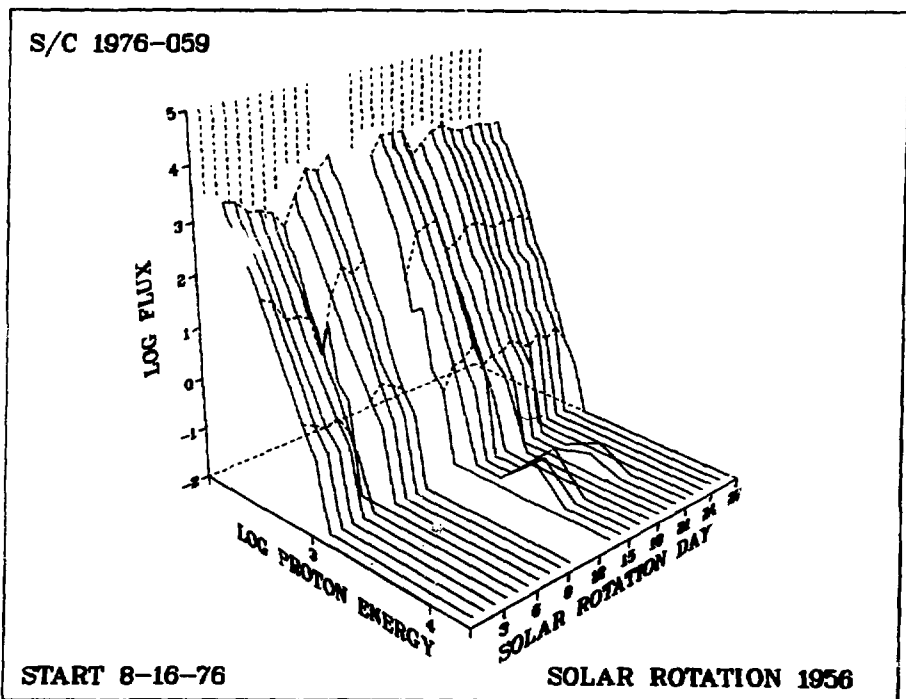
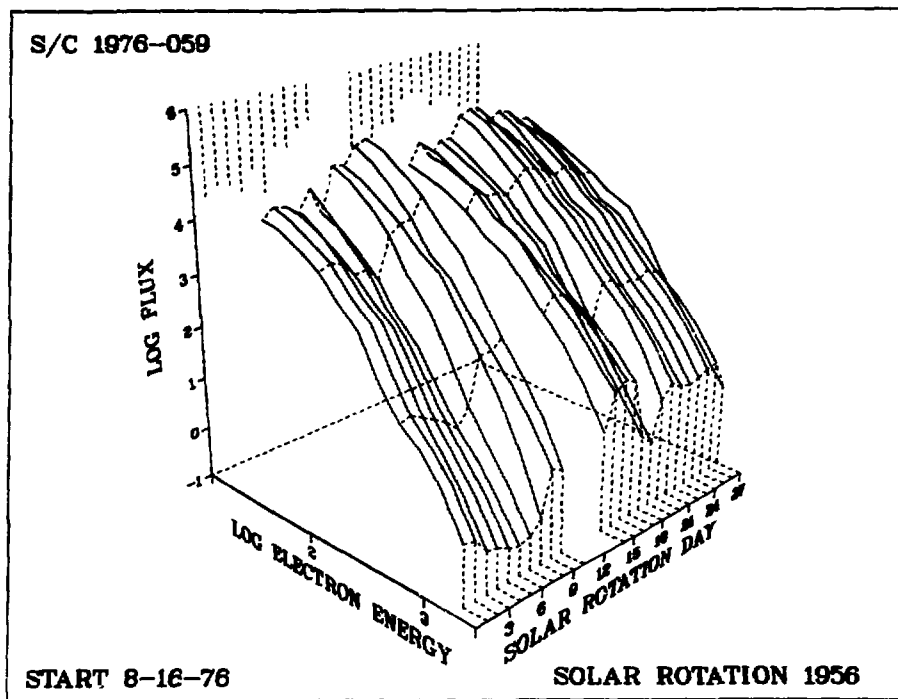
TABLE IV. Integral Energy Thresholds Used in the Flux Probability Plots

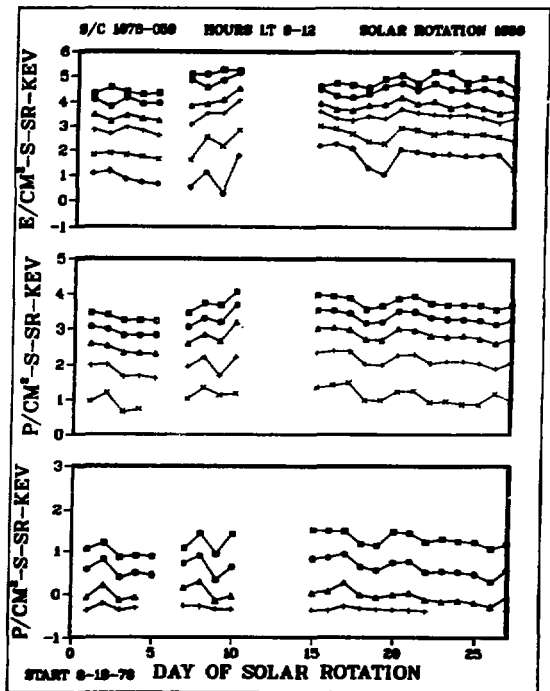
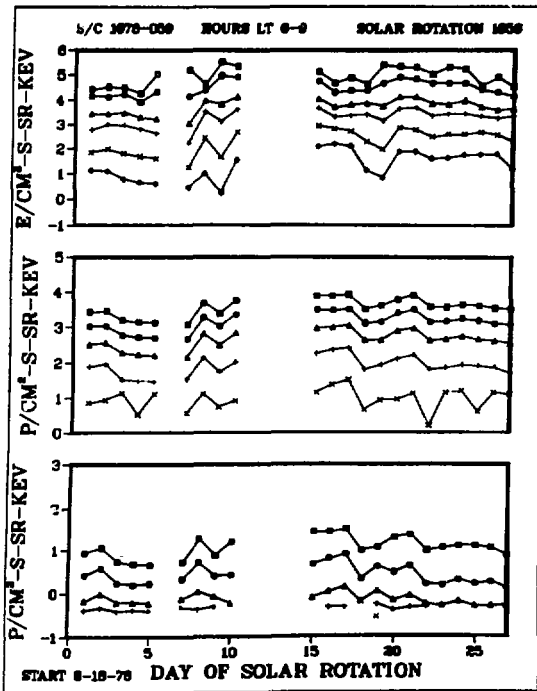
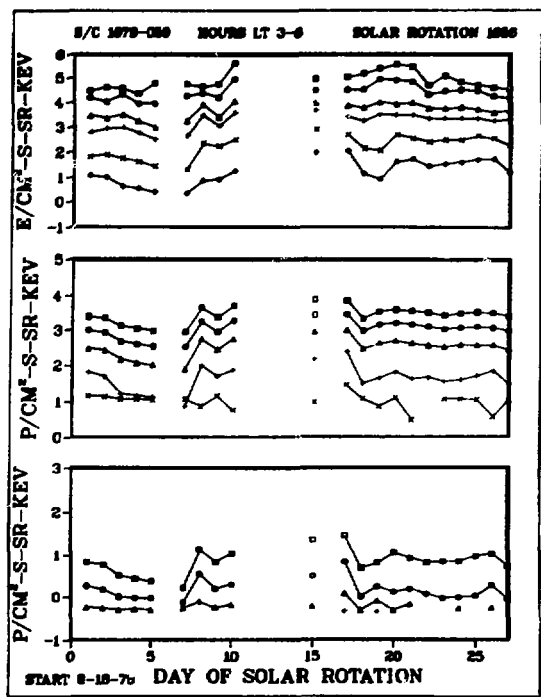
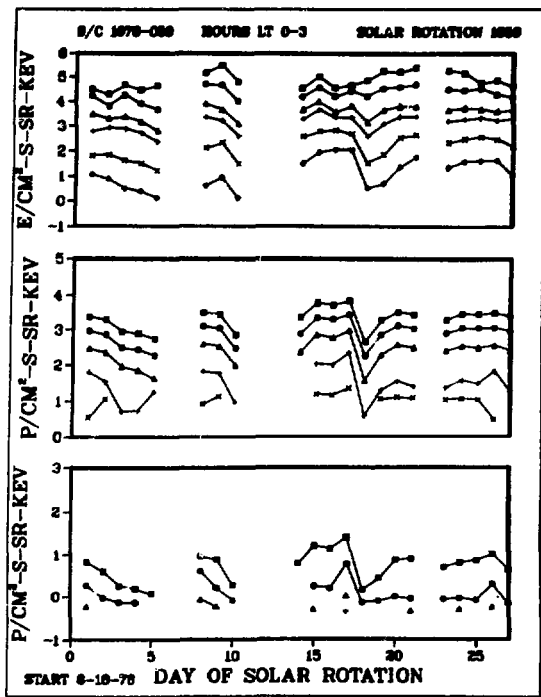
Electrons		Protons	
Energy	Plotting Symbol	Energy	Plotting Symbol
>30 KeV	..	>145 keV	..
65	o	175	o
140	△	215	△
200	+	290	+
430	x	400	x
930	◊	500	◊
		1000	..

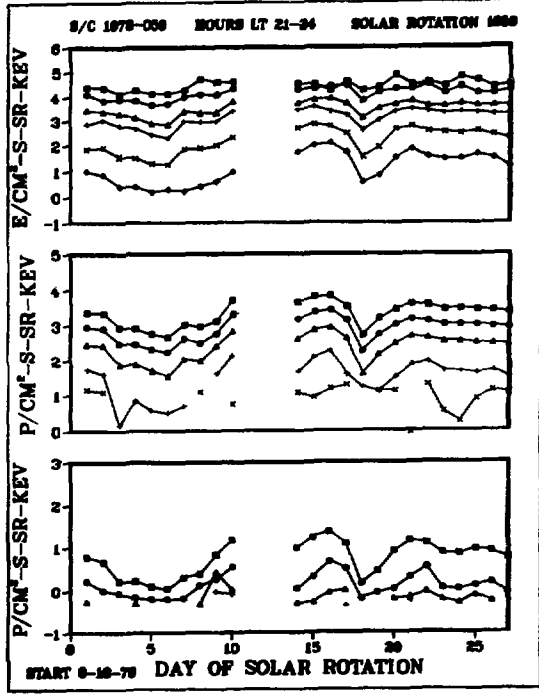
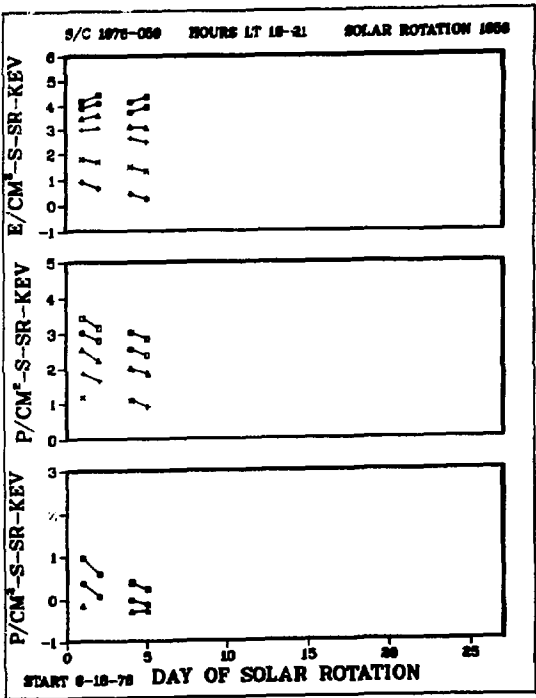
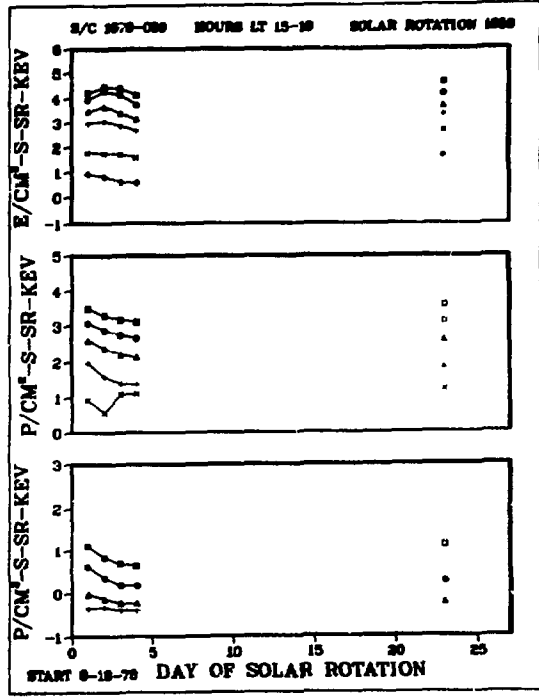
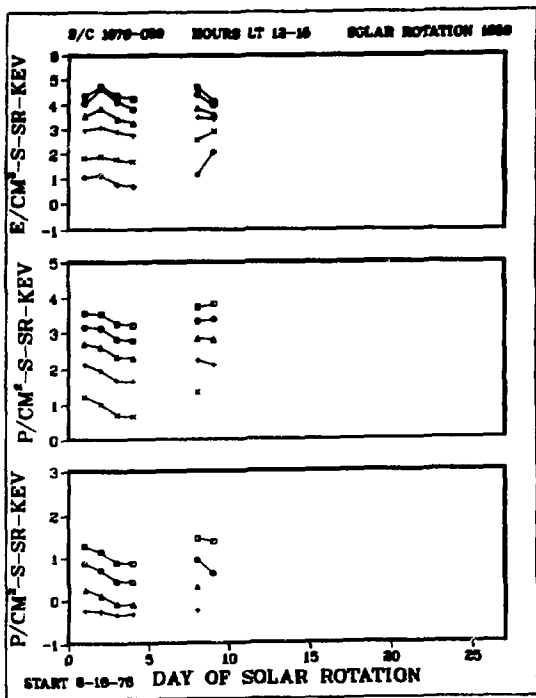




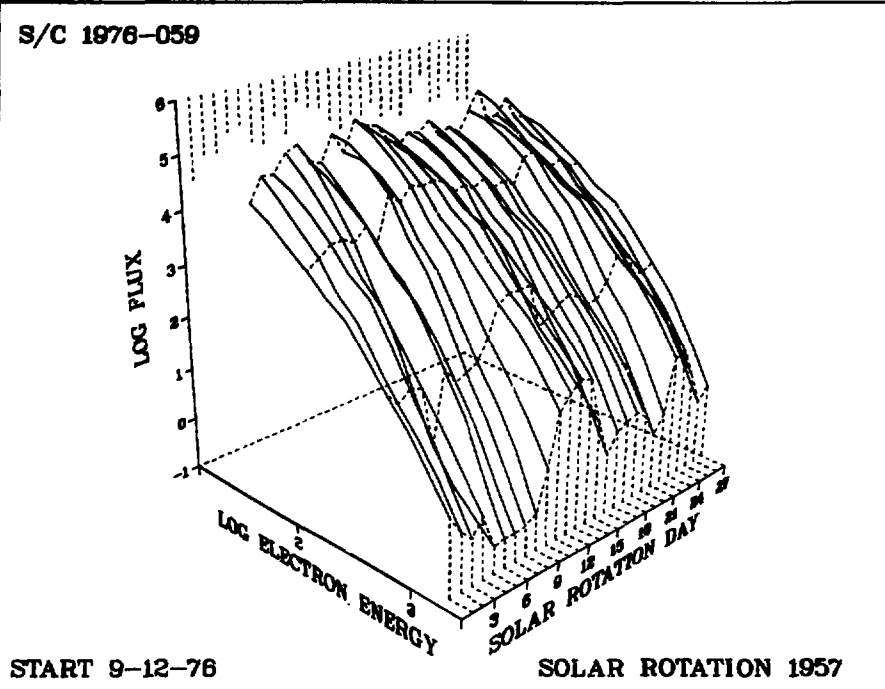




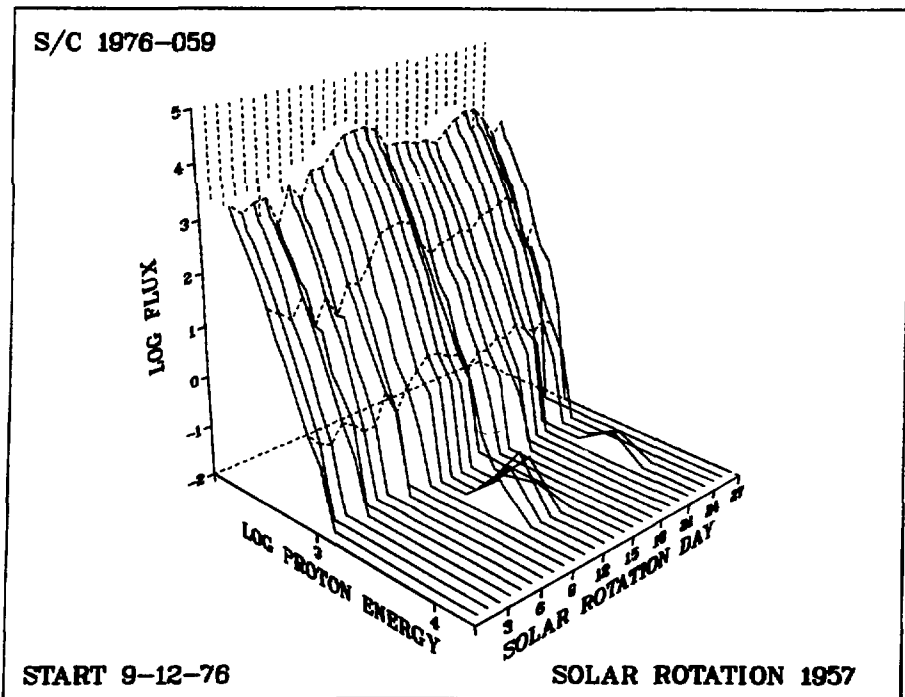


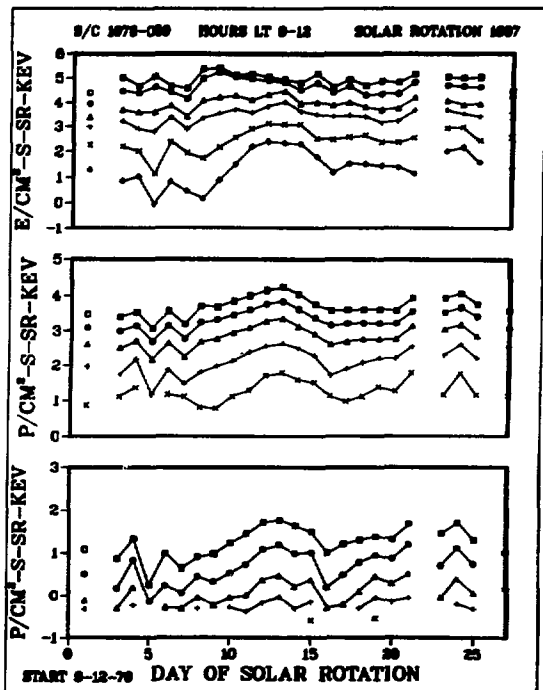
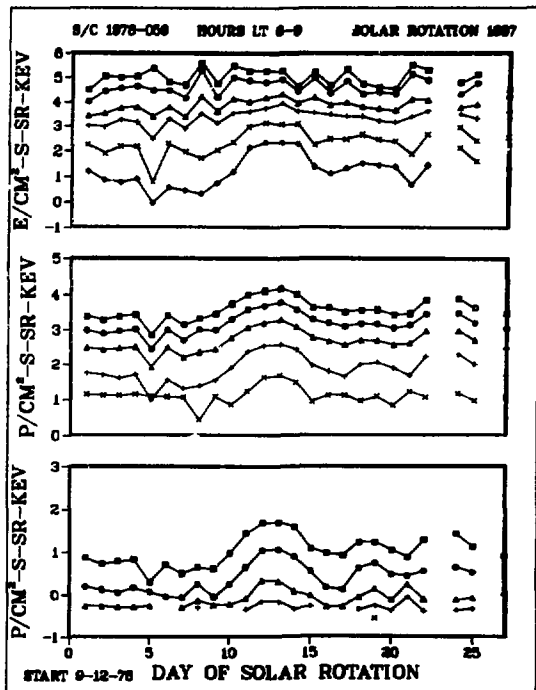
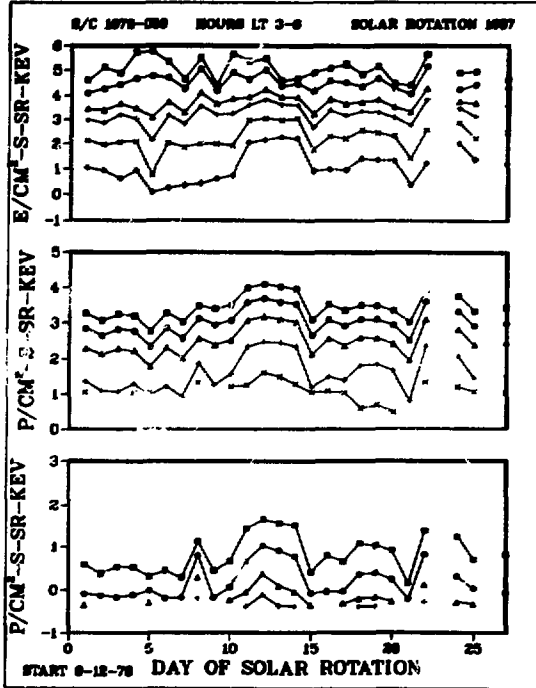
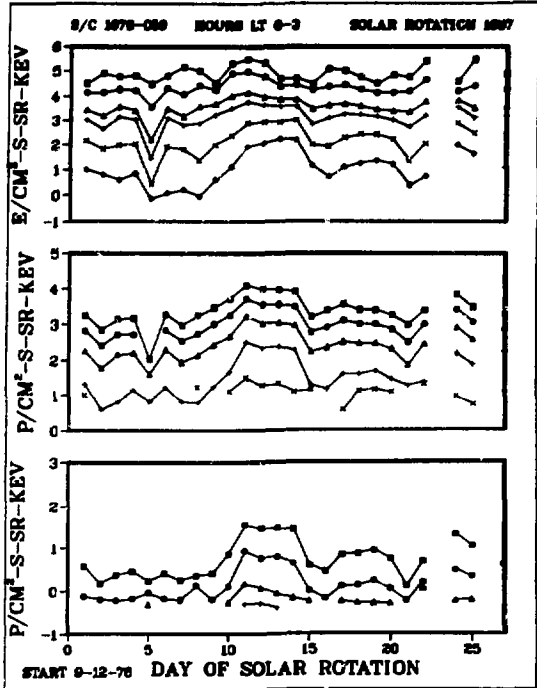


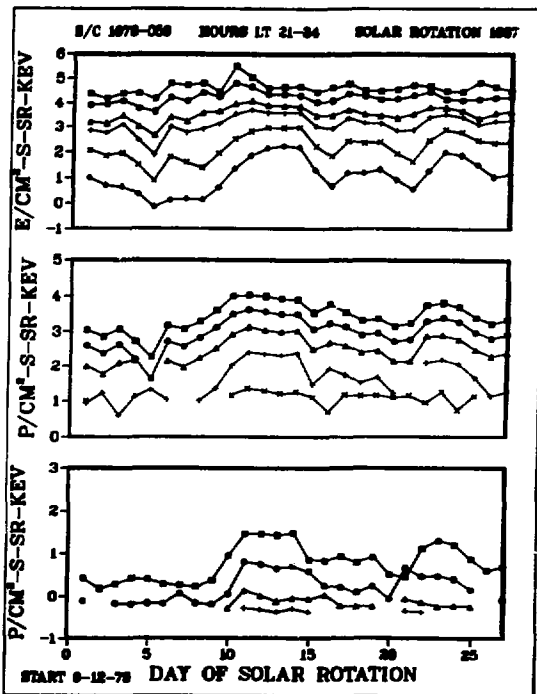
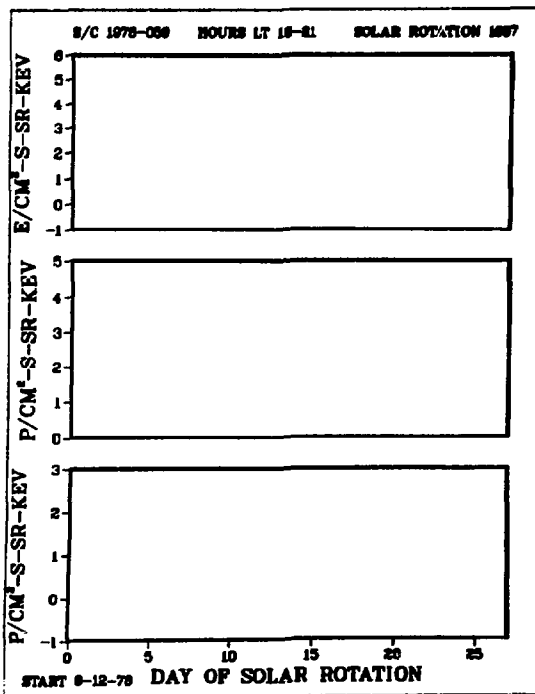
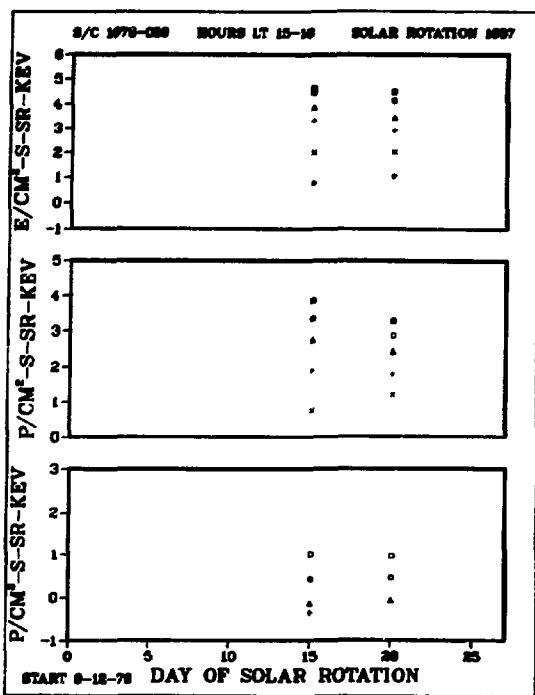
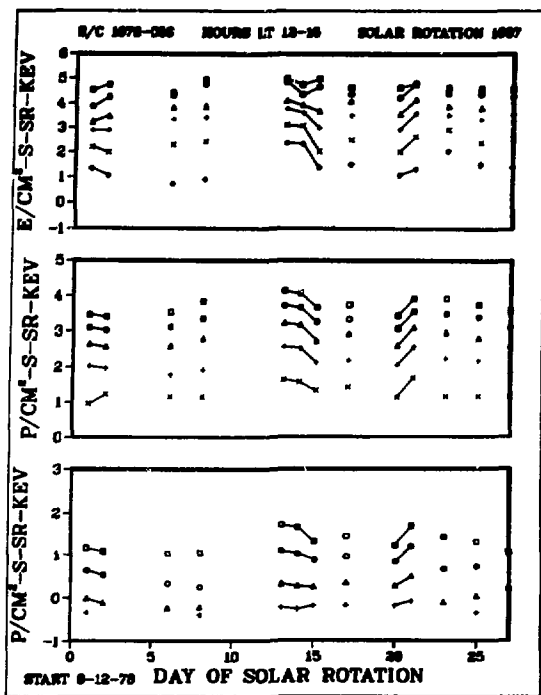
S/C 1976-059

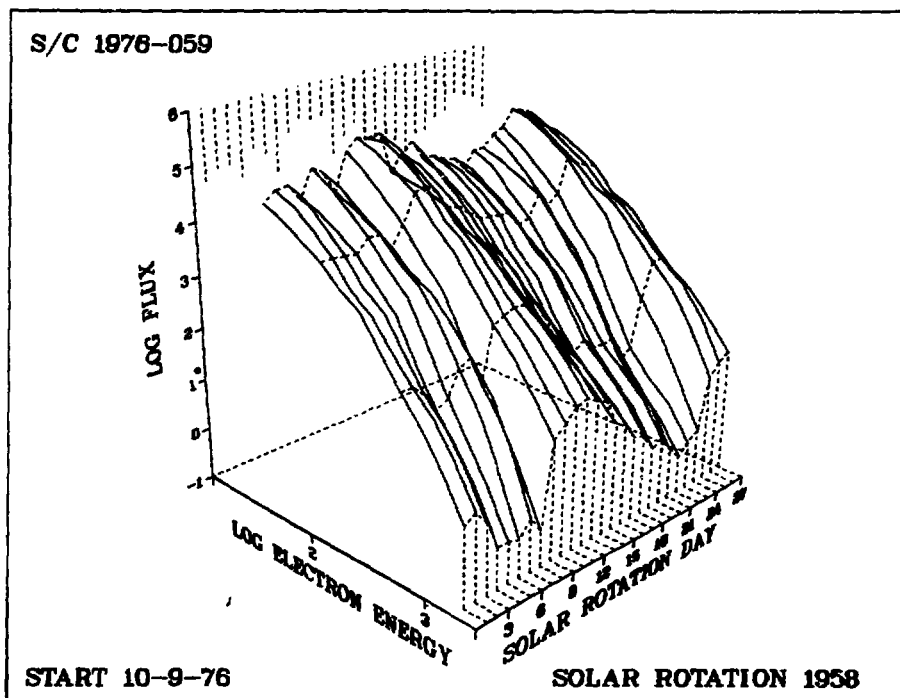
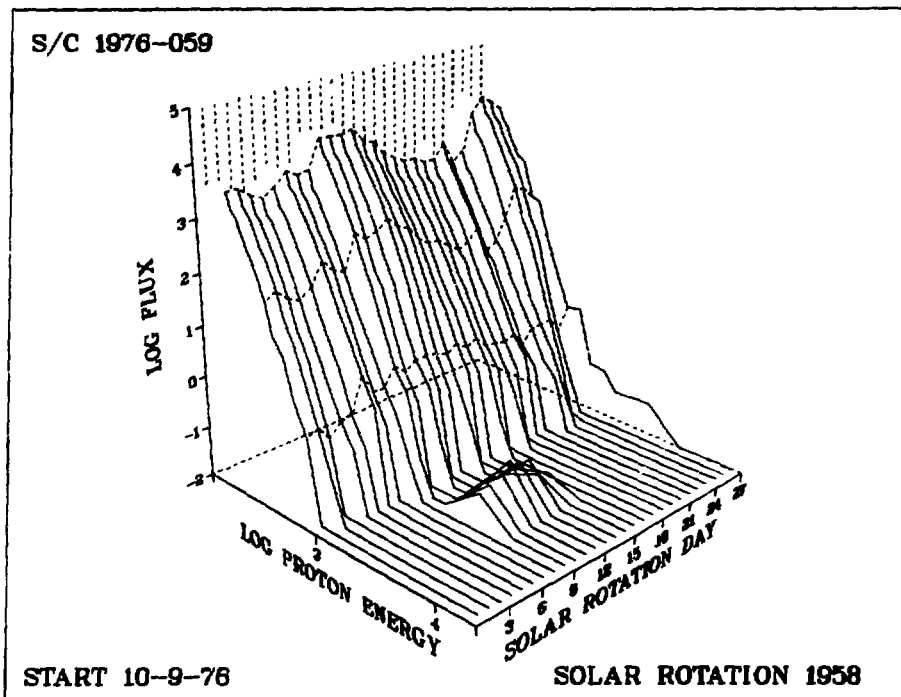


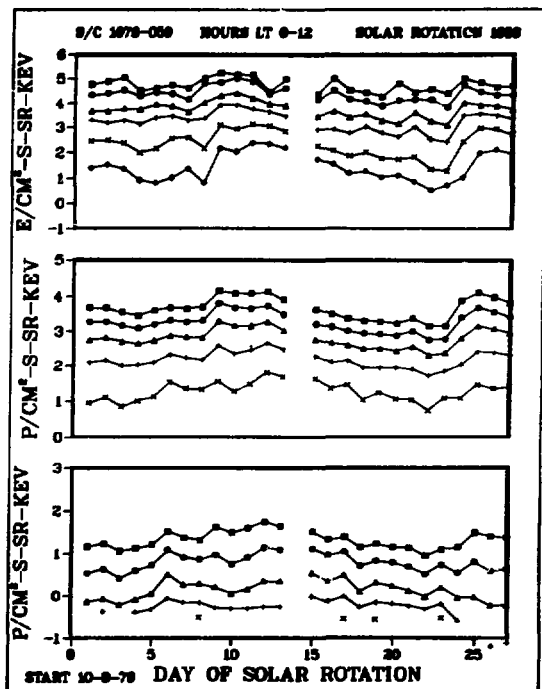
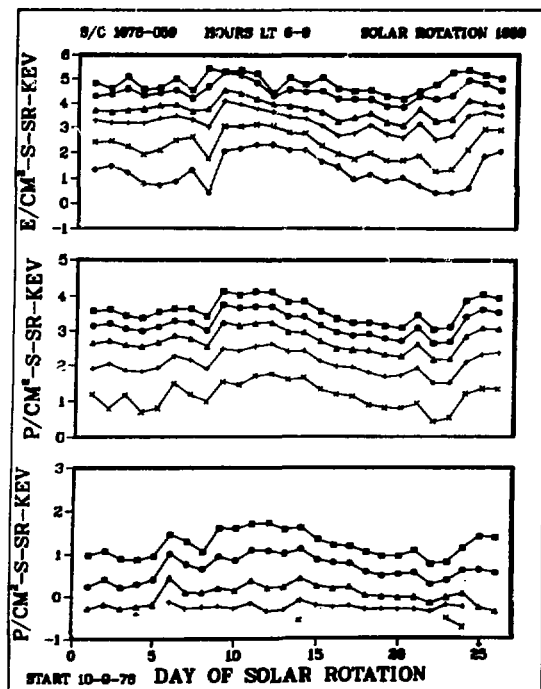
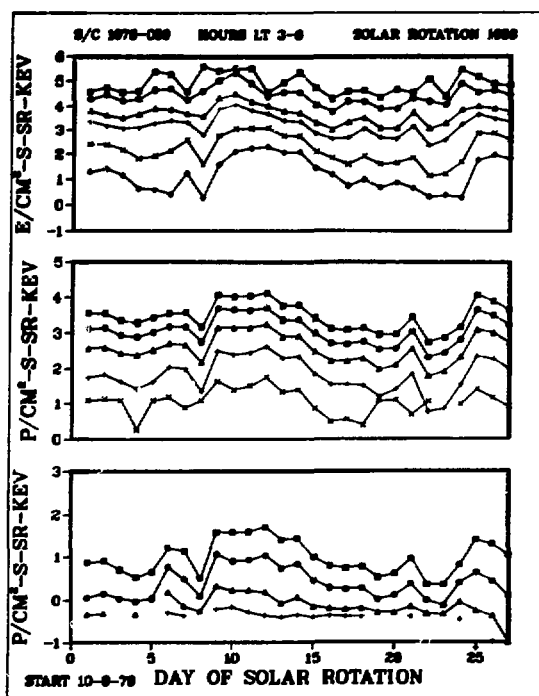
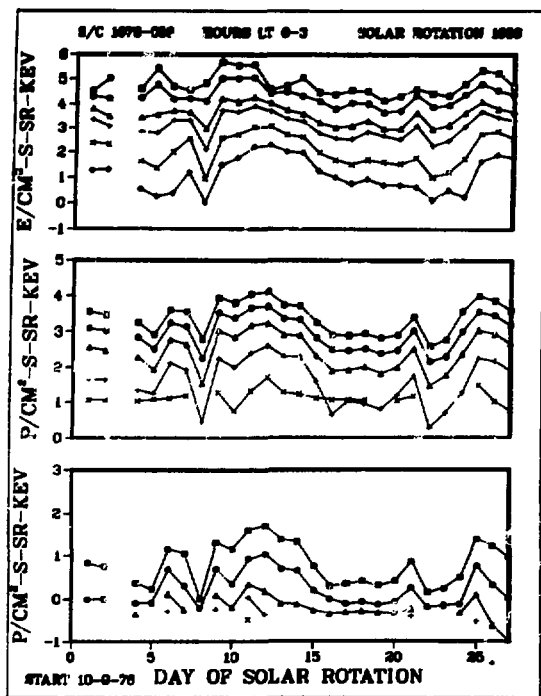
S/C 1976-059

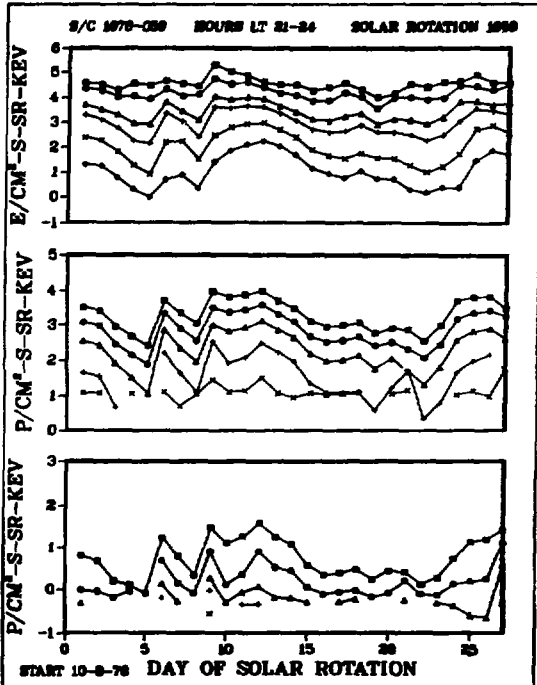
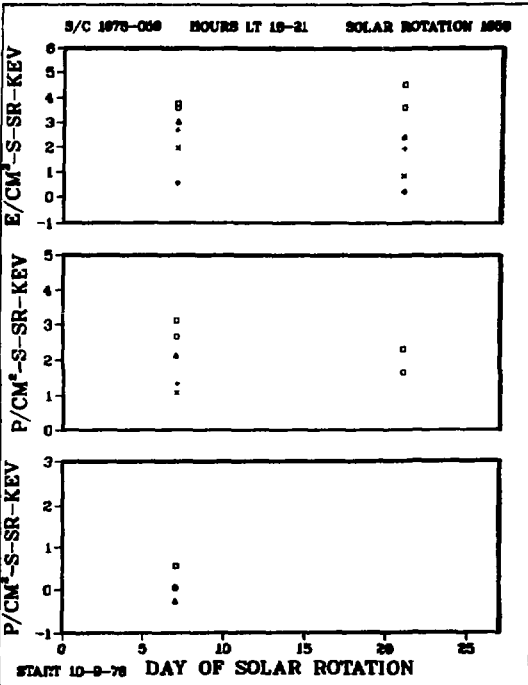
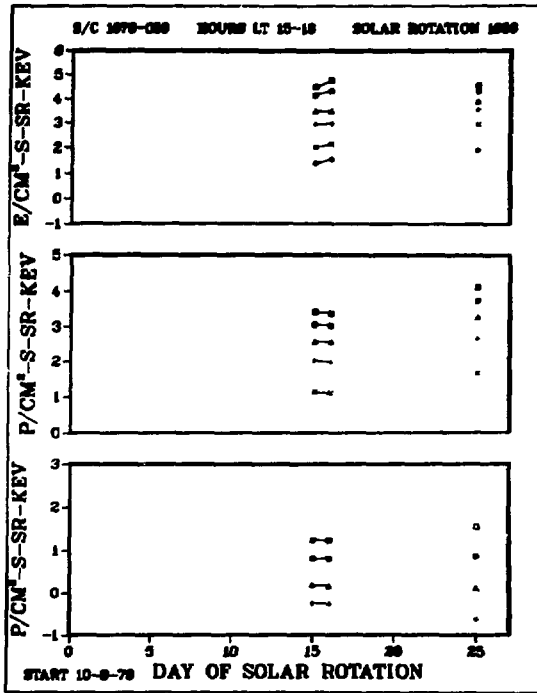
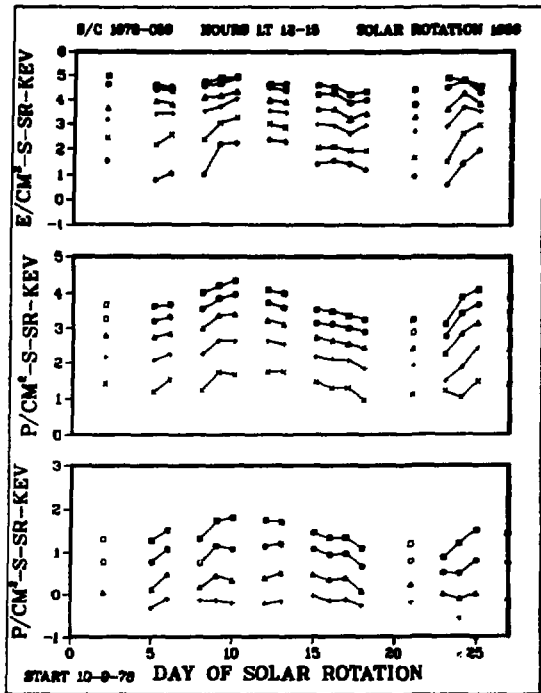




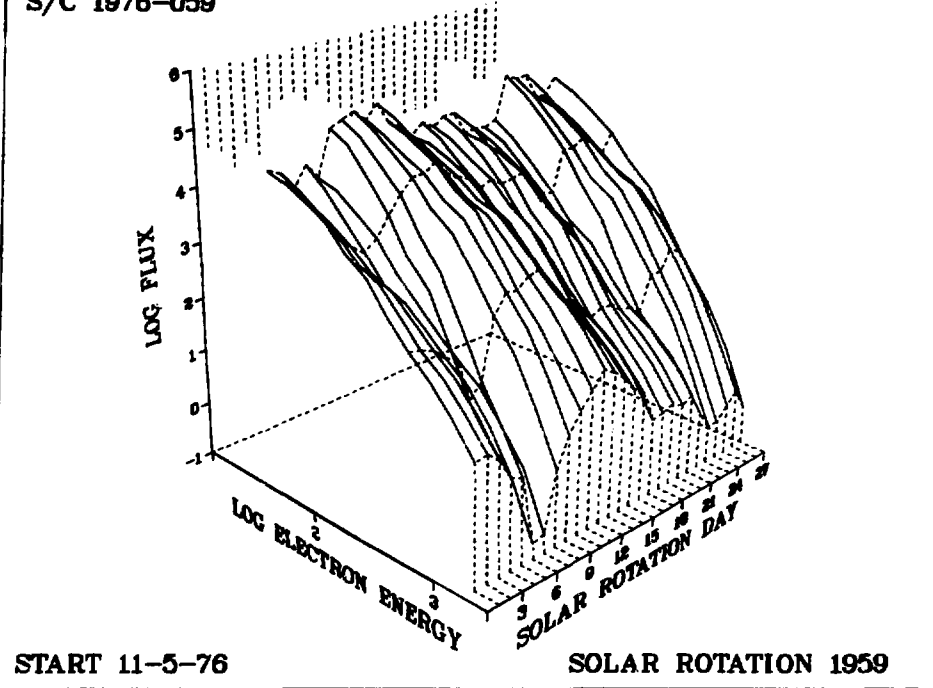




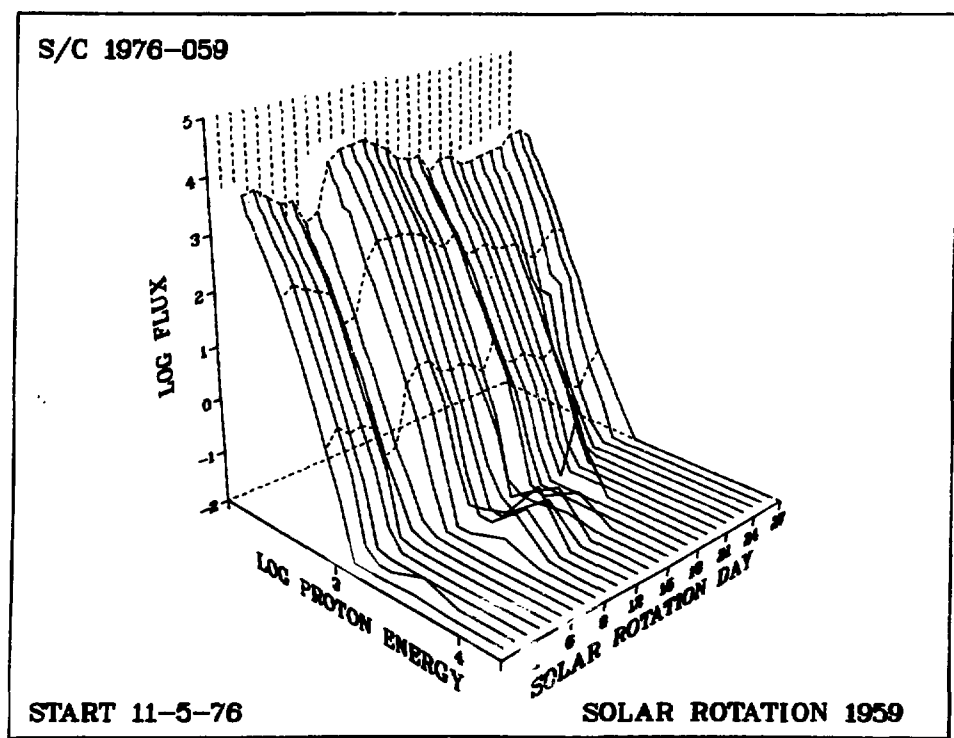


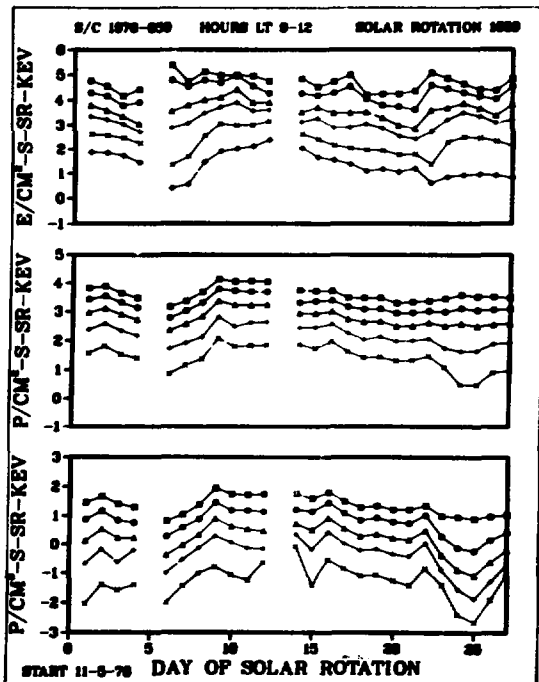
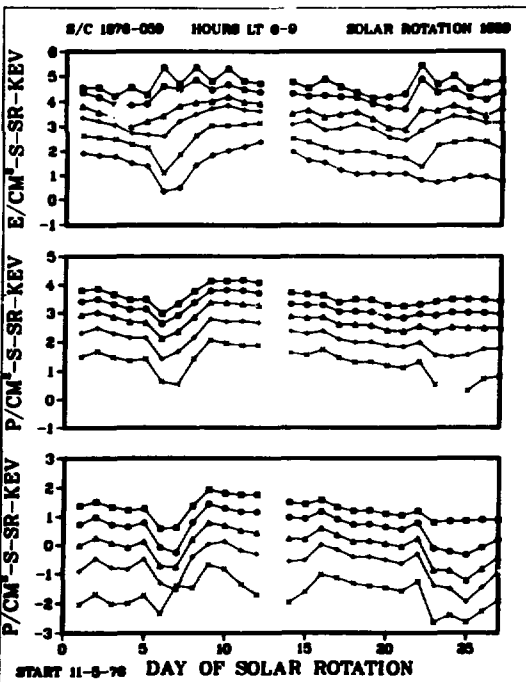
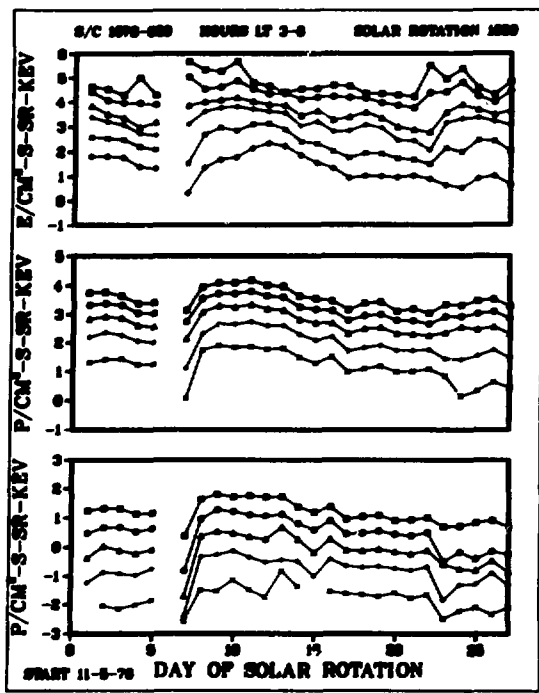
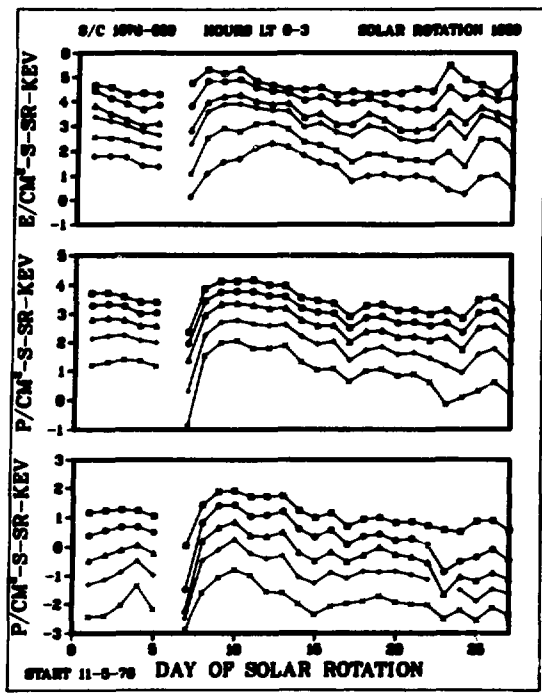


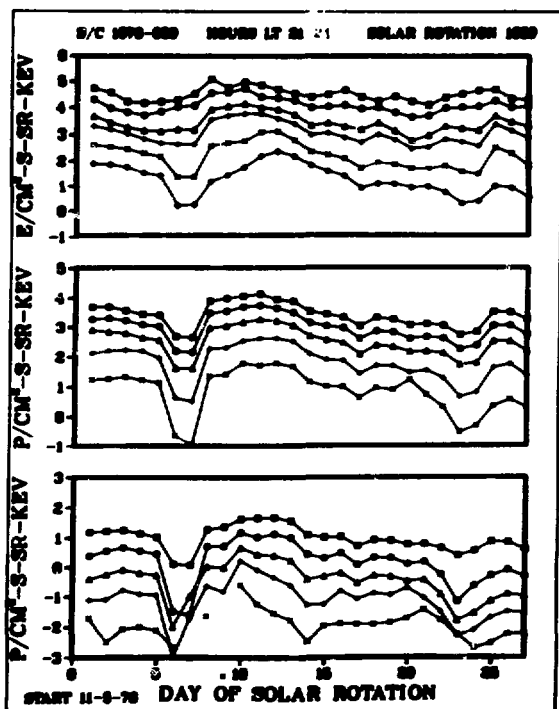
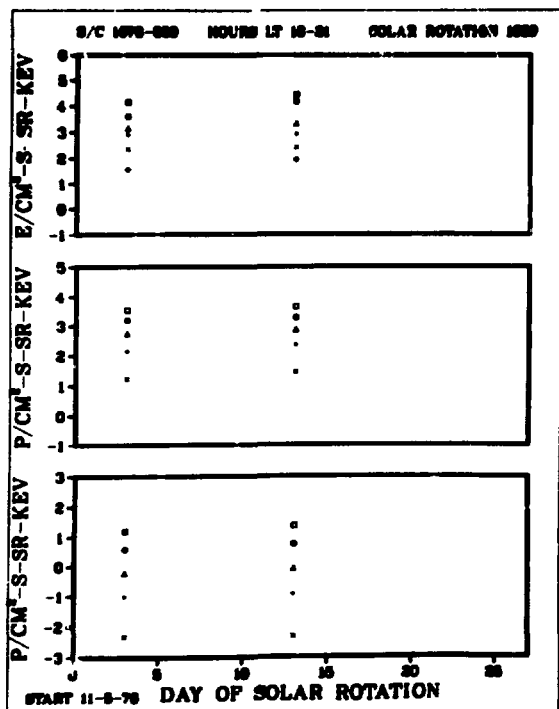
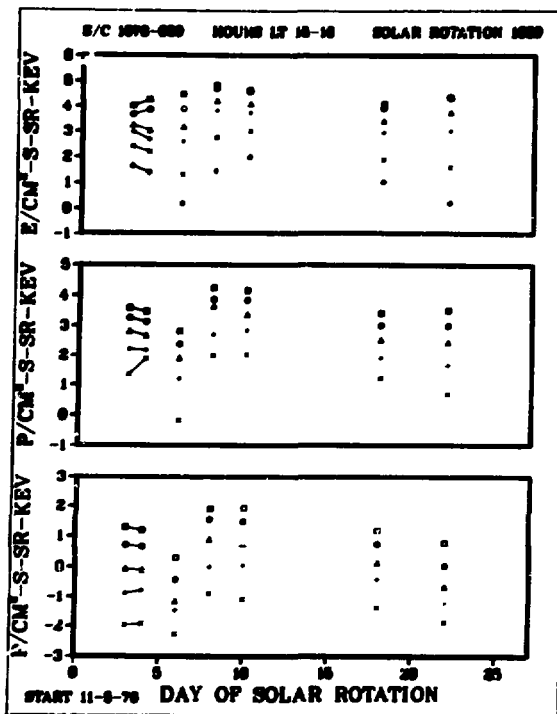
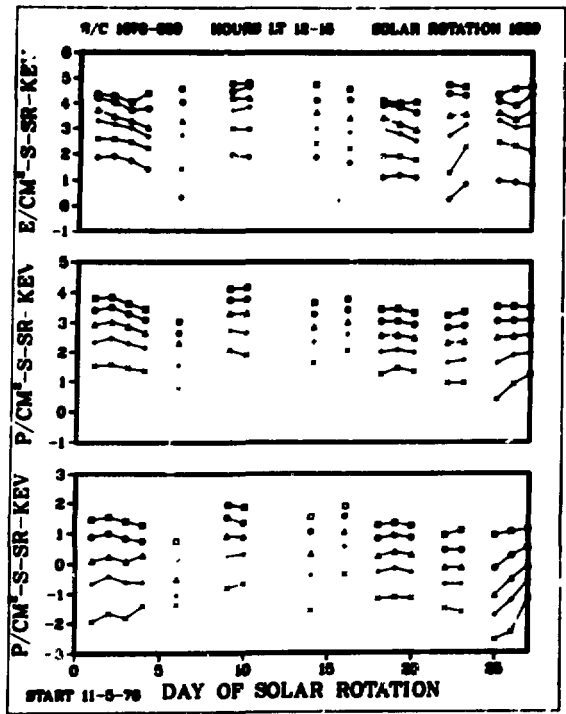
S/C 1976-059



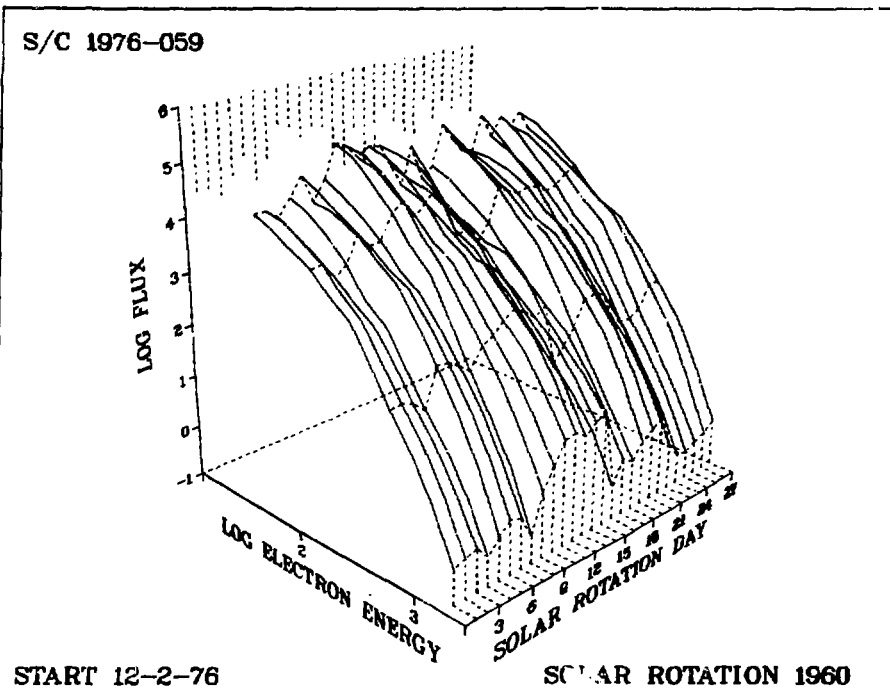
S/C 1976-059



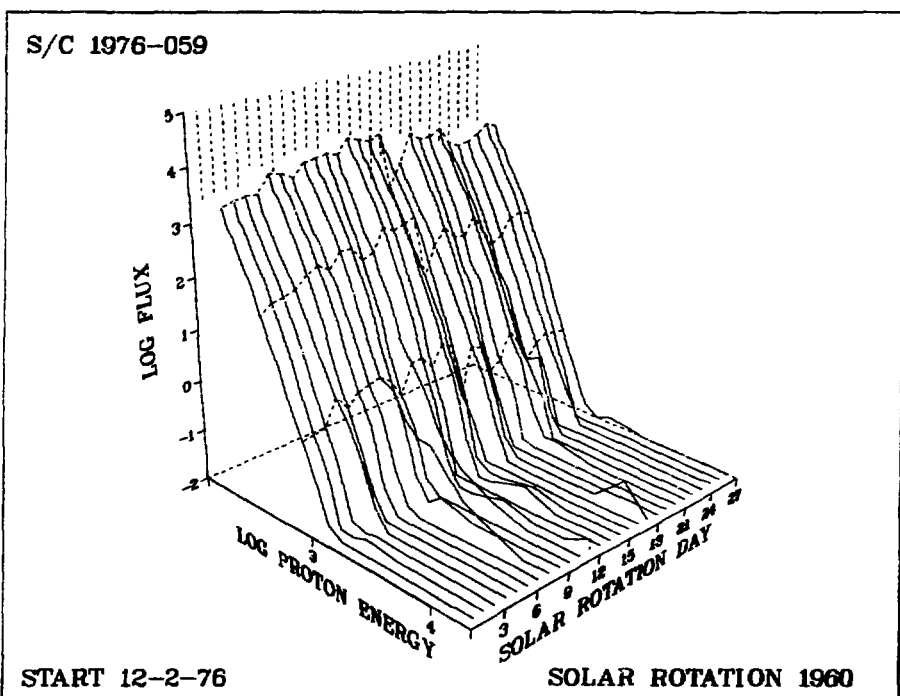


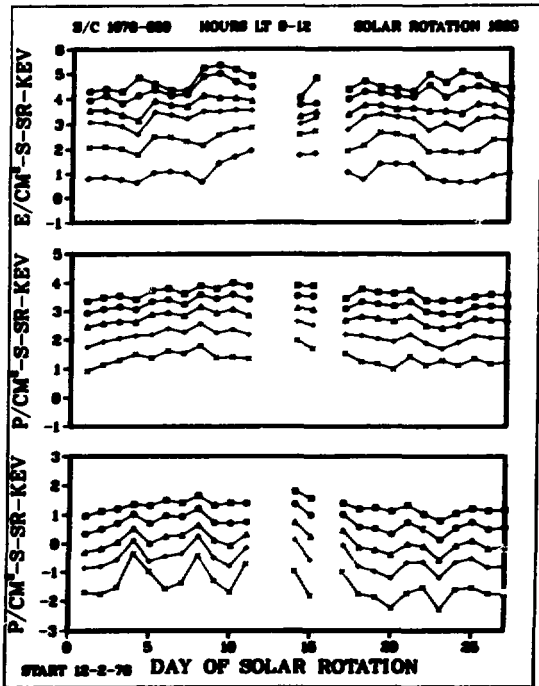
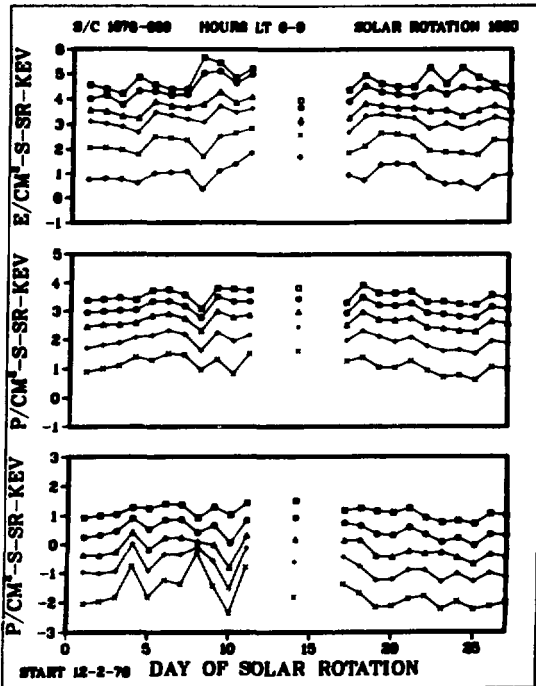
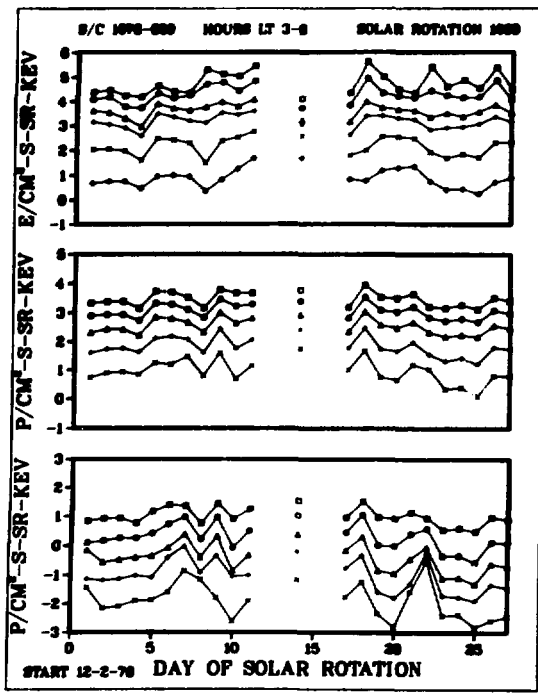
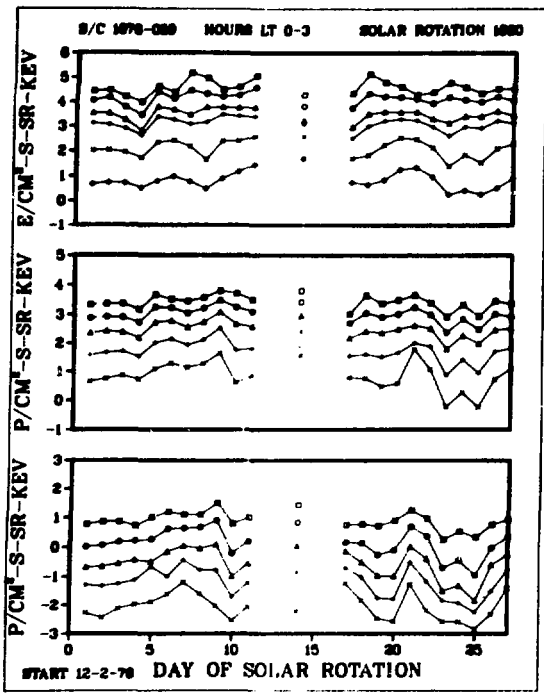


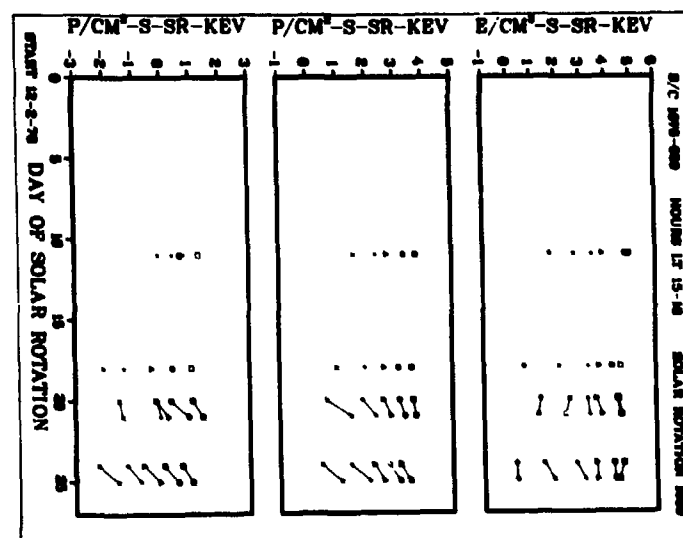
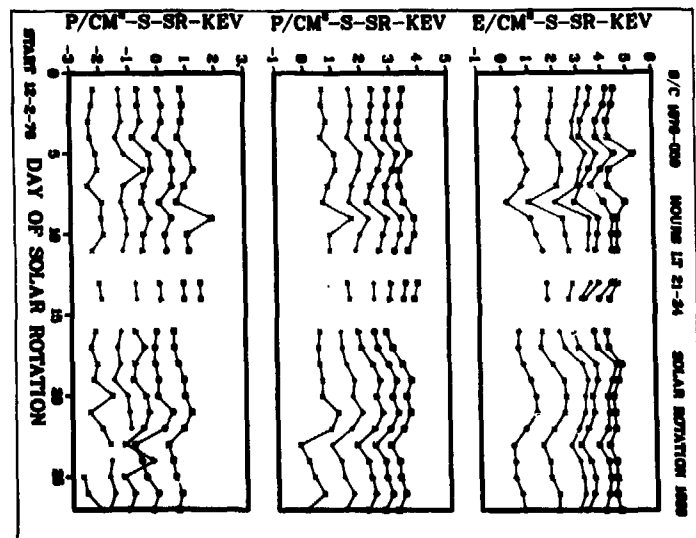
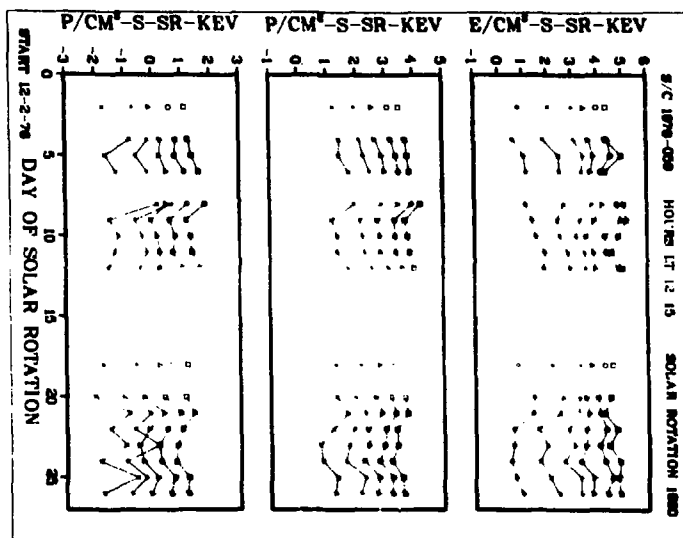
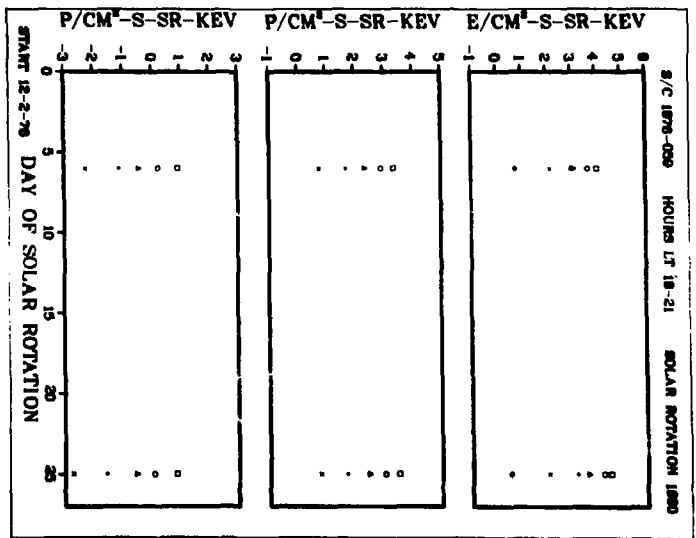
S/C 1976-059



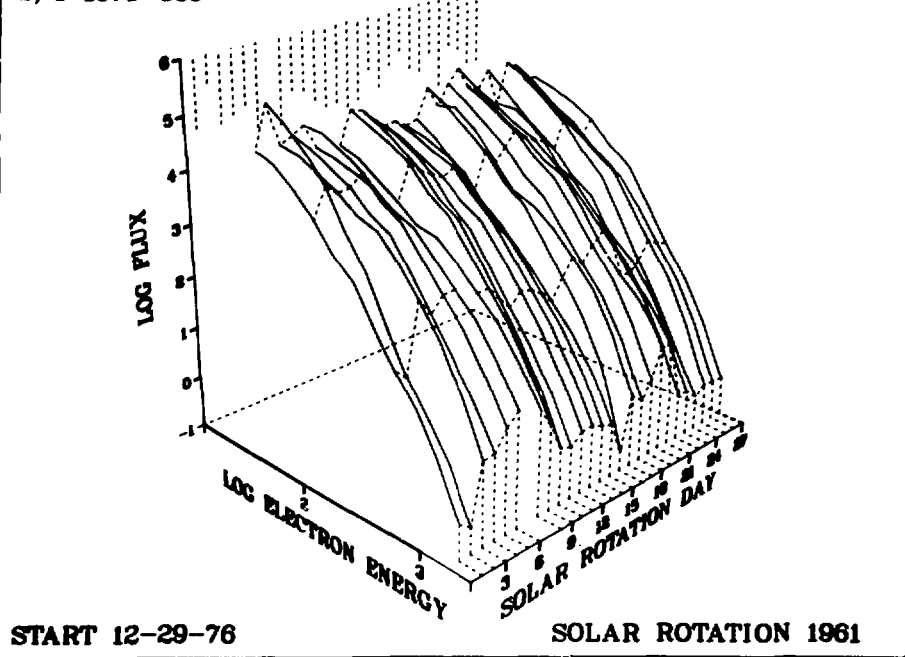
S/C 1976-059



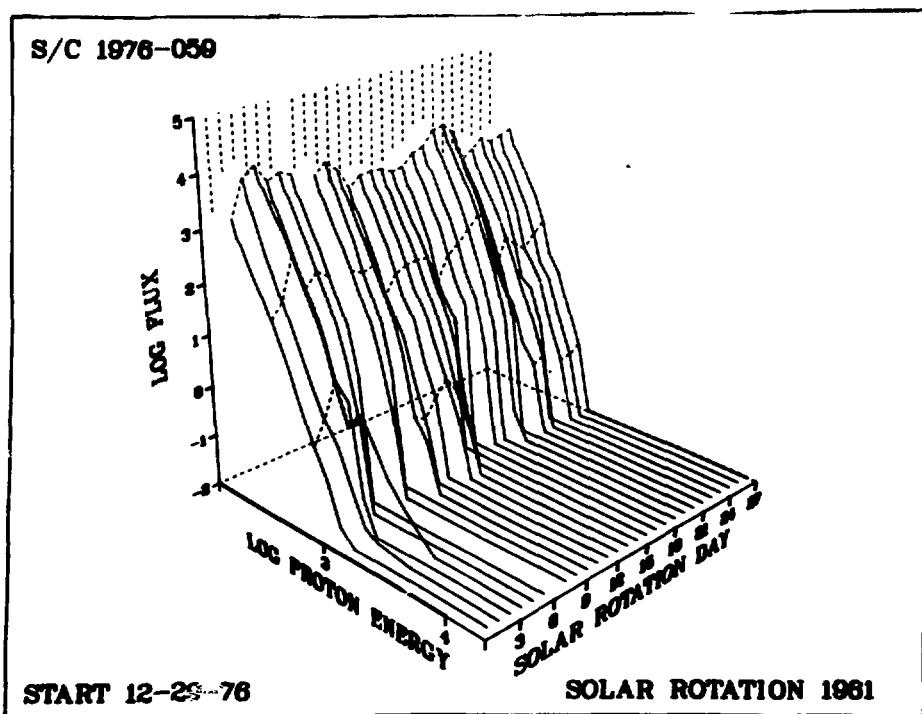


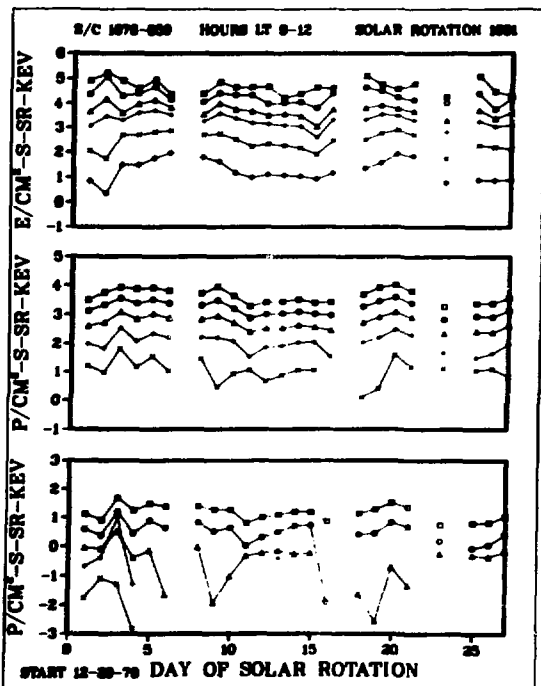
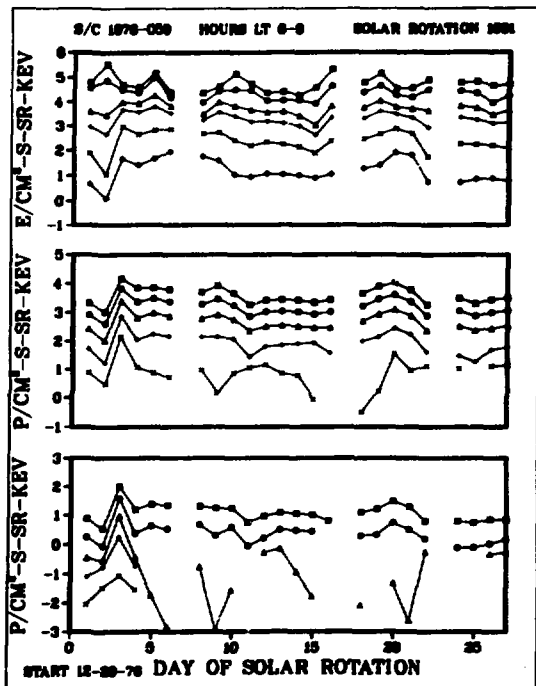
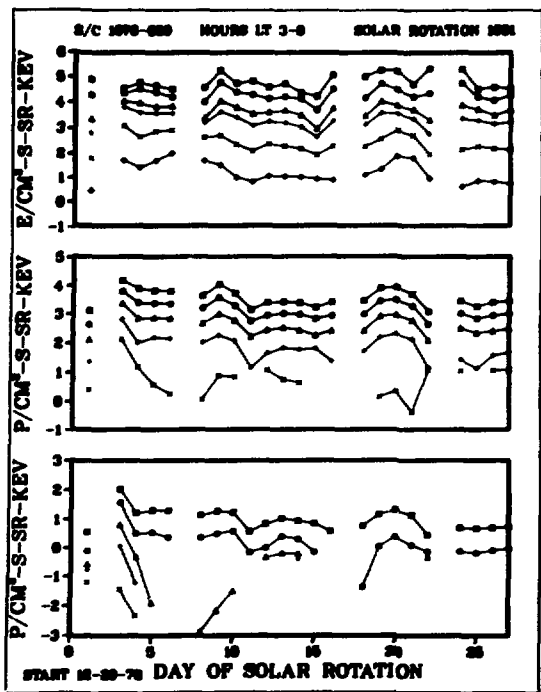
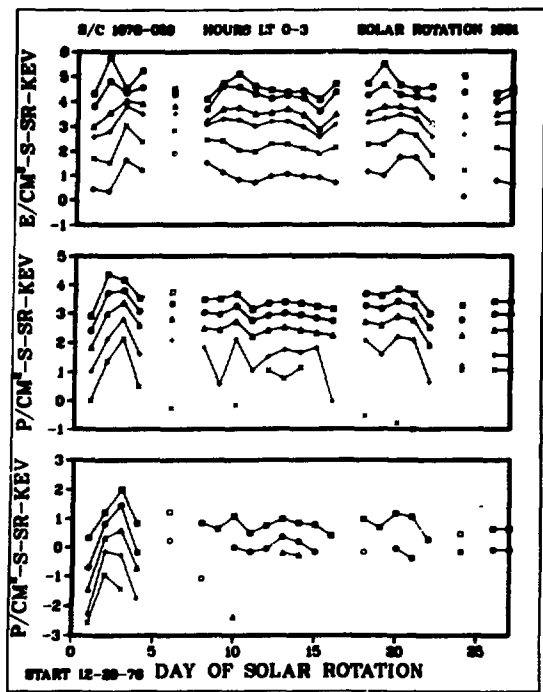


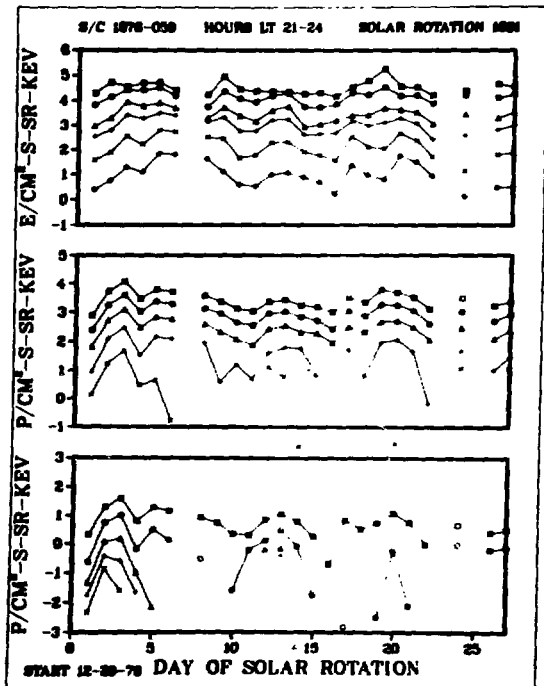
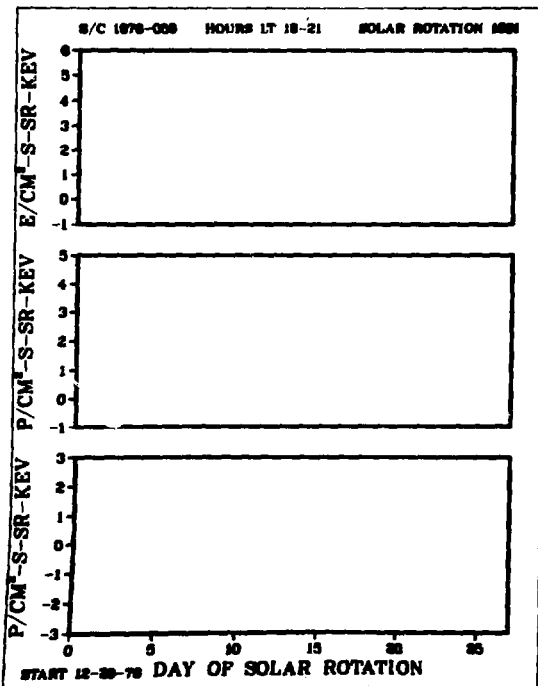
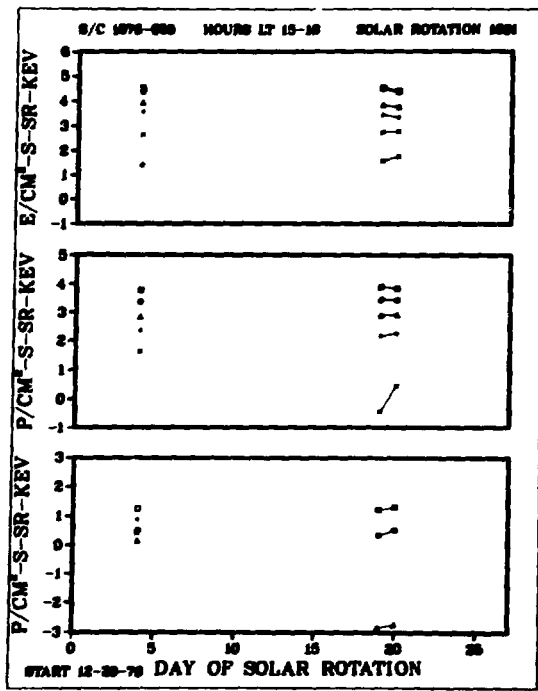
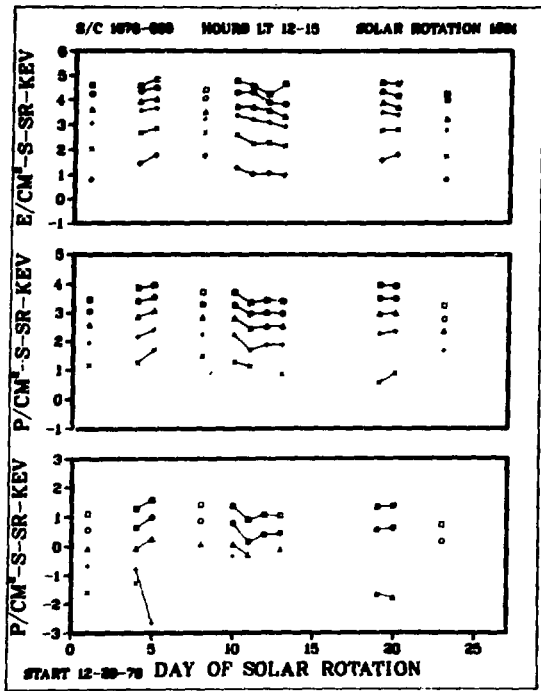
S/C 1976-059



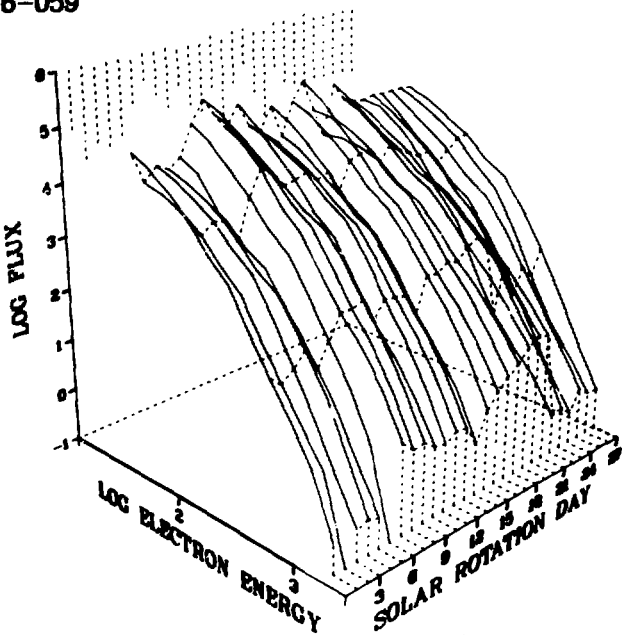
S/C 1976-059







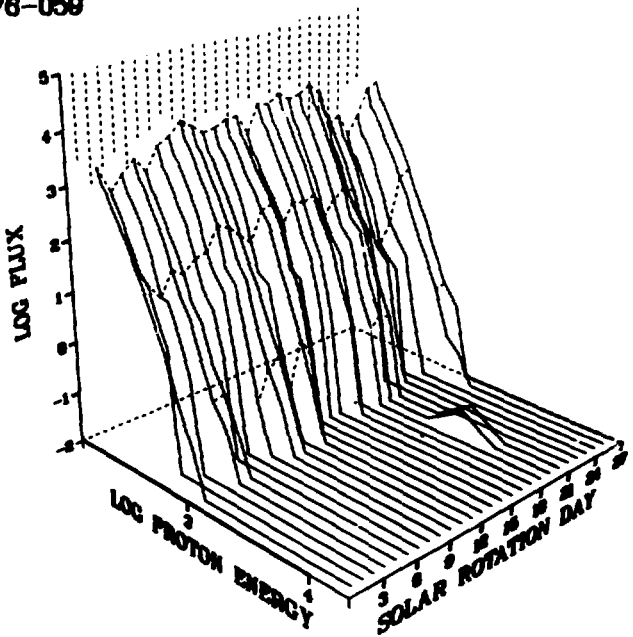
S/C 1976-059



START 1-25-77

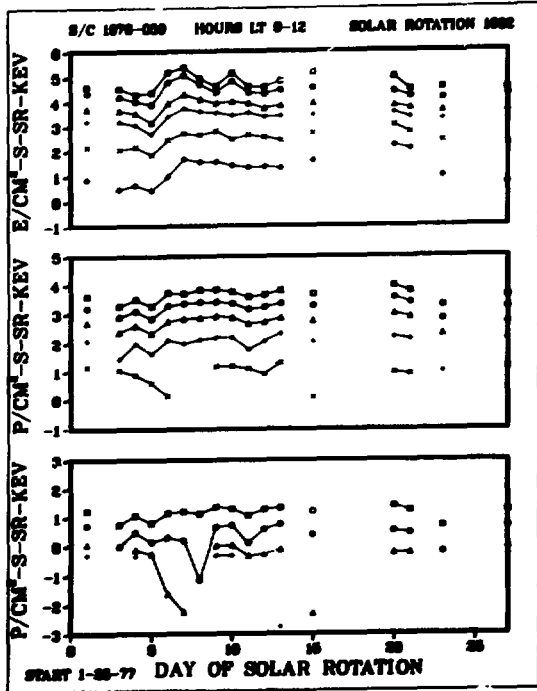
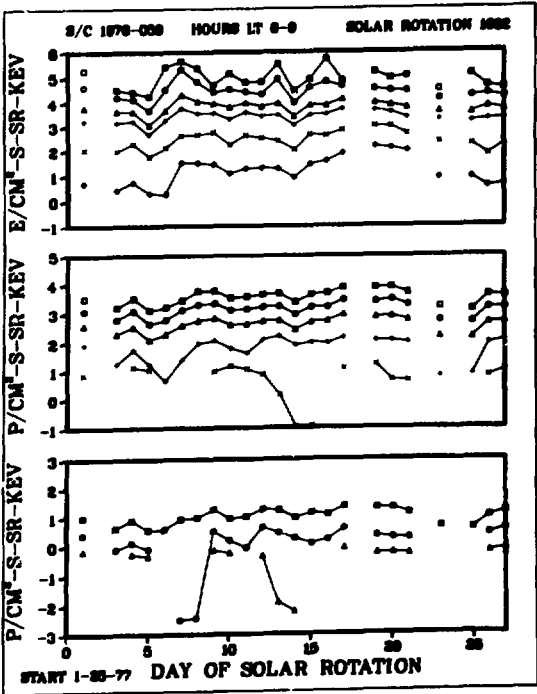
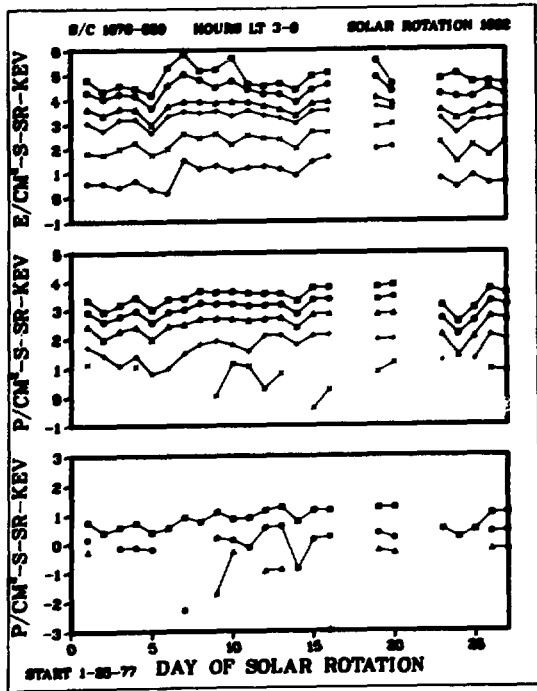
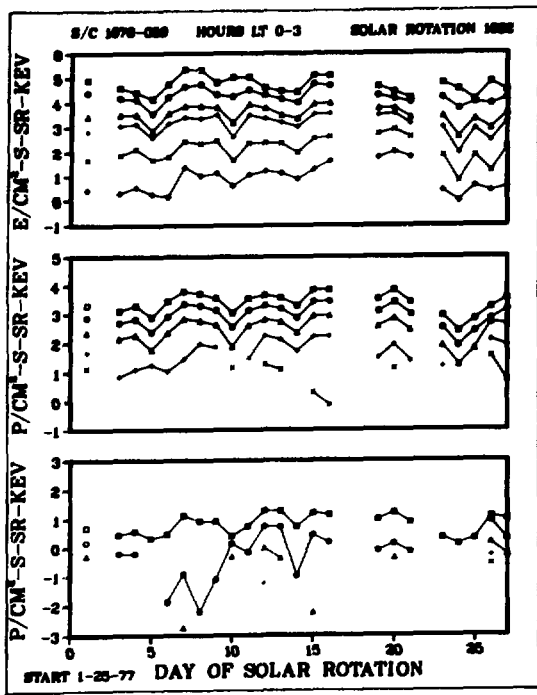
SOLAR ROTATION 1982

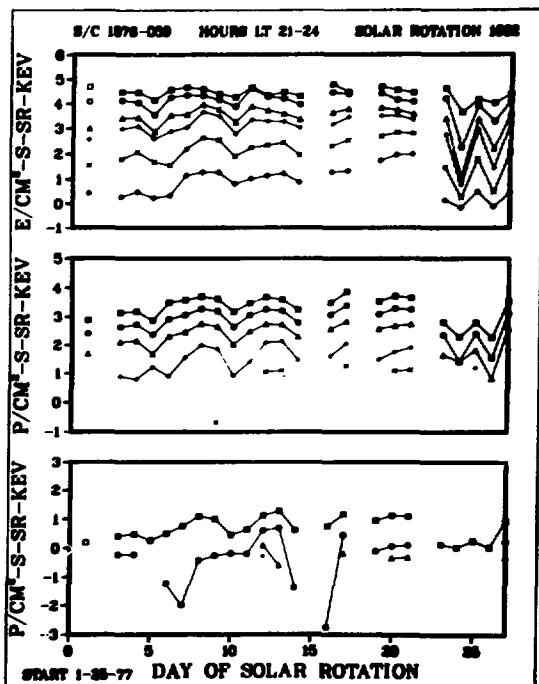
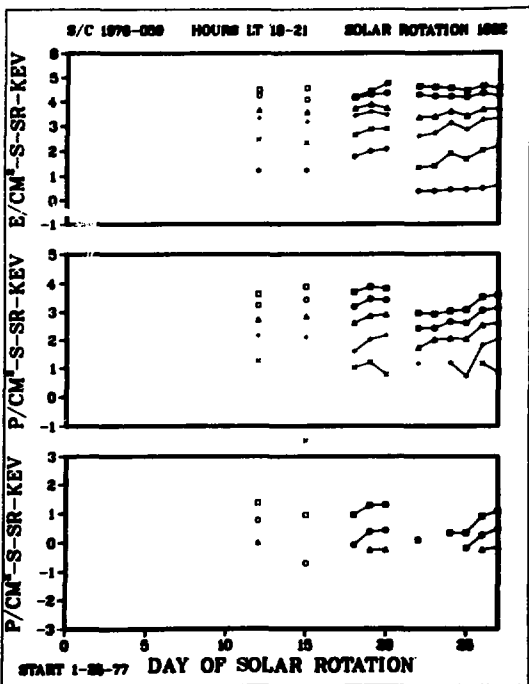
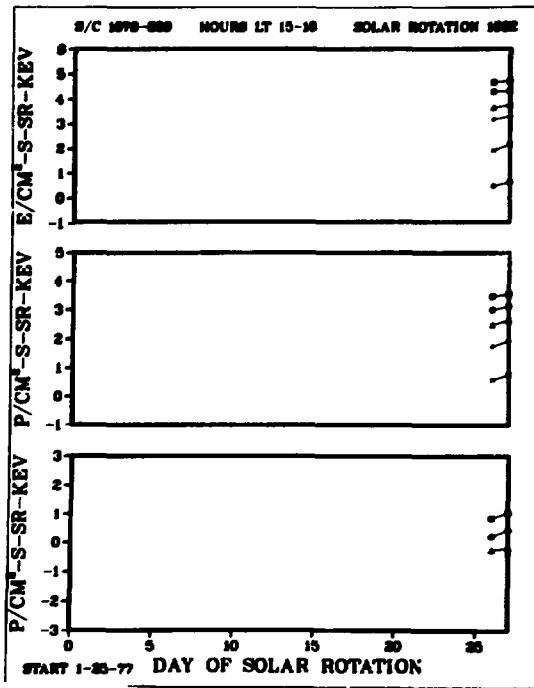
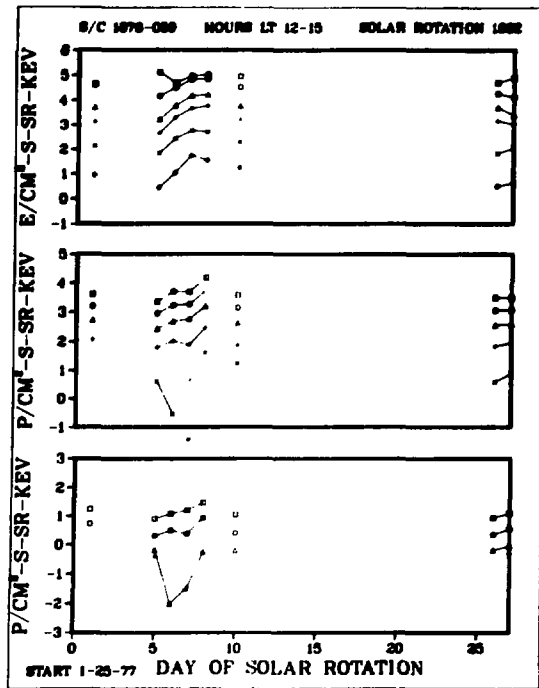
S/C 1976-059



START 1-25-77

SOLAR ROTATION 1982

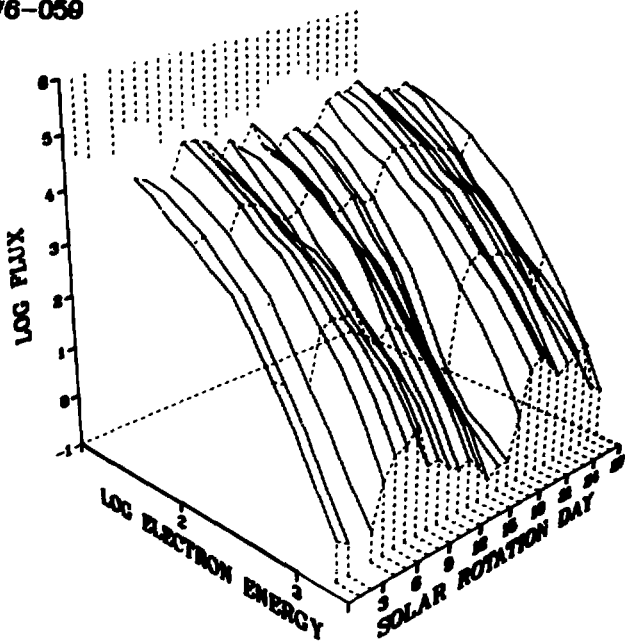




S/C 1976-059

START 2-21-77

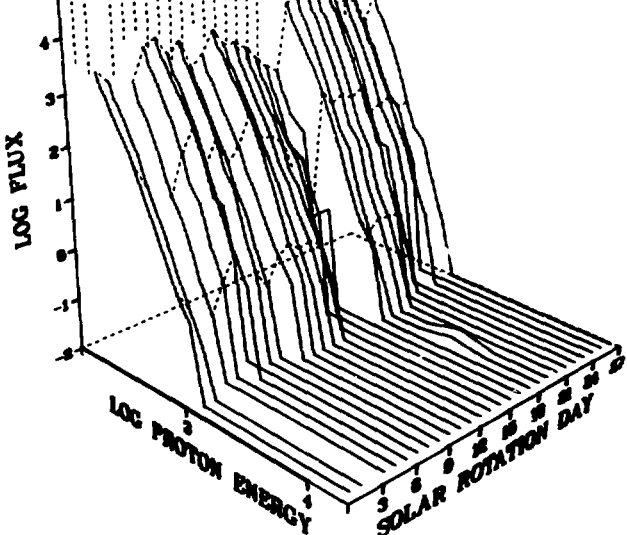
SOLAR ROTATION 1963

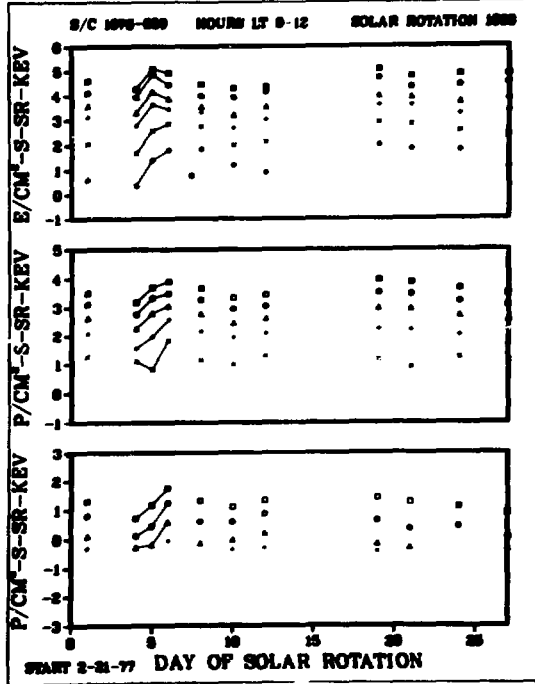
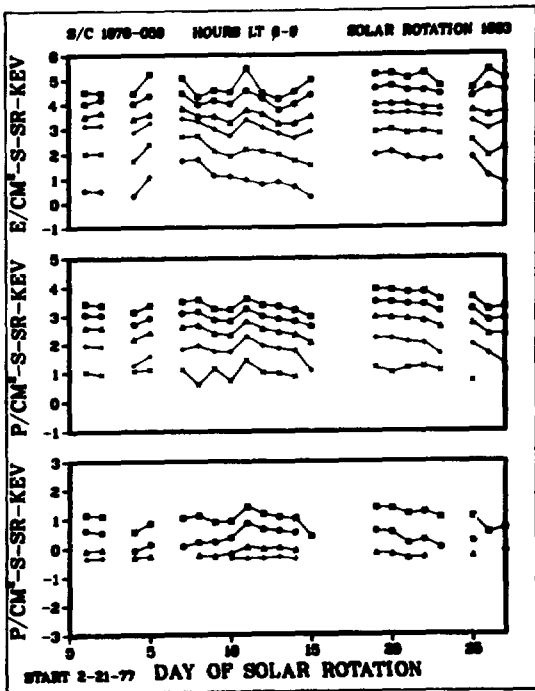
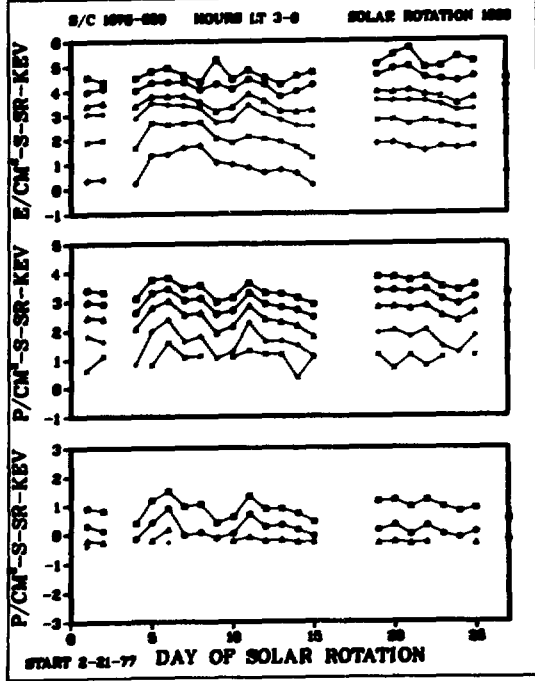
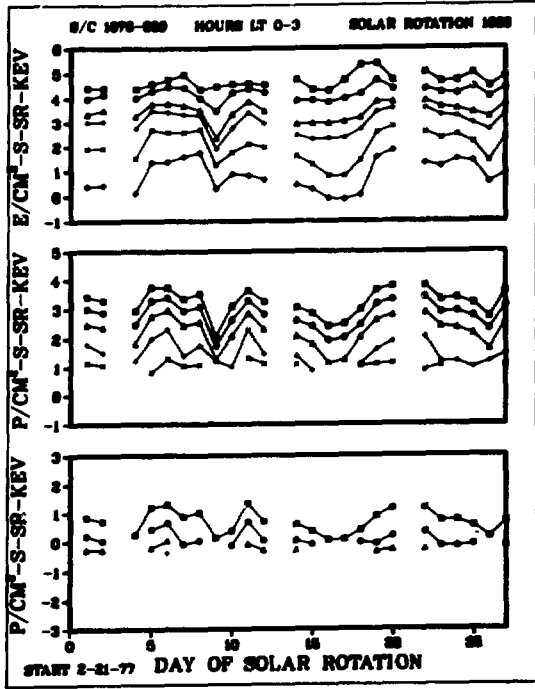


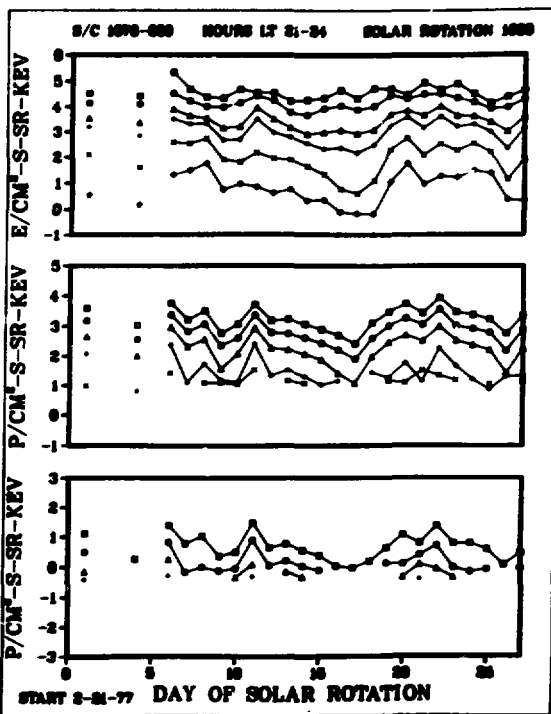
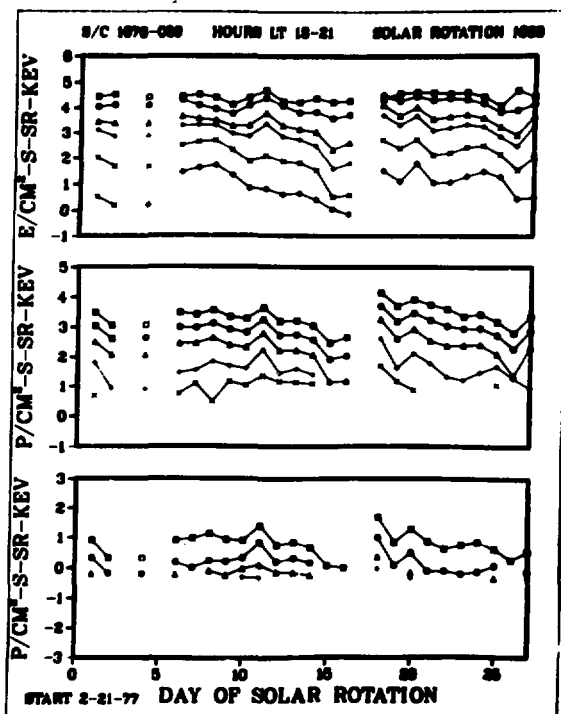
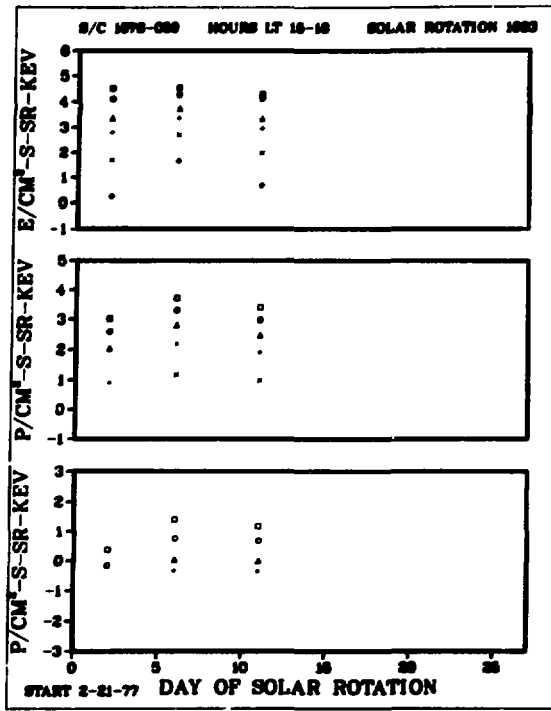
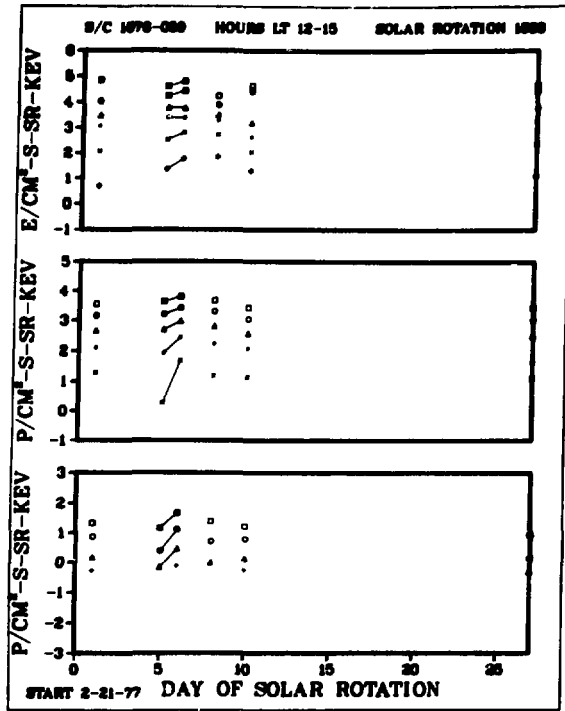
S/C 1976-059

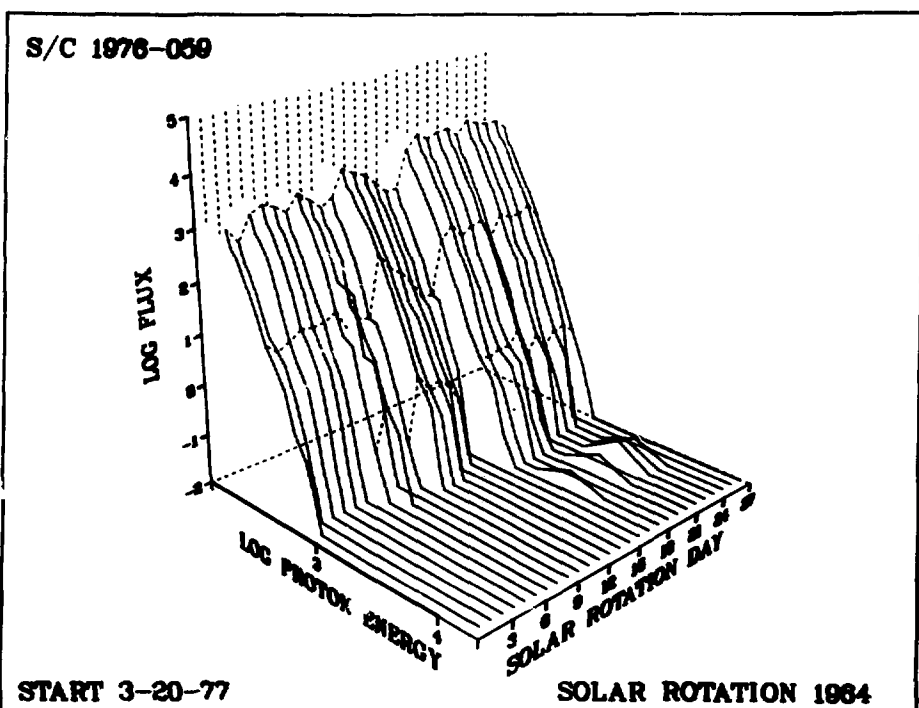
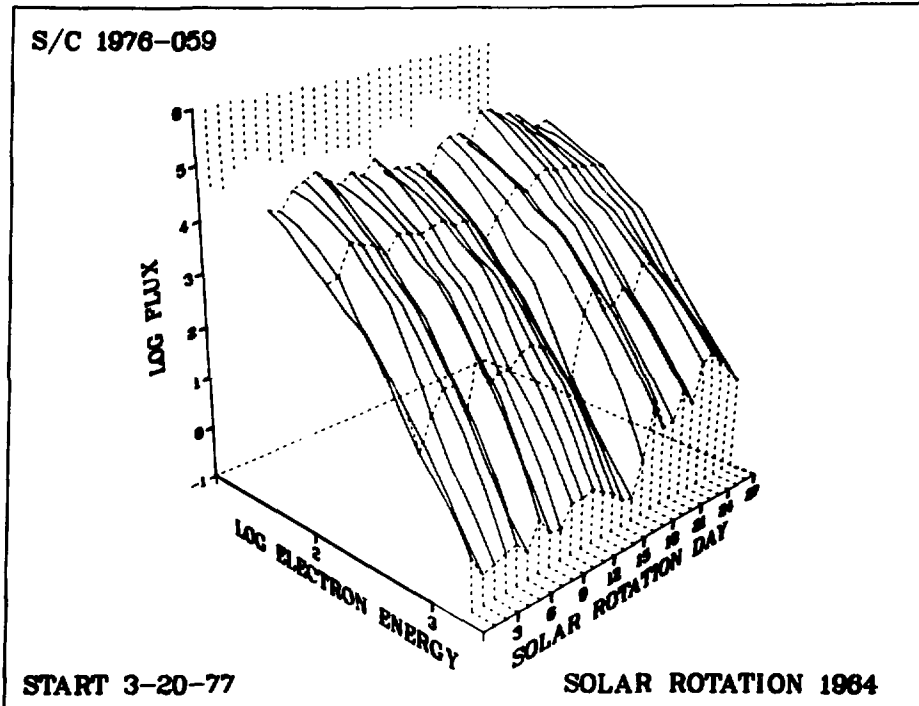
START 2-21-77

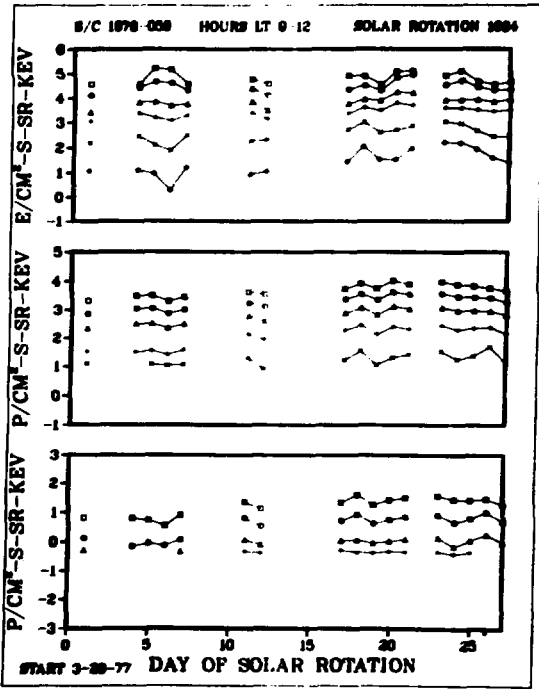
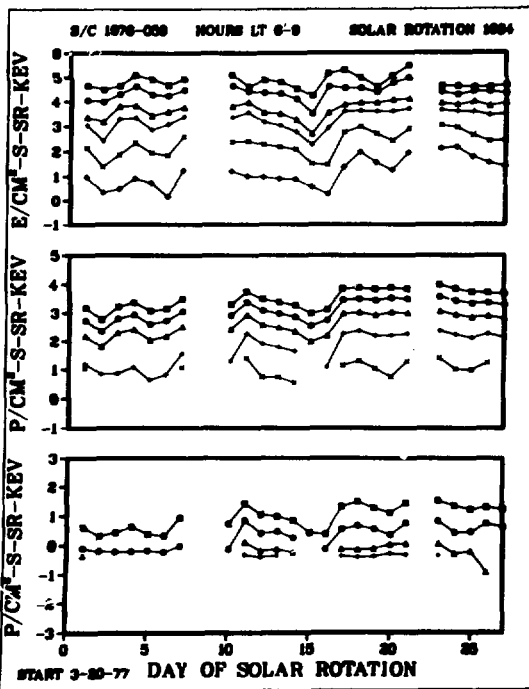
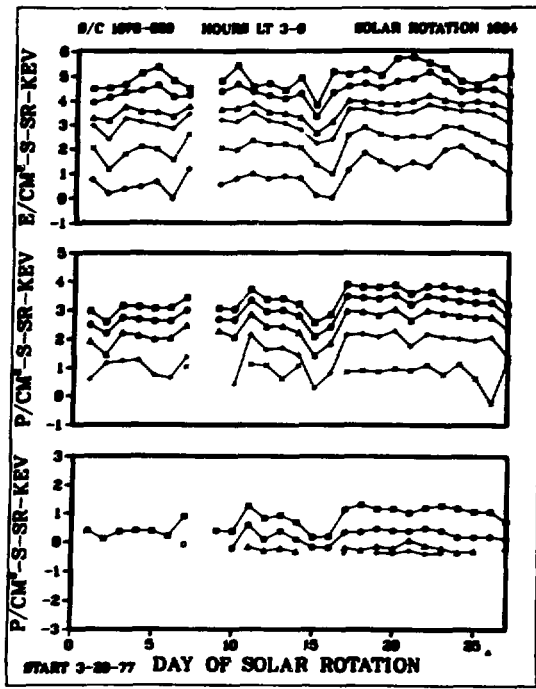
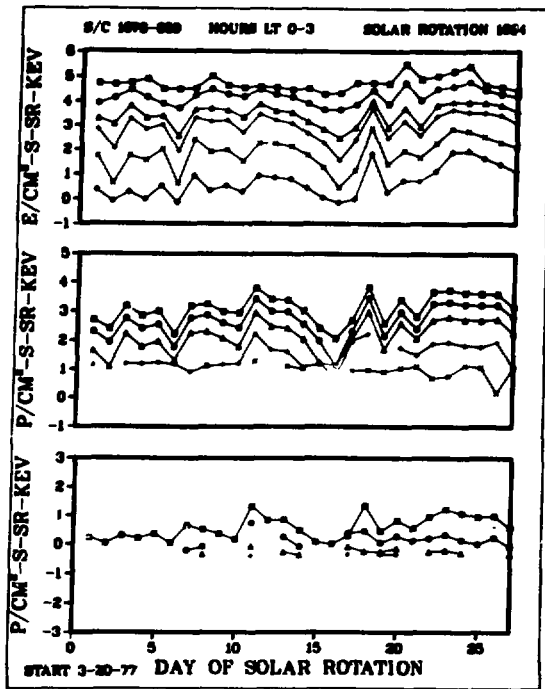
SOLAR ROTATION 1963

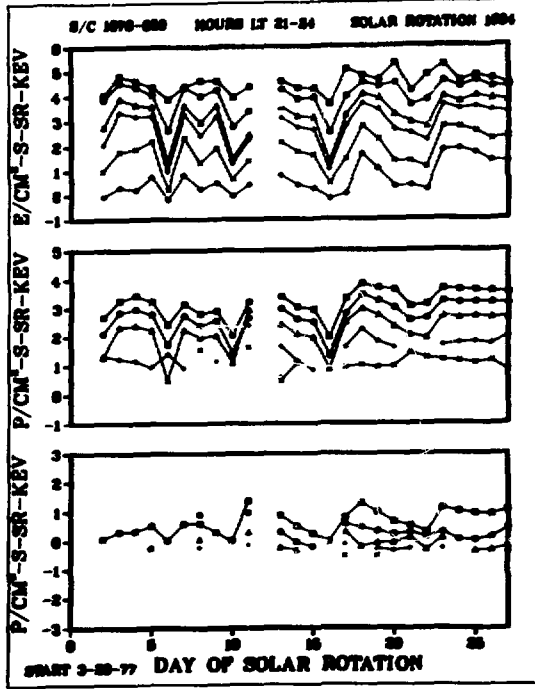
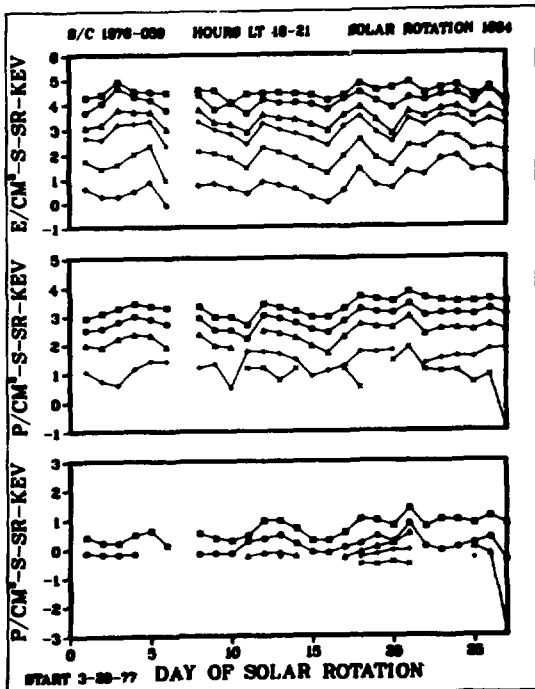
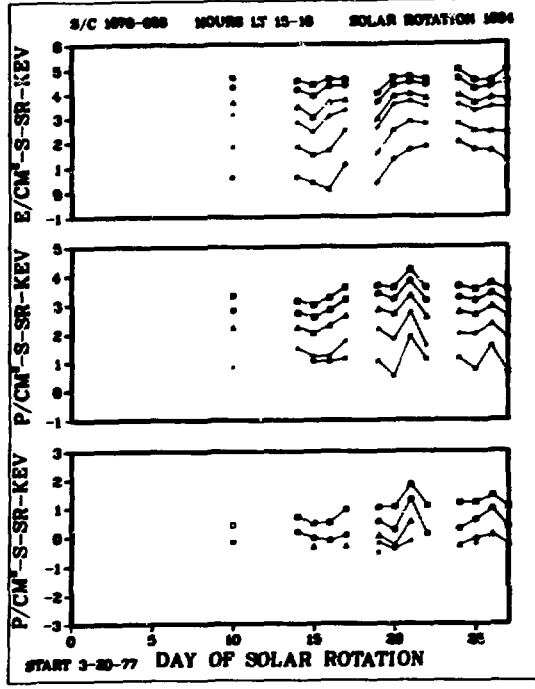
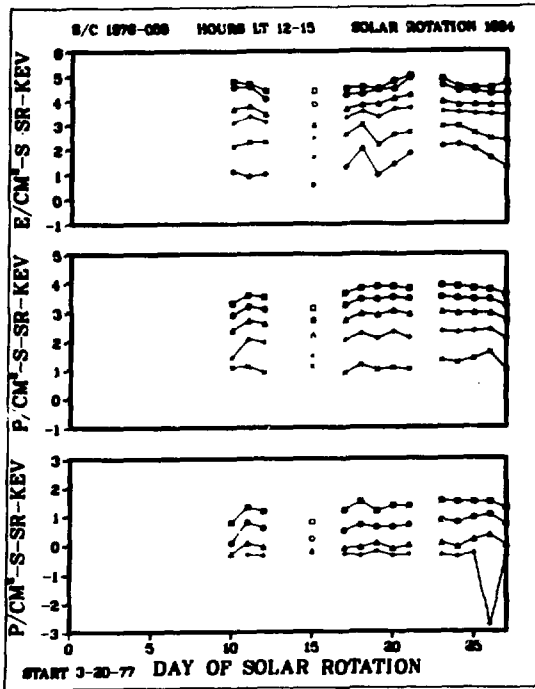




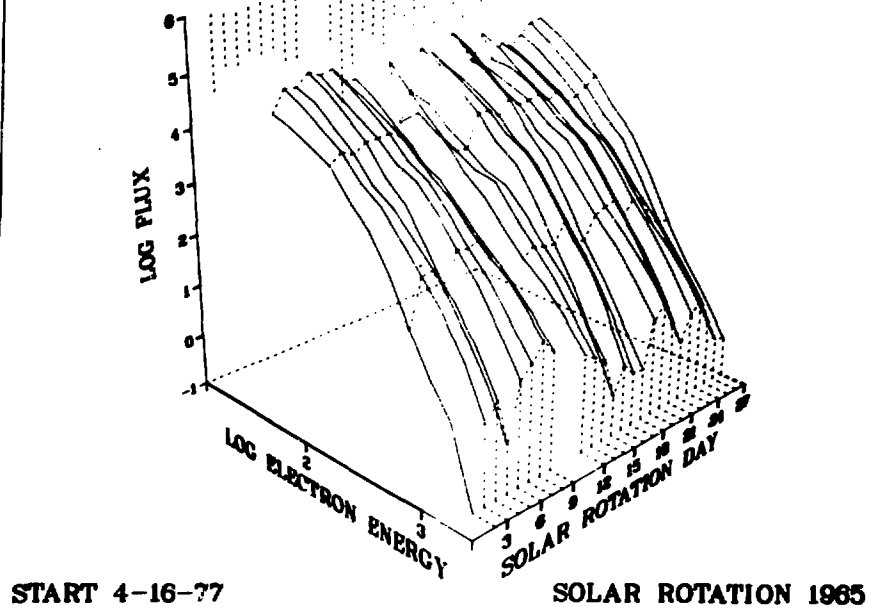




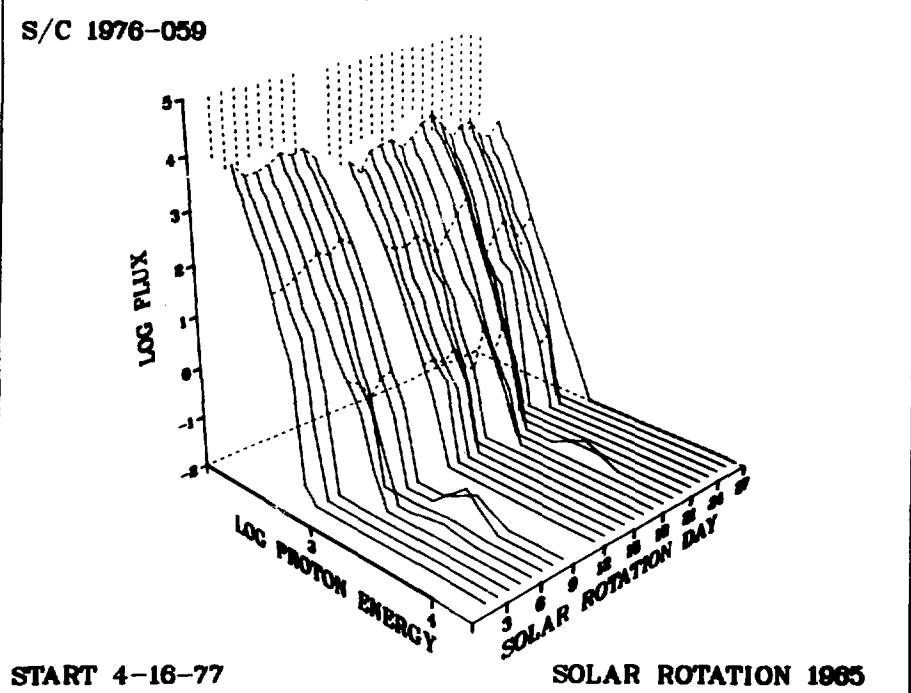


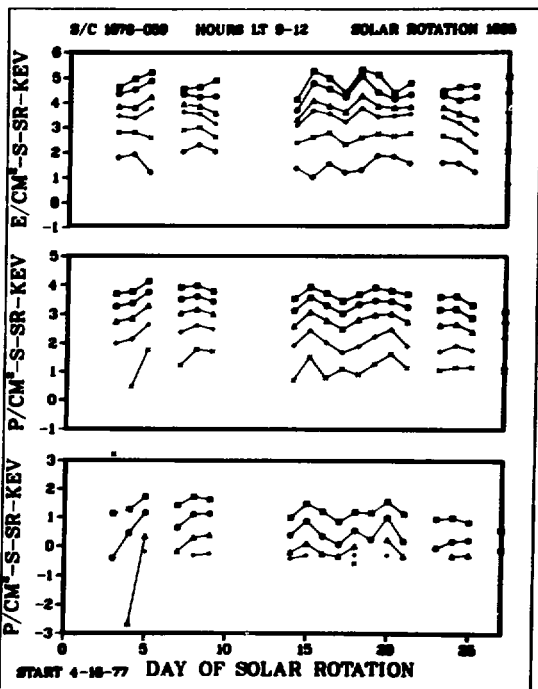
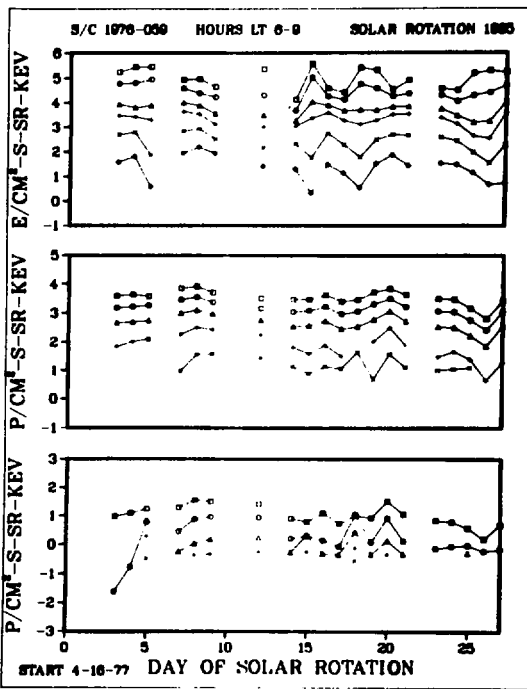
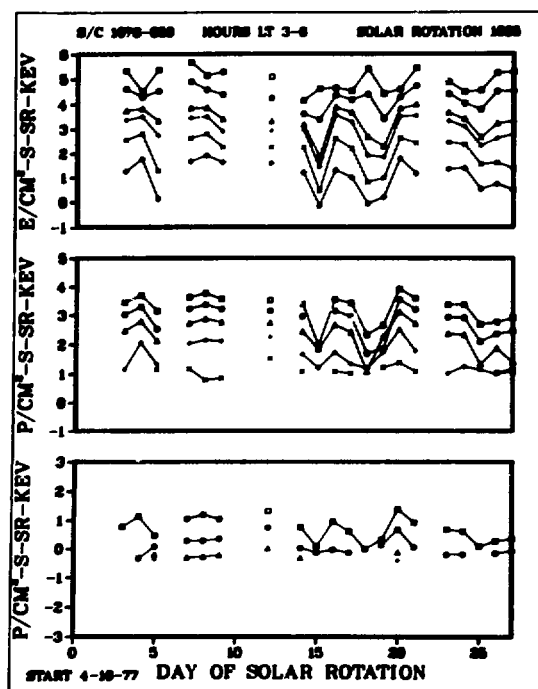
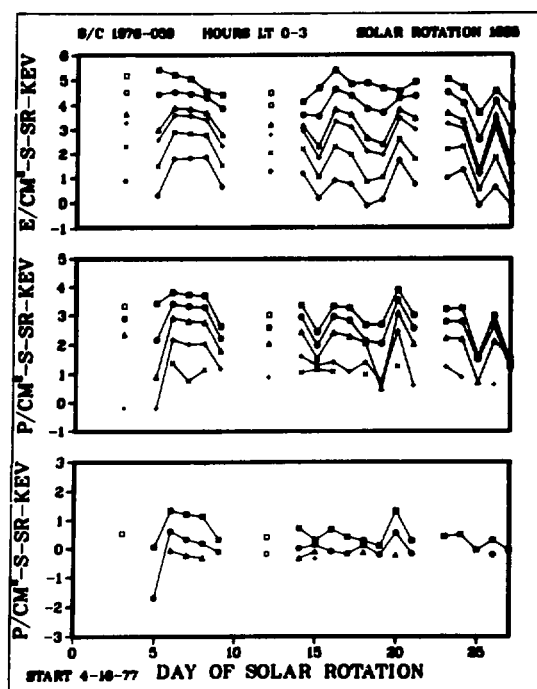


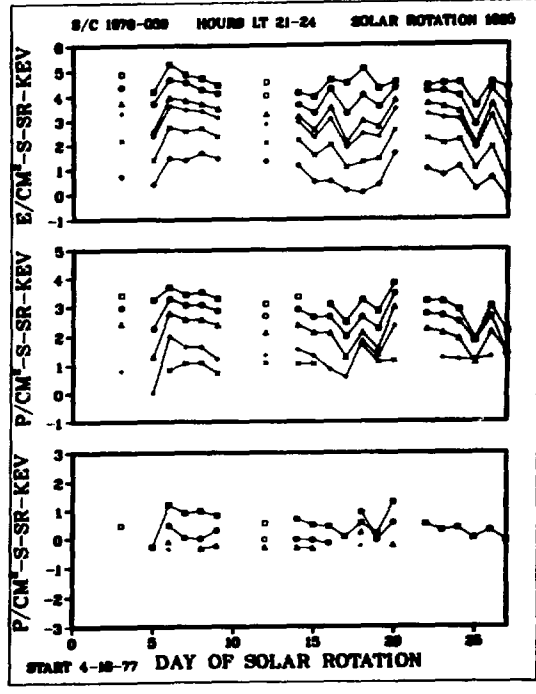
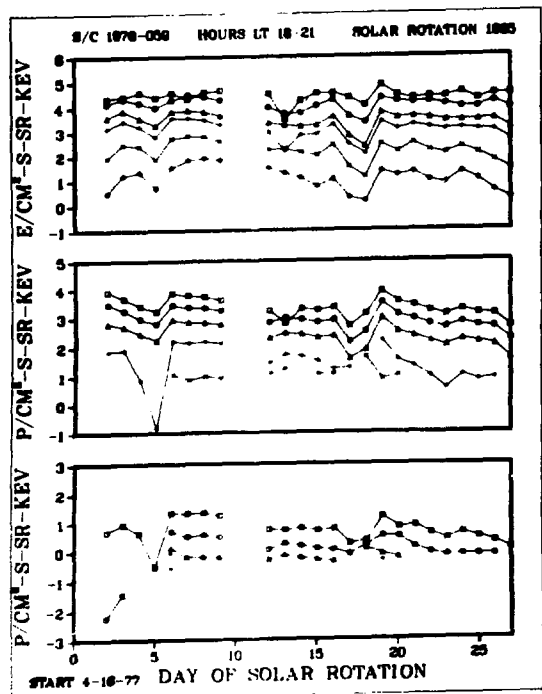
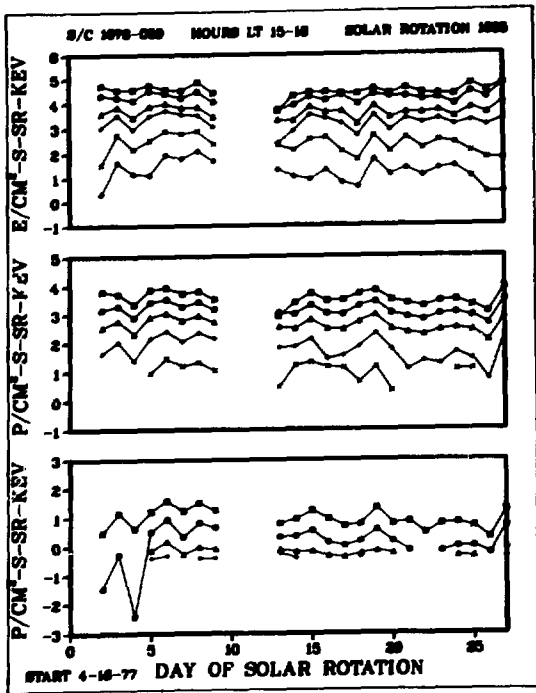
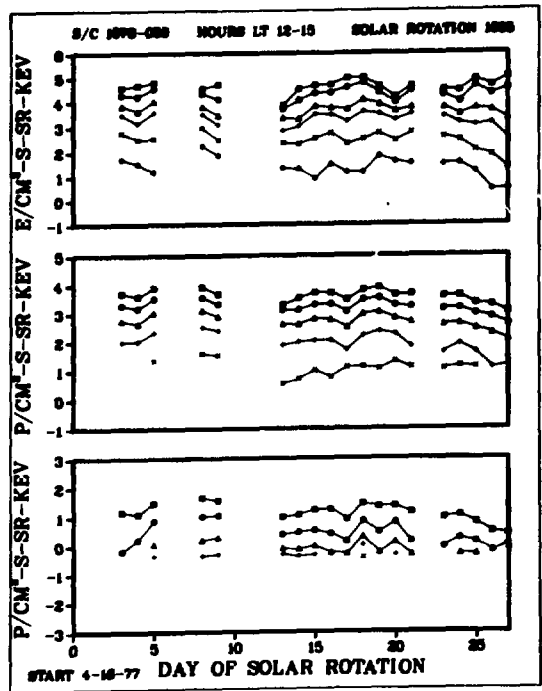
S/C 1976-059



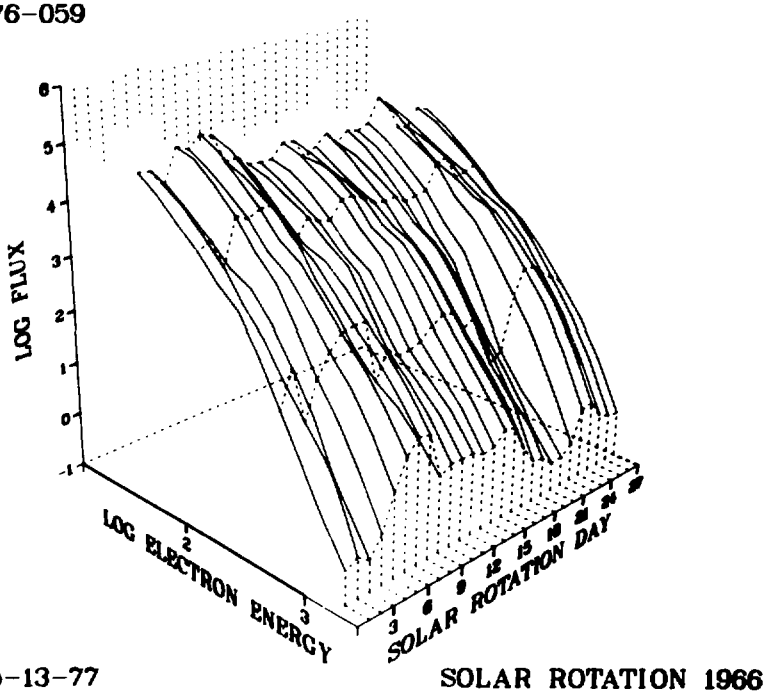
S/C 1976-059







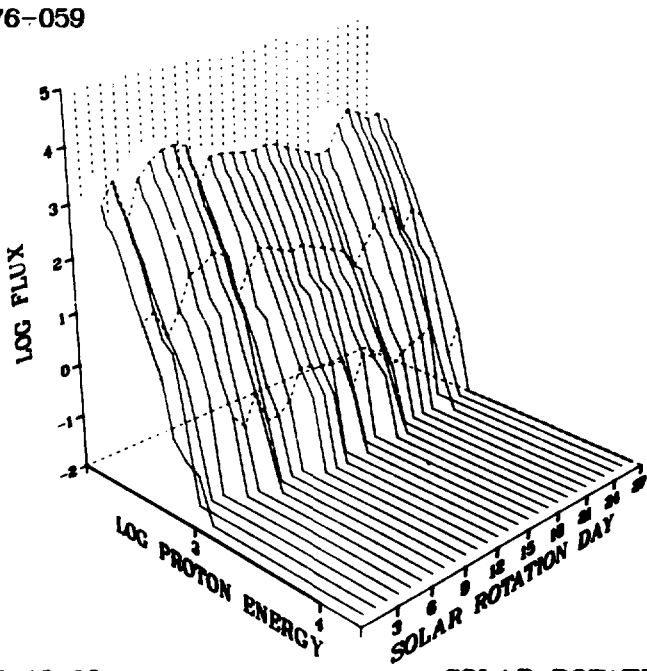
S/C 1976-059



START 5-13-77

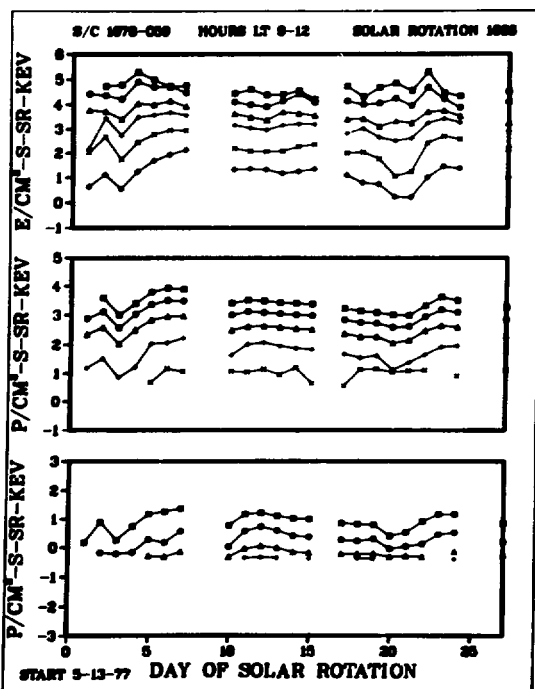
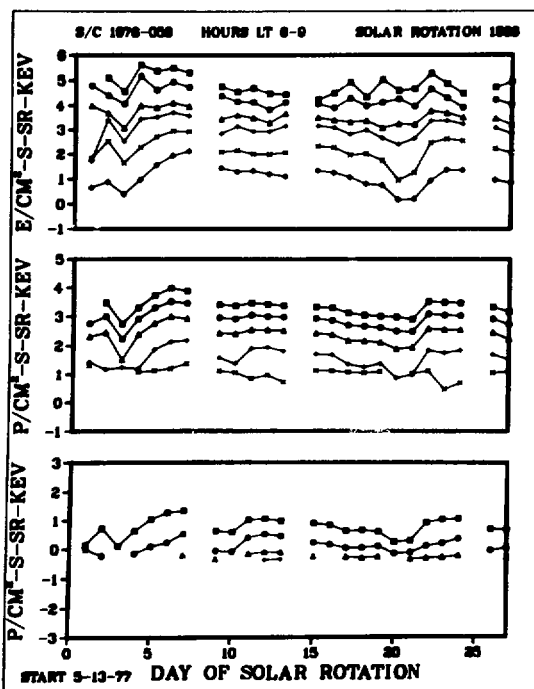
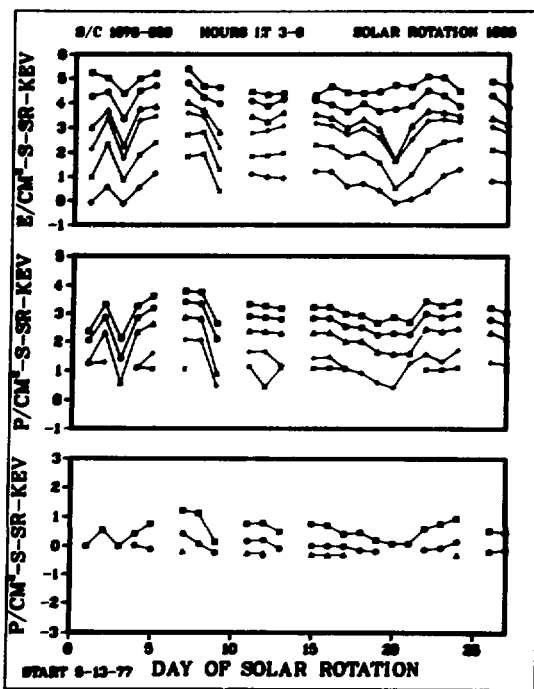
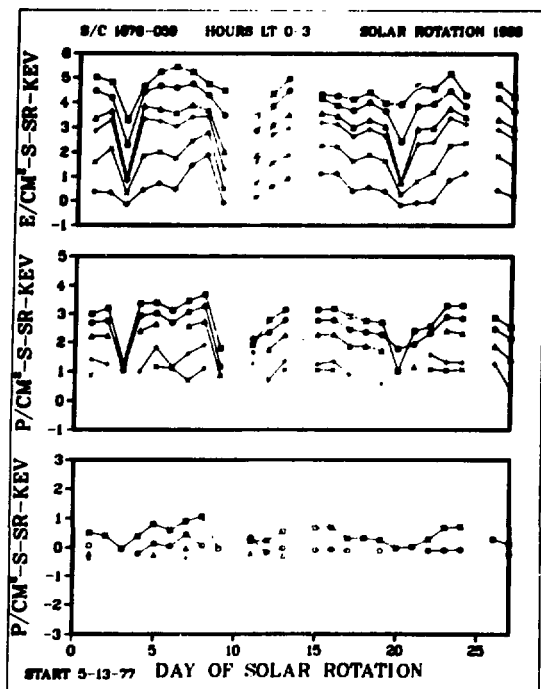
SOLAR ROTATION 1966

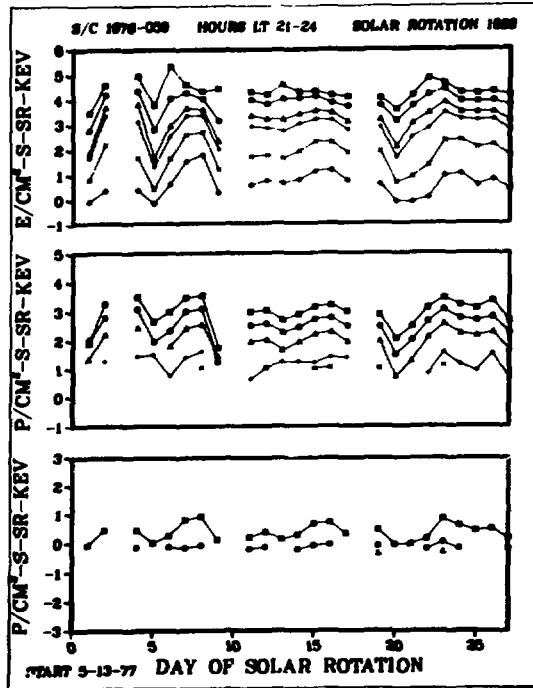
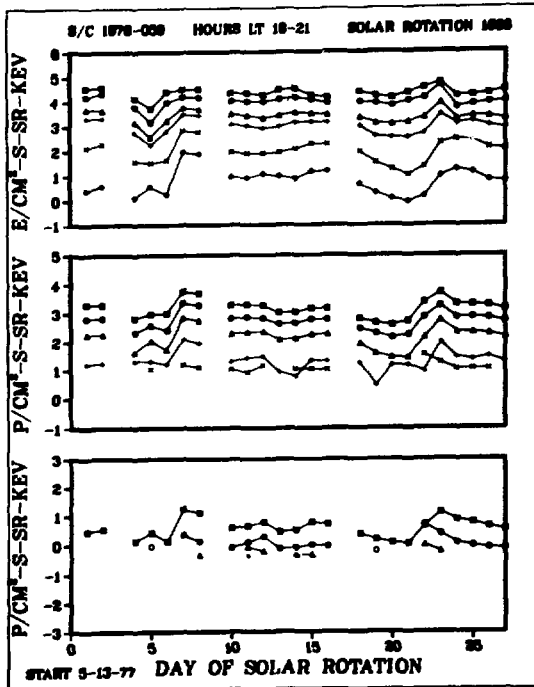
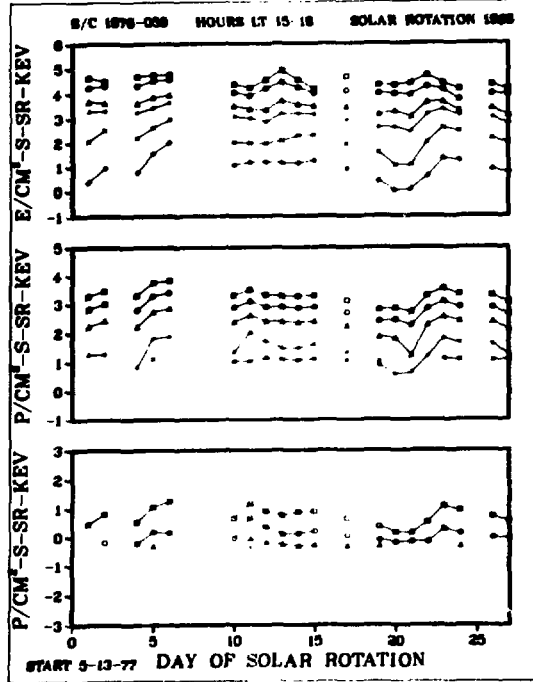
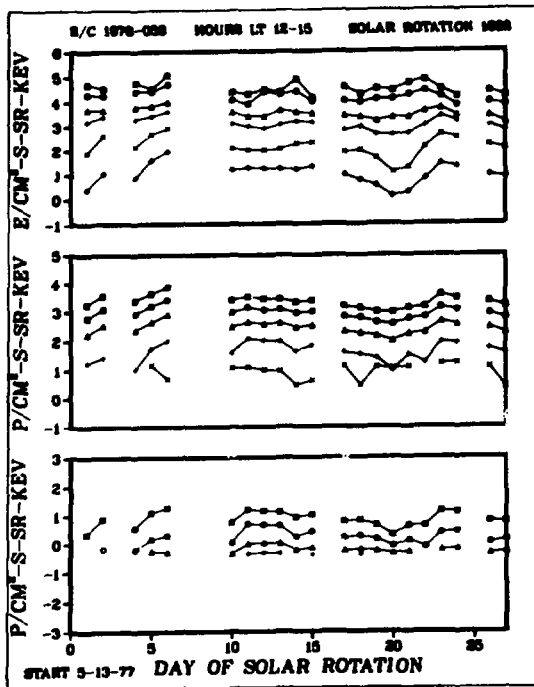
S/C 1976-059



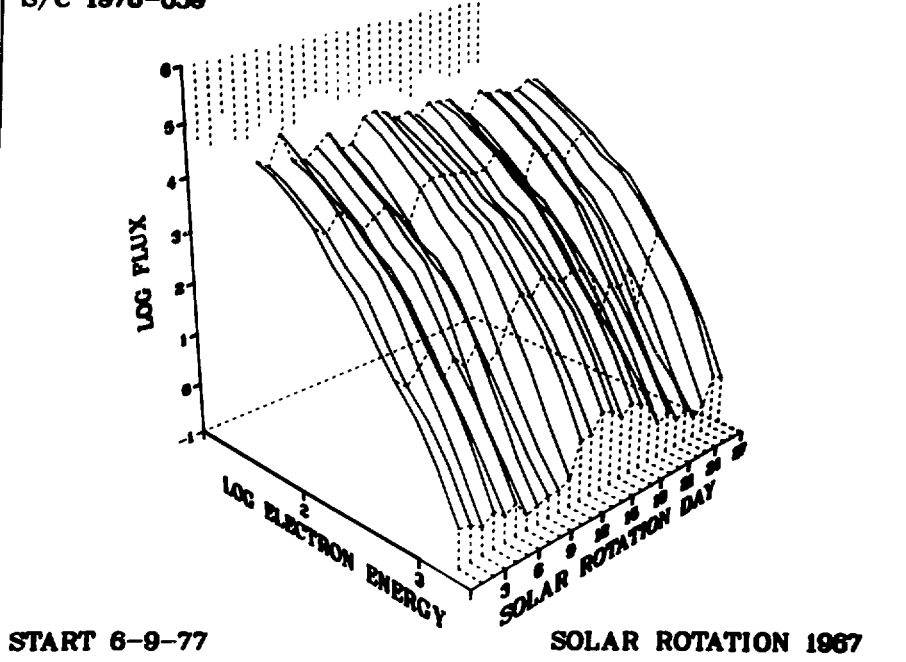
START 5-13-77

SOLAR ROTATION 1966

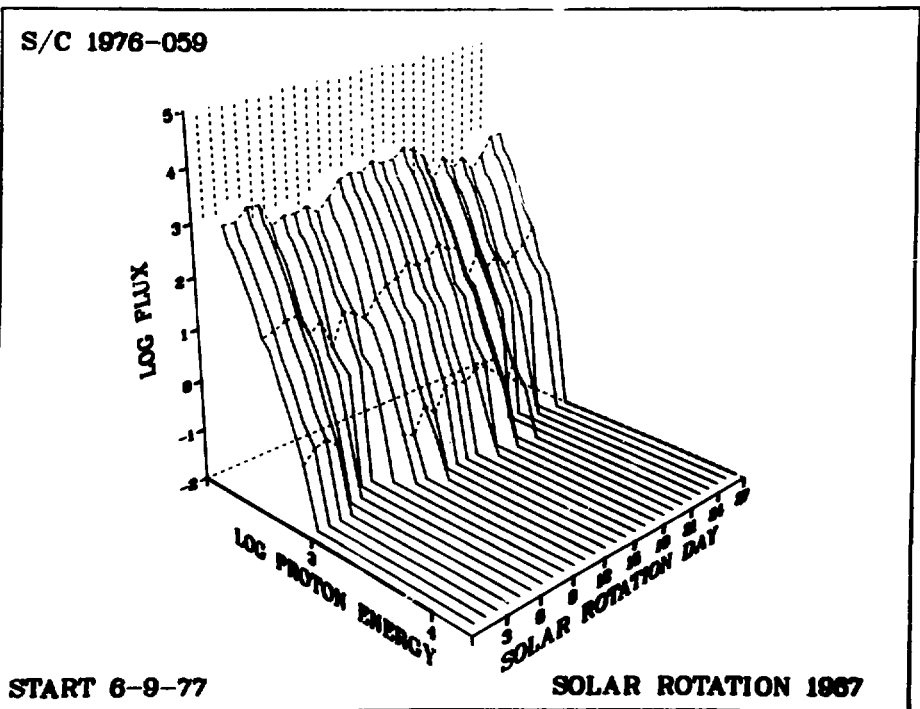


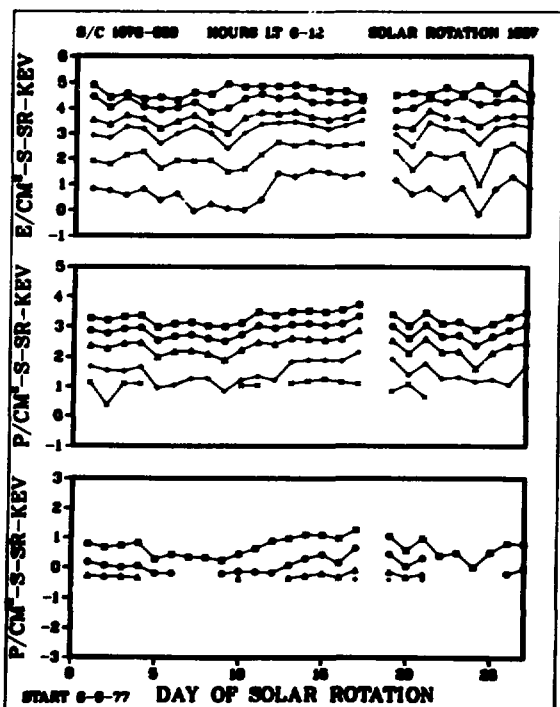
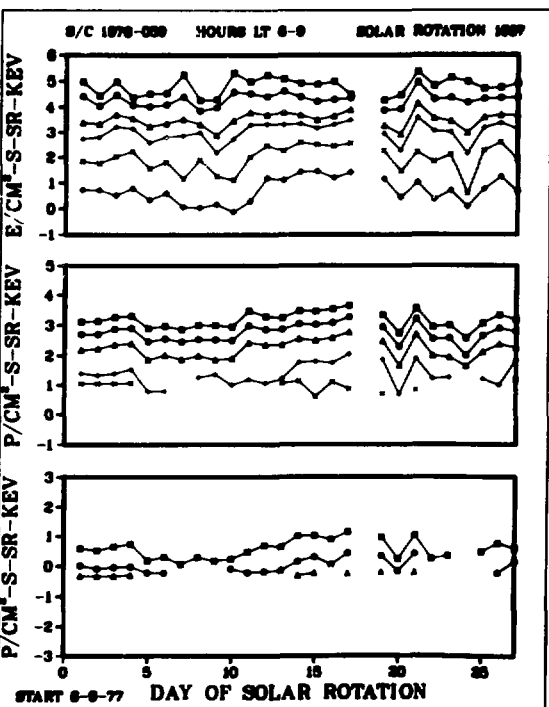
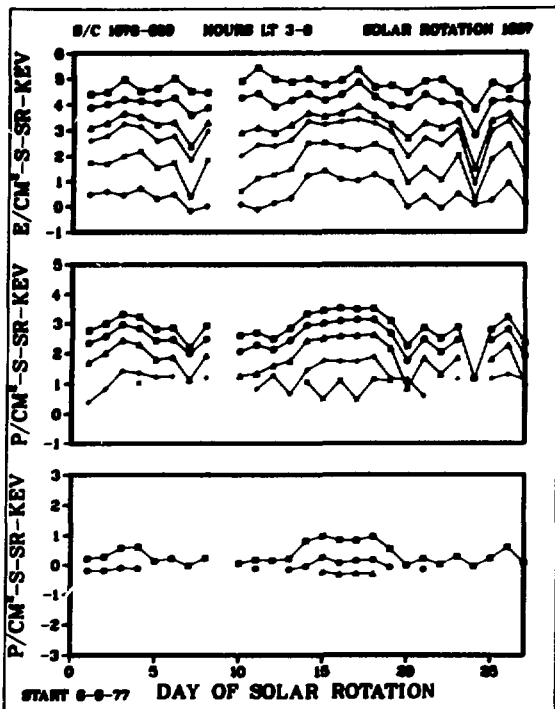
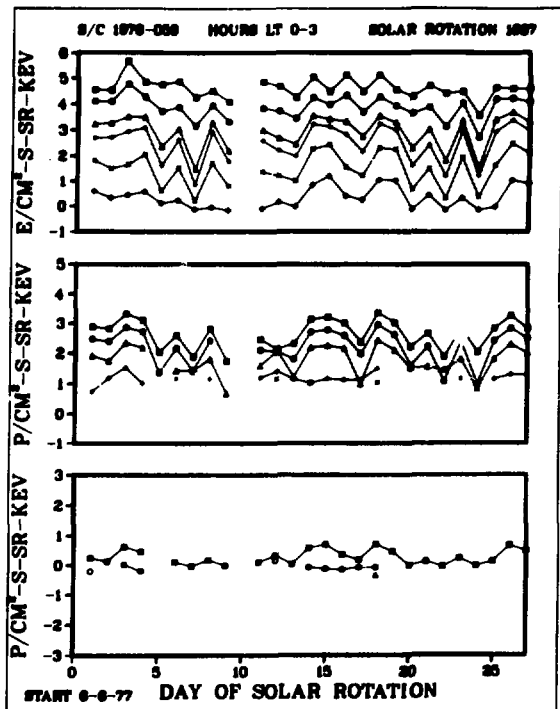


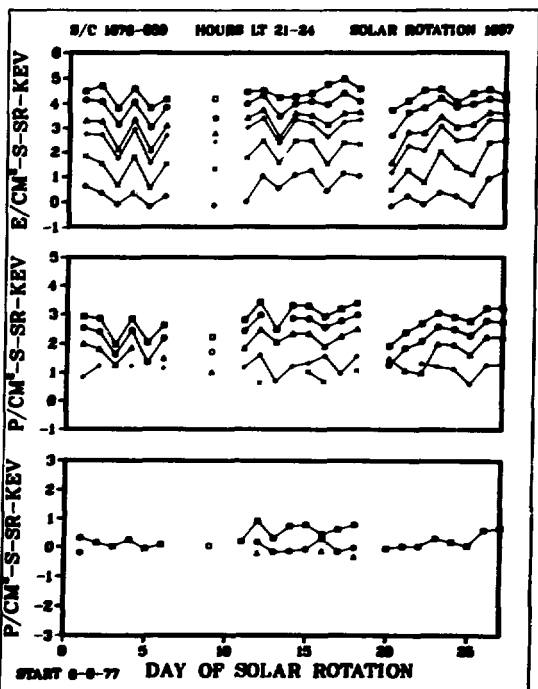
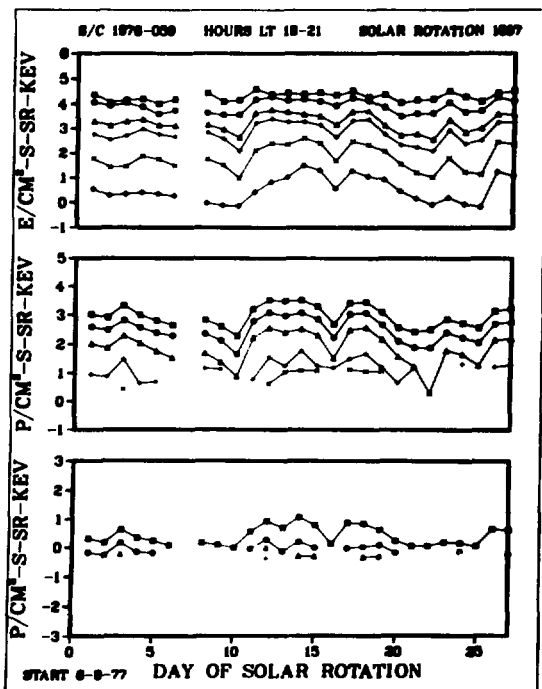
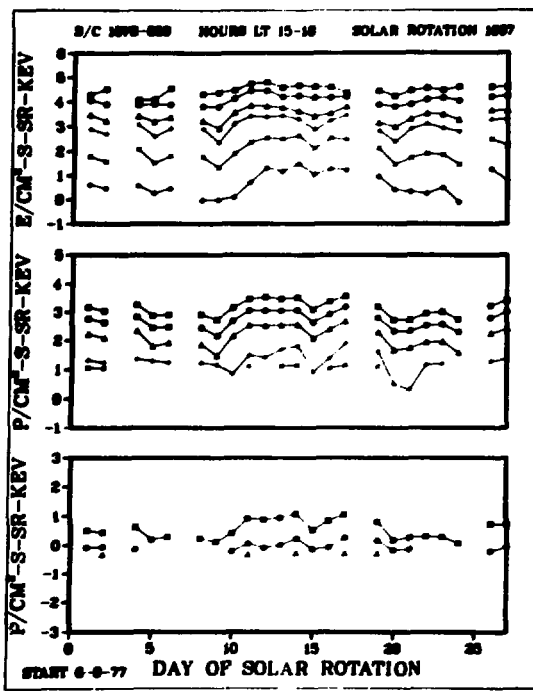
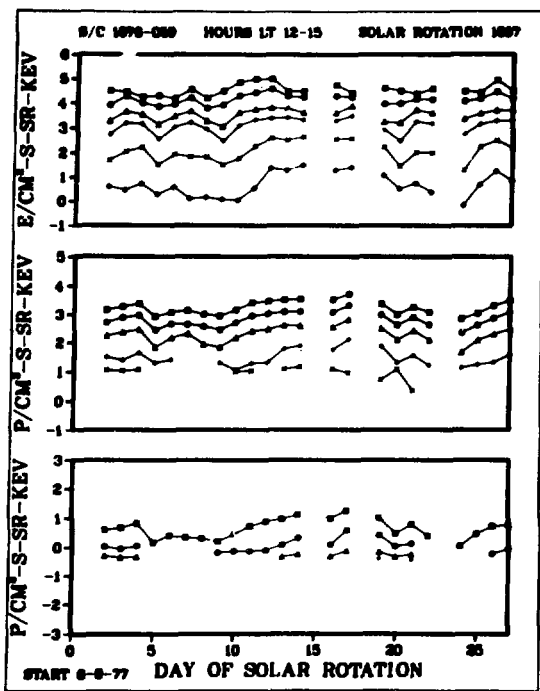
S/C 1976-059



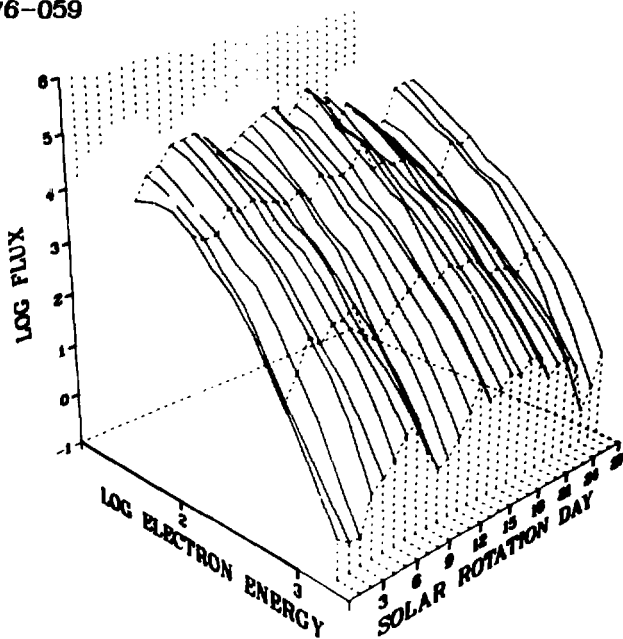
S/C 1976-059







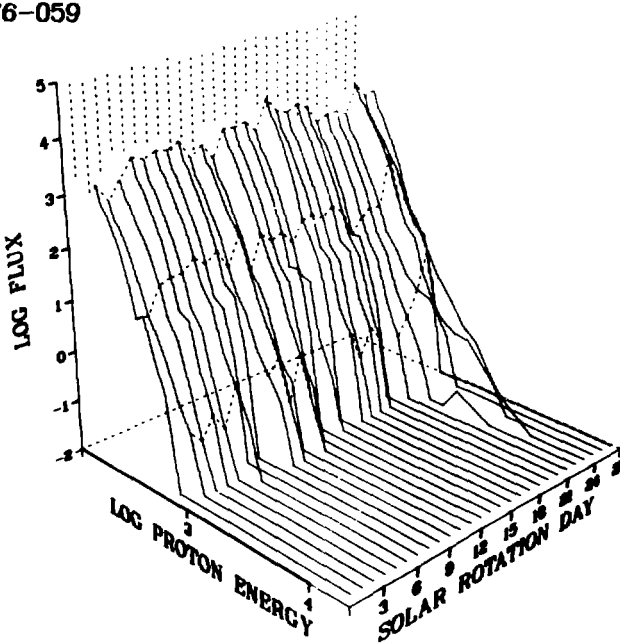
S/C 1976-059



START 7-6-77

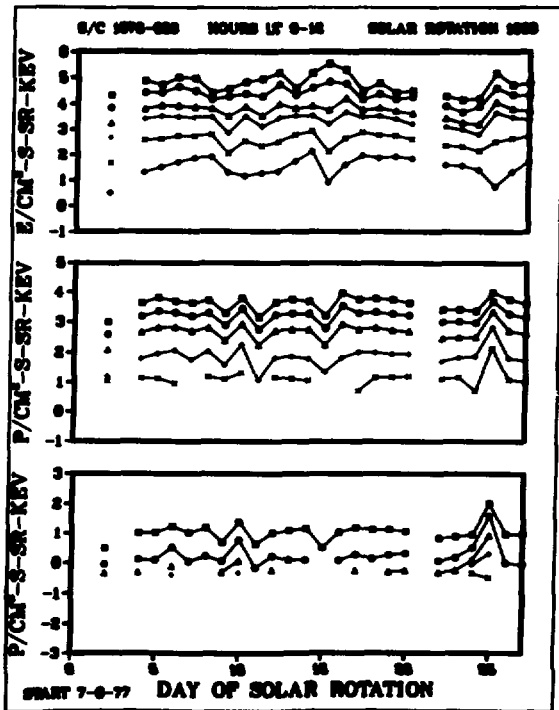
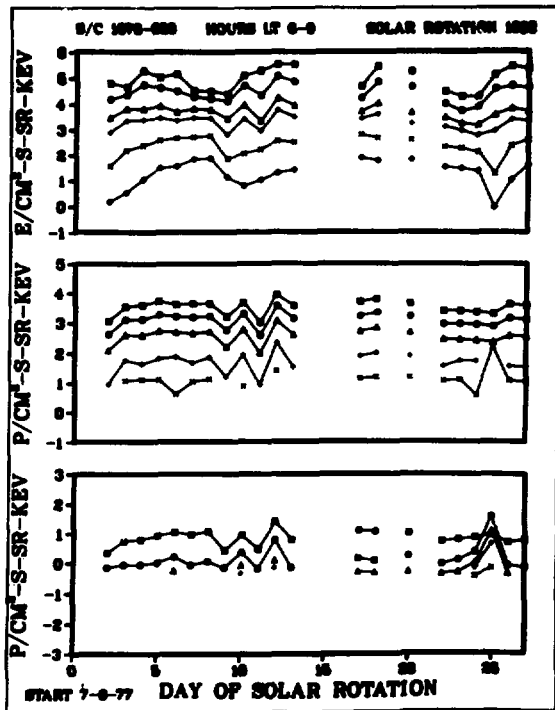
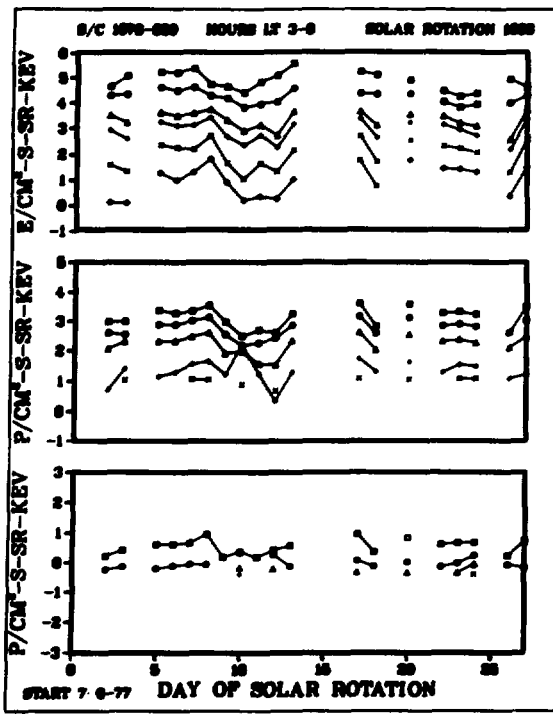
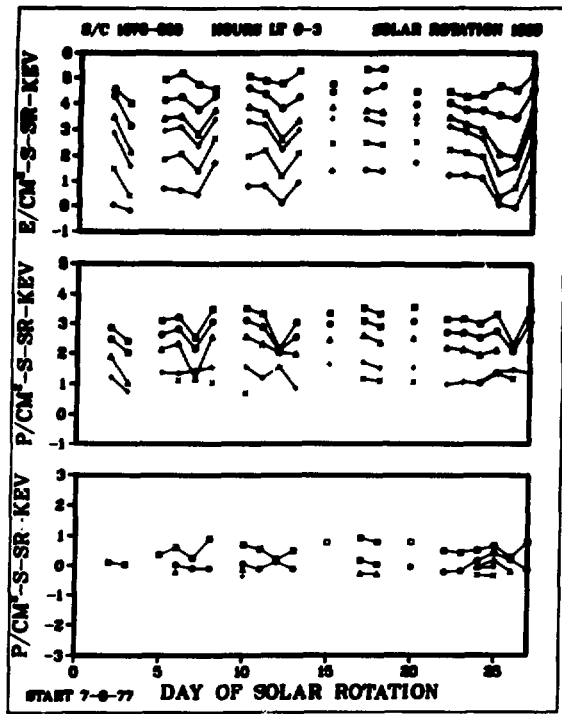
SOLAR ROTATION 1968

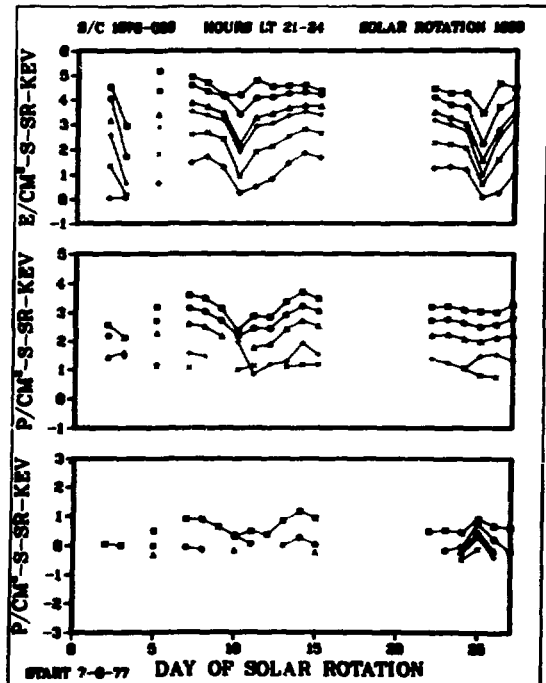
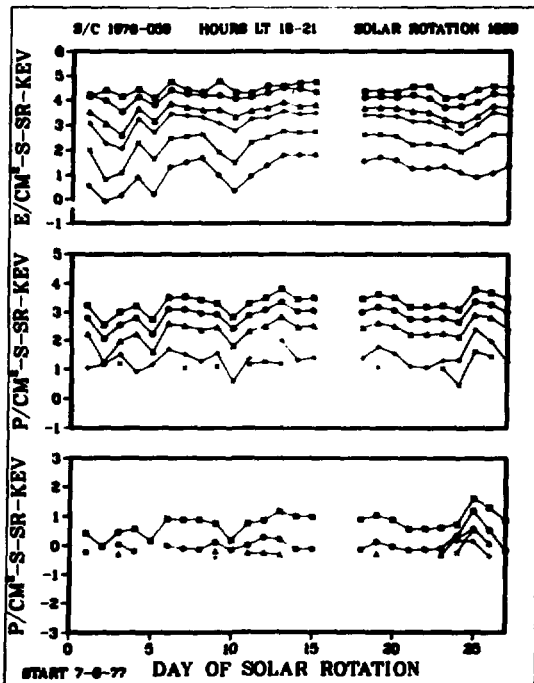
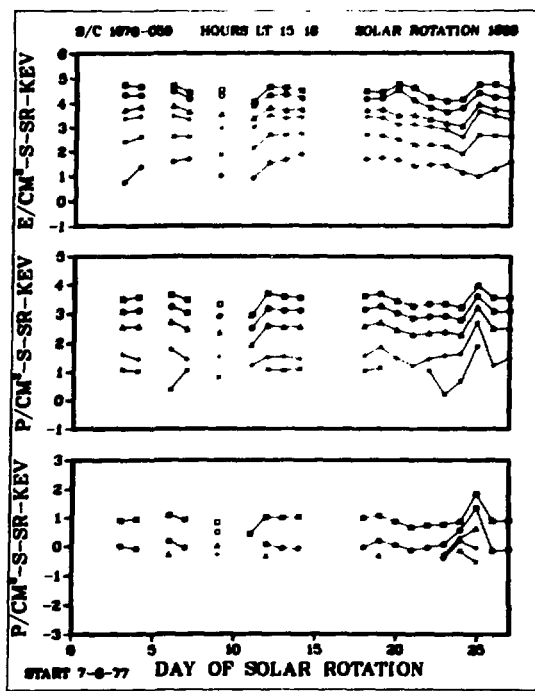
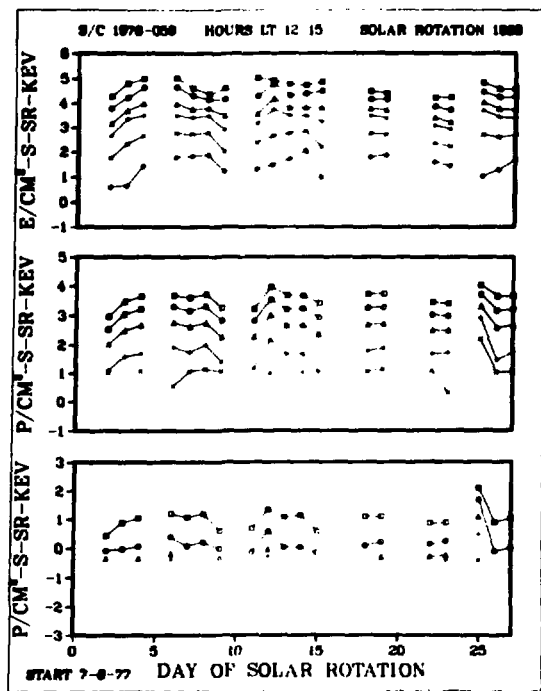
S/C 1976-059



START 7-6-77

SOLAR ROTATION 1968

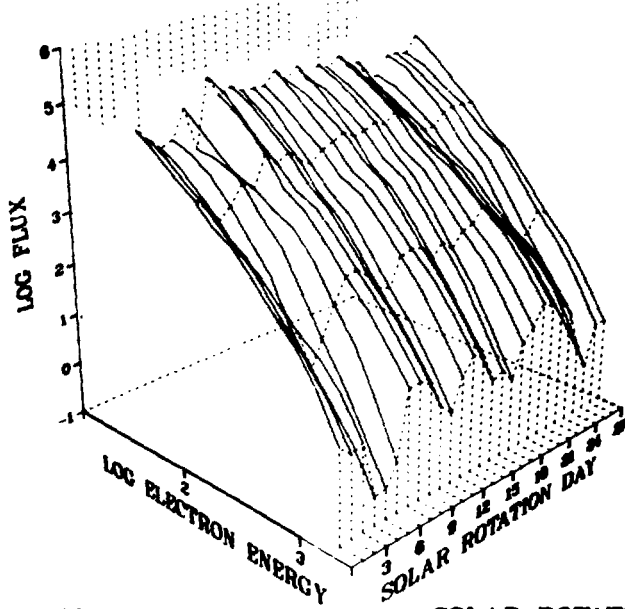




S/C 1976-059

START 8-2-77

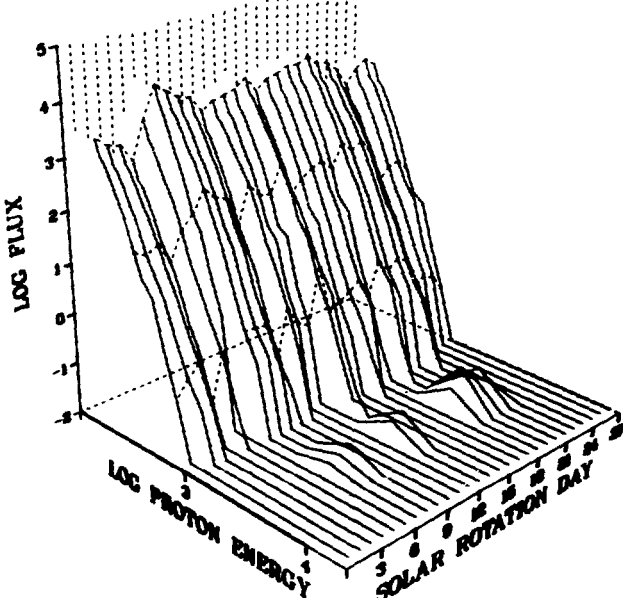
SOLAR ROTATION 1969

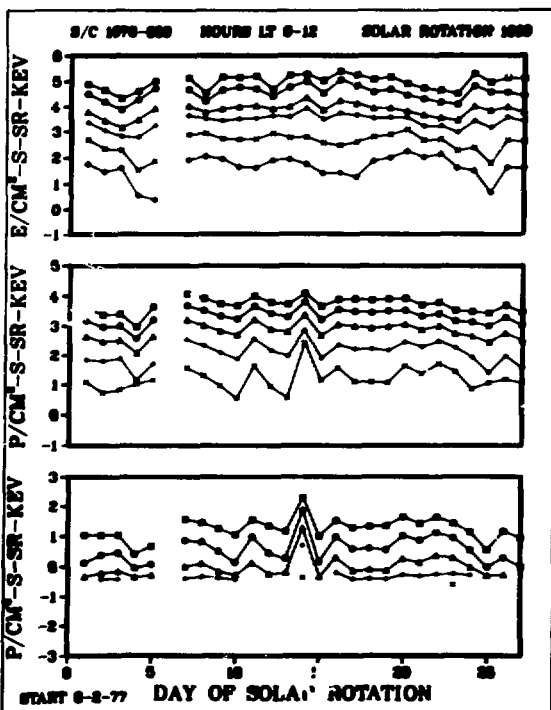
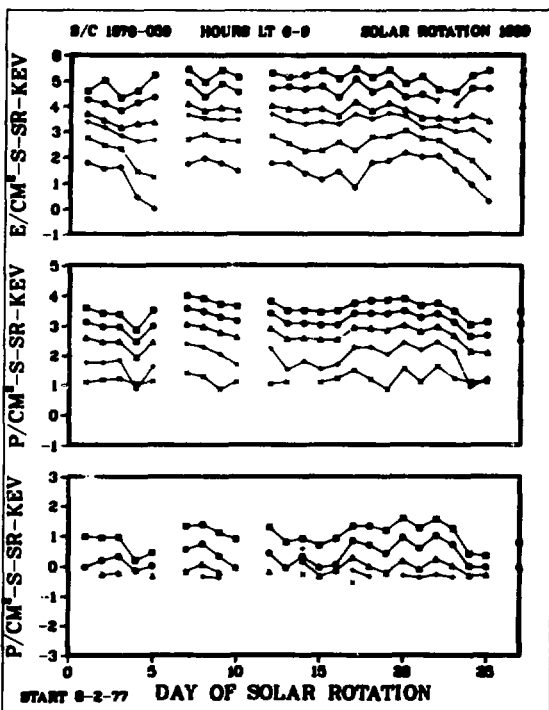
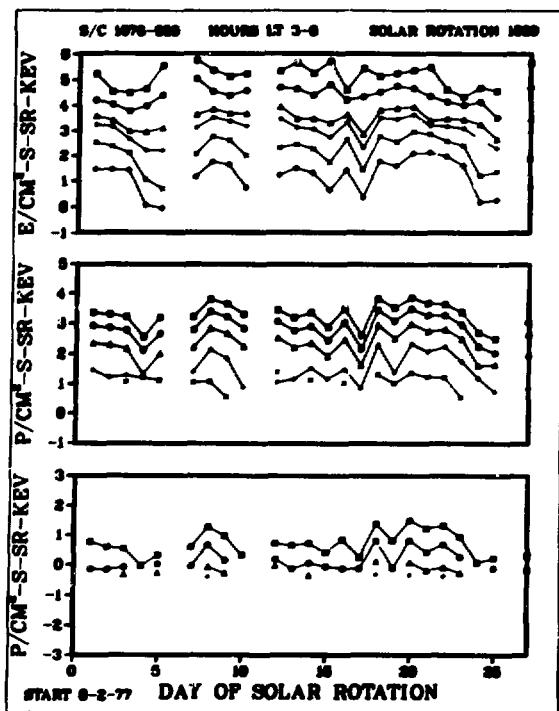
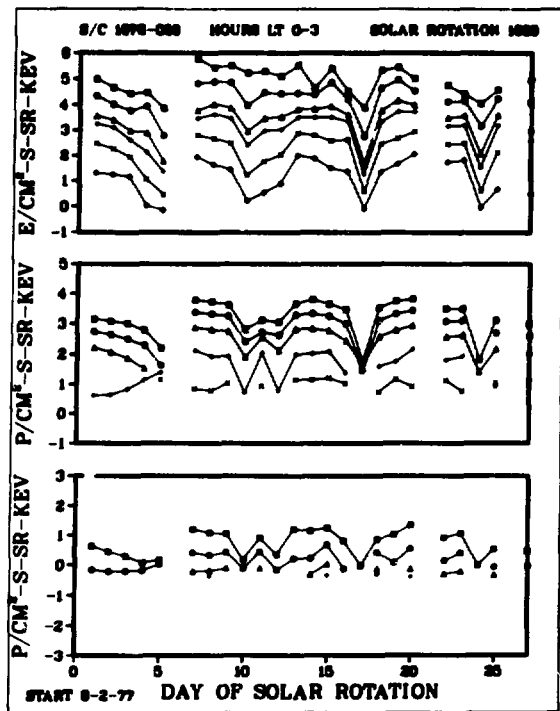


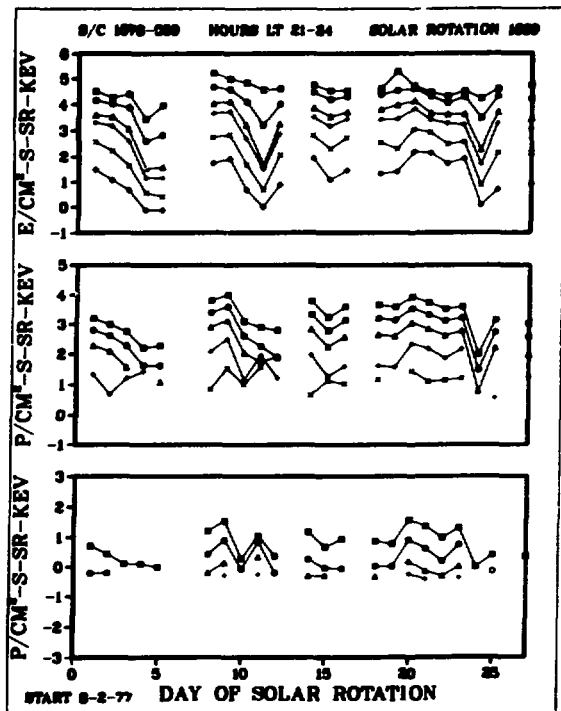
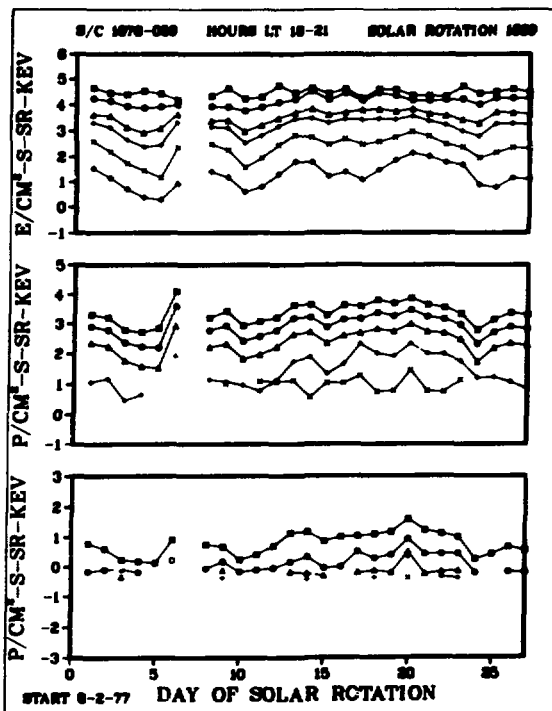
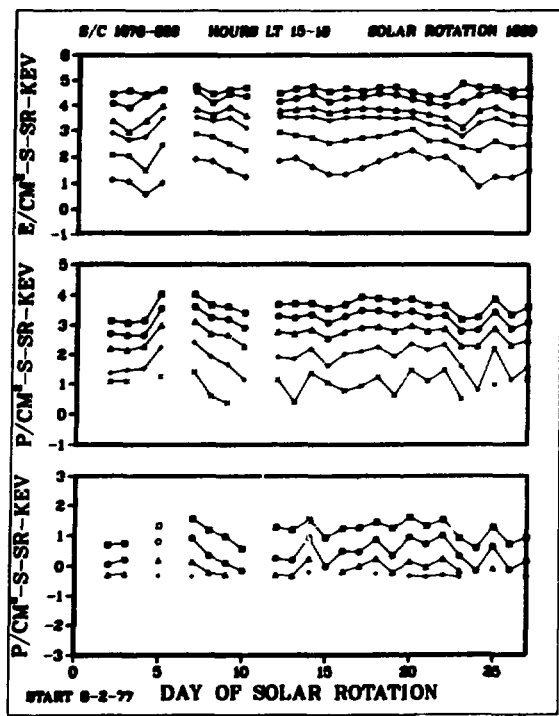
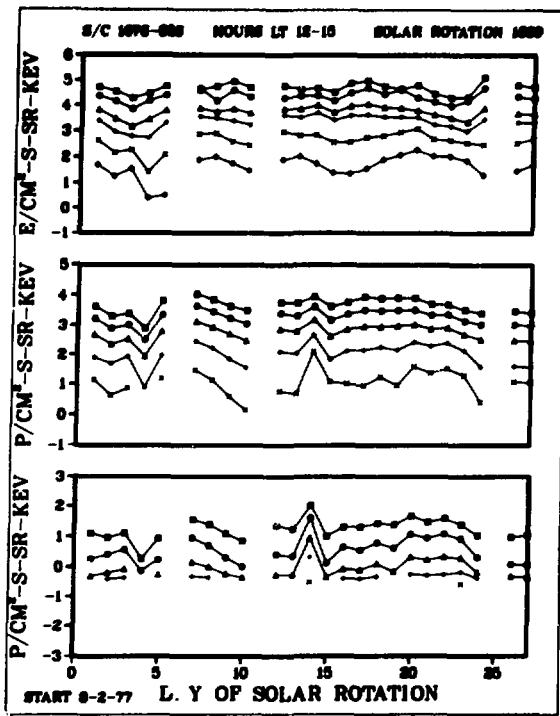
S/C 1976-059

START 8-2-77

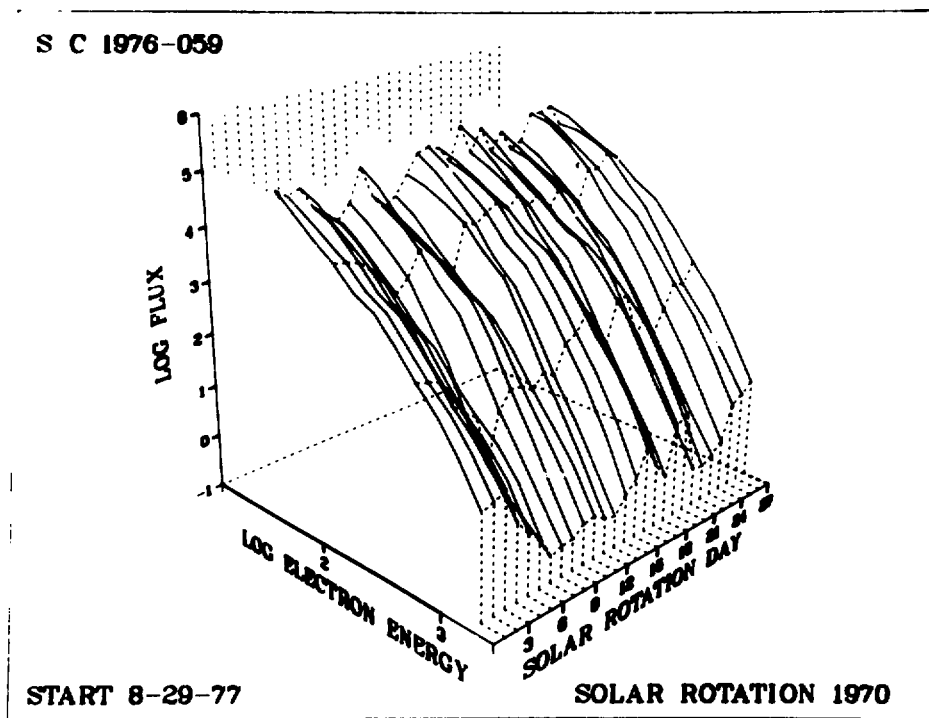
SOLAR ROTATION 1969



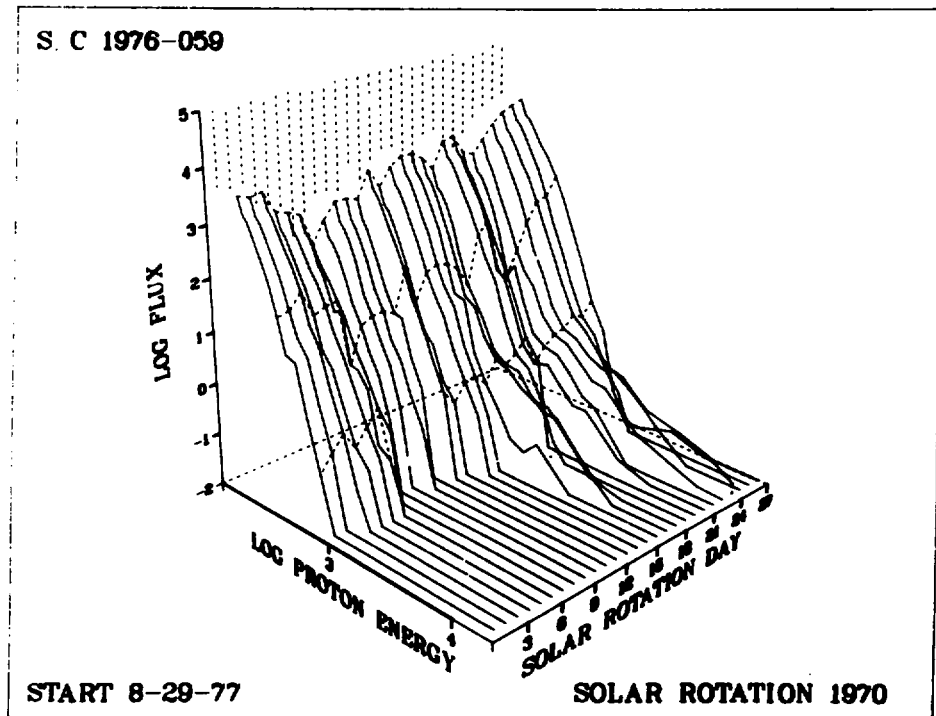


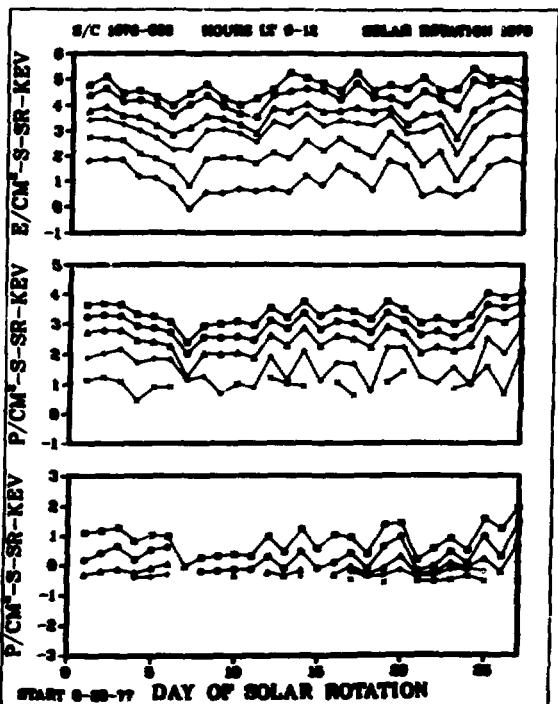
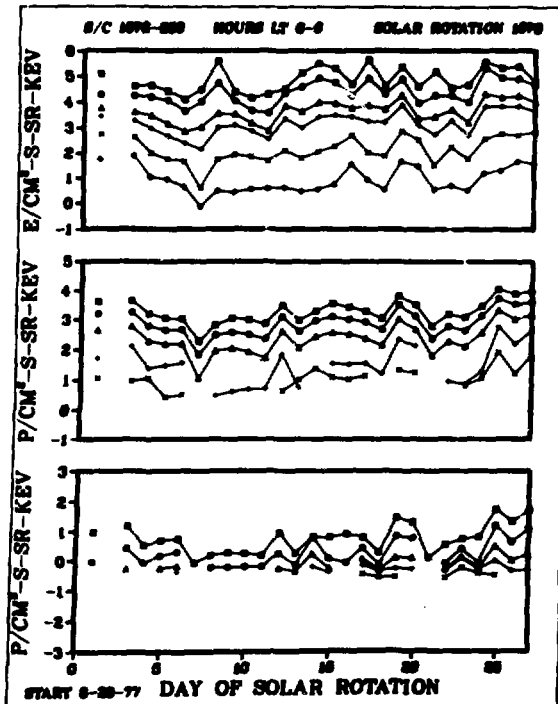
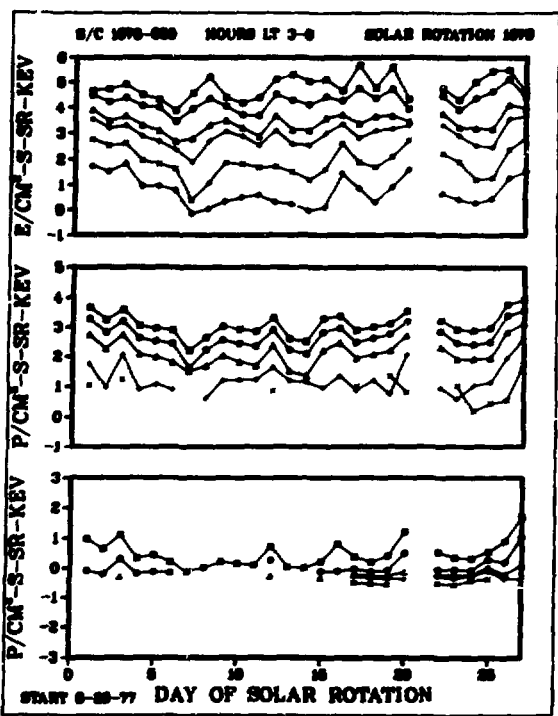
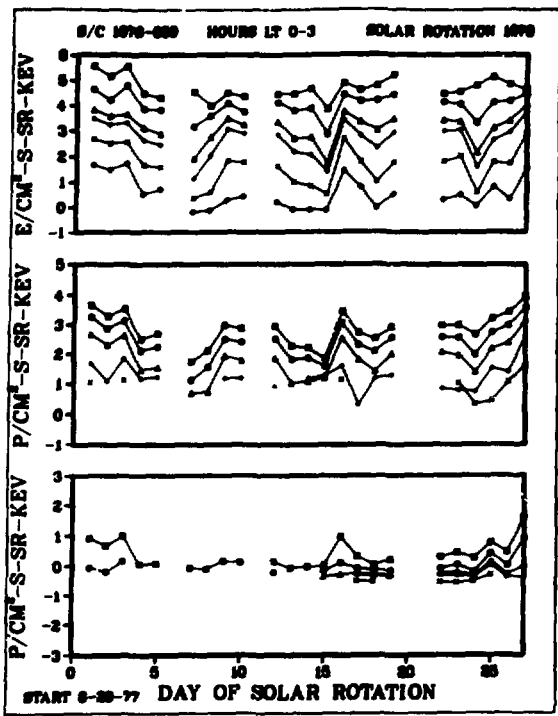


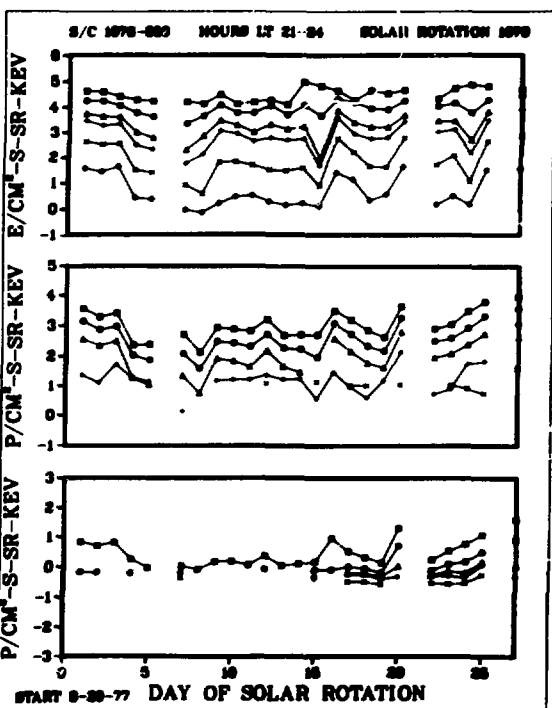
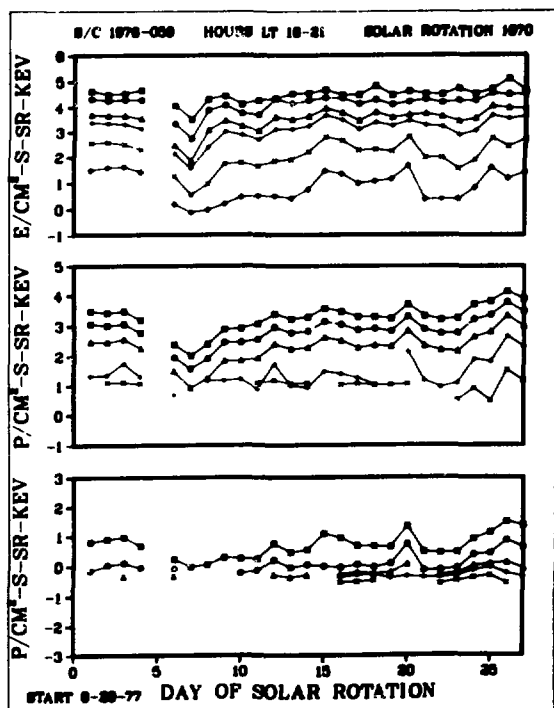
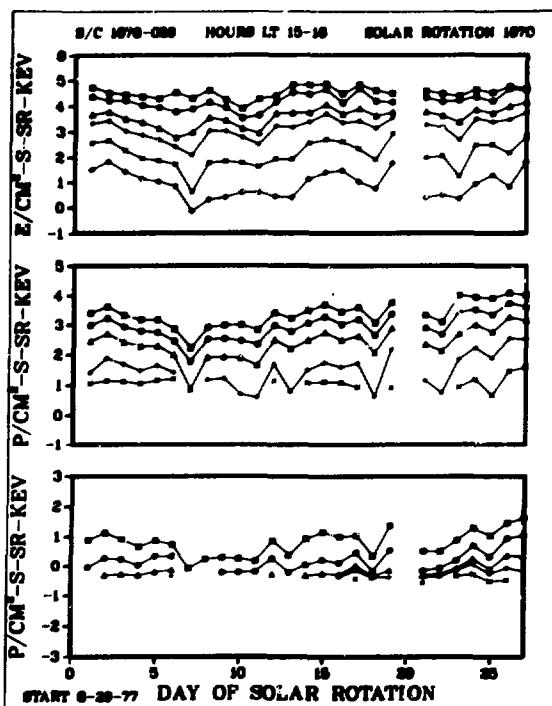
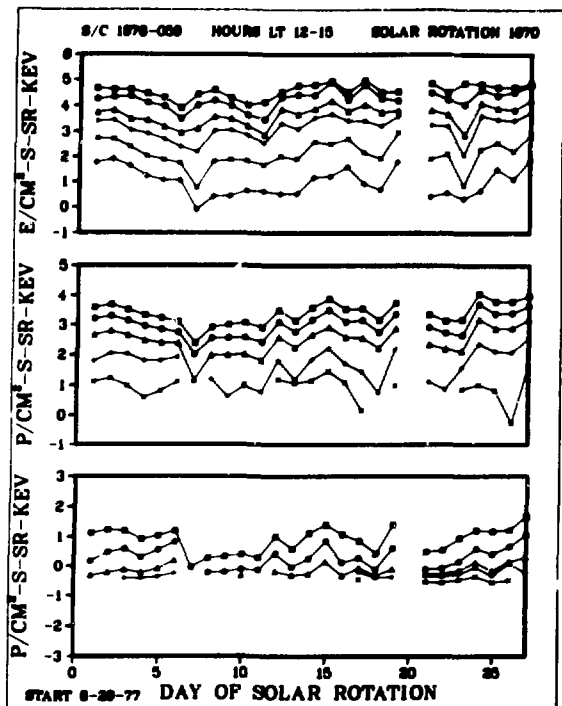
S C 1976-059



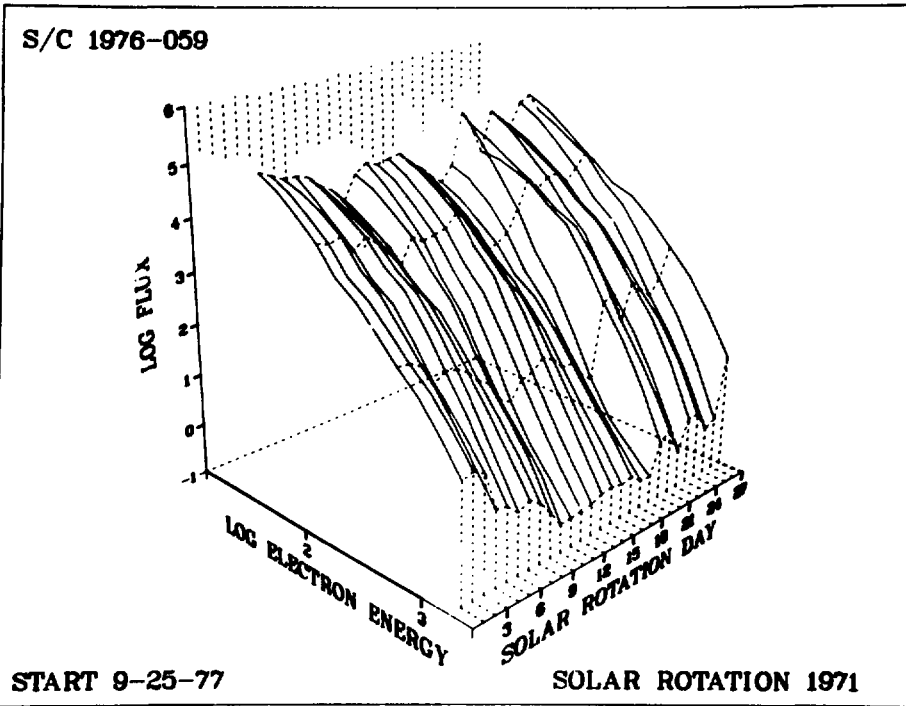
S. C 1976-059



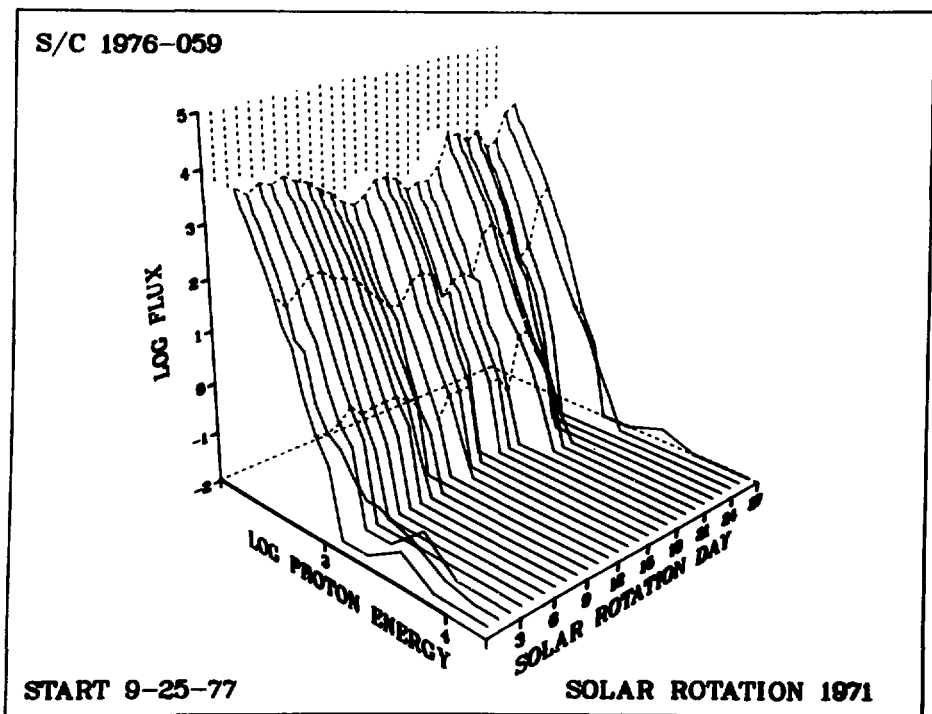


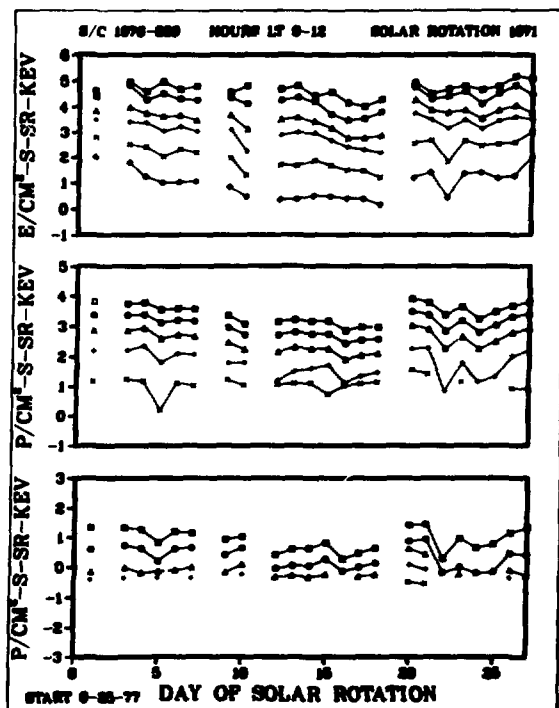
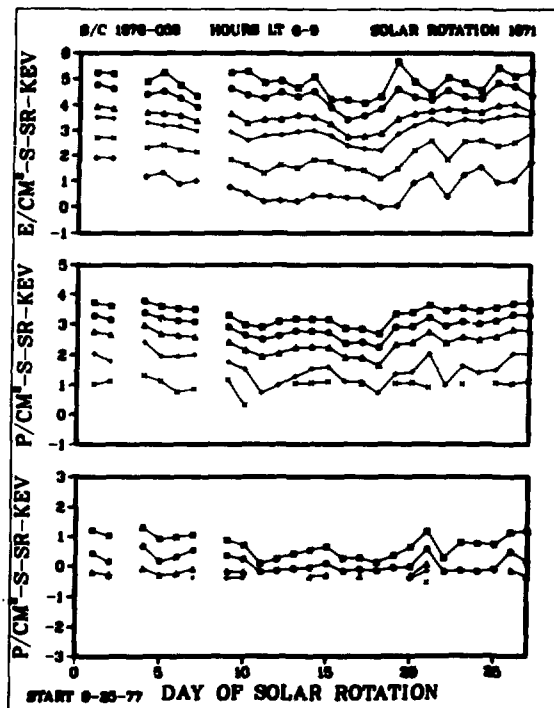
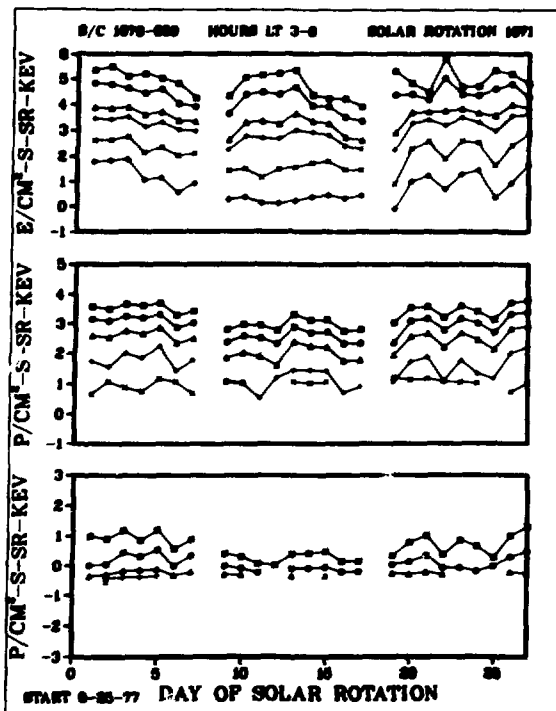
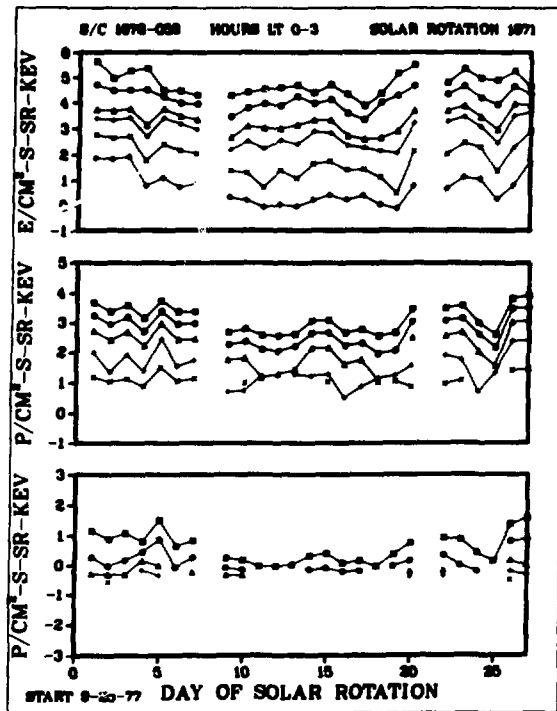


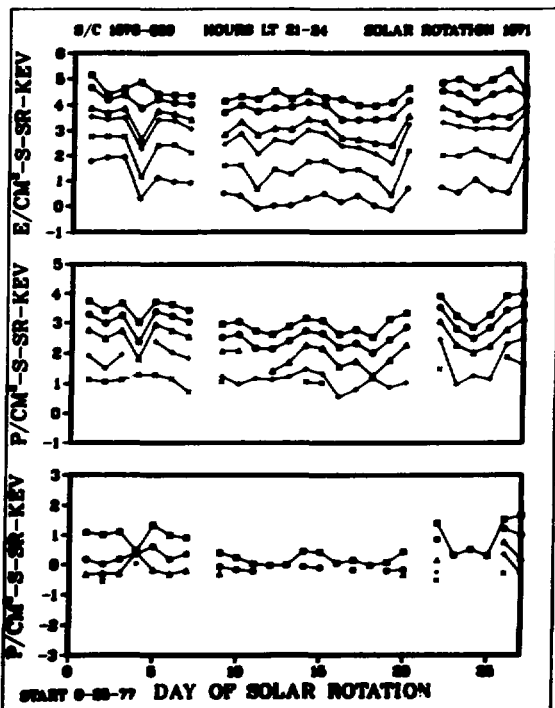
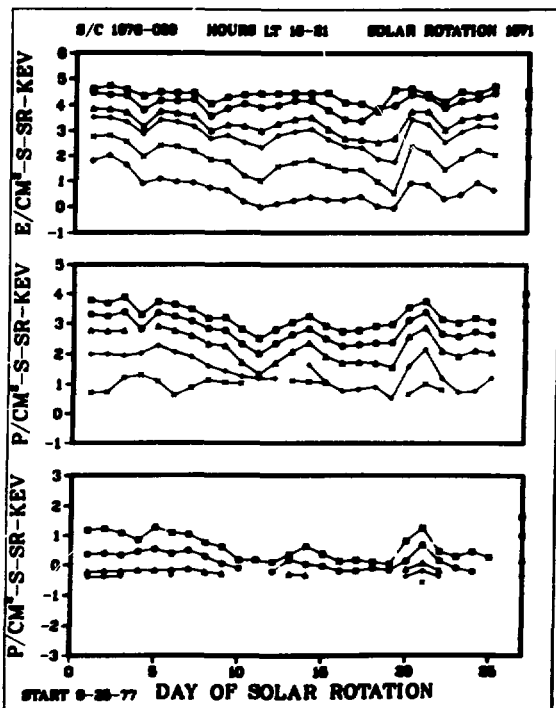
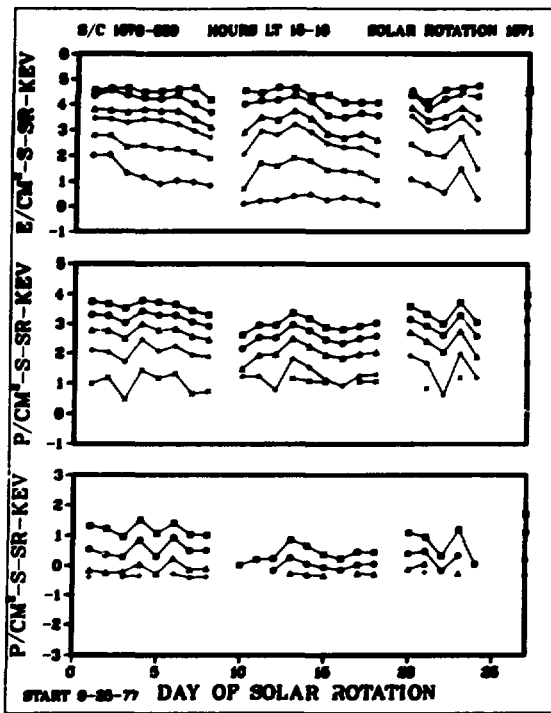
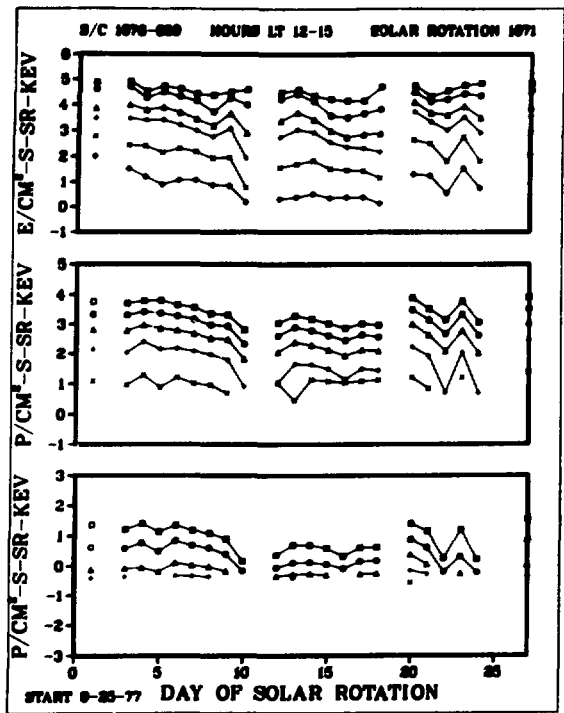
S/C 1976-059



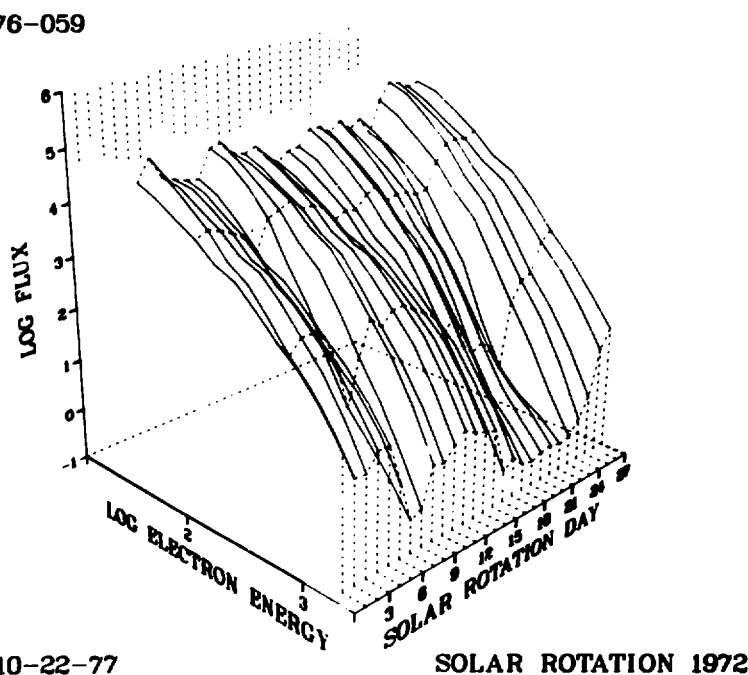
S/C 1976-059







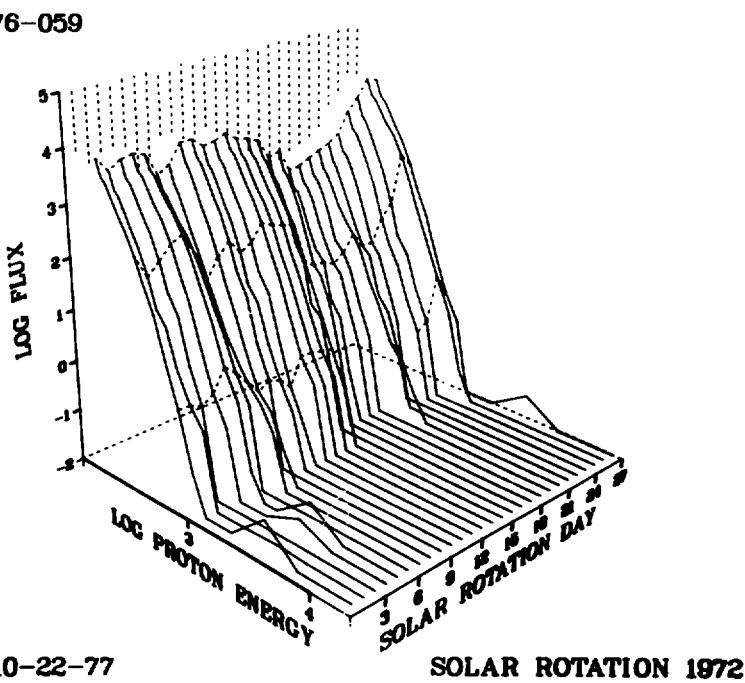
S/C 1976-059



START 10-22-77

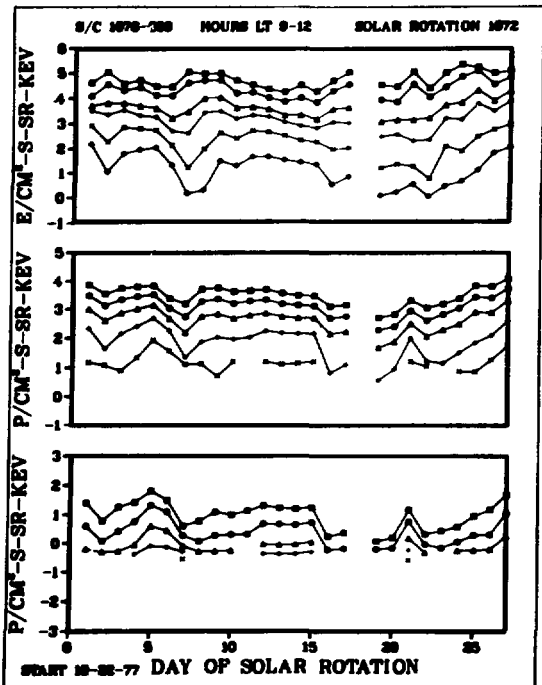
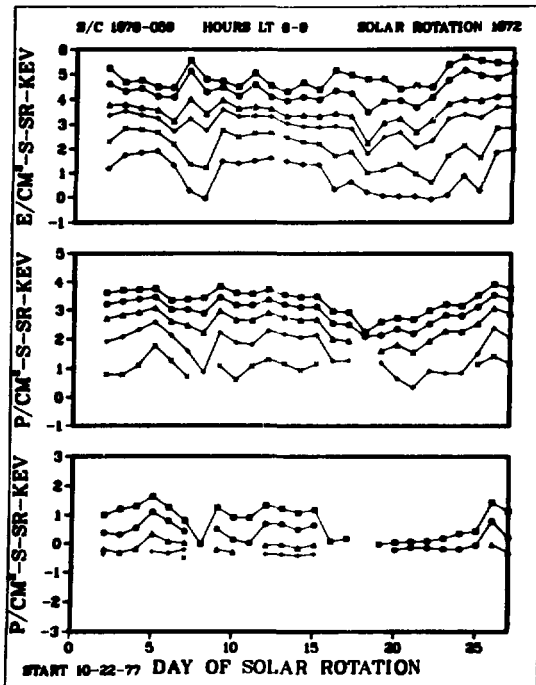
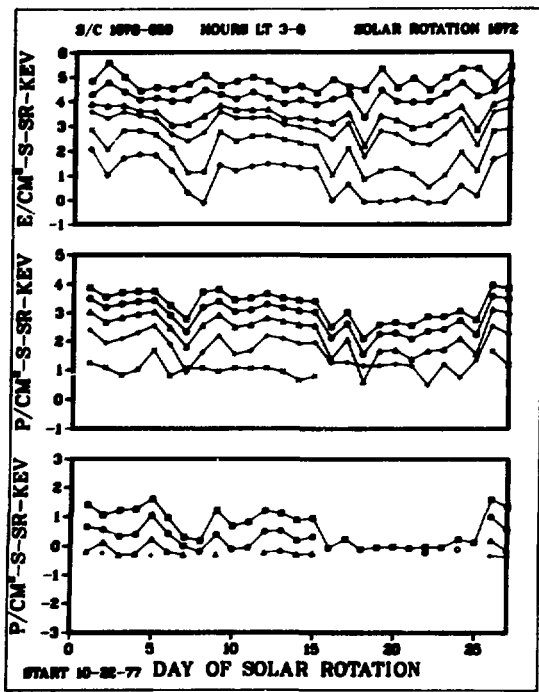
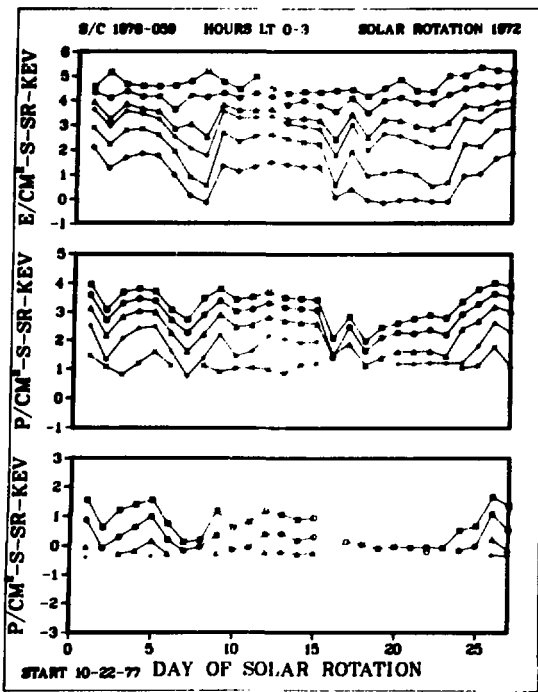
SOLAR ROTATION 1972

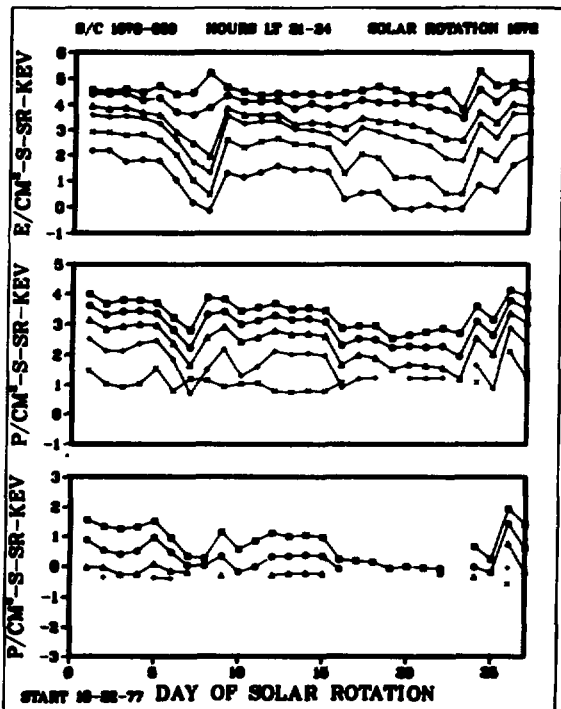
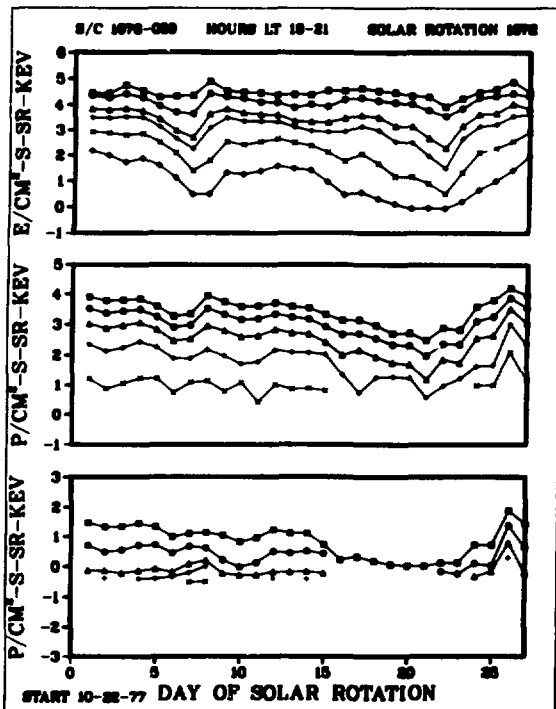
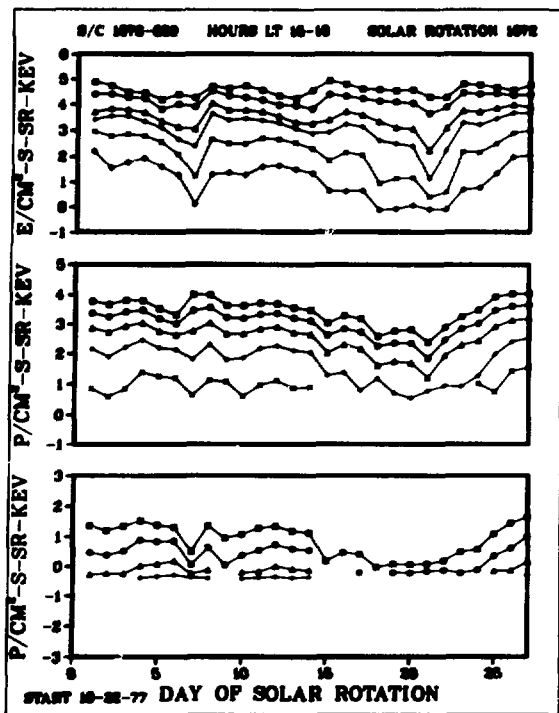
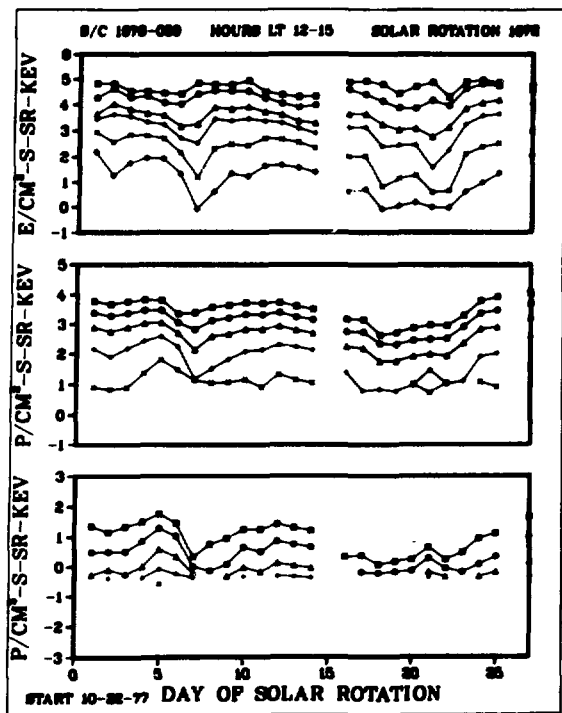
S/C 1976-059



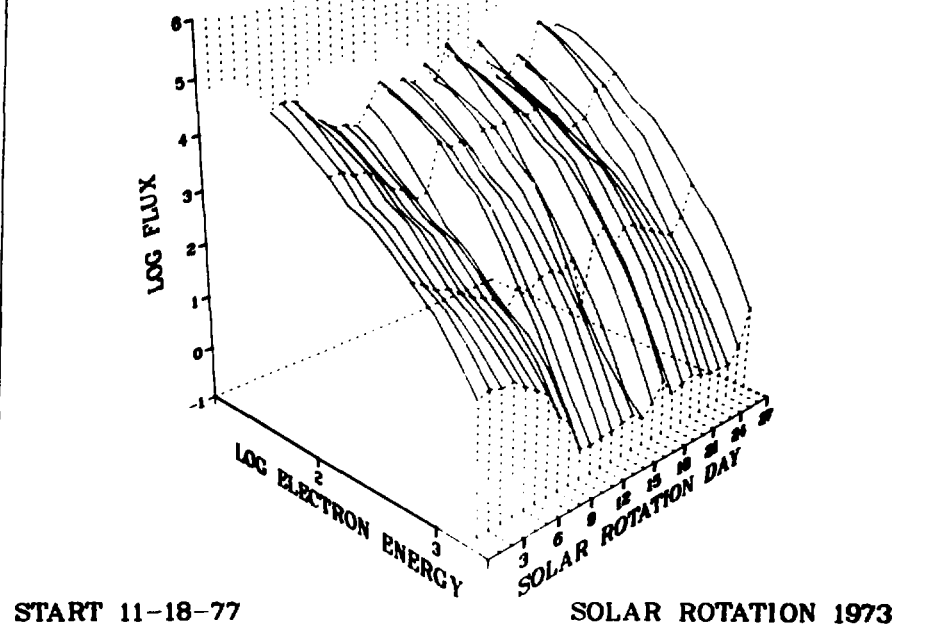
START 10-22-77

SOLAR ROTATION 1972

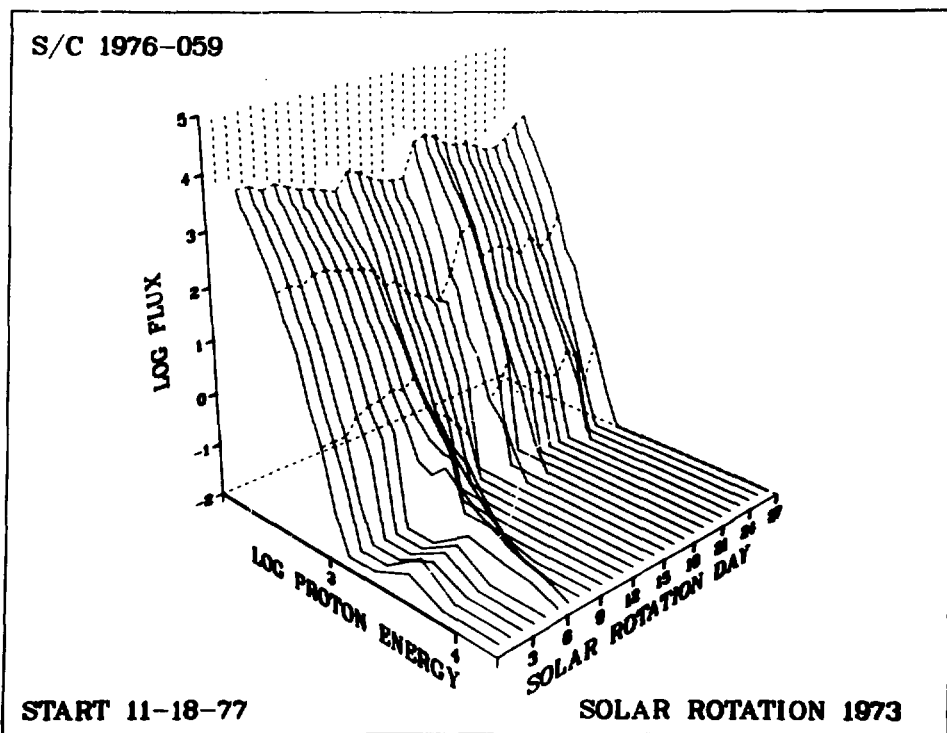


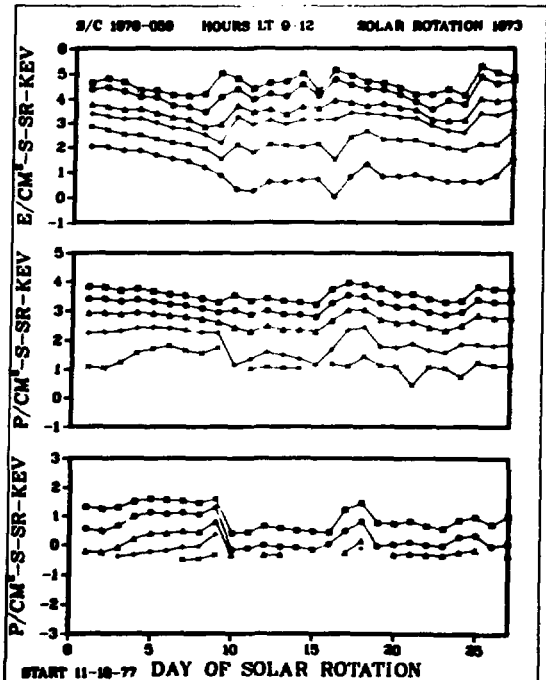
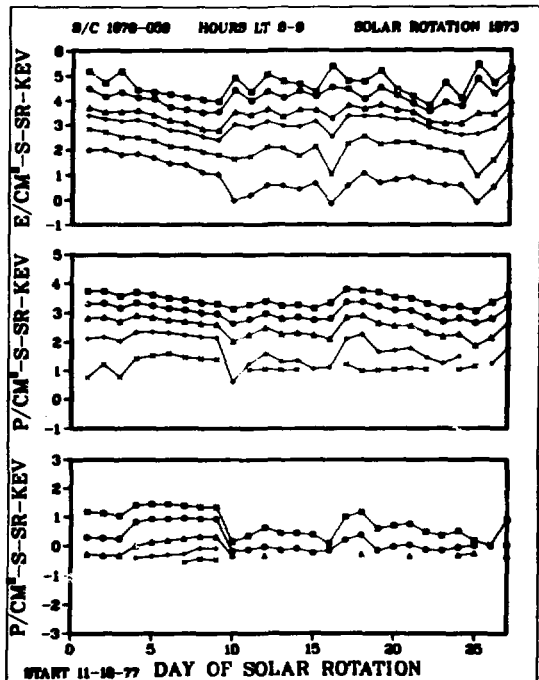
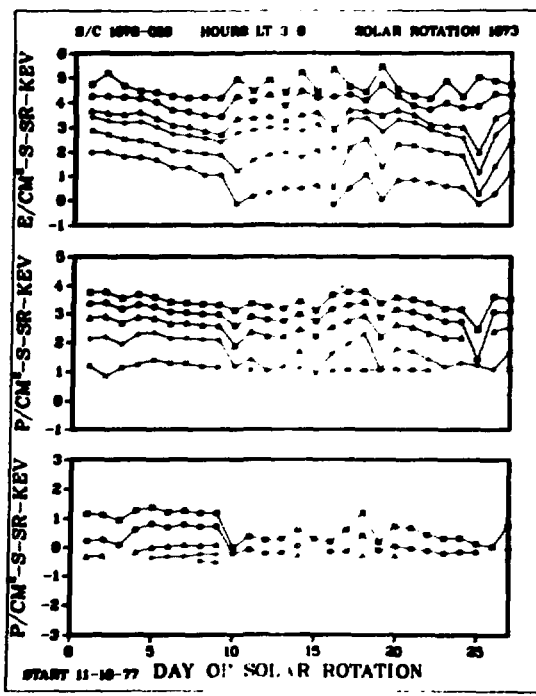
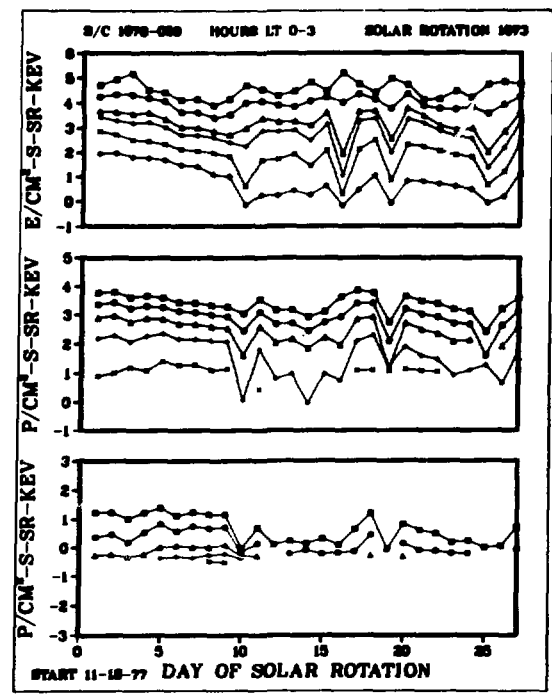


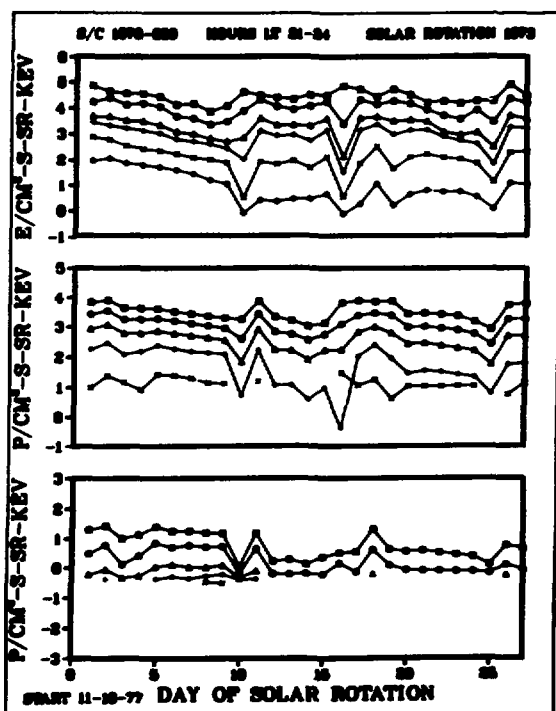
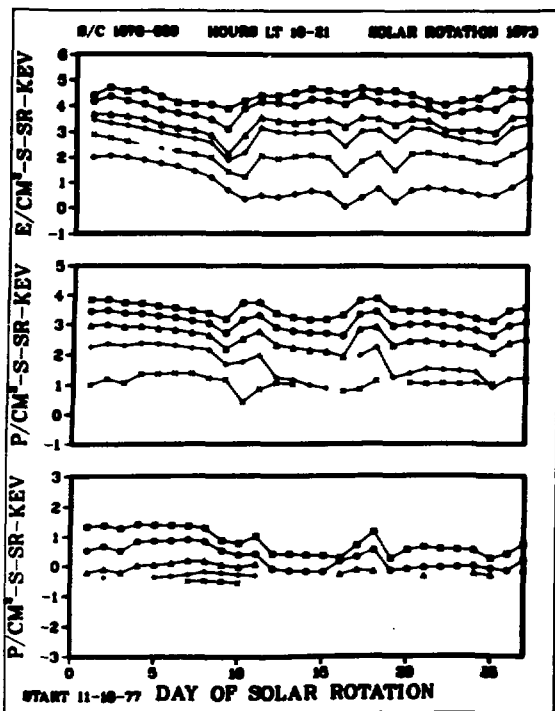
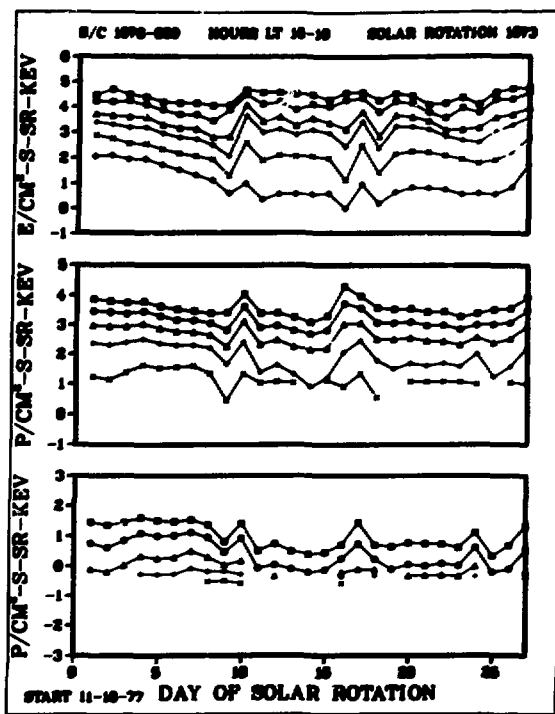
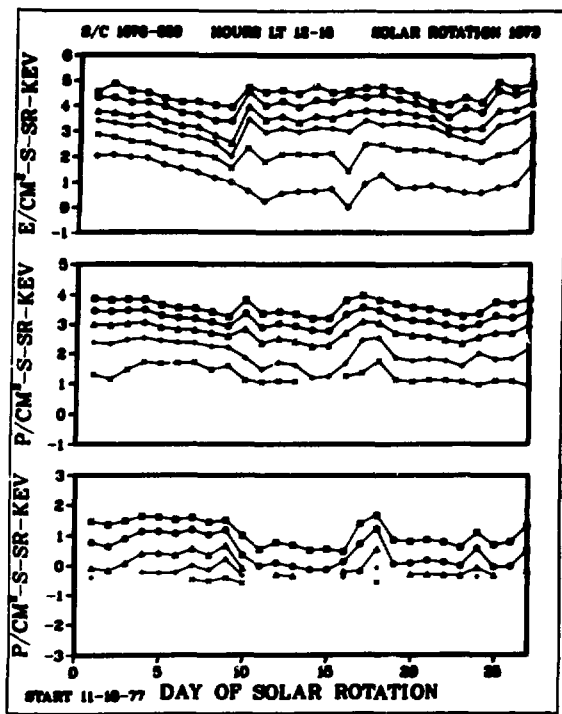
S/C 1976-059



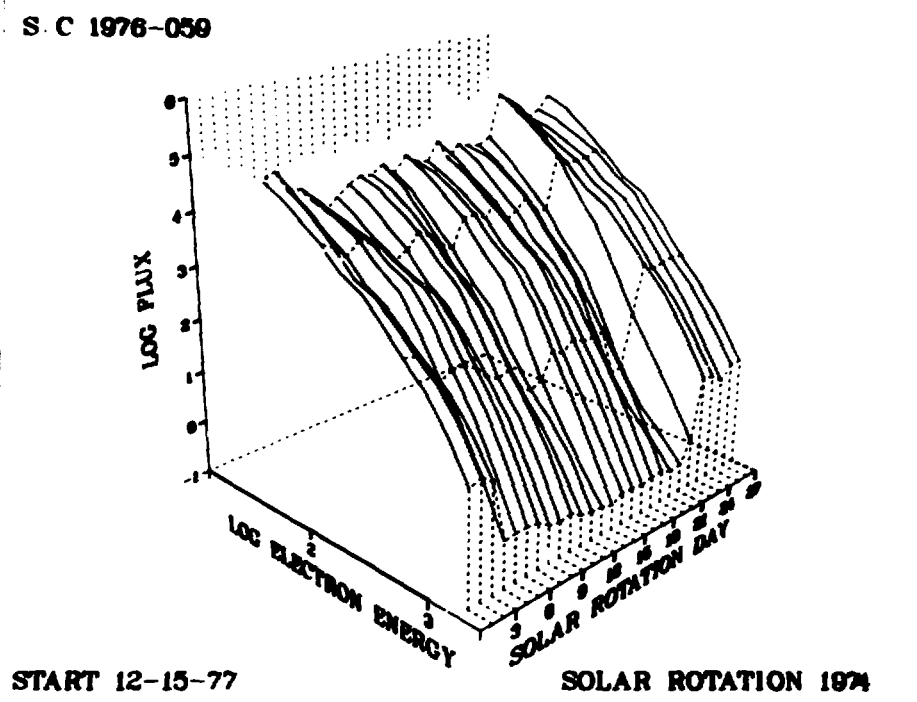
S/C 1976-059



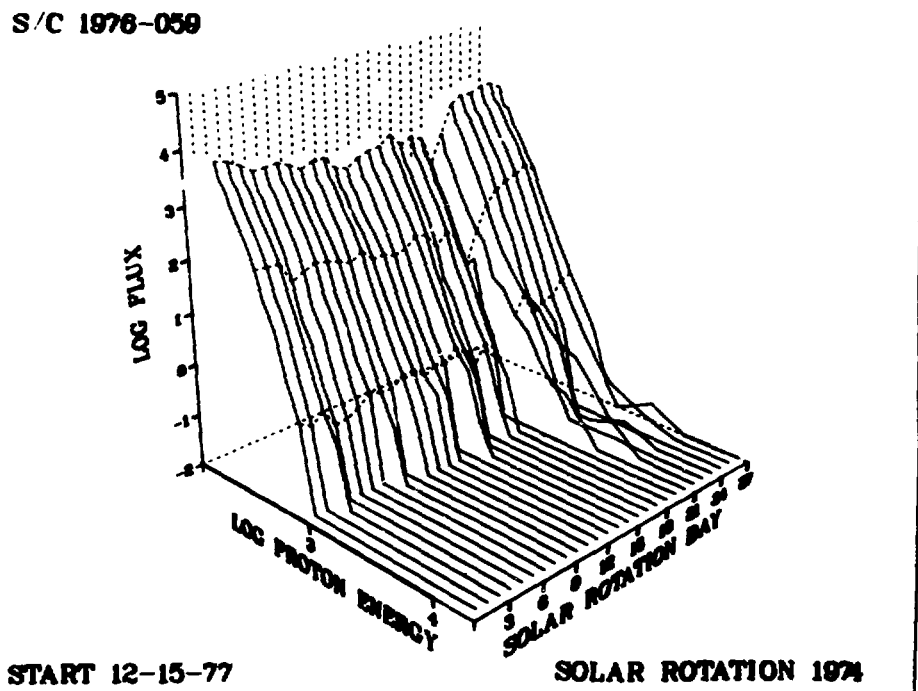


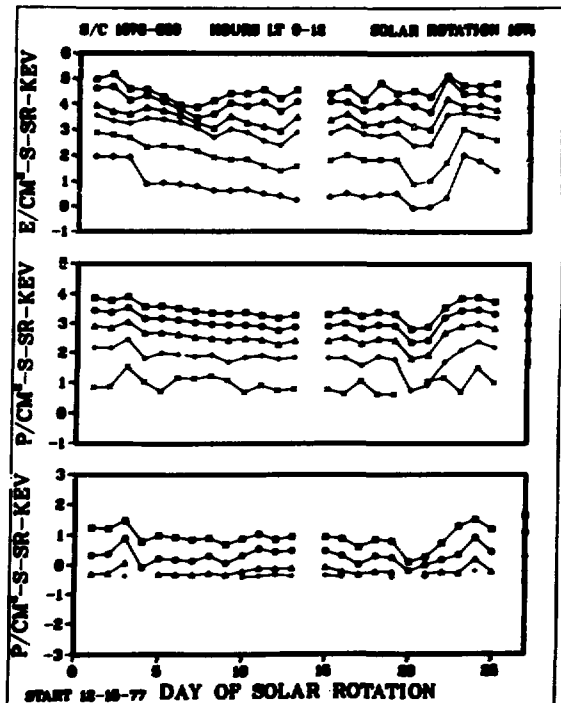
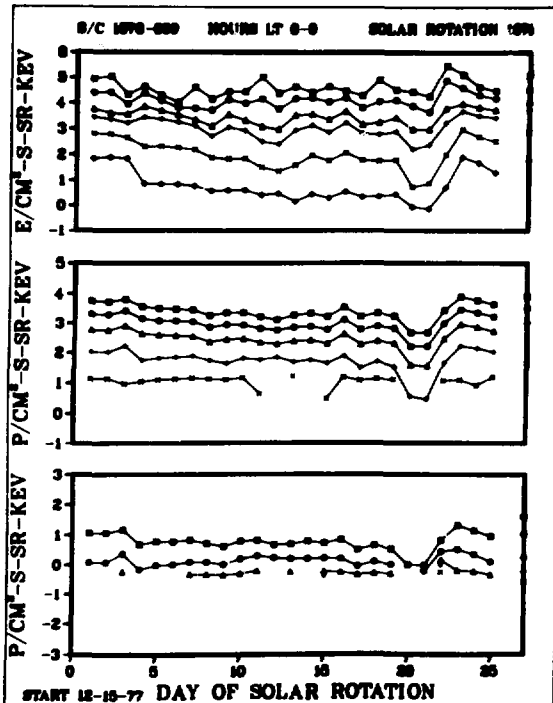
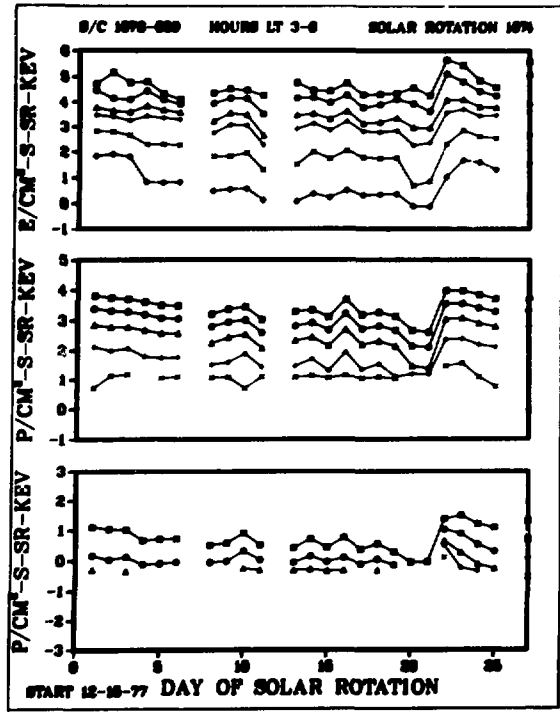
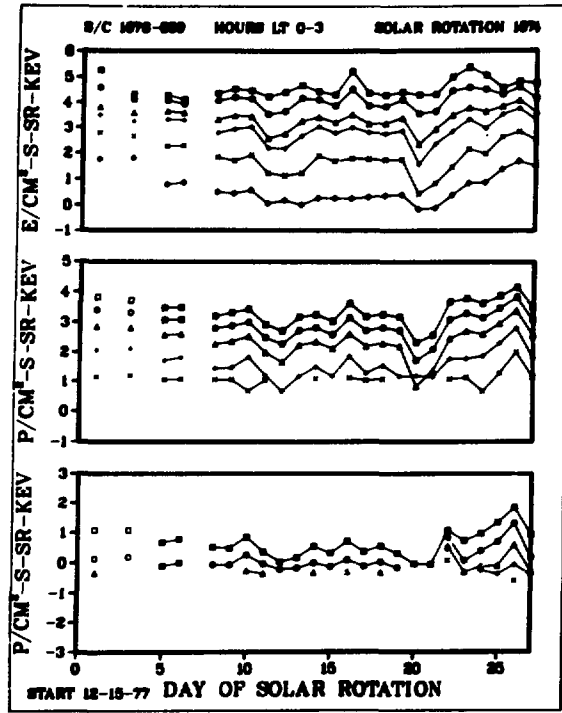


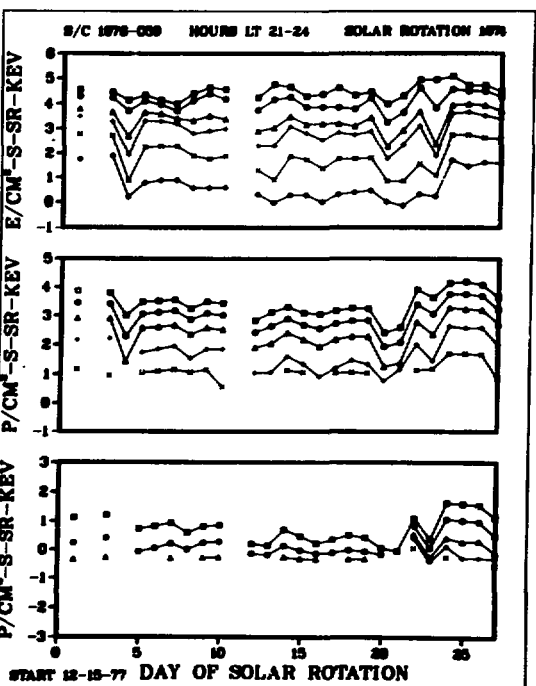
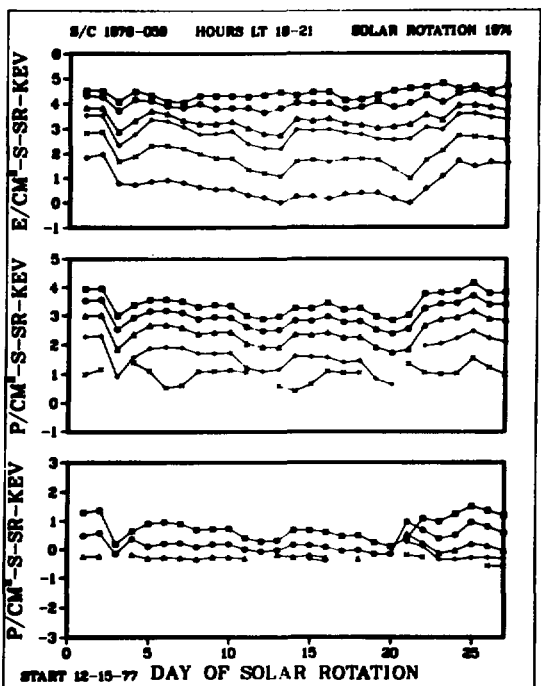
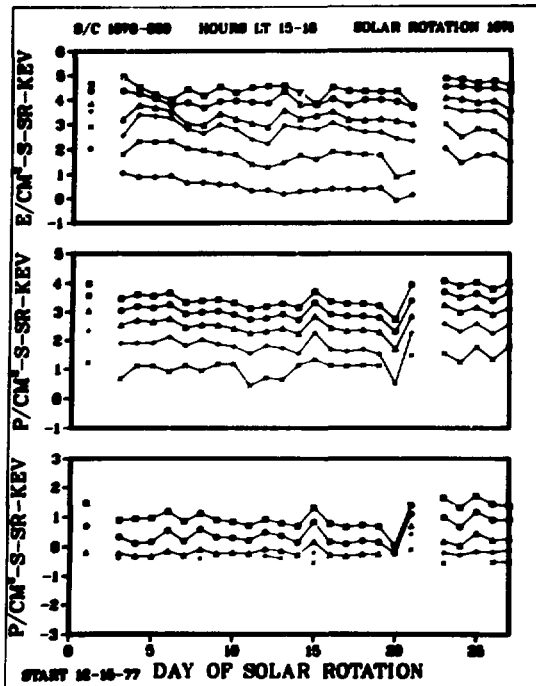
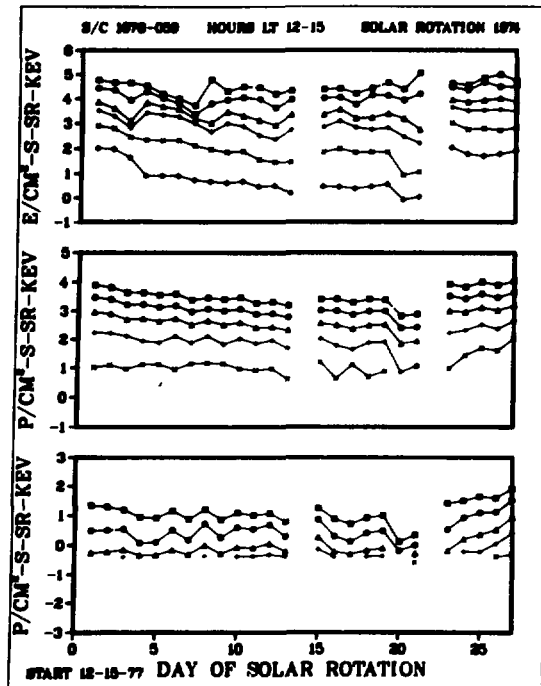
S/C 1976-059

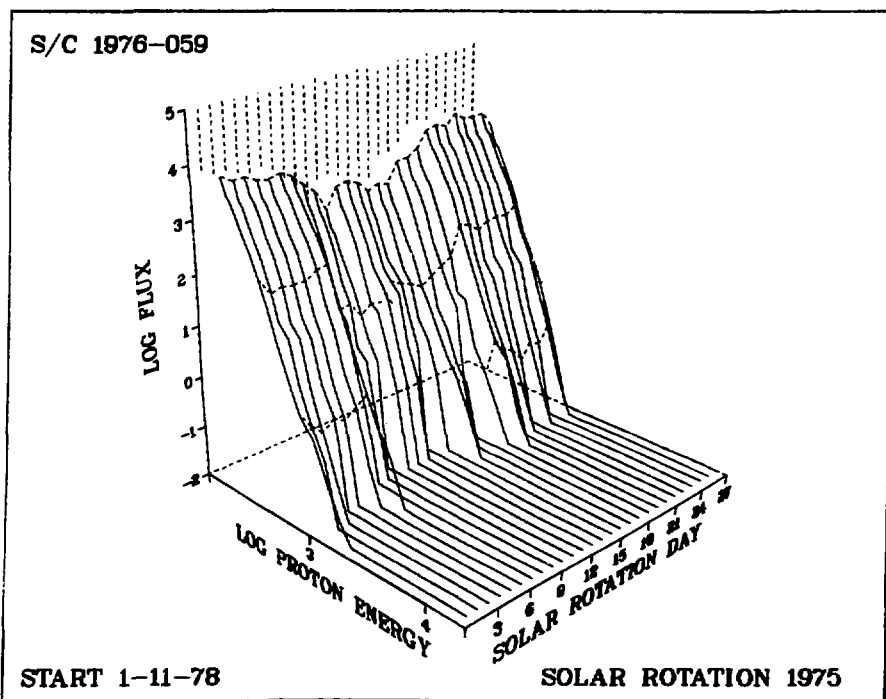
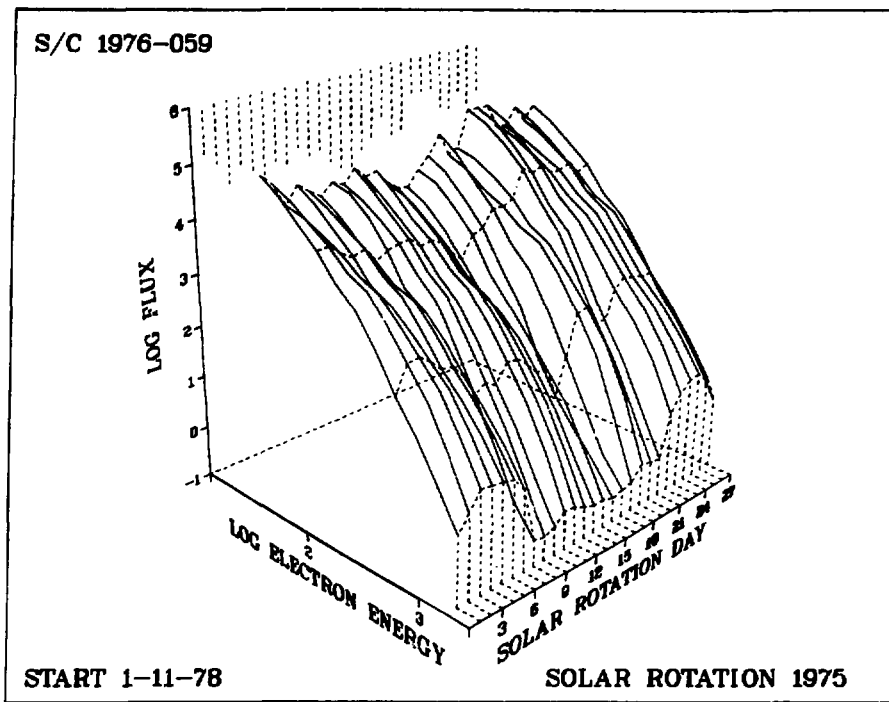


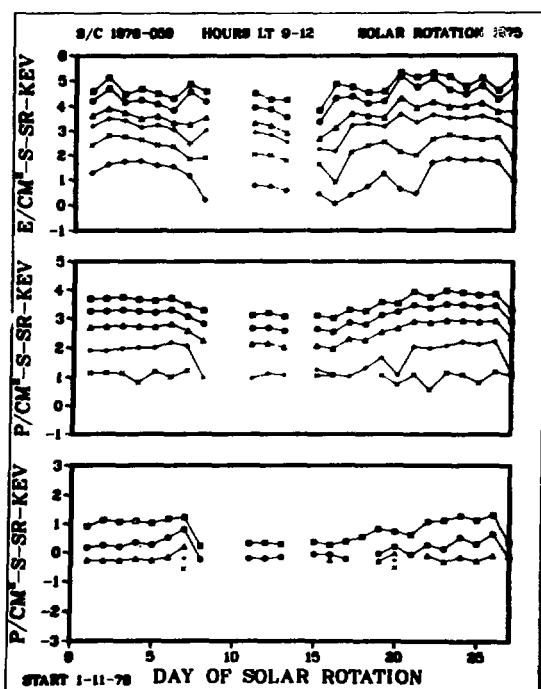
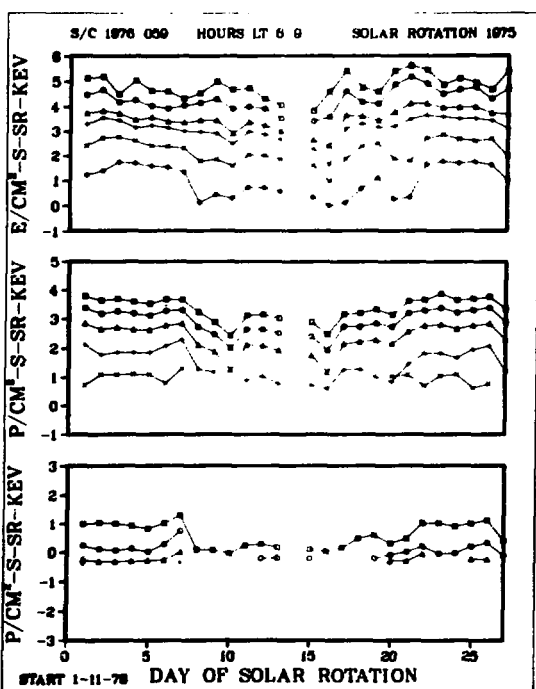
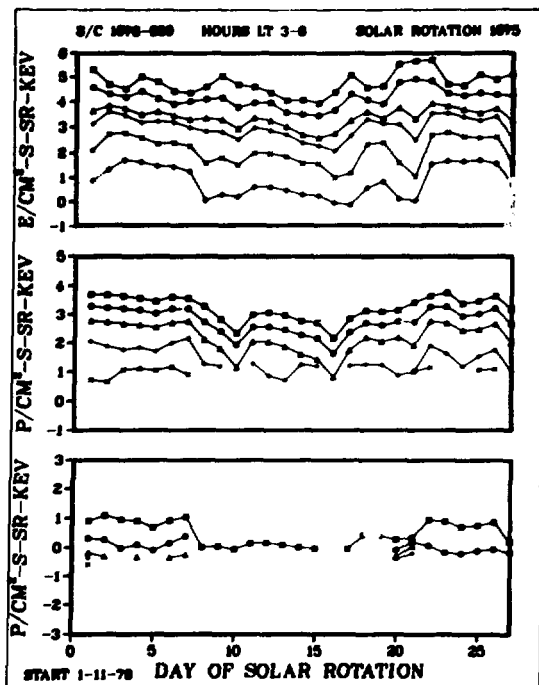
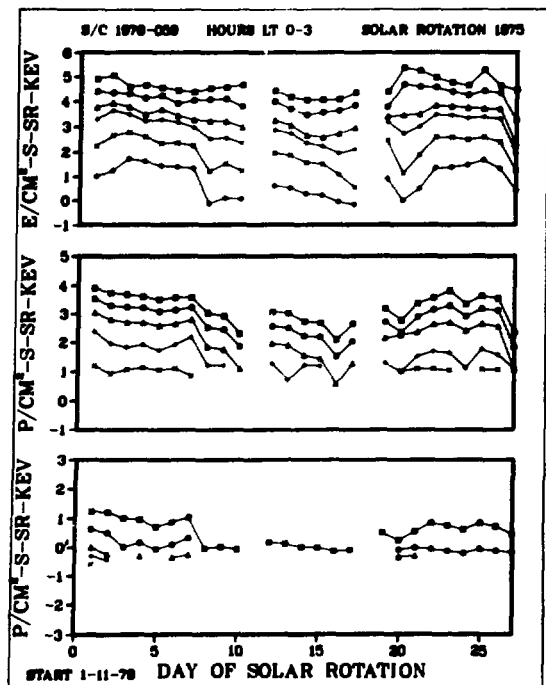
S/C 1976-059

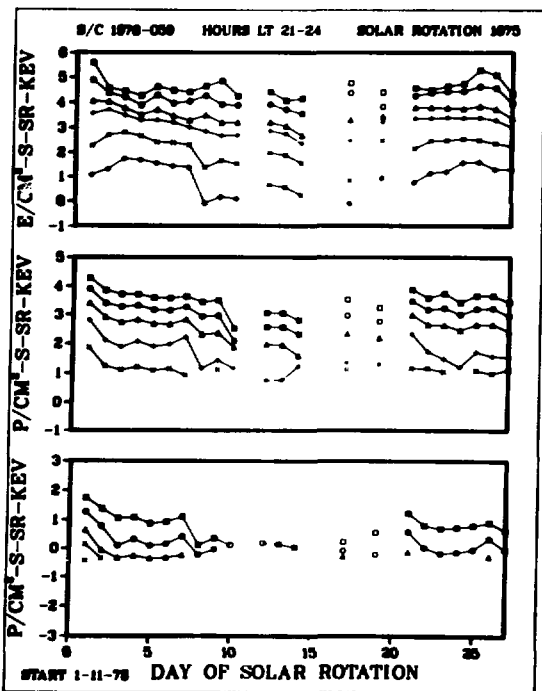
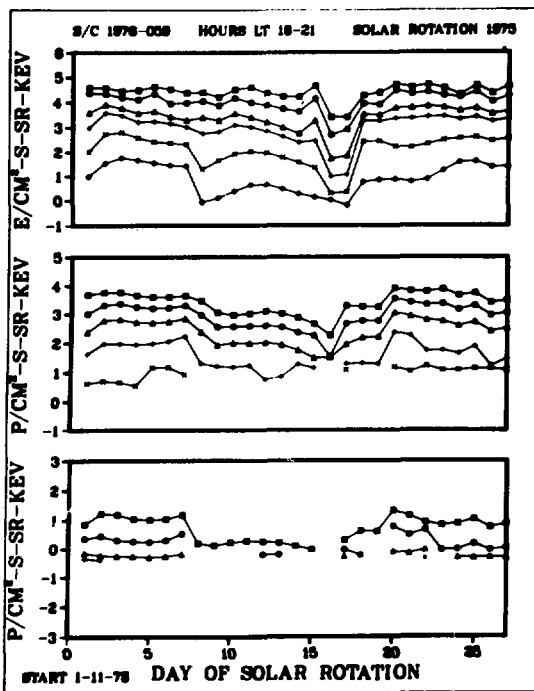
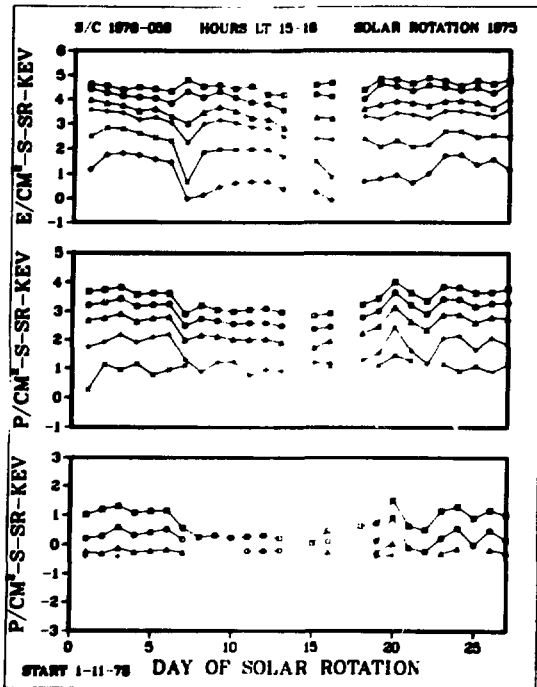
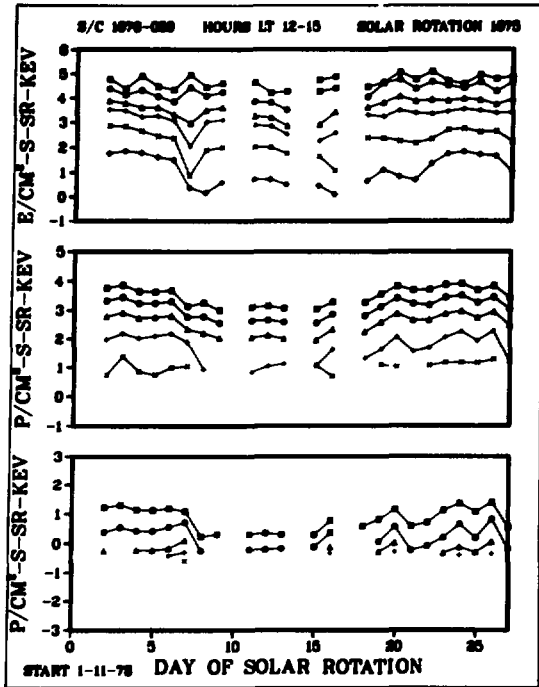


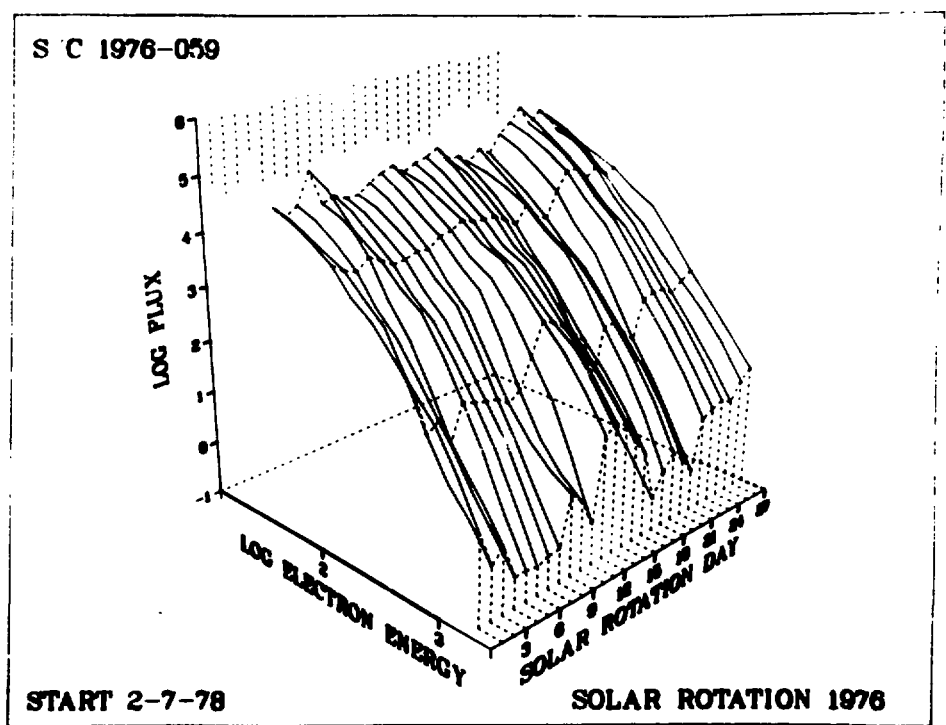
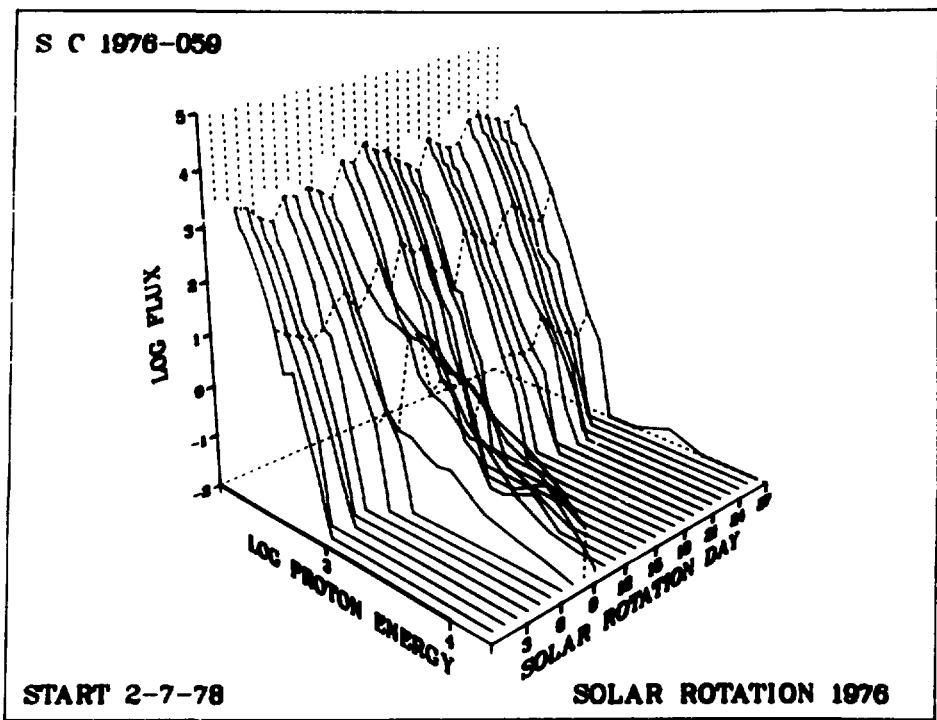


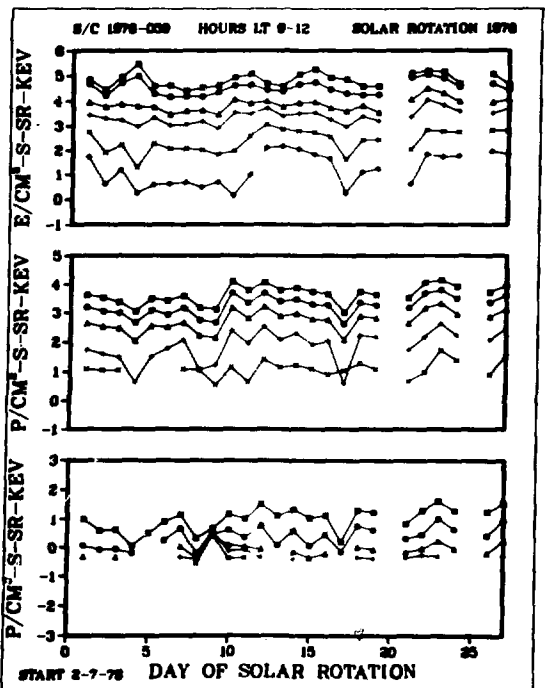
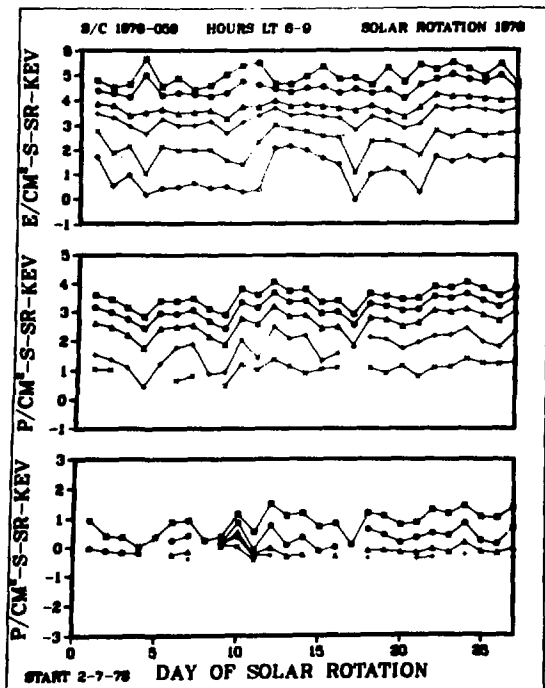
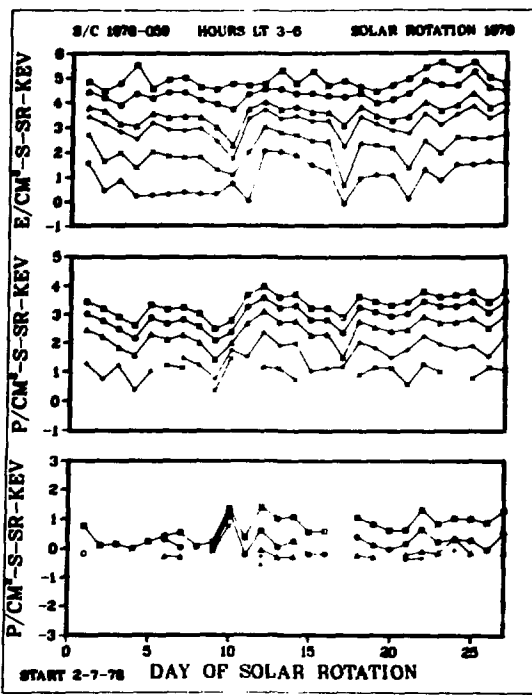
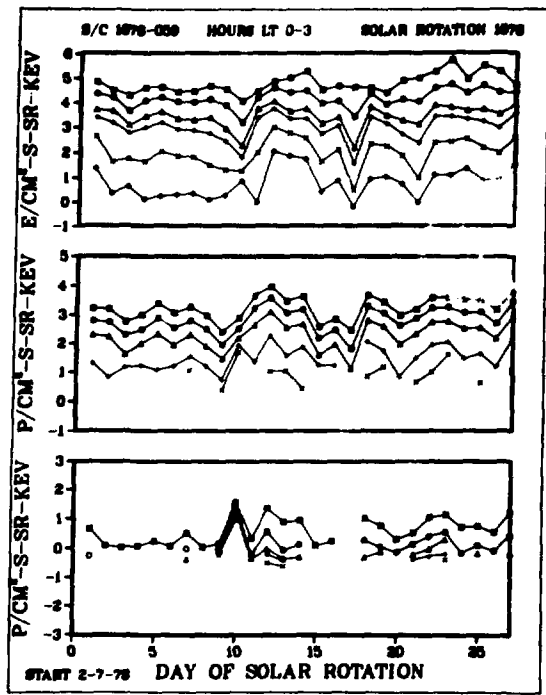


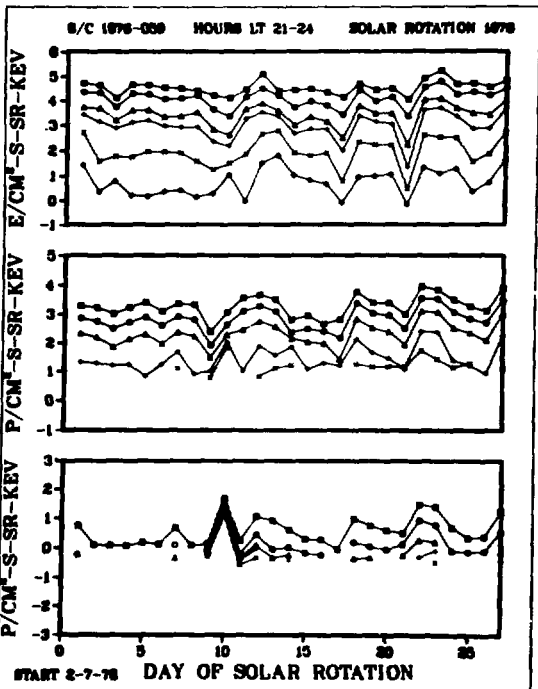
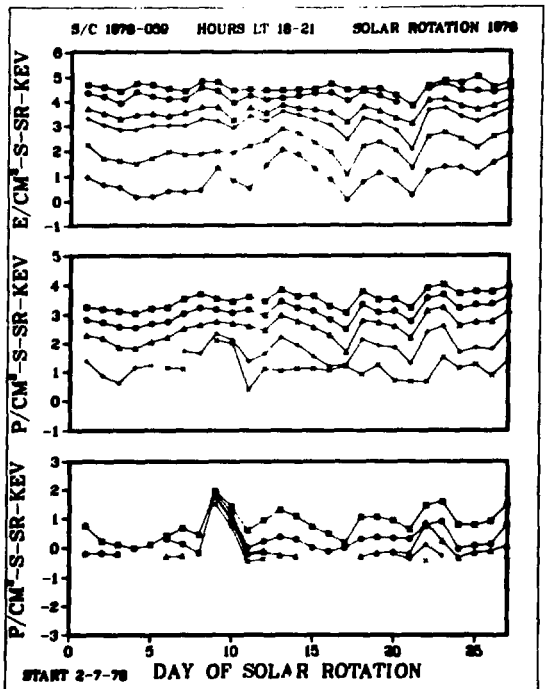
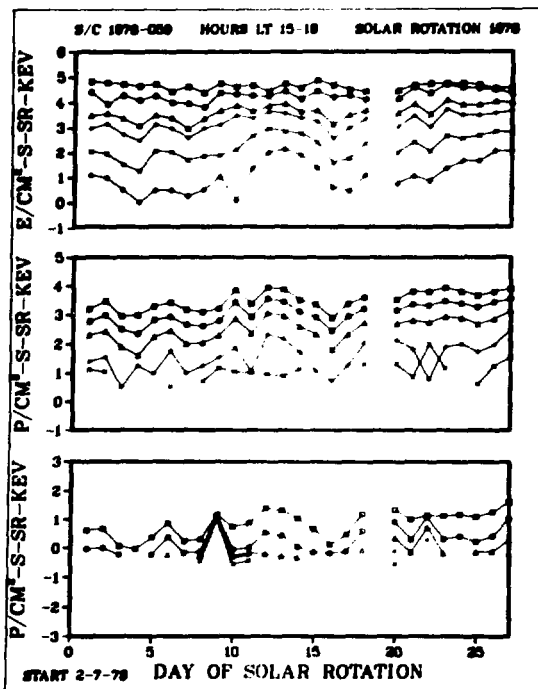
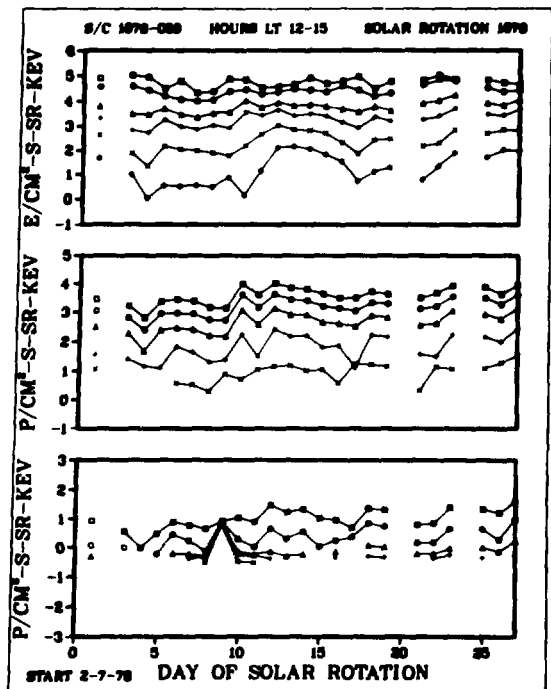




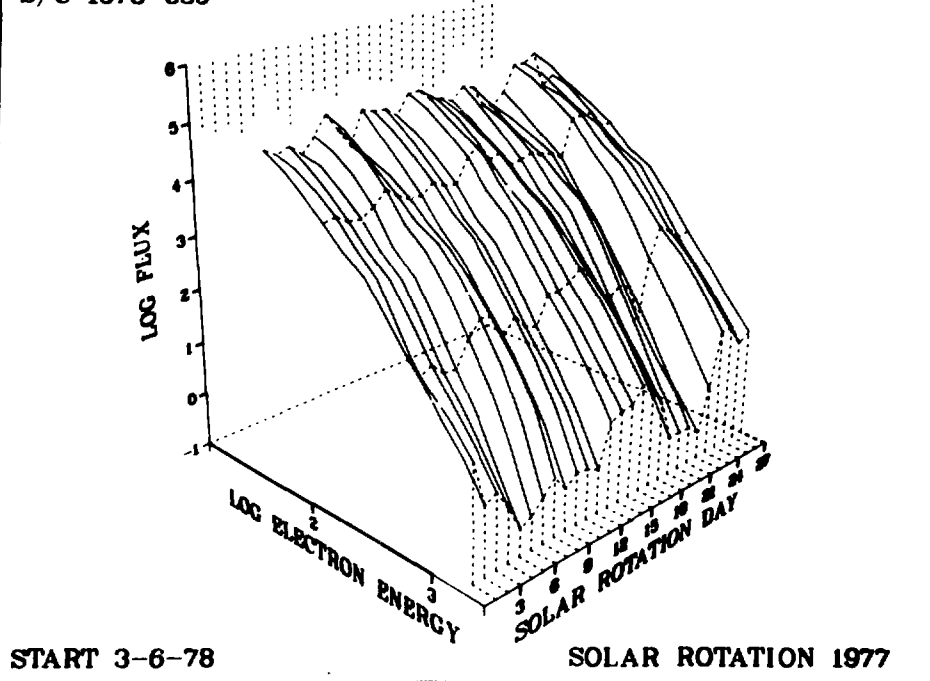




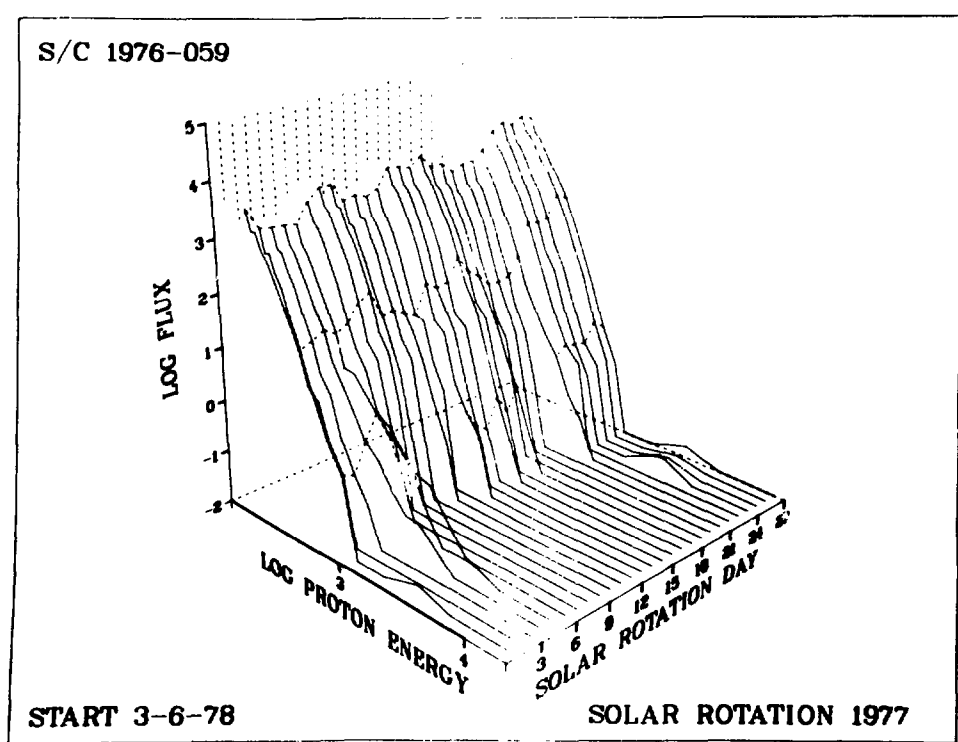


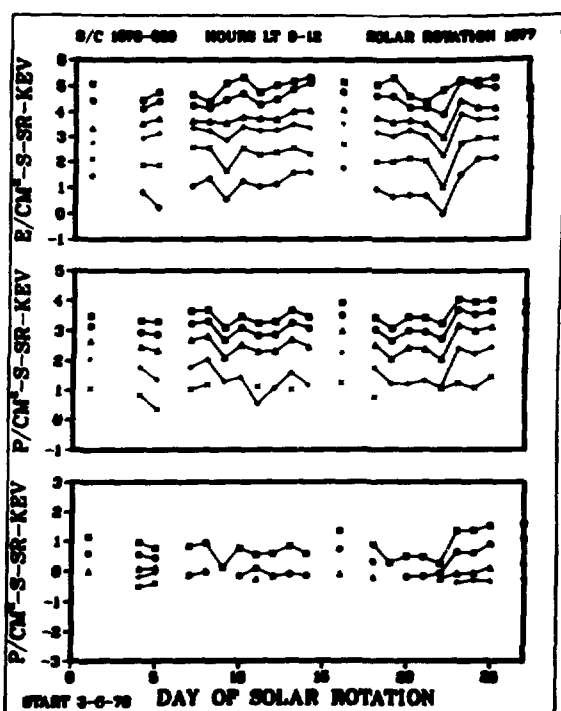
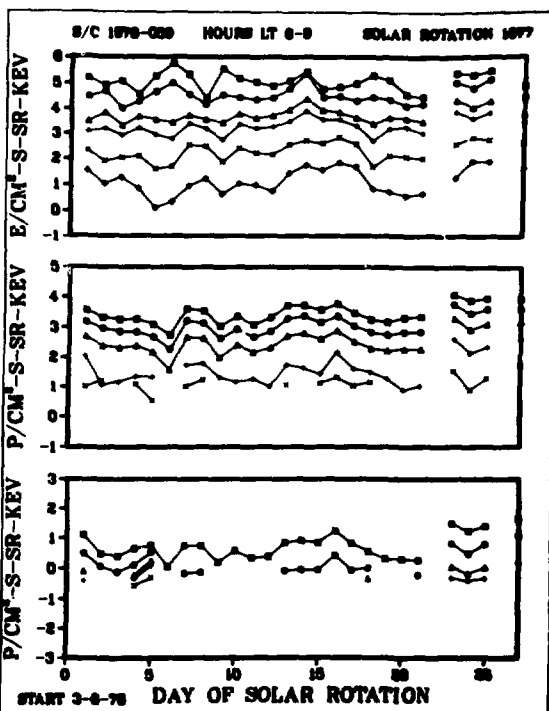
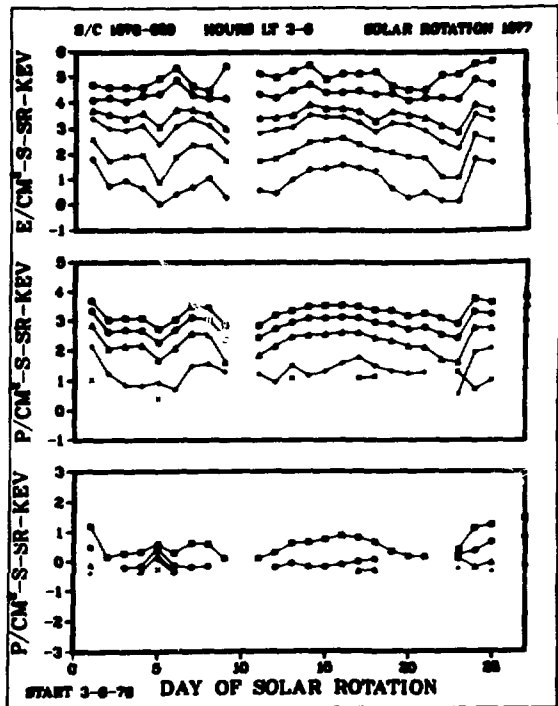
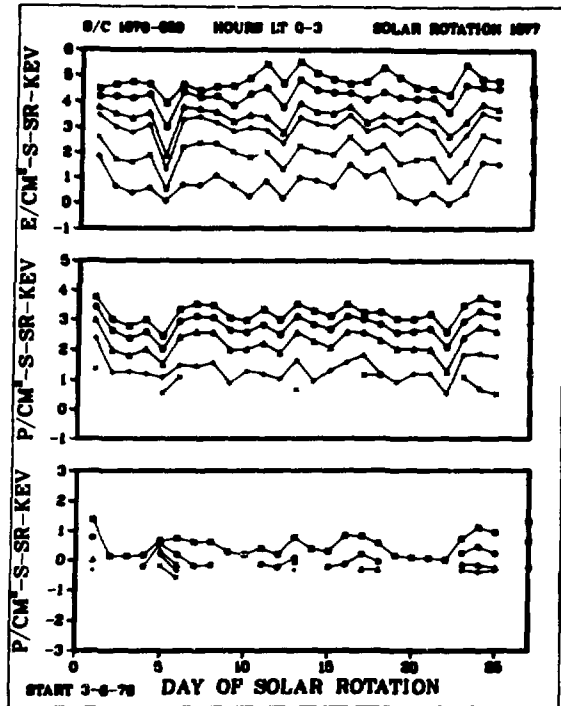


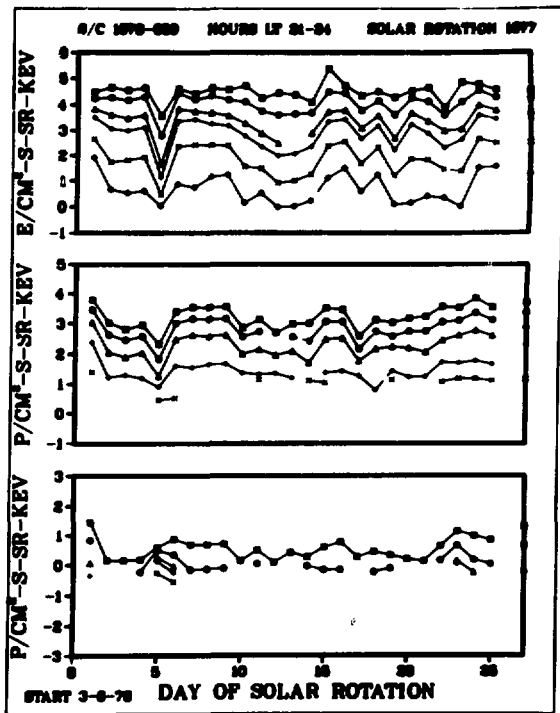
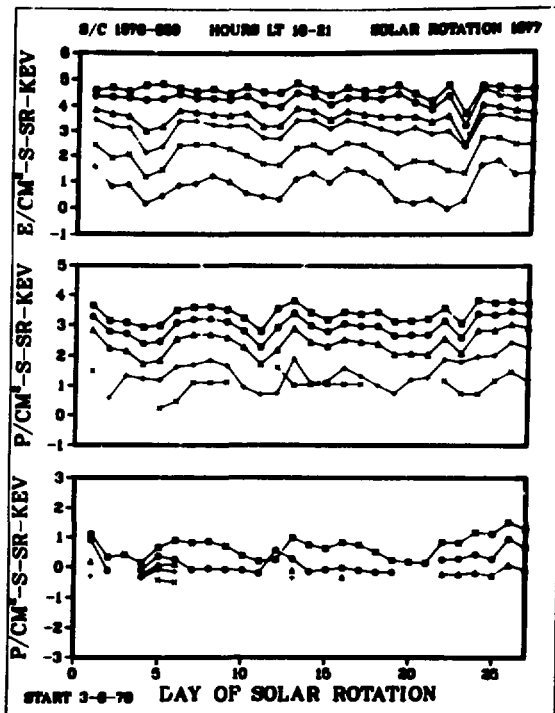
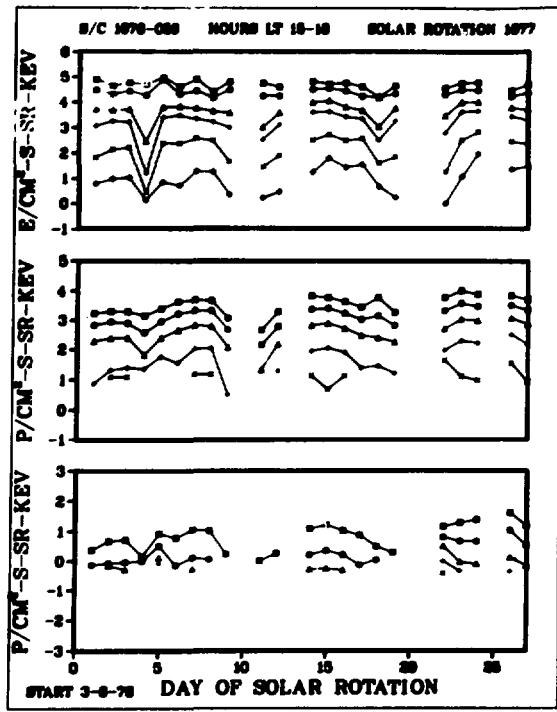
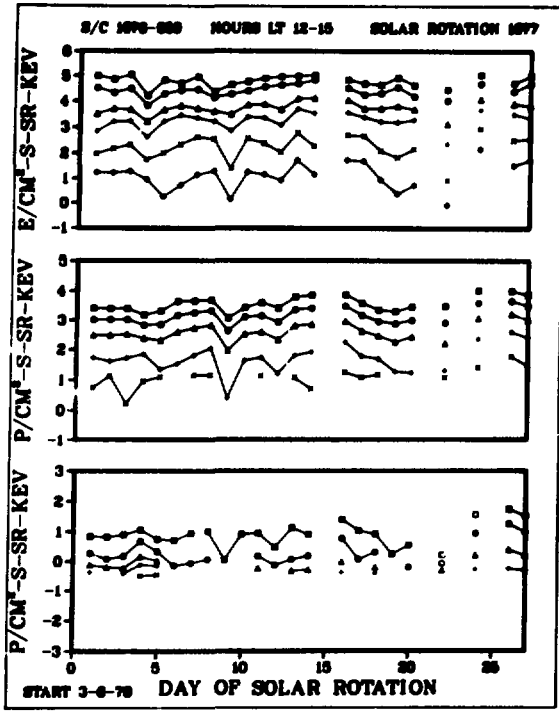
S/C 1976-059



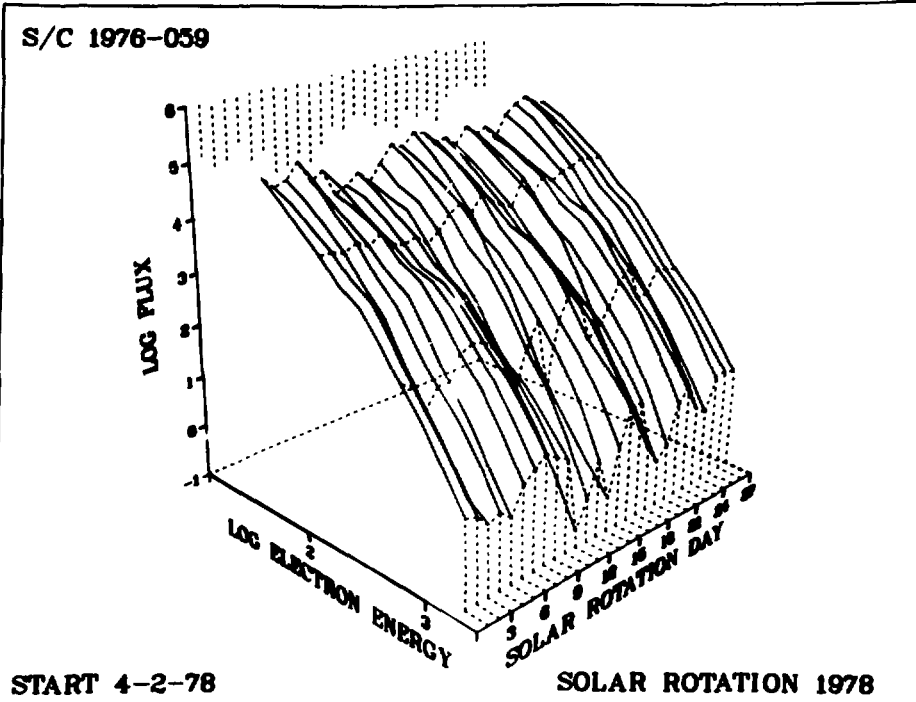
S/C 1976-059



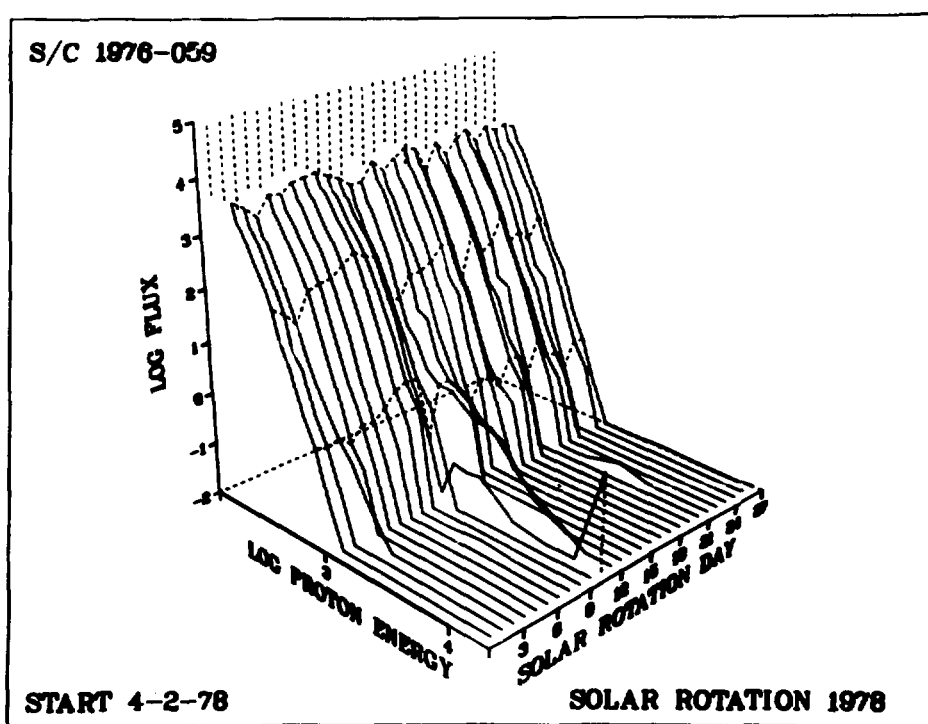


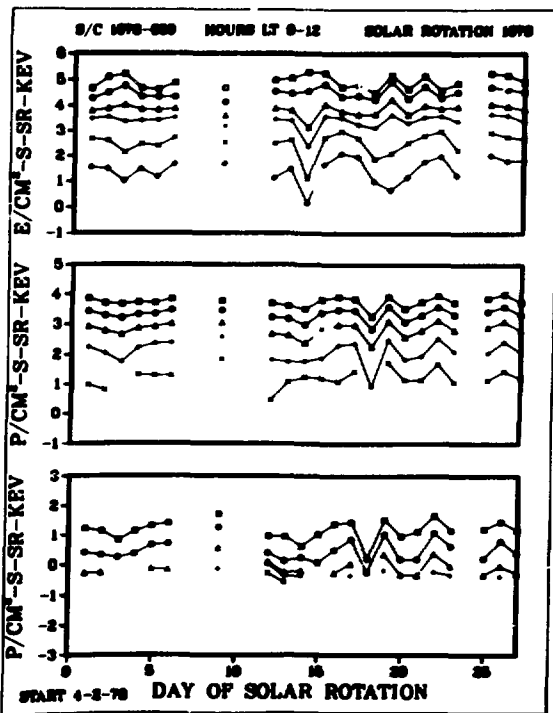
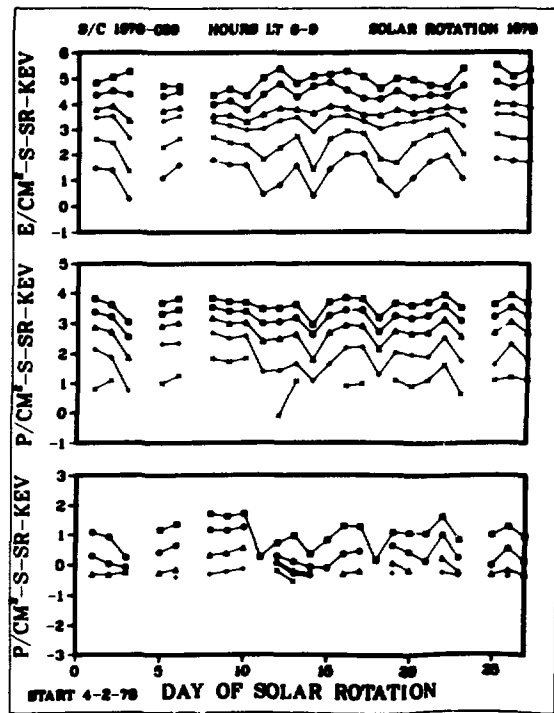
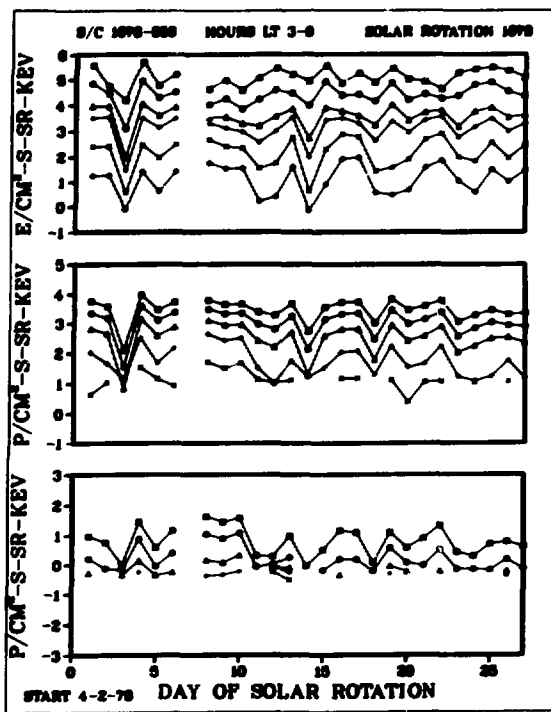
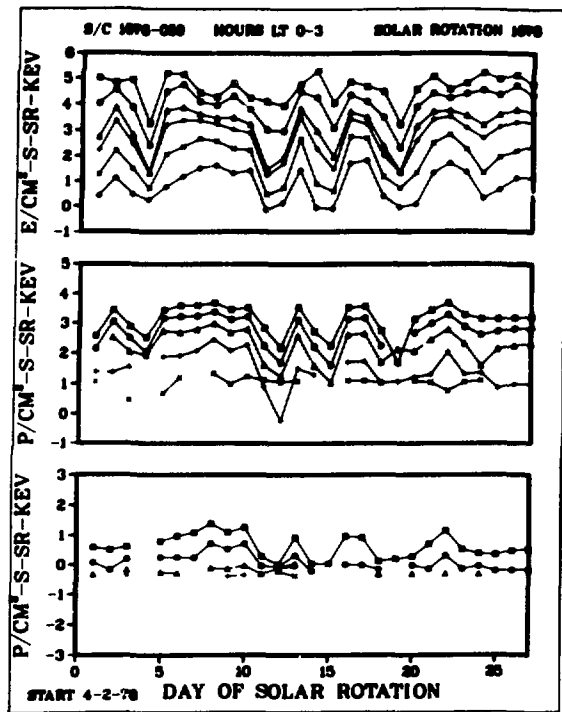


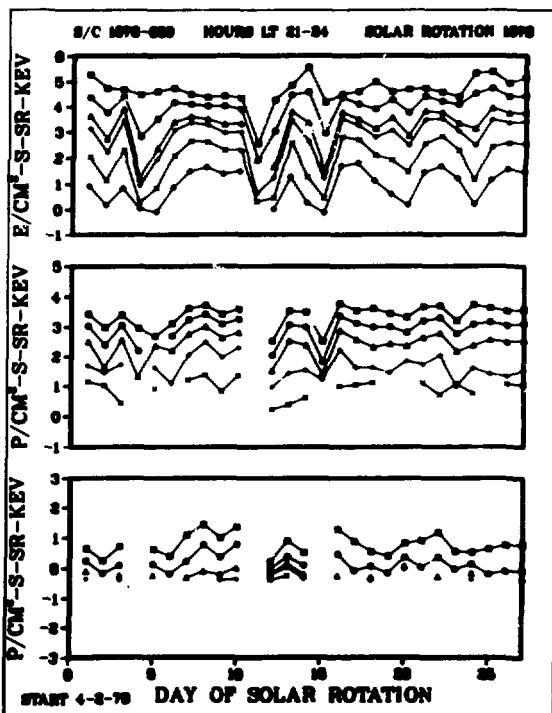
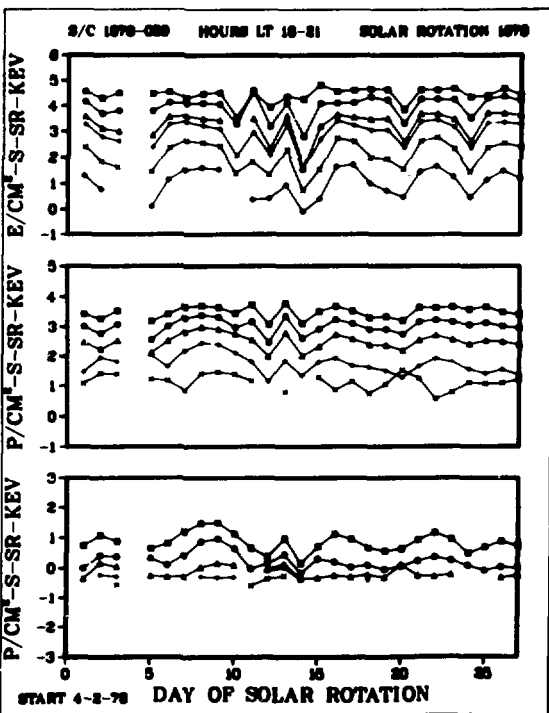
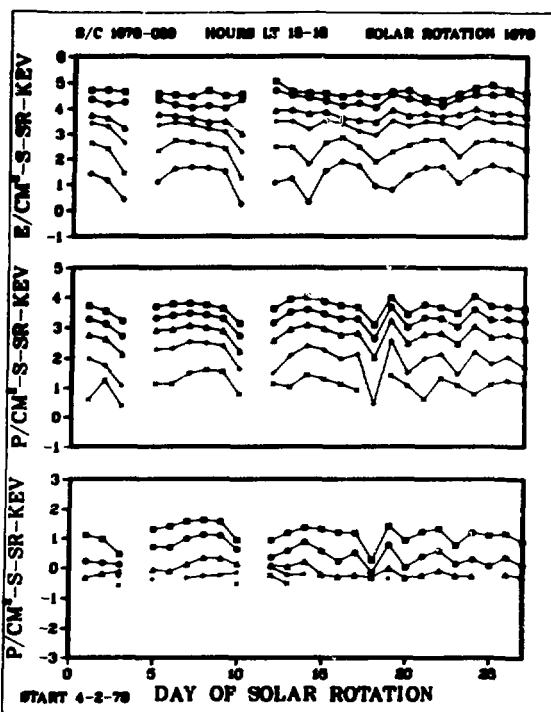
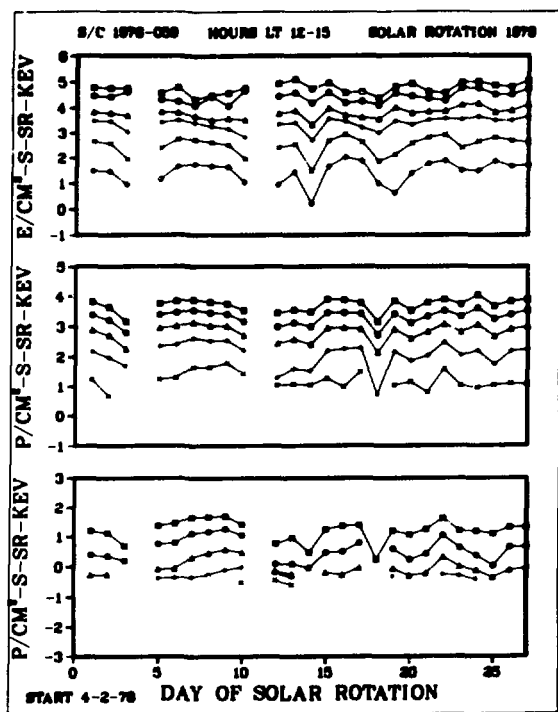
S/C 1976-059



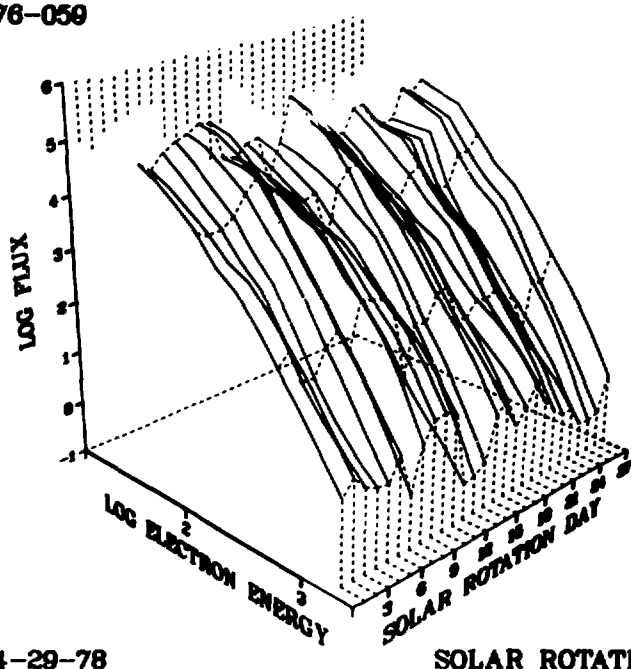
S/C 1976-059







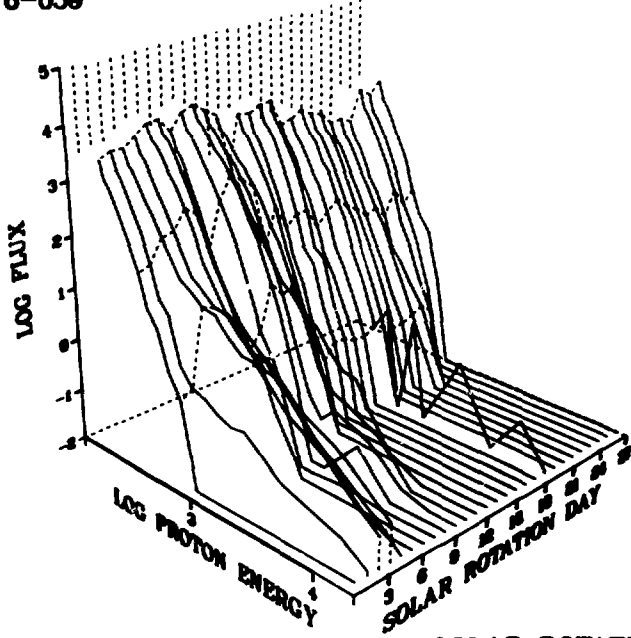
S/C 1976-059



START 4-29-78

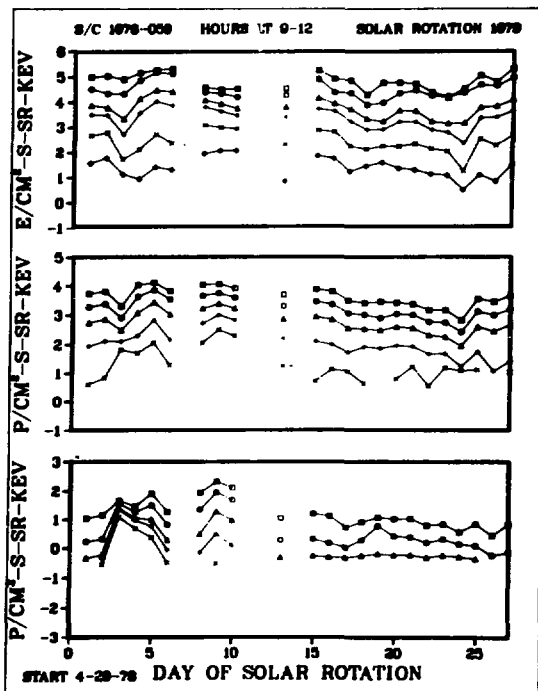
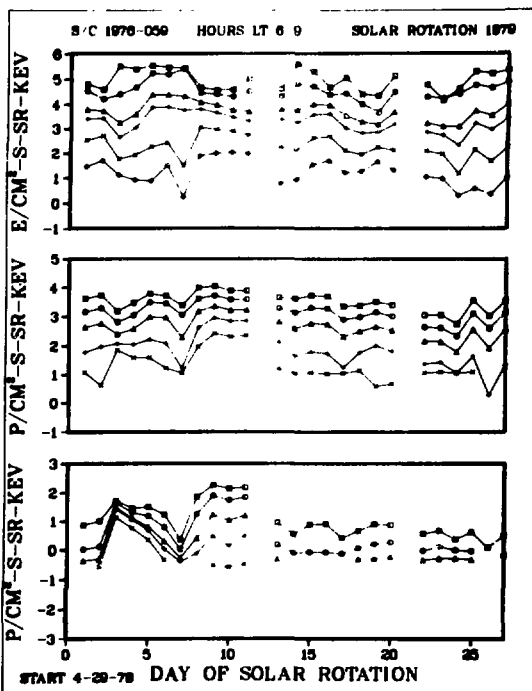
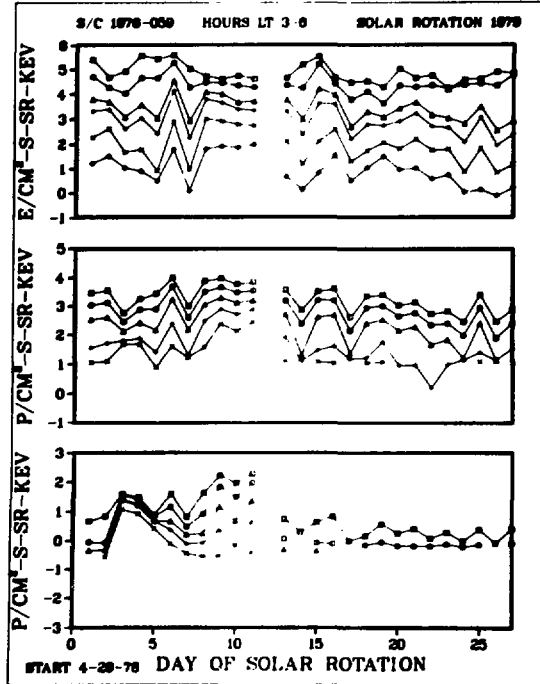
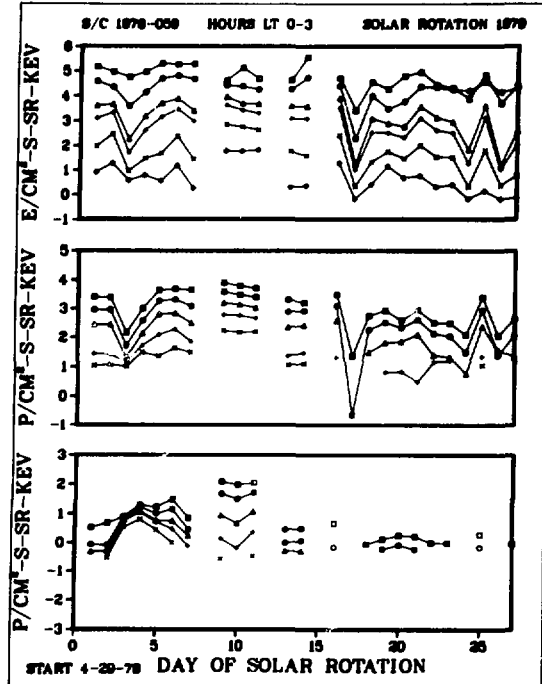
SOLAR ROTATION 1979

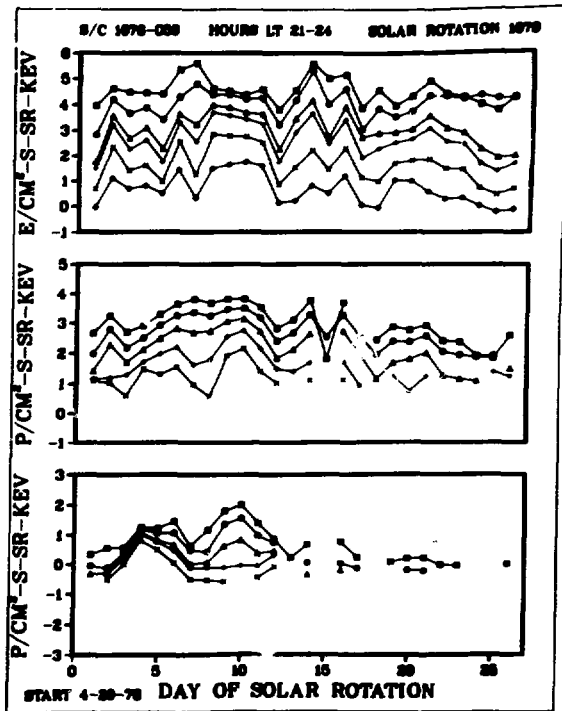
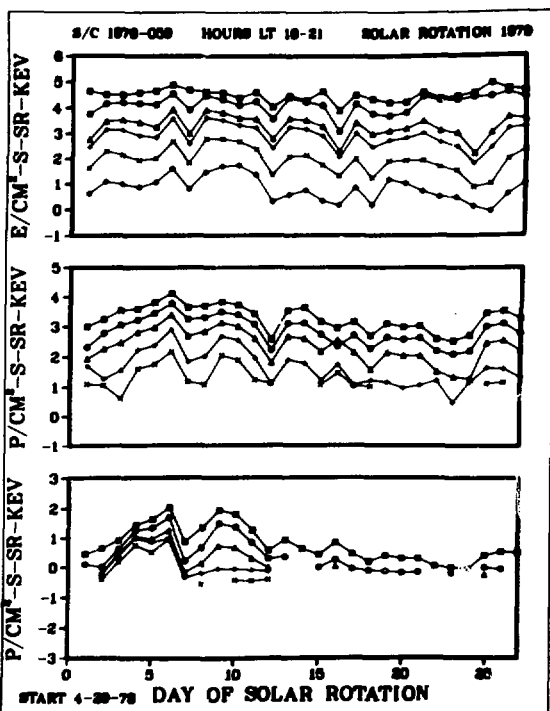
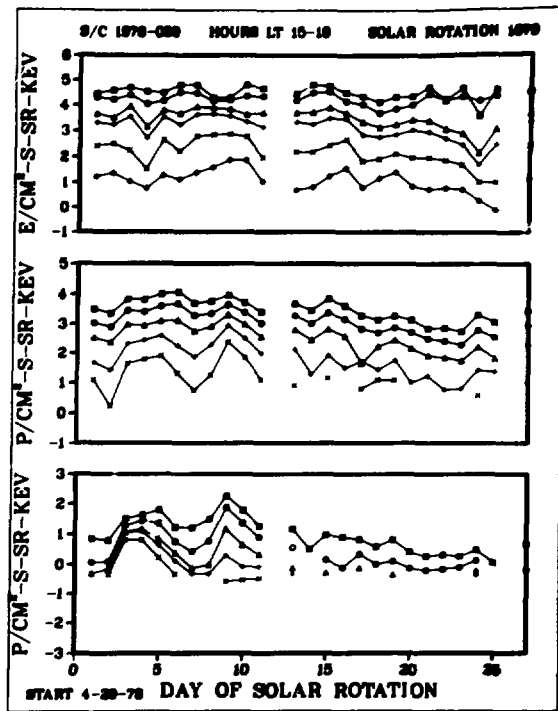
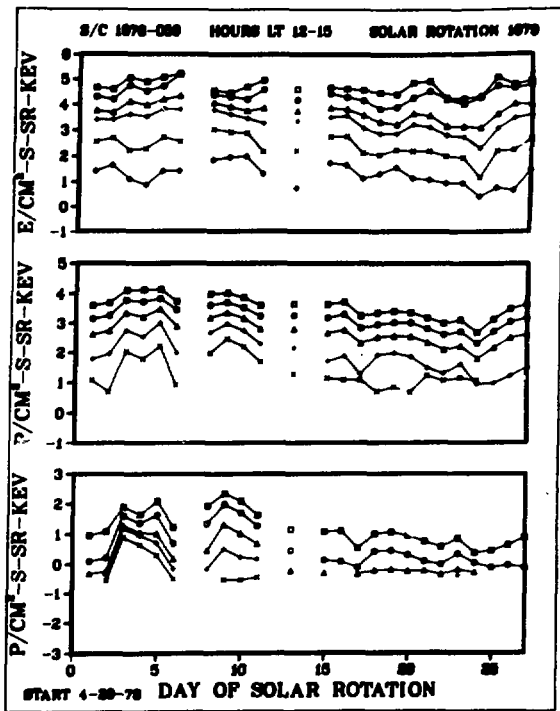
S/C 1976-059



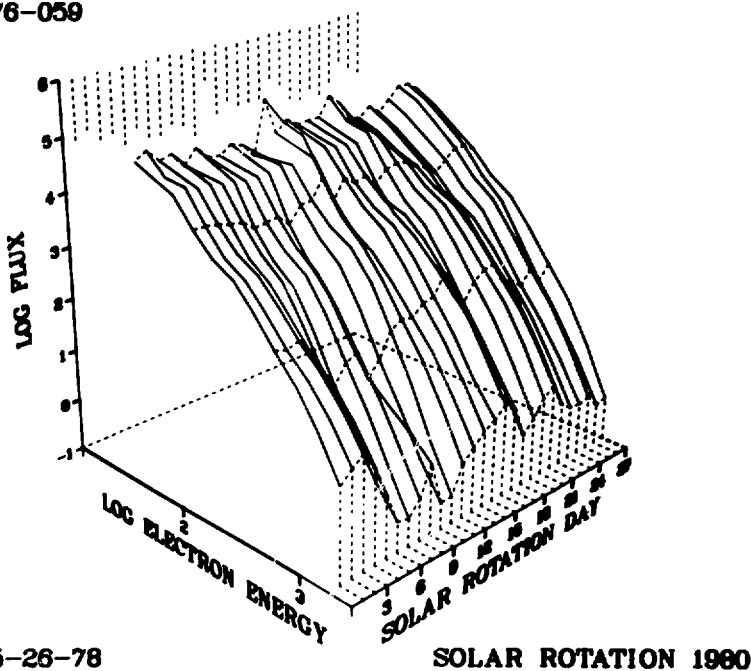
START 4-29-78

SOLAR ROTATION 1979





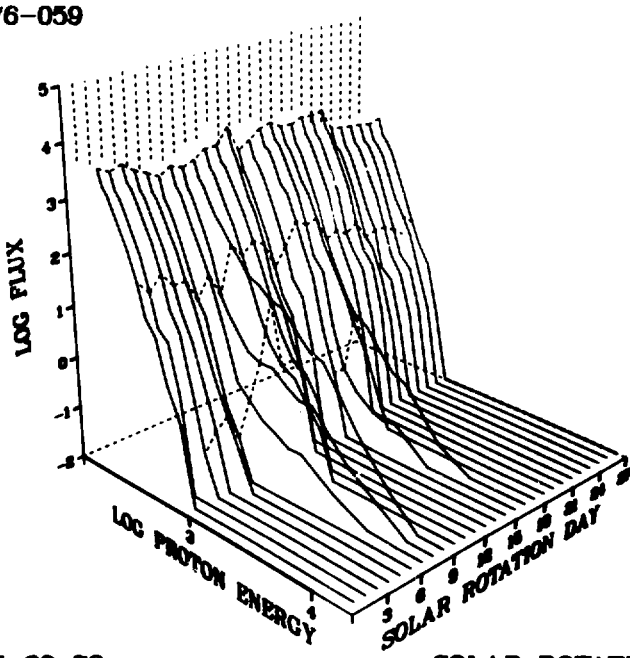
S/C 1976-059



START 5-26-78

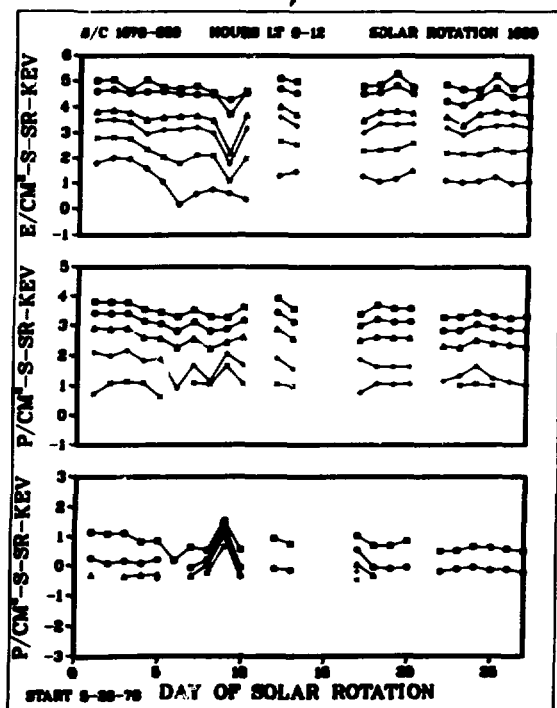
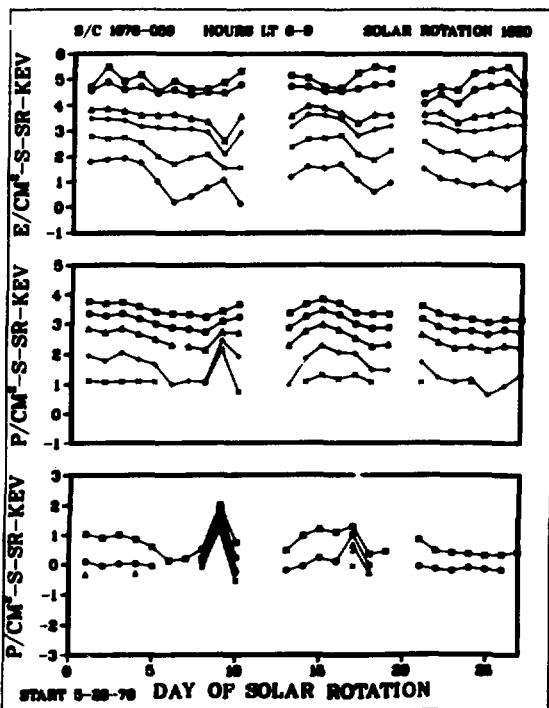
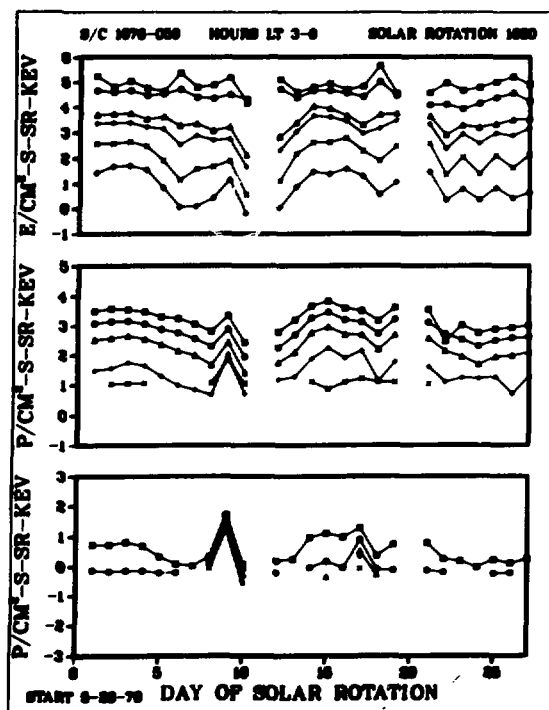
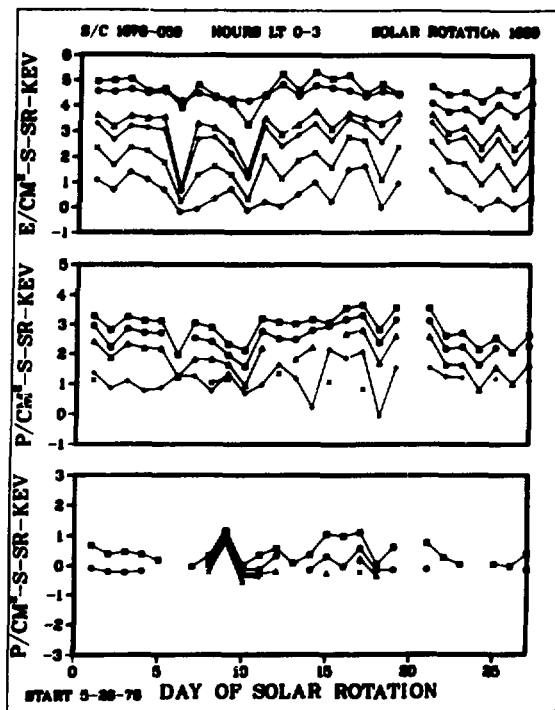
SOLAR ROTATION 1980

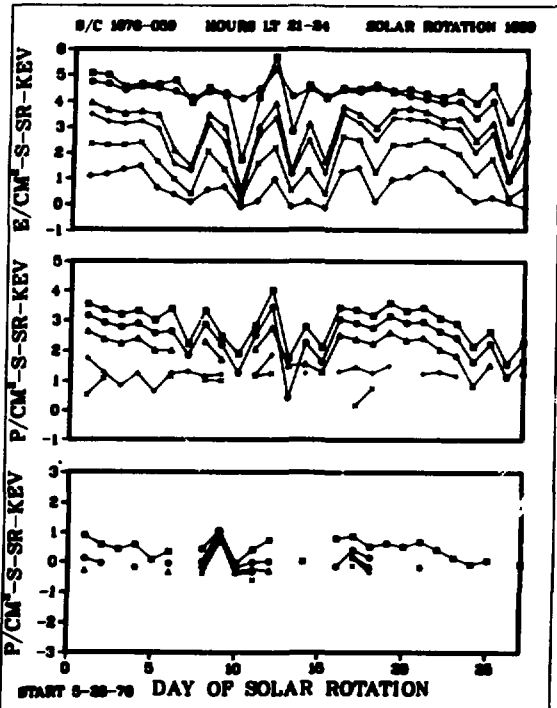
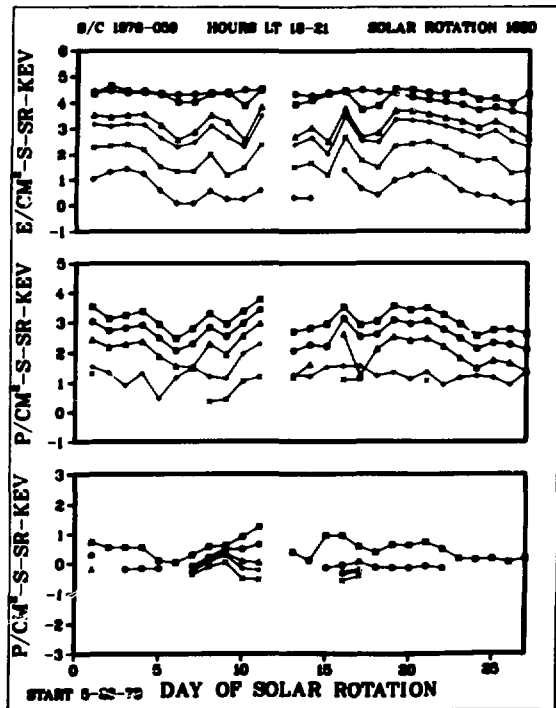
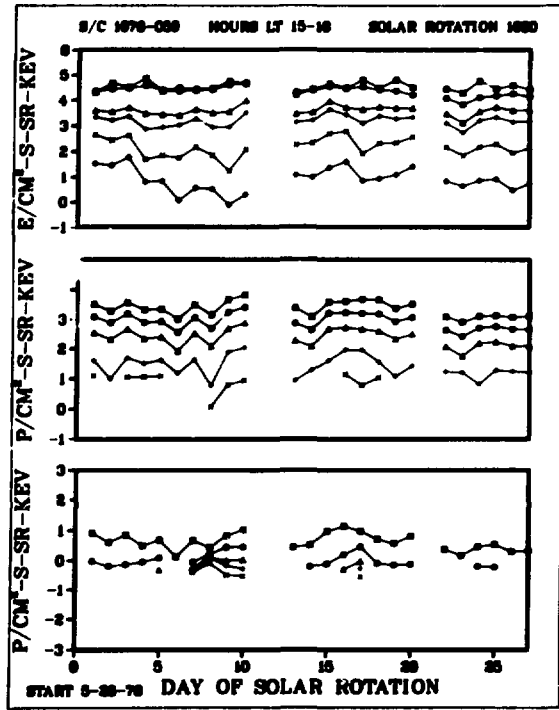
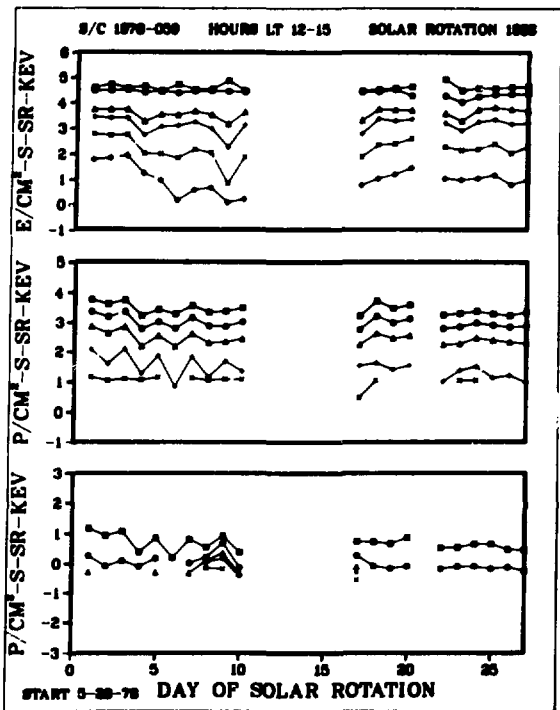
S/C 1976-059



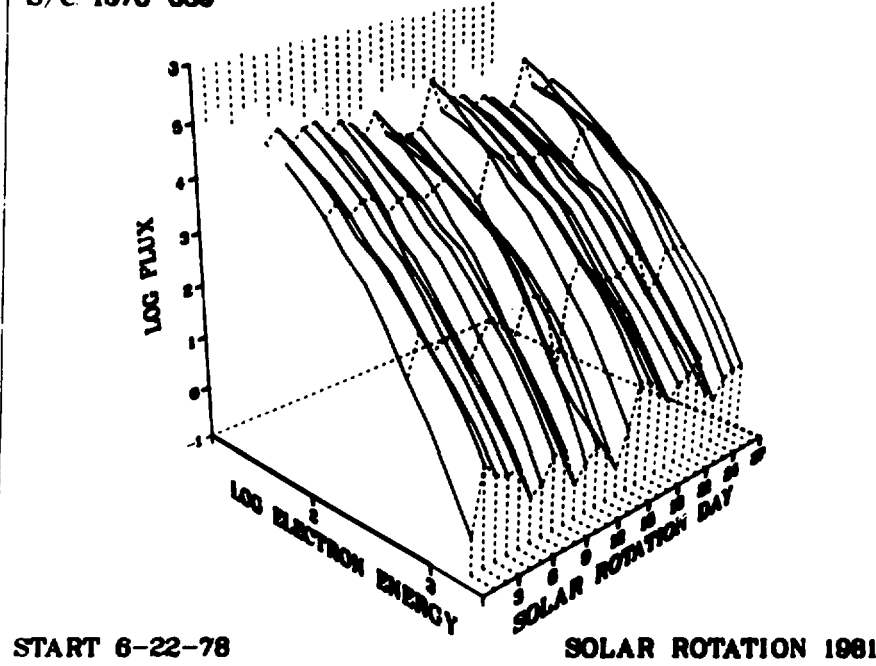
START 5-26-78

SOLAR ROTATION 1980

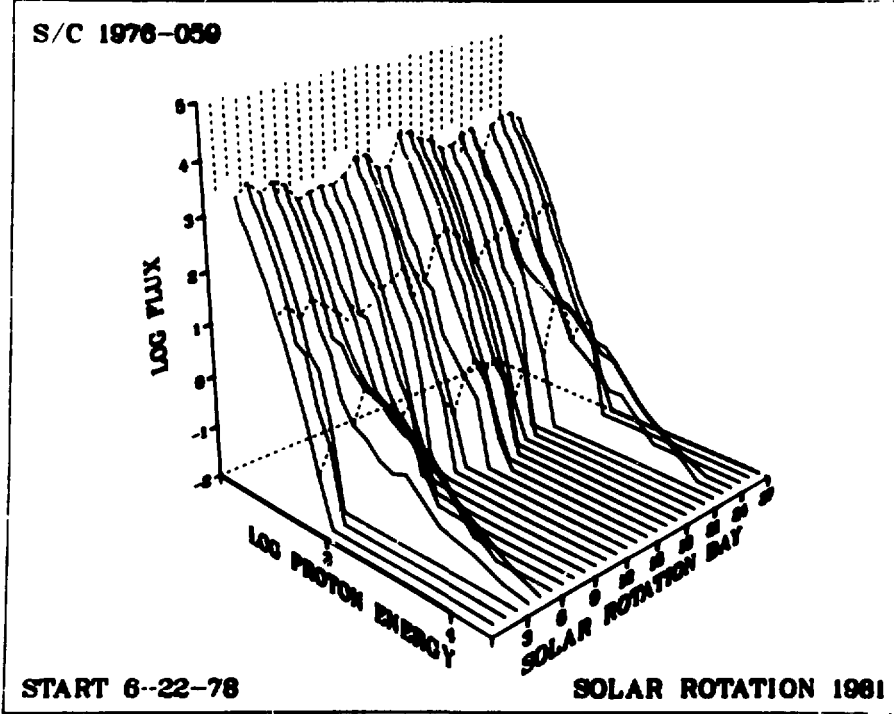


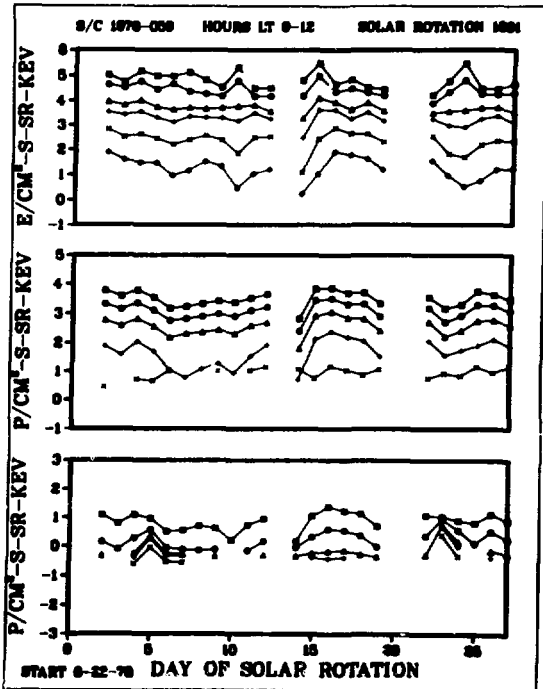
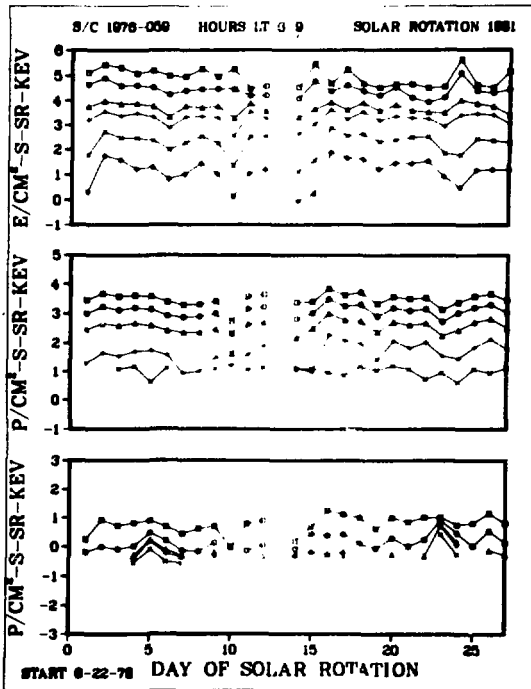
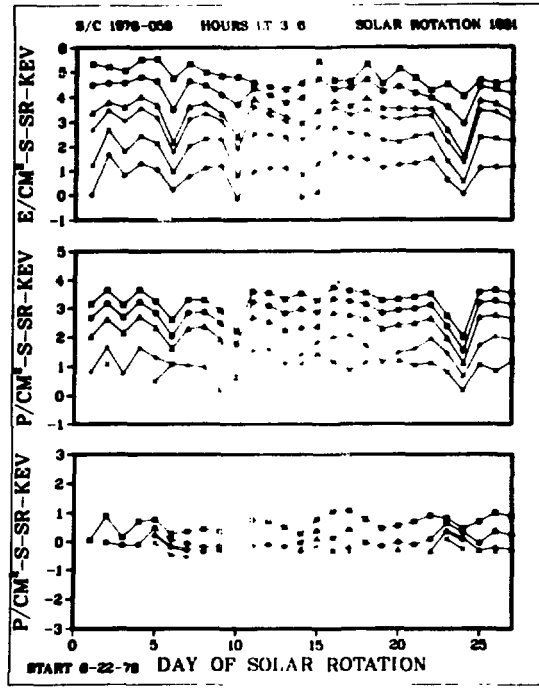
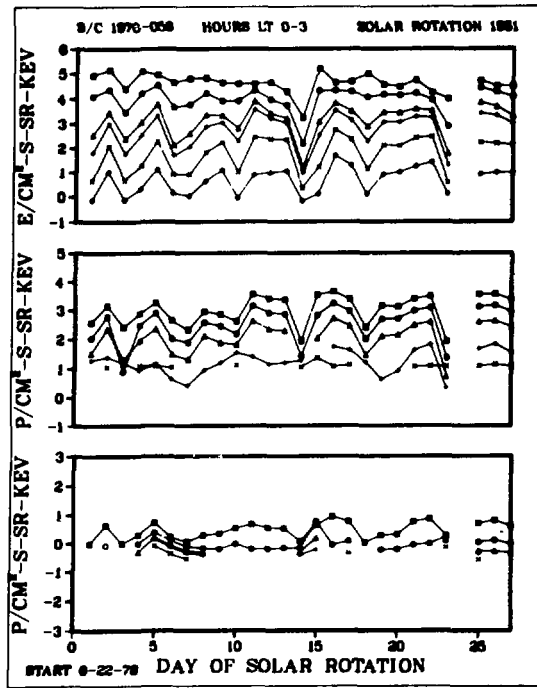


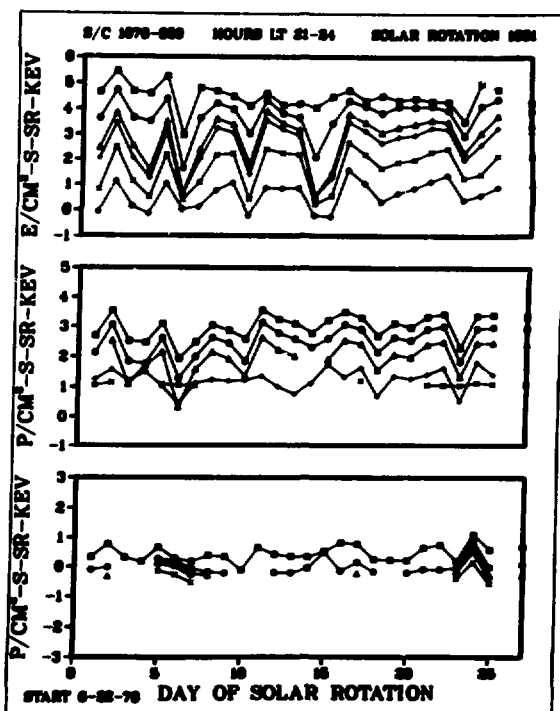
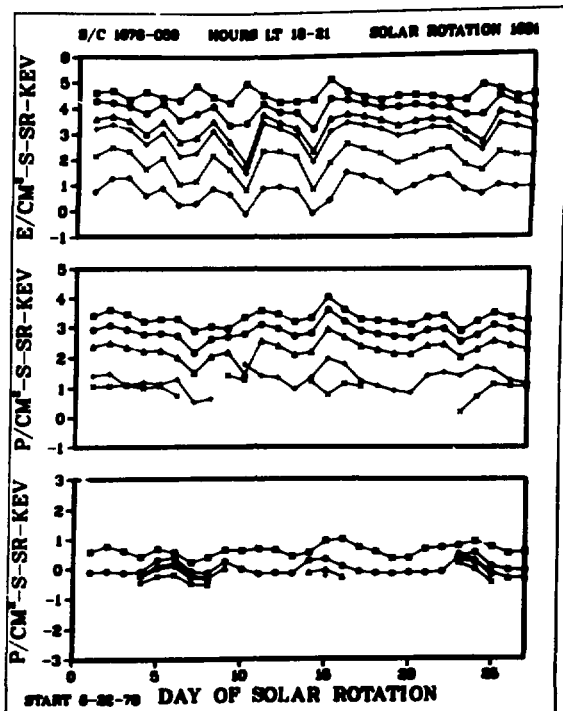
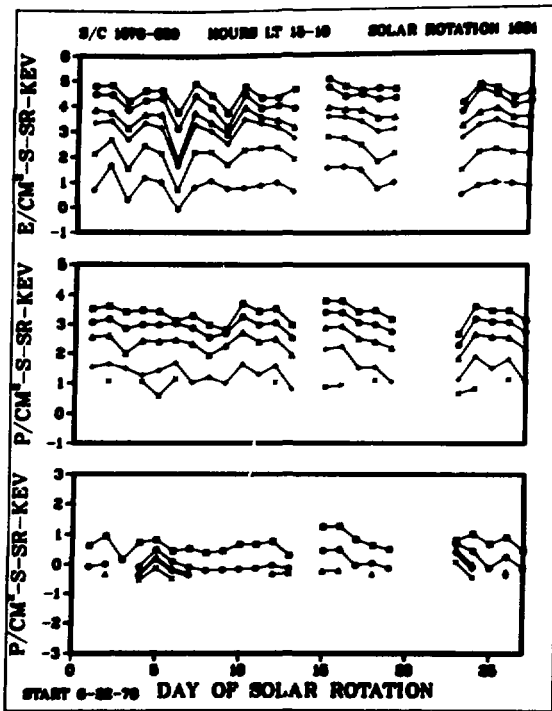
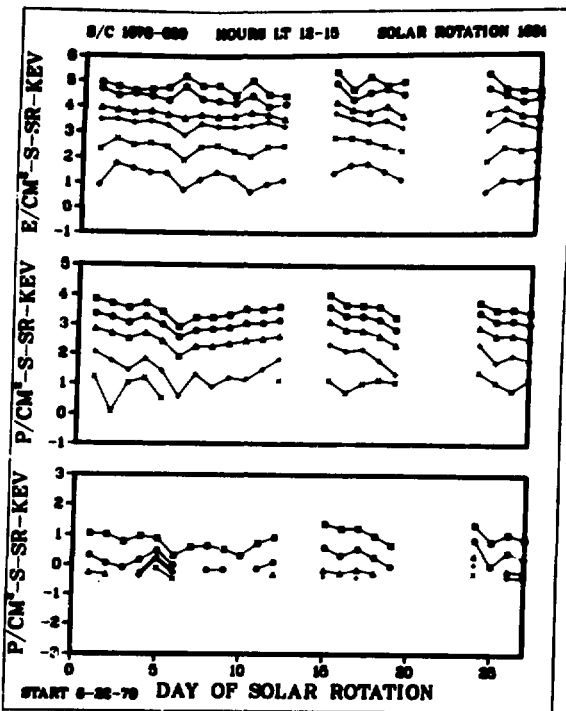
S/C 1976-059



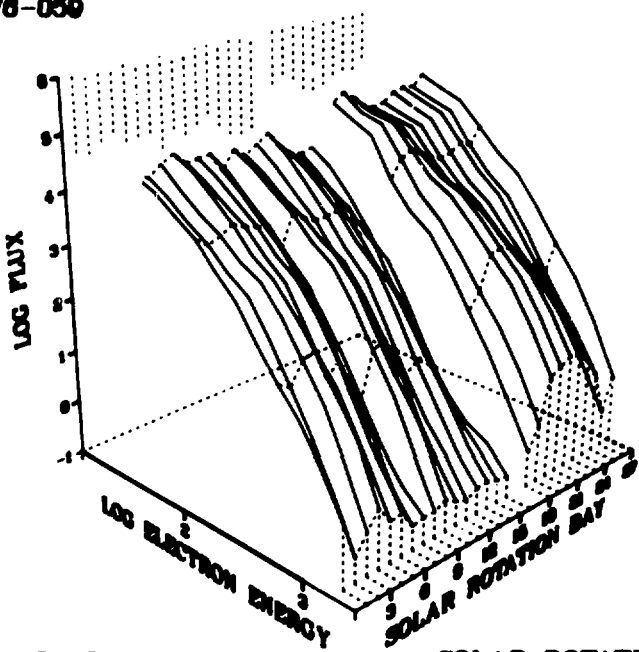
S/C 1976-059







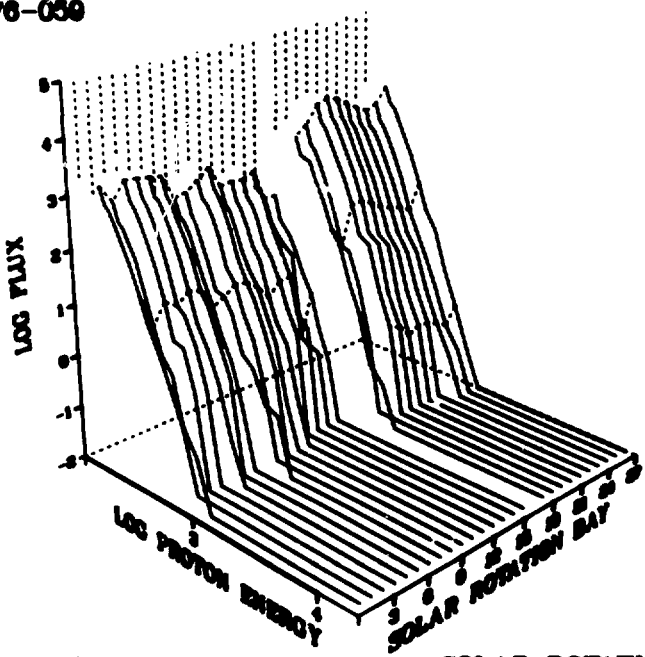
S/C 1970-059



START 7-19-78

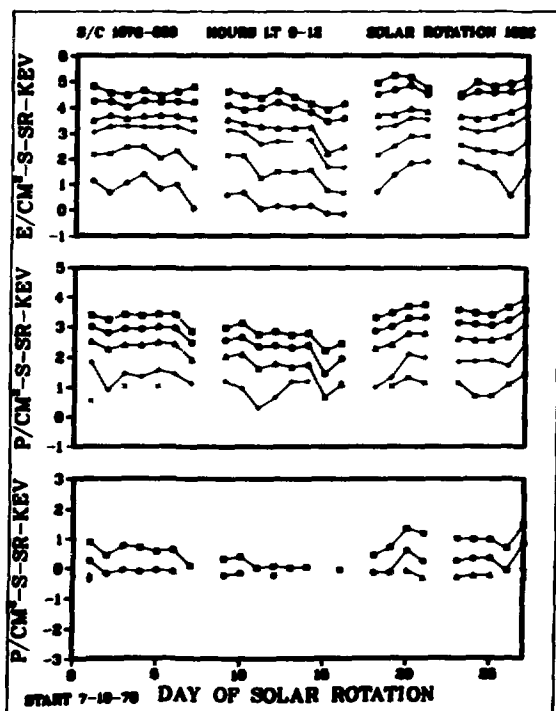
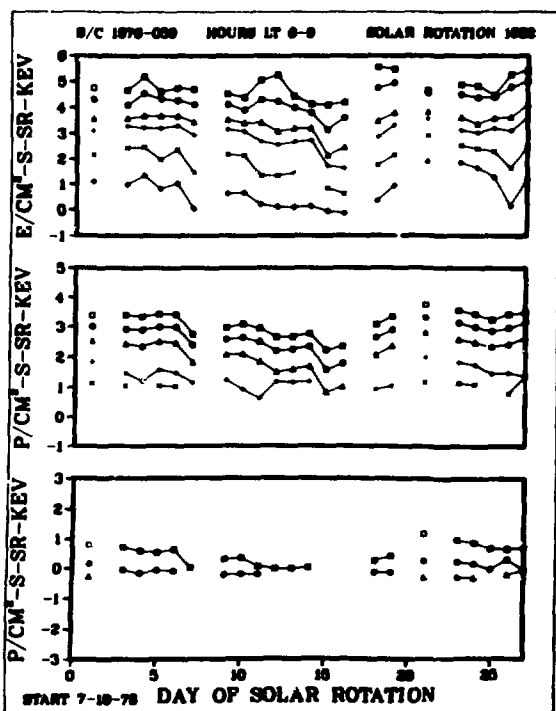
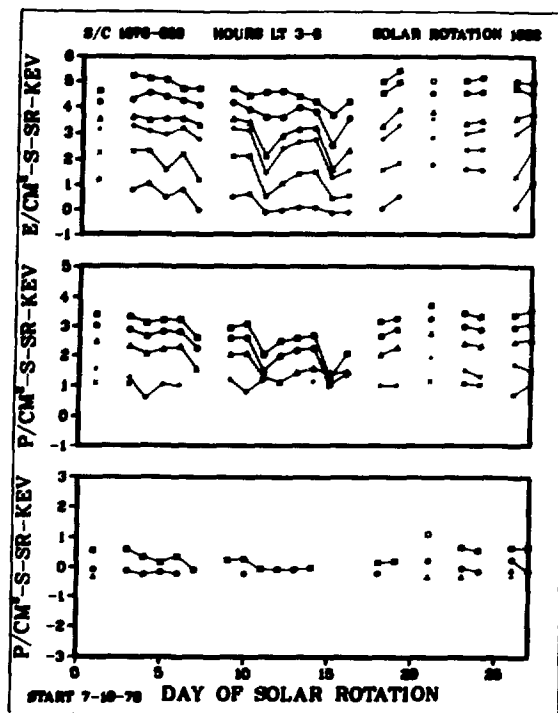
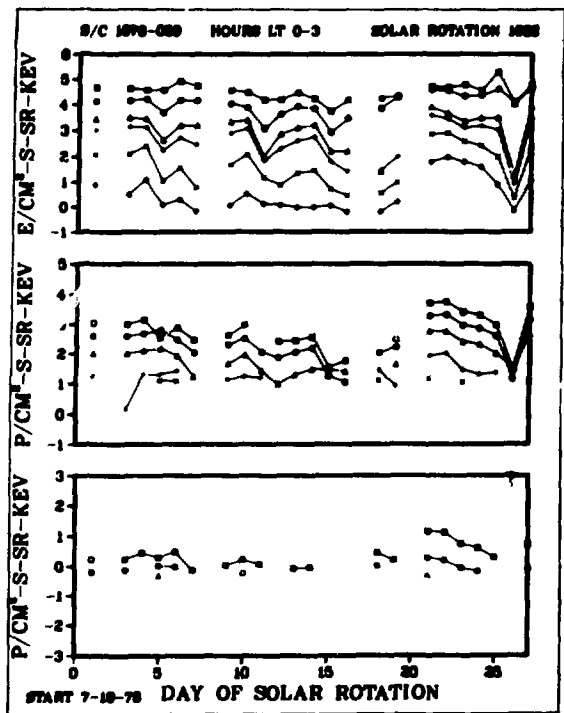
SOLAR ROTATION 1982

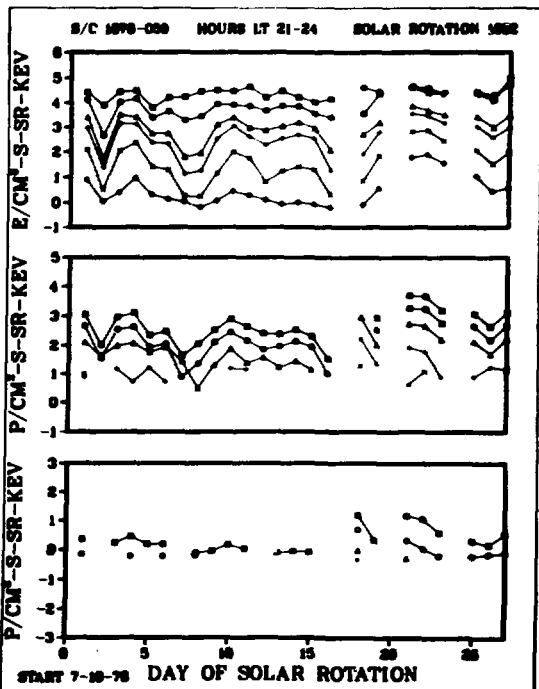
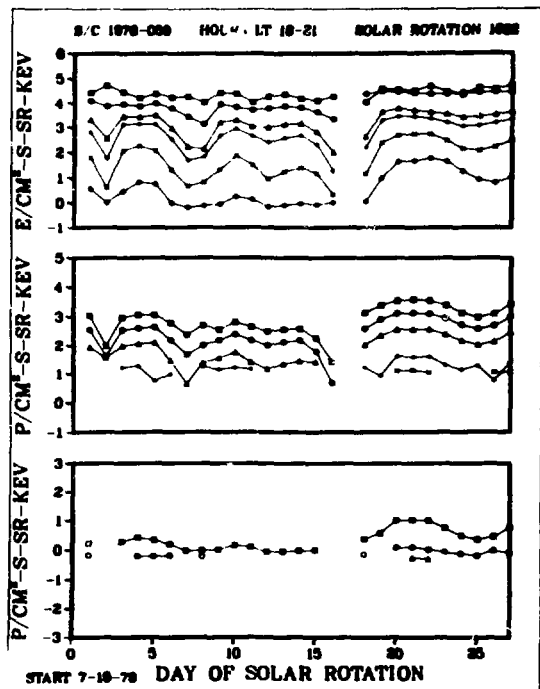
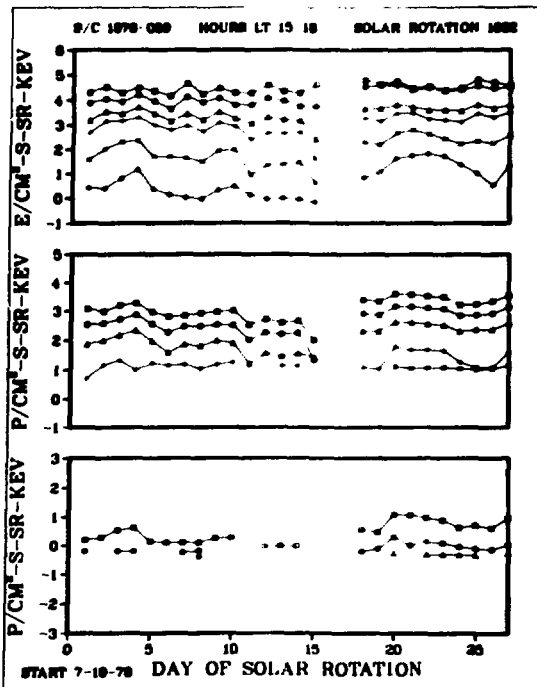
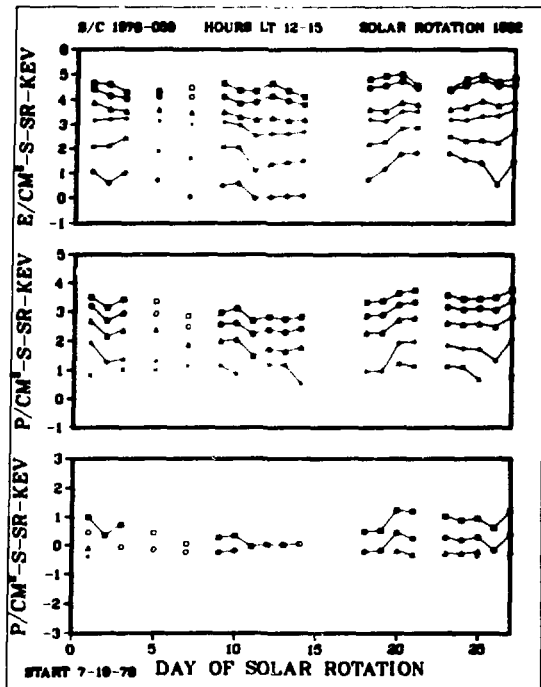
S/C 1970-059



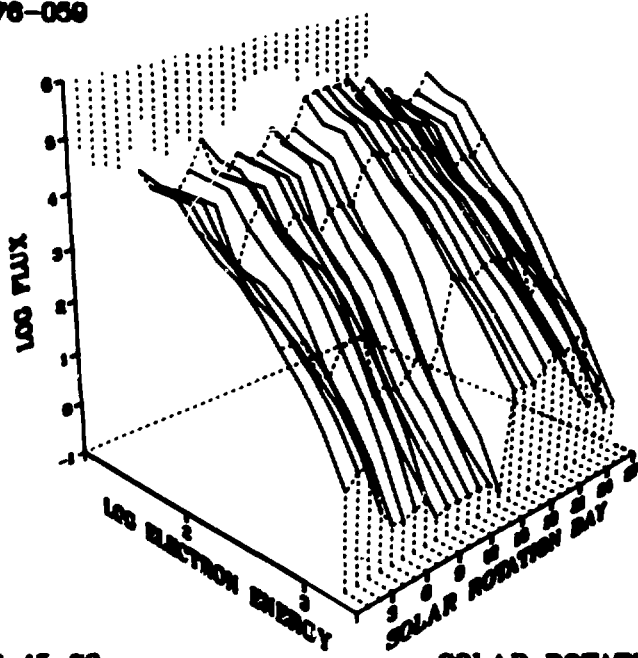
START 7-19-78

SOLAR ROTATION 1982

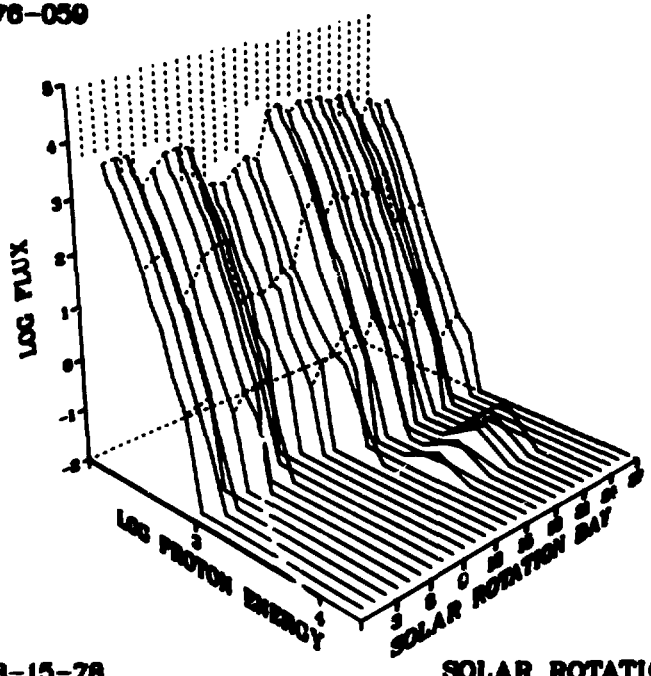


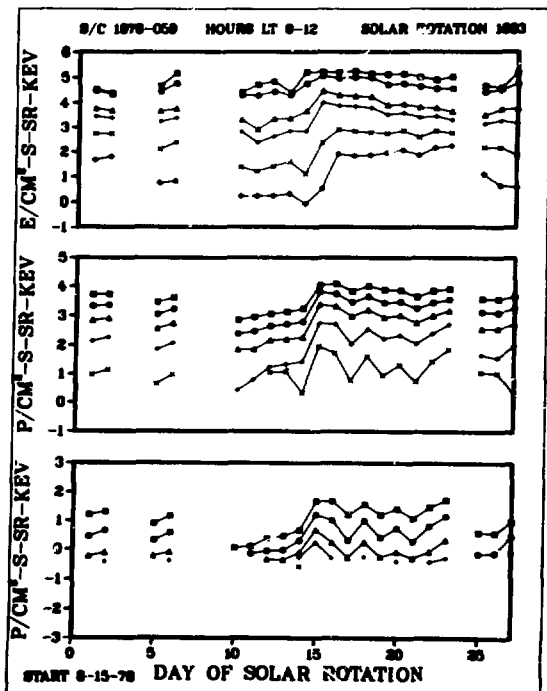
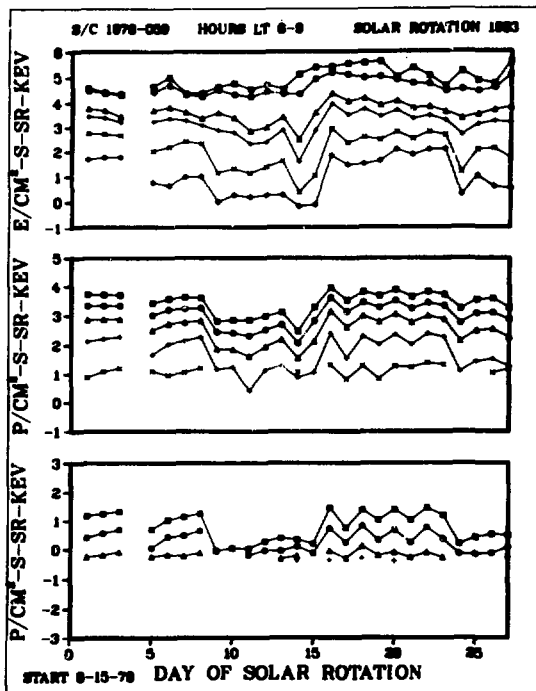
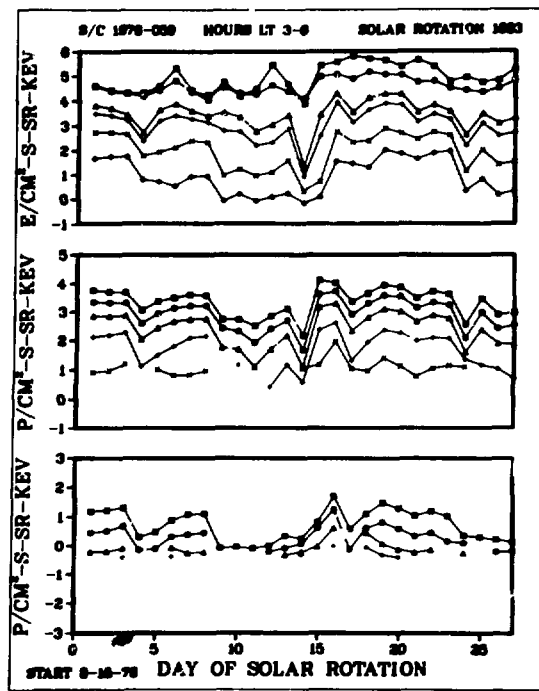
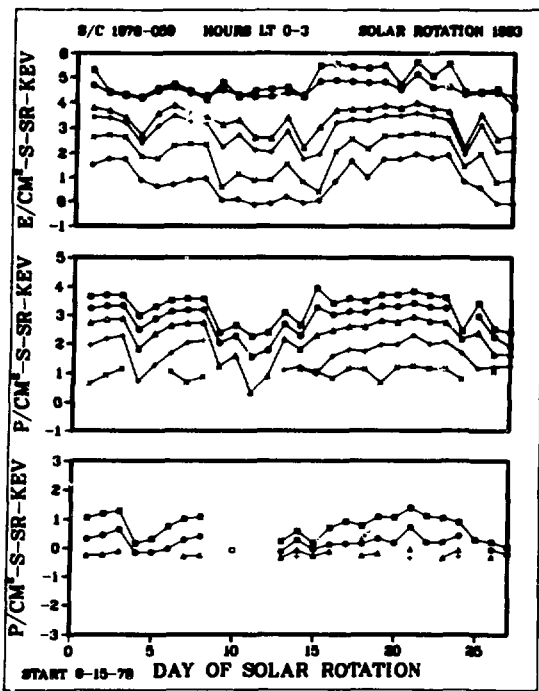


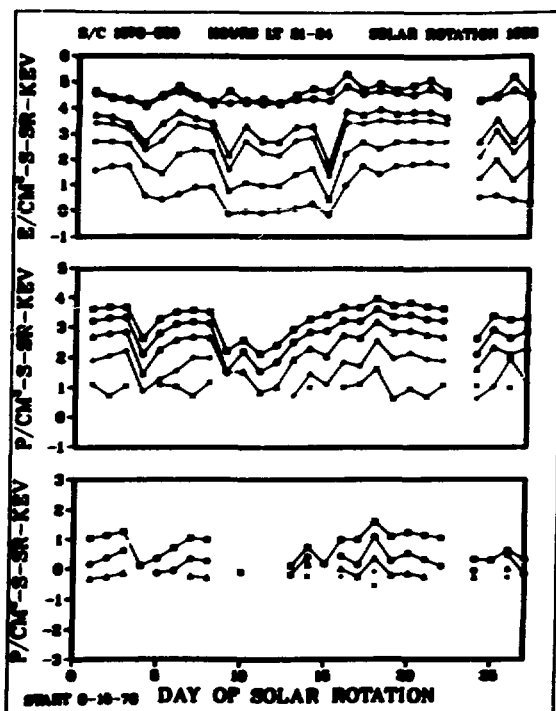
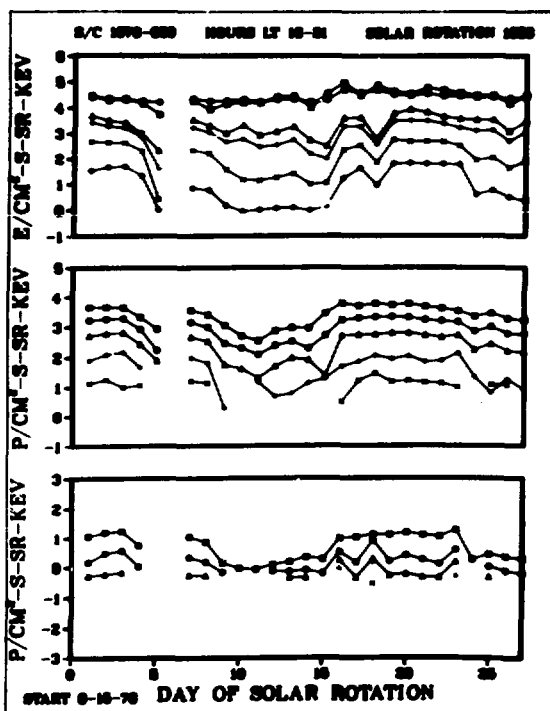
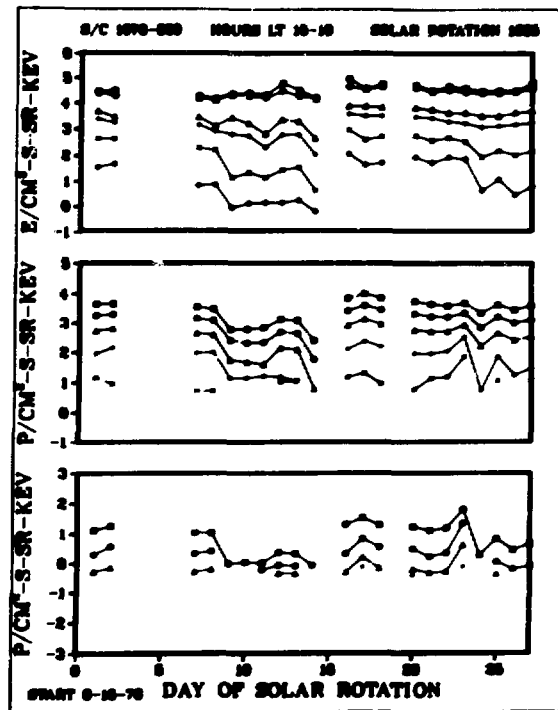
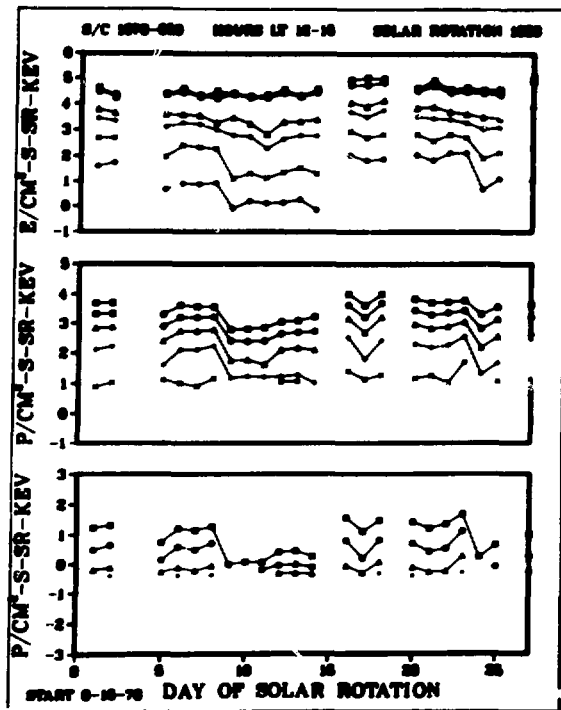
S/C 1976-050

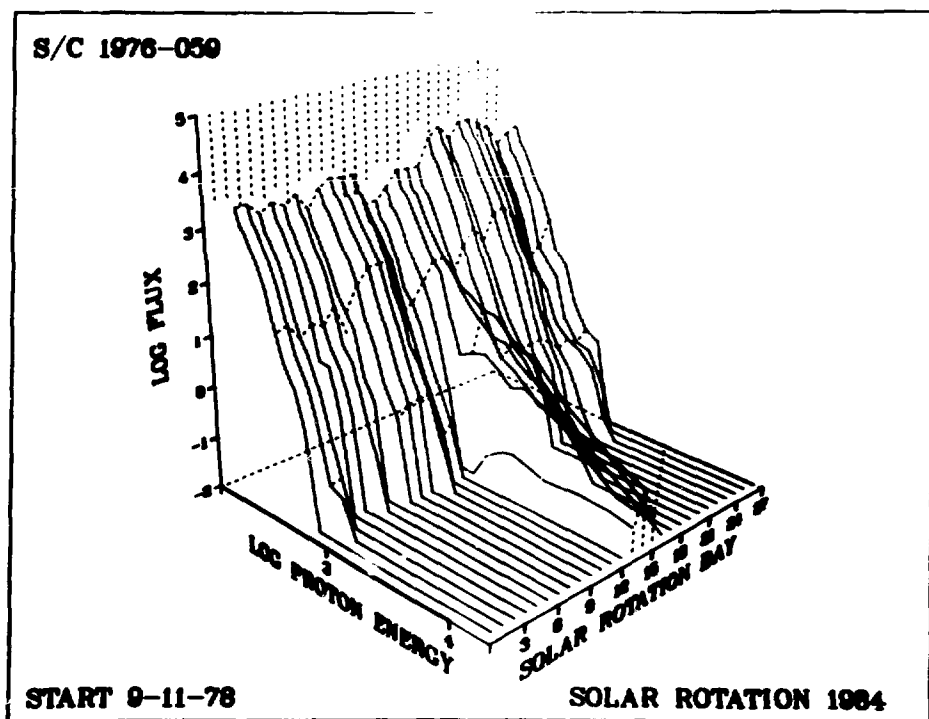
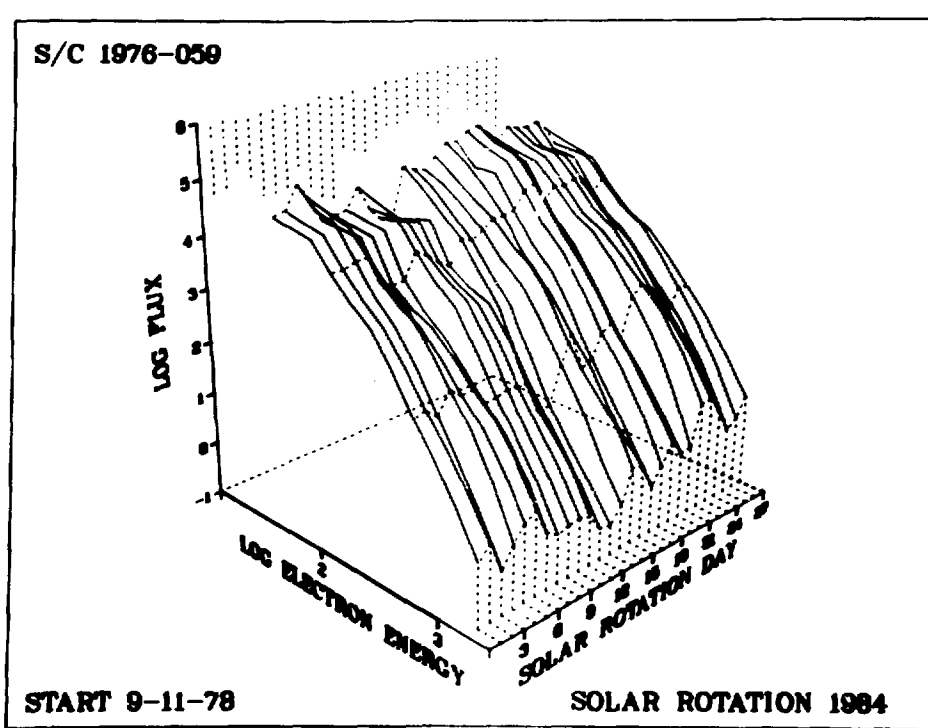


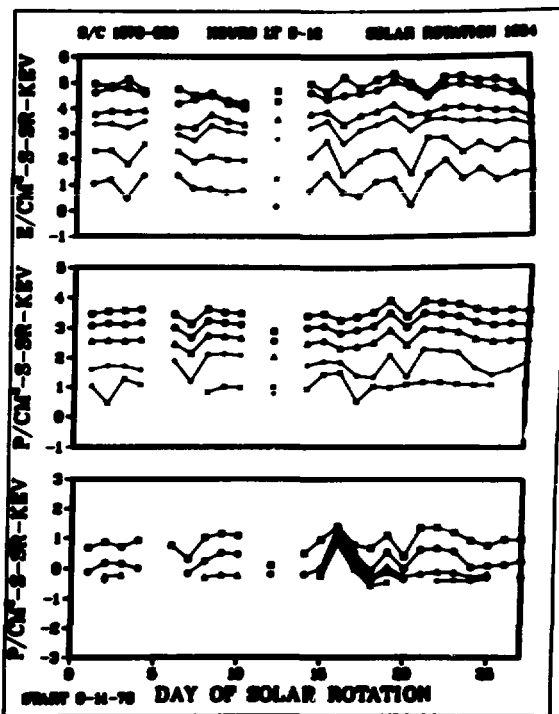
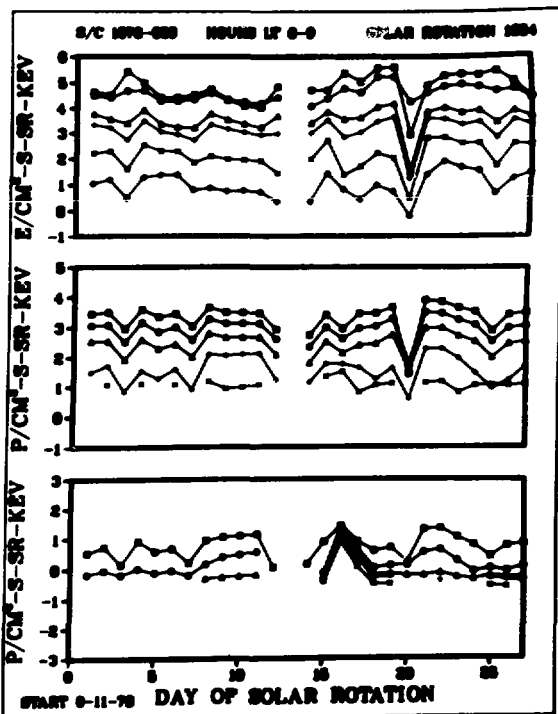
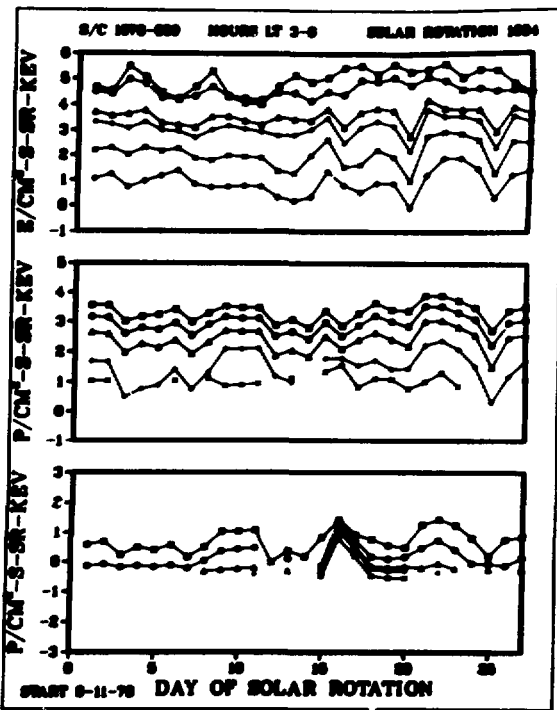
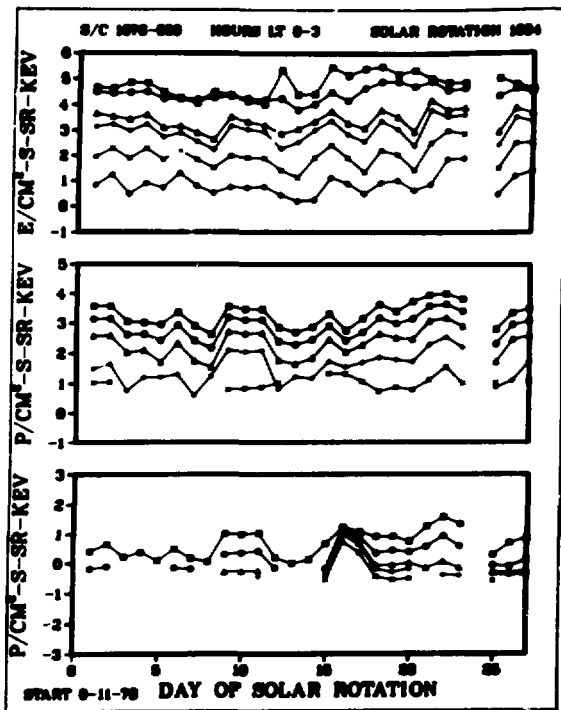
S/C 1976-050

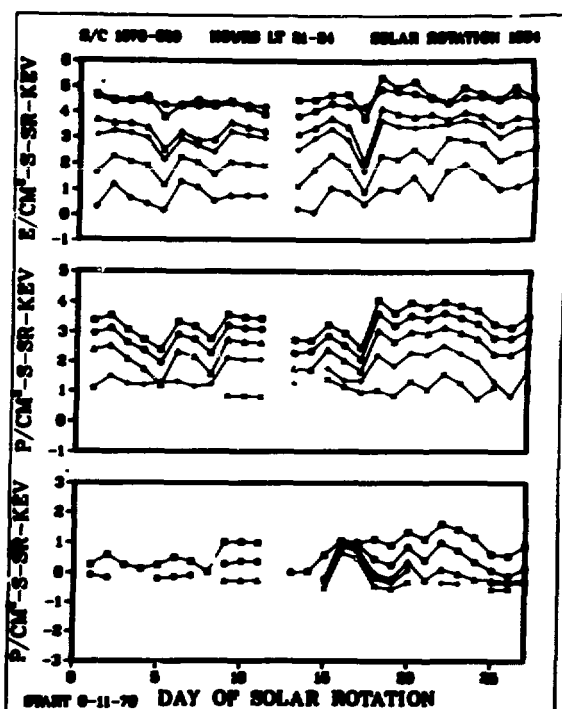
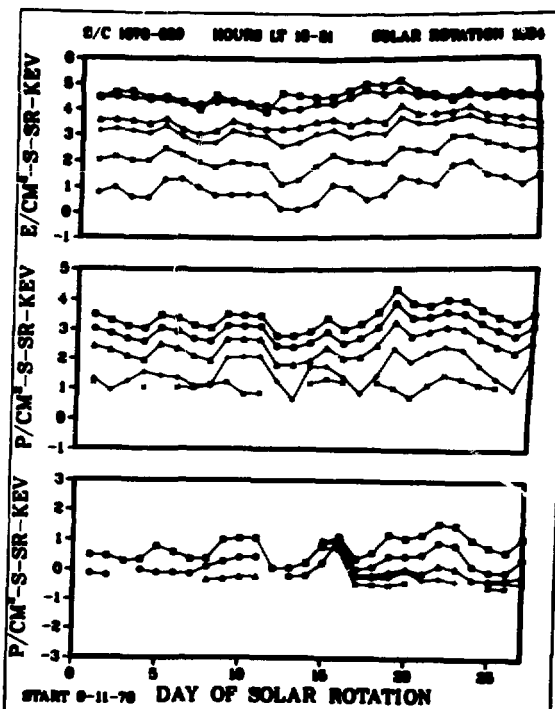
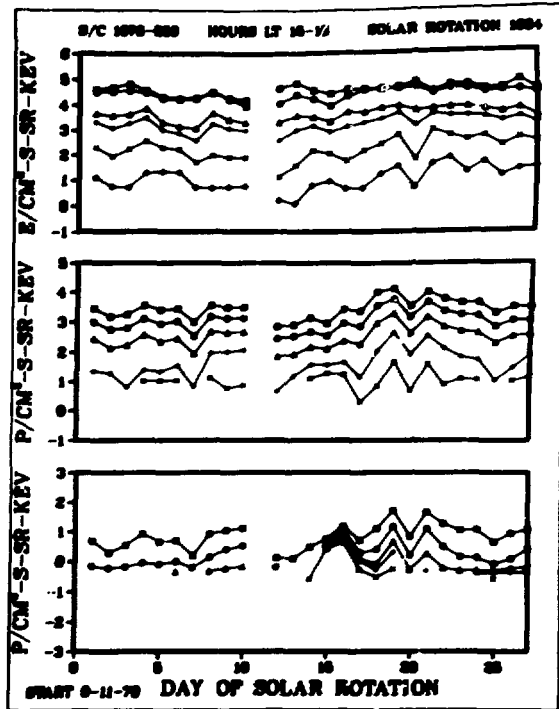
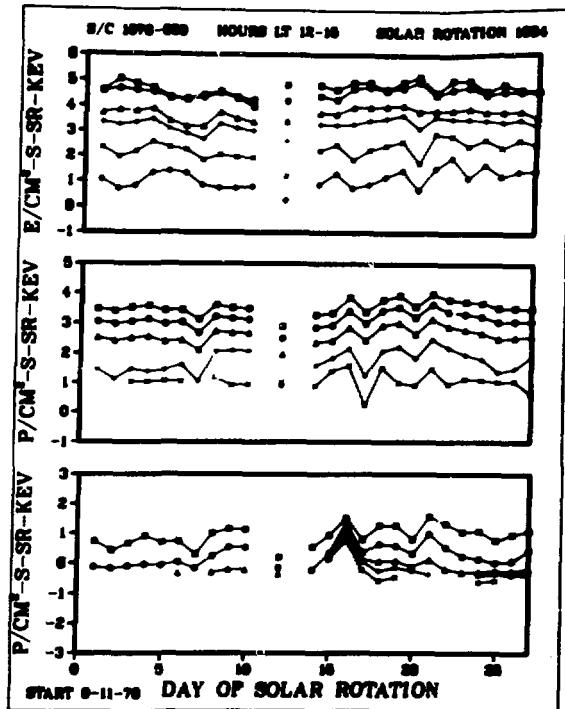




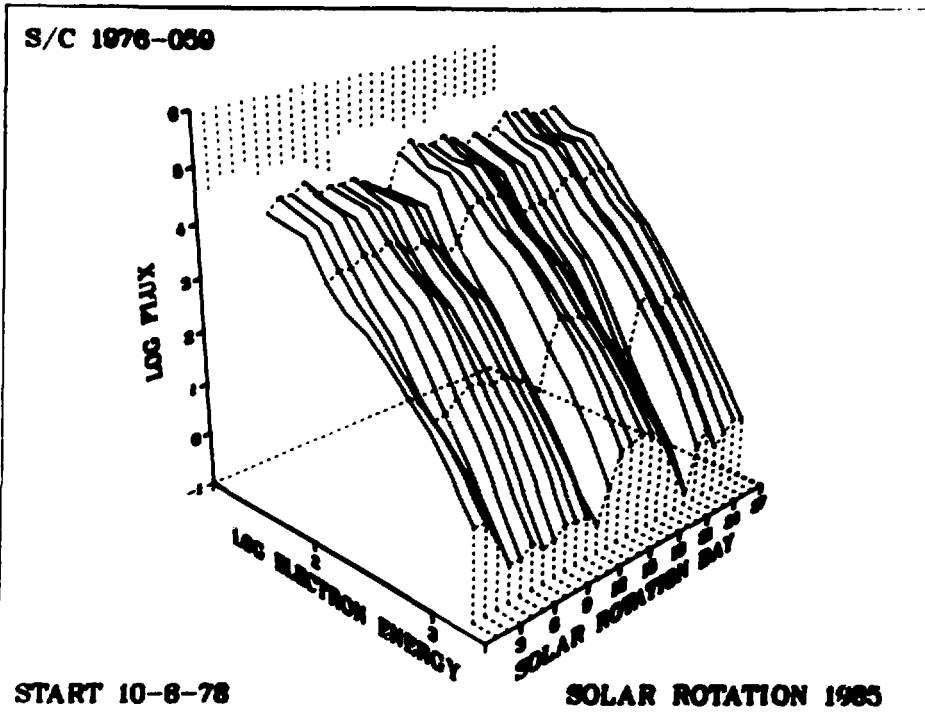




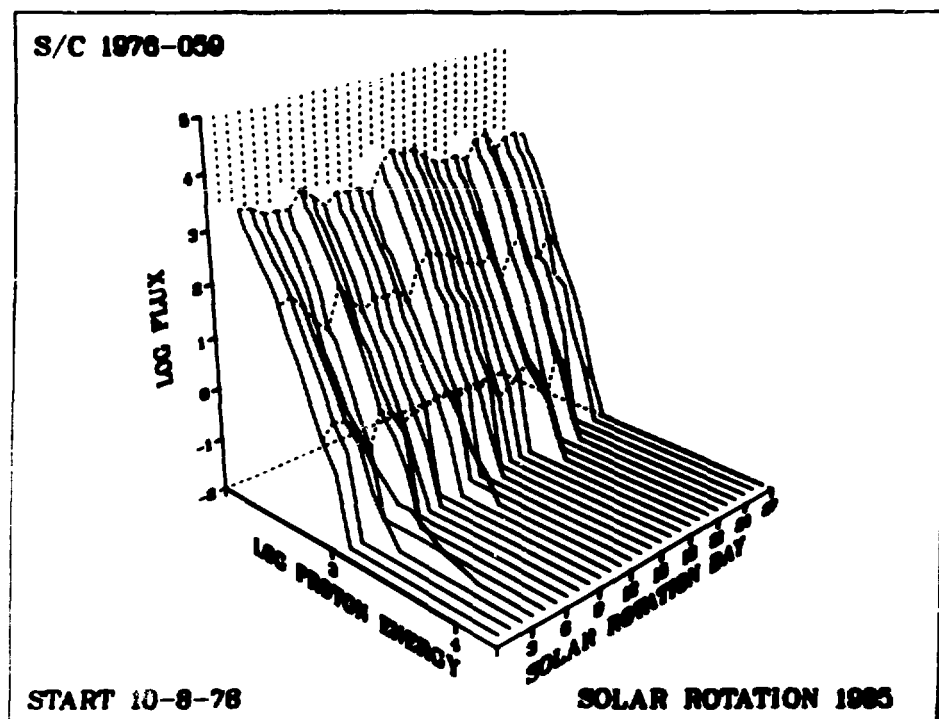


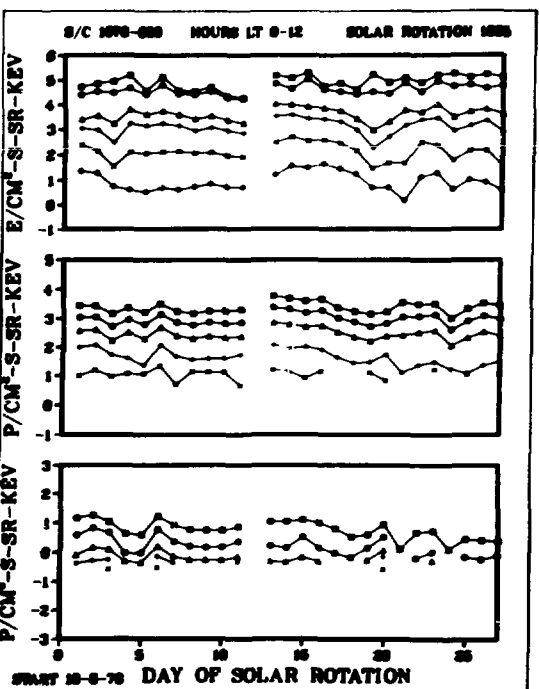
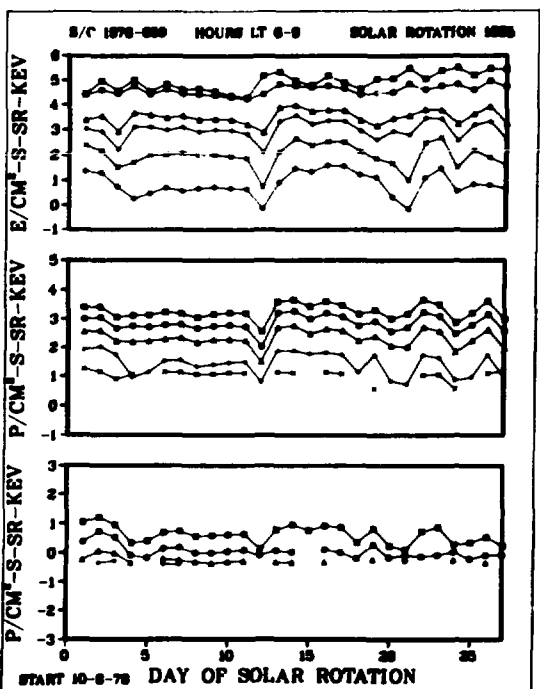
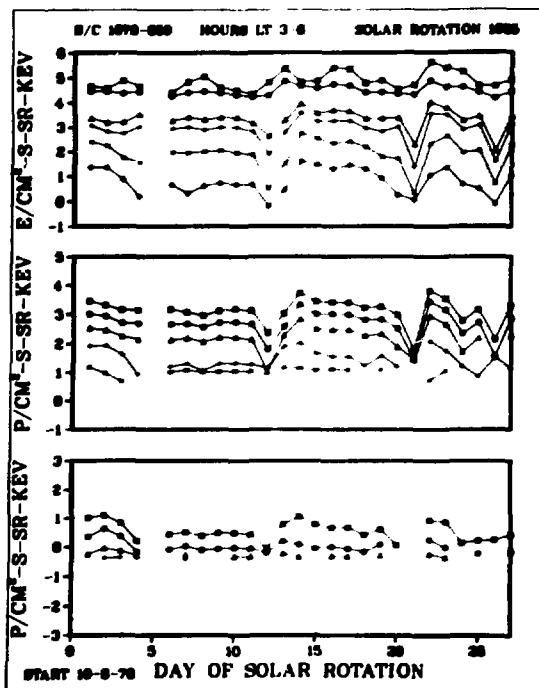
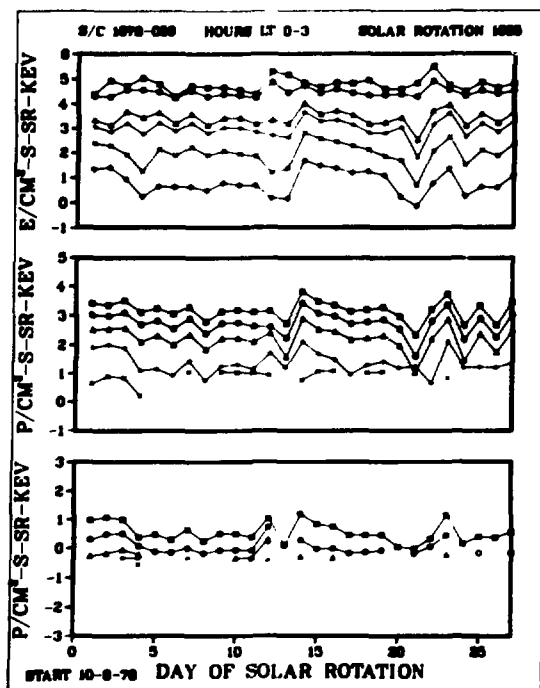


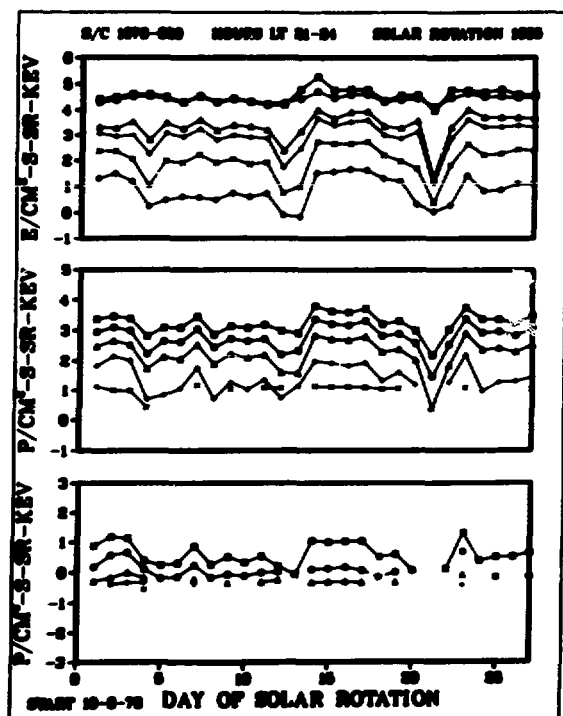
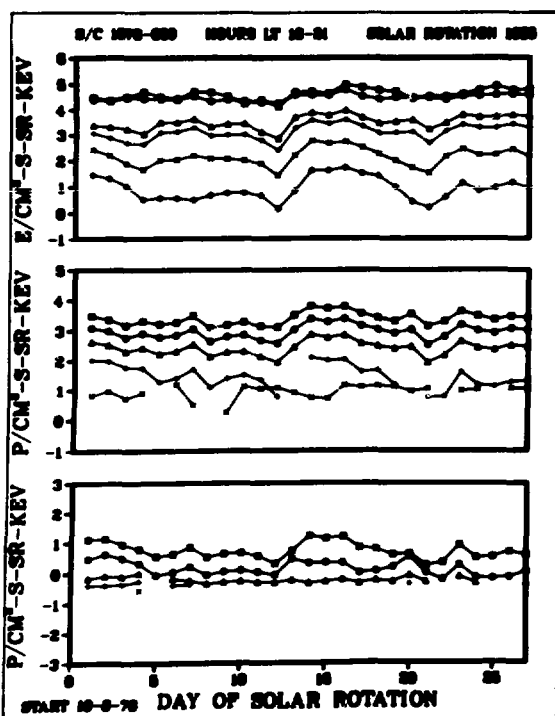
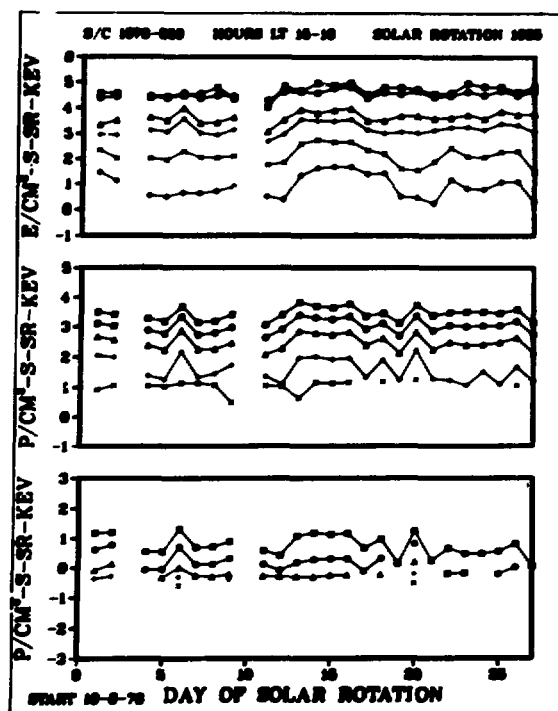
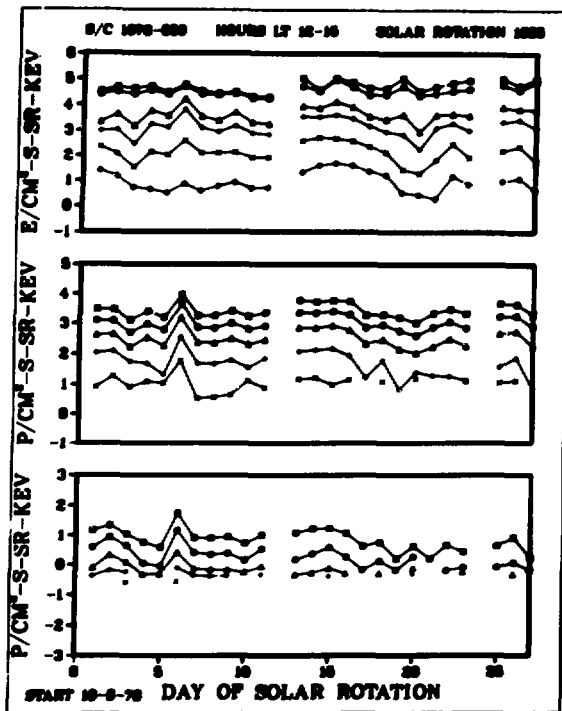
S/C 1976-059



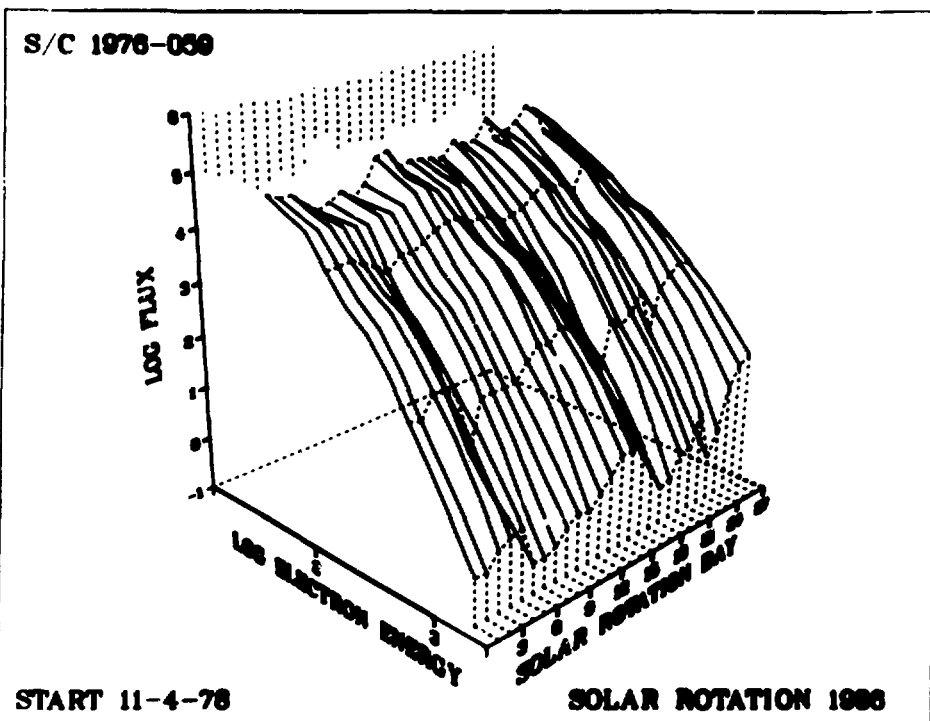
S/C 1976-059



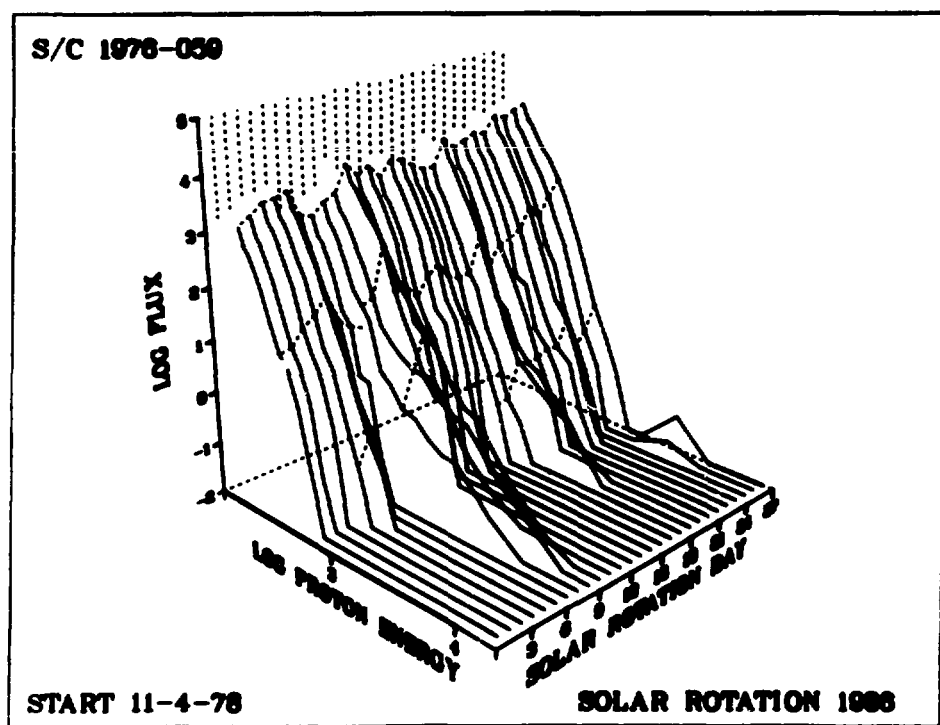


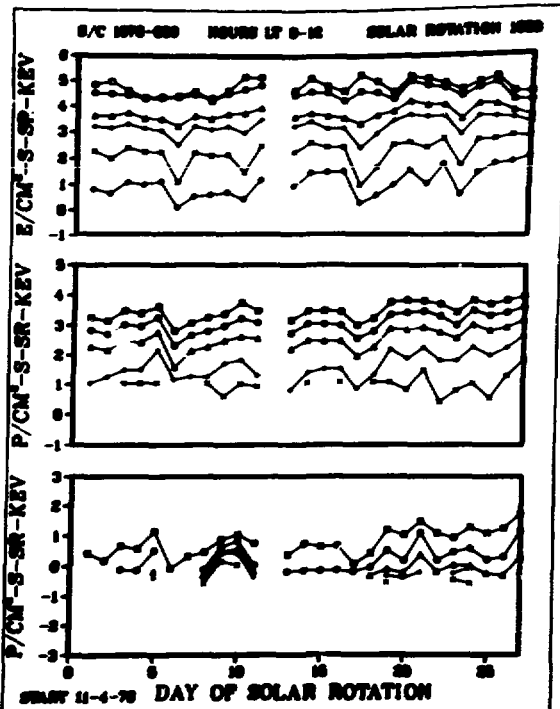
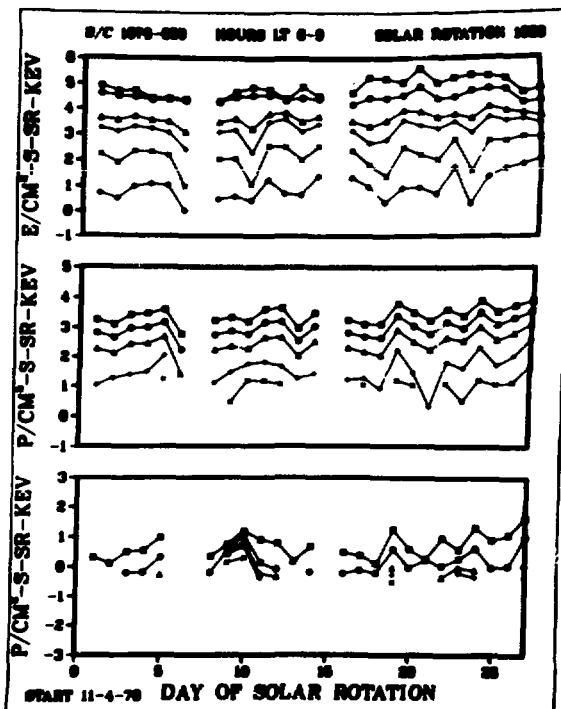
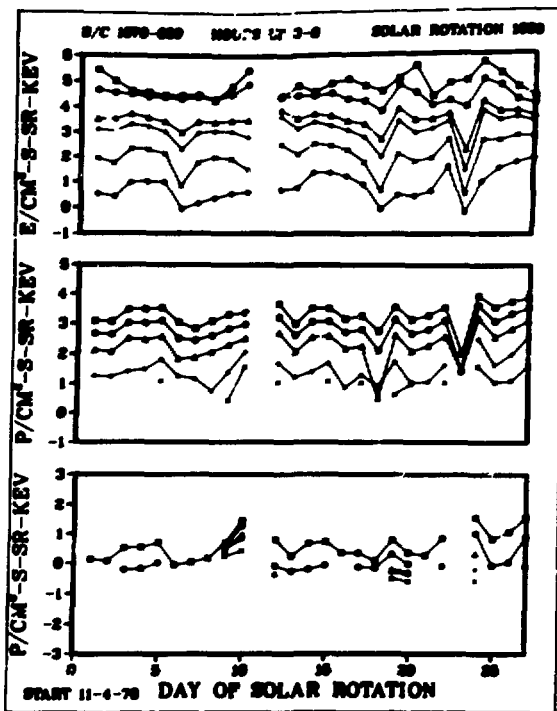
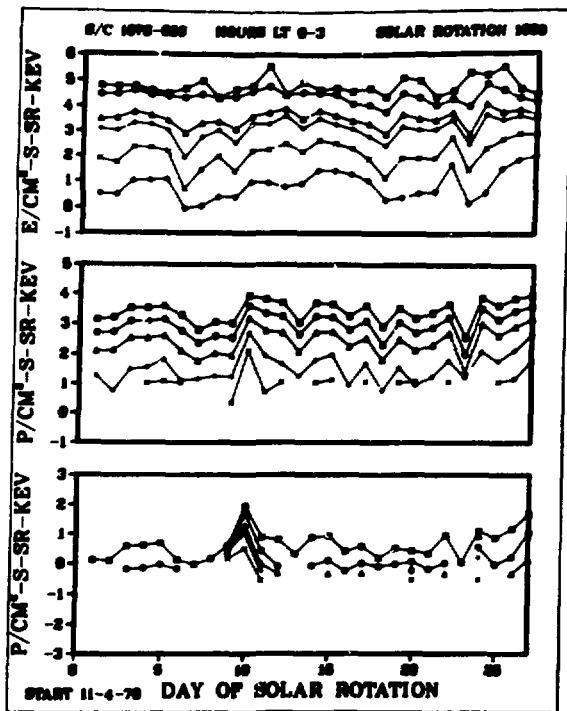


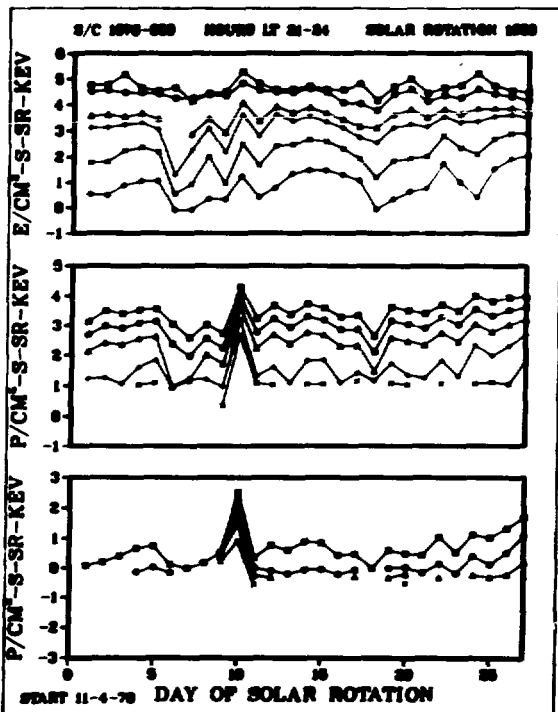
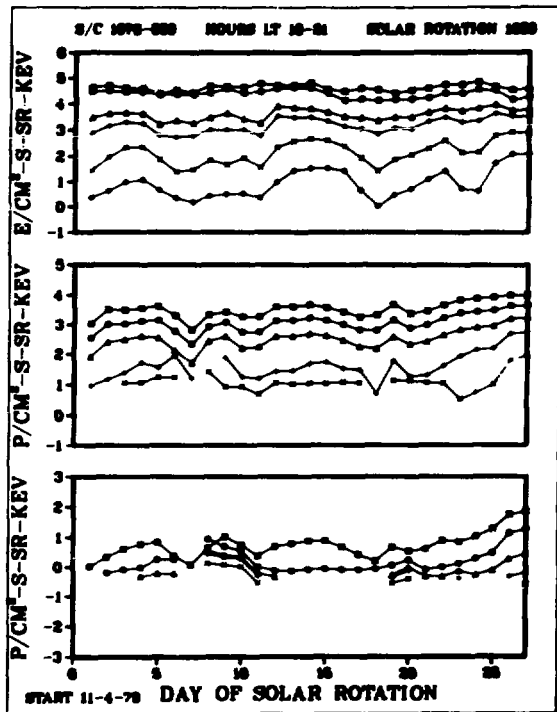
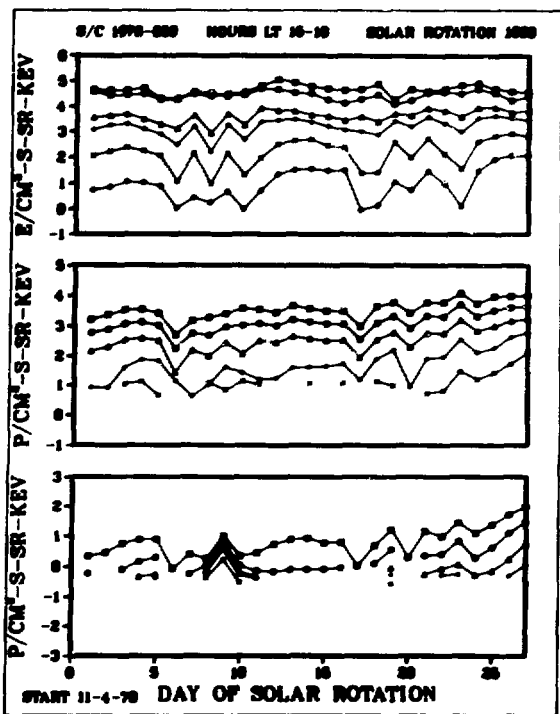
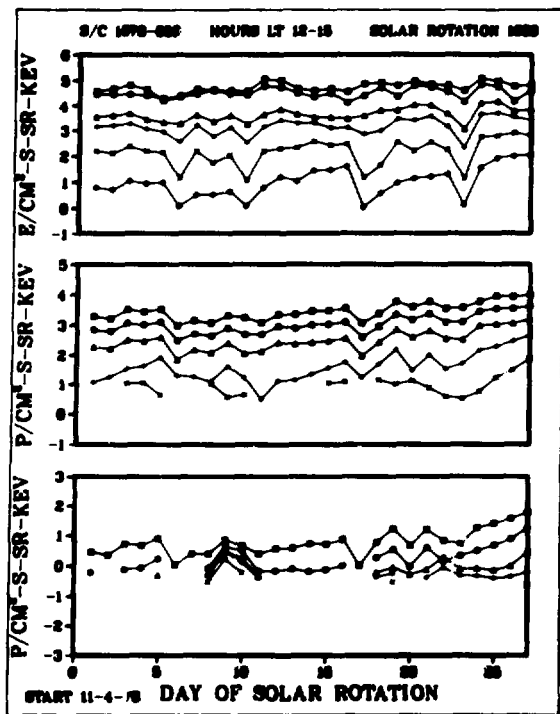
S/C 1976-039



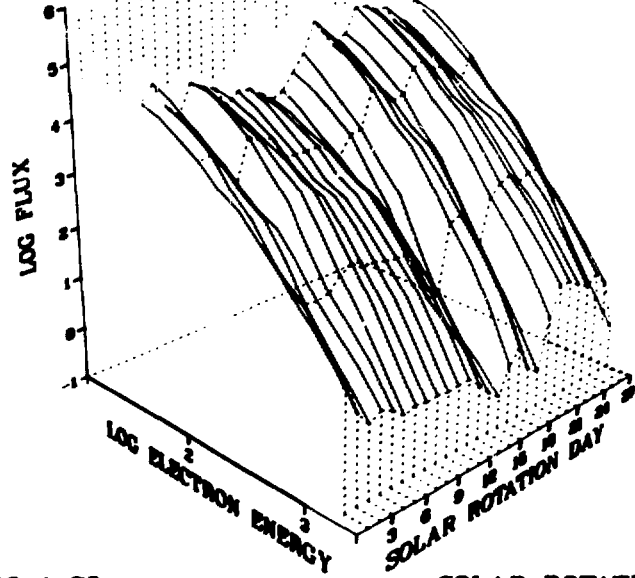
S/C 1976-039







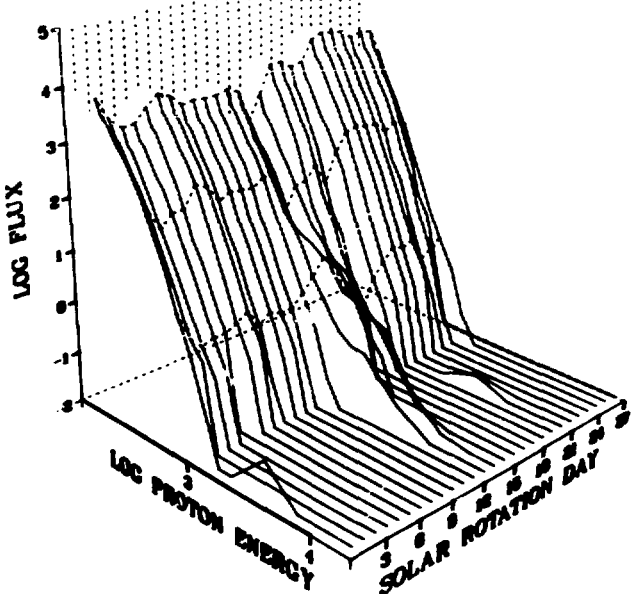
S C 1976-059



START 12-1-78

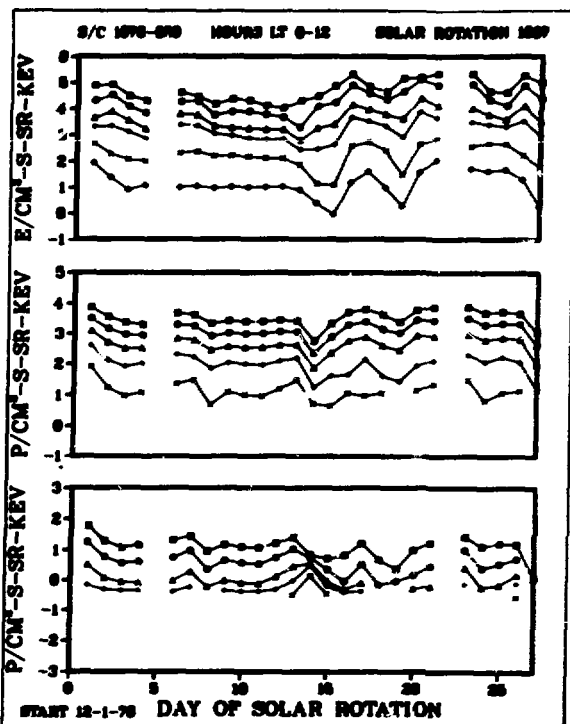
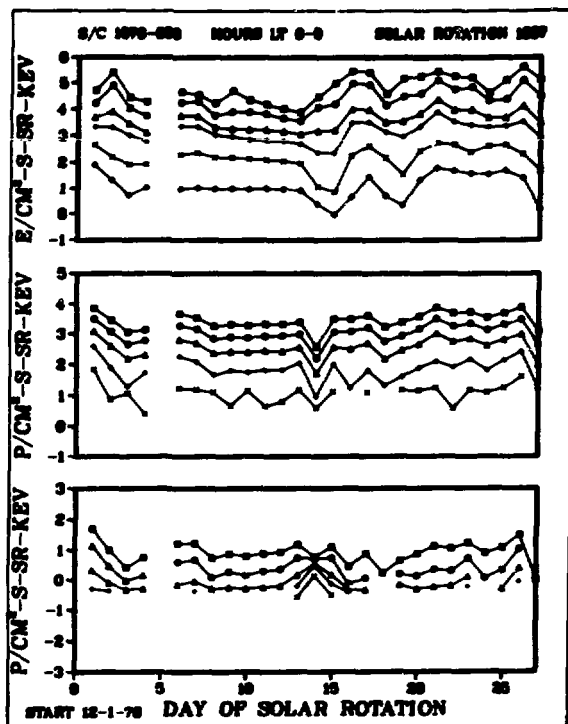
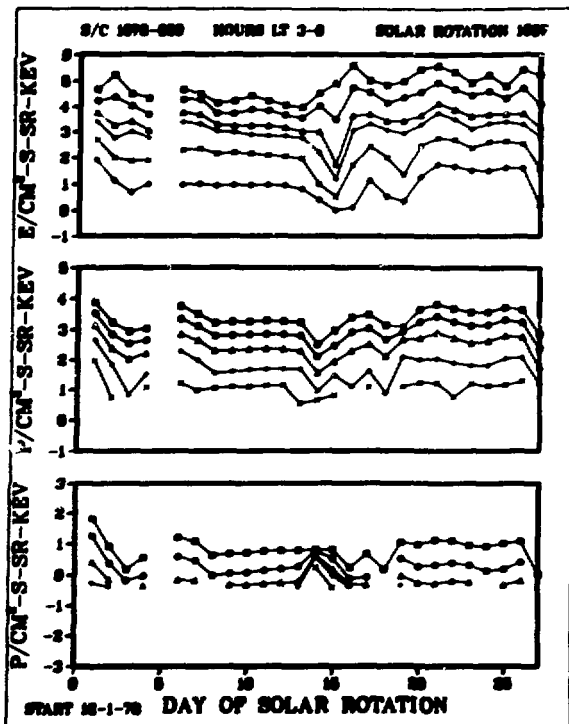
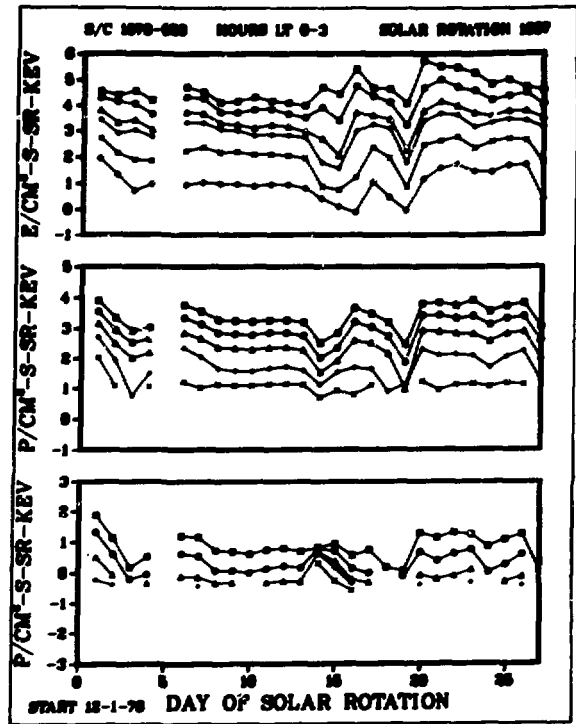
SOLAR ROTATION 1987

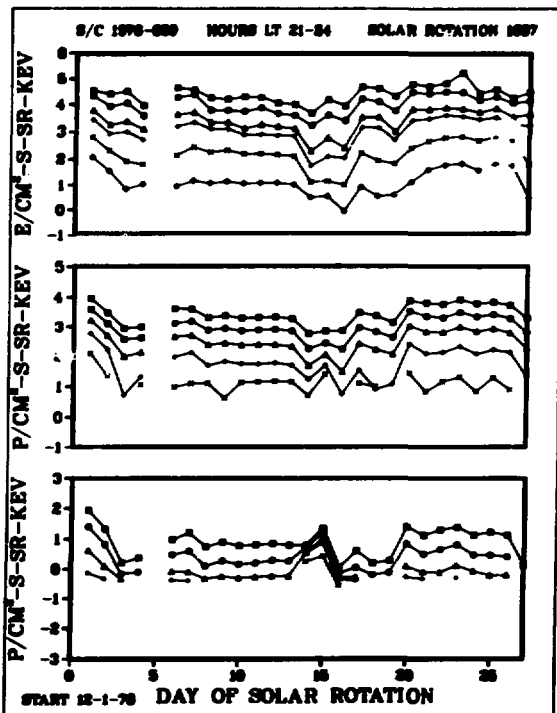
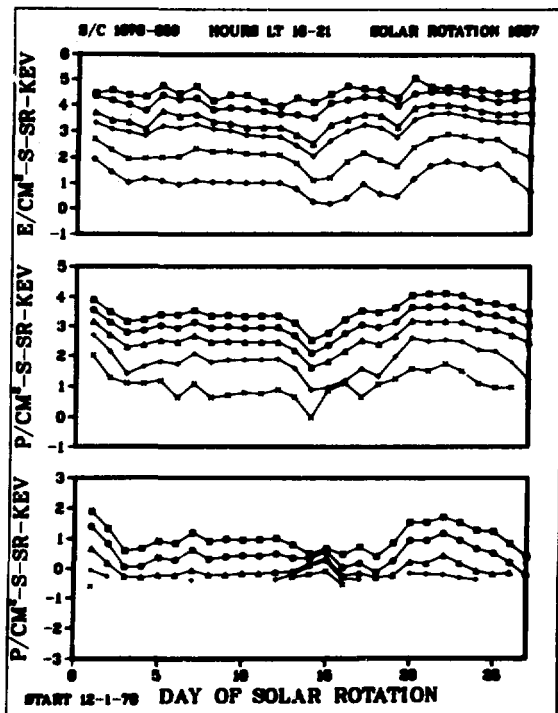
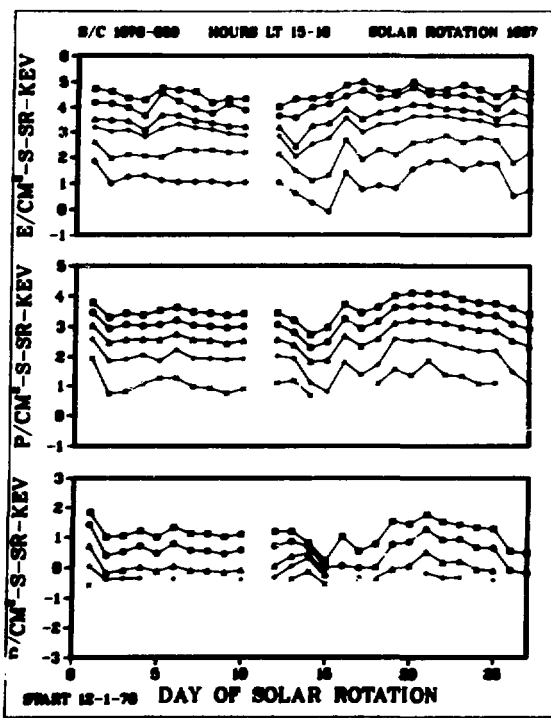
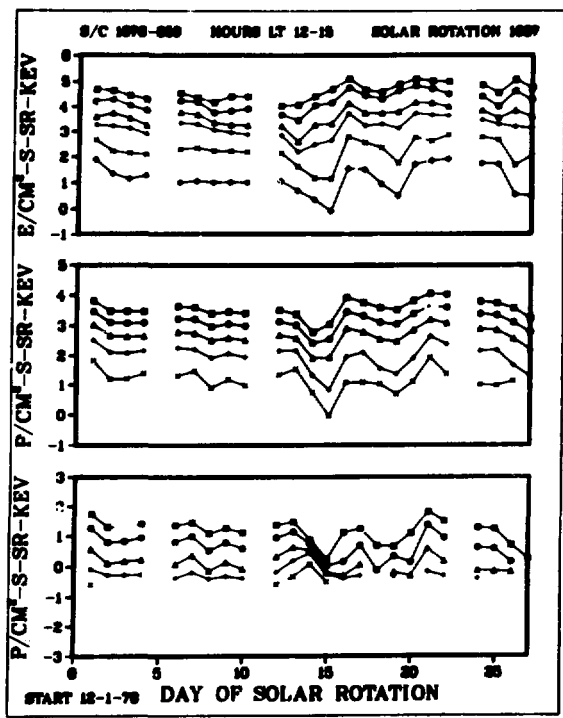
S C 1976-059



START 12-1-78

SOLAR ROTATION 1987

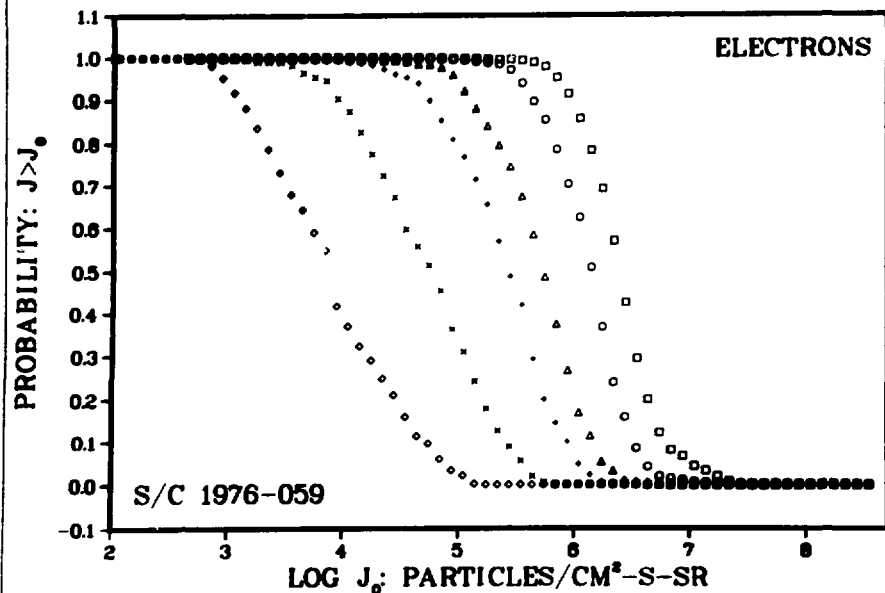




LOCAL TIME: 21-03

PERIOD: 070176-123176

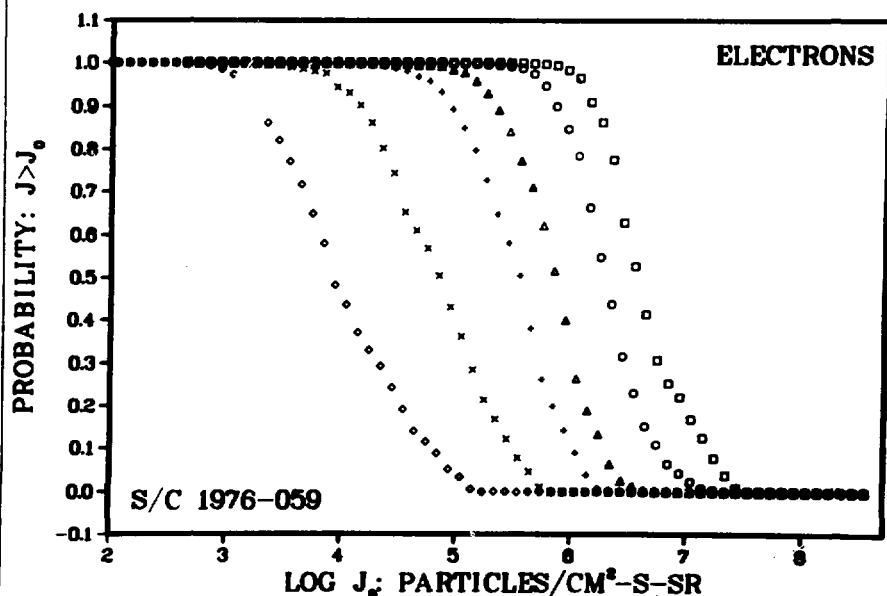
FLUX PROBABILITIES



LOCAL TIME: 03-09

PERIOD: 070176-123176

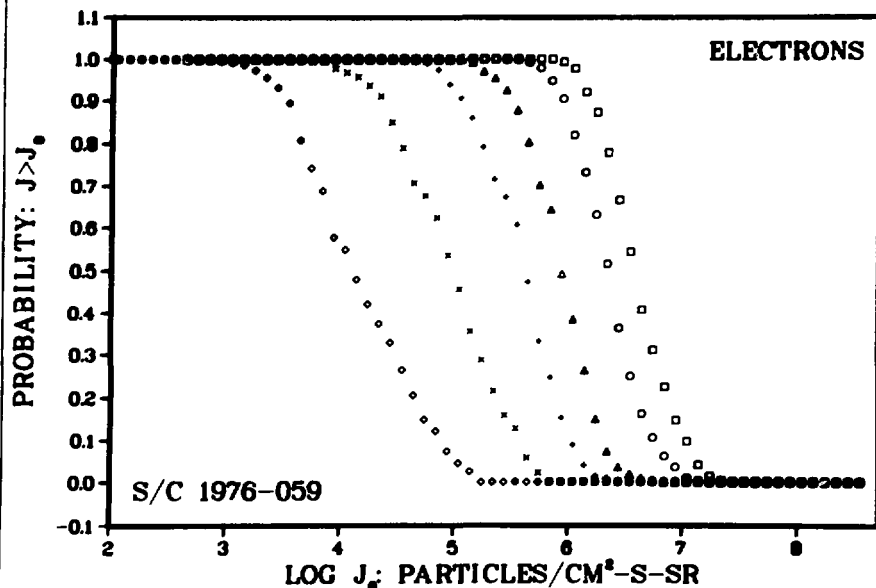
FLUX PROBABILITIES



LOCAL TIME: 09-15

PERIOD: 070176-123176

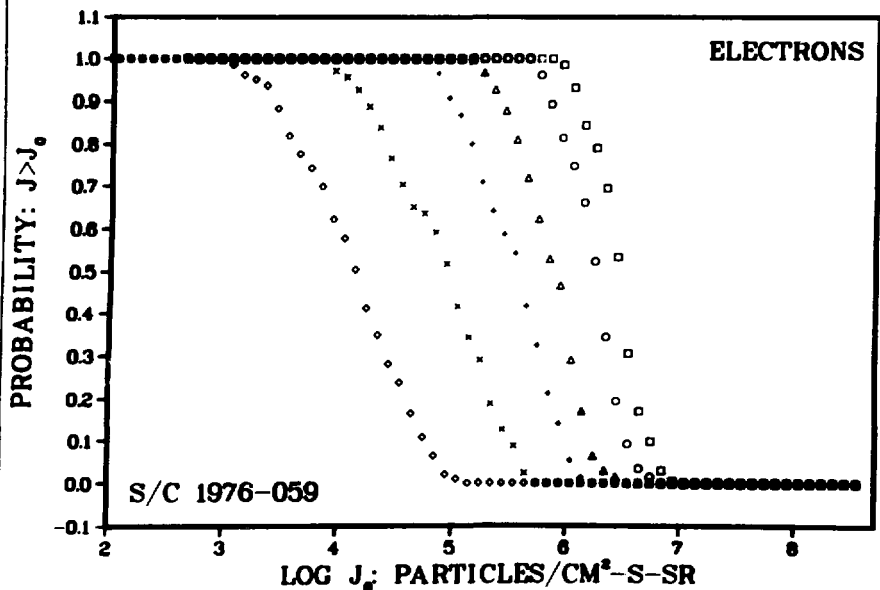
FLUX PROBABILITIES



LOCAL TIME: 15-21

PERIOD: 070176-123176

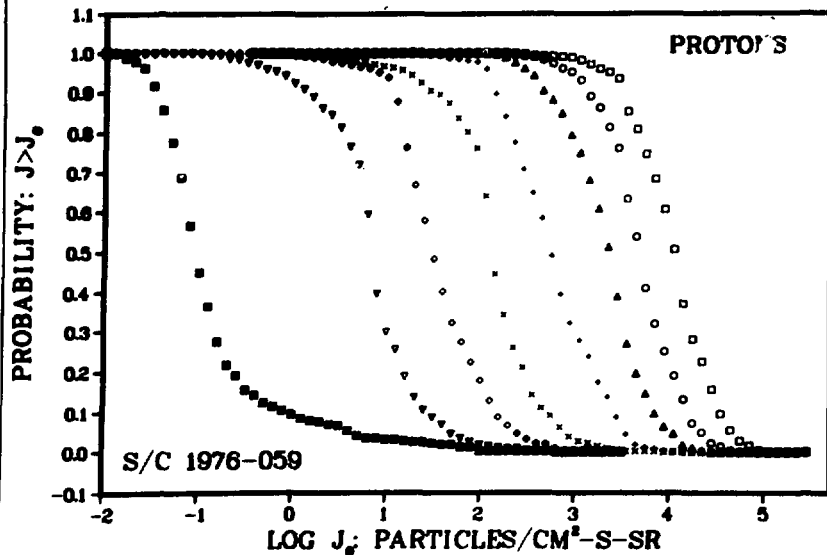
FLUX PROBABILITIES



LOCAL TIME: 21-03

PERIOD: 070176-123176

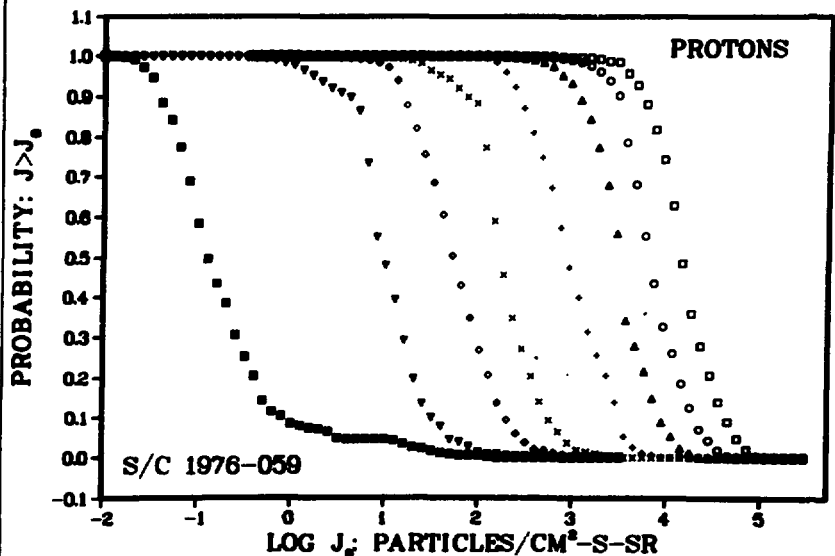
FLUX PROBABILITIES



LOCAL TIME: 03-09

PERIOD: 070176-123176

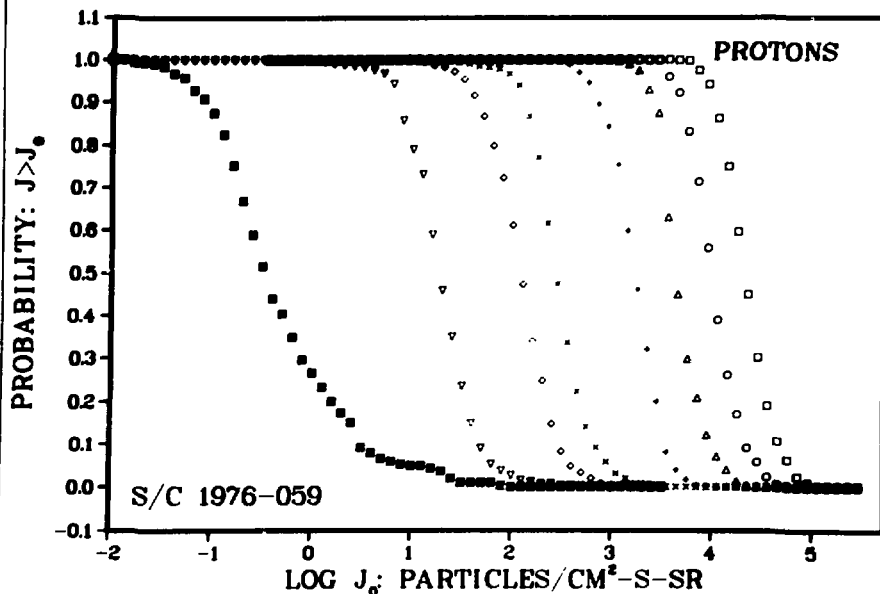
FLUX PROBABILITIES



LOCAL TIME: 09-15

PERIOD: 070176-123176

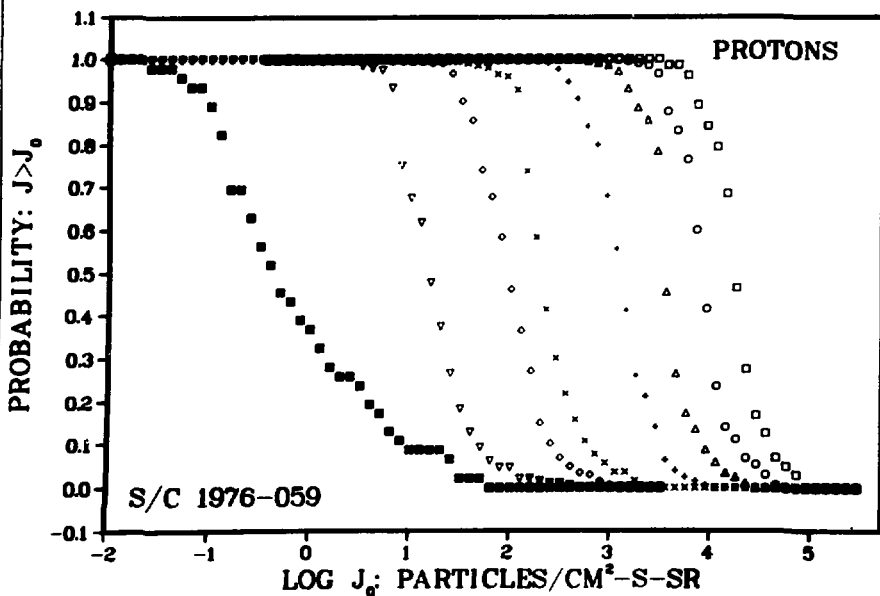
FLUX PROBABILITIES

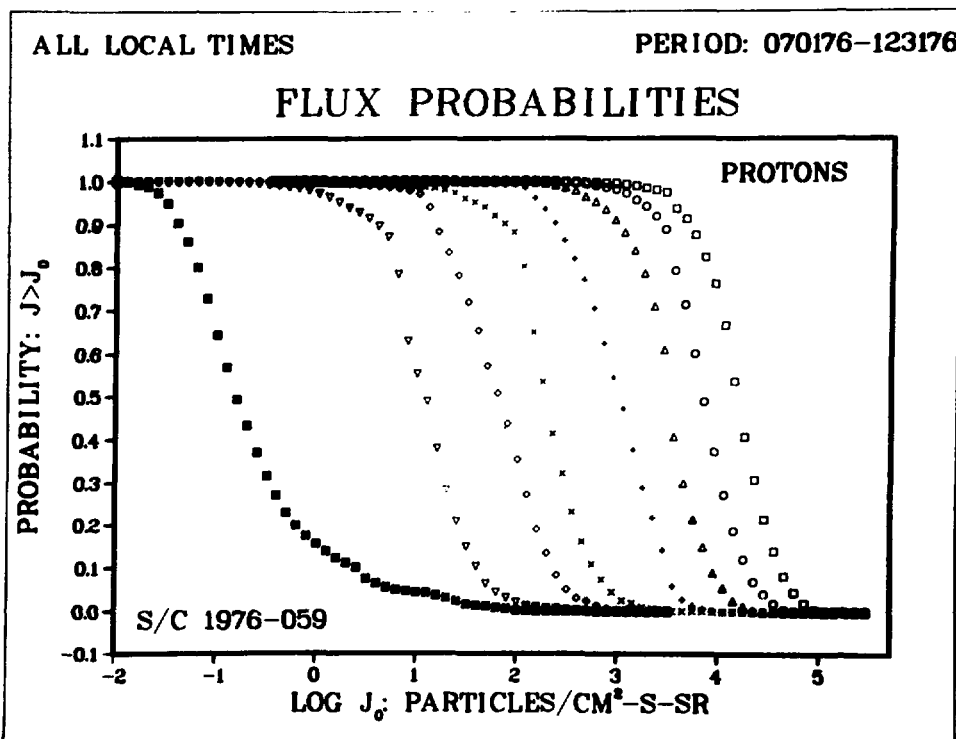
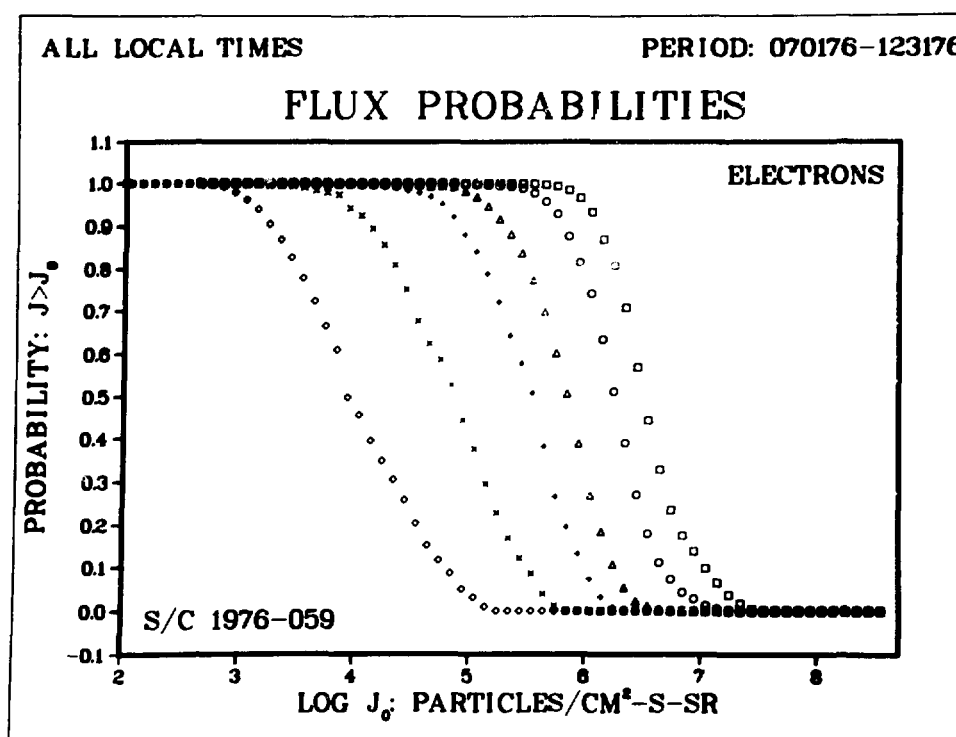


LOCAL TIME: 15-21

PERIOD: 070176-123176

FLUX PROBABILITIES

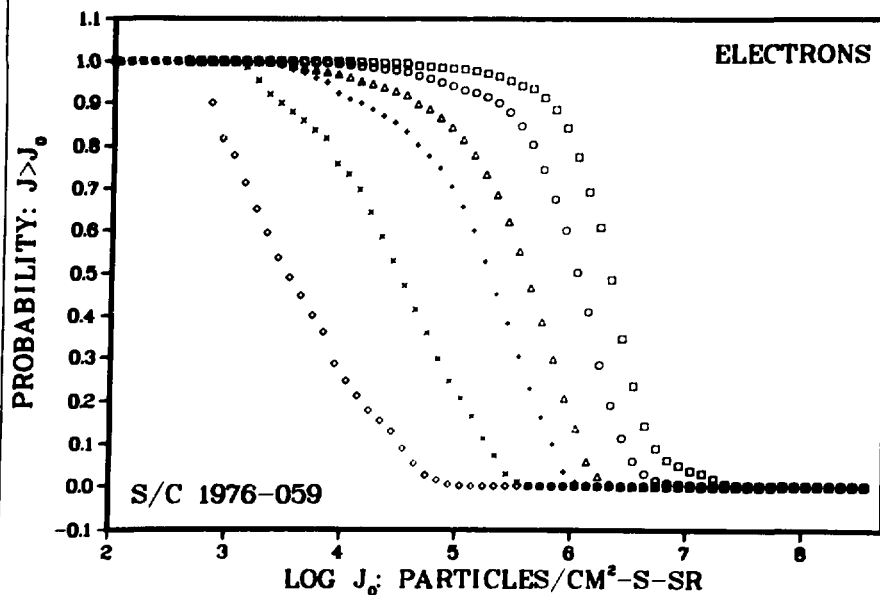




LOCAL TIME: 21-03

PERIOD: 010177-123177

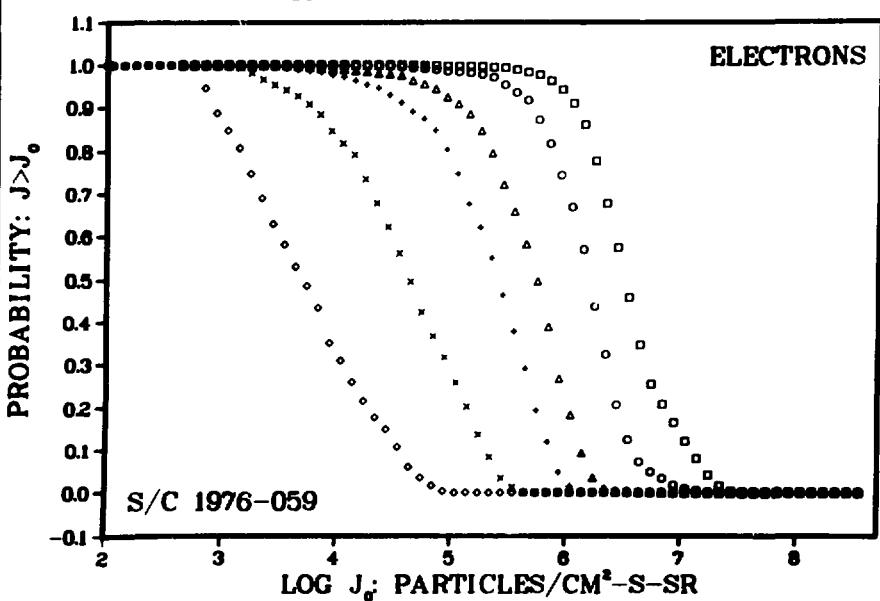
FLUX PROBABILITIES



LOCAL TIME: 03-09

PERIOD: 010177-123177

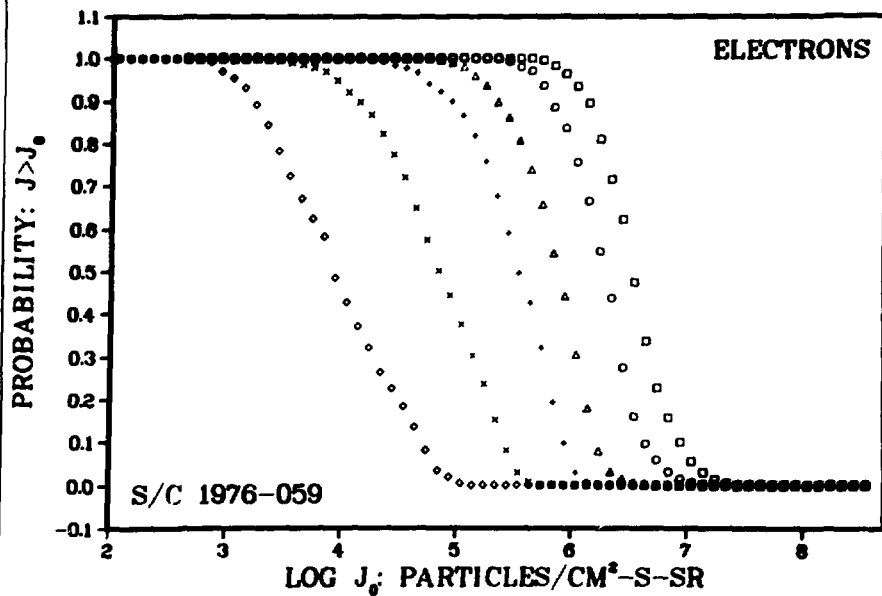
FLUX PROBABILITIES



LOCAL TIME: 09-15

PERIOD: 010177-123177

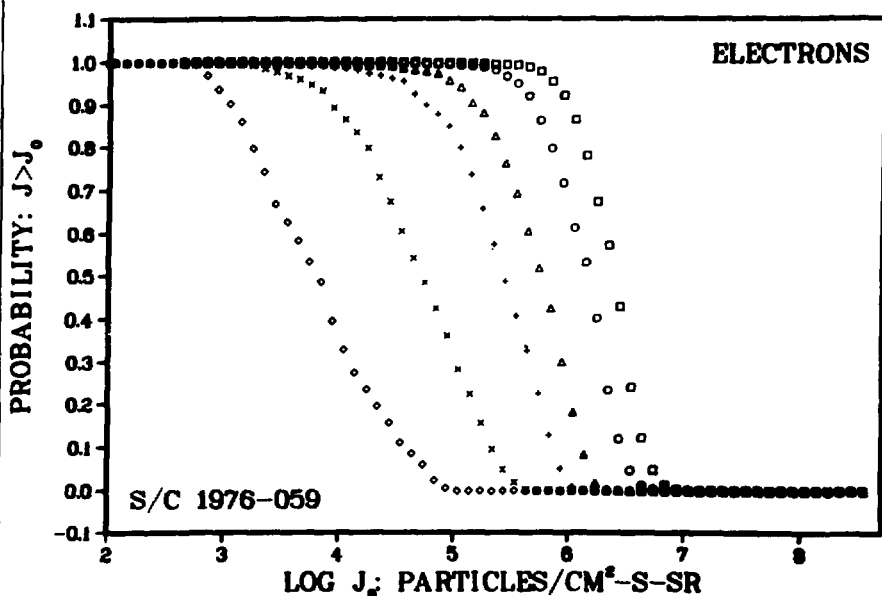
FLUX PROBABILITIES



LOCAL TIME: 15-21

PERIOD: 010177-123177

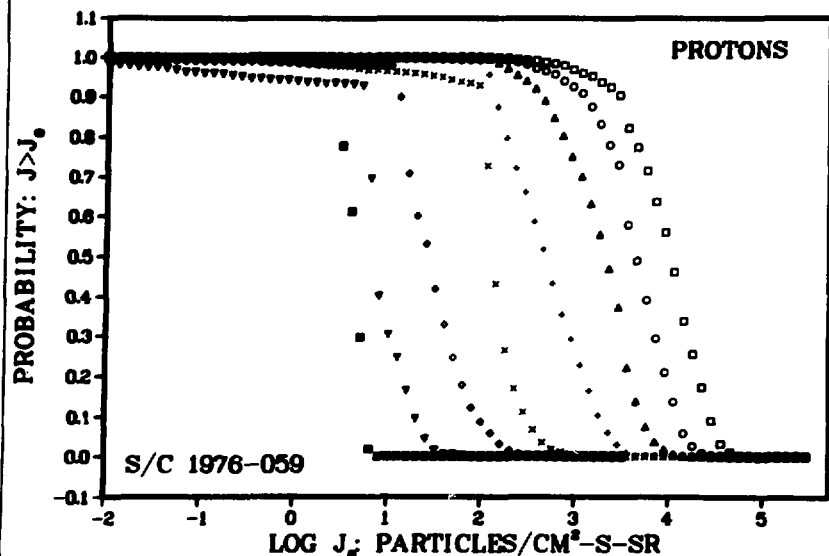
FLUX PROBABILITIES



LOCAL TIME: 03-09

PERIOD: 010177-123177

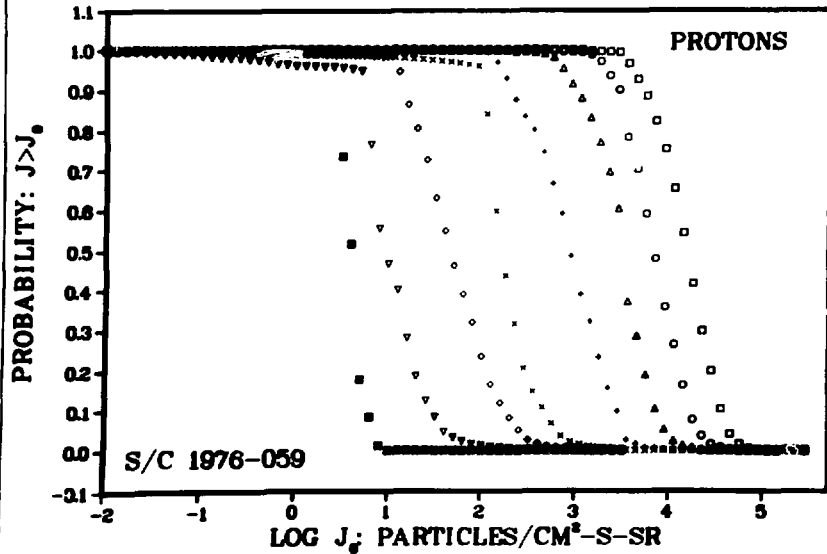
FLUX PROBABILITIES



LOCAL TIME: 09-15

PERIOD: 010177-123177

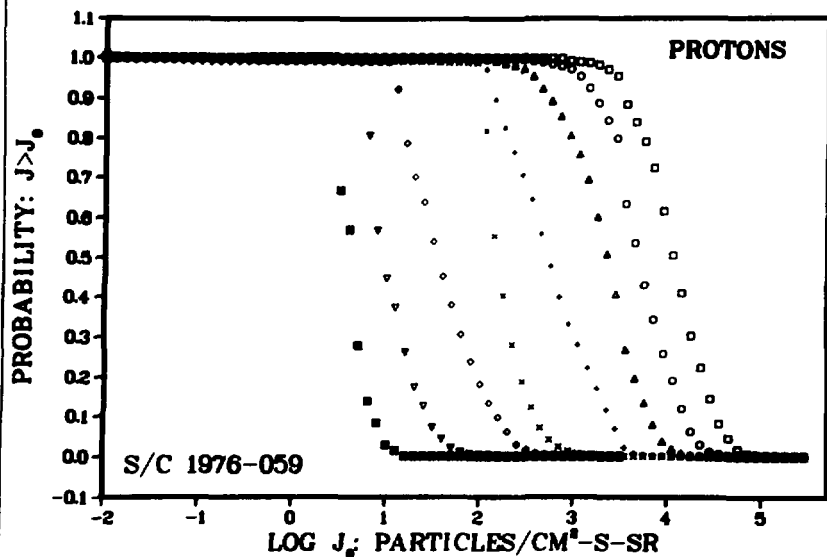
FLUX PROBABILITIES



LOCAL TIME: 15-21

PERIOD: 010177-123177

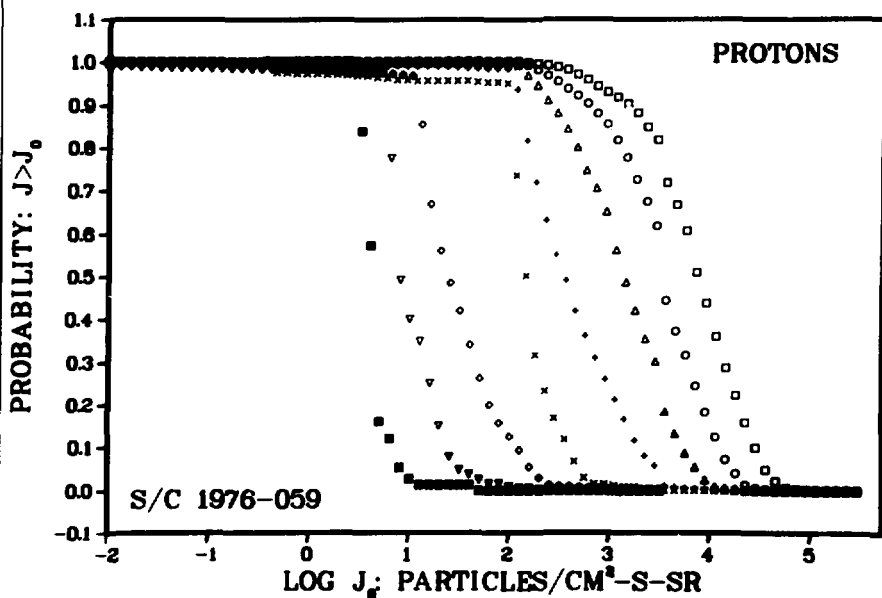
FLUX PROBABILITIES



LOCAL TIME: 21-03

PERIOD: 010177-123177

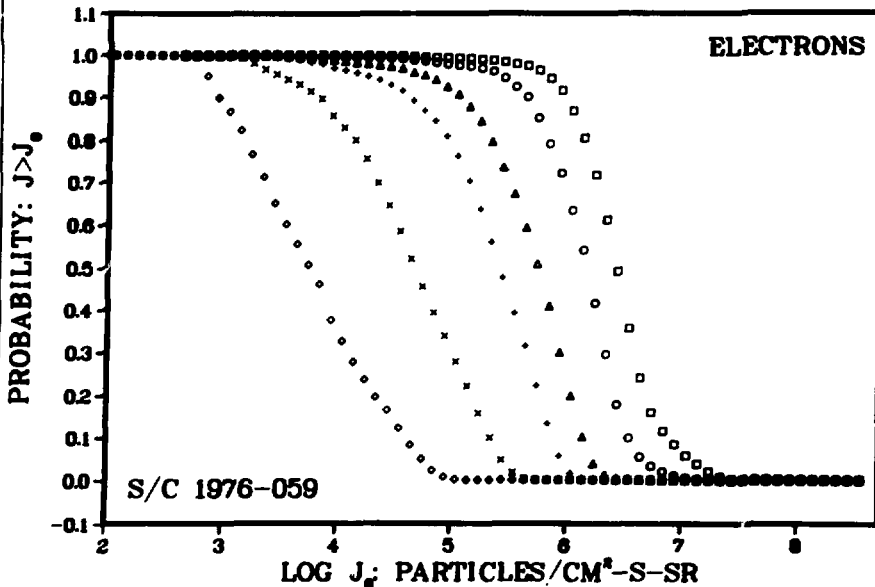
FLUX PROBABILITIES



ALL LOCAL TIMES

PERIOD: 010177-123177

FLUX PROBABILITIES



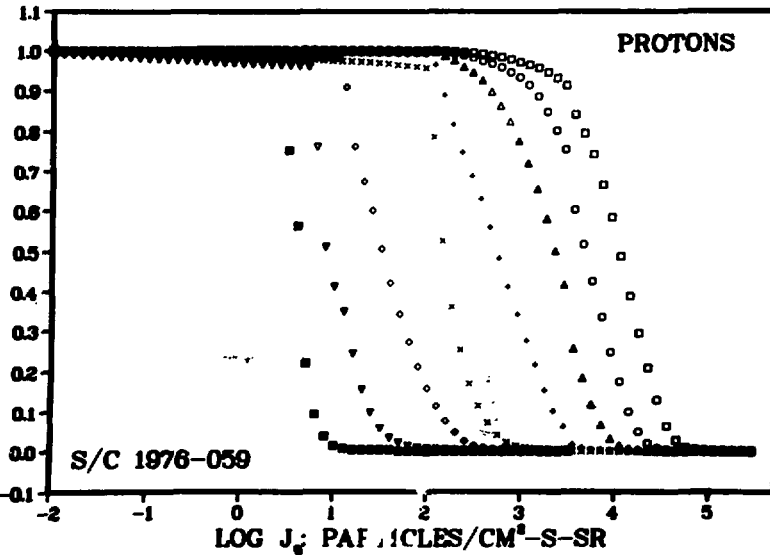
ALL LOCAL TIMES

PERIOD: 010177-123177

FLUX PROBABILITIES

PROBABILITY: $J \geq J_e$

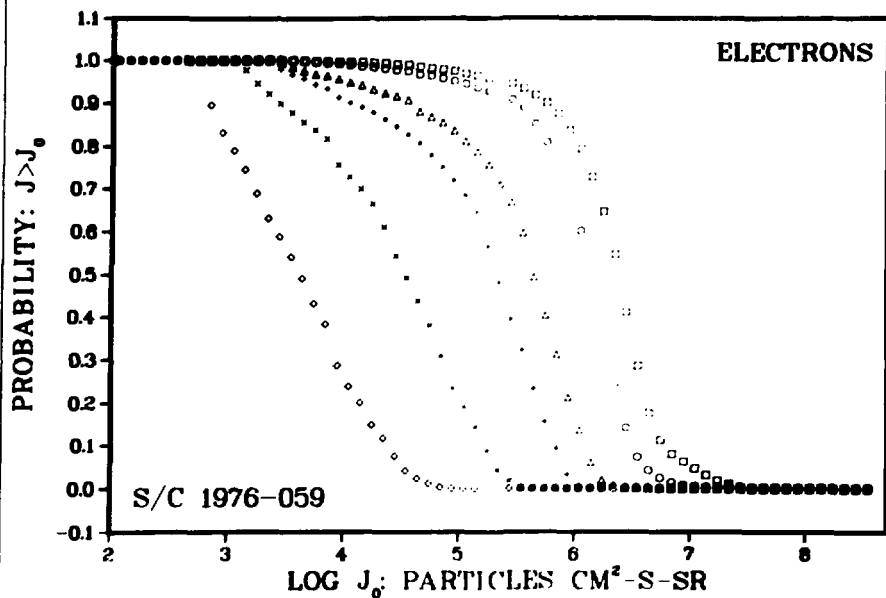
PROTONS



LOCAL TIME: 01-03

PERIOD: 010170-123170

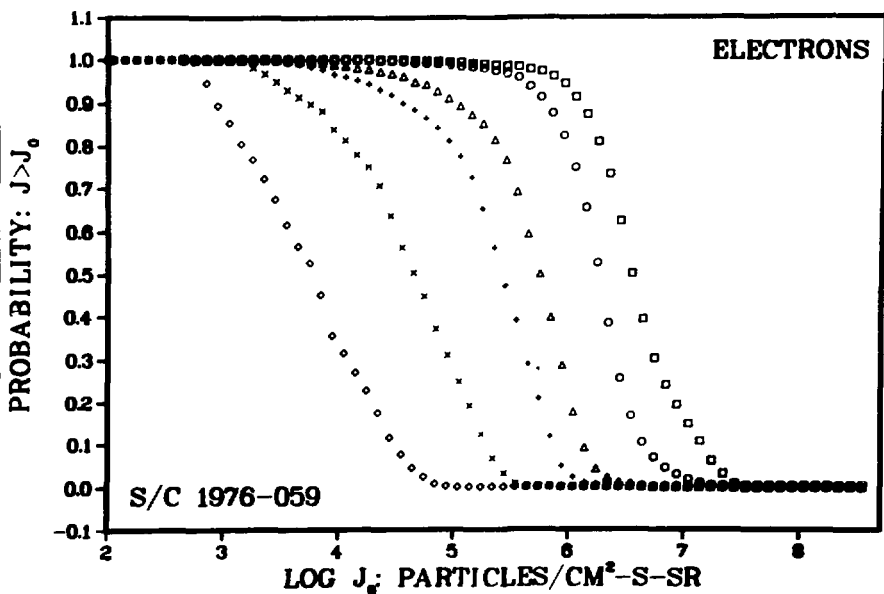
FLUX PROBABILITIES



LOCAL TIME: 03-09

PERIOD: 010178-123178

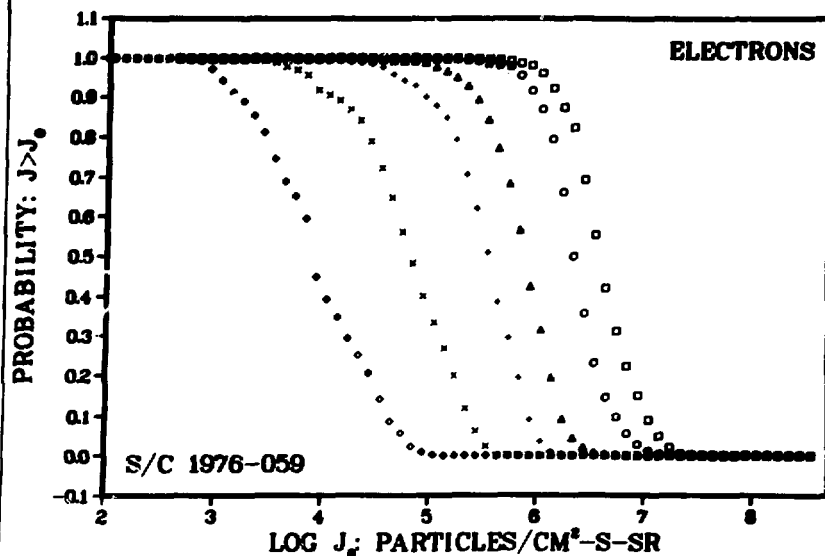
FLUX PROBABILITIES



LOCAL TIME: 09-15

PERIOD: 010178-123178

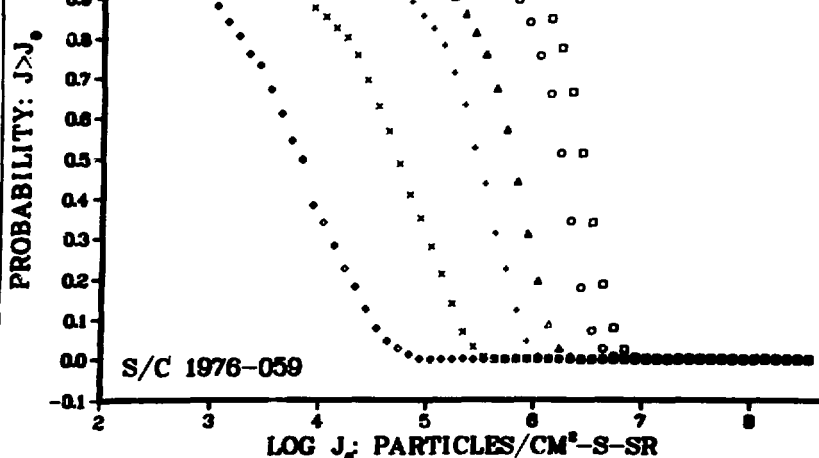
FLUX PROBABILITIES



LOCAL TIME: 15-21

PERIOD: 010178-123178

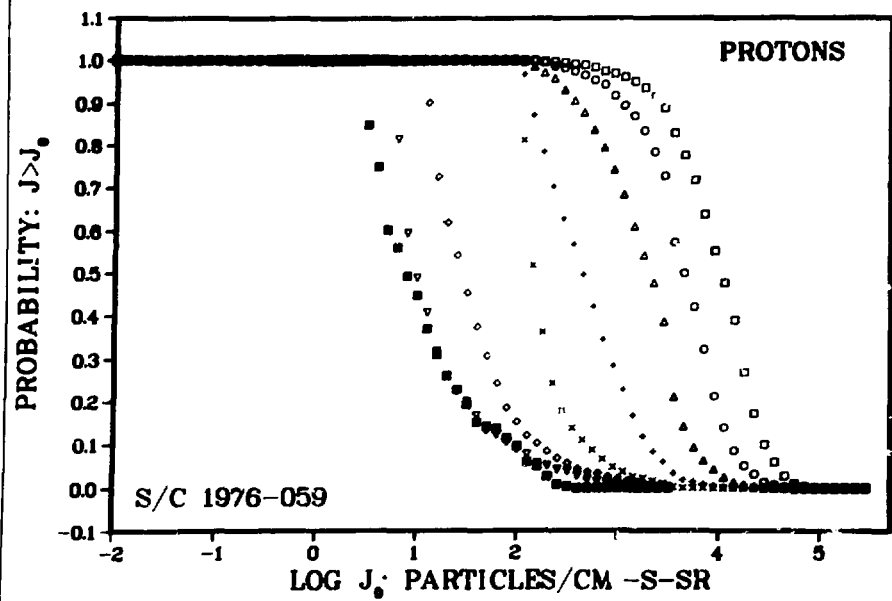
FLUX PROBABILITIES



LOCAL TIME: 03-09

PERIOD: 010178-123178

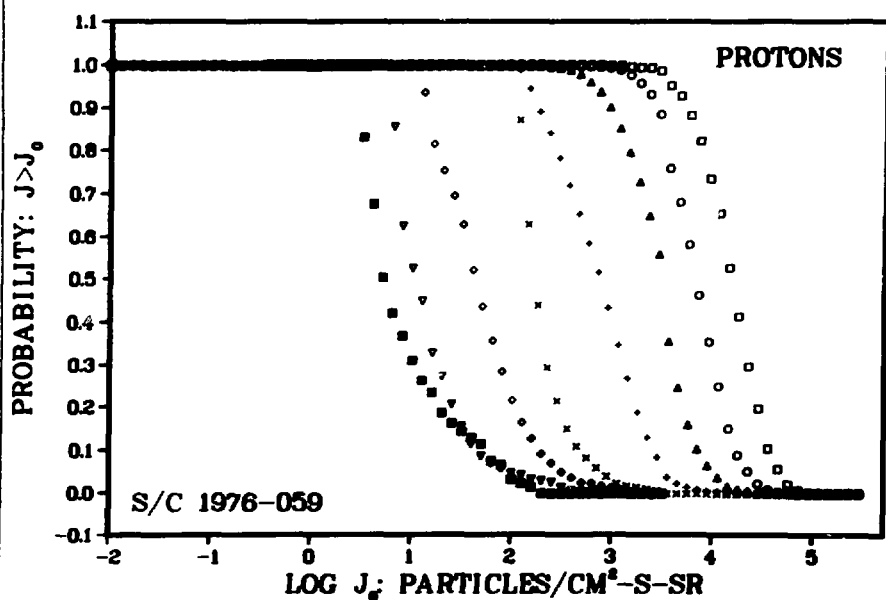
FLUX PROBABILITIES



LOCAL TIME: 09-15

PERIOD: 010178-123178

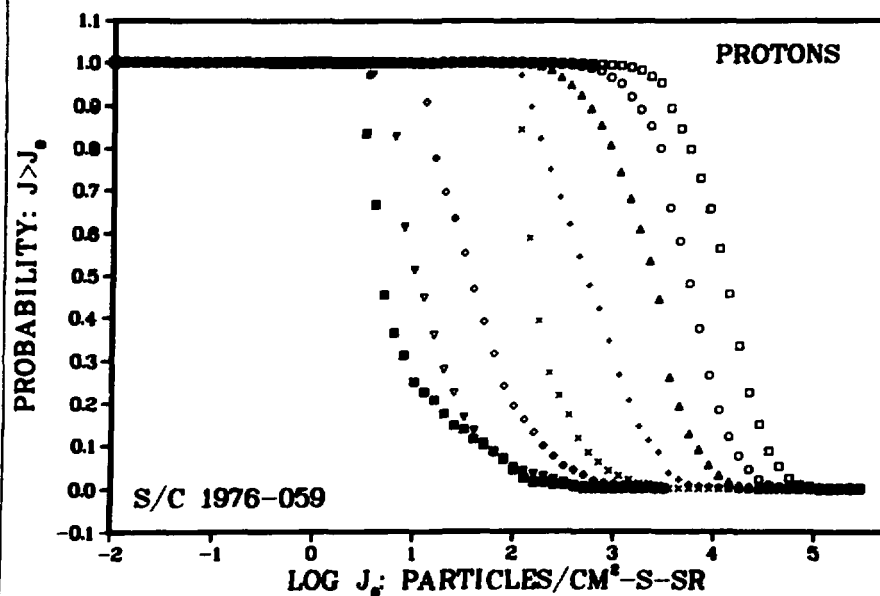
FLUX PROBABILITIES



LOCAL TIME: 15-21

PERIOD: 010178-123178

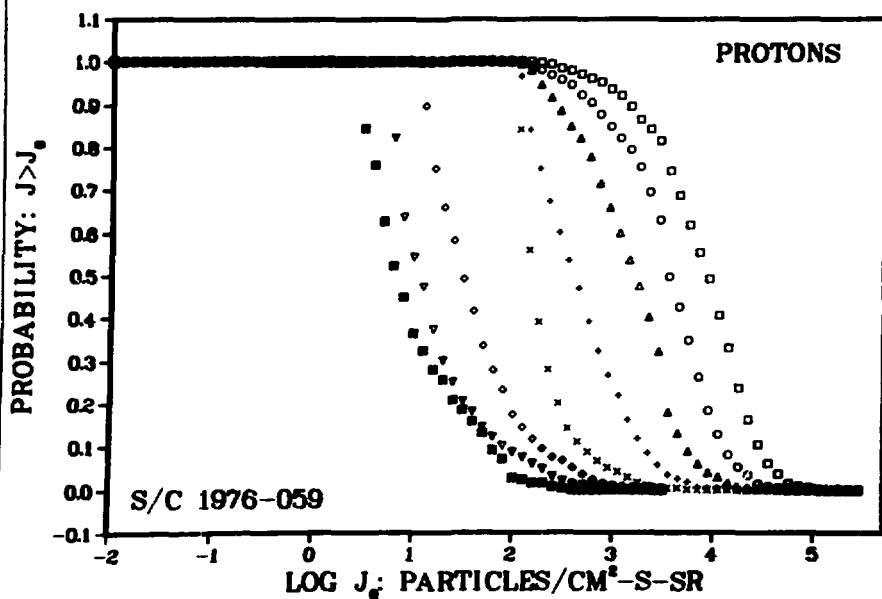
FLUX PROBABILITIES



LOCAL TIME: 21-03

PERIOD: 010178-123178

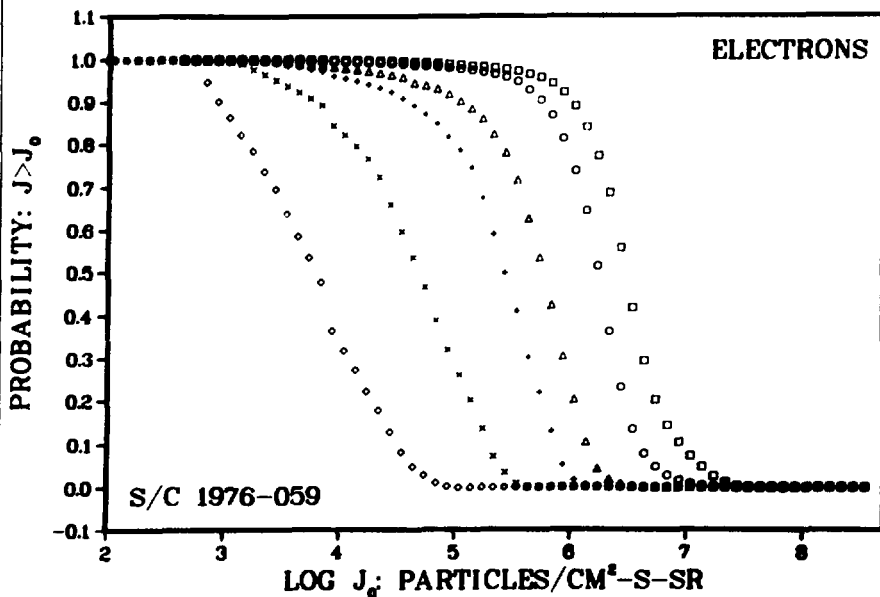
FLUX PROBABILITIES



ALL LOCAL TIMES

PERIOD: 010178-123178

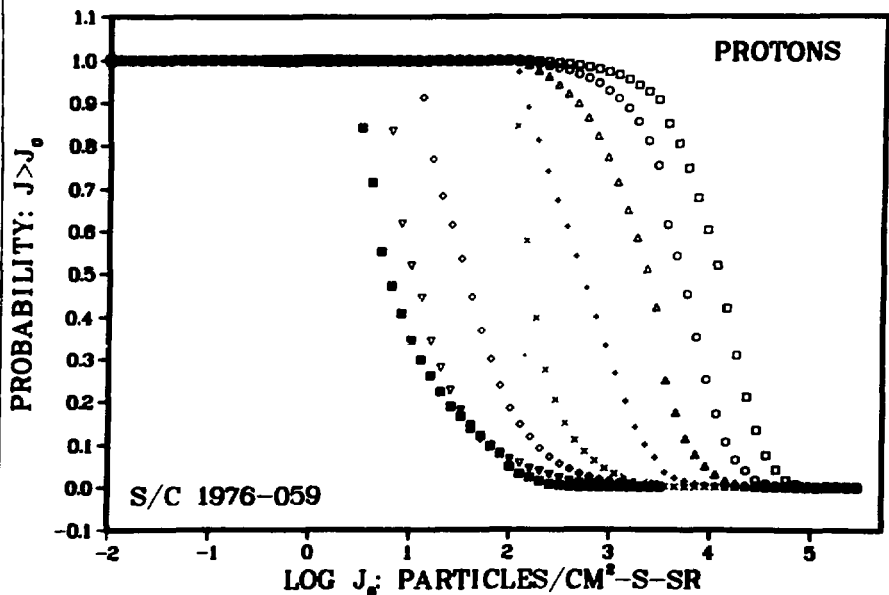
FLUX PROBABILITIES

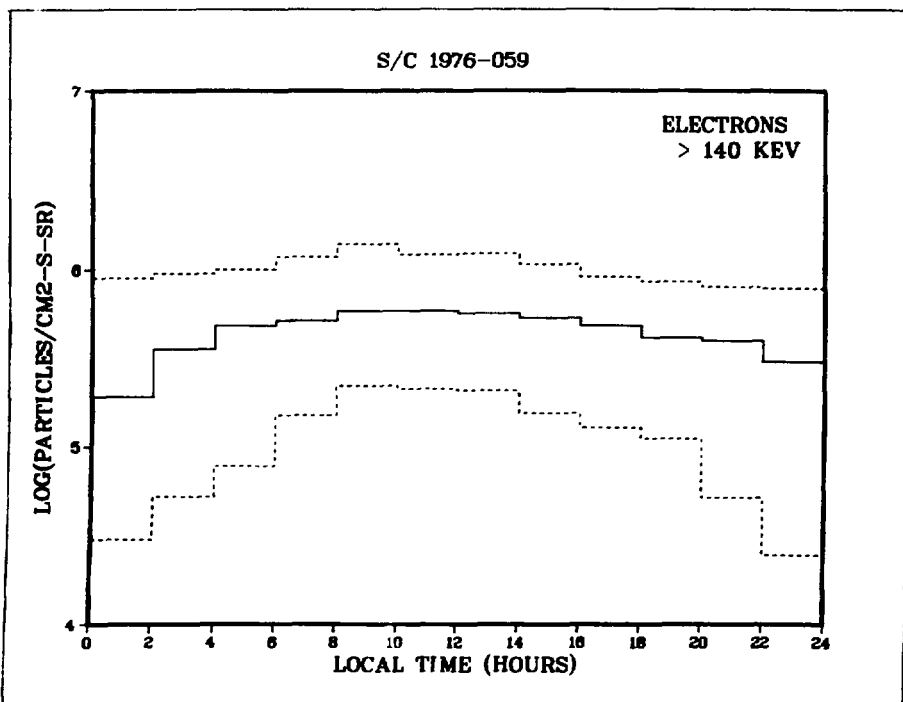
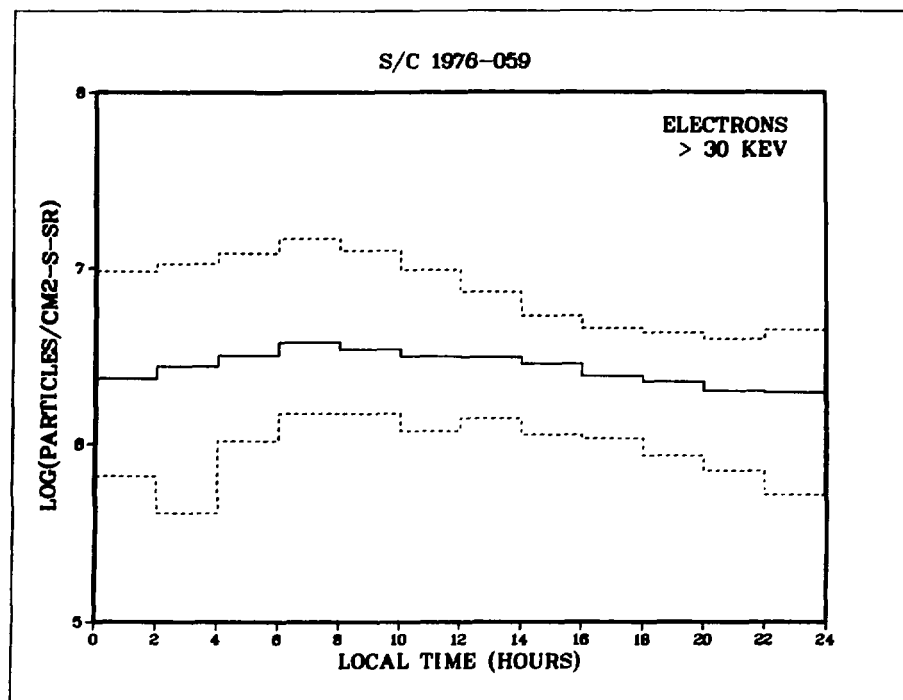


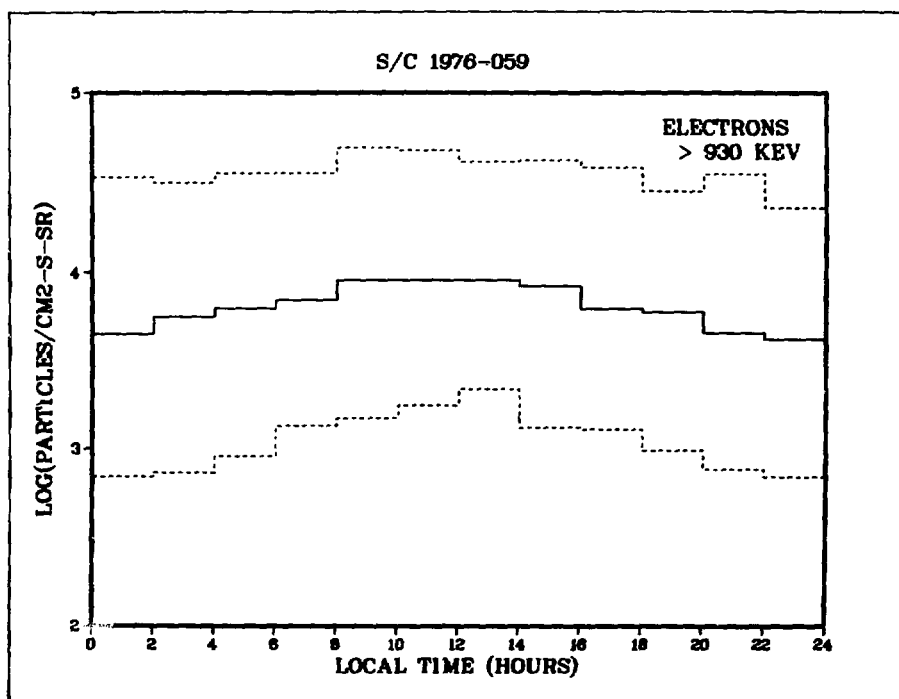
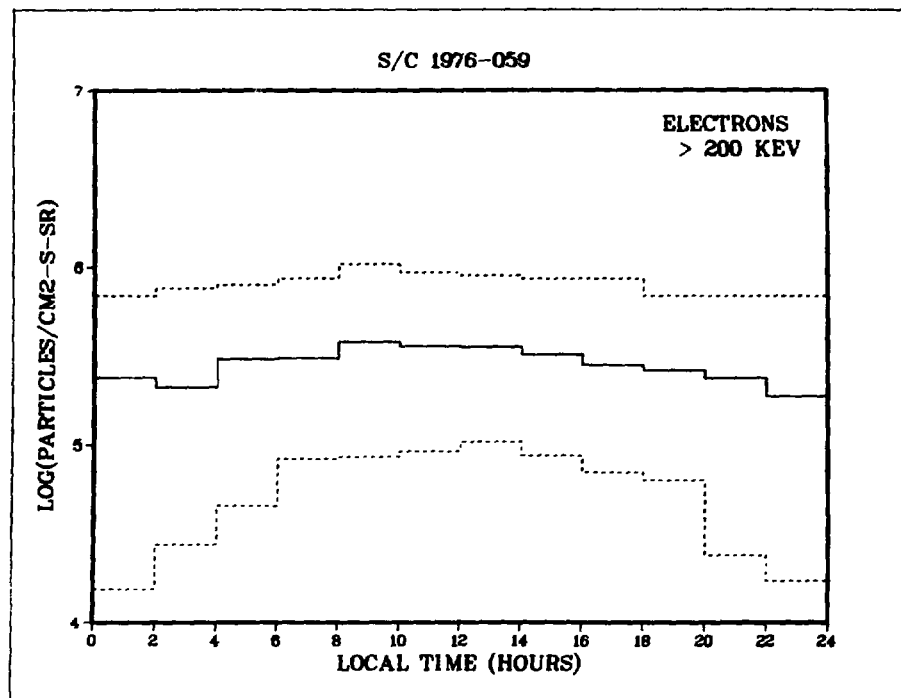
ALL LOCAL TIMES

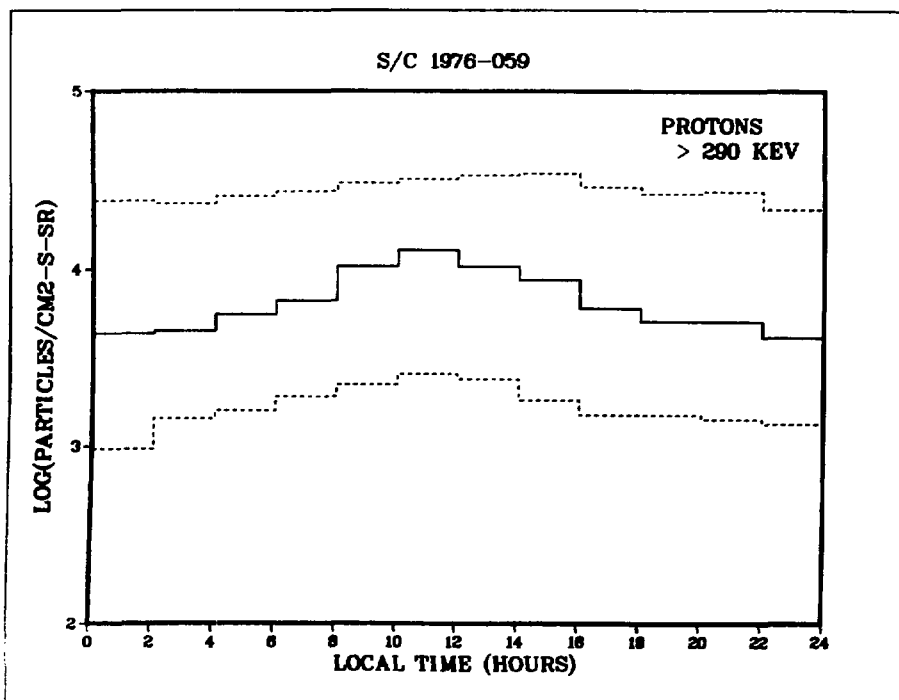
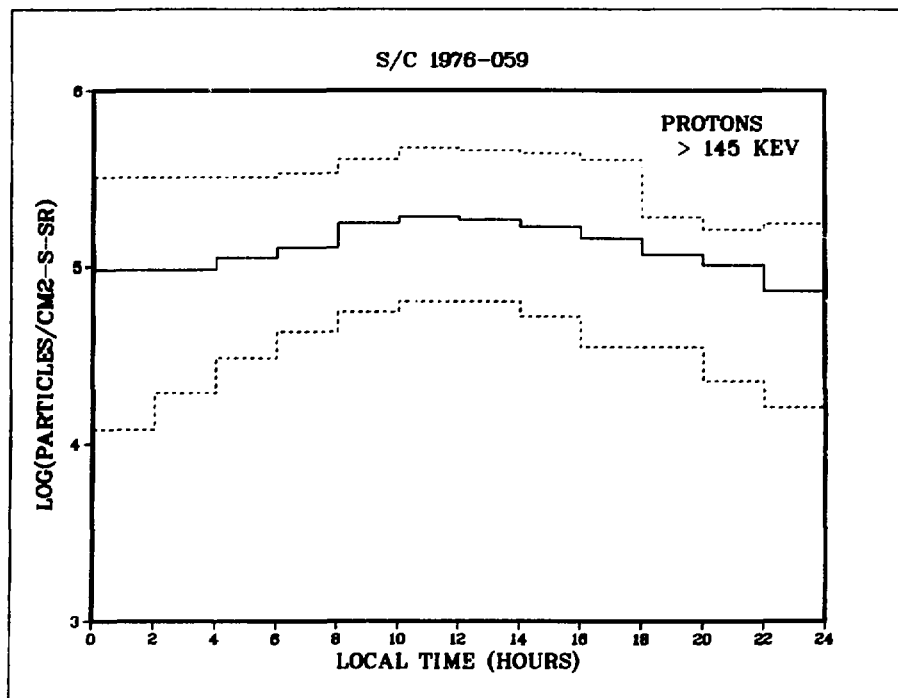
PERIOD: 010178-123178

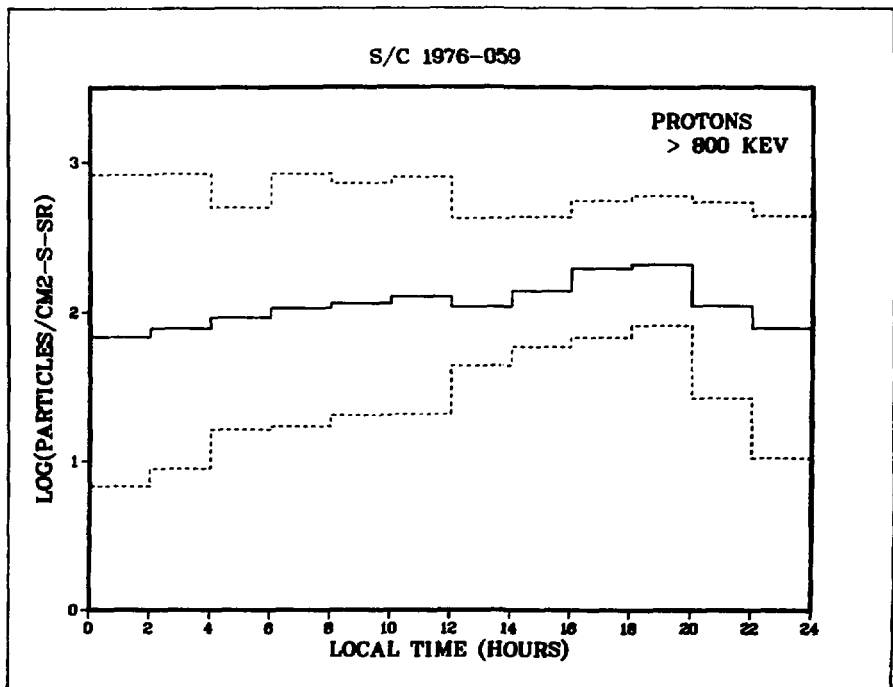
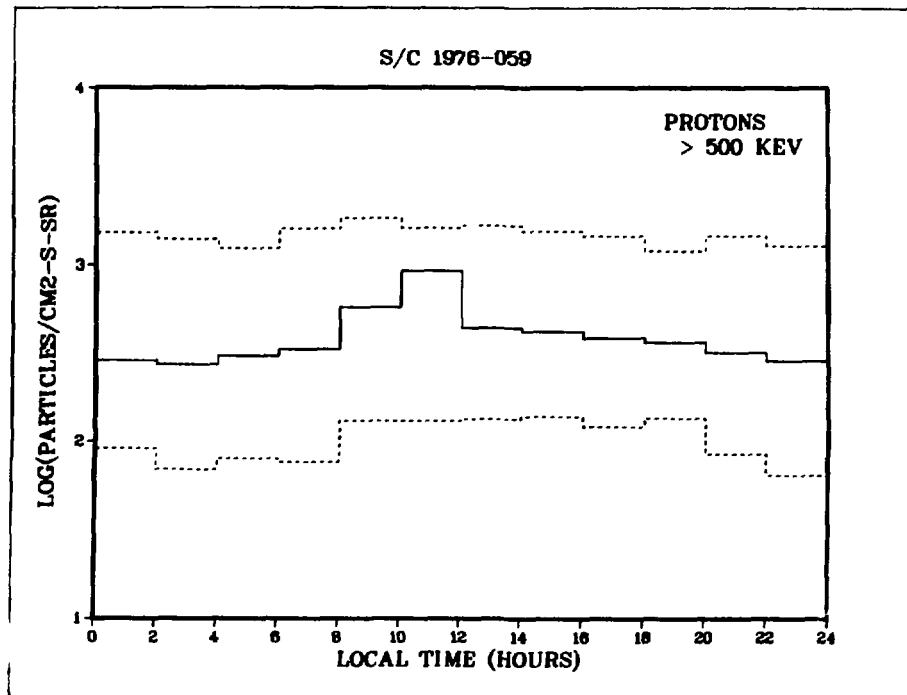
FLUX PROBABILITIES





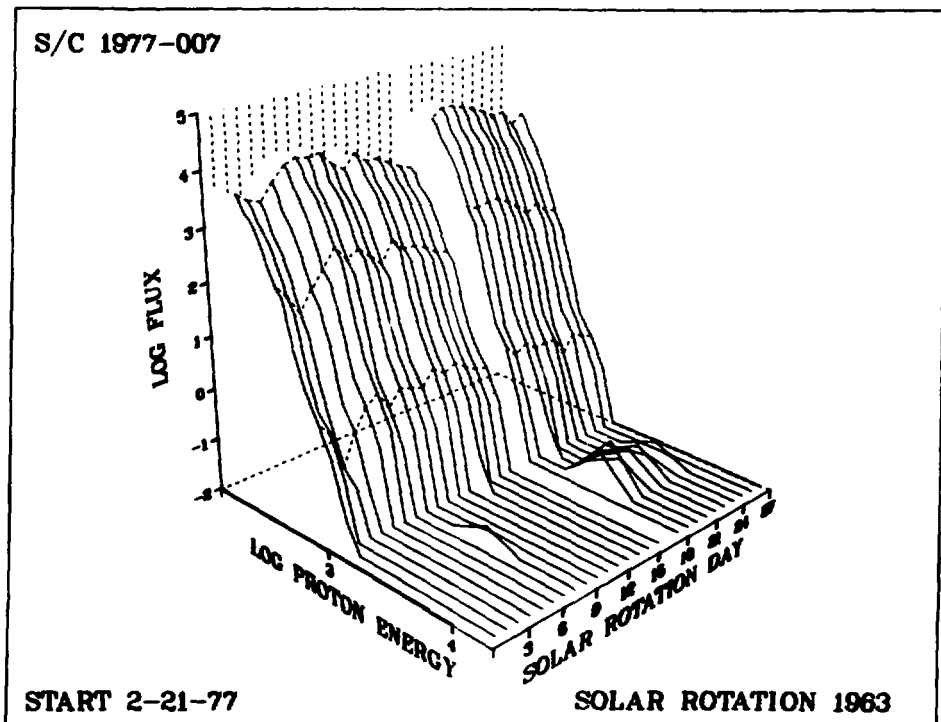
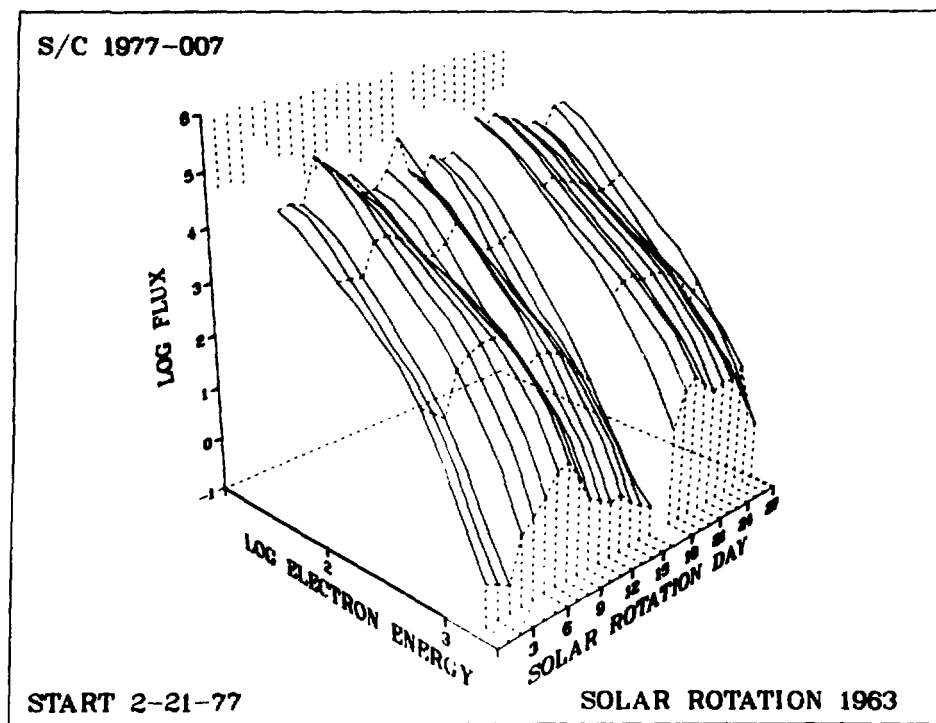


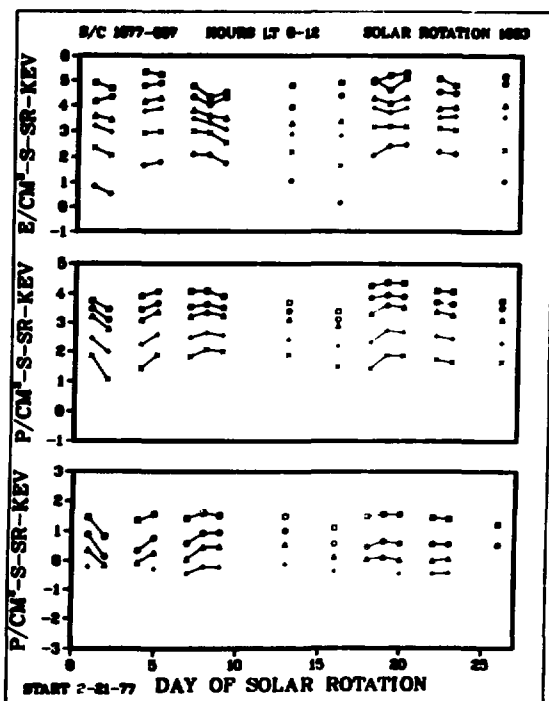
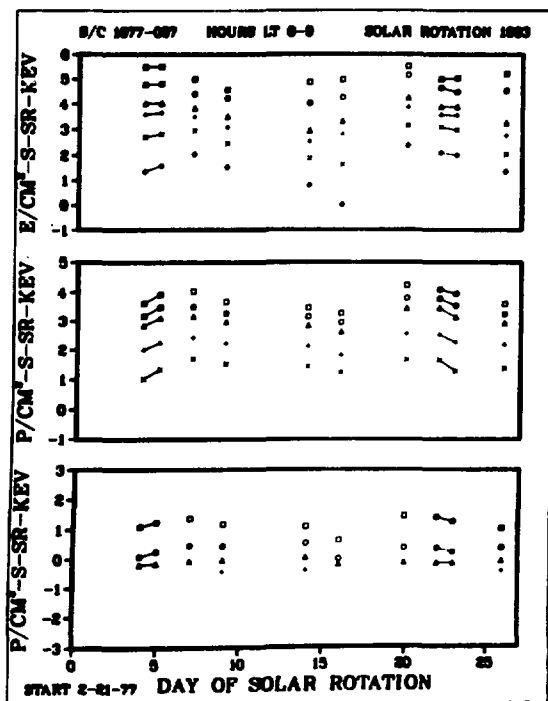
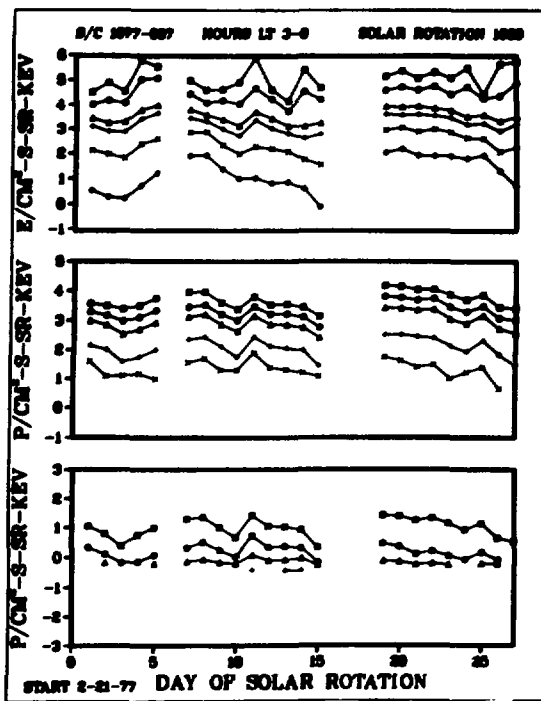
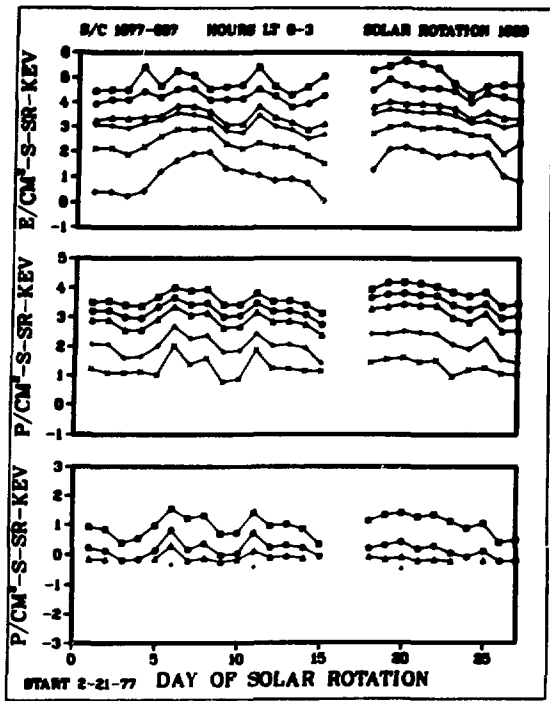


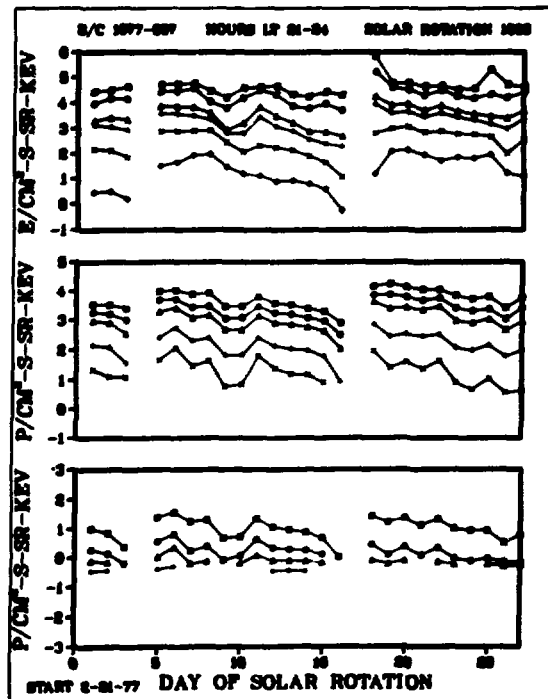
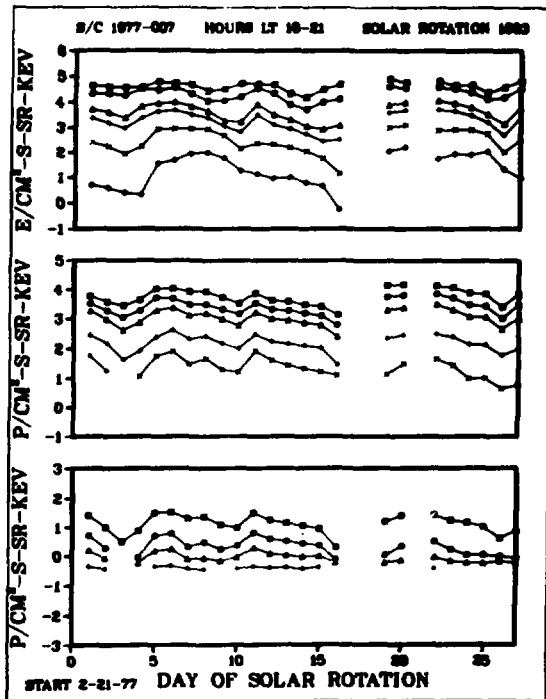
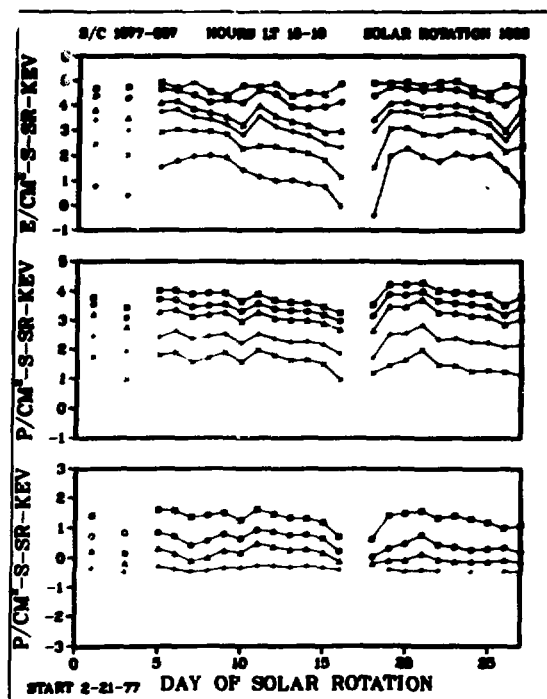
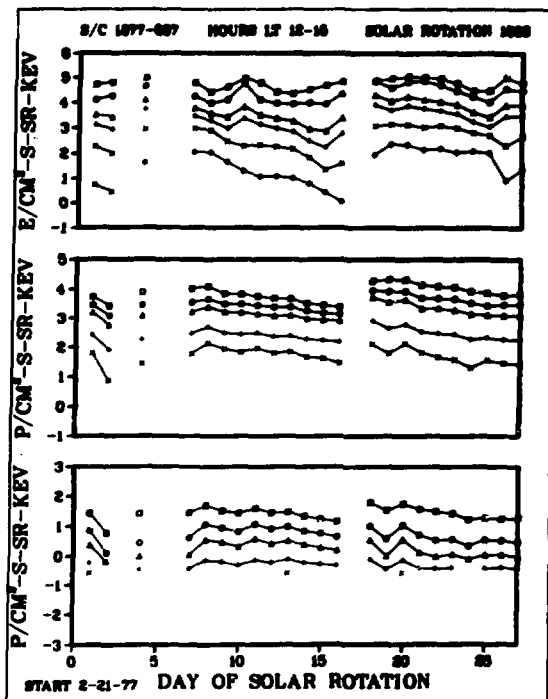


APPENDIX B

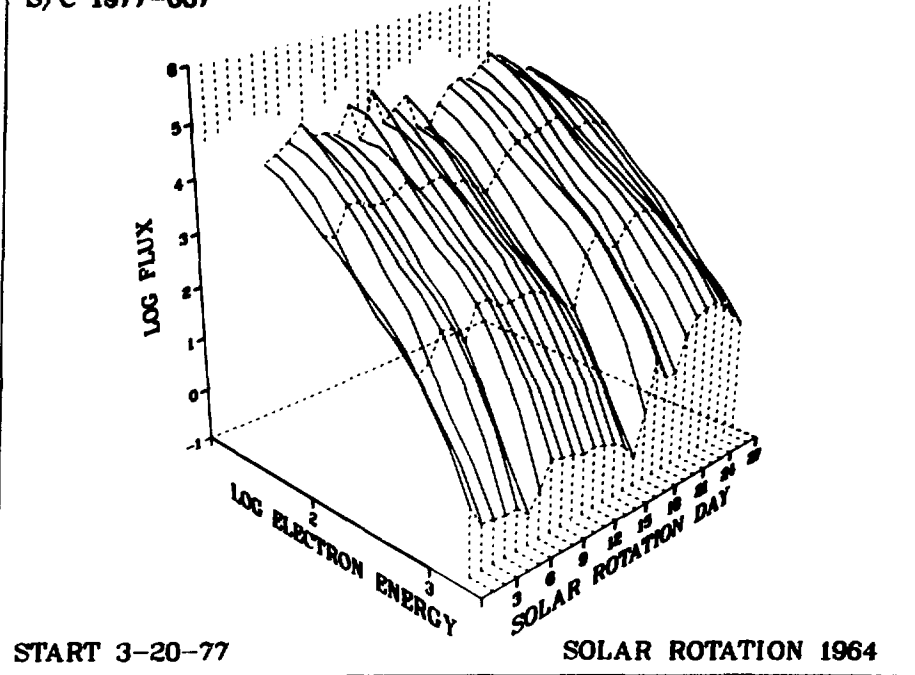
**DATA FOR S/C 1977-007, February 1977—December 1978
(SOLAR ROTATION NUMBERS 1963—1987)**



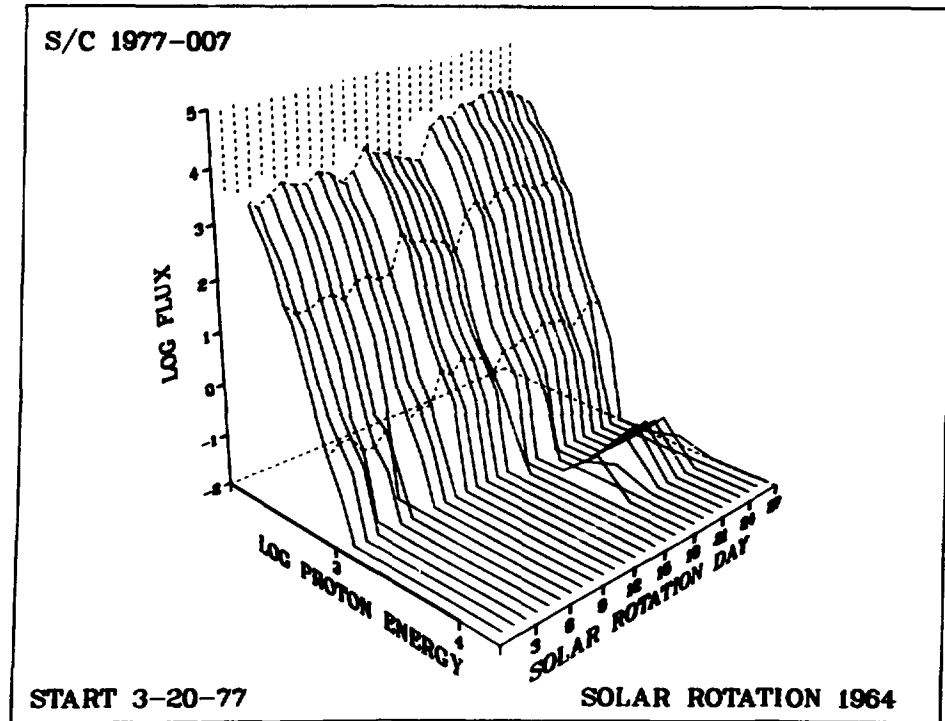


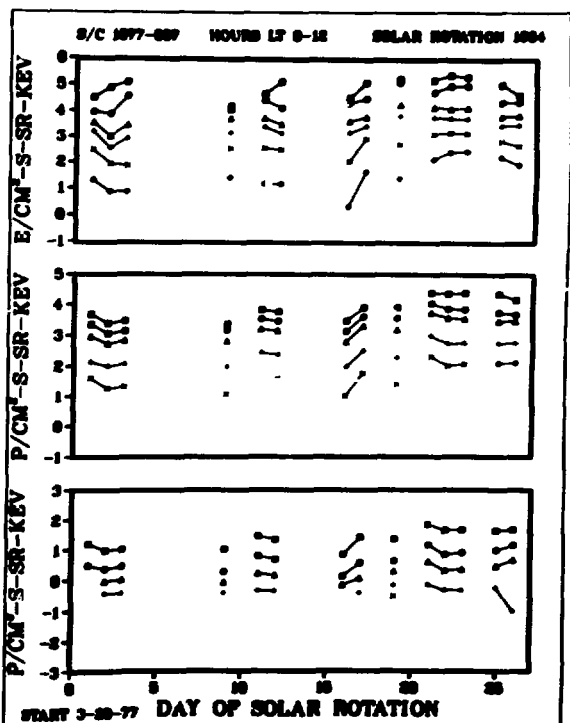
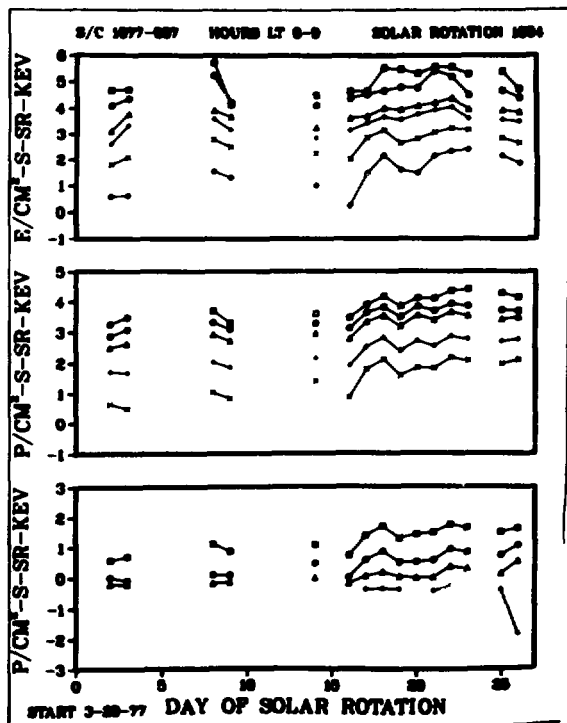
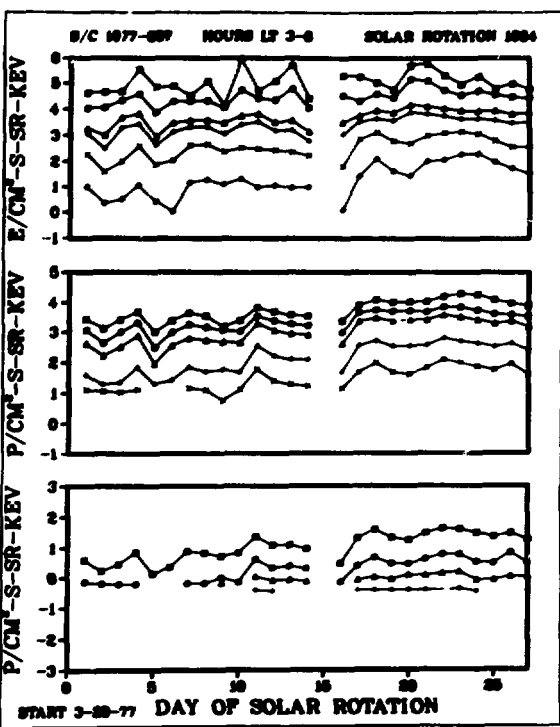
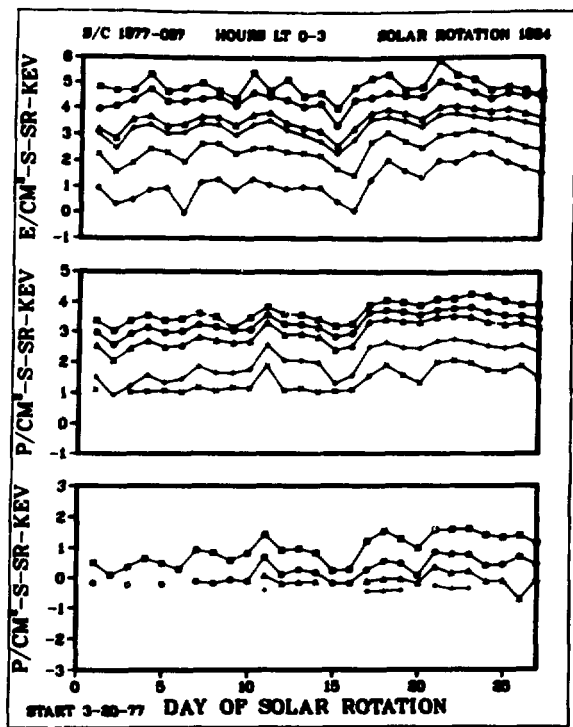


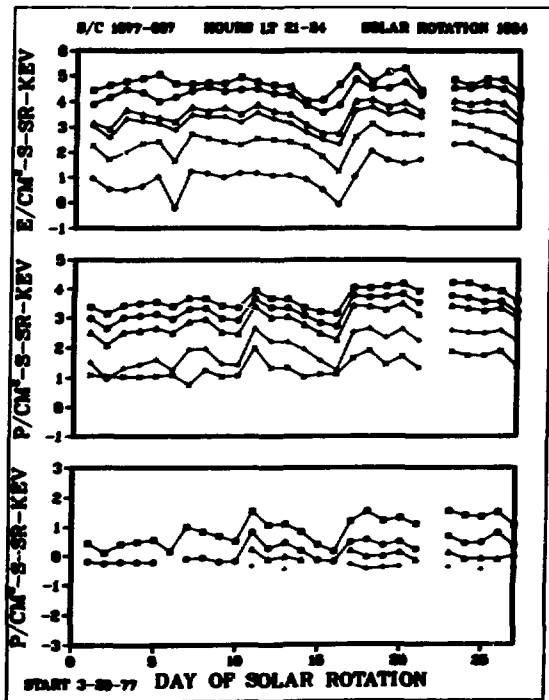
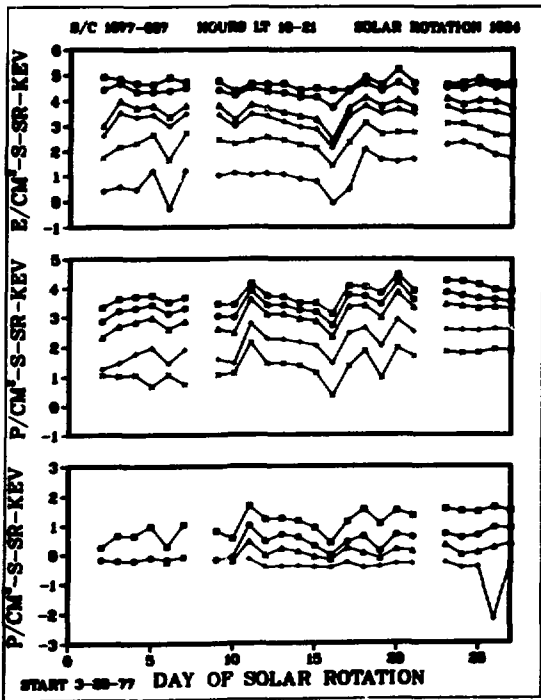
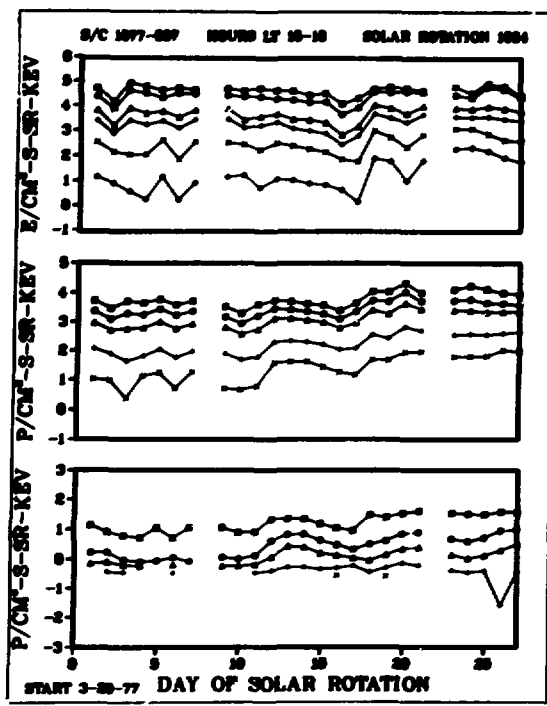
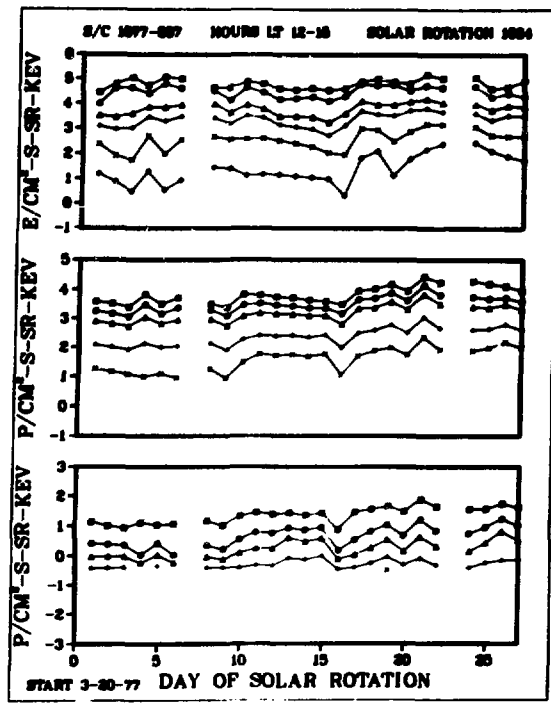
S/C 1977-007



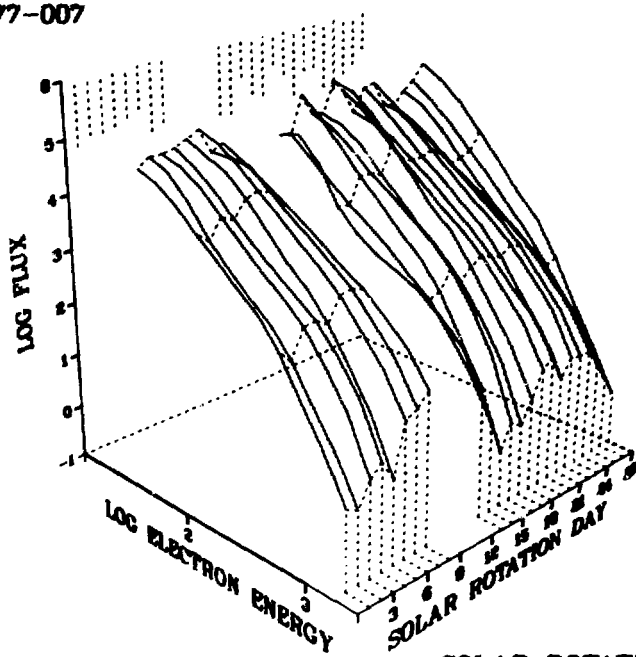
S/C 1977-007







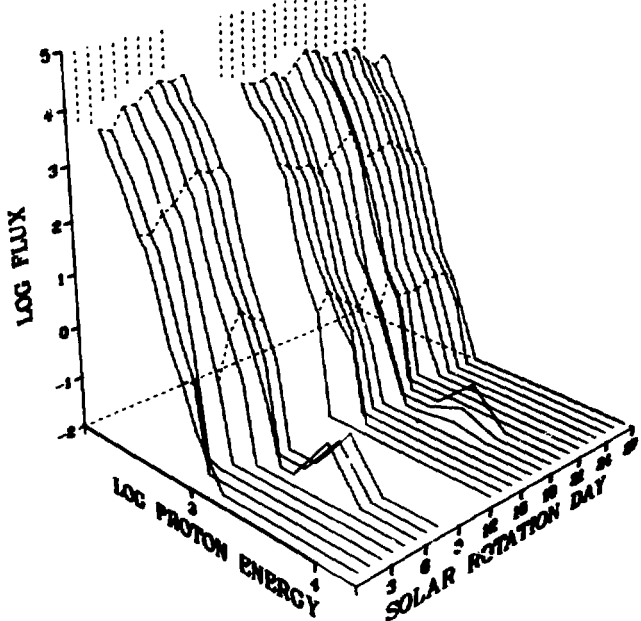
S/C 1977-007



START 4-16-77

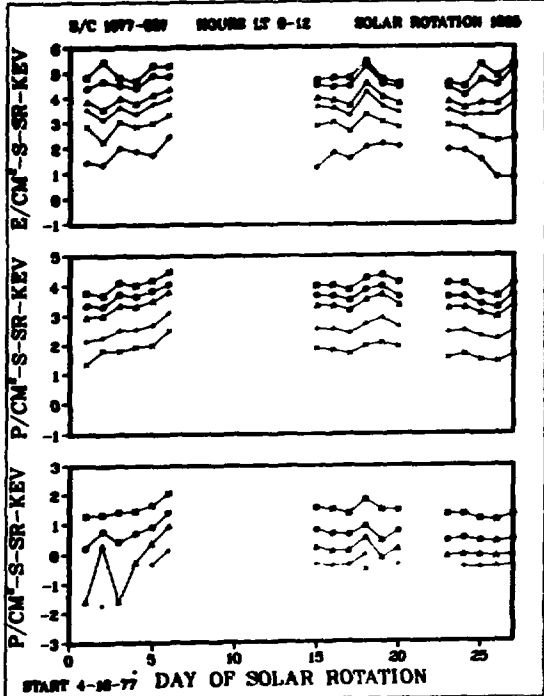
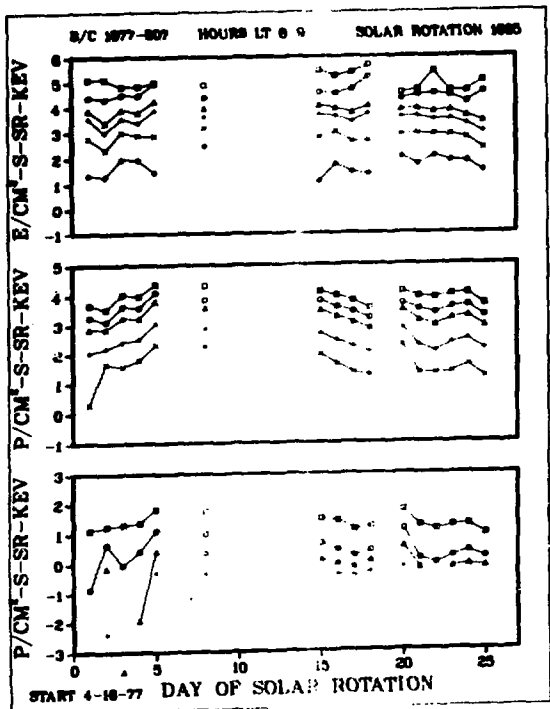
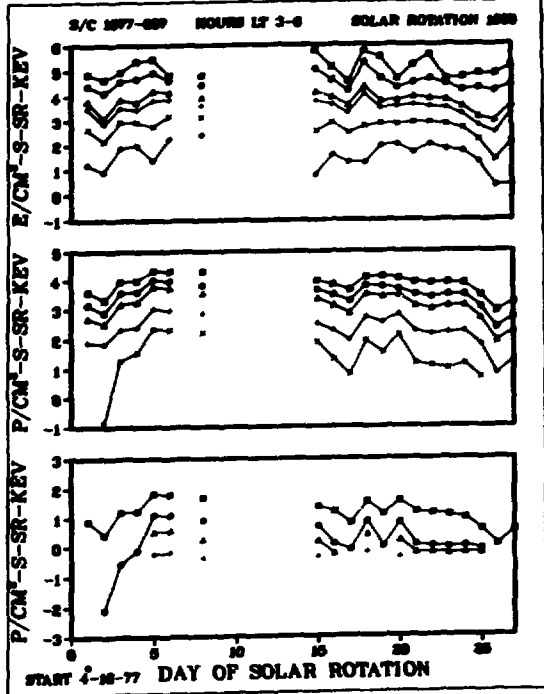
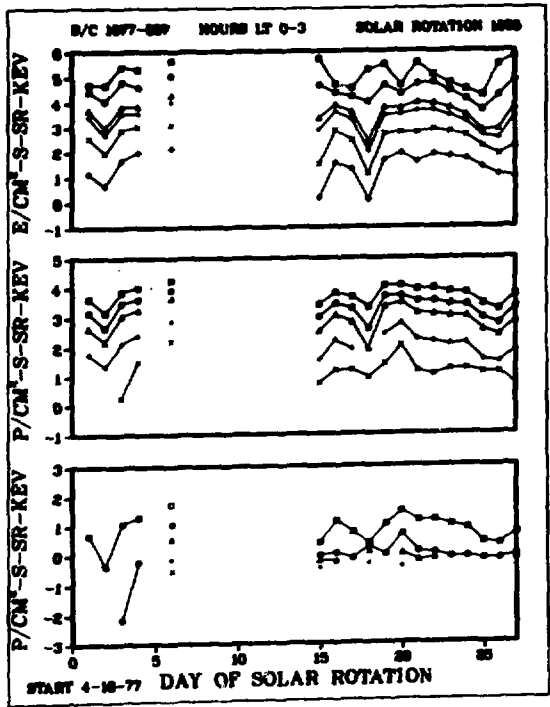
SOLAR ROTATION 1965

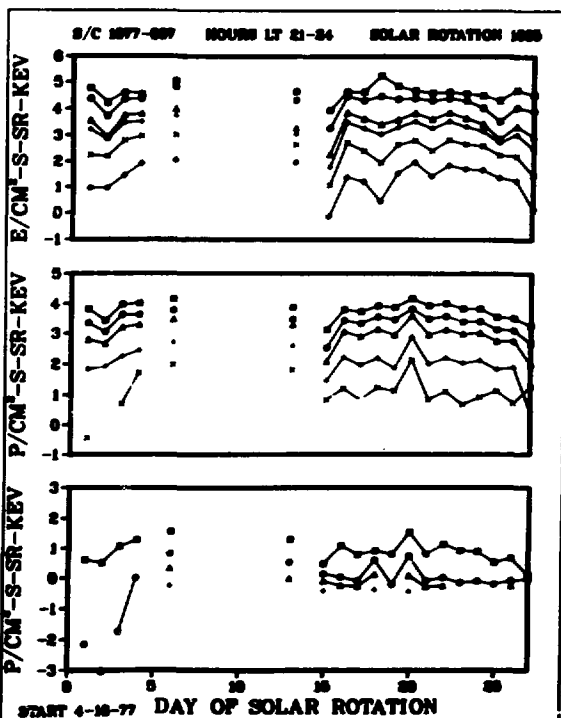
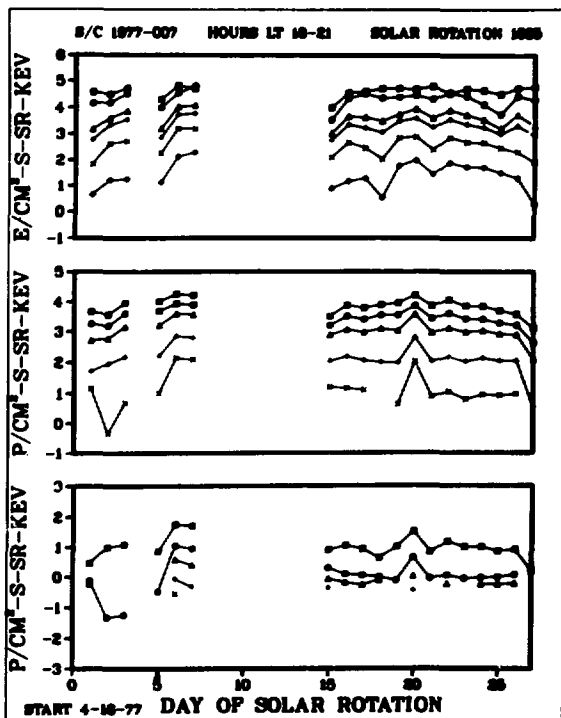
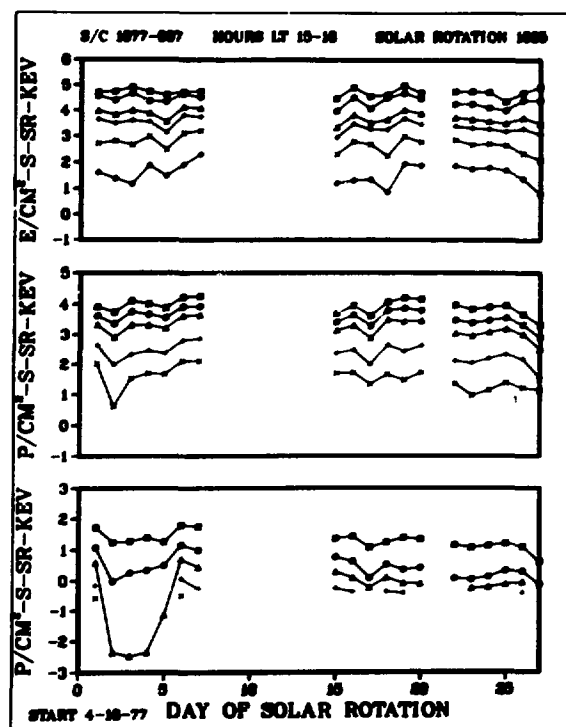
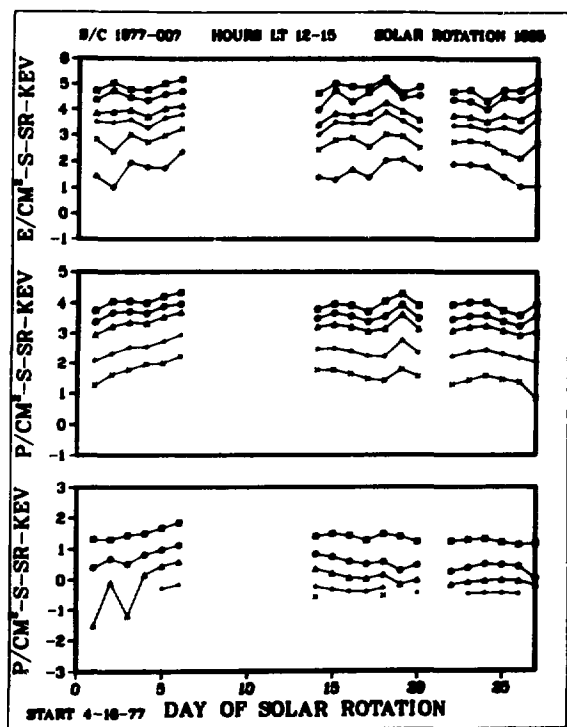
S/C 1977-007

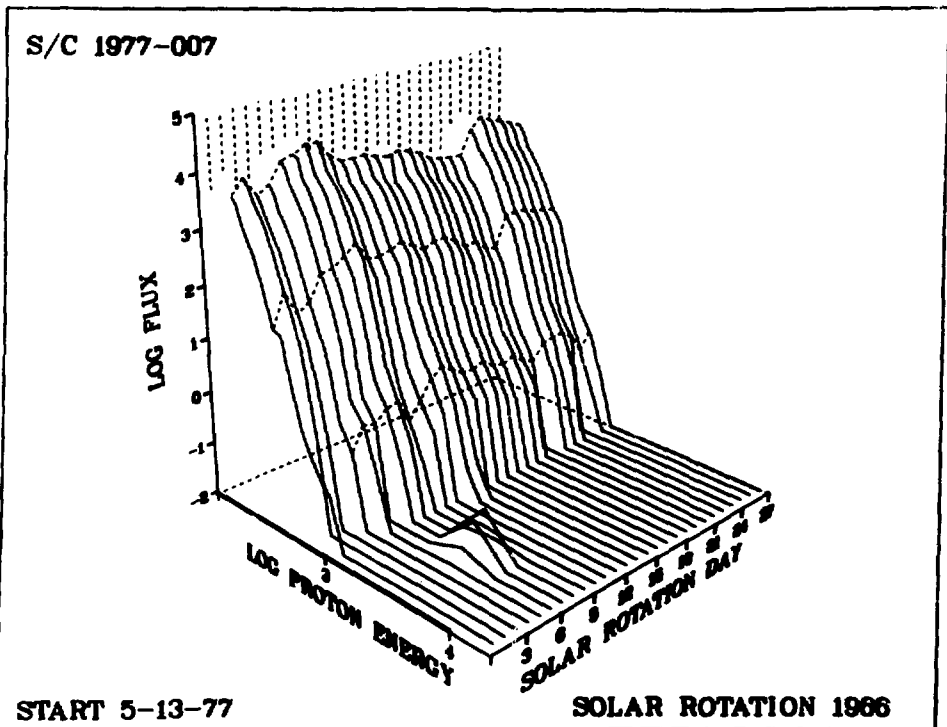
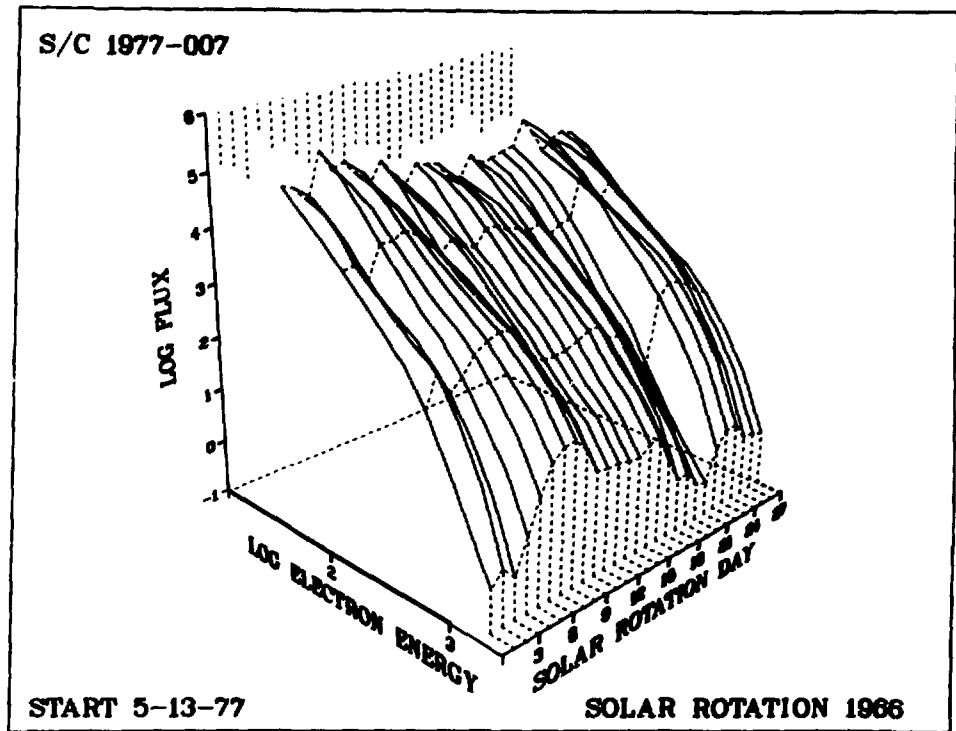


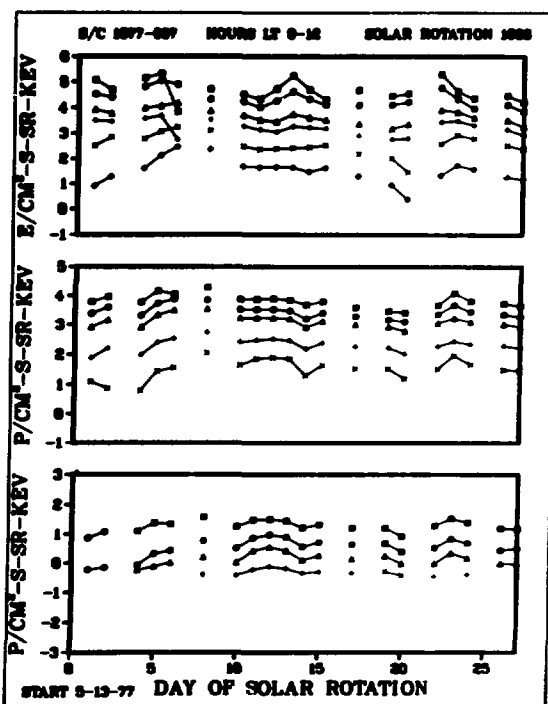
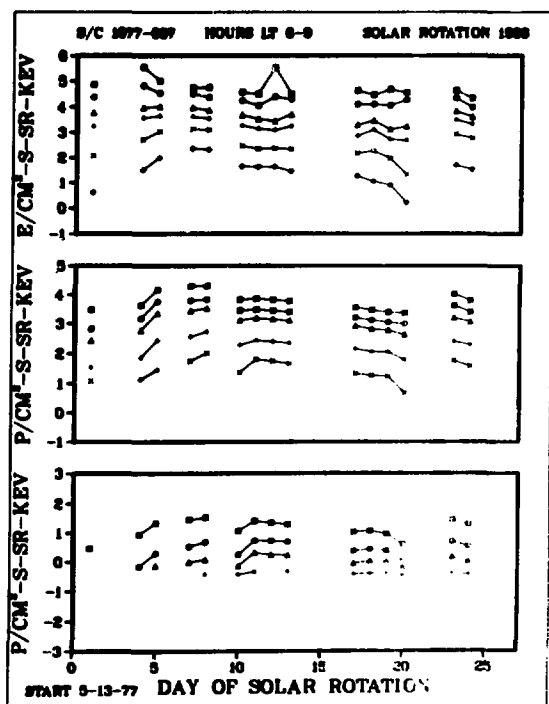
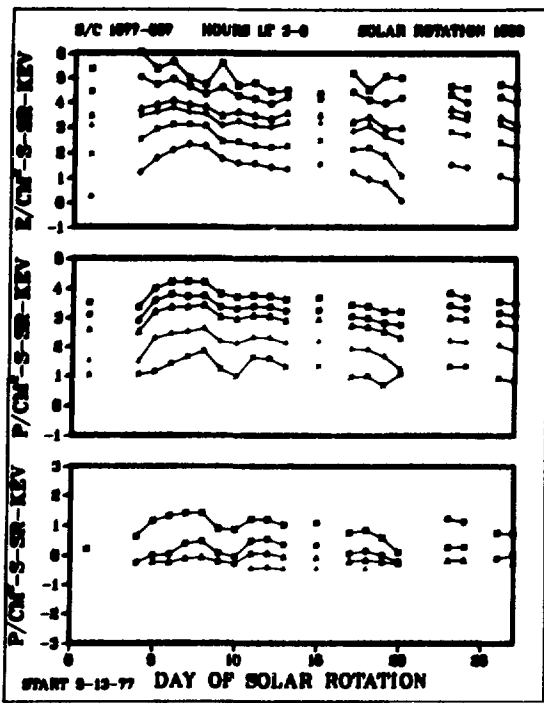
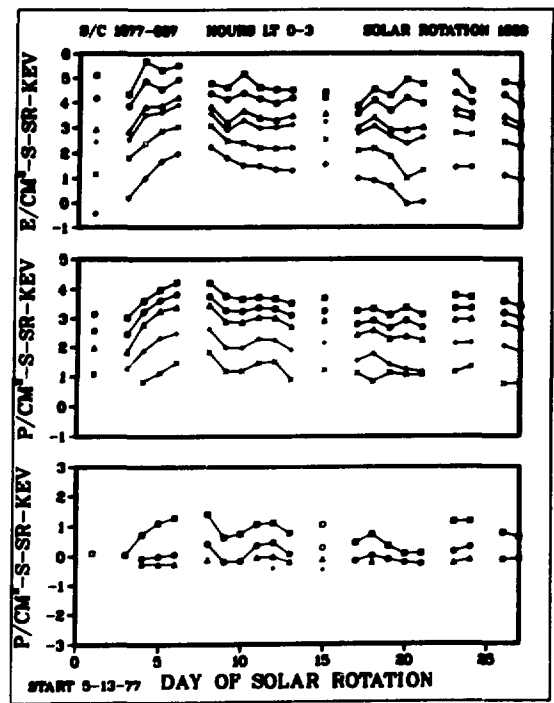
START 4-16-77

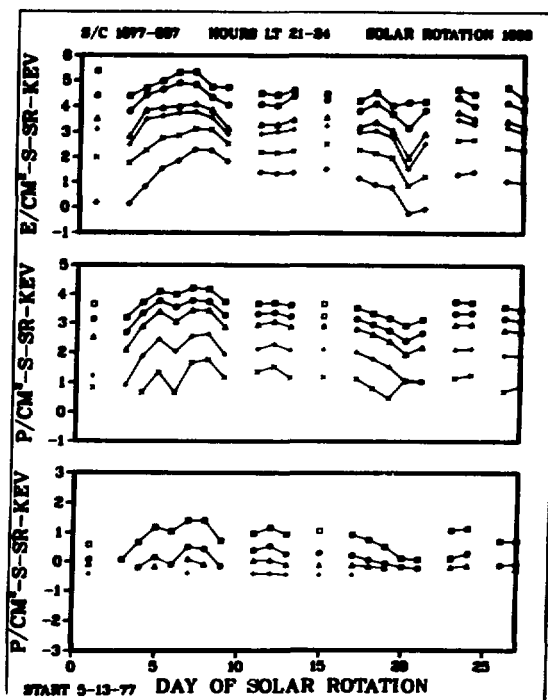
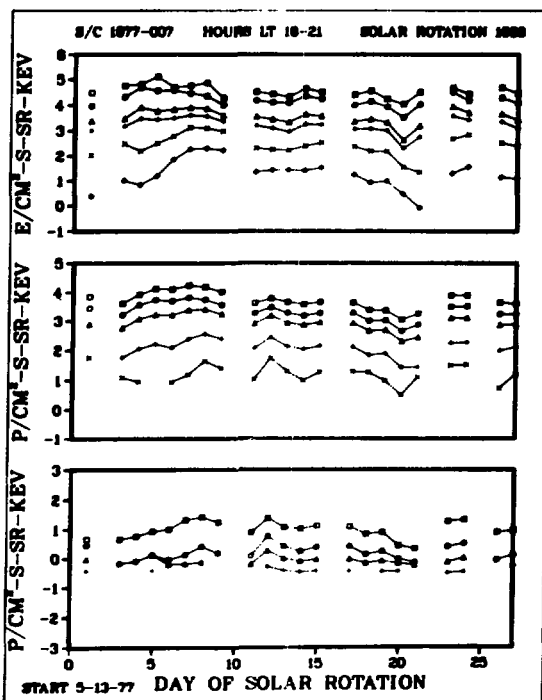
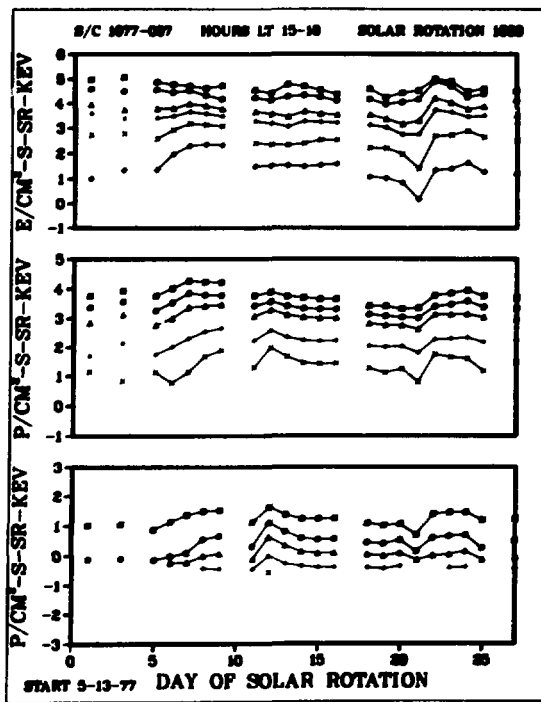
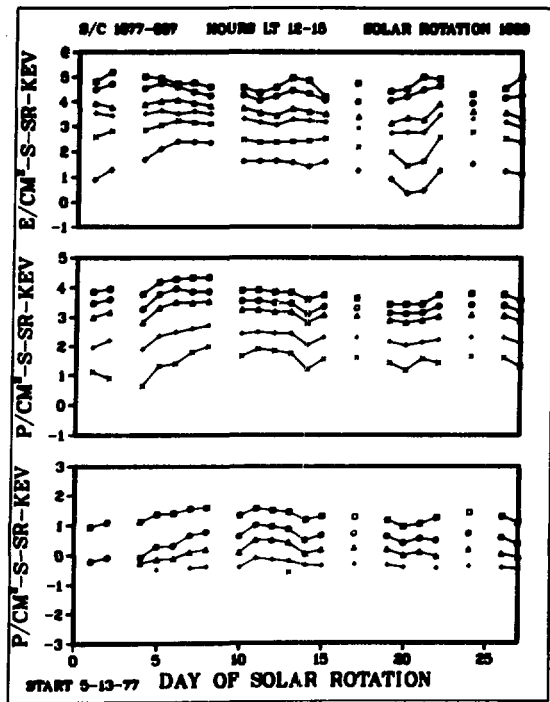
SOLAR ROTATION 1965



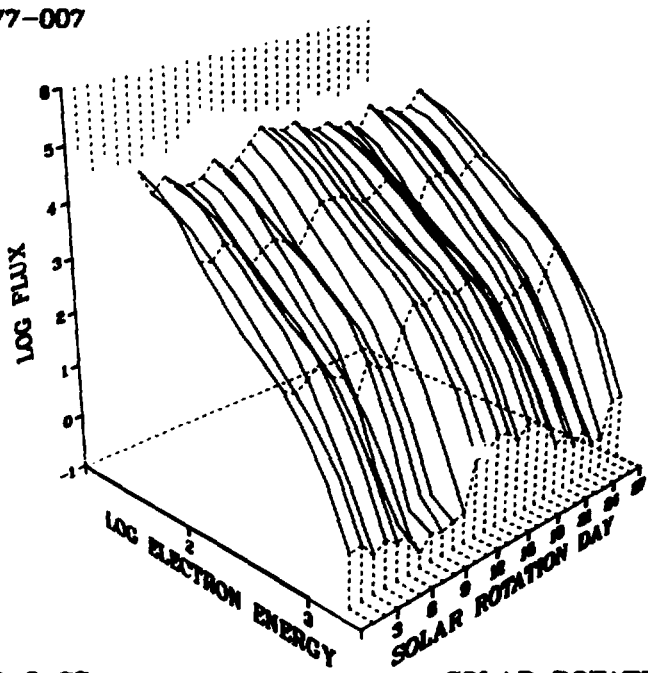








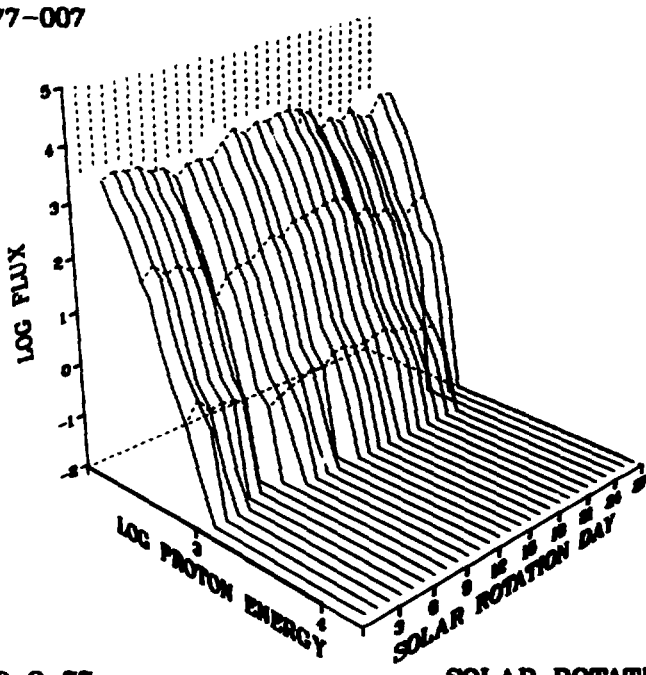
S/C 1977-007



START 6-9-77

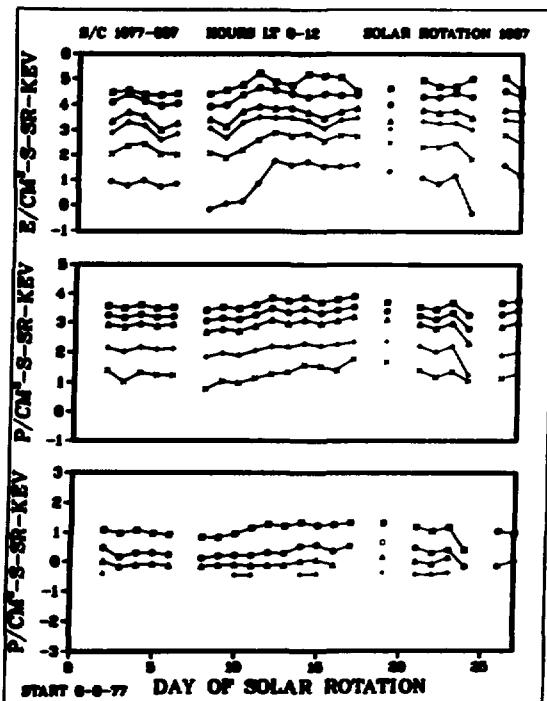
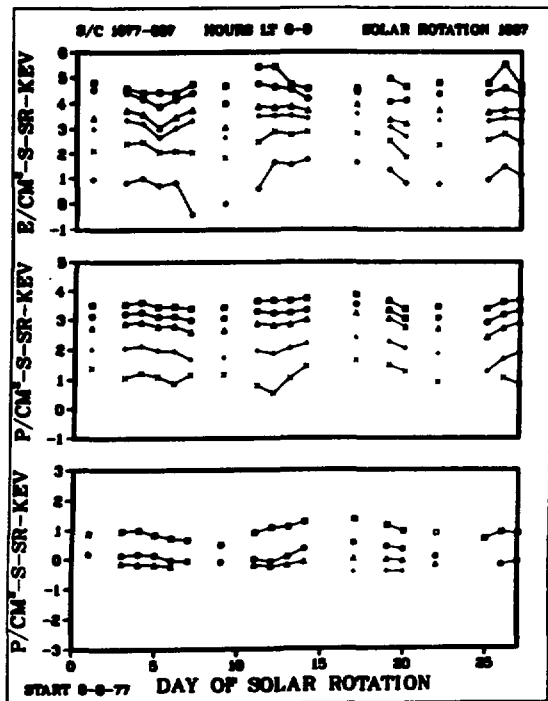
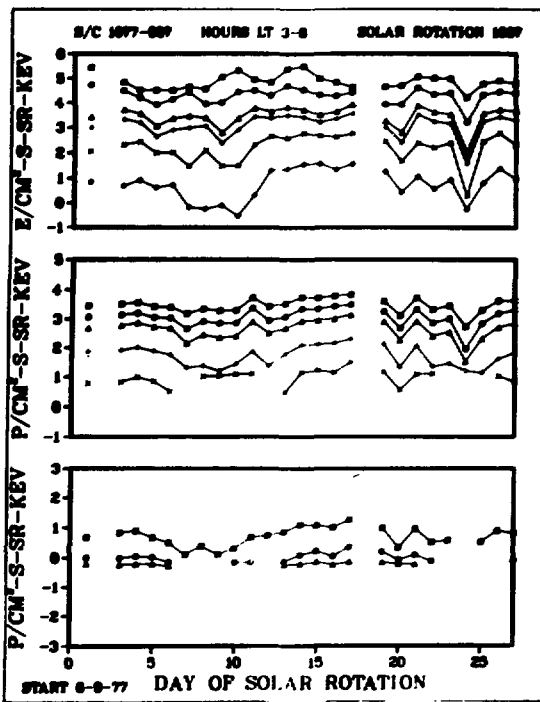
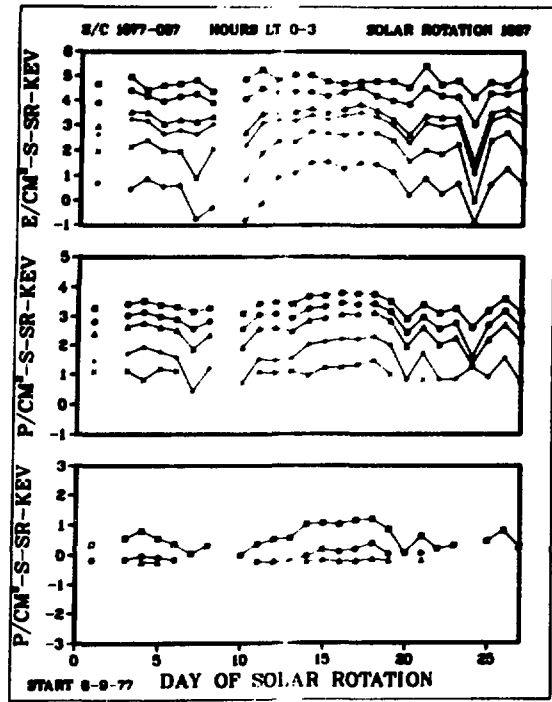
SOLAR ROTATION 1967

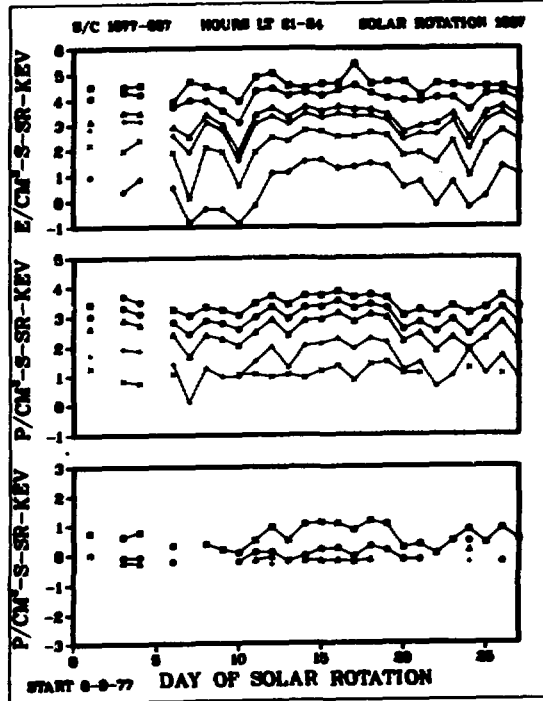
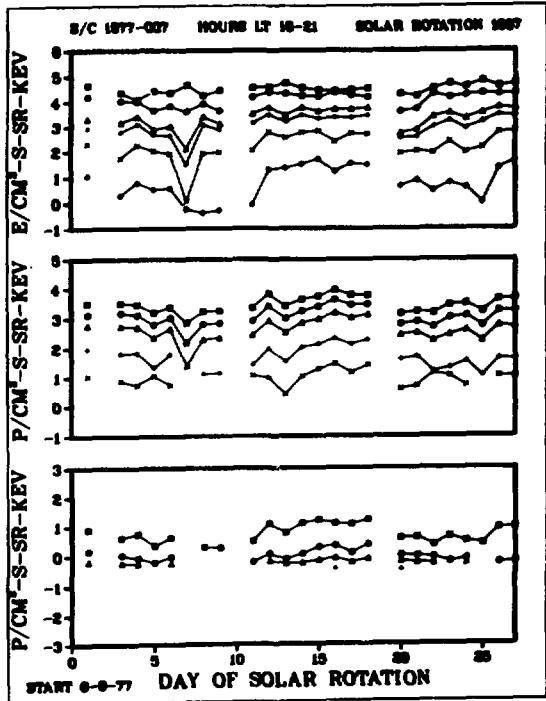
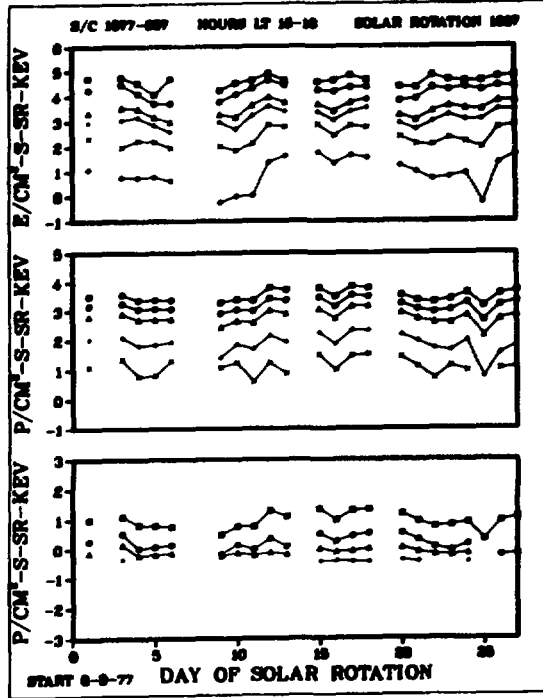
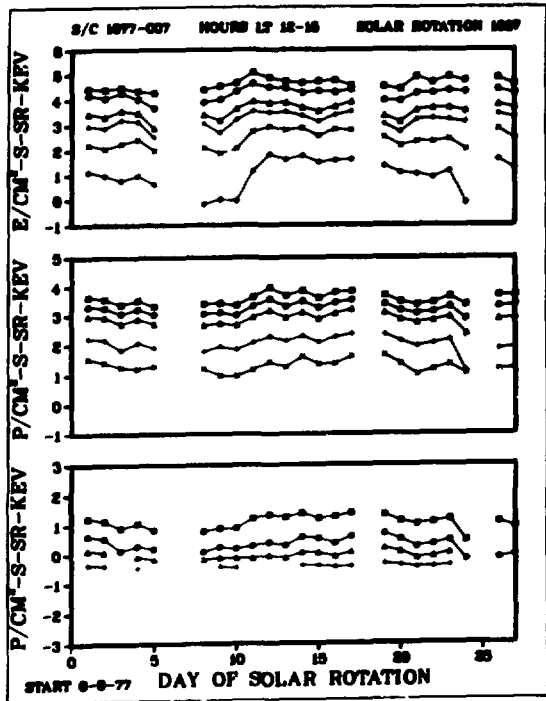
S/C 1977-007



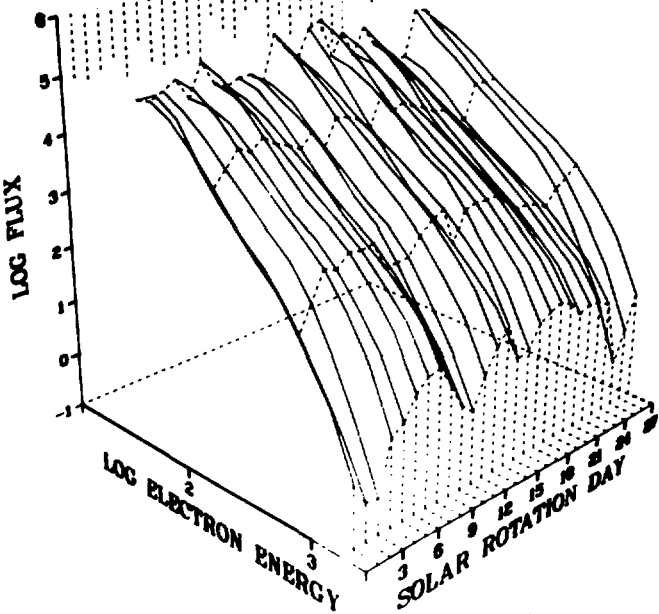
START 6-9-77

SOLAR ROTATION 1967





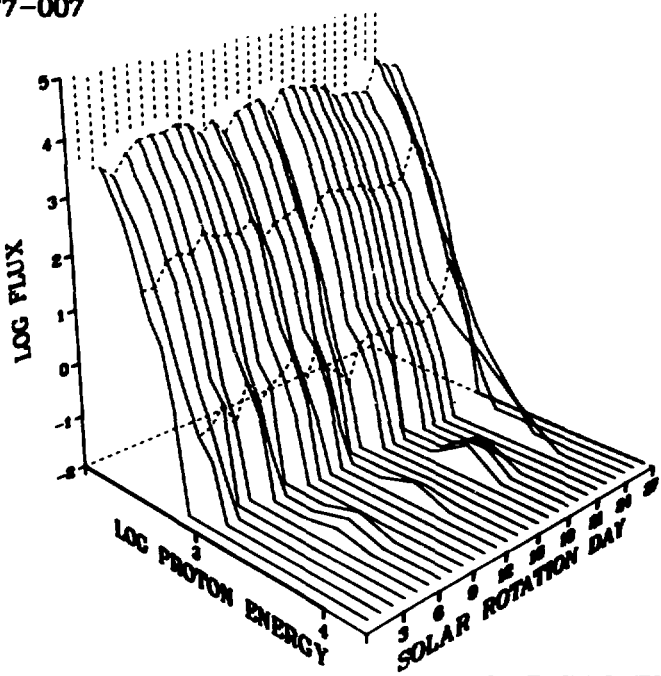
S/C 1977-007



START 7-6-77

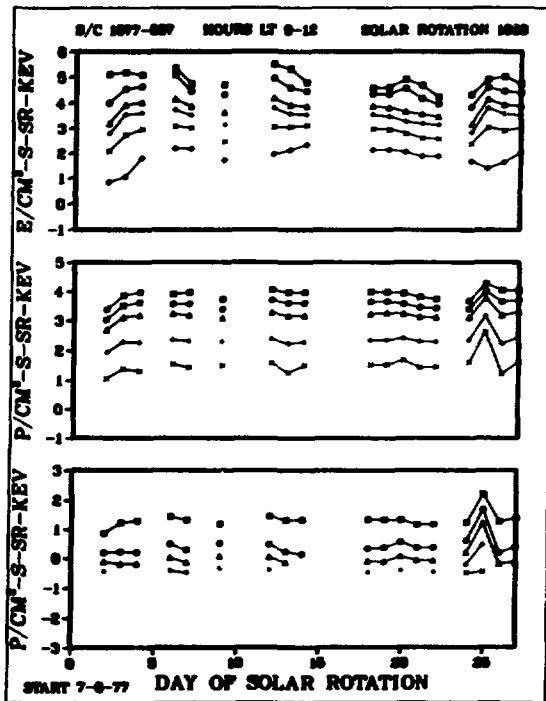
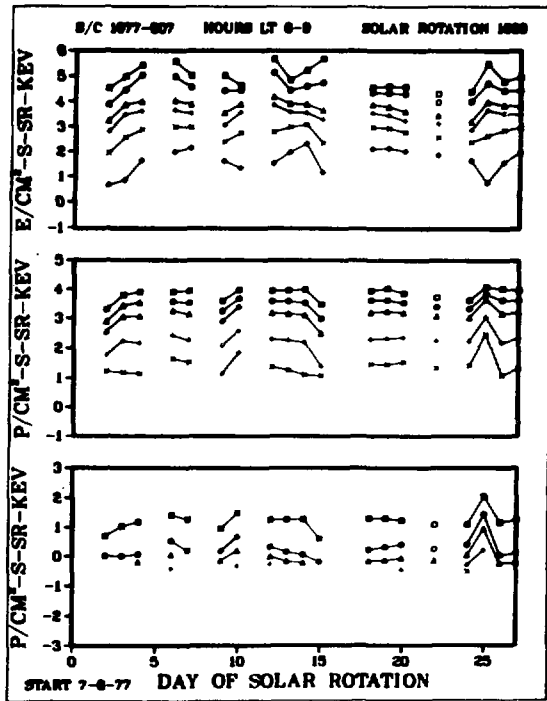
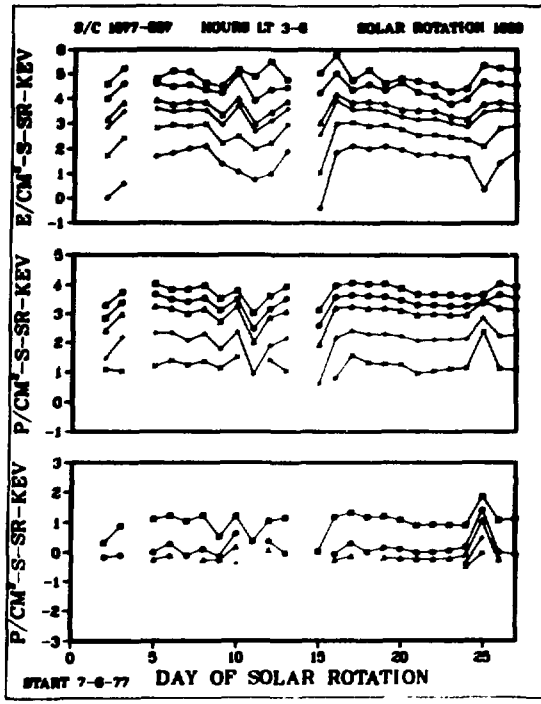
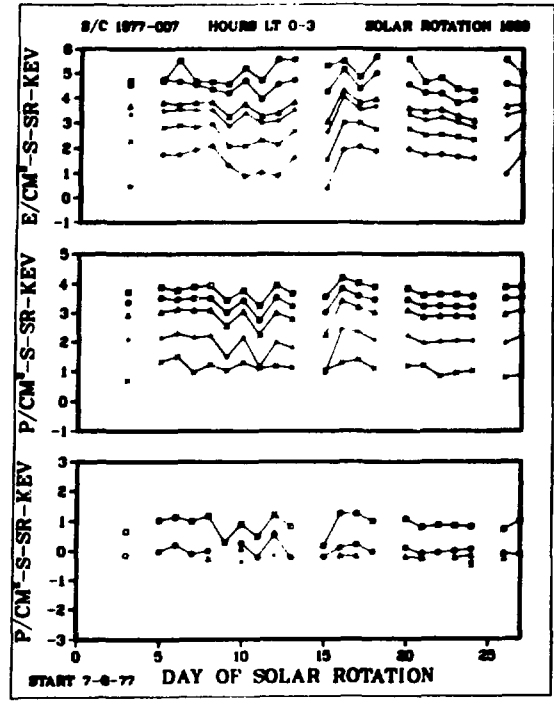
SOLAR ROTATION 1968

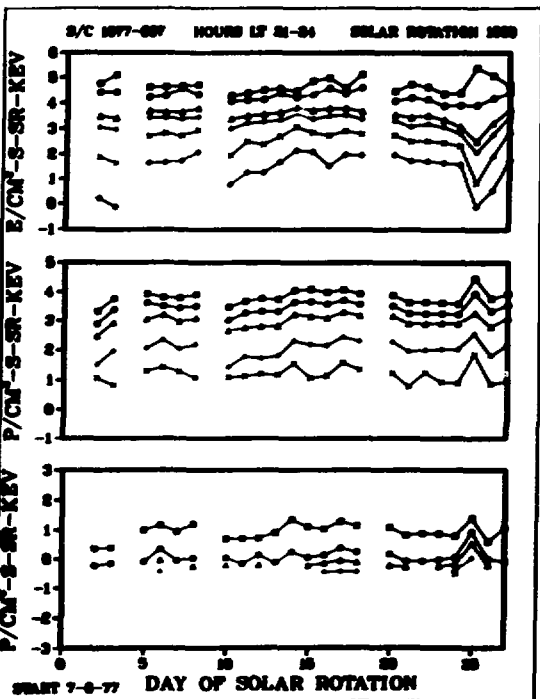
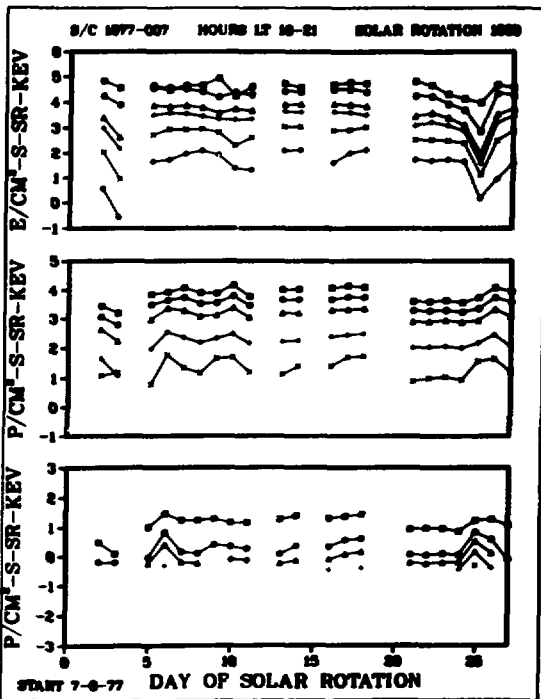
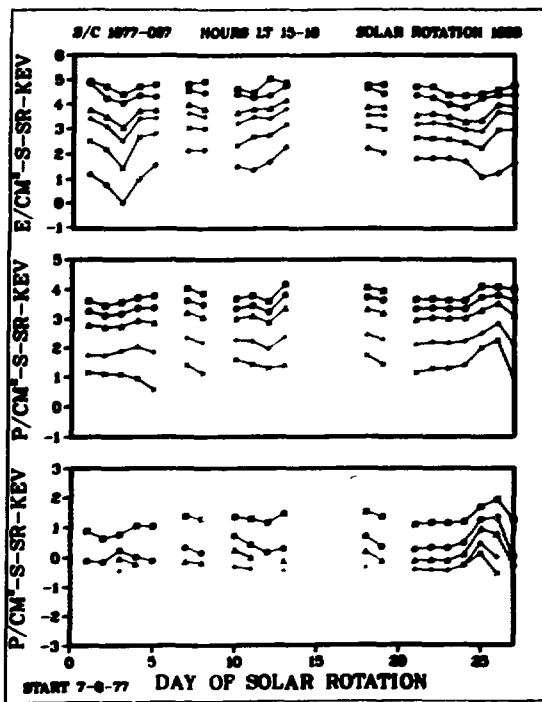
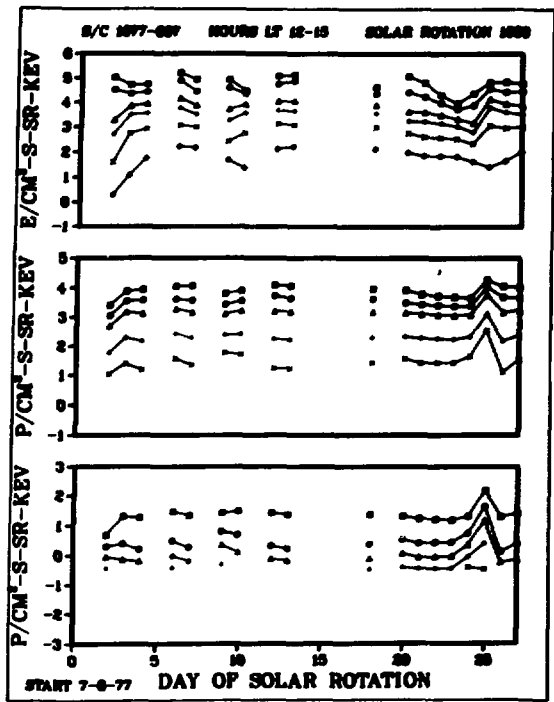
S/C 1977-007

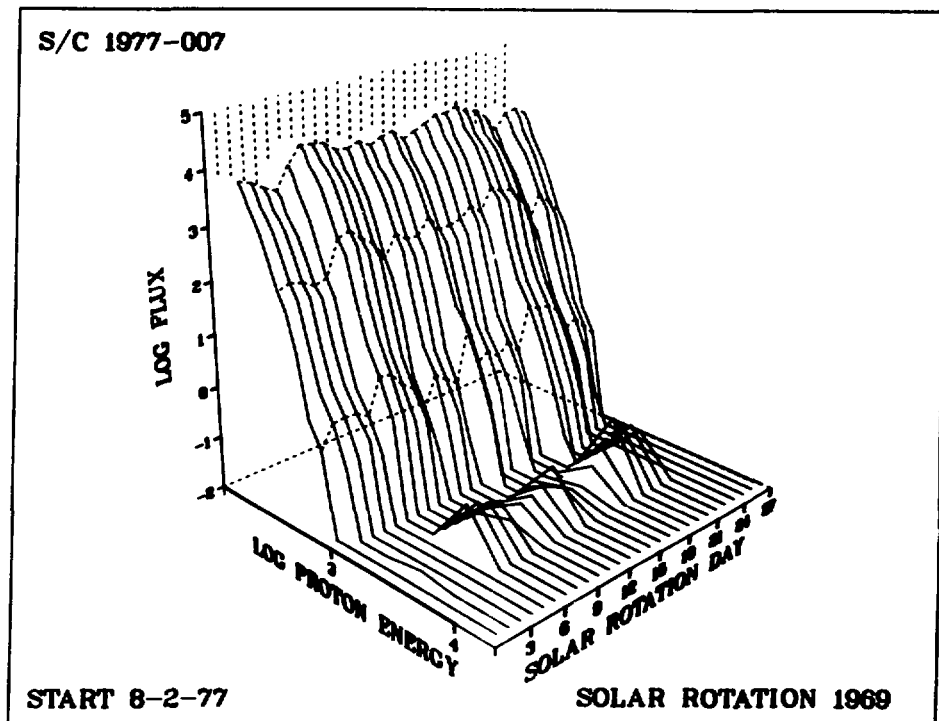
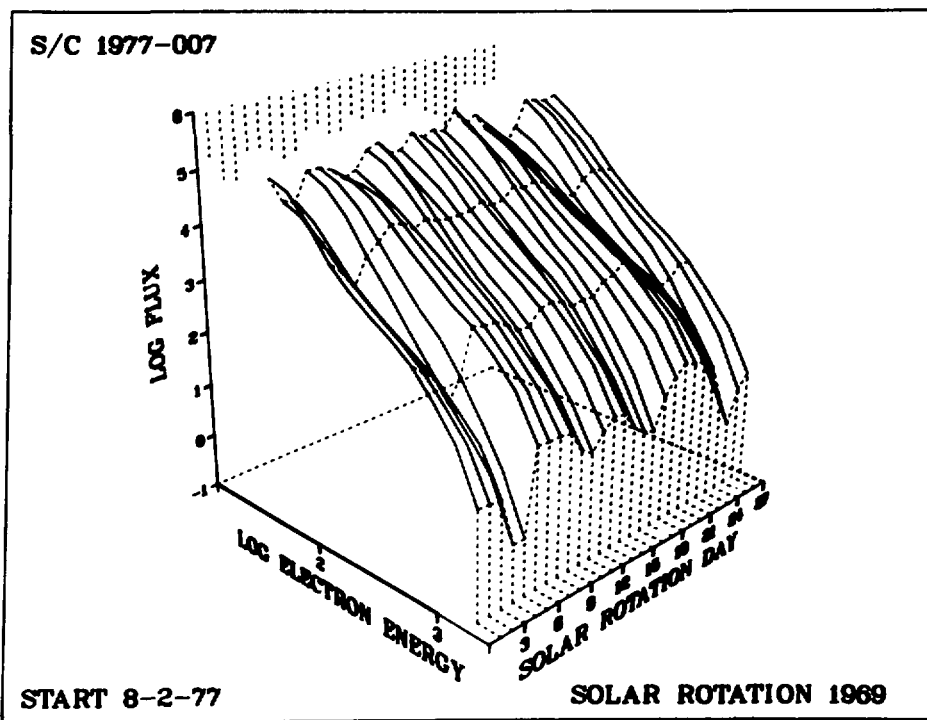


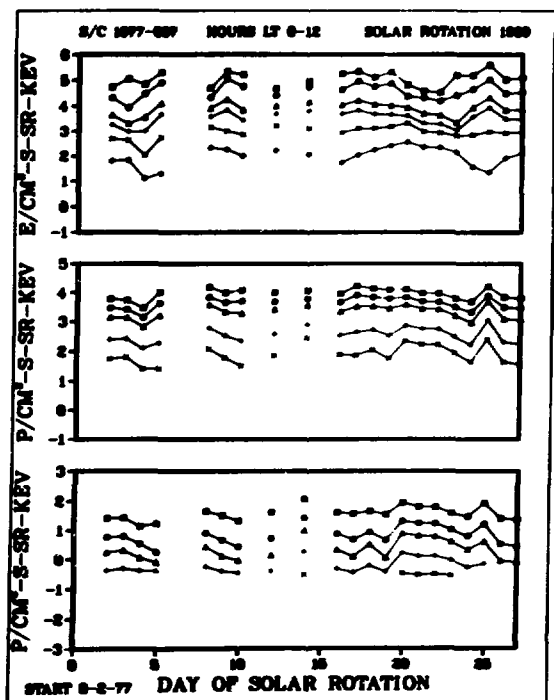
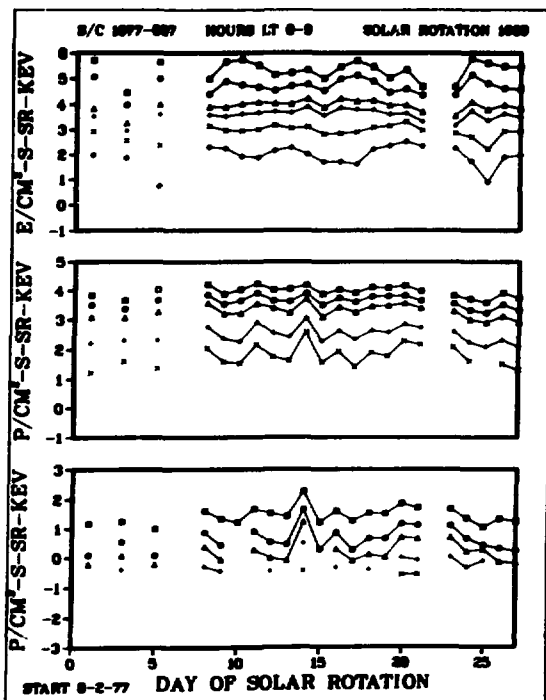
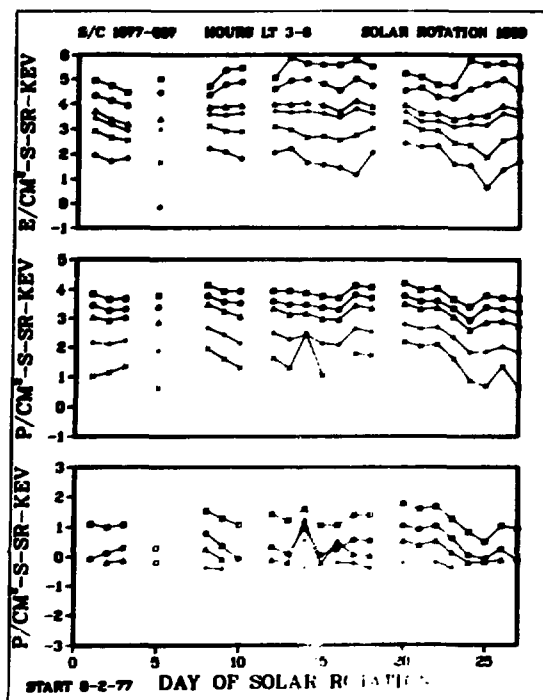
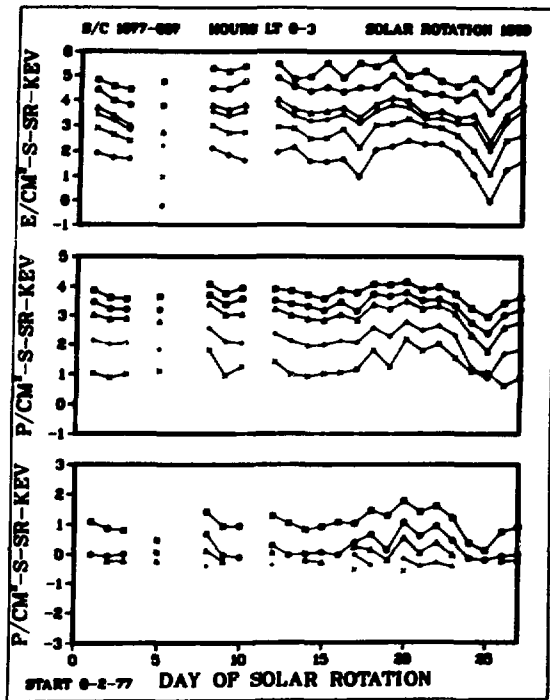
START 7-6-77

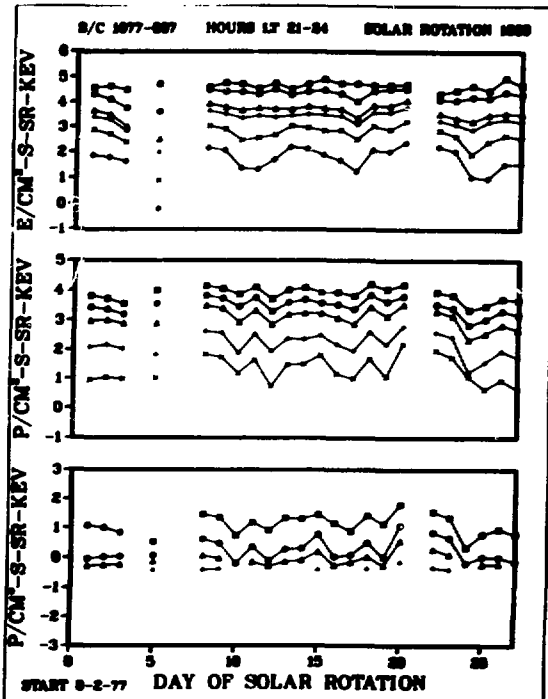
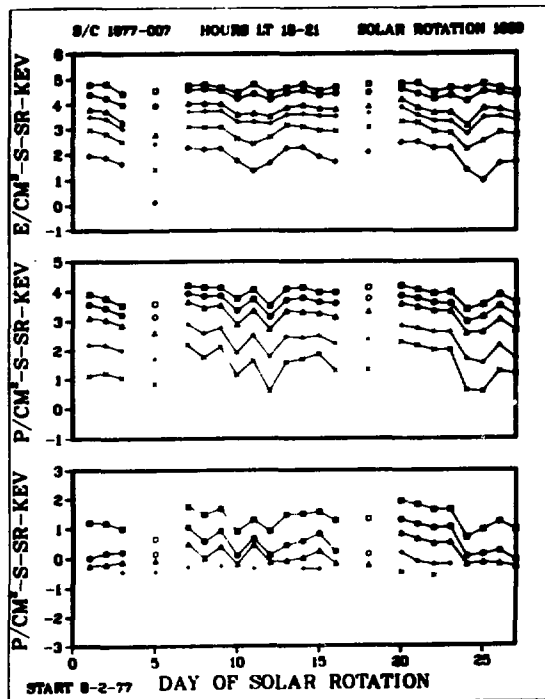
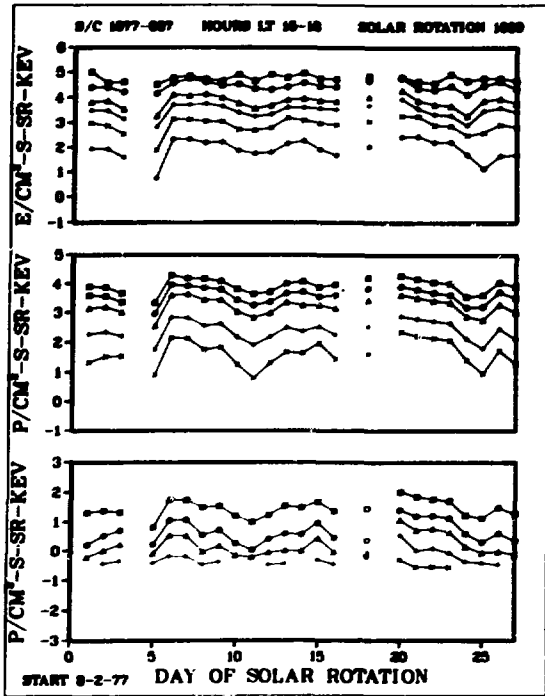
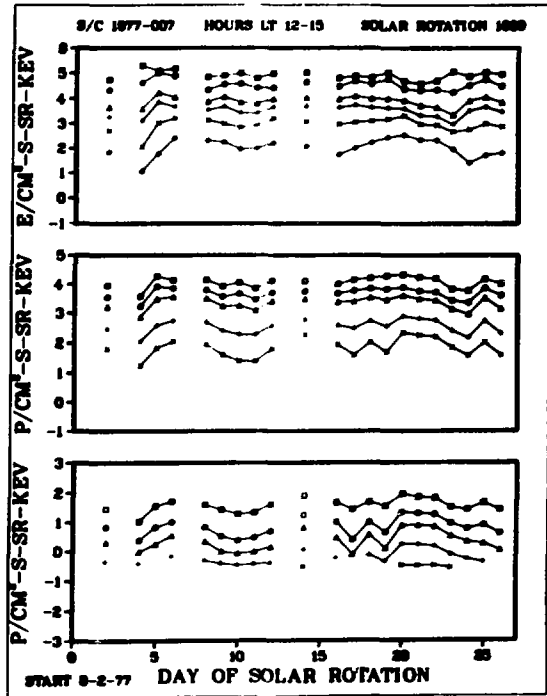
SOLAR ROTATION 1968



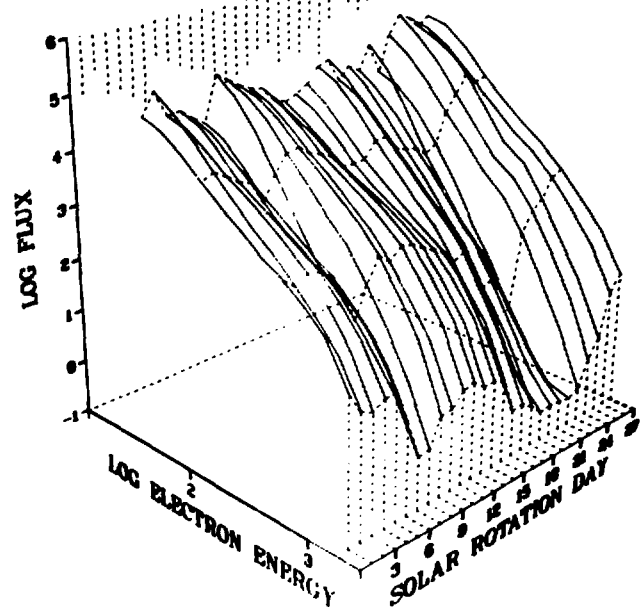








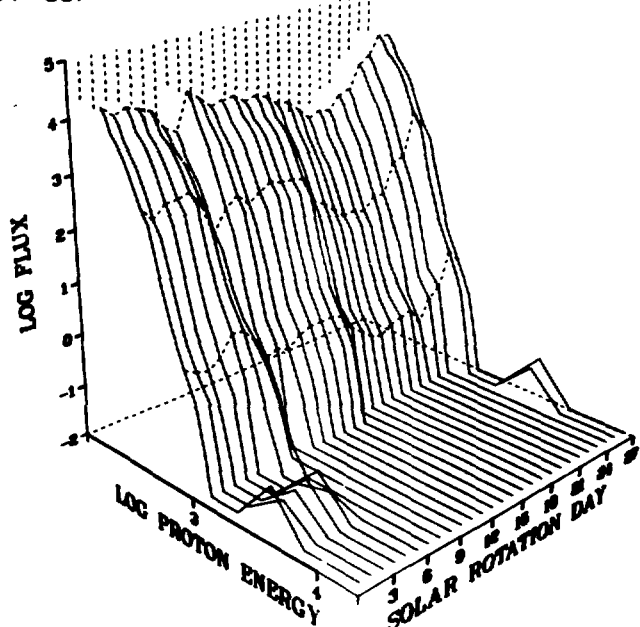
S/C 1977-007



START 10-22-77

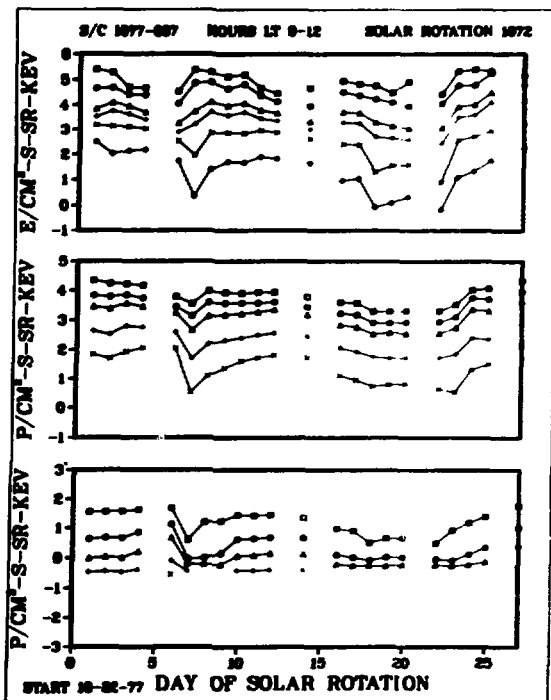
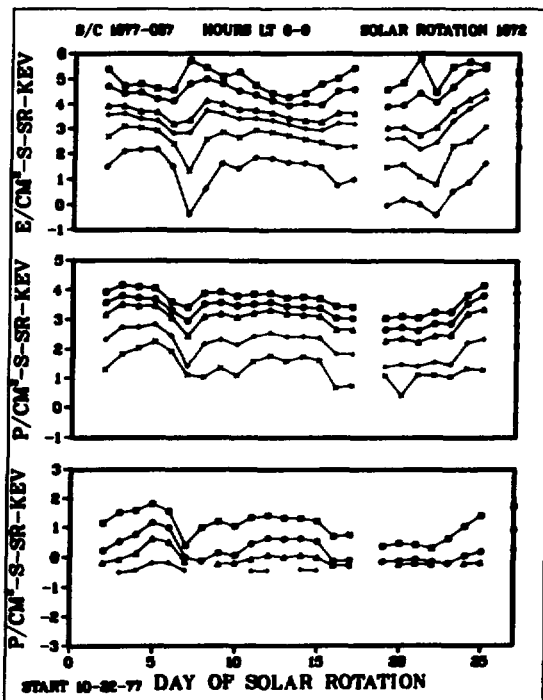
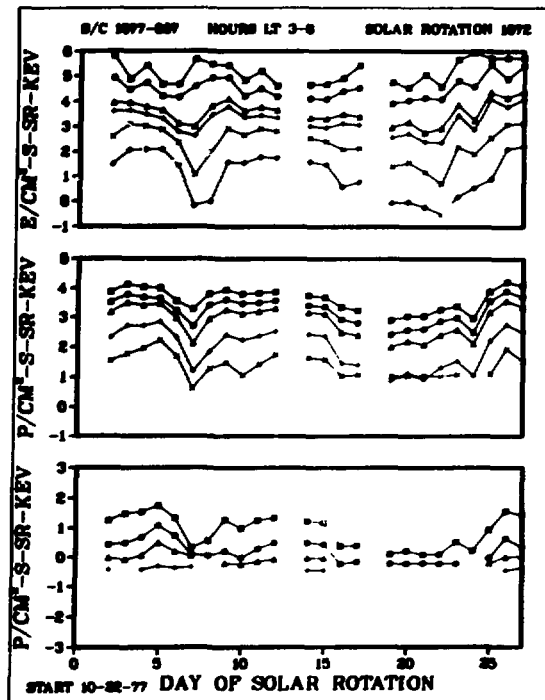
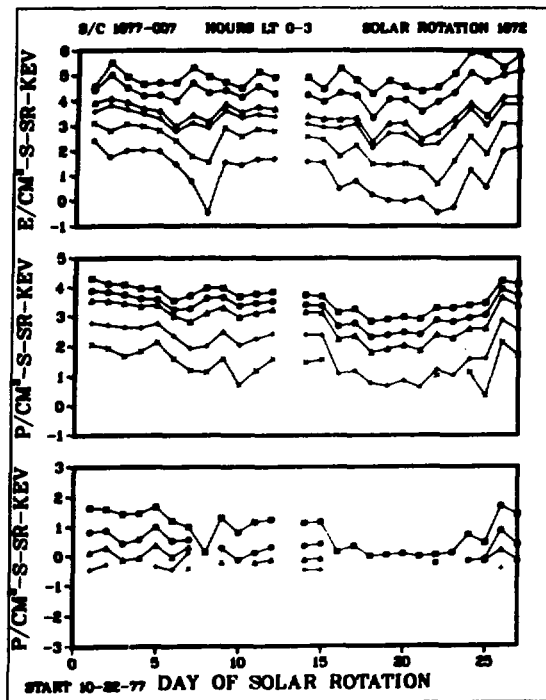
SOLAR ROTATION 1972

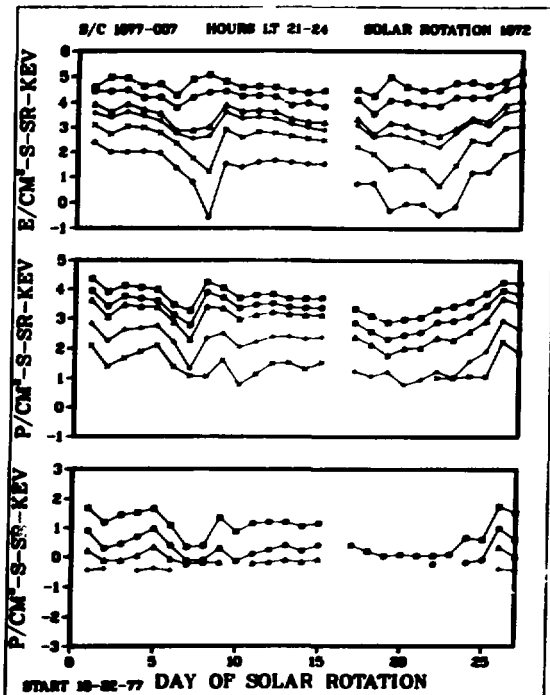
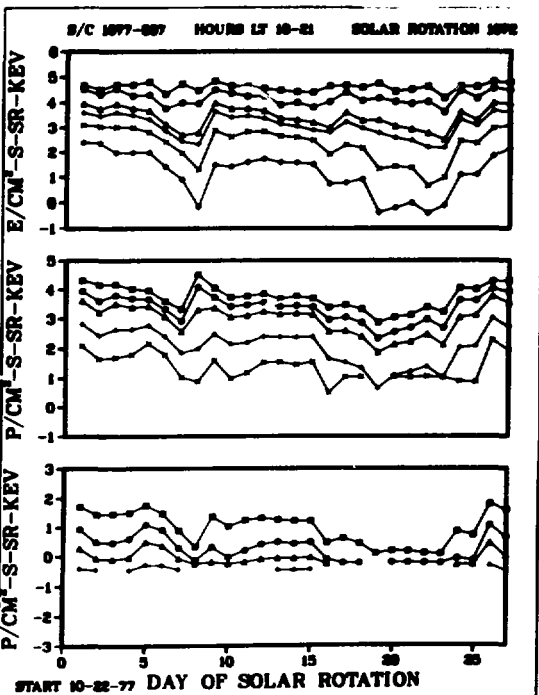
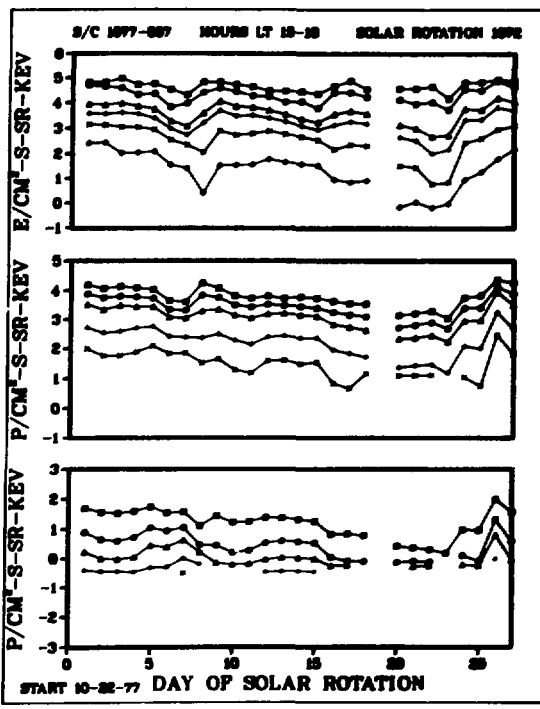
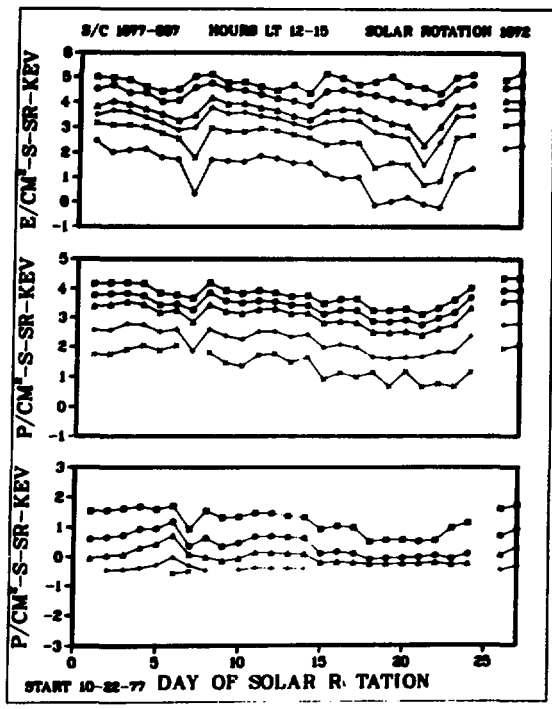
S/C 1977-007



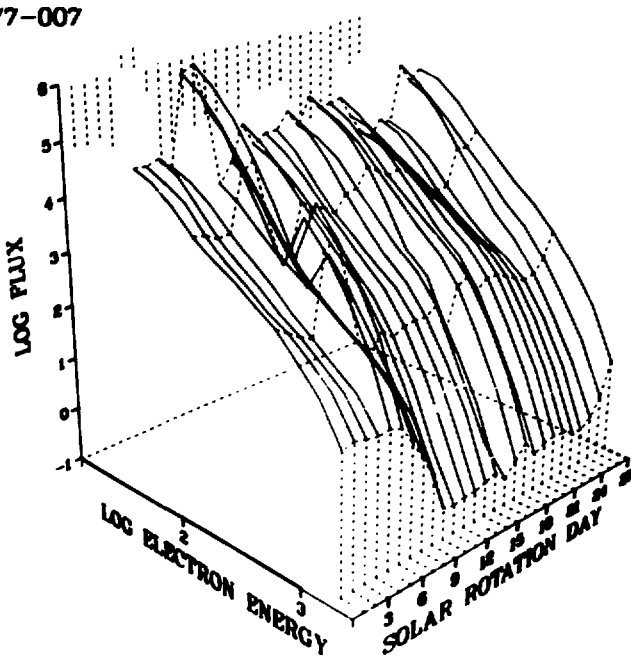
START 10-22-77

SOLAR ROTATION 1972





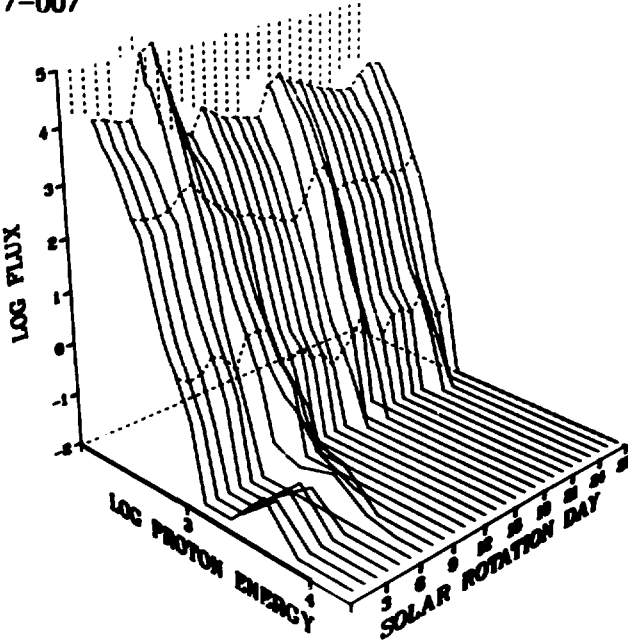
S/C 1977-007



START 11-18-77

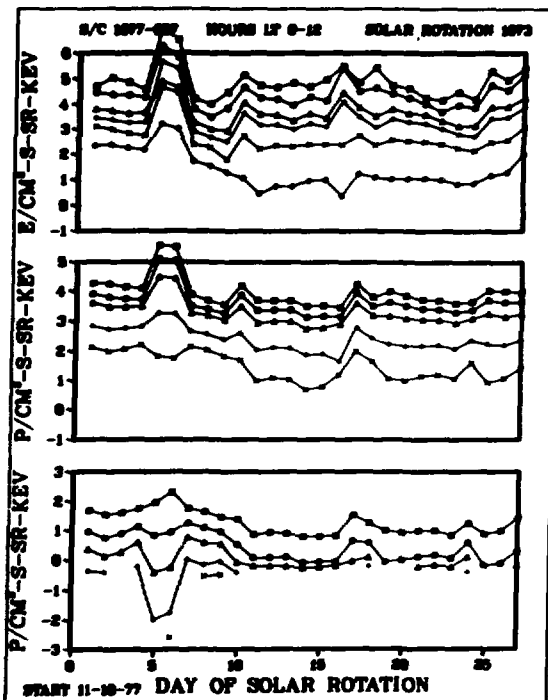
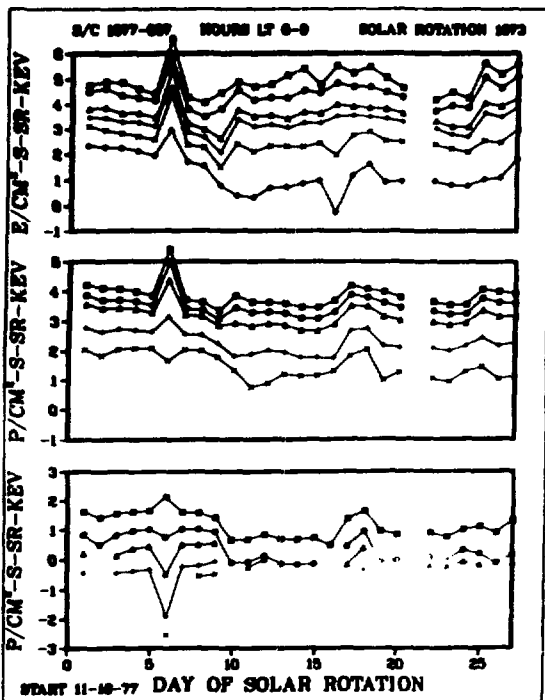
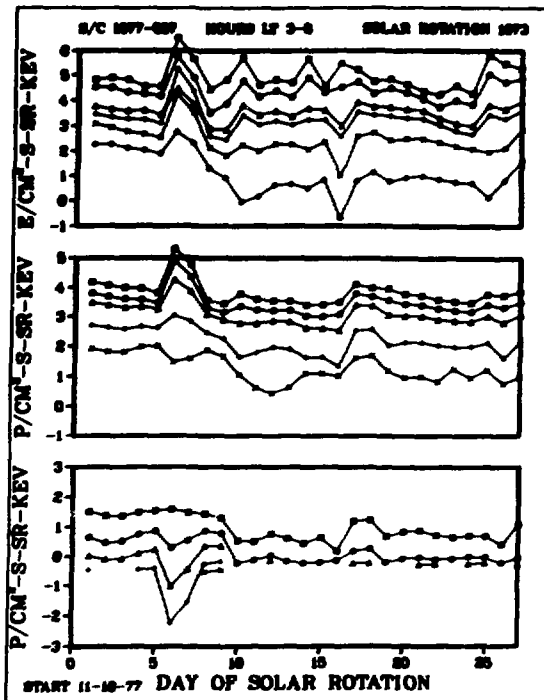
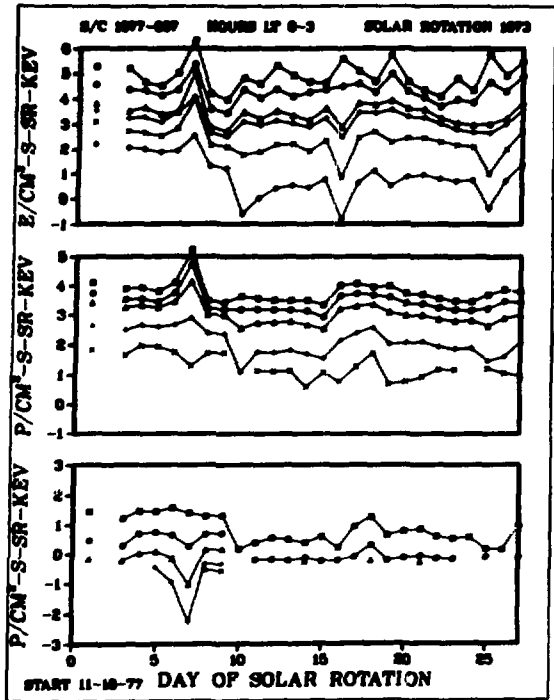
SOLAR ROTATION 1973

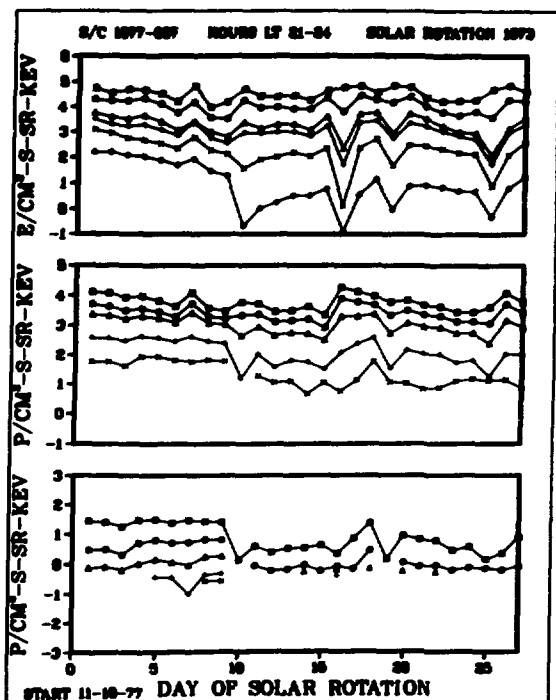
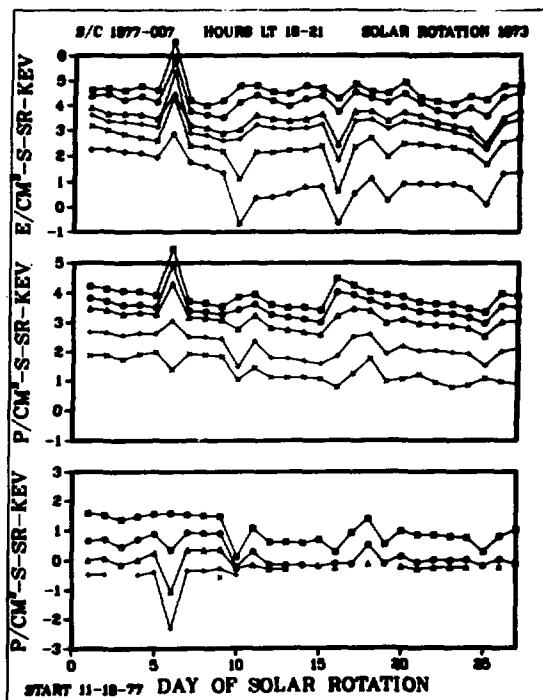
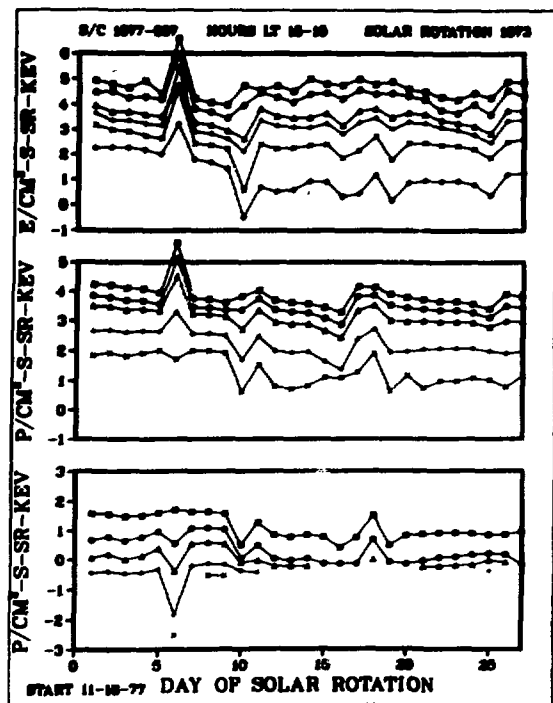
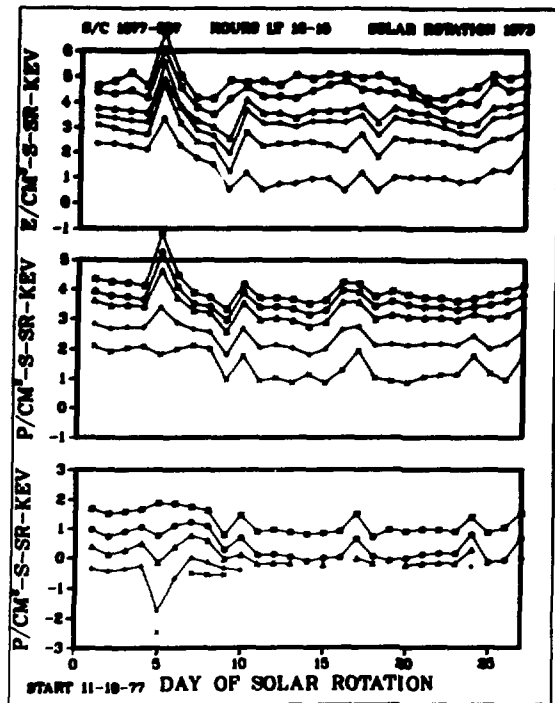
S/C 1977-007



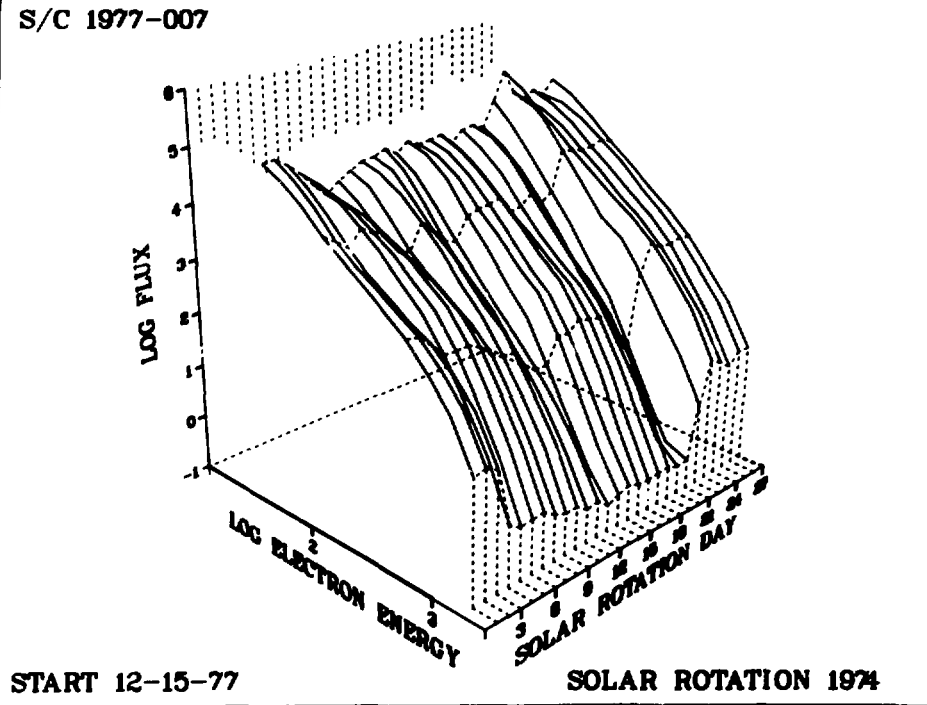
START 11-18-77

SOLAR ROTATION 1973





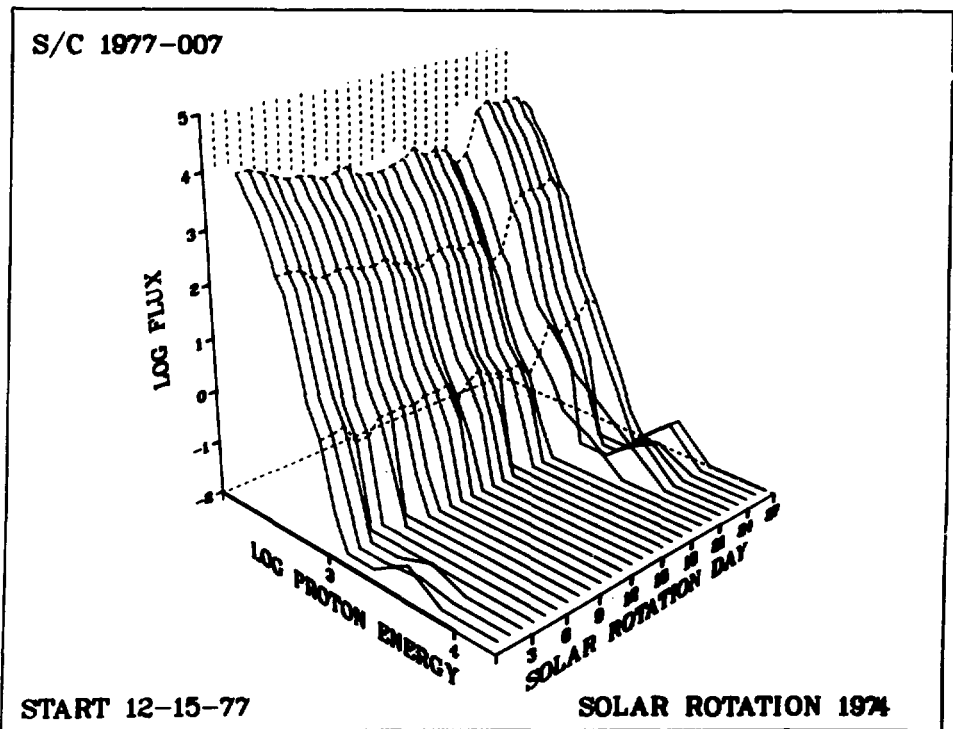
S/C 1977-007



START 12-15-77

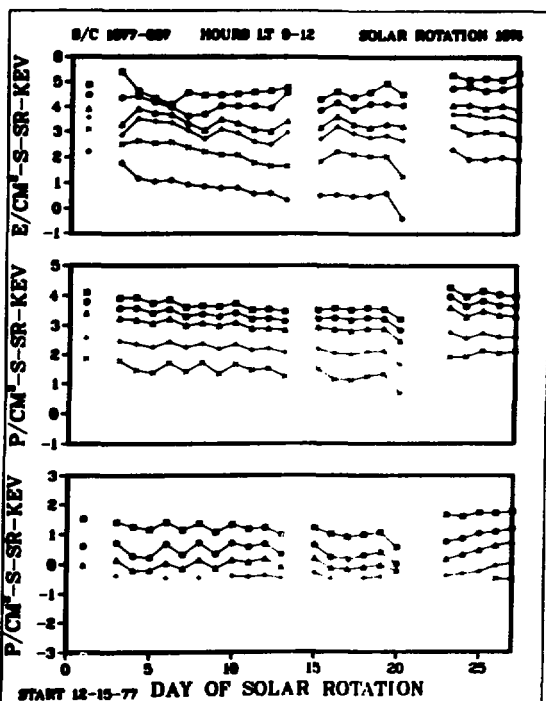
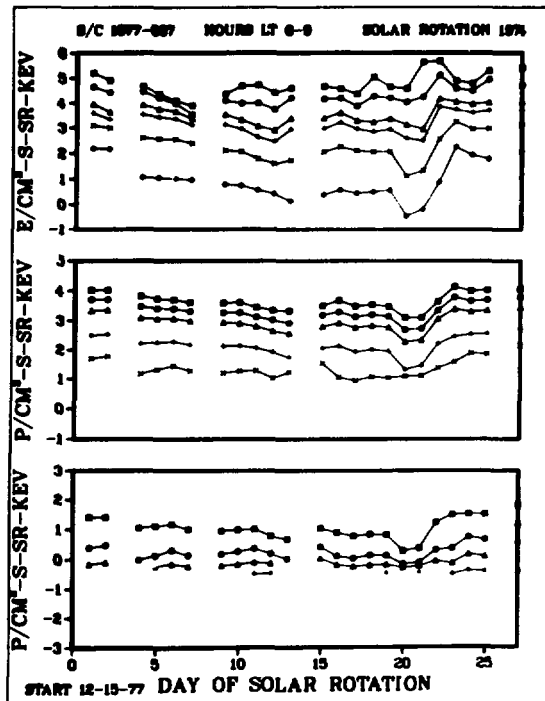
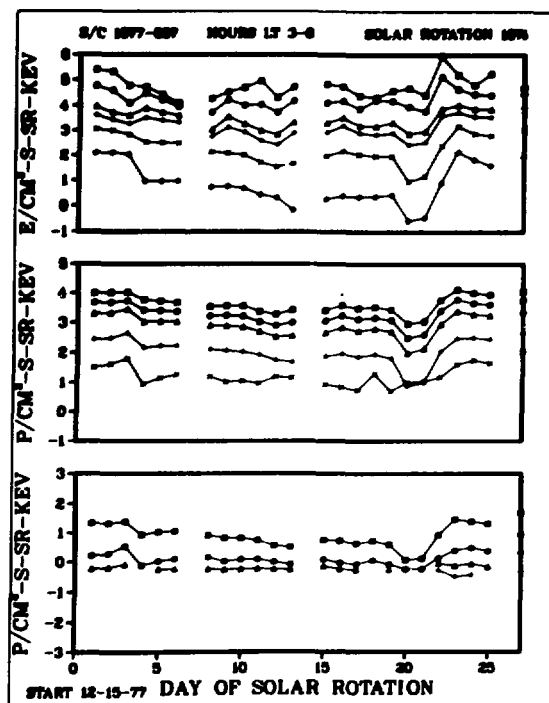
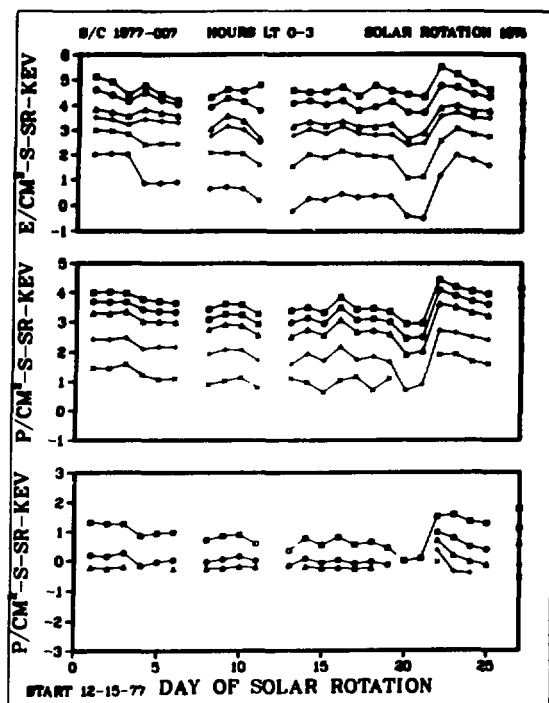
SOLAR ROTATION 1974

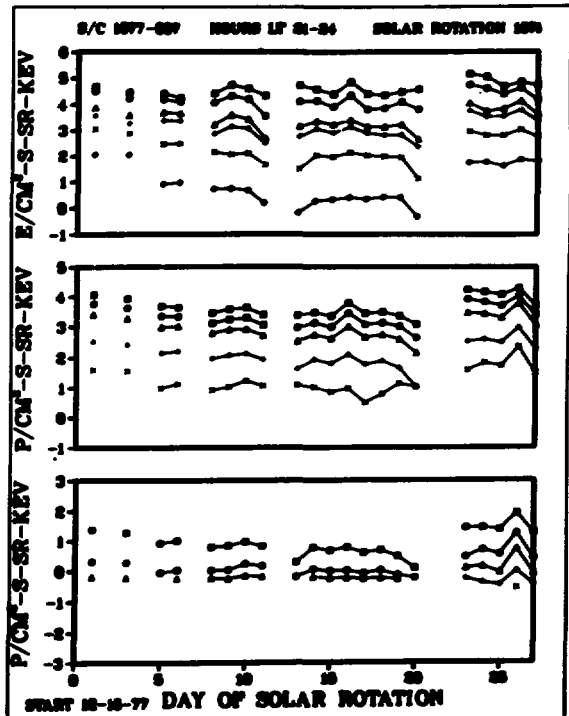
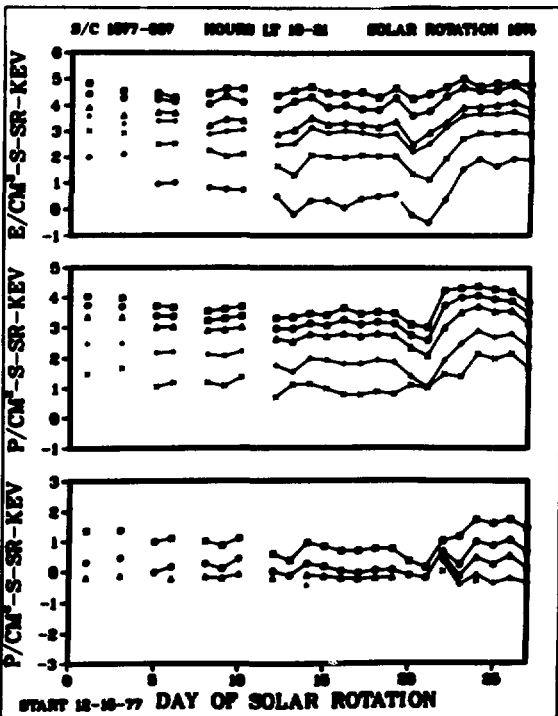
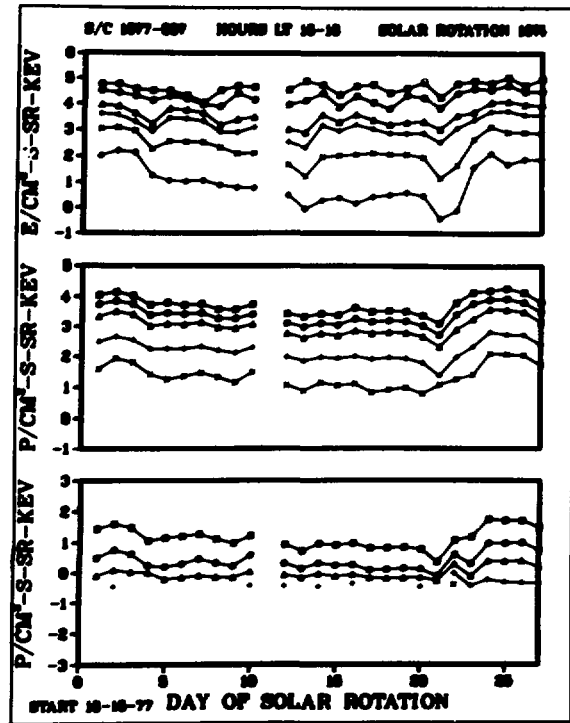
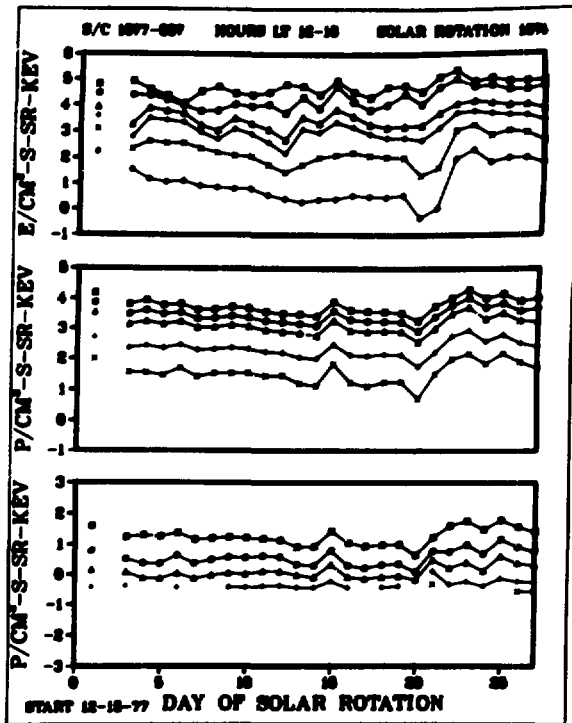
S/C 1977-007

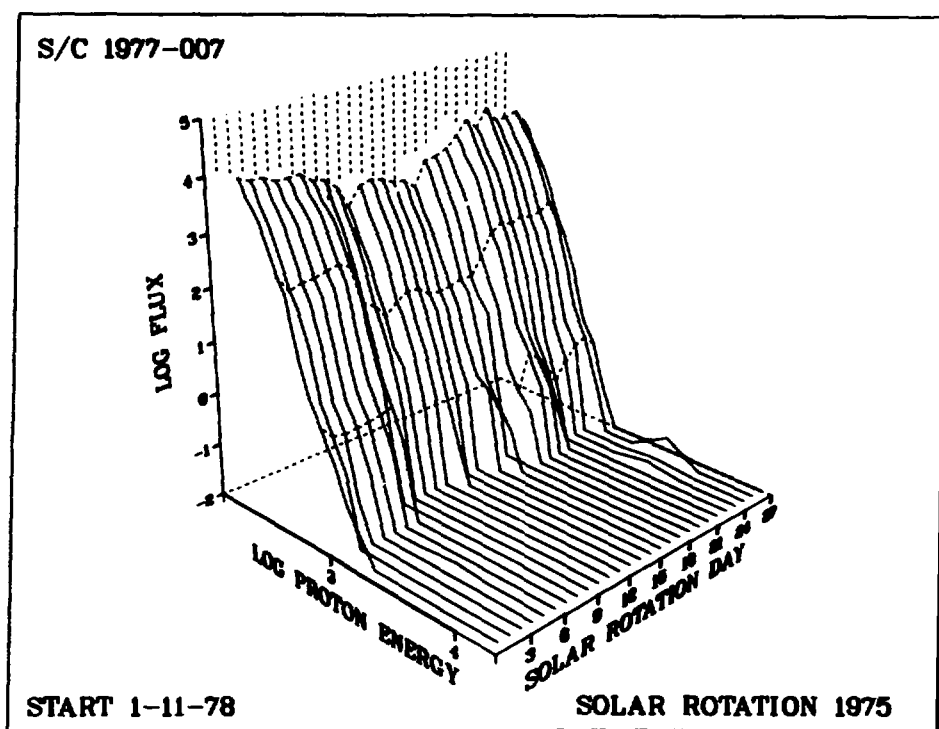
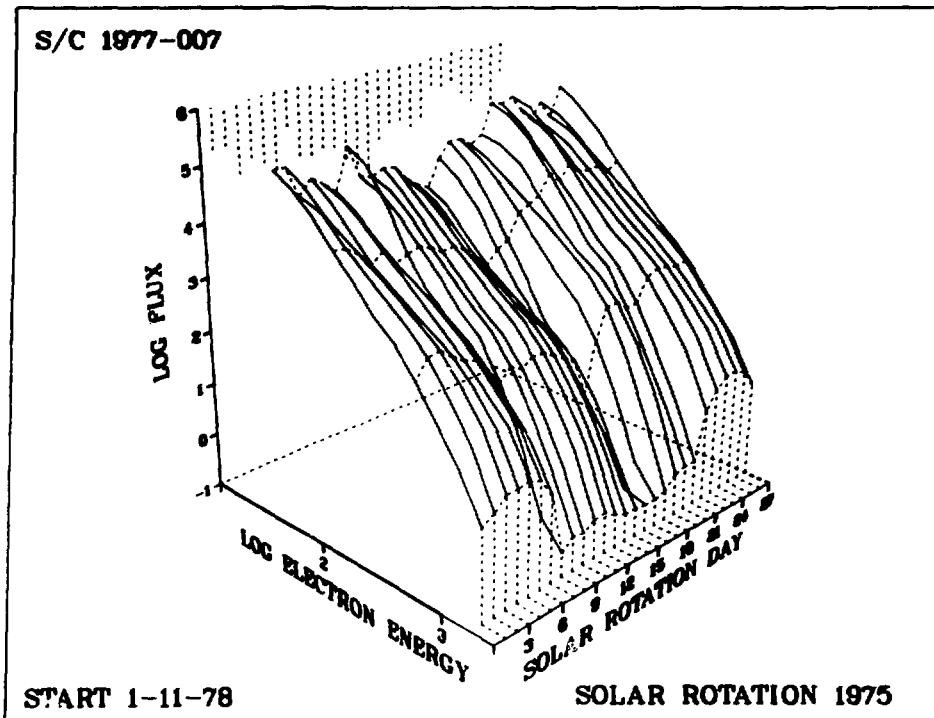


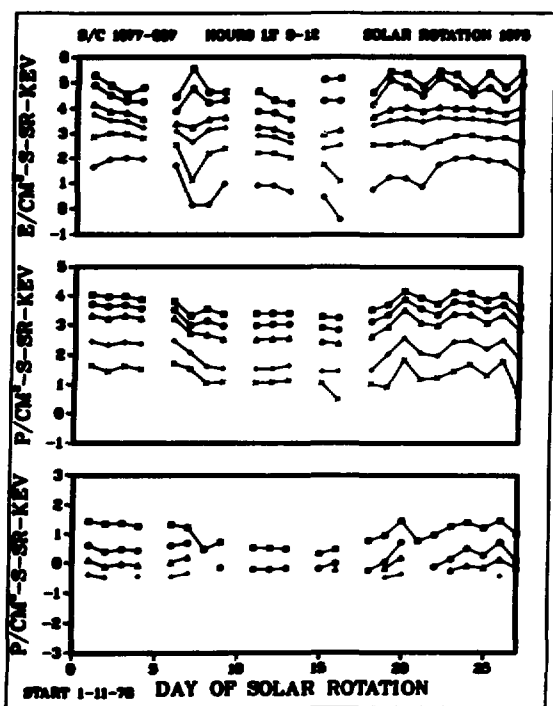
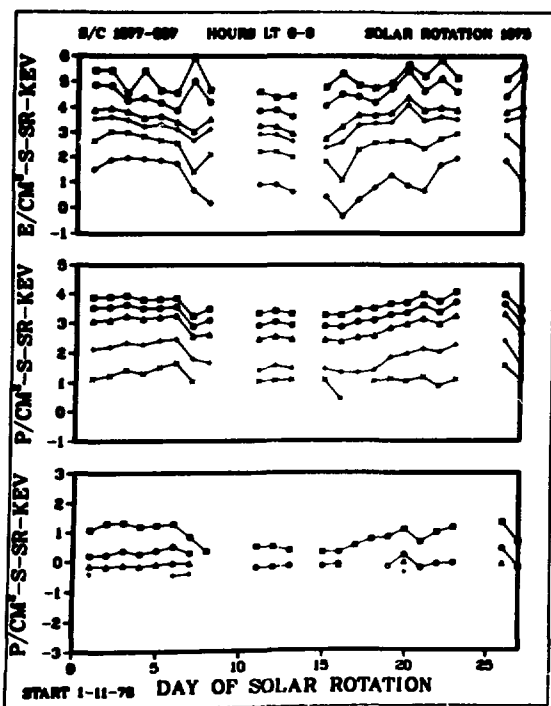
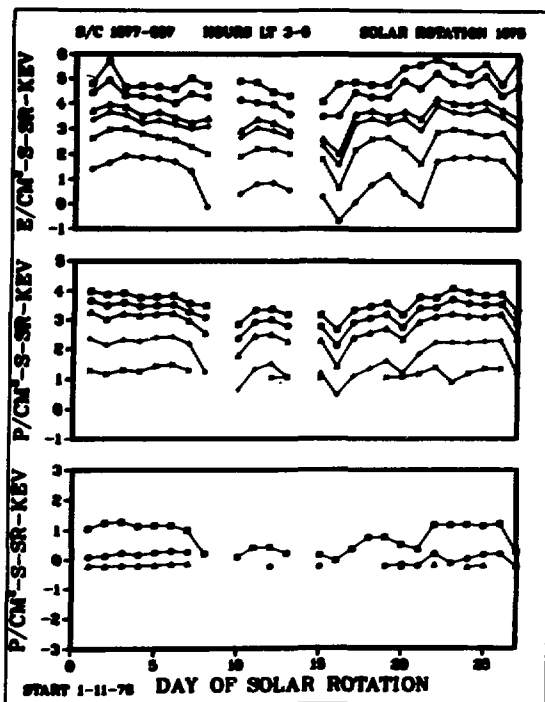
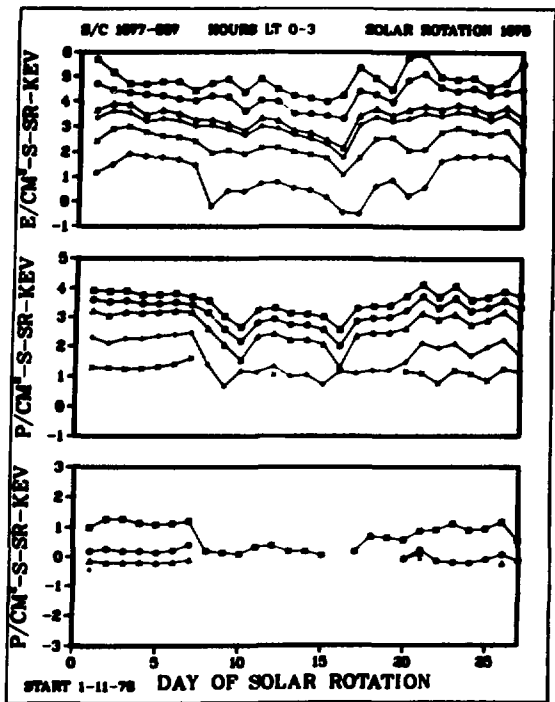
START 12-15-77

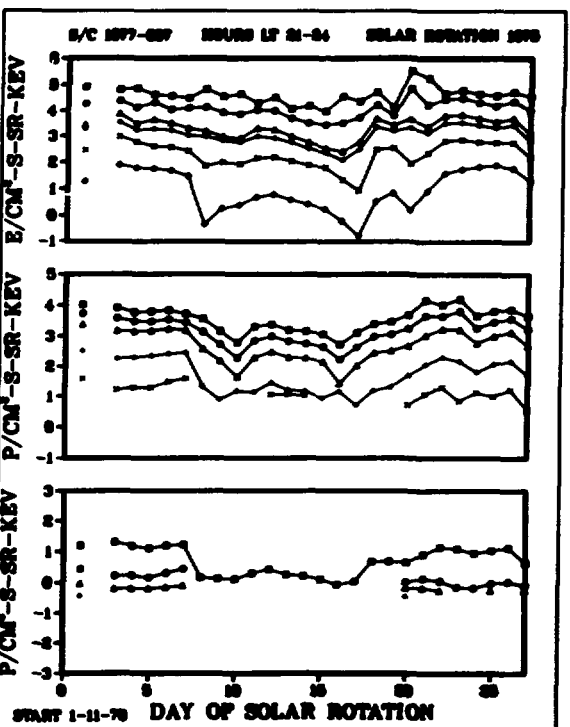
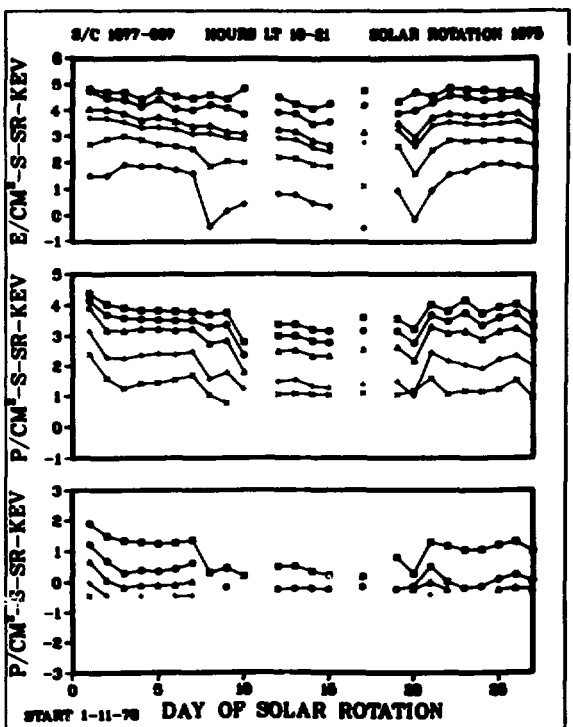
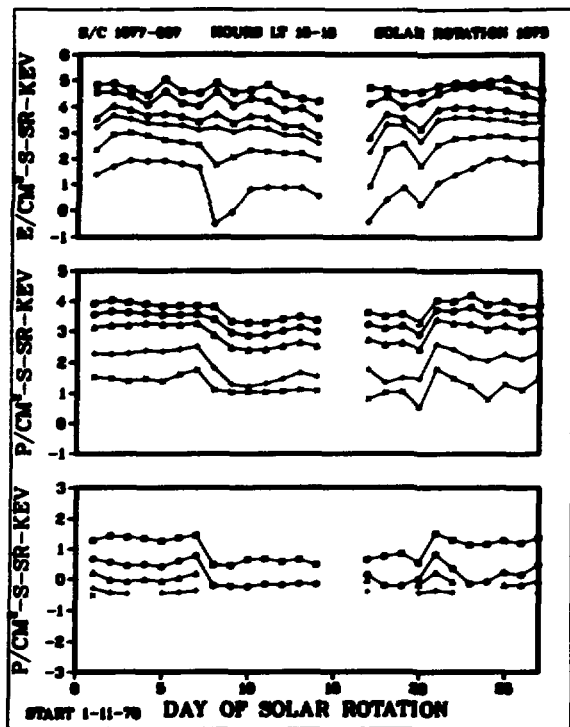
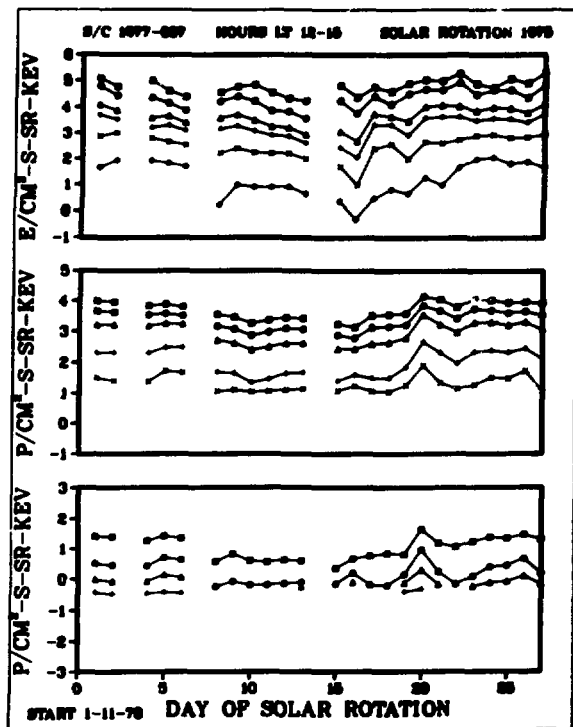
SOLAR ROTATION 1974



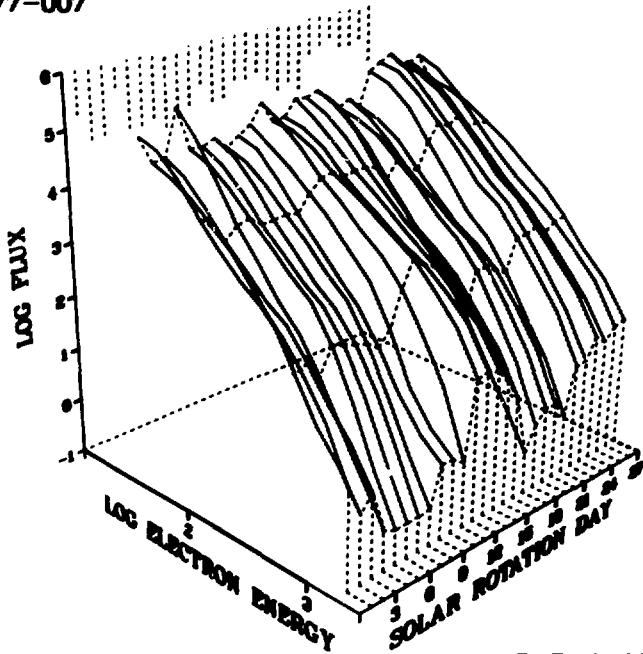








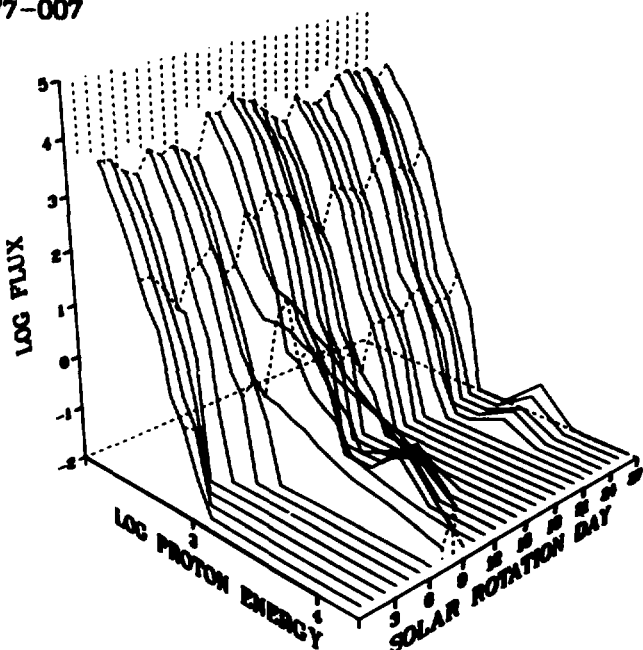
S/C 1977-007



START 2-7-78

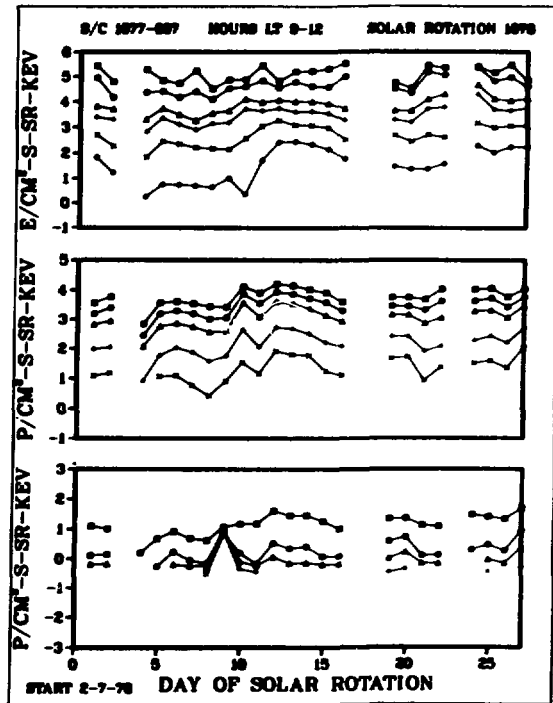
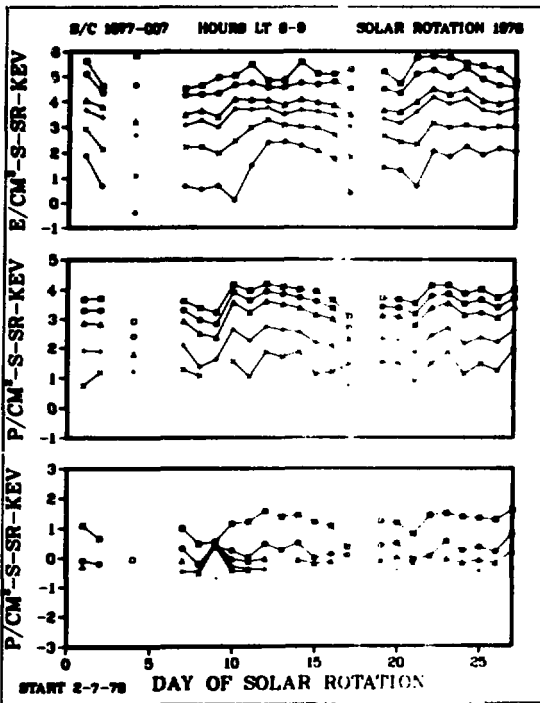
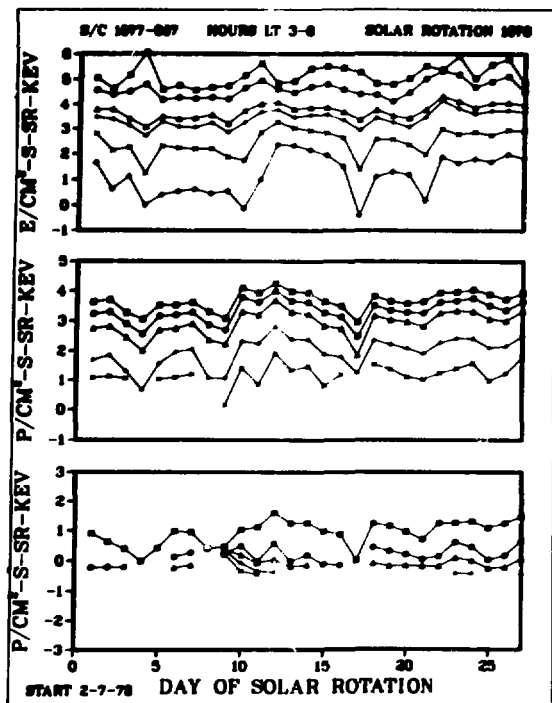
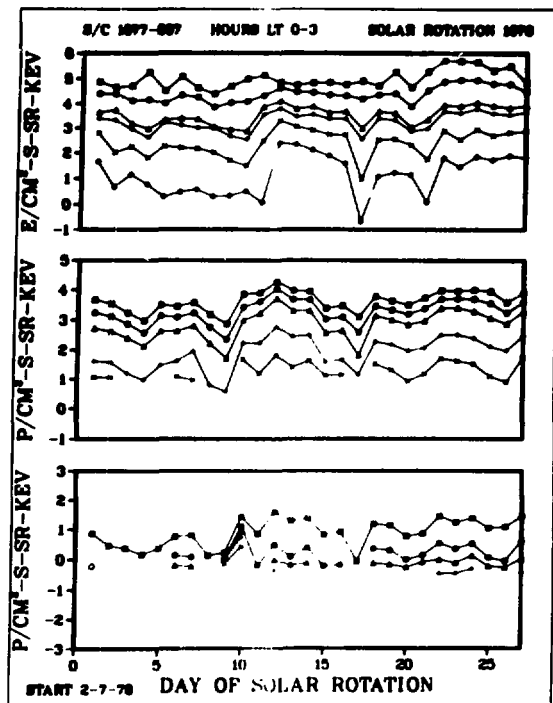
SOLAR ROTATION 1976

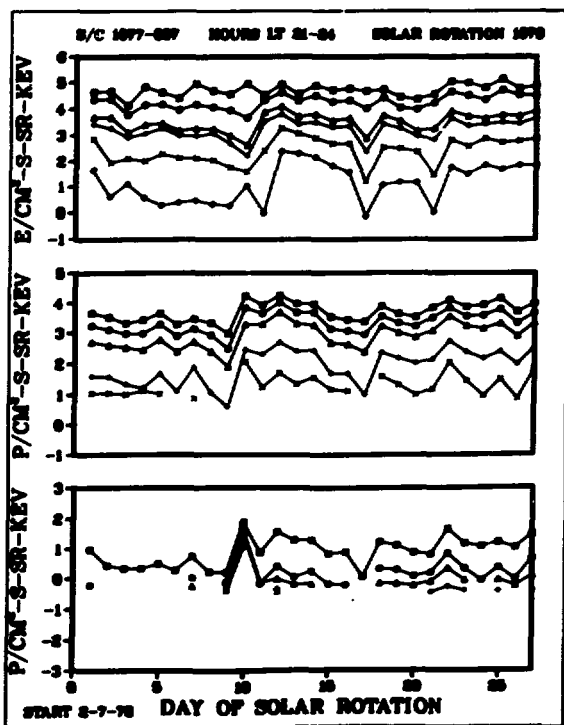
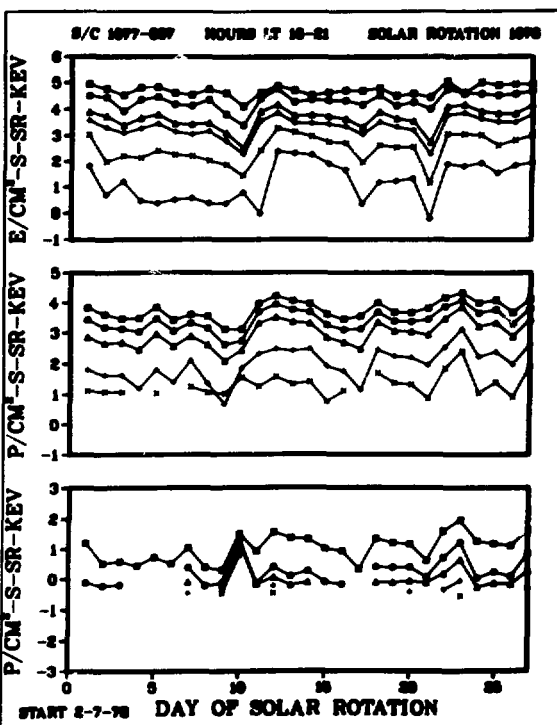
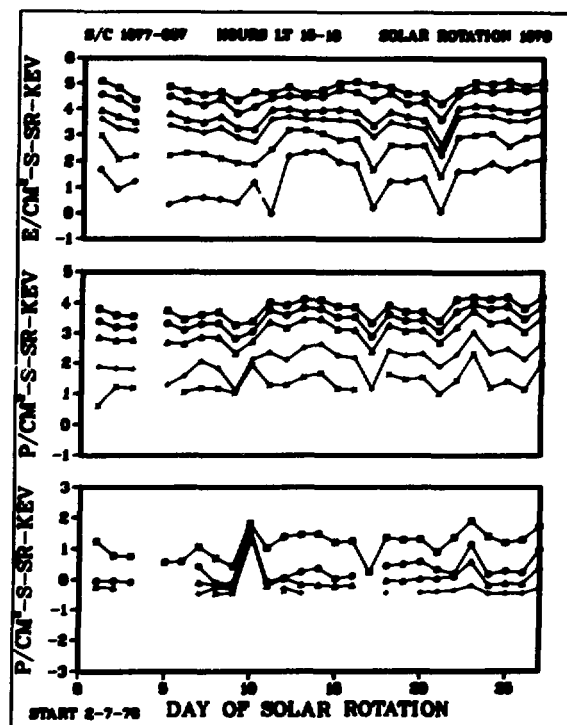
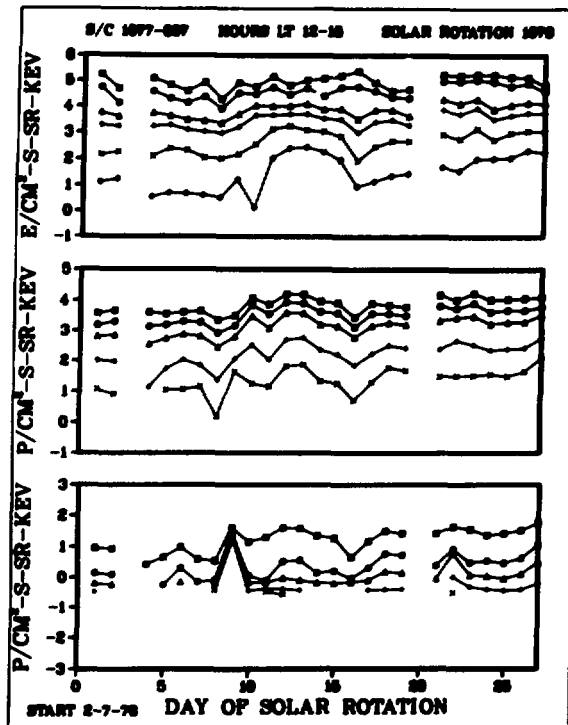
S/C 1977-007

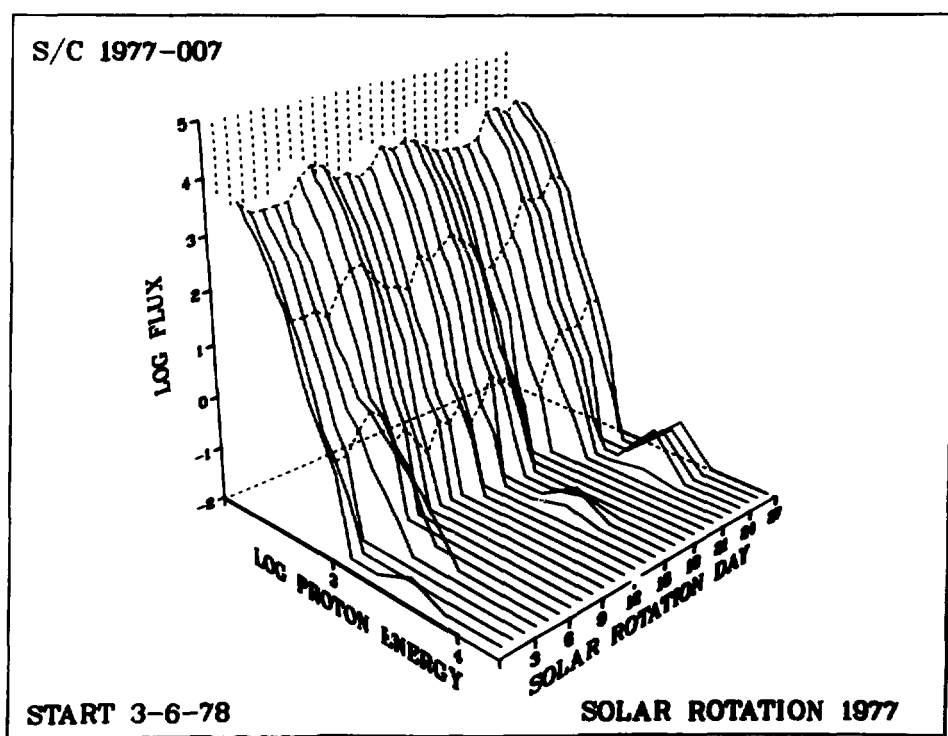
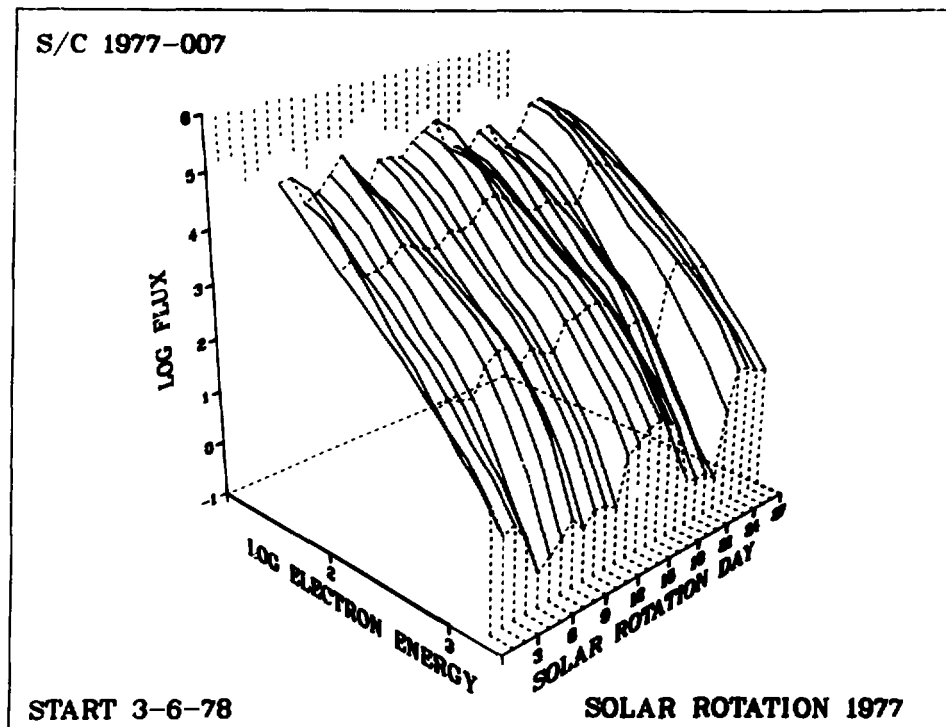


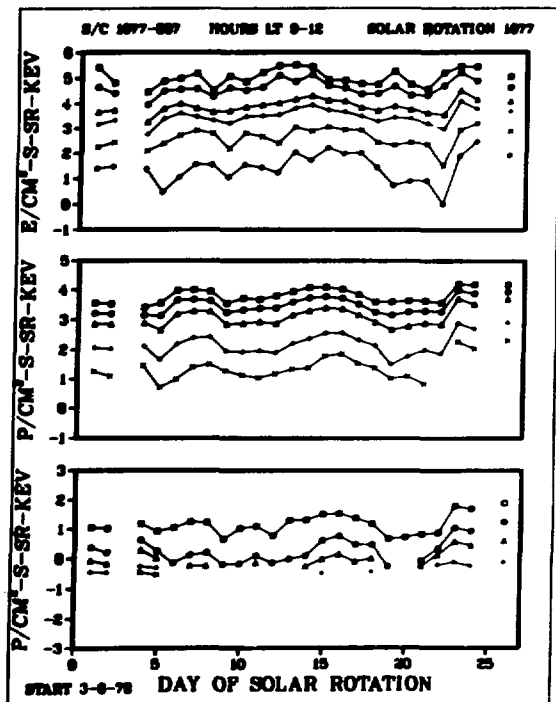
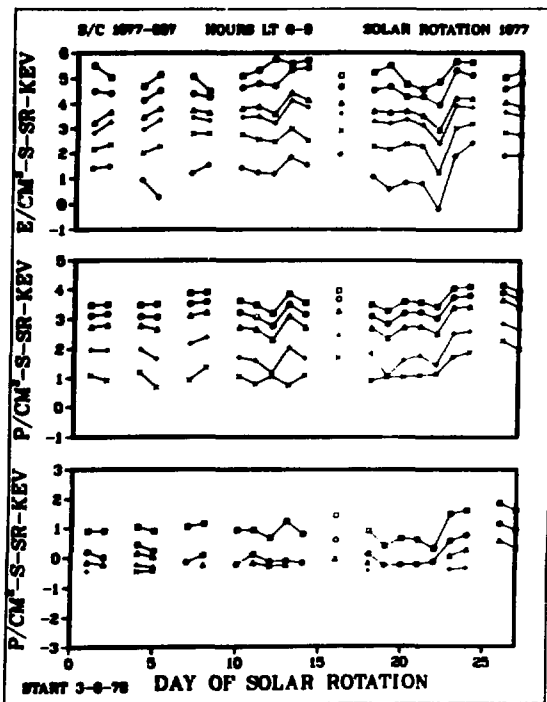
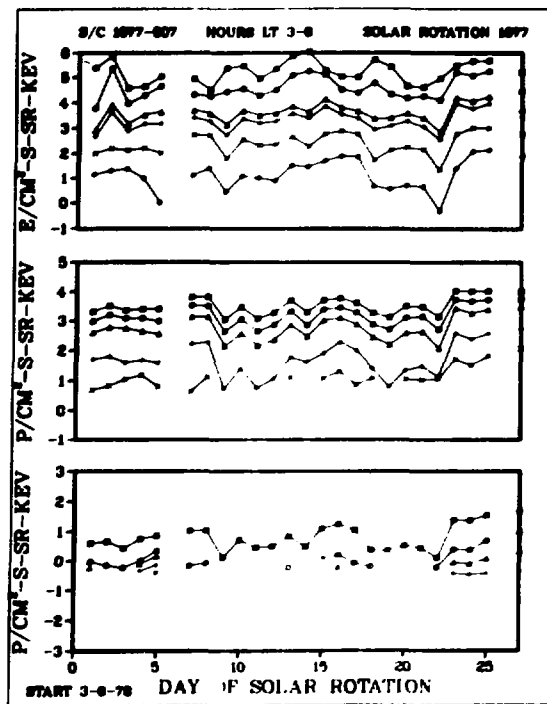
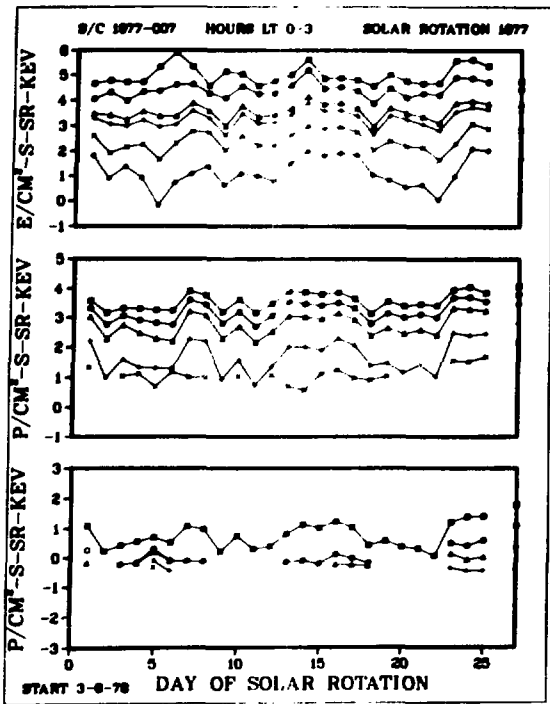
START 2-7-78

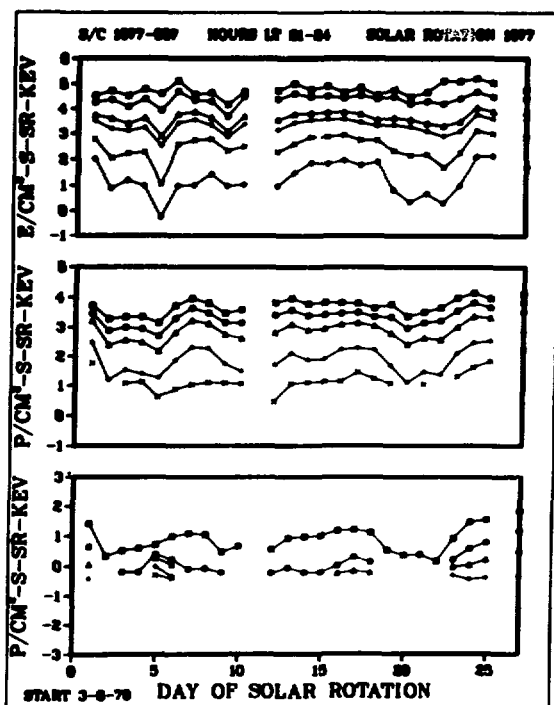
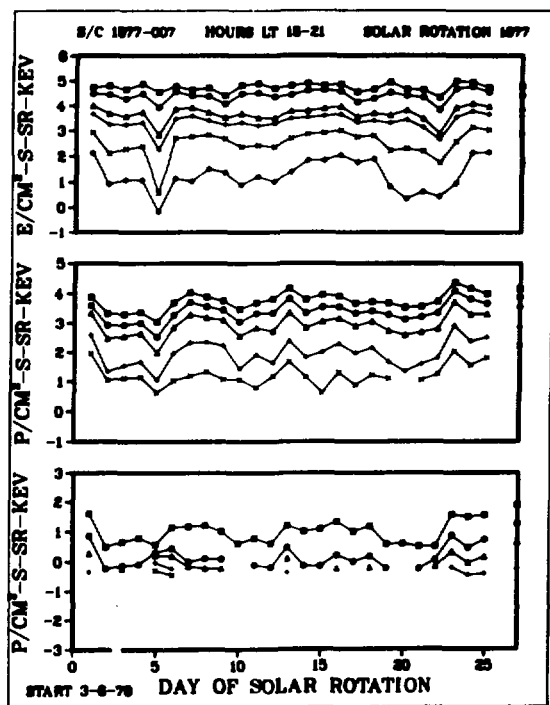
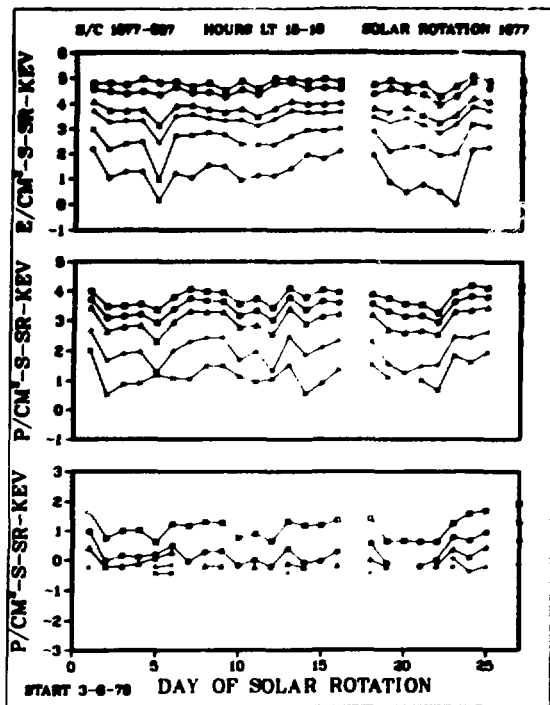
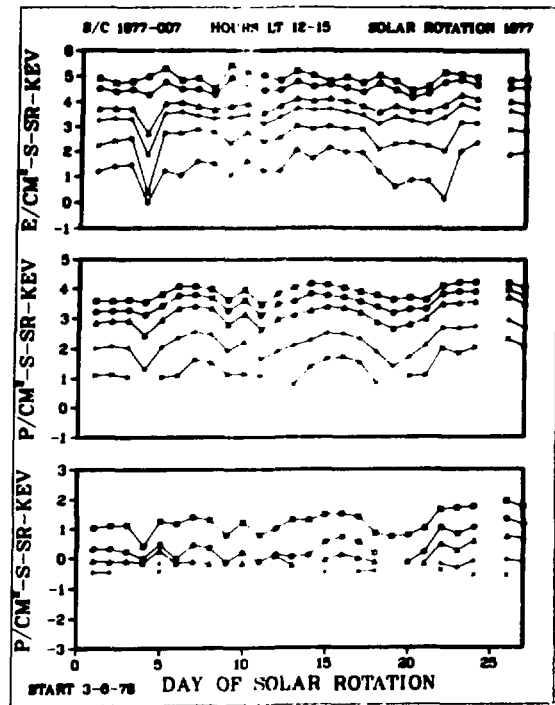
SOLAR ROTATION 1976



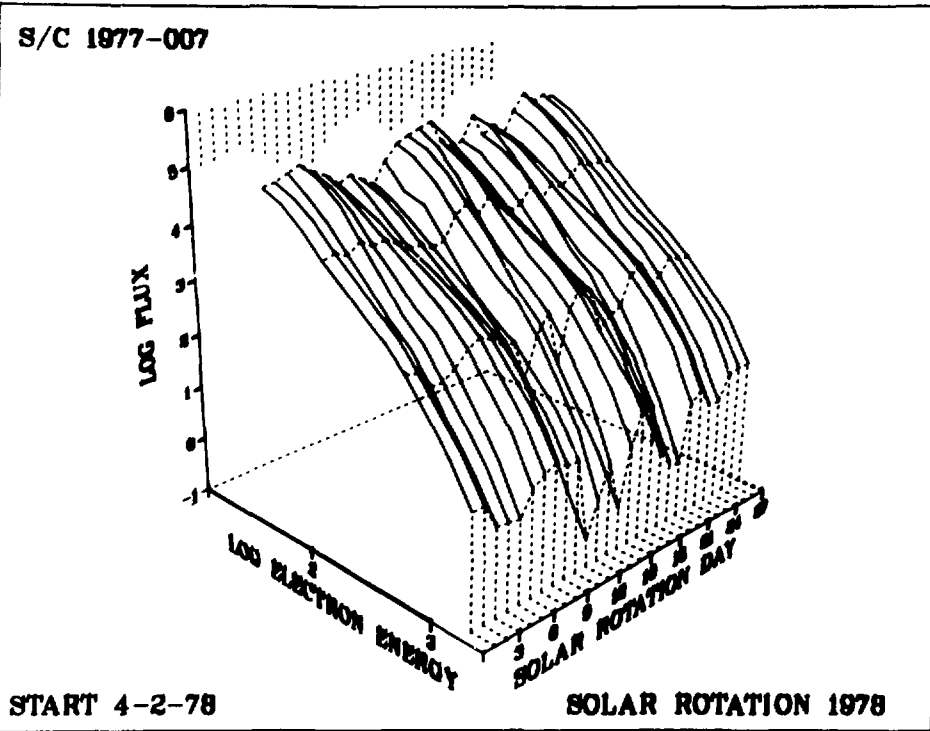




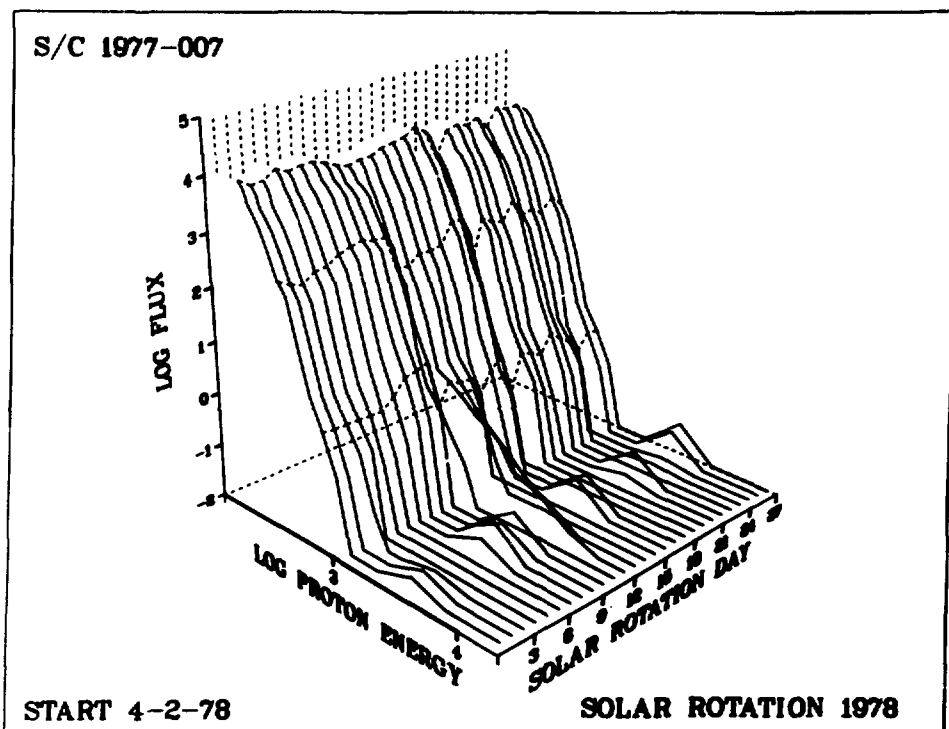


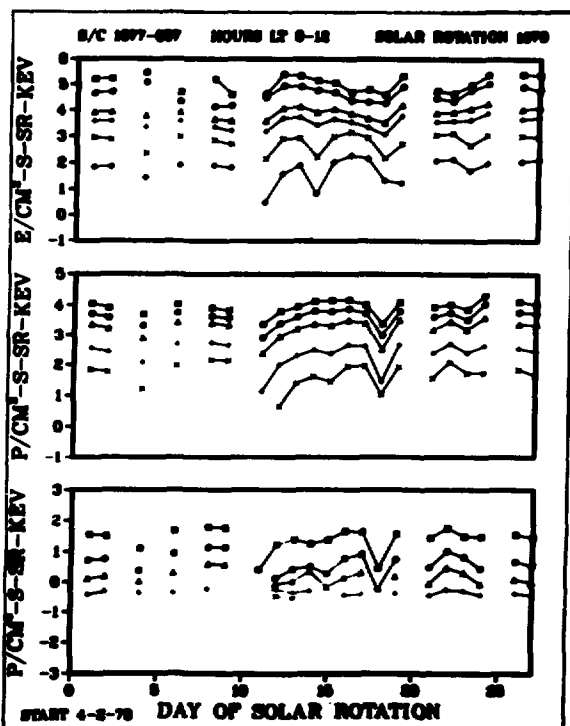
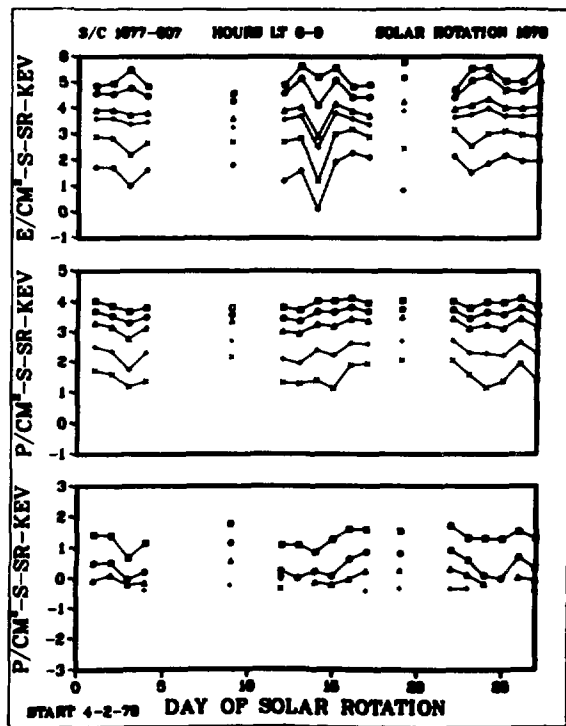
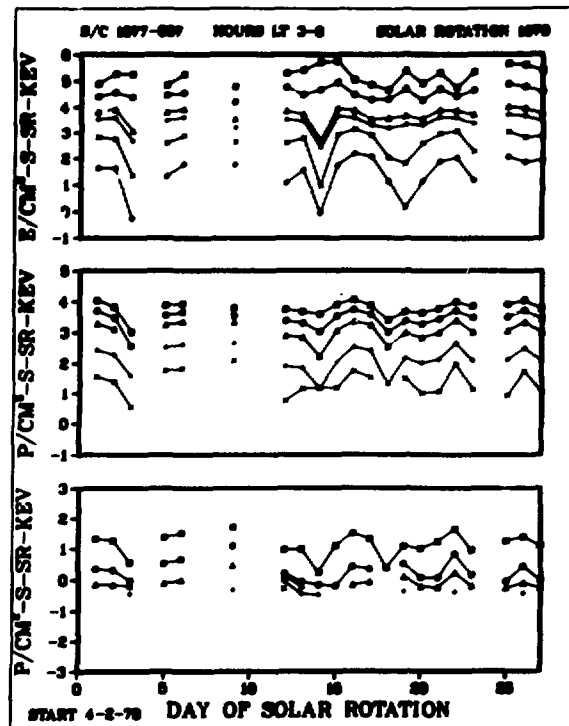
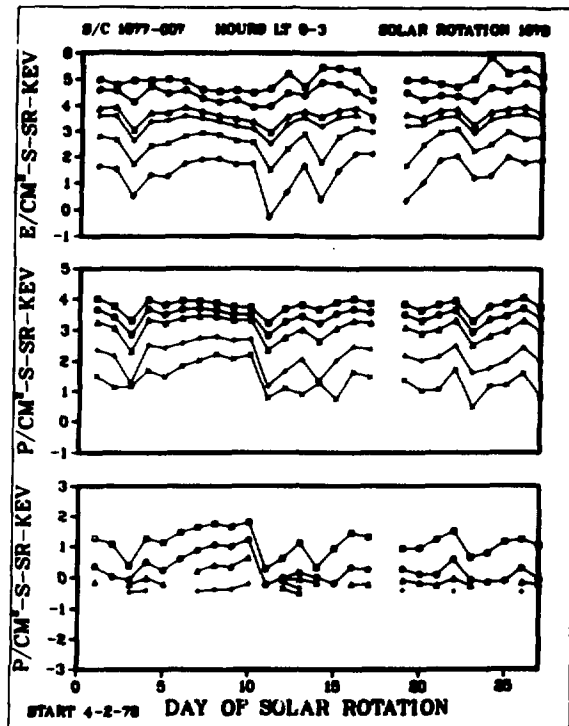


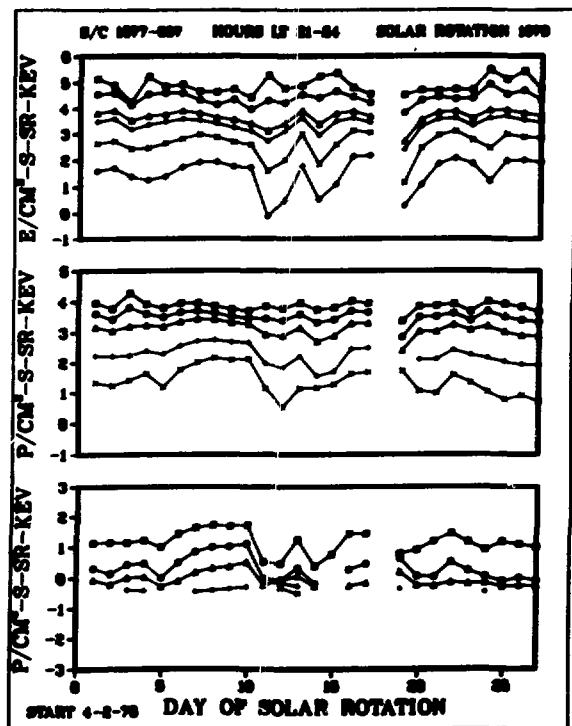
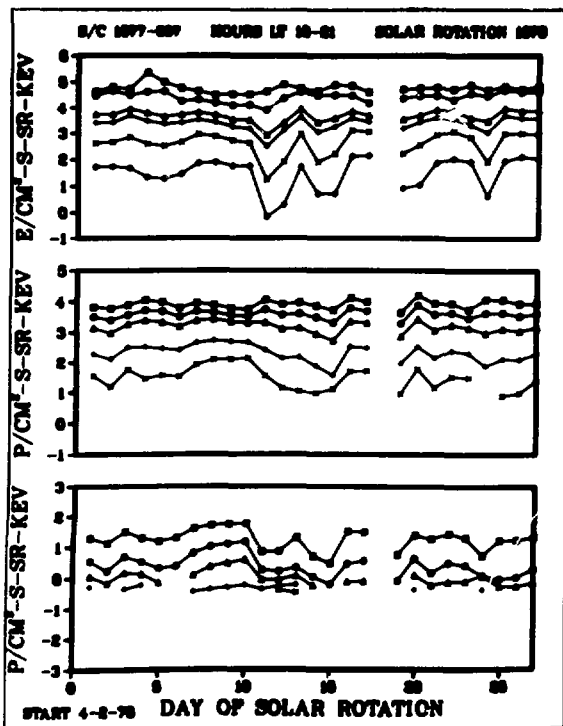
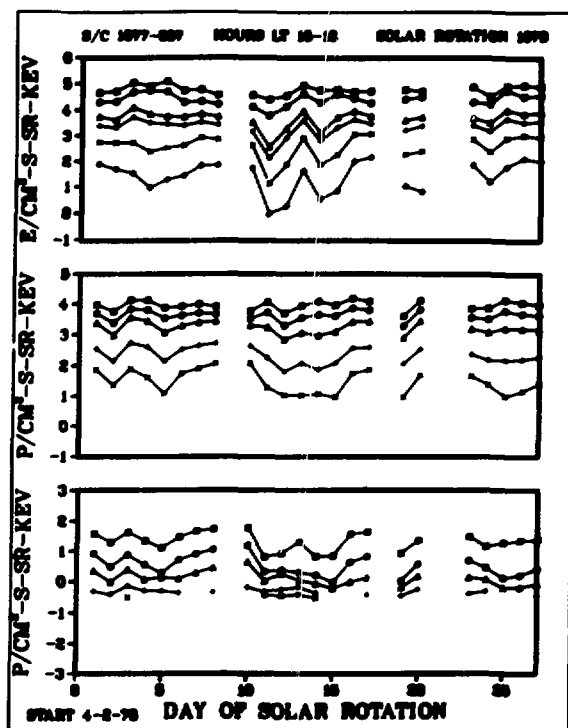
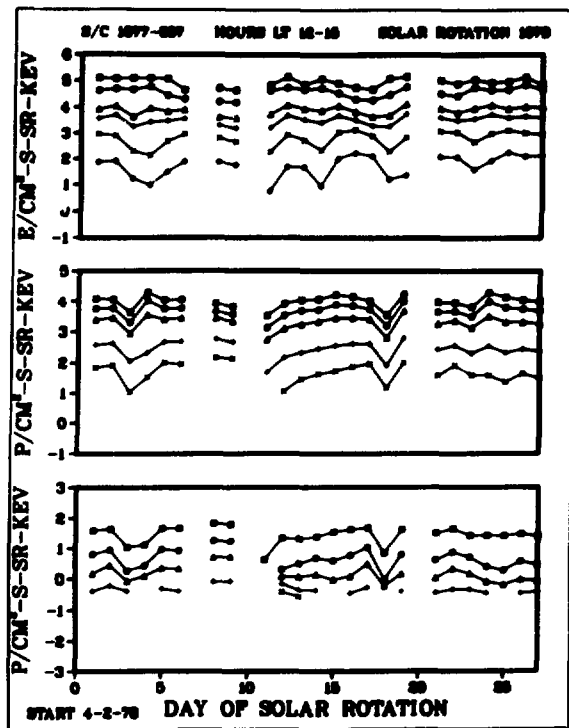
S/C 1977-007

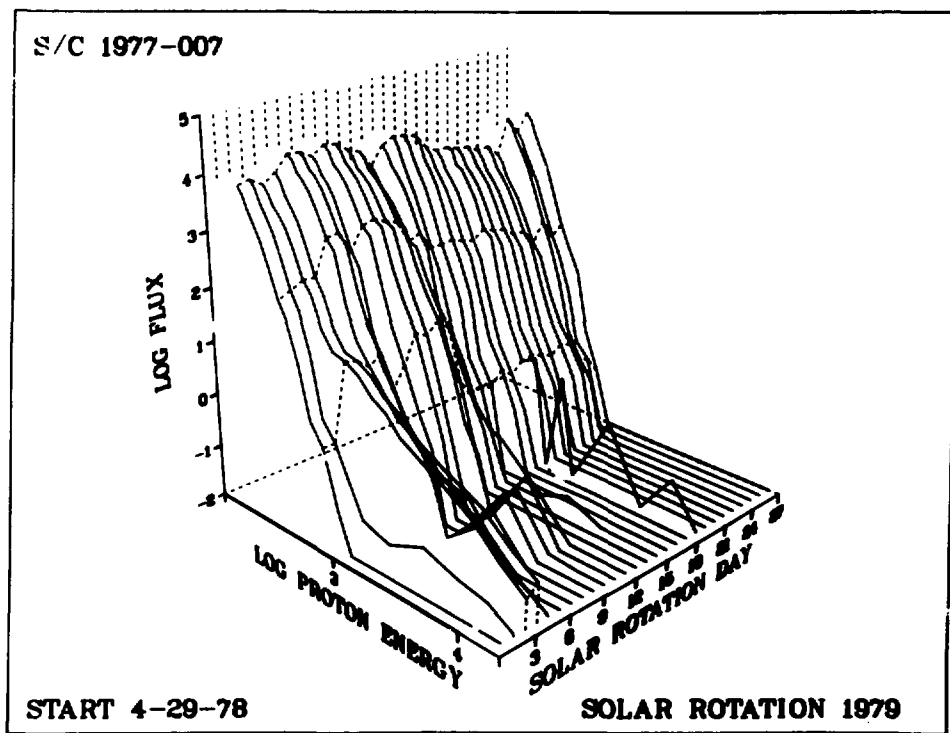
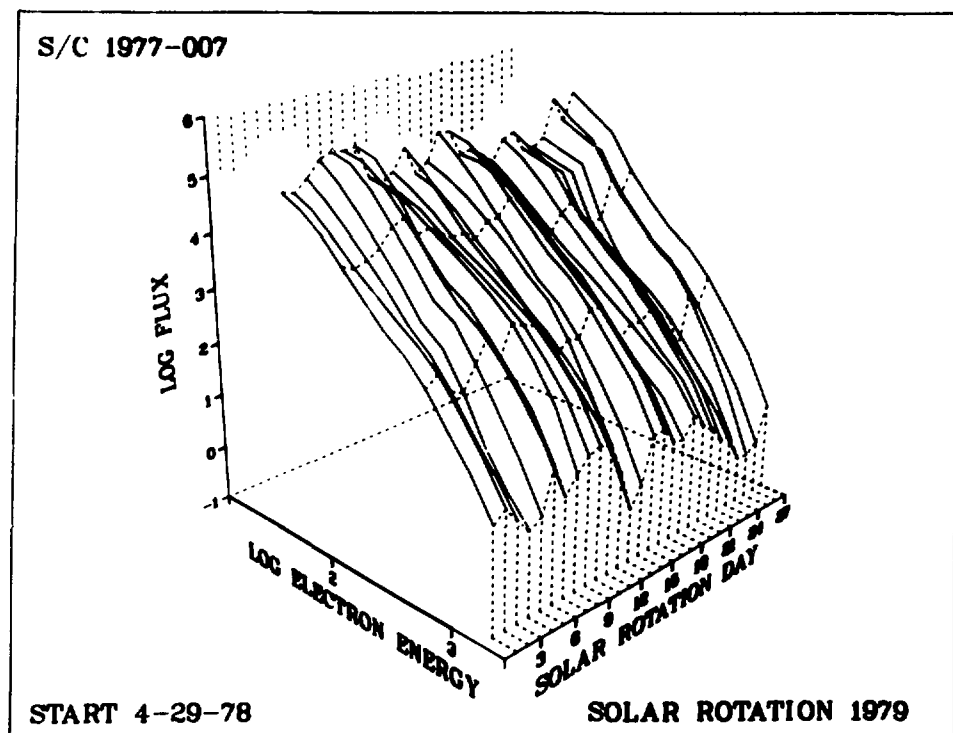


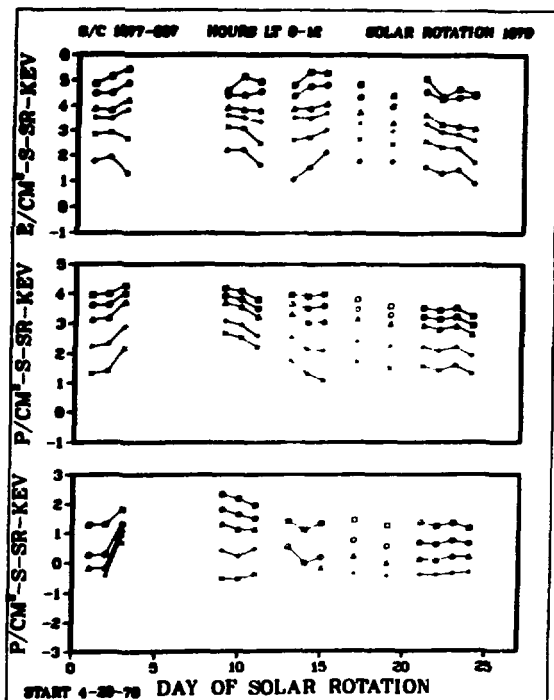
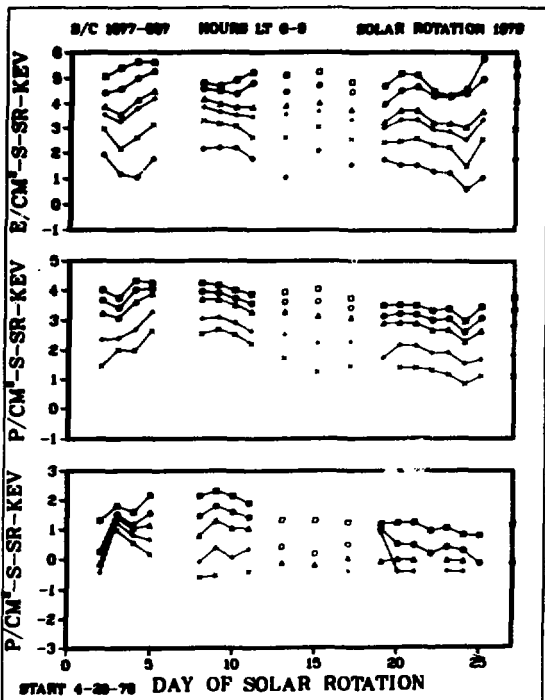
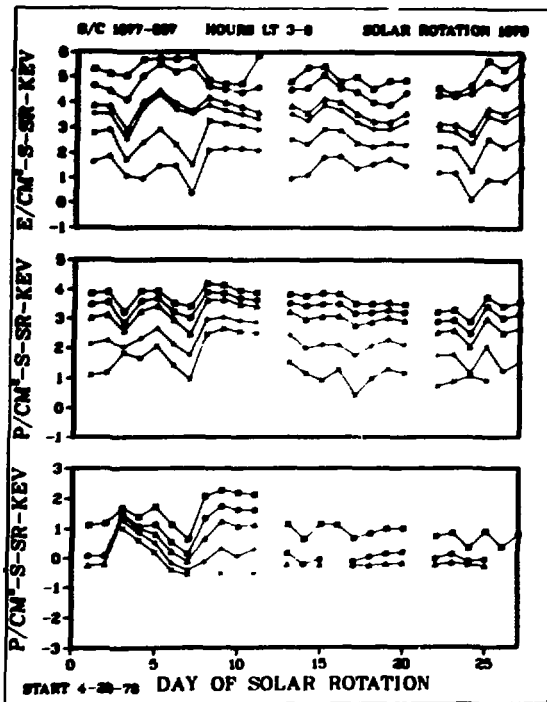
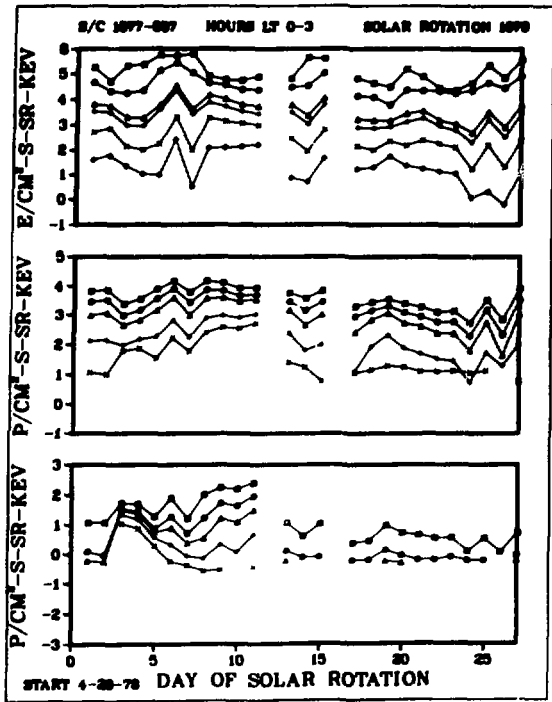
S/C 1977-007

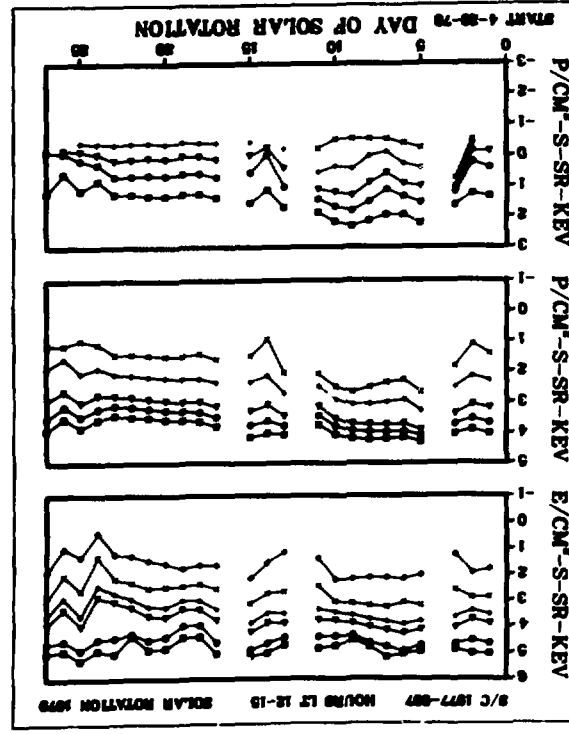
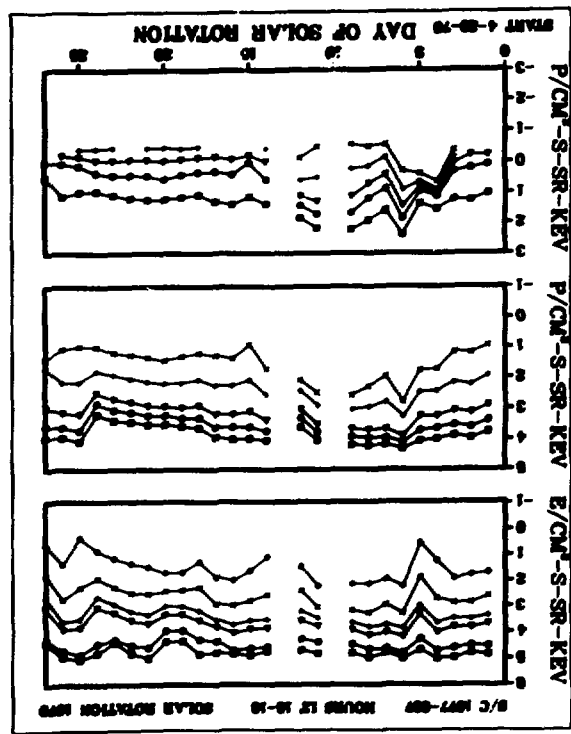
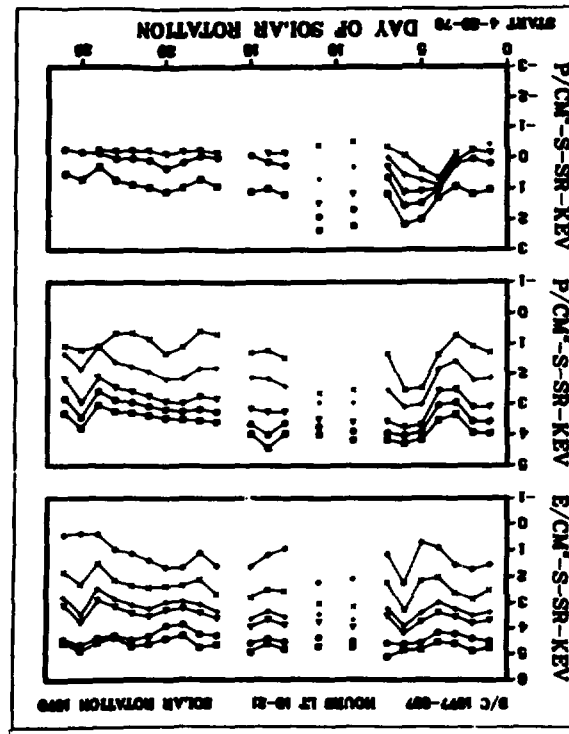
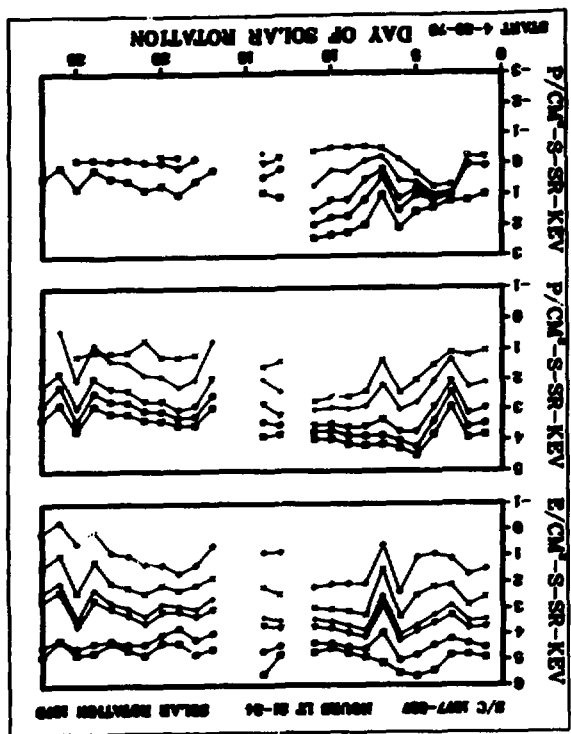




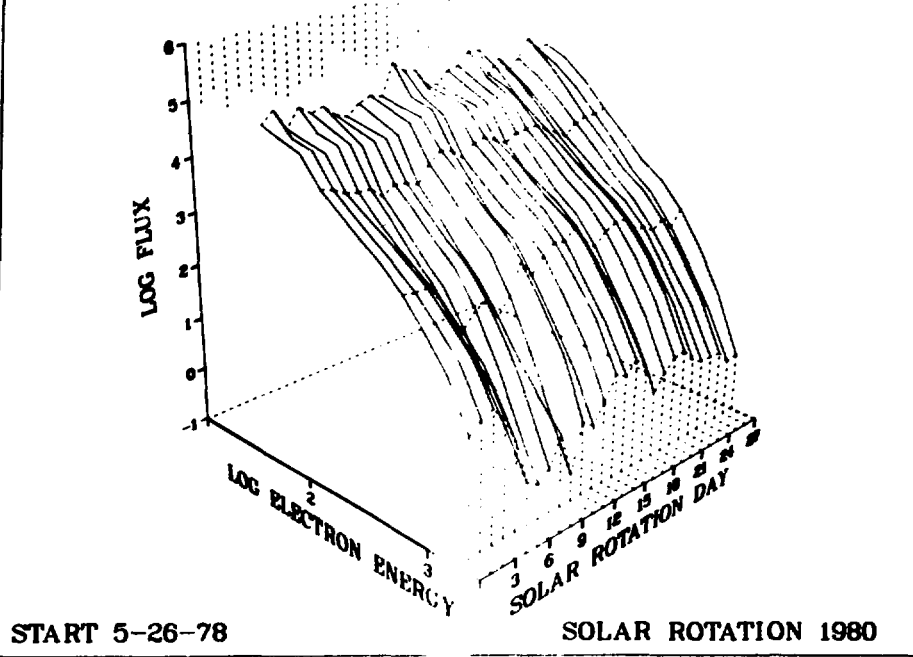




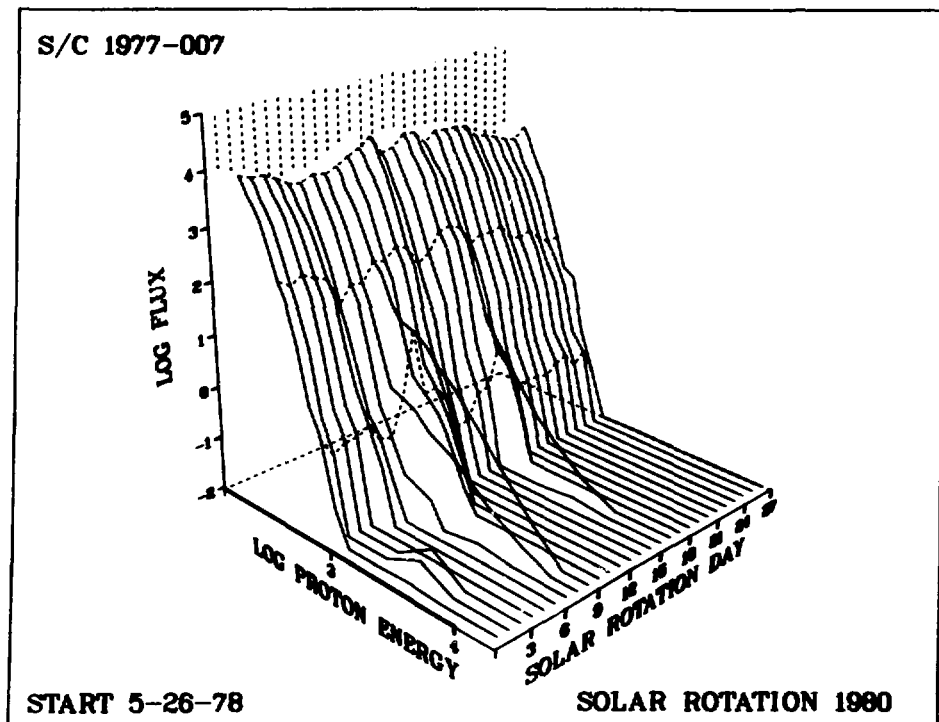


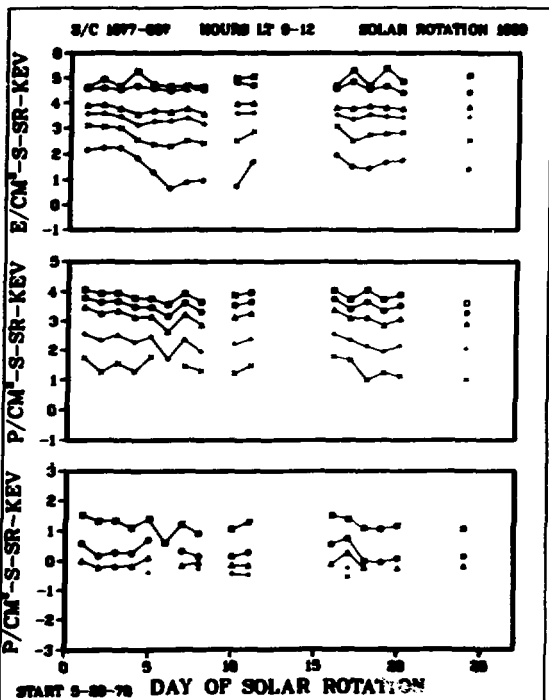
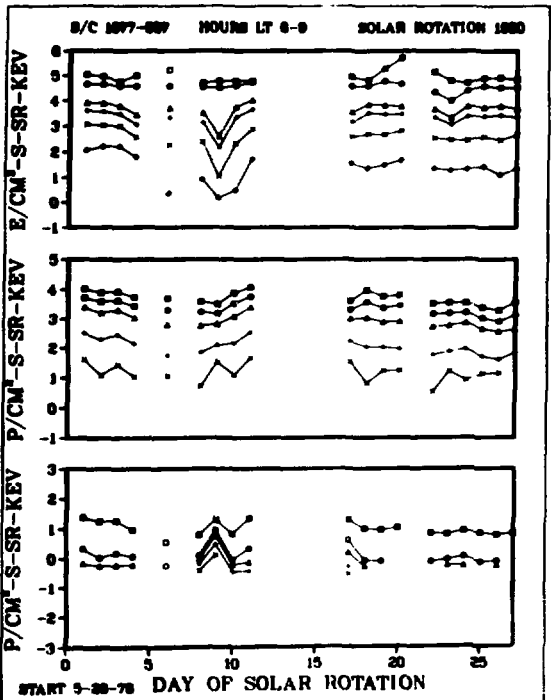
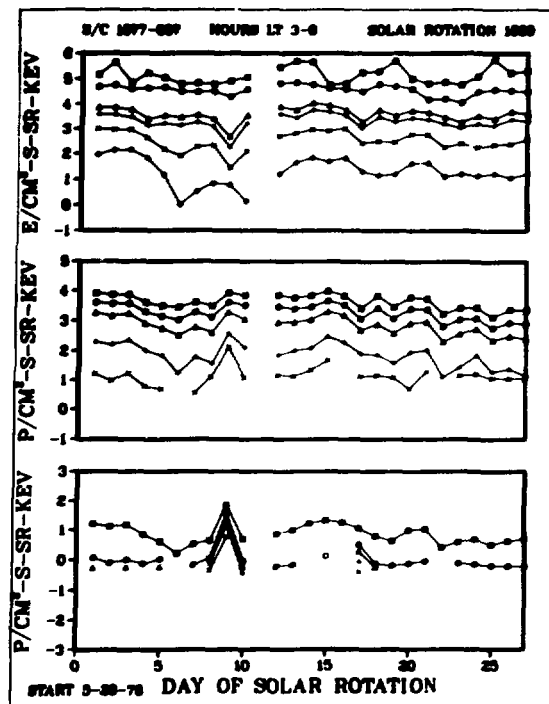
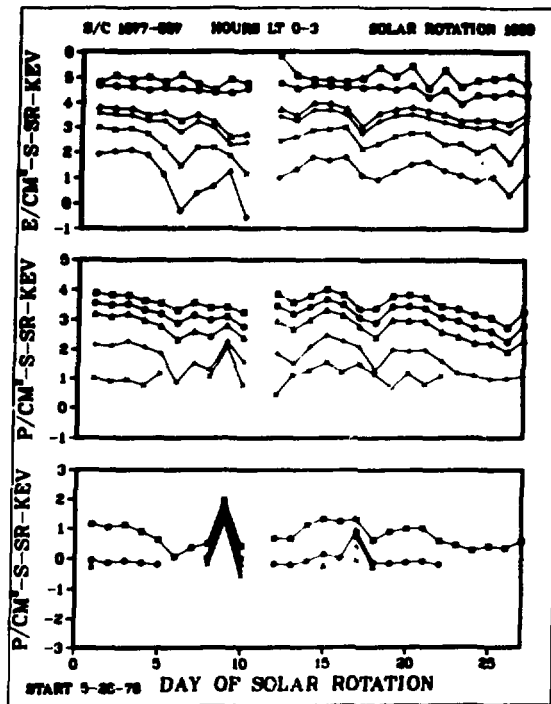


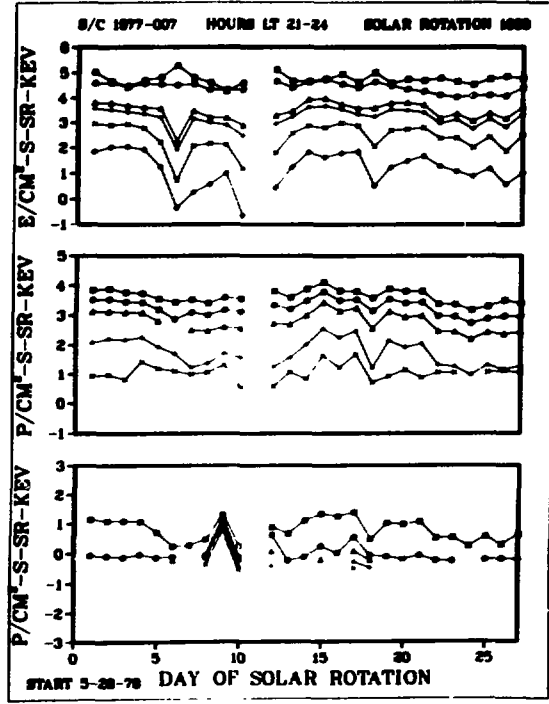
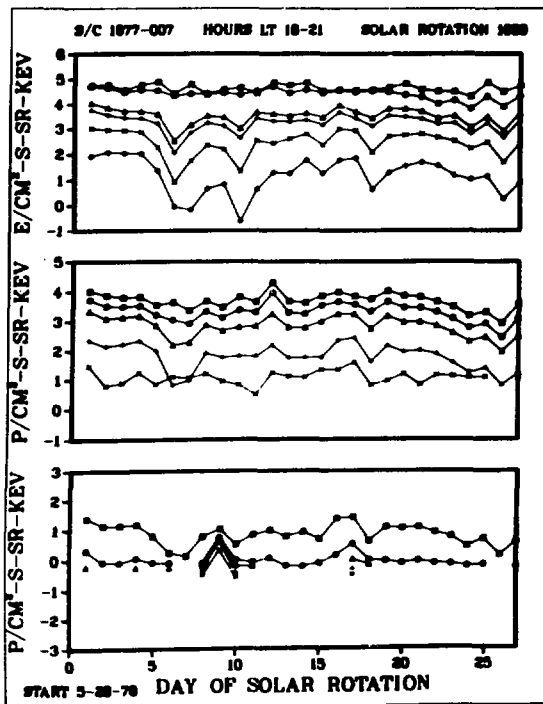
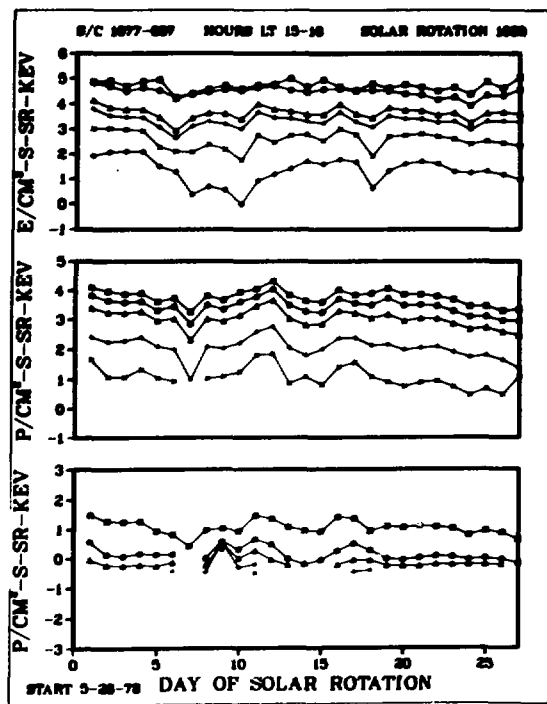
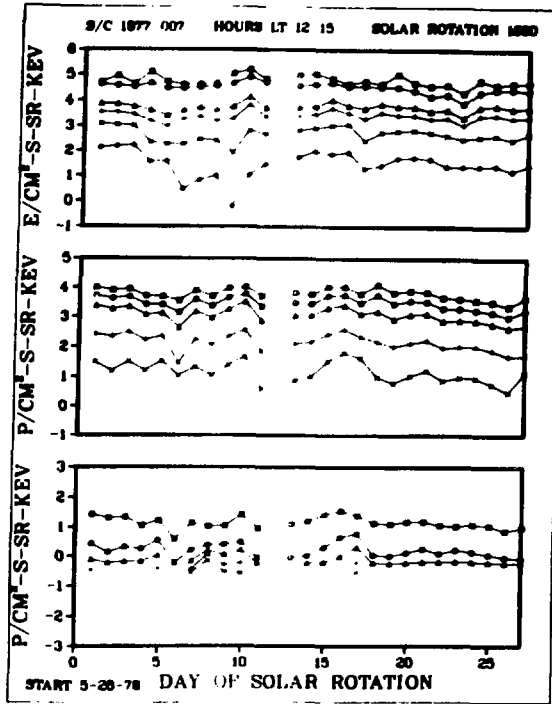
S/C 1977-007

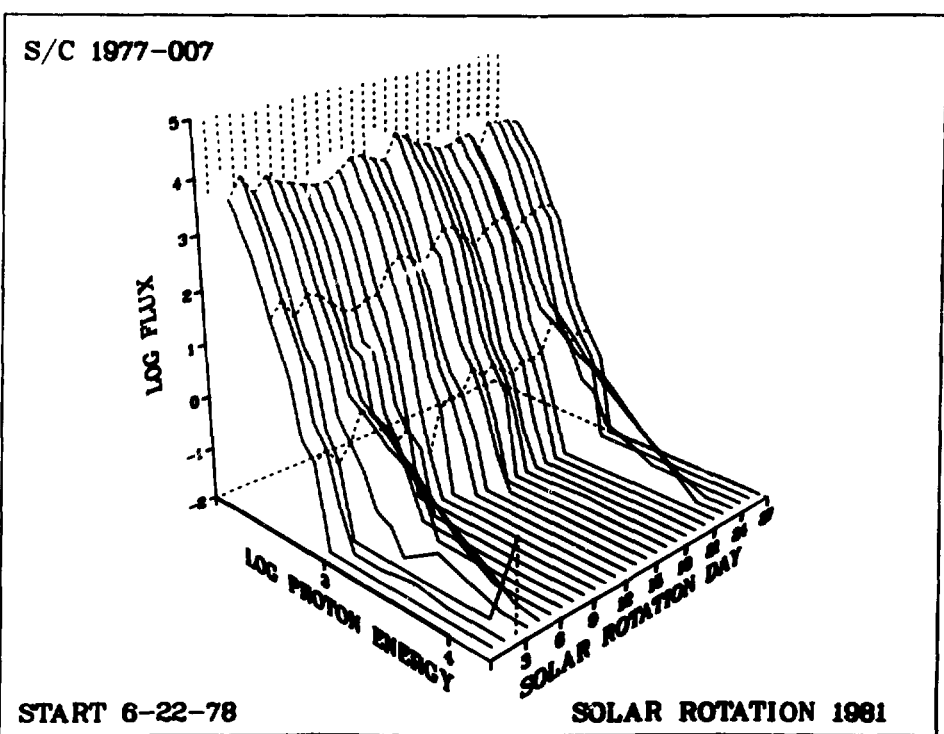
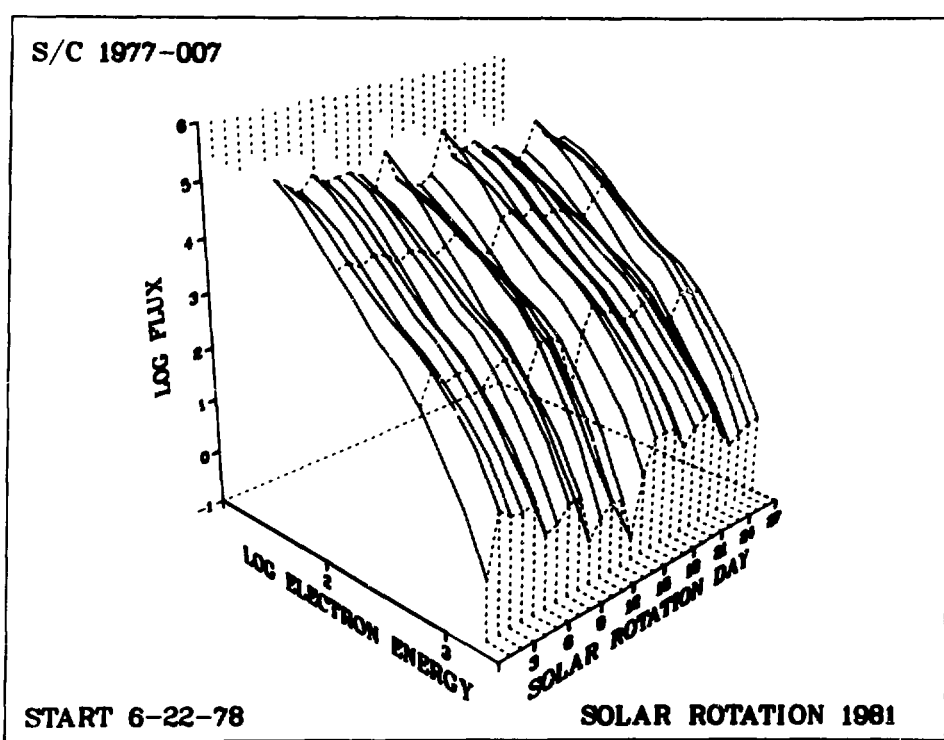


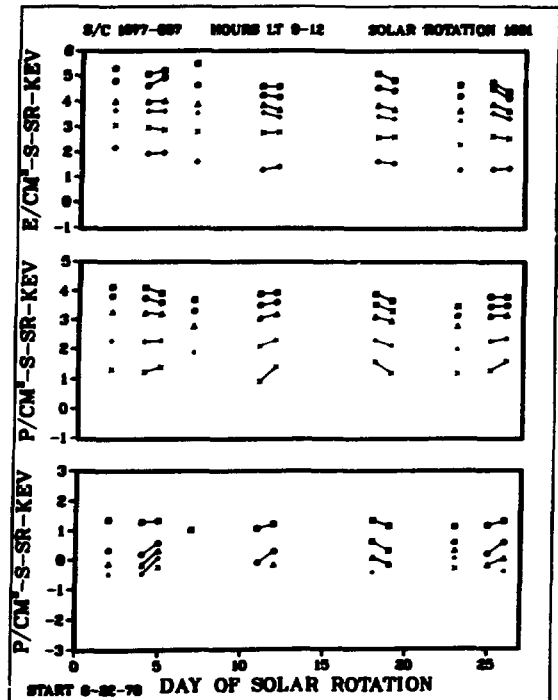
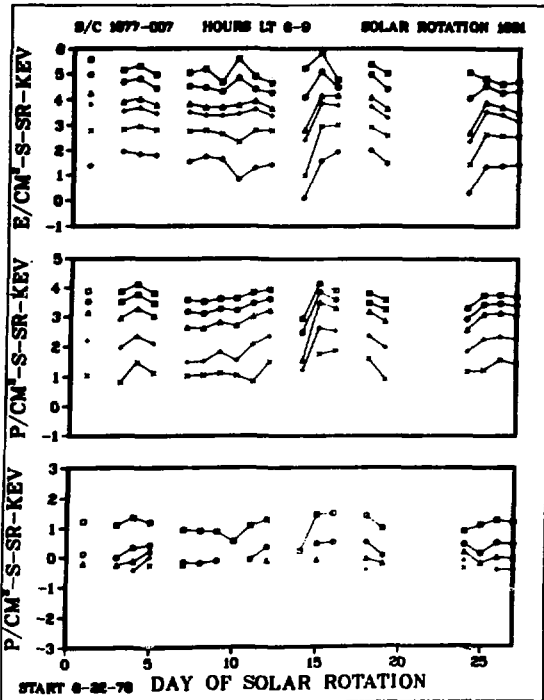
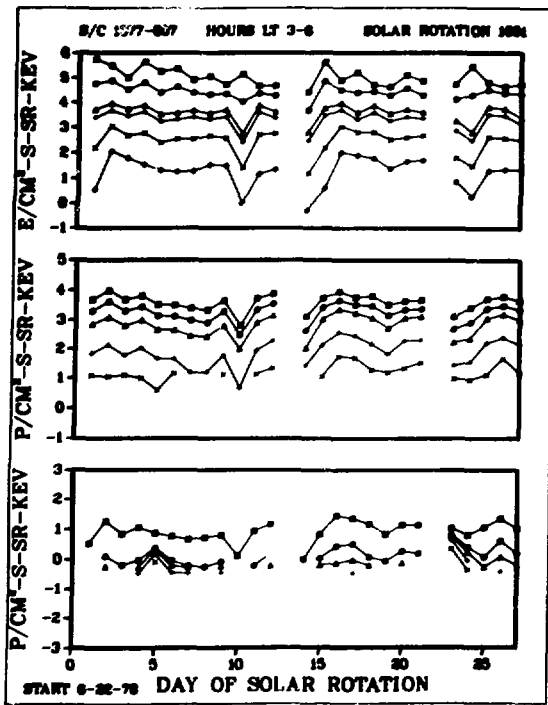
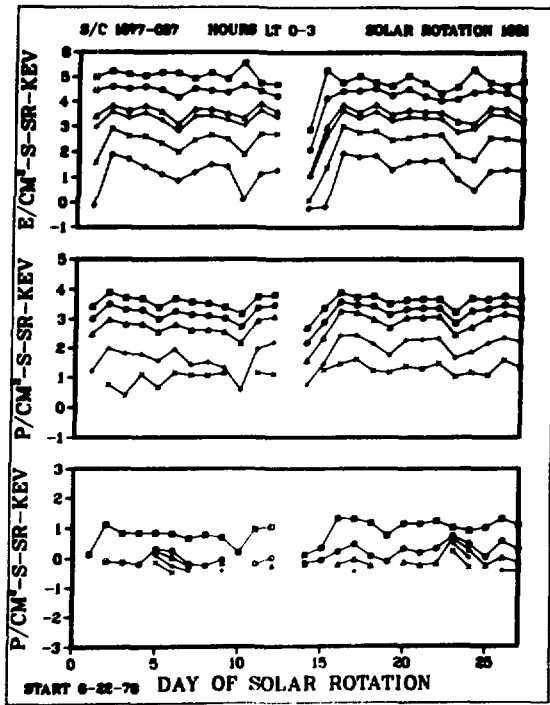
S/C 1977-007

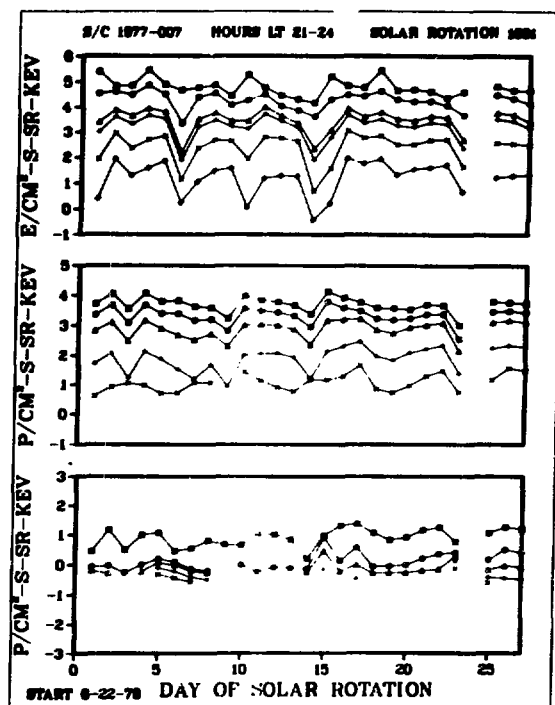
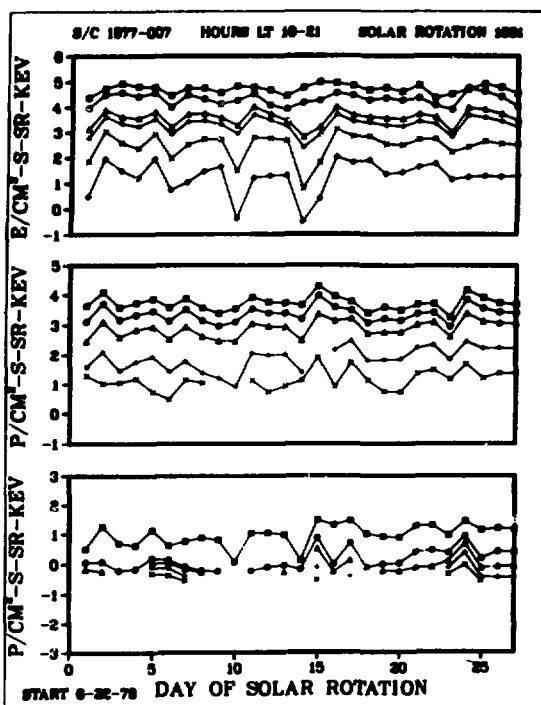
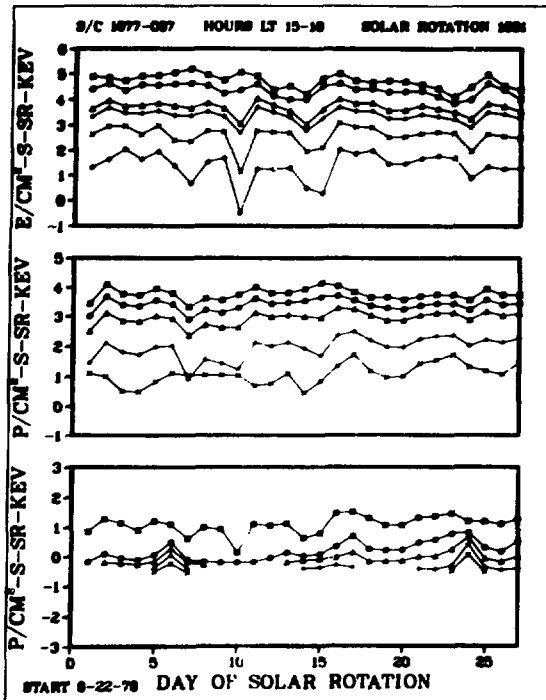
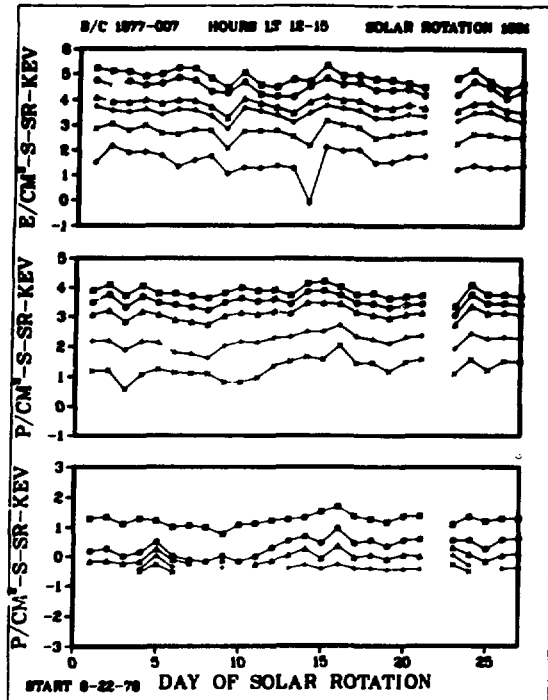




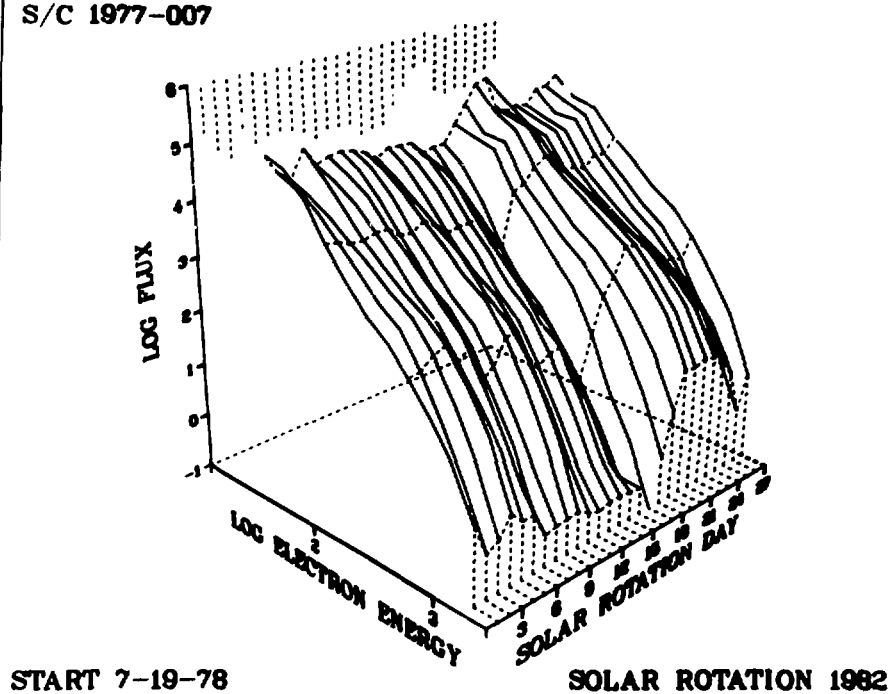




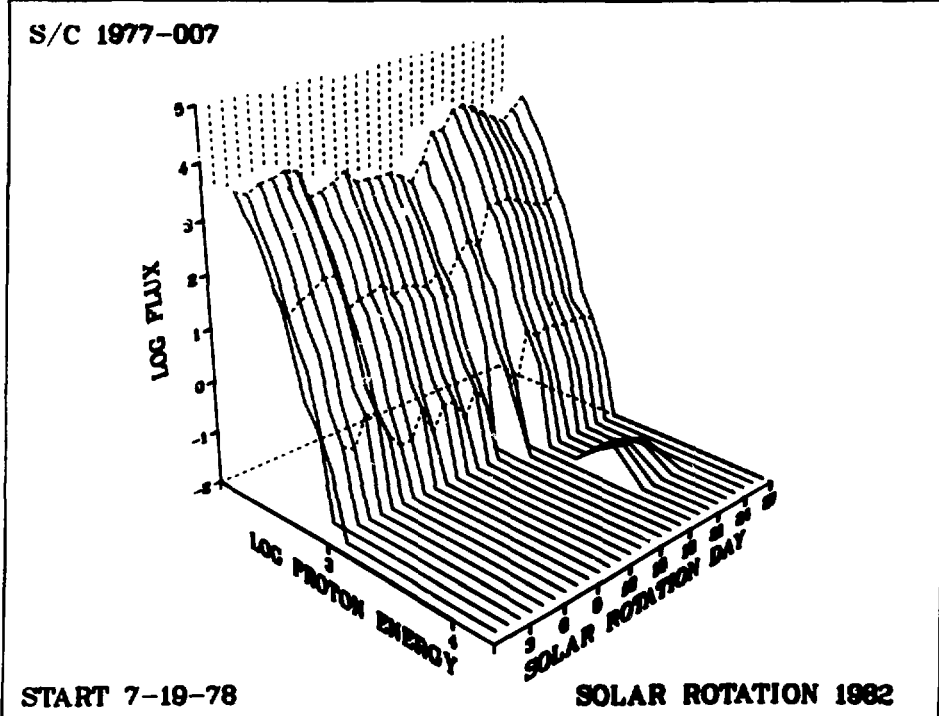


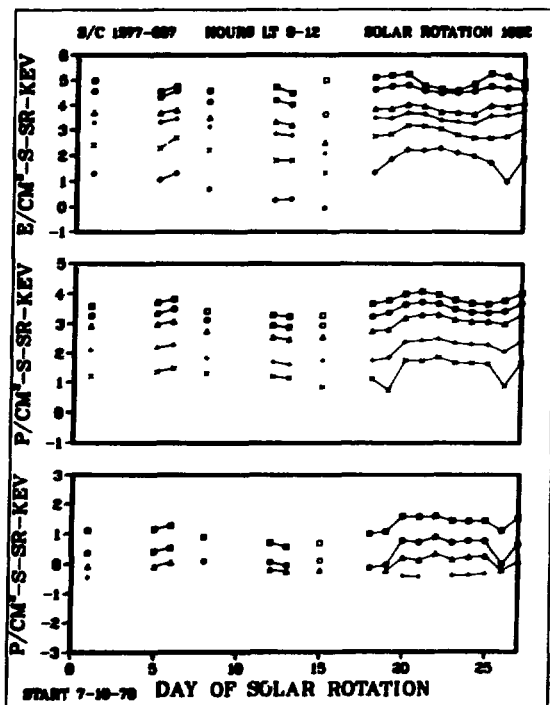
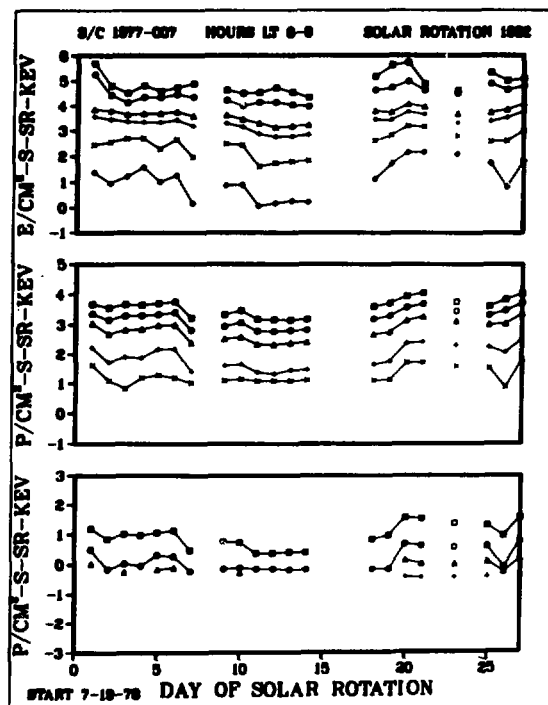
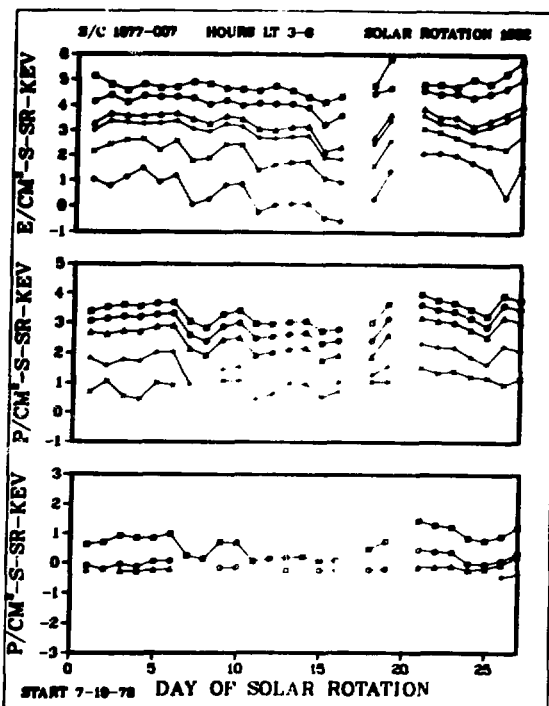
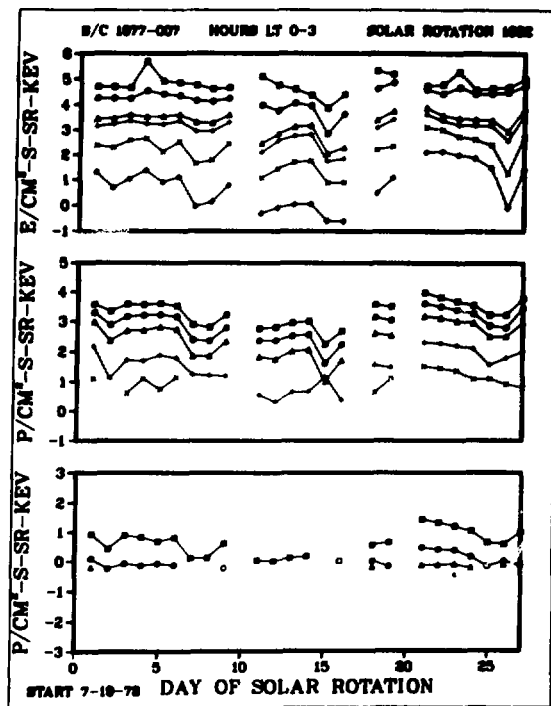


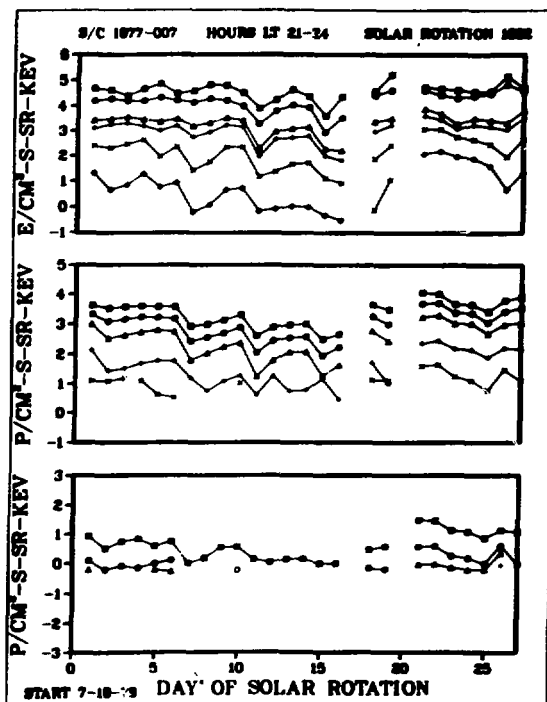
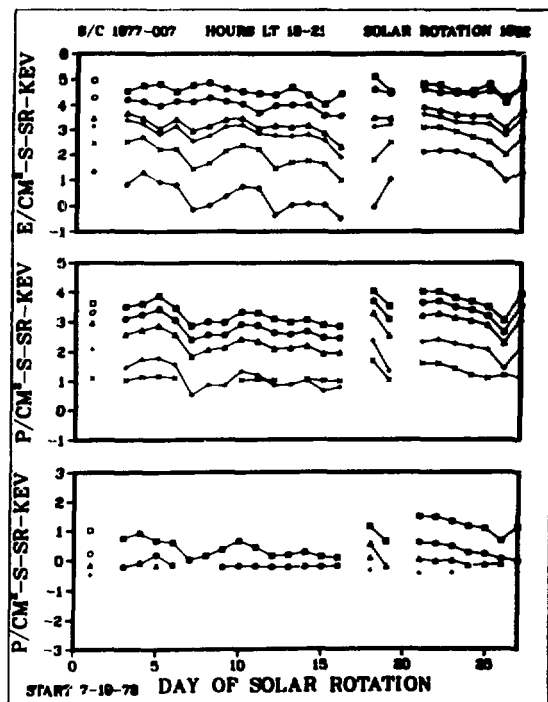
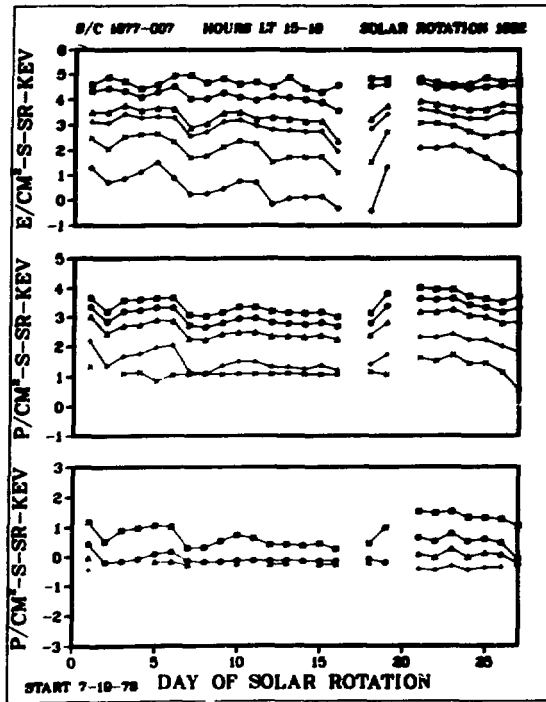
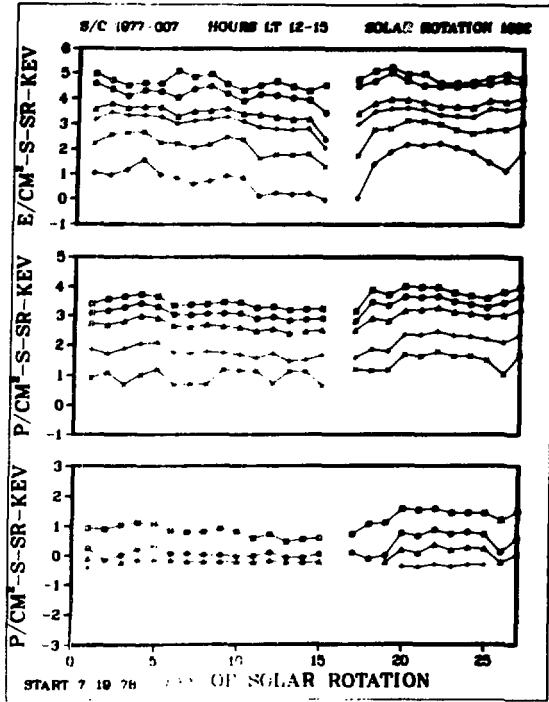
S/C 1977-007



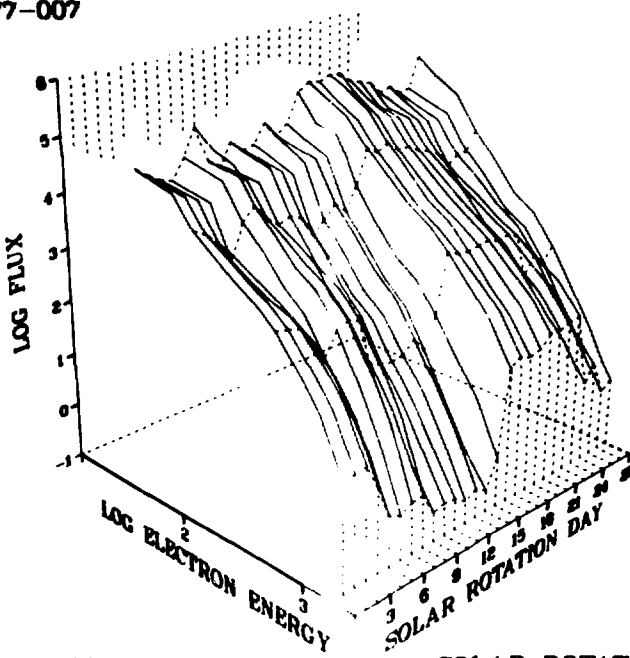
S/C 1977-007







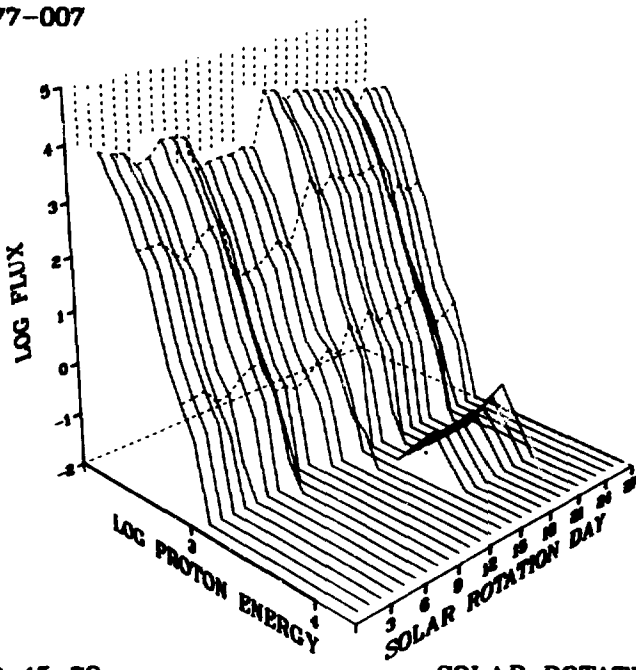
S/C 1977-007



START 8-15-78

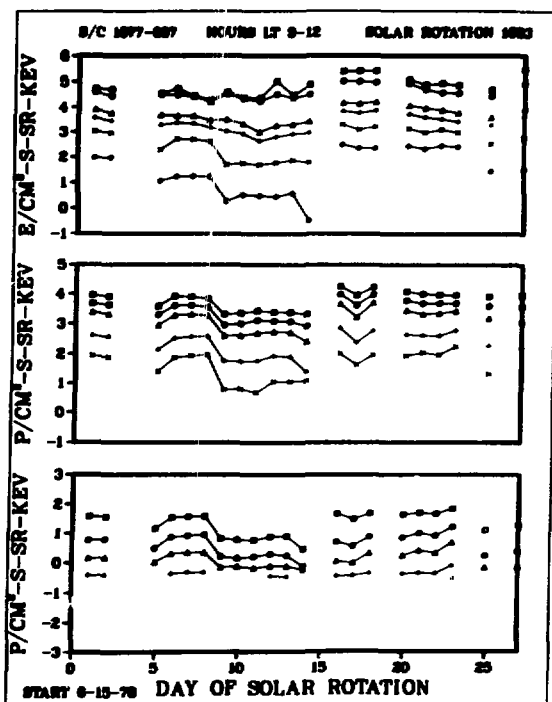
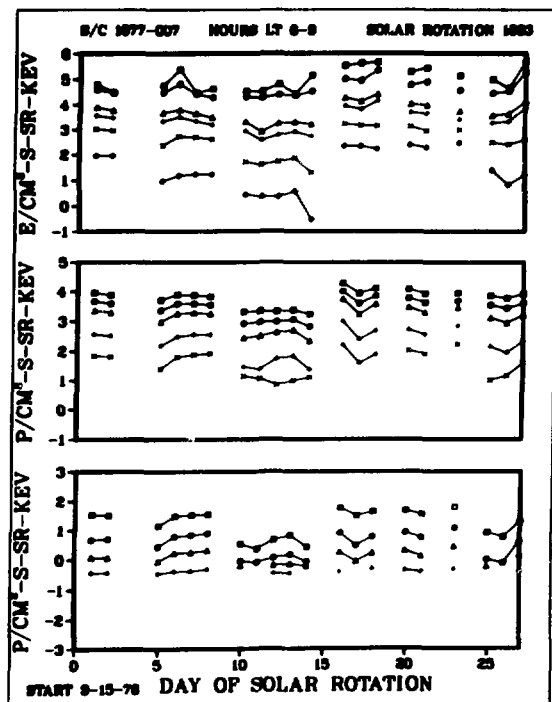
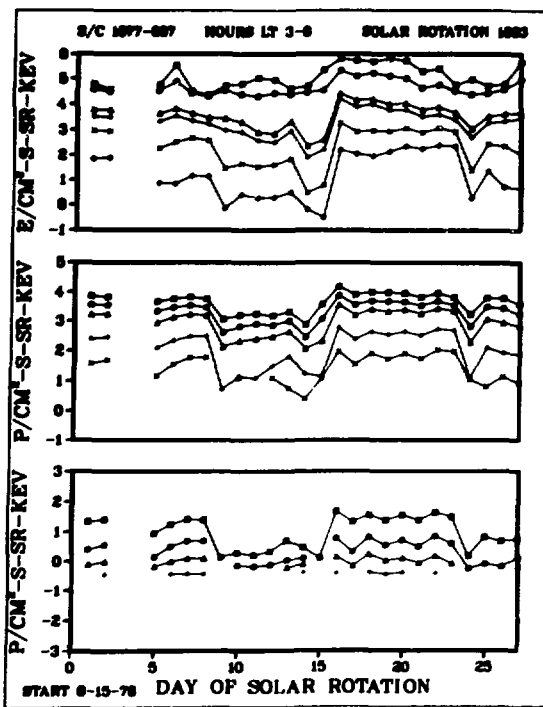
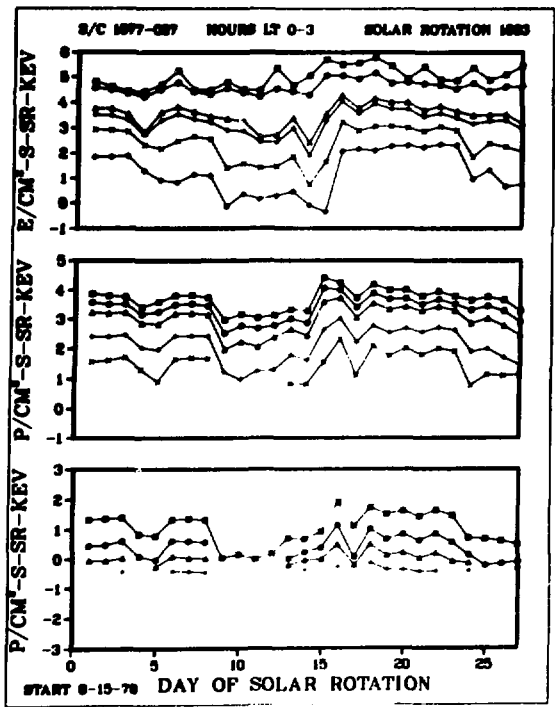
SOLAR ROTATION 1983

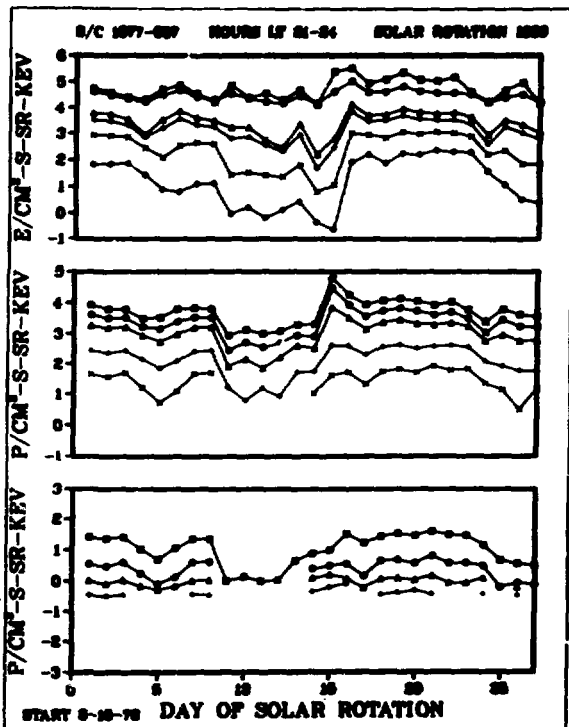
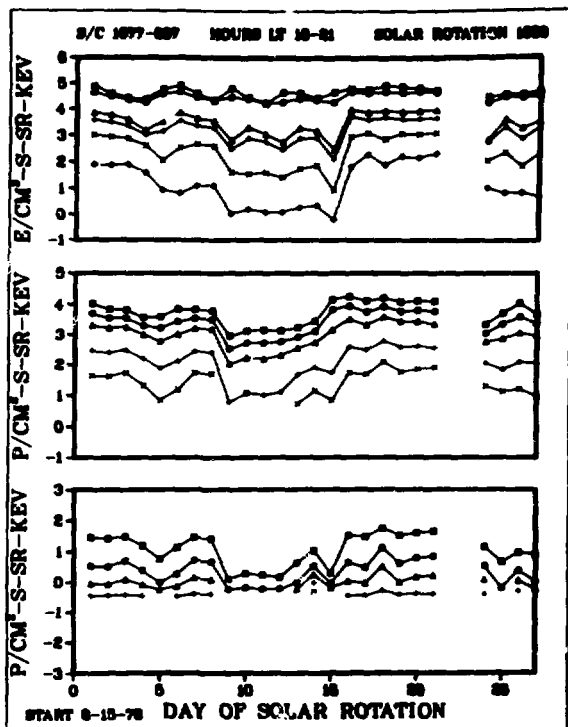
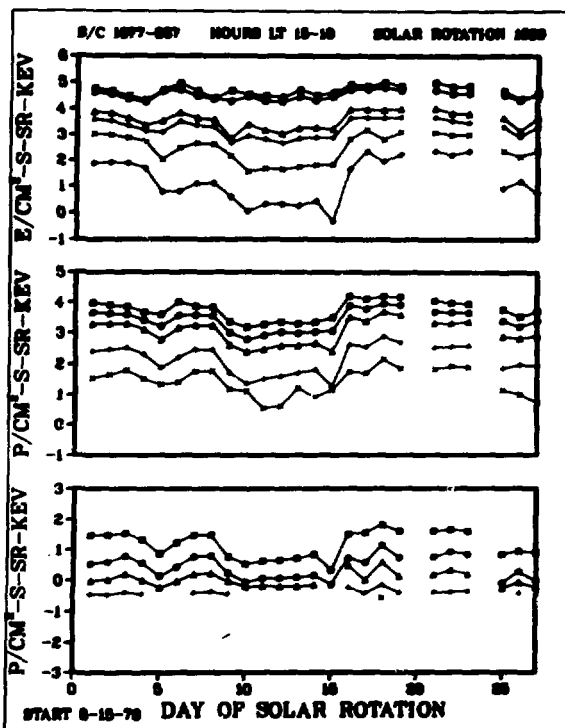
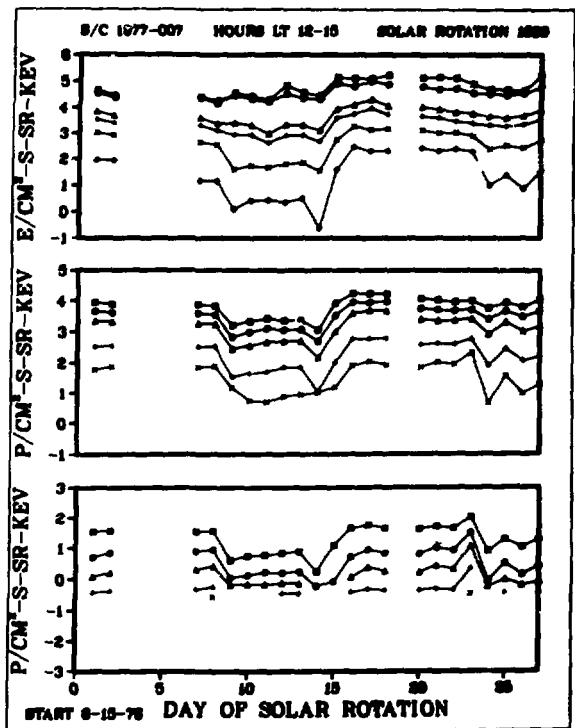
S/C 1977-007



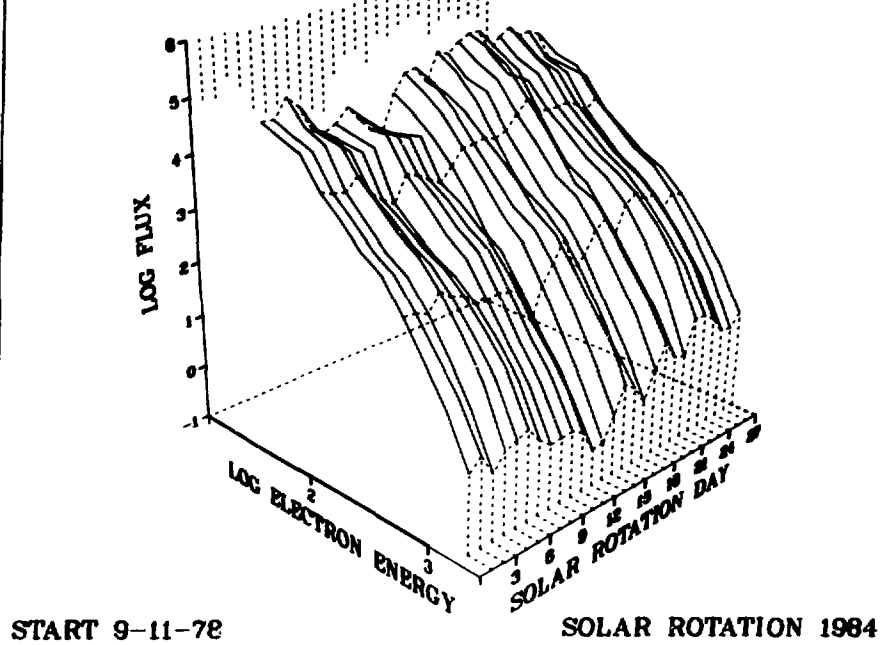
START 8-15-78

SOLAR ROTATION 1983

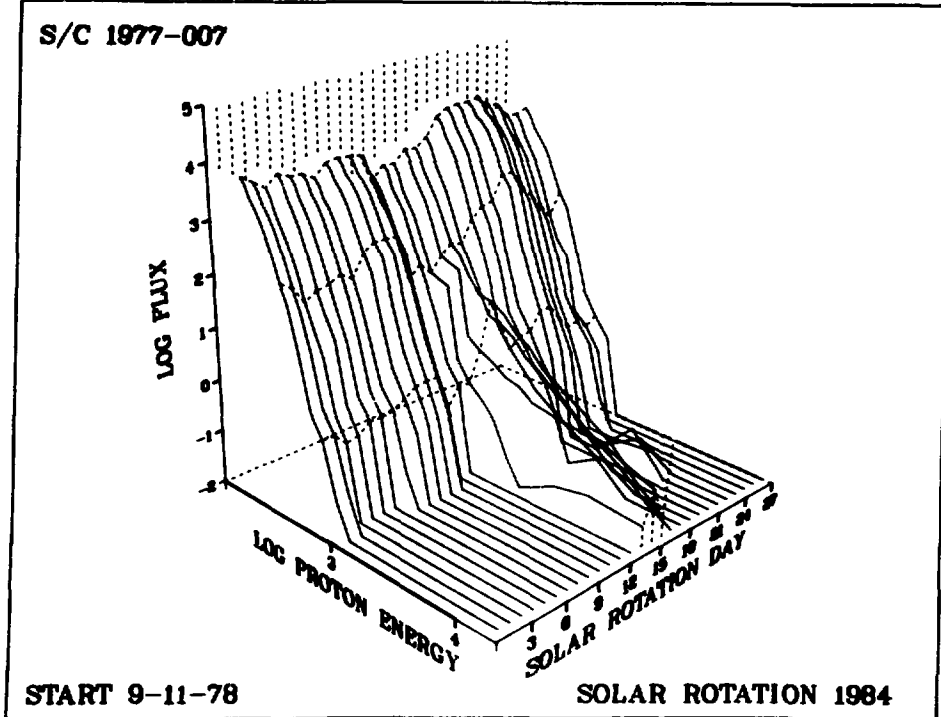


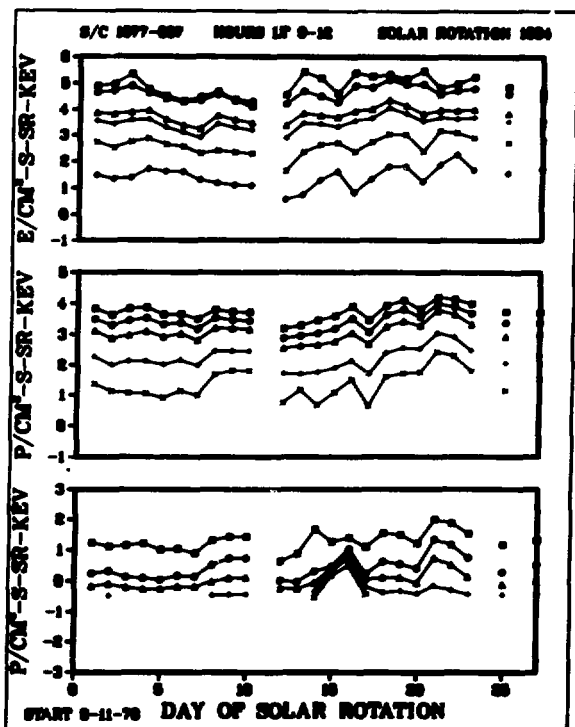
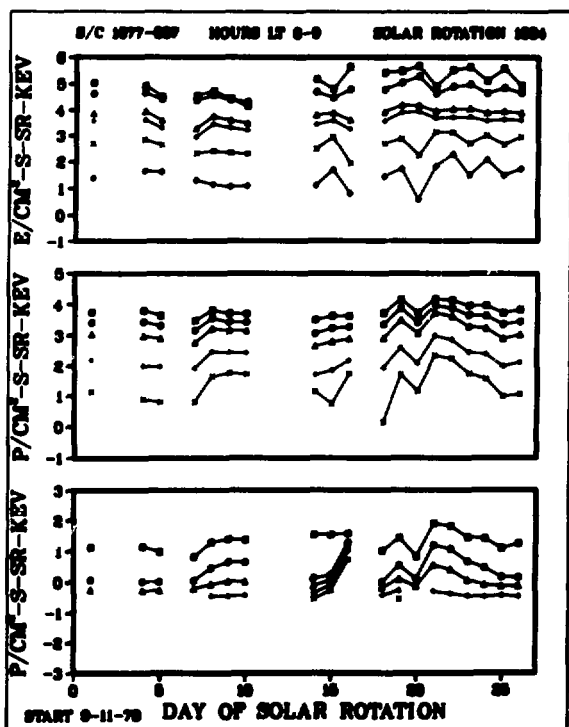
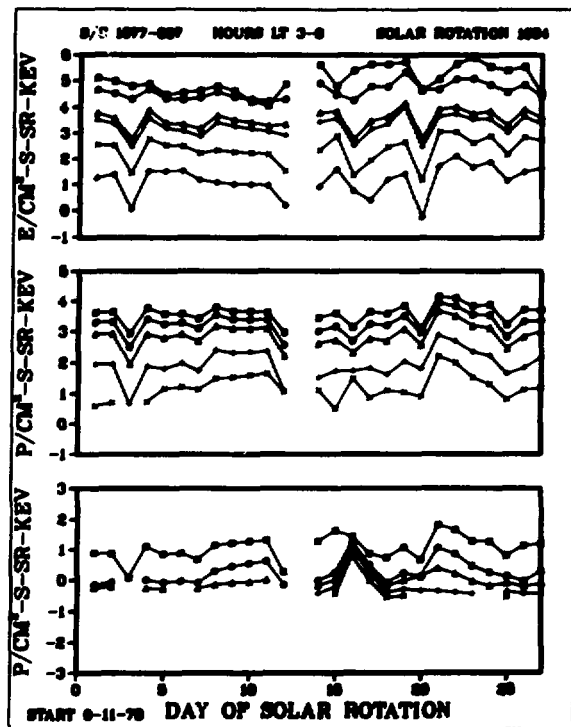
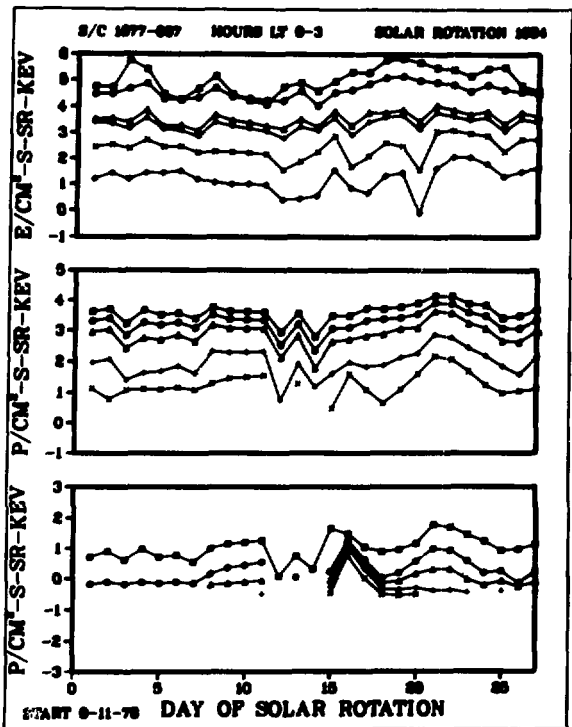


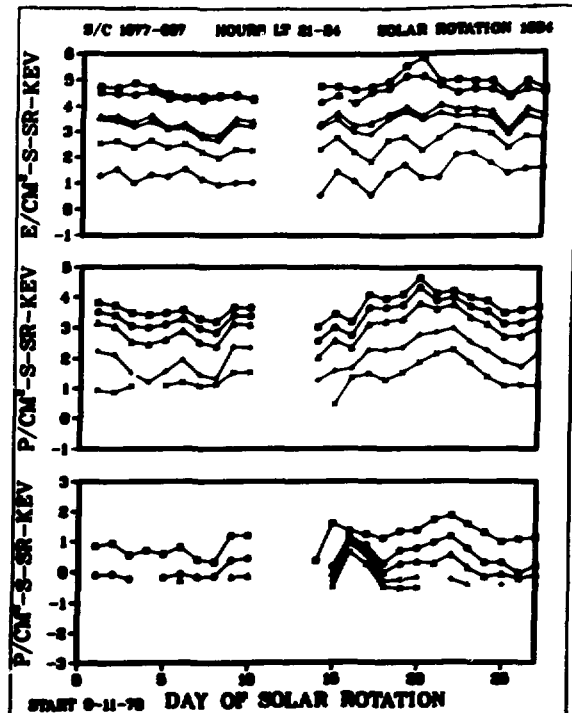
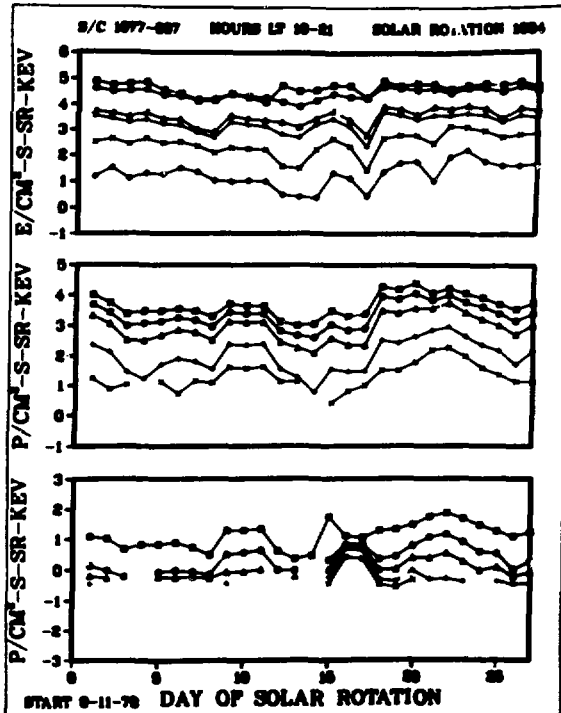
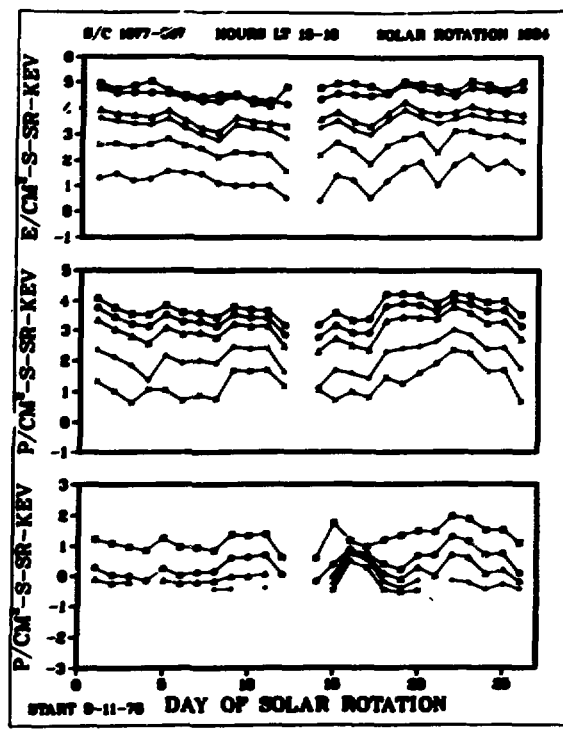
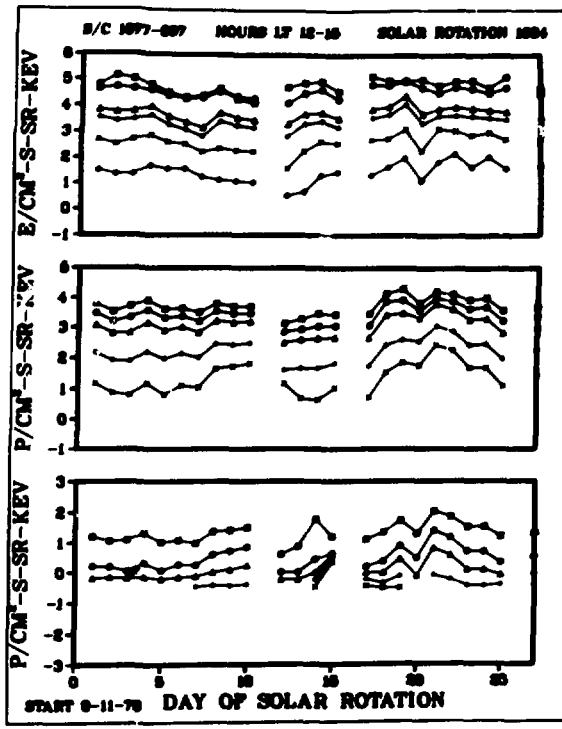
S/C 1977-007

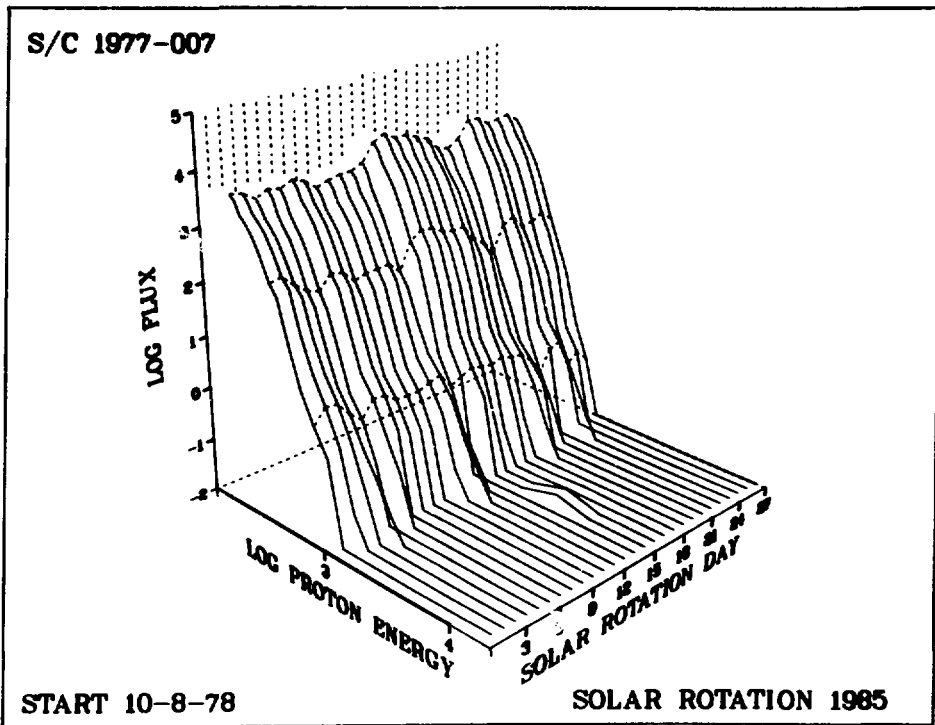
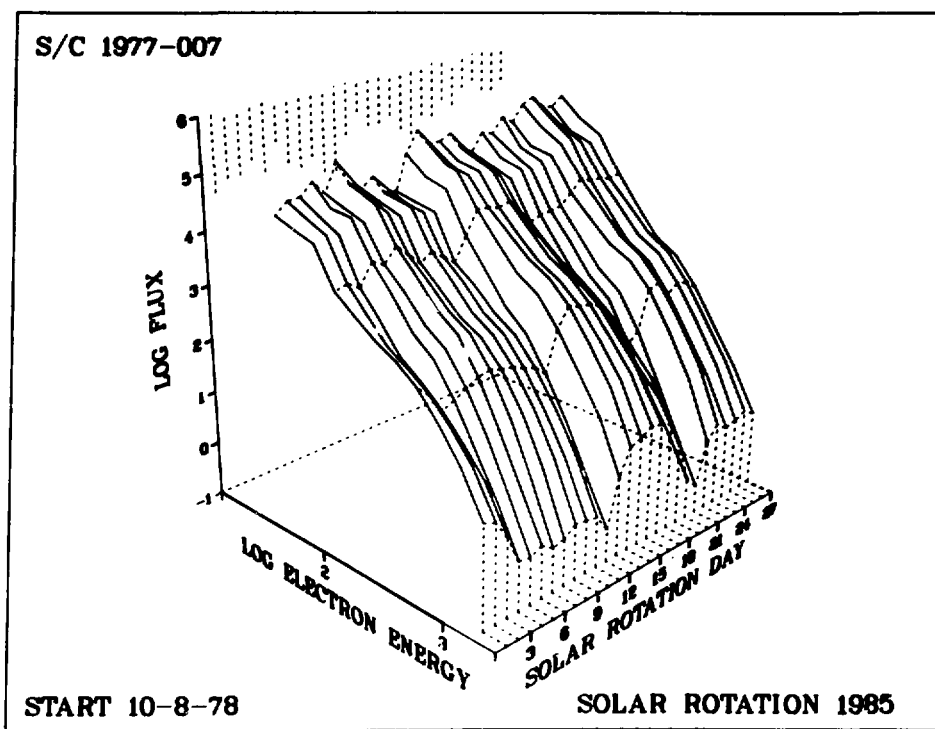


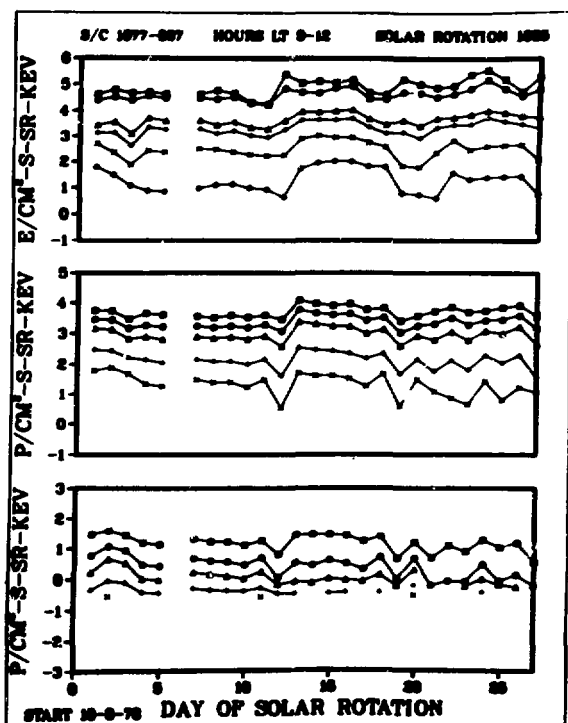
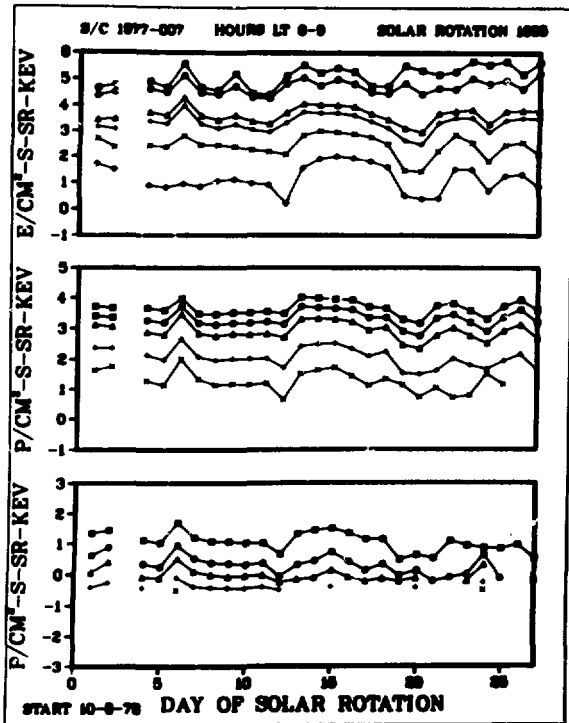
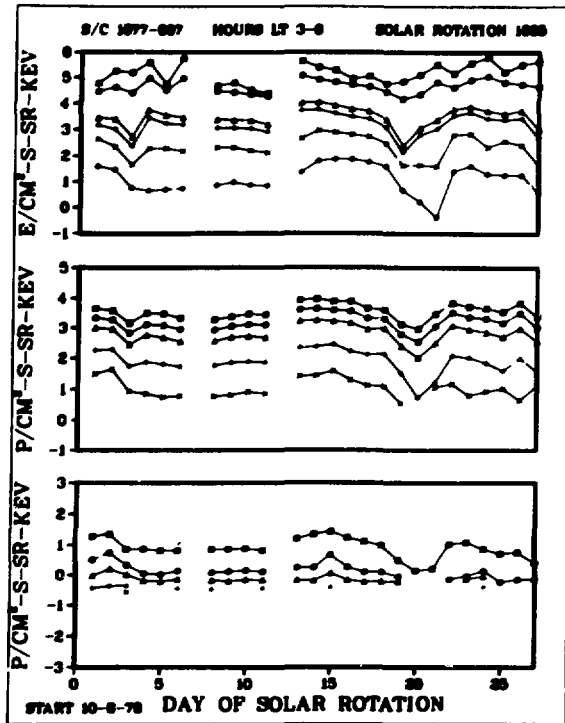
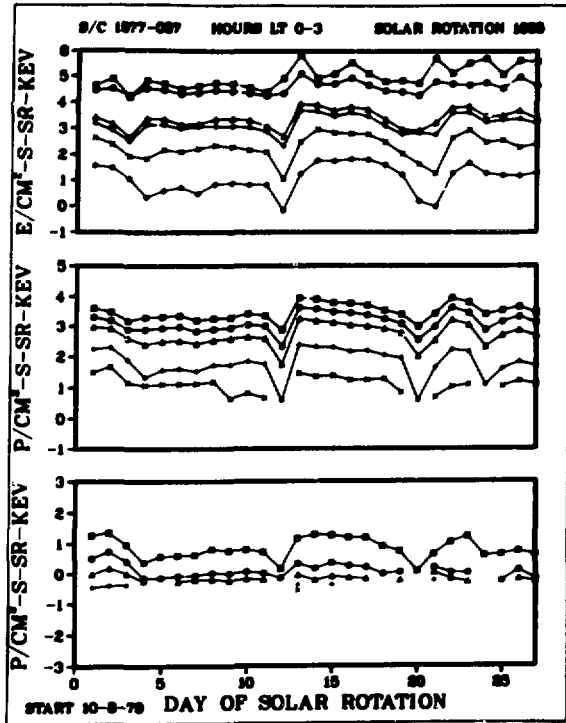
S/C 1977-007

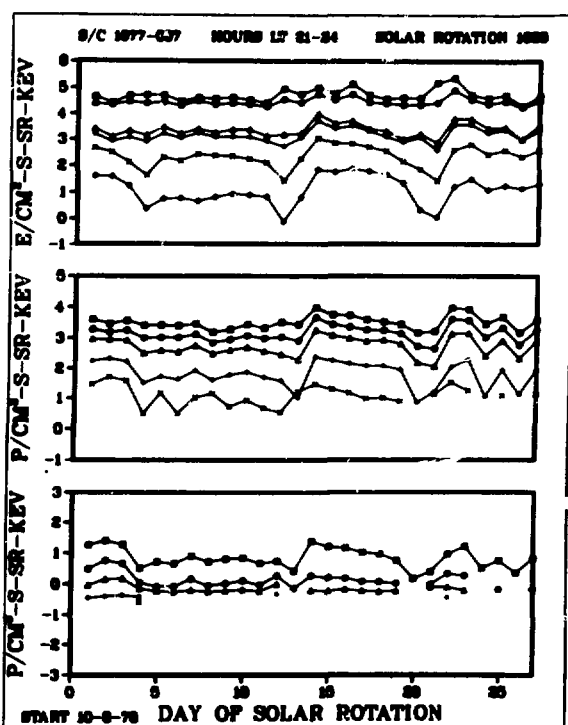
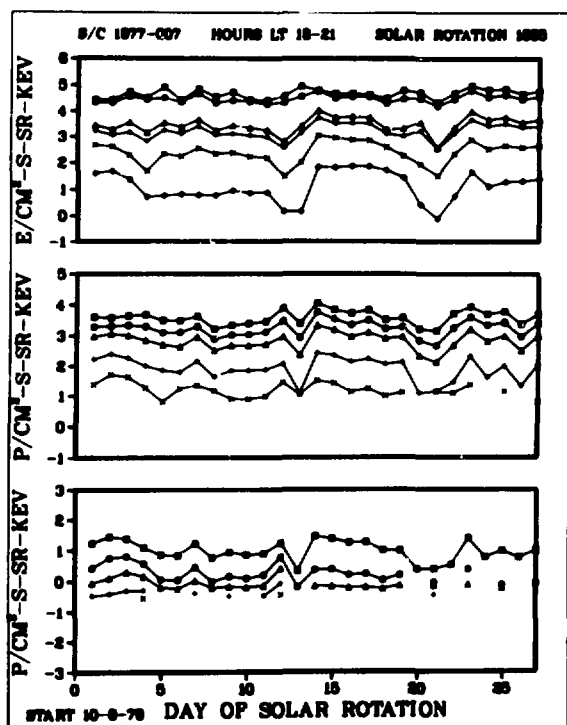
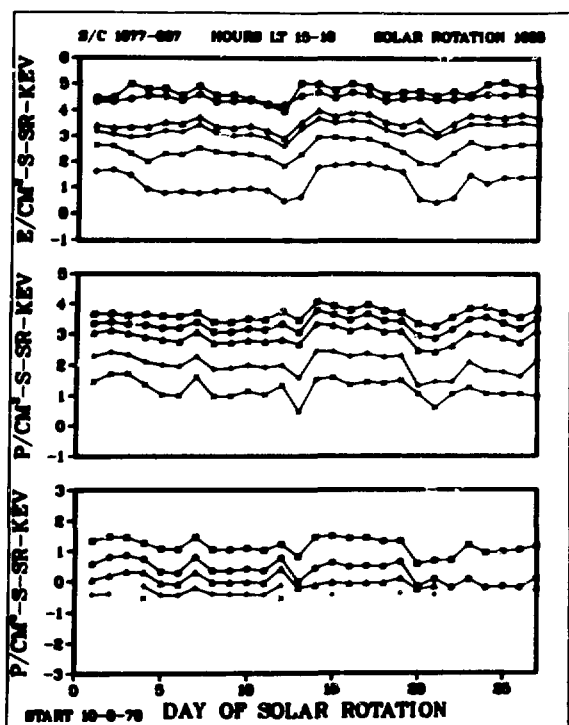
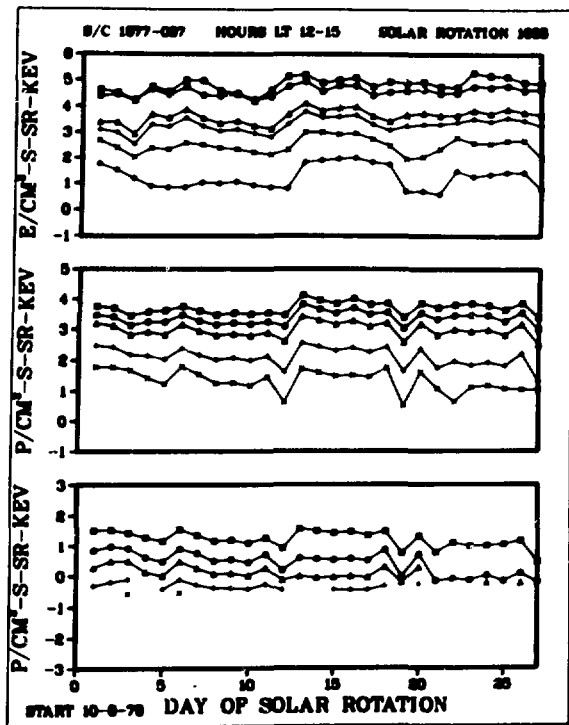




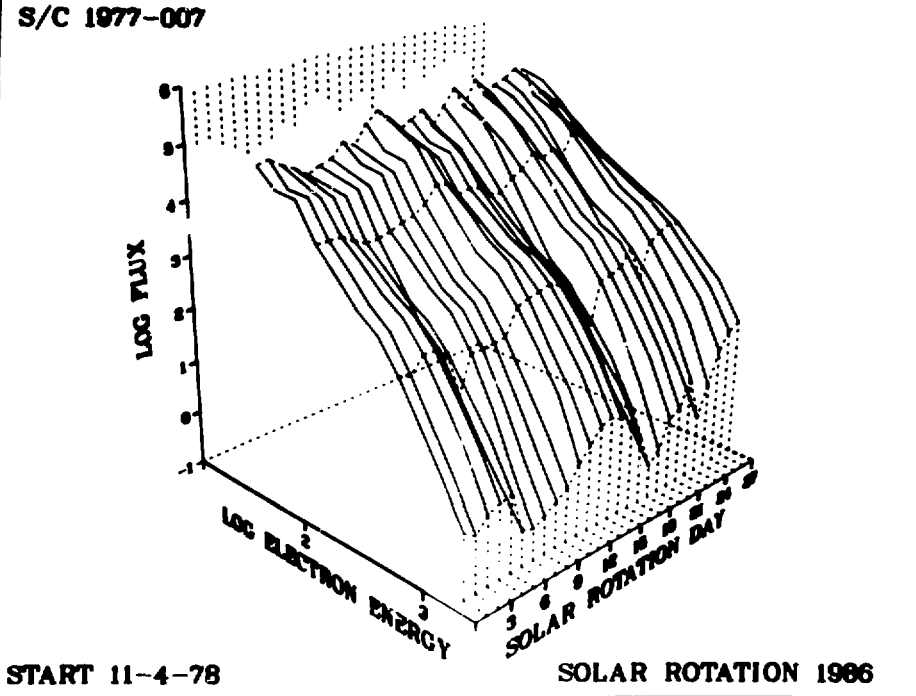




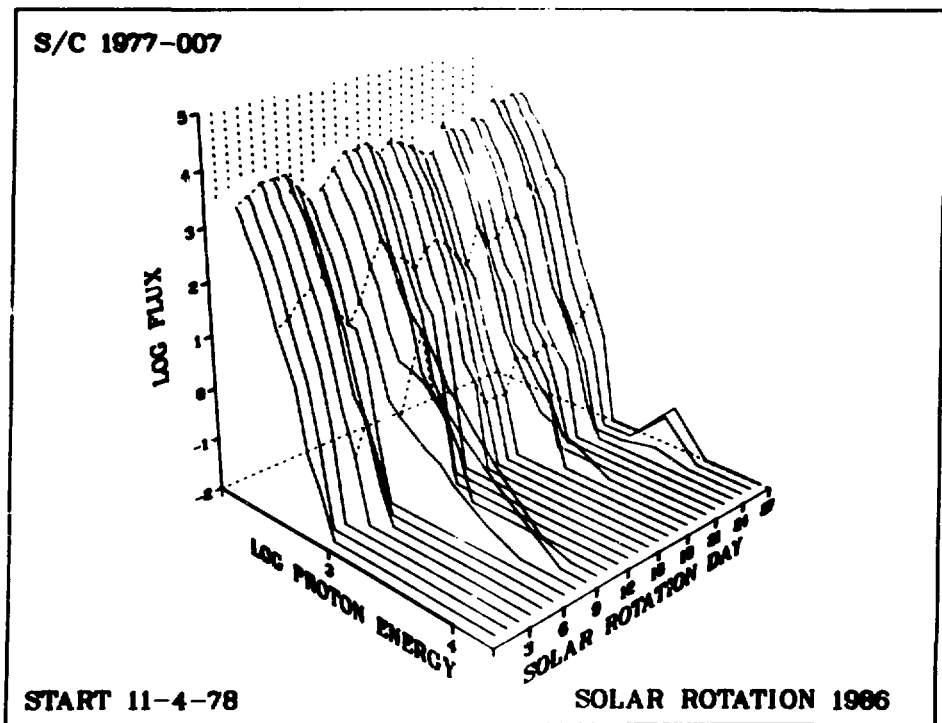


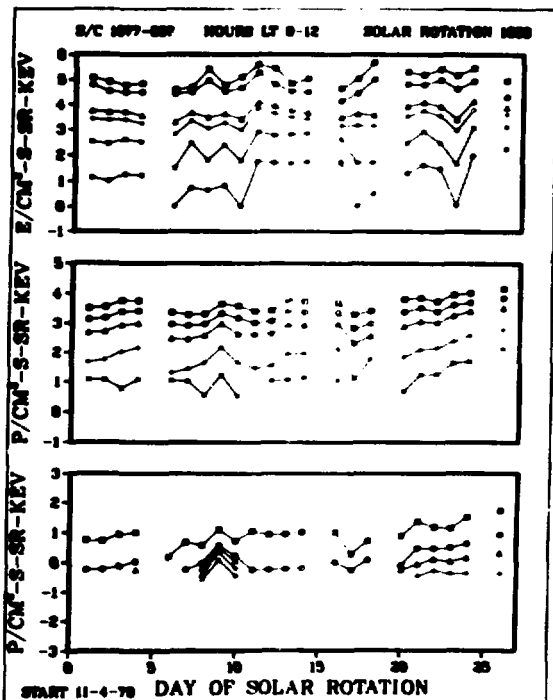
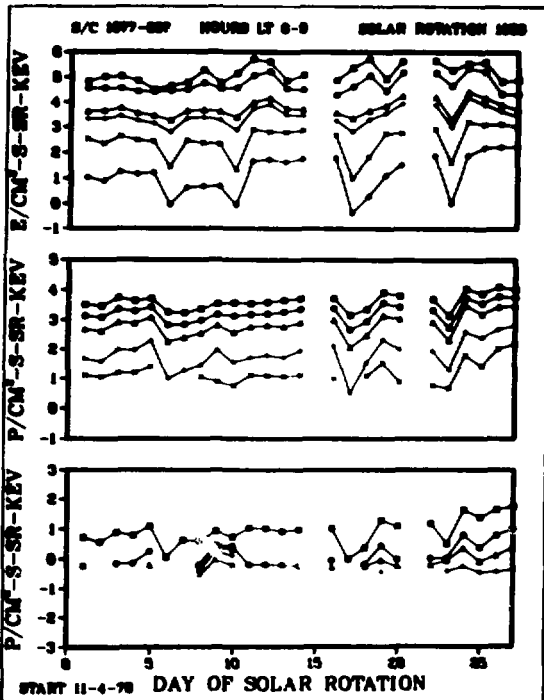
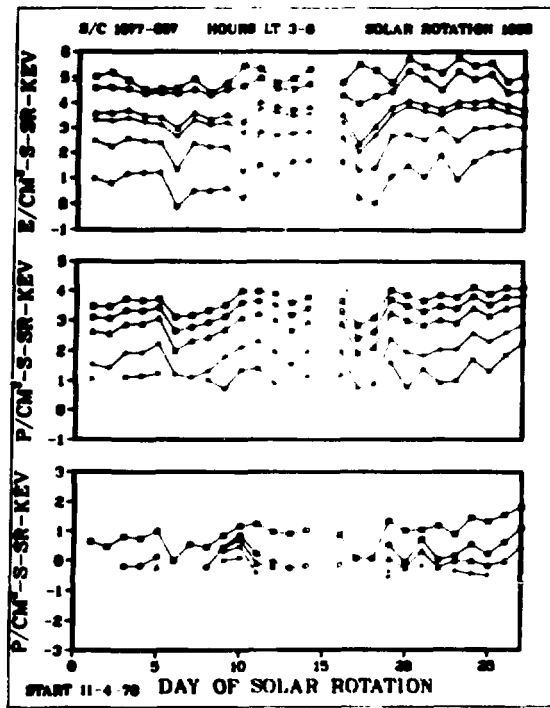
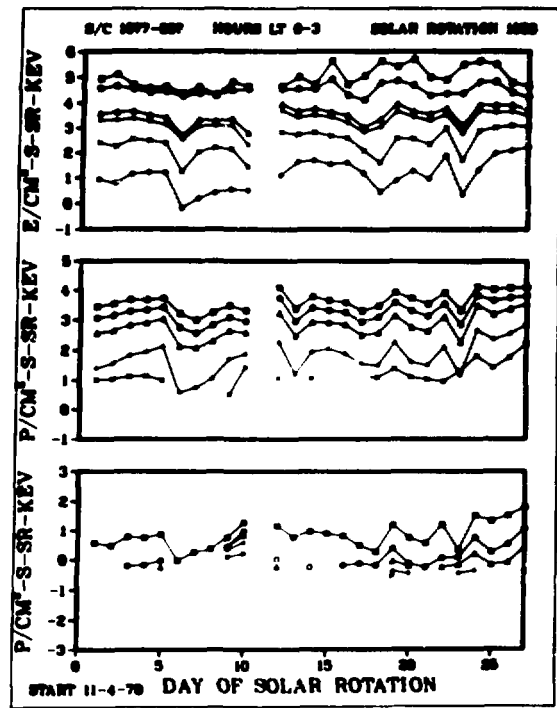


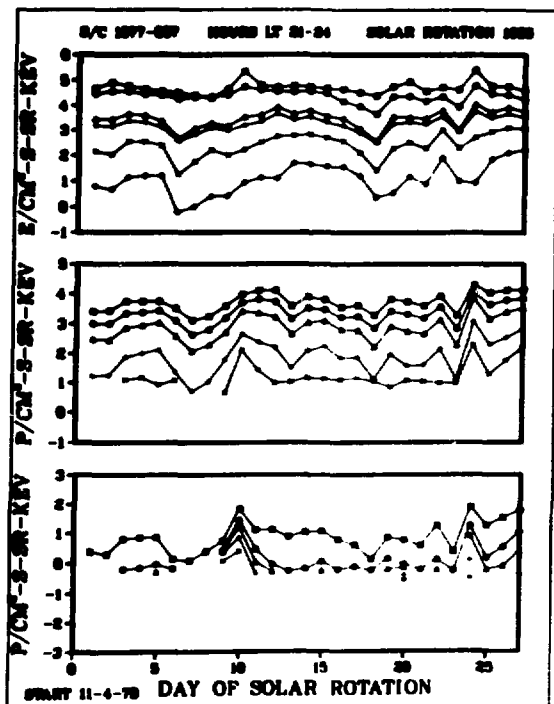
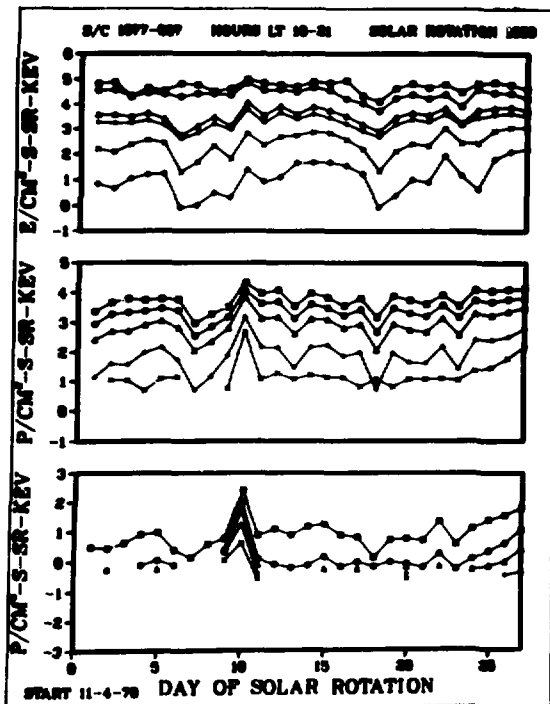
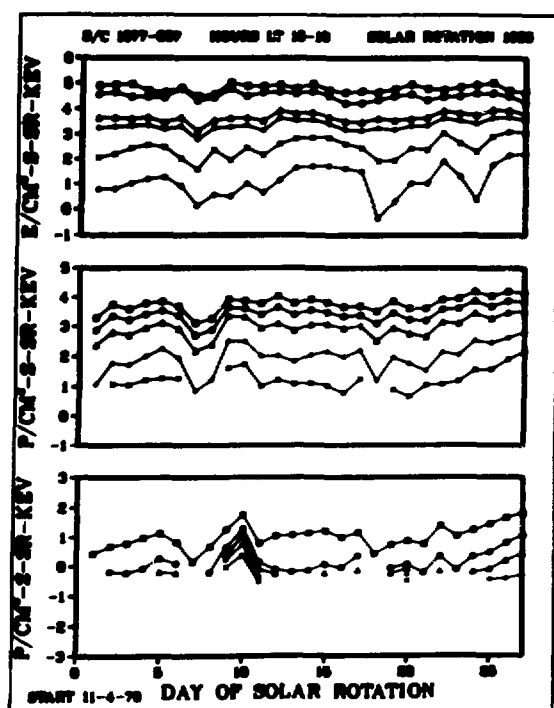
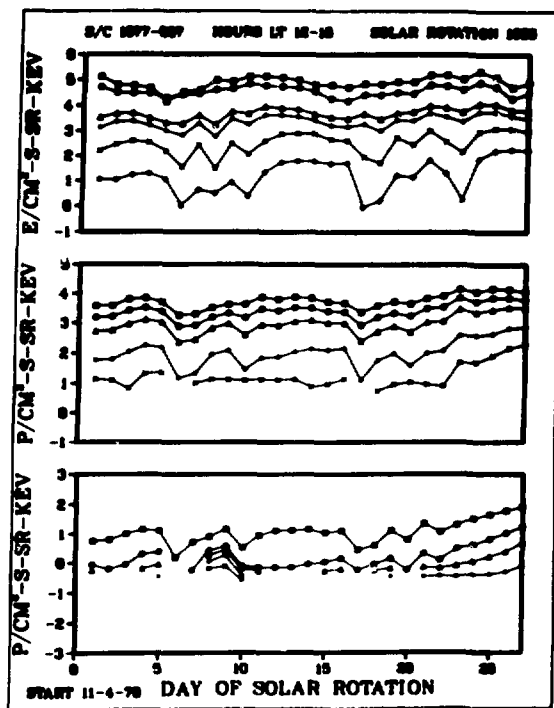
S/C 1977-007



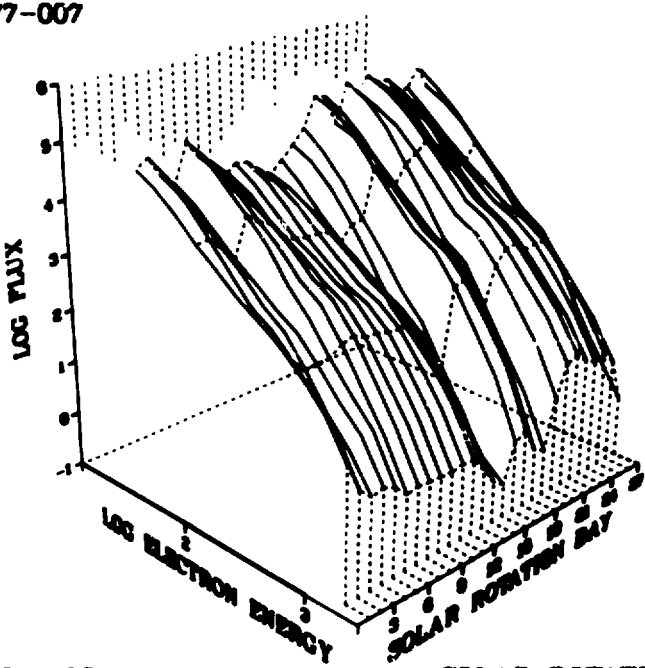
S/C 1977-007







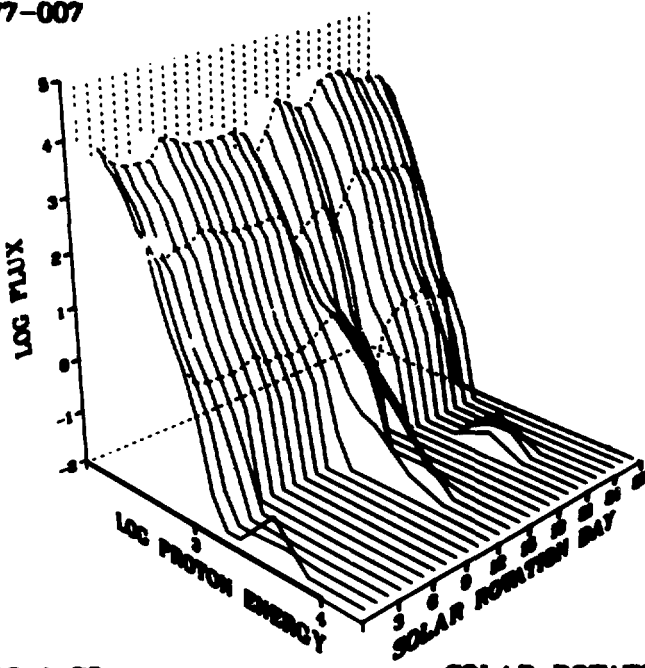
S/C 1977-007



START 12-1-78

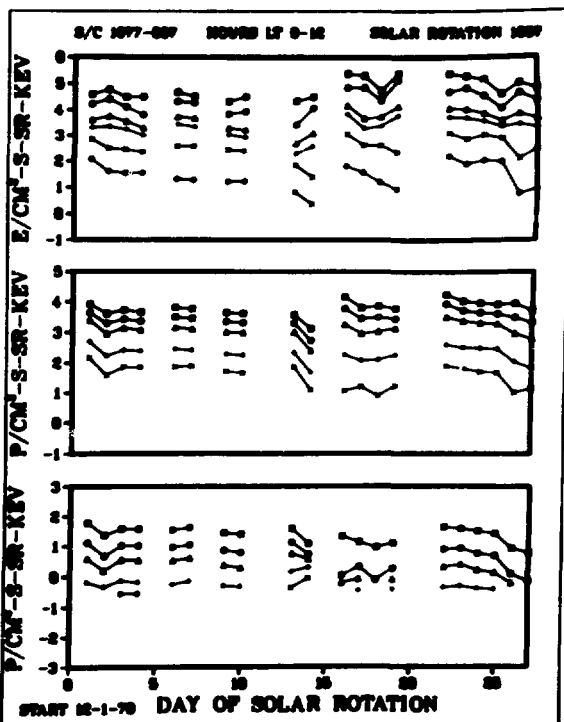
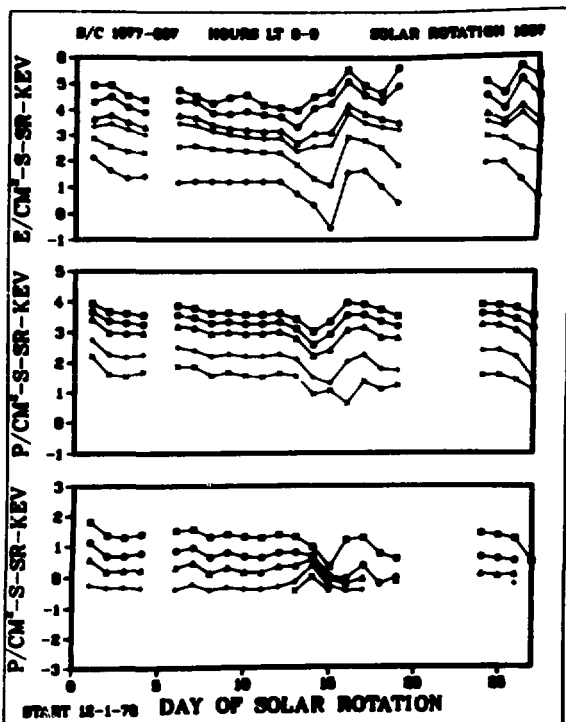
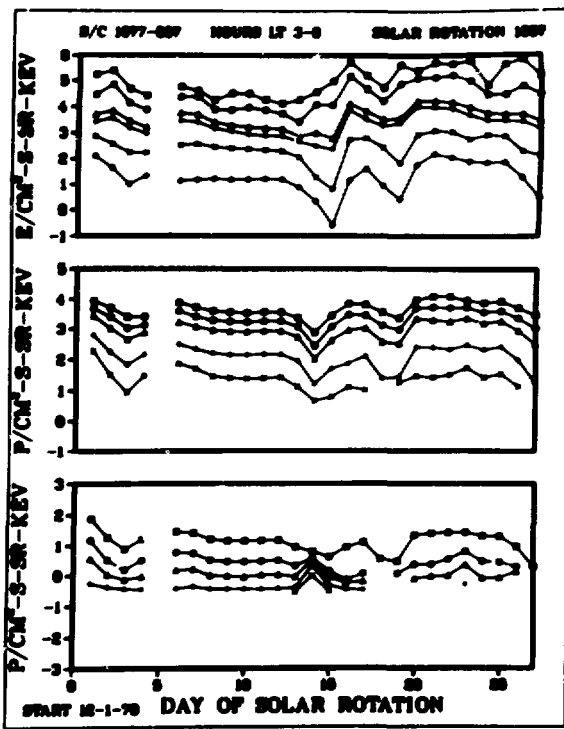
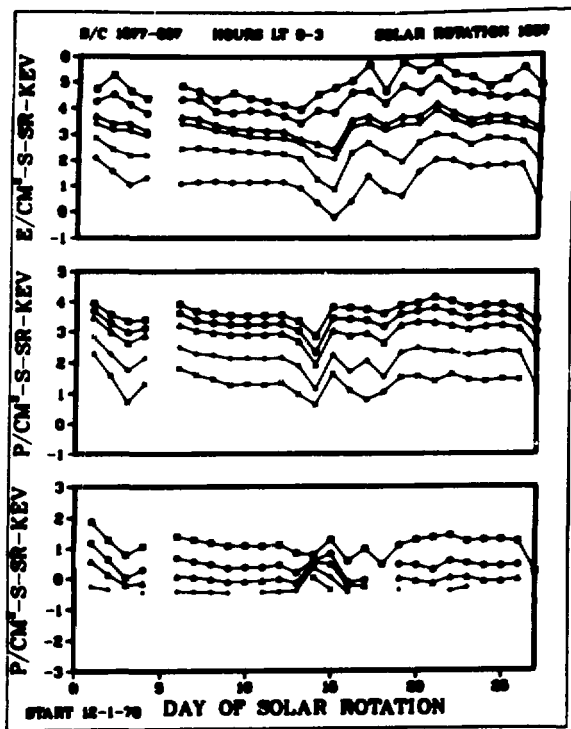
SOLAR ROTATION 1987

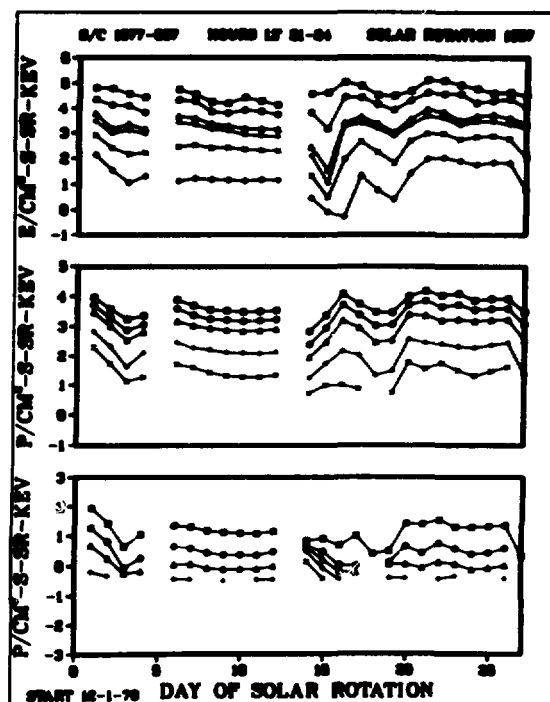
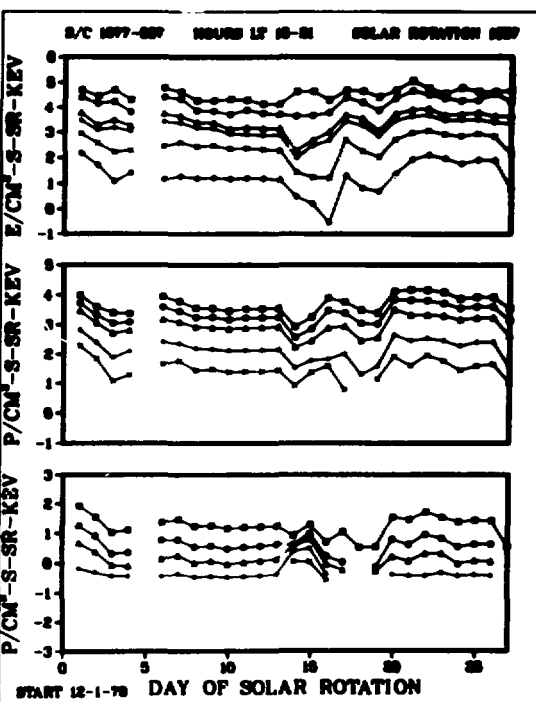
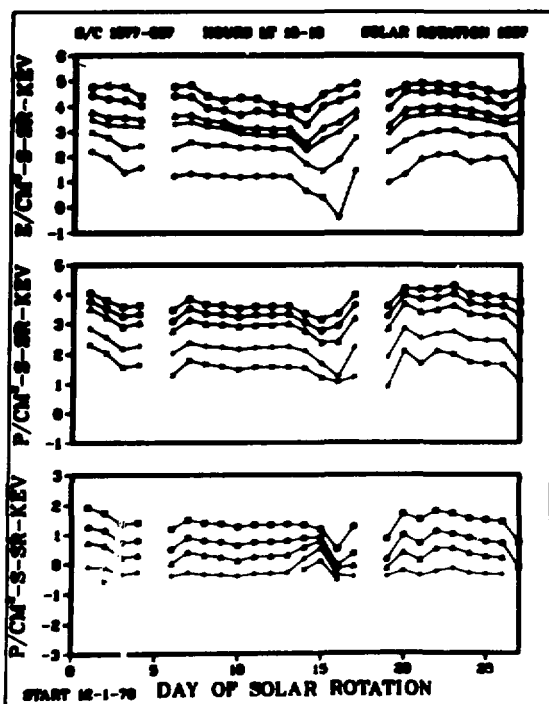
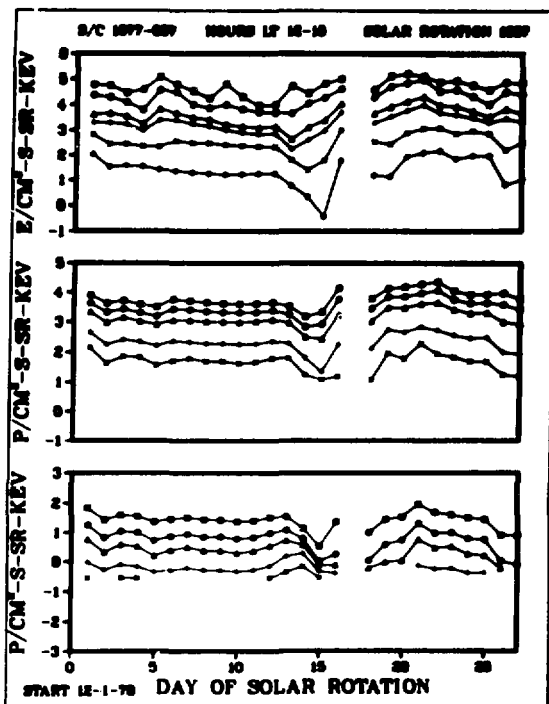
S/C 1977-007



START 12-1-78

SOLAR ROTATION 1987

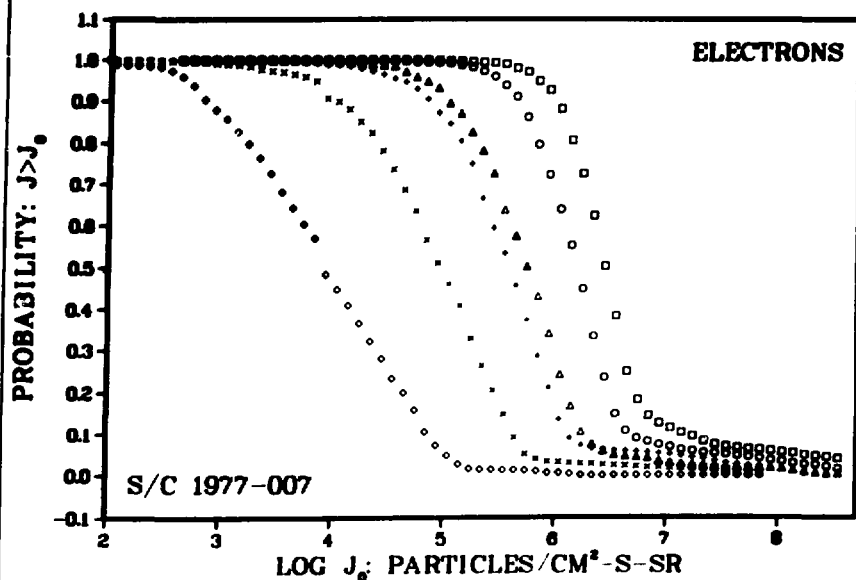




LOCAL TIME: 21-03

PERIOD: 020177-123177

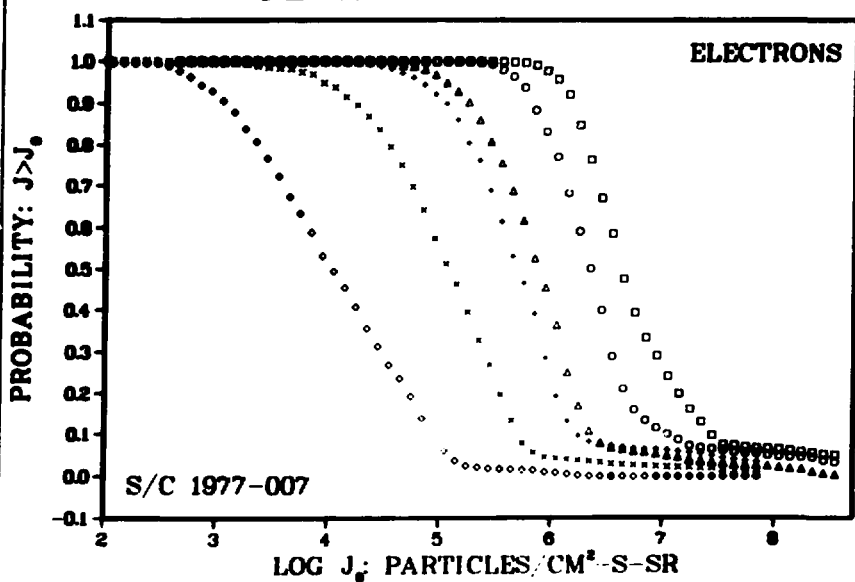
FLUX PROBABILITIES



LOCAL TIME: 03-09

PERIOD: 020177-123177

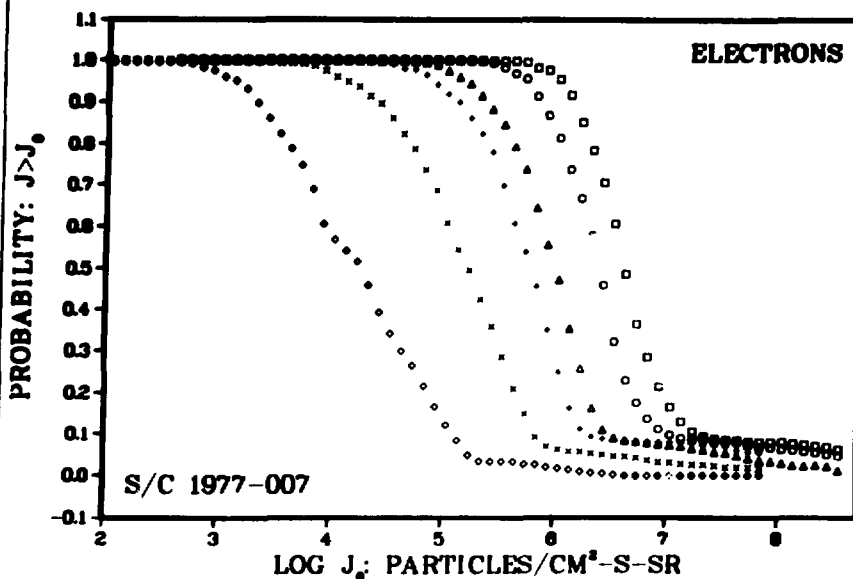
FLUX PROBABILITIES



LOCAL TIME: 09-15

PERIOD: 020177-123177

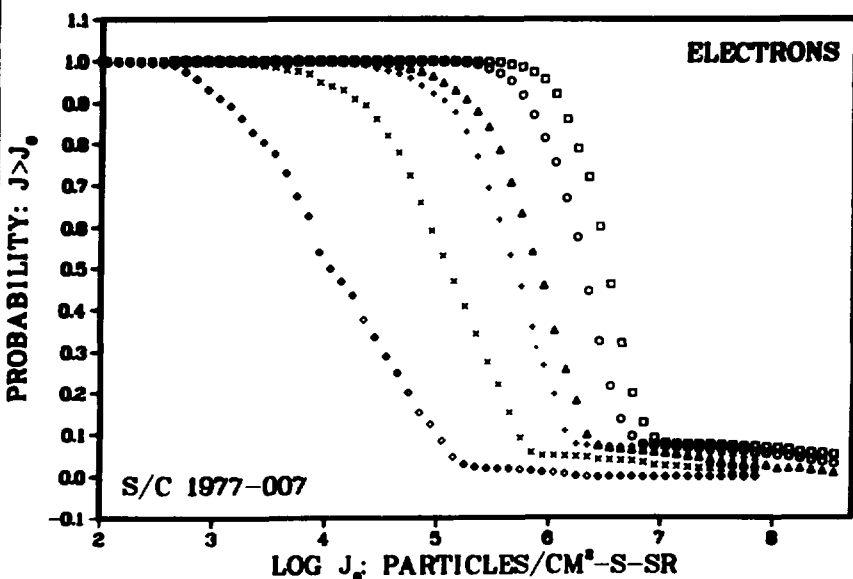
FLUX PROBABILITIES



LOCAL TIME: 15-21

PERIOD: 020177-123177

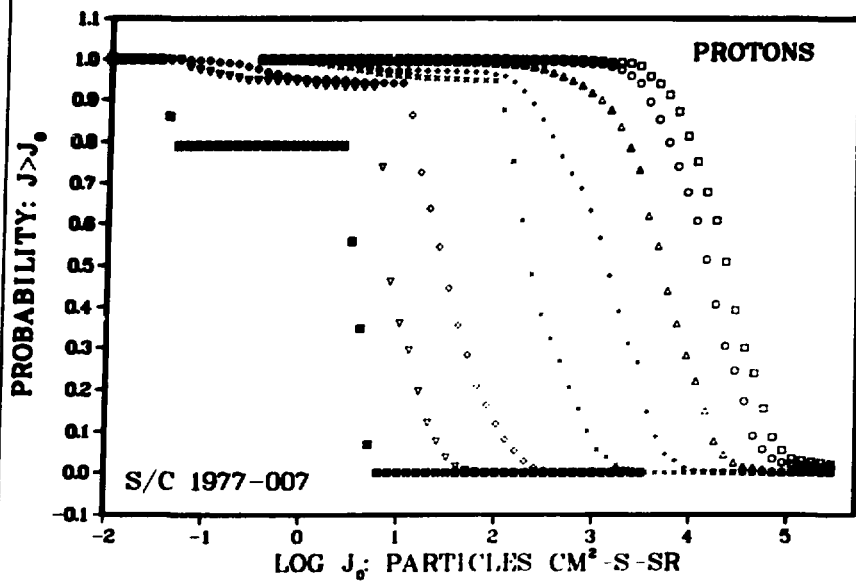
FLUX PROBABILITIES



LOCAL TIME: 21-03

PERIOD: 020177-123177

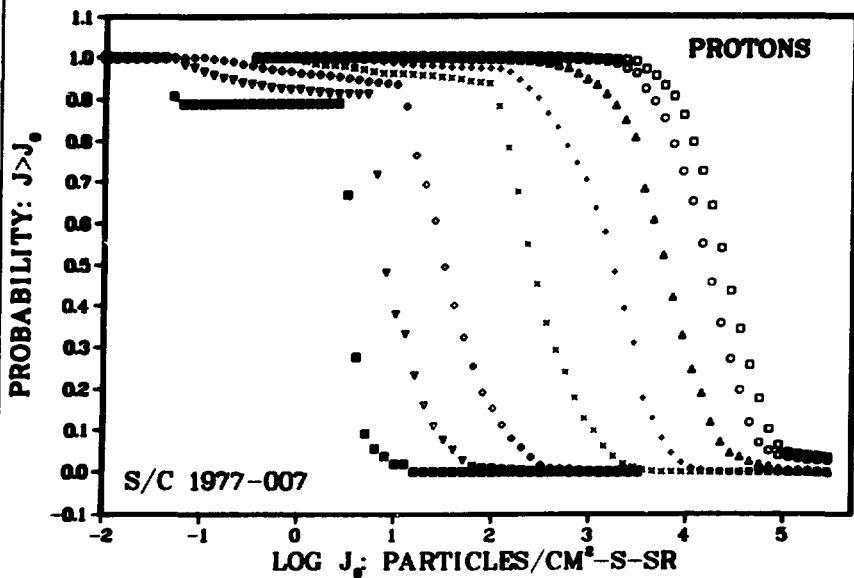
FLUX PROBABILITIES

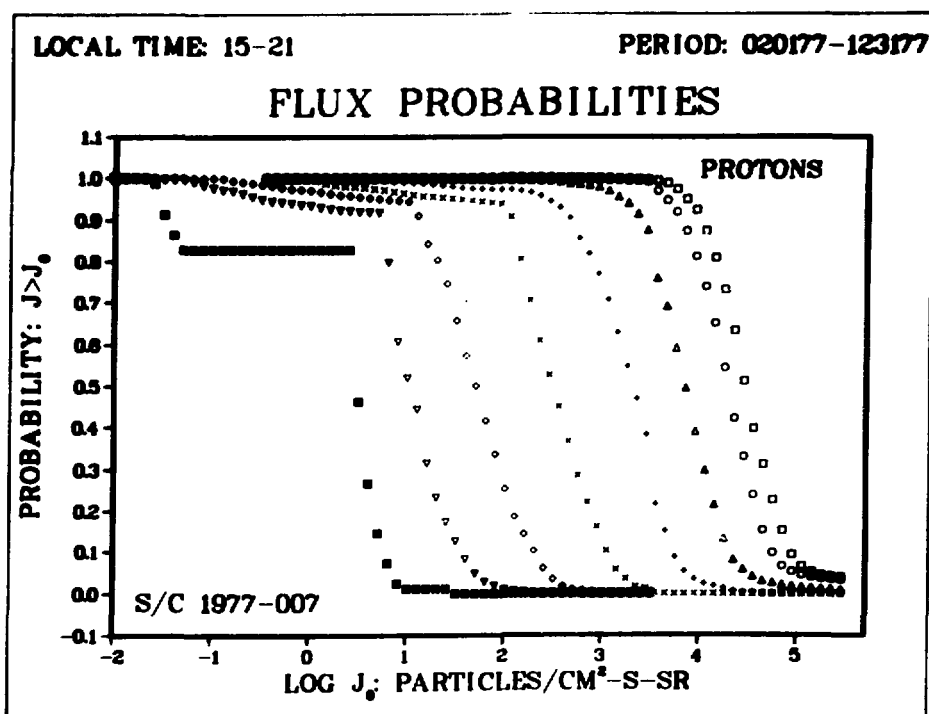
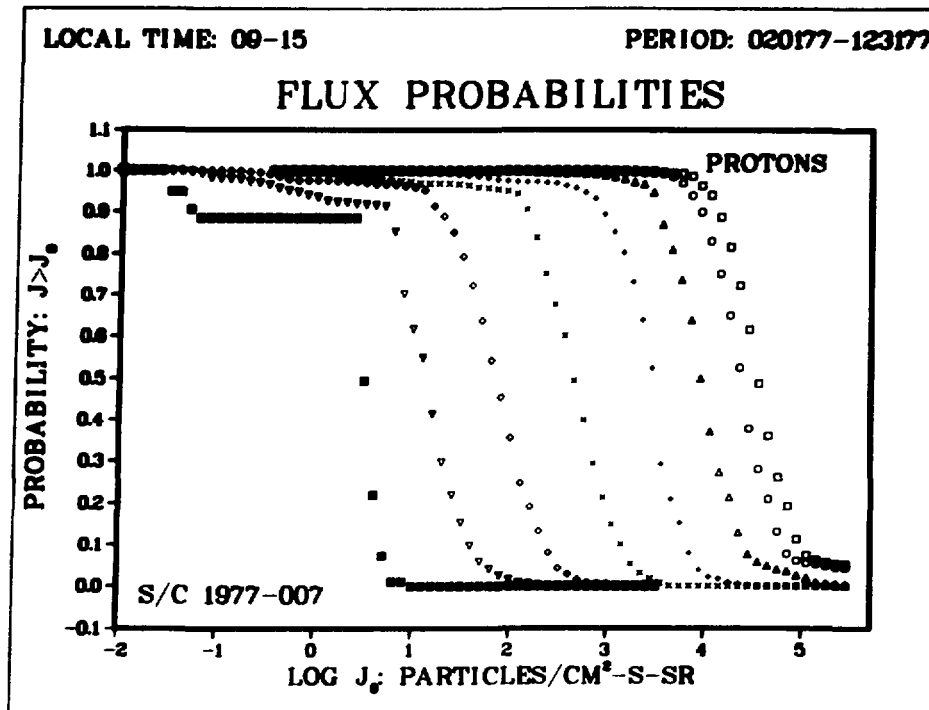


LOCAL TIME: 03-09

PERIOD: 020177-123177

FLUX PROBABILITIES

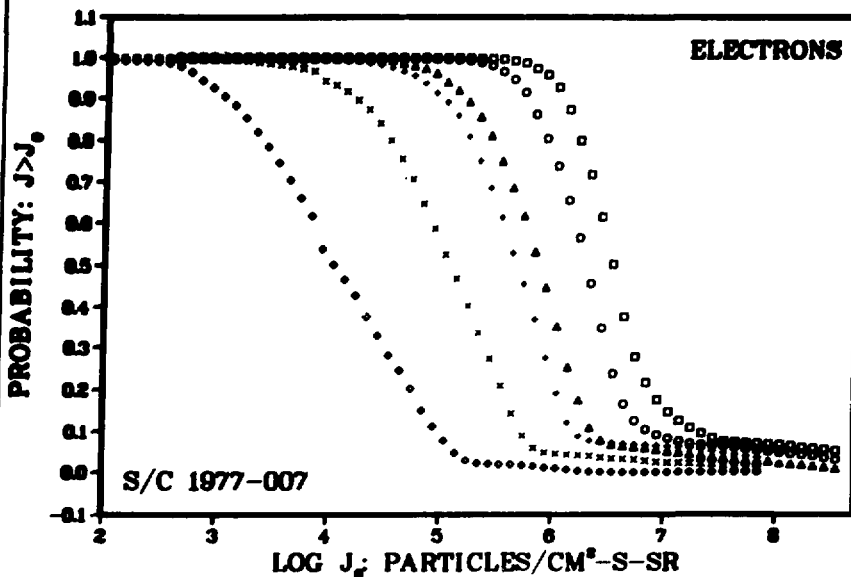




ALL LOCAL TIMES

PERIOD: 020177-123177

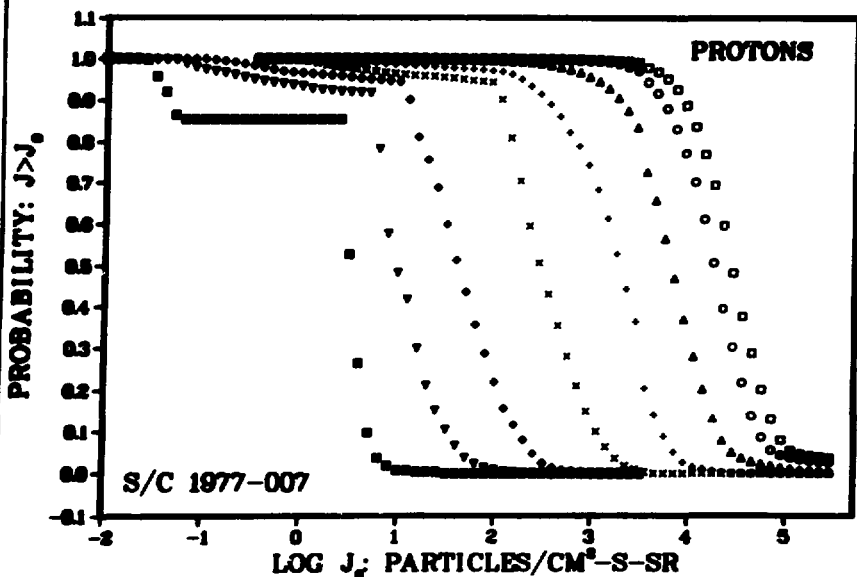
FLUX PROBABILITIES



ALL LOCAL TIMES

PERIOD: 020177-123177

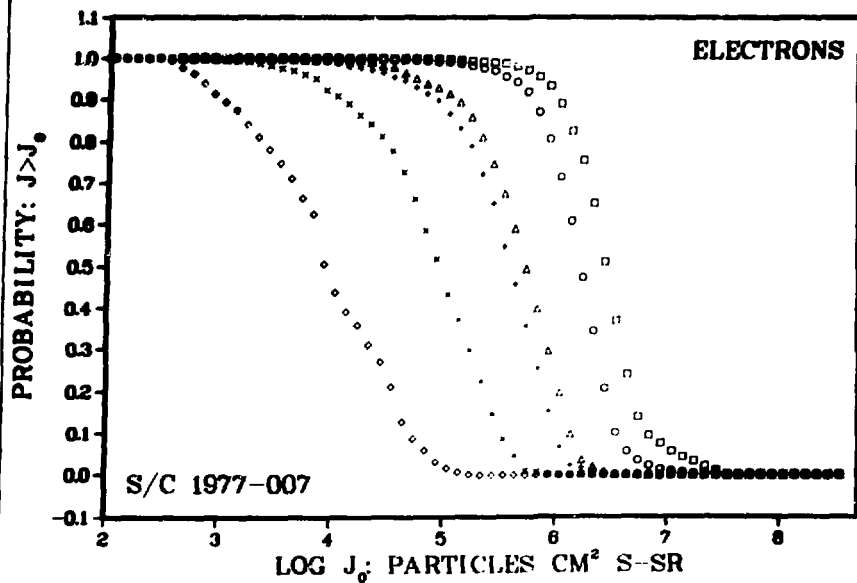
FLUX PROBABILITIES



LOCAL TIME: 21-03

PERIOD: 010178-123178

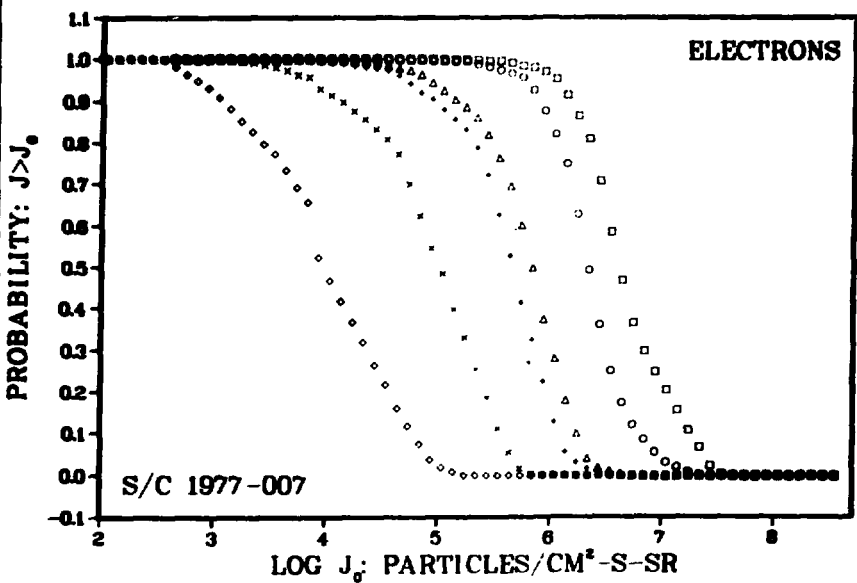
FLUX PROBABILITIES



LOCAL TIME: 03-09

PERIOD: 010178-123178

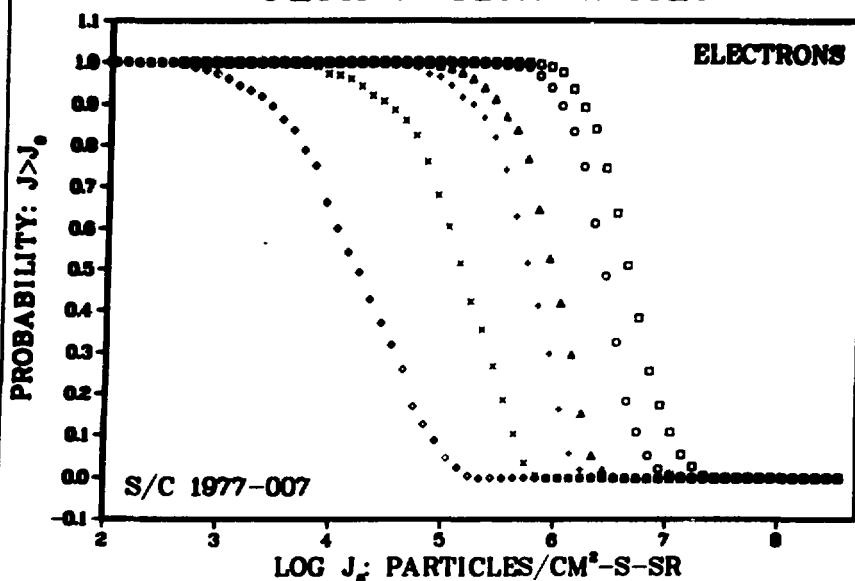
FLUX PROBABILITIES



LOCAL TIME: 09-15

PERIOD: 010178-123178

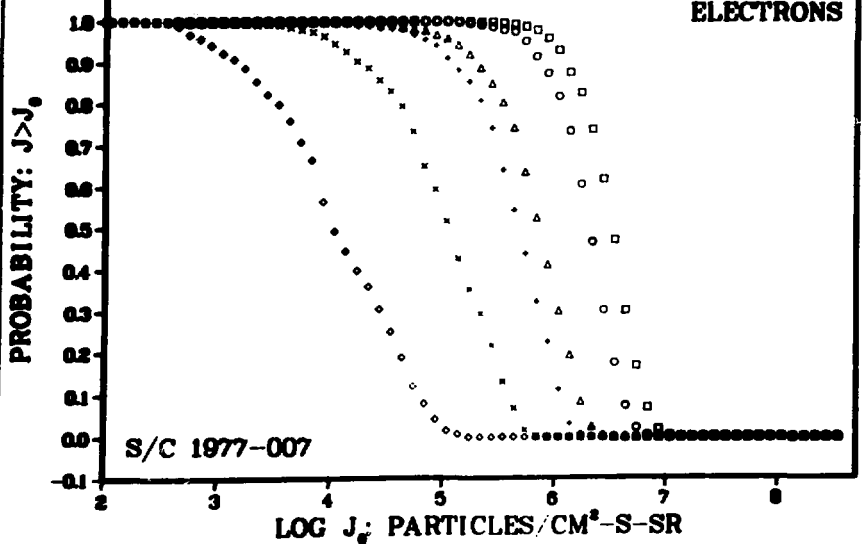
FLUX PROBABILITIES



LOCAL TIME: 15-21

PERIOD: 010178-123178

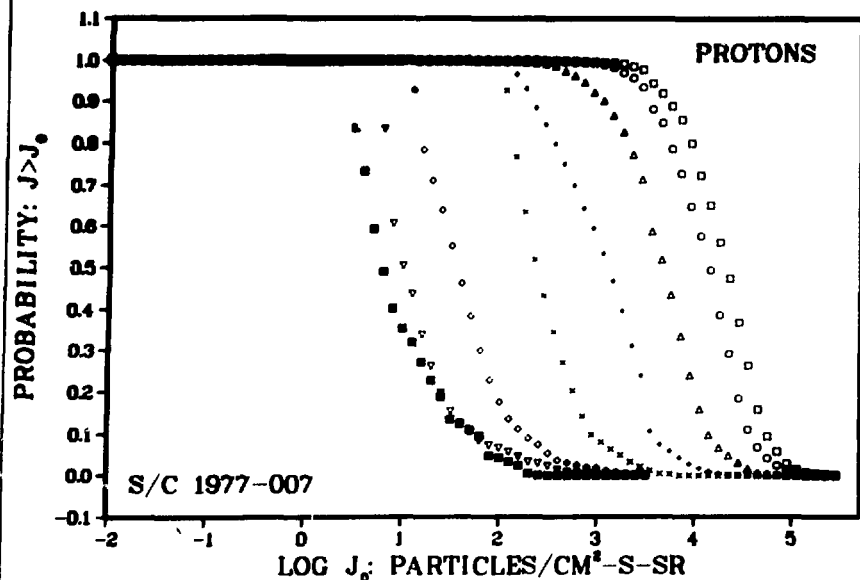
FLUX PROBABILITIES



LOCAL TIME: 21-03

PERIOD: 010178-123178

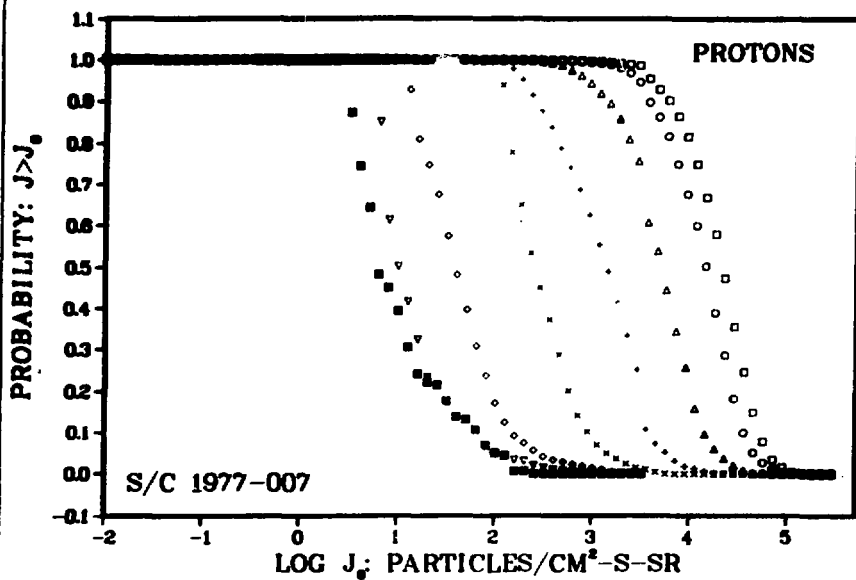
FLUX PROBABILITIES



LOCAL TIME: 03-09

PERIOD: 010178-123178

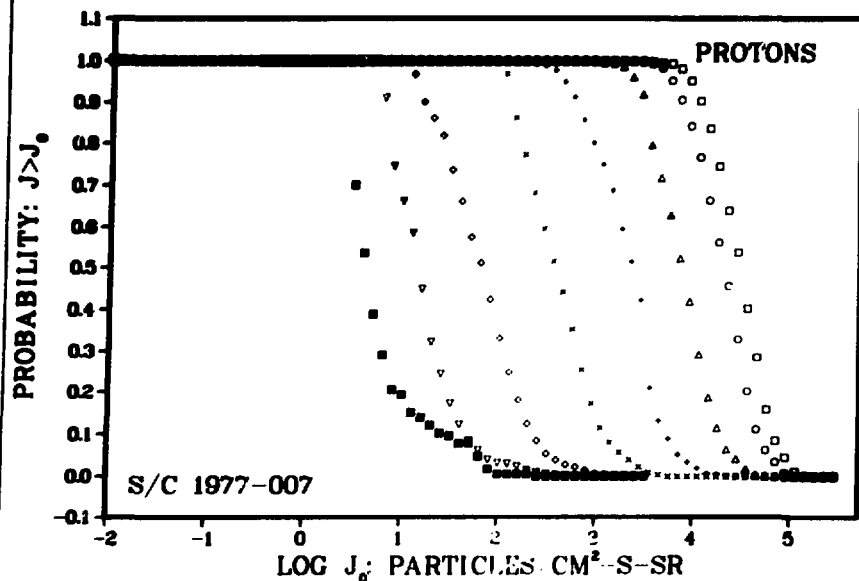
FLUX PROBABILITIES



LOCAL TIME: 09-15

PERIOD: 010178-123178

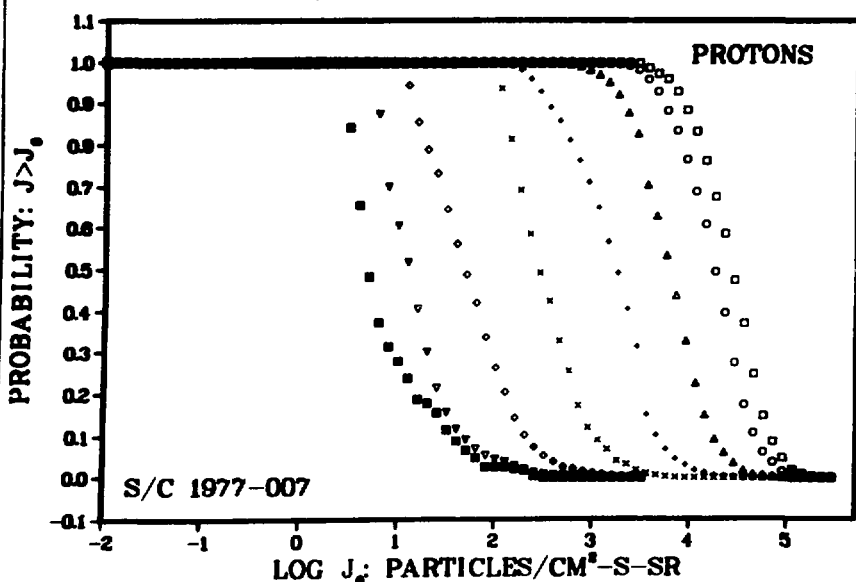
FLUX PROBABILITIES

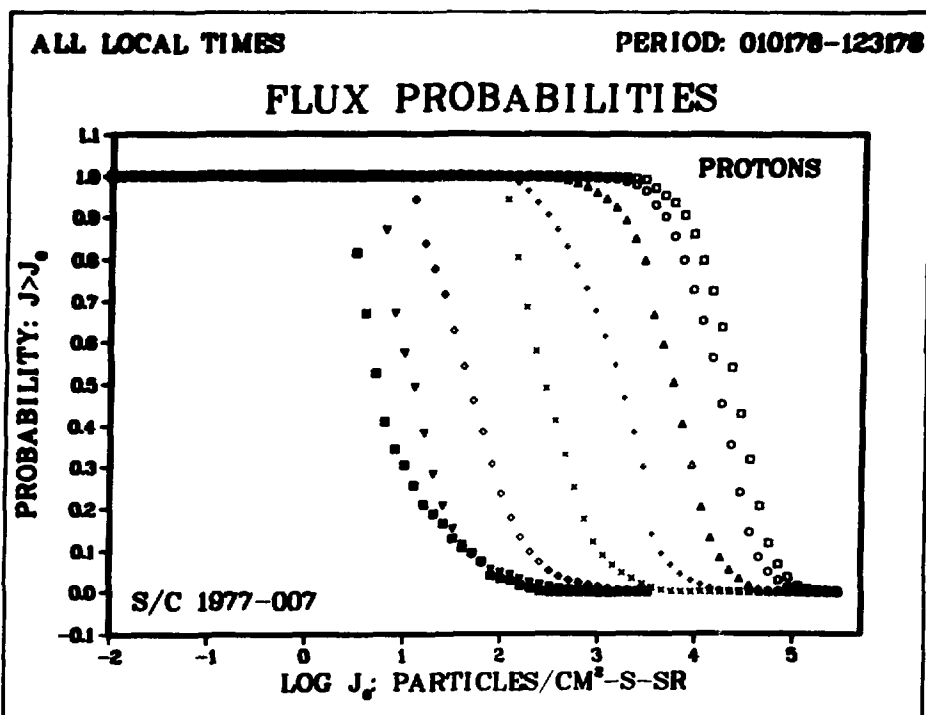
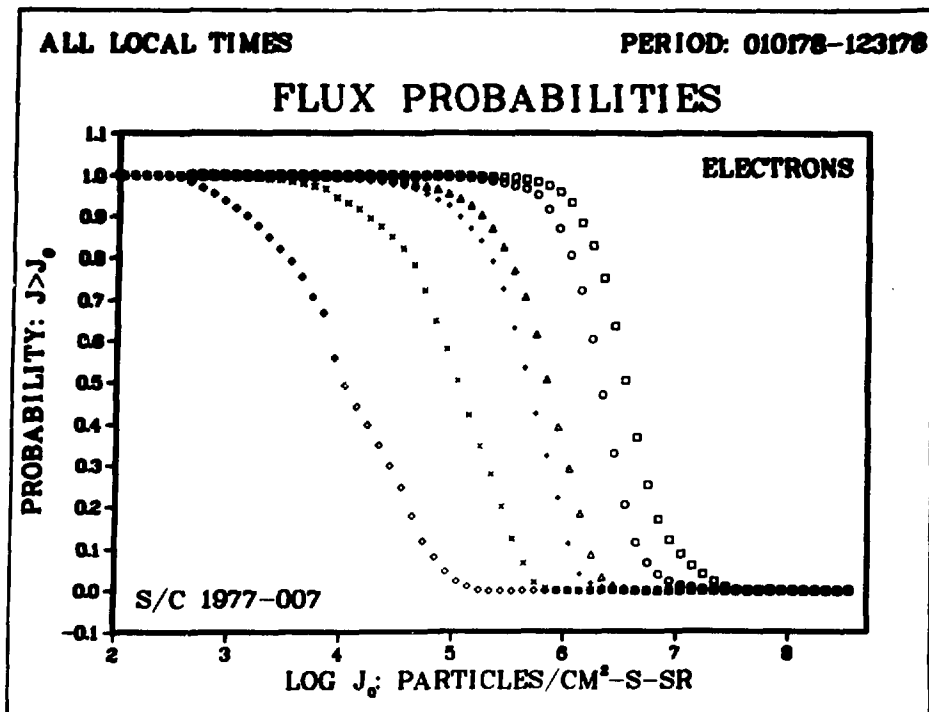


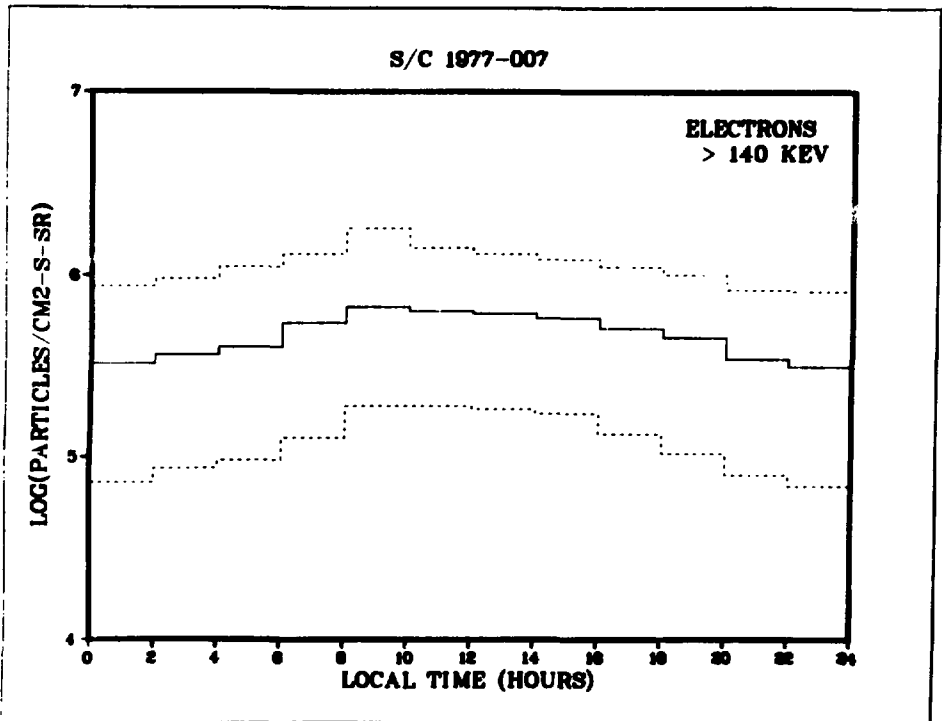
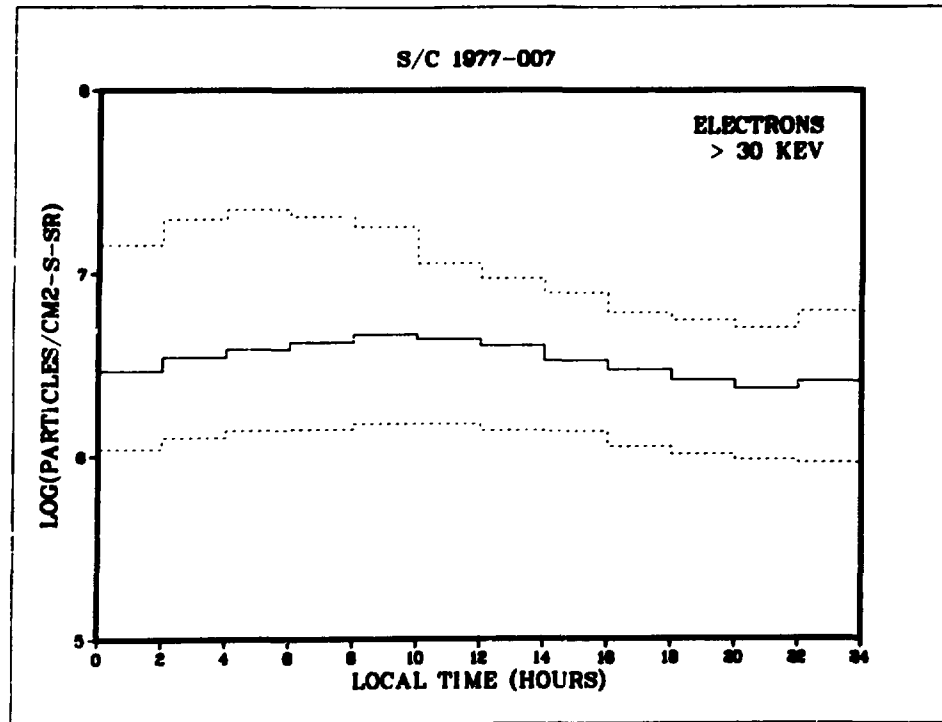
LOCAL TIME: 15-21

PERIOD: 010178-123178

FLUX PROBABILITIES



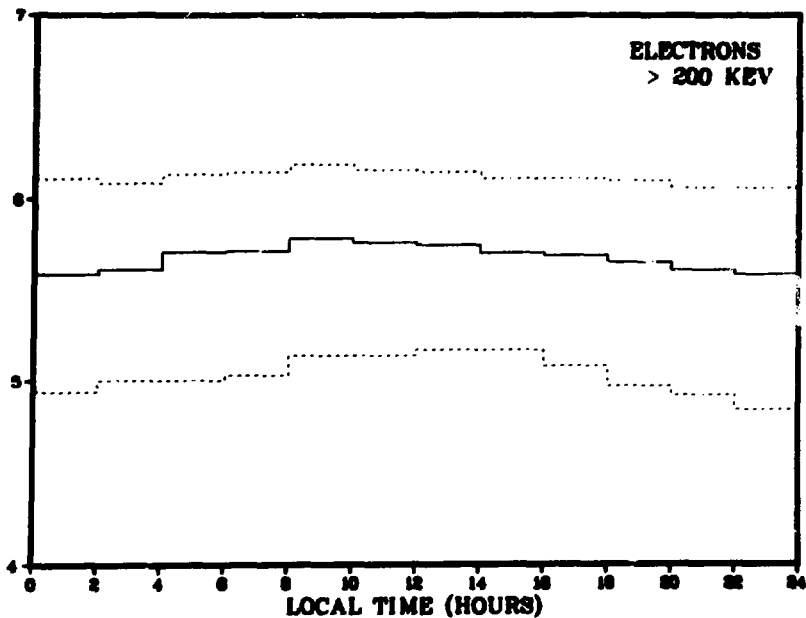




S/C 1977-007

ELECTRONS
> 200 KEV

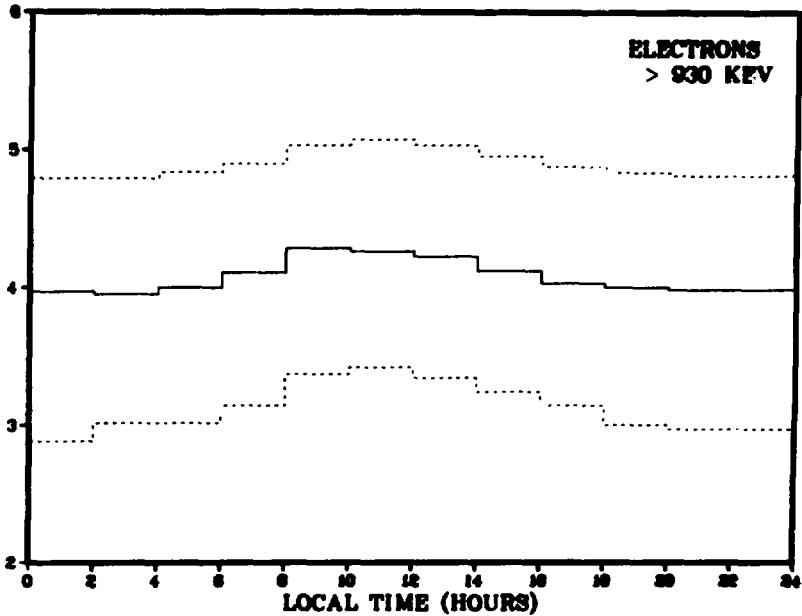
LOG(PARTICLES/CM²-S-SR)

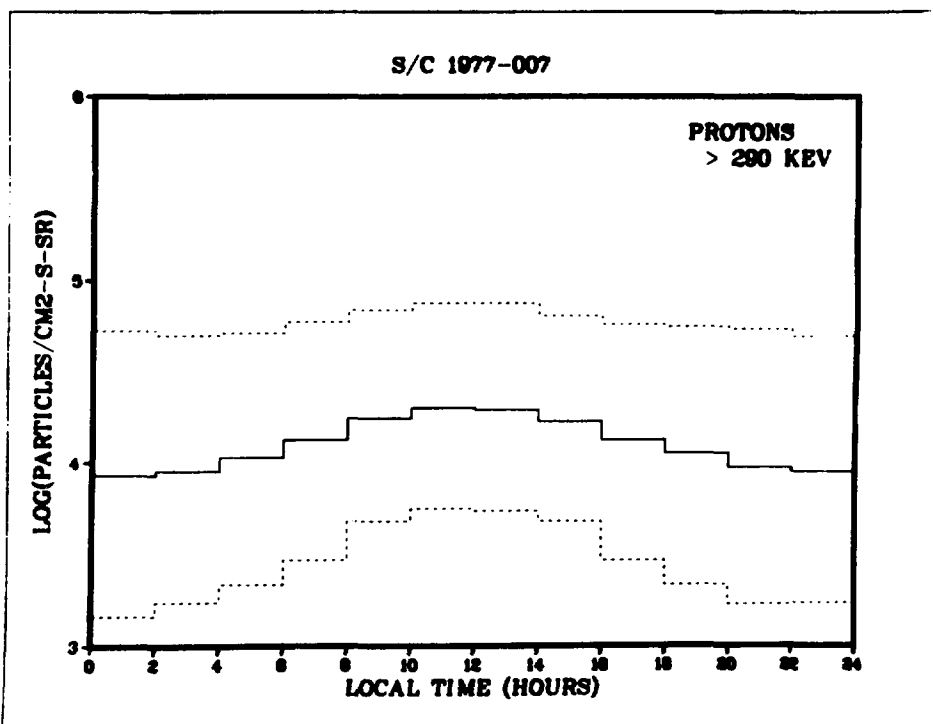
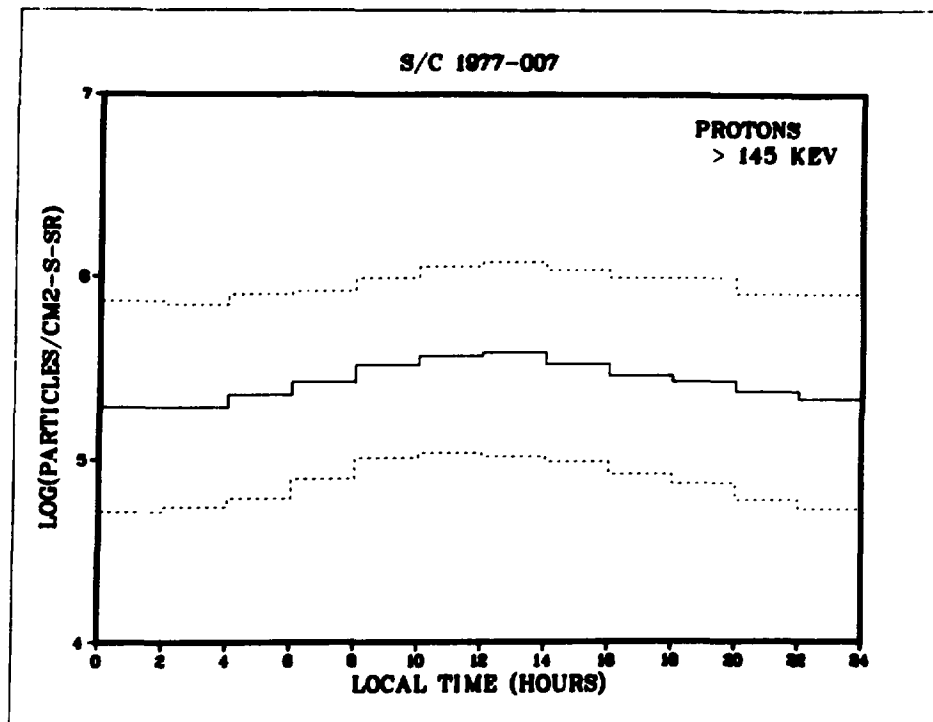


S/C 1977-007

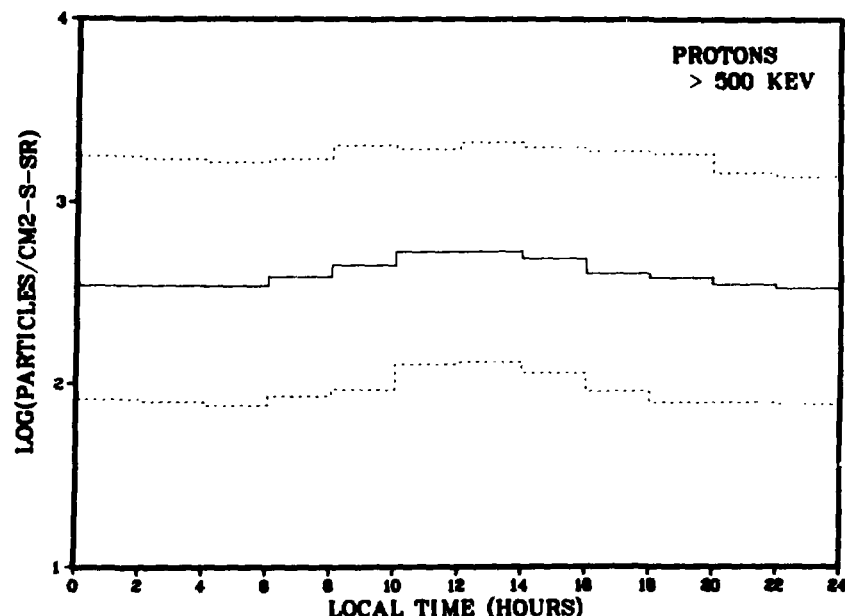
ELECTRONS
> 930 KEV

LOG(PARTICLES/CM²-S-SR)





S/C 1977-007



S/C 1977-007

